Norwegian University of Life Sciences
Faculty of Environmental Sciences
and Natural Resource Management

Philosophiae Doctor (PhD)
Thesis 2020:8

Investigating sensitivity and tolerance to chronic gamma irradiation in the nematode *Caenorhabditis elegans*

En studie av sensitivitet og toleranse for kronisk gammabestråling hos nematoden *Caenorhabditis elegans*

Erica Maremonti

Investigating sensitivity and tolerance to chronic gamma irradiation in the nematode *Caenorhabditis elegans*

En studie av følsomhet og toleranse for kronisk gammabestråling hos nematoden *Caenorhabditis elegans*

Philosophiae Doctor (PhD) Thesis

Erica Maremonti

Norwegian University of Life Sciences

Faculty of Environmental Sciences and Natural Resource Management

Ås (2019)

Thesis: 2020:8

ISSN: 1894-6402

ISBN: 978-82-575-1674-1

"Chaos is merely order waiting to be deciphered"

- José Saramago

Supervisors

Doctor Dag Anders Brede, PhD
Centre for Environmental Radioactivity (CERAD) CoE
Faculty of Environmental Sciences and Natural Resource Management (MINA)
Norwegian University of Life Sciences (NMBU)
E-mail: dag.anders.brede@nmbu.no

Professor Brit Salbu, PhD
Centre for Environmental Radioactivity (CERAD) CoE
Faculty of Environmental Sciences and Natural Resource Management (MINA)
Norwegian University of Life Sciences (NMBU)
E-mail: brit.salbu@nmbu.no

Professor Deborah H. Oughton, PhD
Centre for Environmental Radioactivity (CERAD) CoE
Faculty of Environmental Sciences and Natural Resource Management (MINA)
Norwegian University of Life Sciences (NMBU)
E-mail: deborah.oughton@nmbu.no

Associate Professor Ole-Christian Lind, PhD
Centre for Environmental Radioactivity (CERAD) CoE
Faculty of Environmental Sciences and Natural Resource Management (MINA)
Norwegian University of Life Sciences (NMBU)
E-mail: ole-christian.lind@nmbu.no

Professor Peter Aleström, PhD
Centre for Environmental Radioactivity (CERAD) CoE
Department of Basic Sciences and Aquatic Medicine,
Faculty of Veterinary Medicine
Norwegian University of Life Sciences (NMBU)
E-mail: peter.alestrom@nmbu.no

Evaluation committee

Doctor Christelle Adam-Guillermin
Institut de Radioprotection et de Sûreté Nucléaire, PSE-SANTE, Cadarache,
Saint Paul Lez Durance, France
Phone: +33 4 42 19 94 01
E-mail: christelle.adam-guillermin@irsn.fr

Professor Hilde Loge Nilsen
Department of Clinical Molecular Biology, University of Oslo
Sykehusveien 25, Akershus University Hospital, Epigen B2,
1478 LØRENSKOG, Norway
Phone: +47 67963922
E-mail: h.l.nilsen@medisin.uio.no

Doctor Hans-Christian Teien
Centre for Environmental Radioactivity (CERAD) CoE
Faculty of Environmental Sciences and Natural Resource Management, NMBU
P.O. Box 5003
1432 Ås, Norway
Phone: +47 6723 1893
E-mail: hans-christian.teien@nmbu.no

Acknowledgments

The present PhD project was financially supported by the Norwegian University of Life Sciences (NMBU) through a PhD scholarship and by the Research Council of Norway through its Centre of Excellence (CoE) "Centre for Environmental Radioactivity" funding scheme (CERAD, Project No. 223268/F50). The research work was carried out at the facilities at the Norwegian University of Life Sciences (NMBU).

First of all, I would like to acknowledge my main supervisor, Dr. Dag A. Brede, for offering me this challenge and great opportunity. I cannot express how deeply grateful I am to you, Dag, for giving me your endless support, through wise words, genius ideas and practical guidance, but most importantly for always believing in me. The door of discussion and many times listening was always open, and I really appreciated that.

I would also like to acknowledge all my co-supervisors, for giving me scientific guidance, especially during the writing process, and above all for sharing your knowledge over these years, it has been a very enriching experience for me. Thanks to Prof. Brit Salbu and Dr. Ole-Christian Lind, for giving me the possibility to learn not only from the books and the lectures, but also from the nice stories and from the field. Thanks to Prof. Deborah Oughton for the support, the interesting lectures, but also for the nice dinners and always kind words. Thank you to Prof. Peter Aleström, for giving me the chance to learn more about epigenetic by organizing nice workshops and by opening the door of his lab.

Thank you to all my co-authors and to the CERAD colleagues for their invaluable contribution, but most importantly to Dr. Einar S. Berg, for patiently teaching me all I know about PCR, and for nice discussions about Italian wine. Thanks to Dr. Lisa Rossbach, for being my everyday support as a colleague but especially as a friend. I am very grateful to Dr. Dag Markus Eide, for the statistical and sometimes moral support, and for always helping me find the solution. Thanks to Dr. Yetneberk Kassaye, for the moral and practical support during the development of the Comet assay, Dr. Ann-Karin Olsen for nice discussion and Dr. Fabian Grammes for the bioinformatic support. Thanks to Hilde Raanaas Kolstad, Lene Cecilie Hermansen and Dr. YeonKyeong Lee for nice chats, kind assistance and help during the microscopy analysis. Thanks also to Jan Vermaat, for reading and revising my thesis. A special thanks to Dr. Catherine Lecomte-

Pradines and Rémi Guédon for the warm hospitality in their lab, where I learned more about *C. elegans* and I did not only find nice colleagues, but also valuable friends.

Last but not least, a special thank you to all my lovely colleagues and friends at Isotope lab, for welcoming me since day one, making me feel home, for nice lunches, coffee breaks and amusing dinners, which made even my toughest days more bearable.

Finally, a huge thank you to my family, mamma, papa', Marcello, Visa, zia Giuliana and to my best friends Michele, Sante and Eugenia, for always being there for me, even if at several thousands of kilometres away, you were always at a phone call-distance to me, ready to make me feel better, even in the darkest Norwegian days.

And last to my Ken, thank you for being my family here in Norway, filling my days with laughter and love.

Erica,

Ås, November 2019

Table of Contents

Summary

At the cellular level, excitation and ionization of atoms and molecules constitute the fundamental processes leading to harmful effects induced by exposure to ionizing radiation. However, radiosensitivity, defined as the relative susceptibility of organisms, tissues or cells to the harmful effects of ionizing radiation, differs considerably across species and phyla. Specifically, a lethal dose for most vertebrates (10 Gy) is orders of magnitude lower than the dose required to induce detrimental effects in the utmost radioresistant species (≤1.2 kGy). Living organisms can be exposed to ionizing radiation in the environment due to nuclear accidents, but also due to the routine release from nuclear power plants or reprocessing plants. This can result in chronic exposure at doses above the background levels, with adverse consequences for the population dynamics and sustainability, because sensitive life-stages or vulnerable biological processes are impaired.

Importantly, while most of the research on radioresistant species has focused on acute exposure to high doses, the effects of chronic exposure to low doses remained under appreciated. A ground-breaking study by Buisset-Goussen et al. (2014) revealed that chronic gamma irradiation caused significant reprotoxic effects from relatively low total doses in the radioresistant nematode *Caenorhabditis elegans*. However, the molecular mechanisms causing this adverse effect needed a better understanding.

The current PhD study focused on the investigation of cellular and molecular mechanisms behind the phenotypical adverse effects shown in the nematode *C. elegans* after chronic exposure to ionizing radiation. In particular, the different experiments were designed in order to gain more information about the dose-response reprotoxic and developmental effects, the larval-stage sensitivity as well as the cell and tissue-specific sensitivity. For this purpose, a range of low and high dose-rates of gamma radiation from a ^{60}Co source was selected (0.4 to 1000 mGy·h^{-1}) and a multitude of cellular and molecular biology techniques applied, including the use of GFP reporter strains, epifluorescence microscopy and RNA sequencing. Moreover, this study involved the development and optimization of new methods, including the embryonic cells isolation in order to assess DNA damage via the Comet assay or the droplet digital PCR method, optimized to measure the mitochondrial DNA (mtDNA) copy number variation.

The results demonstrate that chronic exposure during larval development induces reprotoxic effects at doses ≥3.9 Gy (40 mGy·h^{-1}), while acute or chronic irradiation during the post-mitotic larval stage does not induce any adverse effect at doses ≤15 Gy (≤1 Gy·h^{-1}). L1-L4 larval stages were shown to be the most radiosensitive stages of development due to impaired spermatogenesis. Specifically, significant sperm reduction and dysregulation of genes related to sperm meiosis and maturation were identified as the cause of reprotoxicity. At the mechanistic level, these results provide important insight into the radiation induced cellular processes that lead to failed spermatogenesis. These mechanisms may be relevant to other species given the conserved nature of meiosis and the fact that radiation is known to damage spermatogenesis in earthworms, insects, mice, as well as humans.

Adverse effects on proliferative cells were also shown by enhanced germ cell apoptosis in F0 nematodes and significant DNA damage in embryos (F1) of irradiated nematodes, which was corroborated by the dysregulation of genes related to cell-cycle checkpoints, DNA repair, embryonic and post-embryonic development. In contrast to their parents, negative effects on somatic growth but no significant reprotoxic effects were observed in F1 parentally irradiated nematodes. Suggesting that, parental exposure to ionizing radiation induces the activation of defence mechanisms. These aid to ameliorate the severe DNA damage, under control conditions, but may require high energy cost which might explain their significantly reduced somatic growth.

The increased ROS levels together with the enhanced AODs activation was demonstrated *in vivo* and by gene expression analysis after chronic irradiation of F0 nematodes. This was not accompanied by any adverse effect on somatic cell viability or any visible phenotypical effect, indicating tolerance of somatic tissue, despite the cellular redox imbalance. However, the observed redox imbalance suggested a significant contribution of indirect effects, including oxidative damage to DNA, proteins, lipid metabolism and mitochondrial functions from chronic exposure to ionizing radiation. In particular, genes essential for the assembly and proper functioning of the mitochondrial electron transport chain were found significantly down-regulated. For this reason, mitochondria were proposed as a vulnerable target of chronic irradiation. However, by measuring the mt/nDNA-ratio (mitochondrial/nuclear DNA) as read-out for mitochondrial dysfunction, at doses of exposure ≤7.2 Gy, nematodes showed to

maintain a stable mtGenome content. Only doses ≥24 Gy demonstrated a significant increase in the mtDNA copy number, suggesting a potential role of mtDNA replication and maintenance in the intrinsic radioresistance of *C. elegans* somatic cells.

Taken together the main findings of this research contributed to an improved understanding of the molecular and cellular mechanisms of toxicity and tolerance induced after chronic exposure to ionizing radiation in an important model organism, *C. elegans*. The finding that spermatogenesis in a radioresistant nematode is affected by 2.8 Gy, which is approximately three orders of magnitude lower than the reported acute LD90 (lethal dose required to kill 90% of the tested population), demonstrates the importance of characterizing effects of chronic low dose and low dose-rate of ionizing radiation. This information may also be relevant for further comparative analysis with other species, expressing different degrees of sensitivity, as well as for multi or trans-generational studies performed on the same model organism.

Sammendrag

Ioniserende stråling forårsaker skadelige effekter i alle typer celler via to fundamentale prosesser: eksitasjon eller ionisering av atomer og molekyler. Strålingssensitivitet er definert som den relative følsomheten av organismer, vev eller celler overfor skadelige effekter av ioniserende stråling, er svært forskjellig mellom ulike arter og phyla.

En dose på ti Gray (10 Gy) vil forårsake død hos de fleste vertebrater, mens de mest stråleresistente artene må ha over hundre ganger denne dosen (≤1.2 kGy) før de viser tegn til skade. Organismer kan bli eksponert for ioniserende stråling i miljøet som følge av atomulykker eller fra rutineutslipp fra atomkraftverk og nukleære reprosesserings-anlegg. Dette kan gi kronisk eksponering for betydelig høyere doserater sammenlignet med naturlig bakgrunnsstråling. Dette kan i noen tilfeller ha negativ effekt på sensitive livsstadier eller sårbare biologiske prosesser, hvilket kan medføre adverse effekter på populasjondynamikk eller levedyktighet.

Forskning på strålingsresistente arter har fokusert på akutt eksponering ved høye doser. Effekter av lavdose kronisk eksponering har til sammenligning vært lite vektlagt inntil en gjennombruddstudie (Buisset-Goussen et al., 2014) viste signifikante reproduksjonsdefekter hos den strålingsresistente nematoden *Caenorhabditis elegans*. De underliggende molekylære mekanismene som forårsaket slike adverse effektene var ikke kjent.

Denne PhD-studien har fokusert på cellulære og molekylære mekanismer knyttet til fenotypiske adverse effekter av kronisk eksponering til ioniserende stråling i nematoden *C. elegans*. Studien ble designet for å få innsikt i dose-respons sammenhenger i reprotoksisitet, utviklingsdefekter, sensitive celletyper og livsstadier. Denne studien har derfor omfattet et spenn fra lave til høye doserater (0.4 til 1000 $mGy \cdot h^{-1}$), kombinert med en rekke cellulære, molekylære teknikker, inkludert GFP-reporterstammer, epifluorescens-mikroskopi og RNA-sekvensering. Det har også vært nødvendig å utvikle og optimalisere nye metoder inkludert isolering av embryoceller for å kunne måle DNA-skade via COMET, og kvantitativ måling av mitokondrie DNA (mtDNA) kopitall via 'digital dråpe basert PCR' (ddPCR). Resultatene viste at kronisk eksponering gjennom larveutviklingen induserer reprotoksiske effekter ved ≥3.8 Gy (≥40 $mGy \cdot h^{-1}$), mens akutt eller kronisk bestråling av post-mitotiske larver hadde ingen

detekterbare effekter ≤15 Gy (≤1000 mGy·h^{-1}). L1-L4 stadiene ble vist å være det mest strålingssenitive delen av nematodens utvikling pga defekt spermatogenese. Signifikant redusert spermproduksjon og dysregulering av gener involvert i sperm-meiose og modning ble identifisert som årsak til reprotoksisitet. Disse resultatene er viktig og gir ny innsikt i strålingsinduserte cellulære effekter som skader spermatogenesen. Disse mekanismene kan være relevante for andre arter pga mange prosesser i sperm-meiosen er konservert, og fordi stråling er vist å skade spermatogenese i meitemark, insekter, mus og mennesker.

Adverse effekter ble påvist i prolifererende celler, både ved økt apoptose i kjønnsceller i F0 nematoder, og ved signifikant DNA skade i F1 embryo av bestrålte nematoder. Disse effektene ble underbygget av dysregulering av gener involvert i cellesyklus sjekkpunkter, DNA-reparasjon, samt embryo og post-embryo utvikling. I motsetning til den bestrålte foreldregenerasjonen (F0), viste avkom (F1) signifikant redusert vekst men ingen reprotoksisitet. Dette kan tyde på en sterk aktivering av forsvarsmekanismer, f.eks DNA-reparasjon, men at disse har en kostnad i form av høyere energiforbruk og redusert vekst.

Økt produksjon av reaktive oksygenforbindelser (ROS) og aktivering av antioksidant forsvar (AOD) i kronisk bestrålte nematoder, ble vist in vivo og ved genekspresjonsanalyser. Til tross for signifikant redoks ubalanse ble det ikke observert fenotypiske endringer eller redusert viabilitet i somatiske celler. Den observerte redoks-ubalansen viser et signifikant potensiale for indirekte effekter og oksidative skader på DNA, protein, lipidmetabolisme og mitokondriefunksjon ved kronisk eksponering til ioniserende stråling. Genekspresjonsanalyser viste at gener med essensiell funksjon i elektrontransportkjeden var signifikant nedregulerte, og indikerte at mitokondriefunksjoner kunne være sensitive for ioniserende stråling. Dette ble videre undersøkt ved å bruke mitokondriell/nukleær (mt/n) DNA-ratio som endepunkt for å vurdere mitokondriell dysfunksjon. Resultatene viste ingen effekt på mtDNA kopitall ved doser ≤7.2 Gy. Doser ≥24 Gy førte derimot til en dobling i mtDNA kopitall, hvilket kan tyde på at mitokondrie DNA blir replisert, og vedlikeholds mekanismer bidrar til strålingsresistensen i *C. elegans* somatiske celler.

Samlet sett har hovedfunnene av denne studien bidratt til økt kunnskap om molekylære og cellulære mekanismer knyttet til toksisitet og toleranse hos en viktig

modellorganisme, *C. elegans* ved kronisk eksponering til ioniserende stråling. Funnet av inhibert spermatogenese ved 2.8 Gy i en stråleresistent organisme, noe som er ca 1000 ganger lavere enn akutt LD90 (akutt dose med 90% dødelighet), viser viktigheten av å studere effekter av kronisk lav dose og doserate ioniserende stråling. Disse funnene er relevante for komparative analyser med andre arter med ulik strålingsensitivitet, og danner et fundament for fremtidige studier av multi- eller transgenerasjonelle strålingseffekter i *C. elegans*.

Abstract

A livello cellulare, l'eccitazione e la ionizzazione di atomi e molecole rappresentano il principale meccanismo di tossicitá in risposta alle radiazioni ionizzanti. Tuttavia, il grado di sensibilitá relativa alle radiazioni ionizzanti tra diverse specie e phyla presenta enormi variazioni. In particolare, dosi letali (10 Gy) per la maggior parte dei vertebrati sono di ordini di grandezza inferiore rispetto a dosi necessarie per indurre degli effetti tossici nelle specie piu resistenti (≤1.2 kGy). Oltre che a causa di incidenti nucleari, l'esposizione degli organismi viventi alle radiazioni ionizzanti puó avvenire in conseguanza al normale rilascio da parte di centrali nucleari o di impianti per lo smaltimento delle scorie radioattive. Queste attivitá possono causare l'esposizione cronica a dosi superiori rispetto ai livelli di background, con conseguenze negative per le dinamiche e la sostenibilitá delle popolazioni. Tra le cause di tali effetti negativi ci sono lo sconvolgimento dei naturali processi biologici o l'esposizione di fasi di sviluppo sensibili, come ad esempio la capacitá riproduttiva di una specie o l'esposizione dei primi stadi di sviluppo larvale.

Molti studi si sono concentrati sugli effetti relativi a specie radioresistenti esposte in maniera acuta ad alte dosi di radiazioni, tuttavia gli effetti causati da un'esposizione cronica a dosi inferiori, in tali specie, sono ancora poco chiari. Studi preliminari hanno dimostrato un effetto reprotossico nel nematode radioresistante *Caenorhabditis elegans* (Buisset-Goussen et al., 2014), in consequenza ad un esposizione cronica, ma i meccanismi molecolari scatenanti rimangono ignoti.

Per queste ragioni, il presente studio ha lo scopo di analizzare i meccanismi cellulari e molecolari alla base degli effetti fenotipici osservati nel *C. elegans* esposto a dosi croniche di radiazioni. In particolare, diversi esperimenti sono stati pianificati con l'obiettivo di ottenere maggiori informazioni riguardo agli effetti dose-risposta reprotossici e di sviluppo, alla vulnerabilitá di determinati stadi di sviluppo, o di determinati tipi cellulari.

A tal proposito, un'ampio range di dosi di radiazioni gamma a diversa intensitá provenienti da una sorgente di ^{60}Co è stata selezionata (0.4 to 100 mGy·h-1 e ~1 Gy·h-1). Inoltre, diverse tecniche di biologia cellulare e molecolare sono state applicate, tra cui l'uso di mutanti, la microscopia a fluorescenza e l'espressione genica. In alcuni casi,

questo studio ha richiesto l'ottimizzazione e lo sviluppo di nuove metodologie, come ad esempio l'isolamento di cellule embrionali, al fine di valutare il danno al DNA in embrioni esposti in utero, oppure l'ottimizzazione di un metodo basato sulla PCR digitale per misurare la variazione nel numero di copie di DNA mitocondriale.

I risultati di questo studio dimostrano che l'esposizione cronica durante le diverse fasi di sviluppo larvale induce un effetto reprotossico a dosi ≥3.9 Gy, mentre l'esposizione acuta o cronica a dosi anche piú elevate (≤15 Gy) durante lo sviluppo post-mitotico in organismi adulti non causa alcun danno. In particolare il maggior grado di sensibilitá alle radiazioni e stato dimostrato negli stadi di sviluppo larvale L1-L4, a causa di effetti negativi a carico della spermatogenesi. La riduzione della conta spermatica, insieme alla negativa regolazione di geni essenziali per la meiosi e la maturazione spermatica misurate a dosi ≥2.8 Gy sono state considerate le cause scatenanti dell'effetto reprotossico. Altri effetti negativi sono stati riscontrati a carico di cellule proliferative, come dimostrato dall'aumento di cellule germinali apoptotiche o dal significativo danno genomico misurato nelle cellule embrionali. Tali effetti sono stati ulteriormente validati dalla differente espressione di geni con funzioni essenziali per il ciclo cellulare, e lo sviluppo embrionale e post-embrionale.

L'aumento dei livelli di radicali liberi, insieme all'attivazione di meccanismi antiossidanti, dimostrati *in vivo* ed attraverso il sequenziamento genico, in seguito all'esposizione cronica, hanno indicato uno sbilanciamento nello stato ossidoriduttivo cellulare. Questo sbilanciamento puo essere interpretato come la causa scatenante per l'attivazione di una moltitudine di meccanismi molecolari di difesa, inclusi quelli relativi alla riparazione del danno al DNA, alla degradazione proteica, al metabolismo lipidico e all'alterazione di alcune funzioni mitocondriali. In particolare, la ridotta espressione di geni essenziali per l'assemblamento ed il normale funzionamento della catena di trasporto degli elettroni ha indicato che il mitocondrio potesse essere un target vulnerabile delle radiazioni. Tuttavia il rapporto tra genoma mitocondriale e nucleare non ha dimostrato alcun effetto sul numero di copie di DNA mitocondriale, a dosi di radiazioni simili (≤7.2 Gy). Soltanto dosi superiori ai 24 Gy hanno dimostrato di indurre un aumento significativo nel numero di genomi mitocondriali, effetto che potrebbe suggerire un meccanismo di compensazione a causa dell'eccessivo danno genotossico.

La somma di questi risultati, ottenuti nel corso di questo dottorato di ricerca, contribuisce a far luce sui meccanismi di tossicitá e tolleranza cellulare e molecolare indotti dall'esposizione cronica alle radiazioni nell'organismo resistante *C. elegans*. Queste informazioni possono essere utilizzate per ulteriori analisi comparative con altre specie che possiedono diversi gradi di sensibilitá, oltre che per studi multigenerazionali e transgenerazionali sullo stesso organismo modello.

Abbreviations and acronyms

AODs	antioxidant defences
AOP	adverse outcome pathway
CNV	copy number variation
cpYFP	circularly permuted yellow fluorescent protein
CT	cycle threshold
ddPCR	droplet digital Polymerase Chain Reaction
DDR	DNA damage response
DEGs	differentially expressed genes
DIC	differential interference contrast
dPCR	digital Polymerase Chain Reaction
DSB	double strand break
DTC	distal tip cell
ETC	electron transport chain
FB	fibrous body
GFP	green fluorescent protein
Grx1-roGFP2	Glutaredoxin 1-redox sensitive green fluorescent protein 2
Gy	Gray (SI unit, J/Kg absorbed)
HyPer	Hydrogen Peroxide ratiometric biosensor
HR	homologous recombination
LET	linear energy transfer
MO	membranous organelle
MSP	major sperm protein
mtDNA	mitochondrial DNA
mtGenome	mitochondrial genome
nDNA	nuclear DNA

NER	nucleotide excision repair
NGM	nematode growth media
NHEJ	non-homologous end joining
NORM	naturally occurring radioactive material
PCR	Polymerase Chain Reaction
qRT-PCR	quantitative real-time Polymerase Chain Reaction
RNAi	RNA inhibition
ROS	reactive oxygen species
SPCH	sperm chromatin enriched proteins
TZ	transition zone
UV	ultraviolet

List of papers

This thesis is based on the papers listed below, which are referred to in the text by their Roman numerals.

Paper I

MAREMONTI, E., EIDE, D. M., OUGHTON, D. H., SALBU, B., GRAMMES, F., KASSAYE, Y. A., GUÉDON, R., LECOMTE-PRADINE, C. & BREDE, D. A. 2019. Gamma radiation induces life stage-dependent reprotoxicity in *Caenorhabditis elegans* via impairment of spermatogenesis. *Science of The Total Environment*, 133835.

Paper II

MAREMONTI, E., EIDE, D. M., ROSSBACH, L.M., SALBU, B., LIND, O.C. & BREDE, D. A. 2019. *In vivo* assessment of reactive oxygen species production and oxidative stress effects induced by chronic exposure to gamma radiation in *C. elegans. Accepted for publication. Free Radical Biology and Medicine.* (November 2019)

Paper III

MAREMONTI, E., EIDE, D. M., OLSEN, A-K., BREDE, D. A. & BERG, E. S. 2019. Development of droplet digital PCR method for the assessment of mitochondrial DNA copy number variation in response to ionizing radiation in the nematode *Caenorhabditis elegans*. M*anuscript.*

1. Introduction

1.1 Background

All organisms are exposed to low level background of environmental radiation with little detriment to their existence. Nevertheless, ionizing radiation associated with naturally occurring radioactive material (NORM), mining sites, or from anthropogenic release from nuclear power plants or nuclear accidents, have the potential to pose a significant environmental risk (UNSCEAR, 2000).

The ability of organisms to tolerate radiation exposure can vary by more than 1000-fold (Andersson et al., 2009). Therefore, the environmental consequences of ionizing radiation contamination are highly dependent on species composition in a given ecosystem (Garnier-Laplace et al., 2013). Understanding of the factors influencing species radiosensitivity thus constitutes an important research area to assess the risk of adverse effects at species, population and ecosystem functions level (Pentreath et al., 2014).

An acute dose of 10 Gy would cause lethal effects in most vertebrate species, whereas, the most radioresistant organism known (the extremophile bacterium *Deinococcus radiodurans*) is hardly affected at doses of 12 kGy (Daly et al., 1994). Intermediate tolerance has been shown in invertebrates composed primarily of post-mitotic tissues, such as adult fruitflies (Parashar et al., 2008) and the nematode *Caenorhabditis elegans* (Johnson and Hartman, 1988, Daly, 2009). Moreover, differences in radiation sensitivity are also dependent on exposure scenario (acute or chronic exposure), the biology of the organism, the stage of development at which the irradiation occurs and the evolved cellular and molecular defence mechanisms (Adam-Guillermin et al., 2018). For instance, a highly efficient DNA repair mechanism via homologous recombination, or the capacity to scavenge reactive oxygen species (ROS) through a robust antioxidant defence (AOD) system, can render an organism more tolerant towards ionizing radiation (Zahradka et al., 2006, Krisko et al., 2012a).

While effects of acute exposure on radioresistant species have been extensively studied (Hartman, 1982, Cox and Battista, 2005, Horikawa et al., 2006, Gladyshev and Meselson, 2008b, Hashimoto et al., 2016), the consequences of low dose and low dose-rate chronic

exposure are less clear. However, accumulating experimental evidence indicates that under certain circumstances long-term exposure to ionizing radiation can induce adverse effects at lower doses than acute exposures, and that adversity can be transmitted over multiple generations (Merrifield and Kovalchuk, 2013, Adam-Guillermin et al., 2018, Kamstra et al., 2018, Horemans et al., 2019). Reproduction constitutes a particular sensitive target of chronic exposure to ionizing radiation, most likely because actively dividing and functionally undifferentiated cells are vulnerable to the effects of radiation (UNSCEAR, 1996). Even tolerant species have shown loss of their reproductive capacity when chronically irradiated (Hertel-Aas et al., 2007, Buisset-Goussen et al., 2014, Parisot et al., 2015, Yushkova, 2019). Thus, biological processes involving rapid cell division, such as germ cell proliferation and embryonic development, can represent susceptible targets, and their impairment can have severe consequences for the survival of populations. For these reasons, once adverse effects have been identified, understanding the underlying mechanisms for radiosensitivity of specific tissues and cell-types between different species is of high relevance.

1.2 Aim and hypotheses of the study

The aim of this study was to assess the effects of chronic exposure to low-dose ionizing gamma radiation in the radioresistant nematode *Caenorhabditis elegans,* through a systematic investigation of life stage, tissue, cellular and molecular responses, in order to connect phenotypical effects with molecular mechanisms of toxicity. For this purpose, the following hypotheses were defined to address radiosensitivity and tolerance mechanisms in *C. elegans*:

I. Chronic irradiation during larval development is more harmful than exposure of post-mitotic adult larvae.

II. The reproductive apparatus is a vulnerable target for chronic low-dose gamma irradiation due to high cell proliferation in the gonadal tissues.

III. *C. elegans* Antioxidant Defences ameliorate oxidative damage and thereby provide tolerance towards chronic exposure to ionizing radiation.

IV. The mitochondria and mtDNA comprise a sensitive target of chronic exposure to ionizing radiation and nematodes activate defence mechanisms to counteract mitochondrial dysfunction.

1.3 Sources of ionizing radiation in the environment

In the environment, the release of radionuclides from nuclear weapons testing (Salbu, 2008, Wendel et al., 2013, Abella et al., 2019) and nuclear power plant accidents (i.e. Chernobyl, 1986 and Fukushima Daiichi, 2011) (Salbu et al., 1994, Stohl et al., 2012, UNSCEAR, 2008) can be sources of ecotoxicological risk. In addition, other anthropogenic activities generate routine discharges of radioactive material, including releases from nuclear power or reprocessing plants, mining, NORM-sites, nuclear waste from research facilities and medical diagnostic or therapeutic treatments (UNSCEAR, 1996). Combined these sources enhance the probability of an organism to be exposed to ionizing radiation at doses above the background levels of 0.01 - 0.44 $\mu Gy \cdot h^{-1}$ (Copplestone et al., 2001). The exposure scenario, however, will depend on the source and the way the release occurs (Salbu, 2000). In the event of a nuclear accident, the environment will usually be contaminated by a mixture of radionuclides, and different kinds of ionizing radiation, namely alpha (α), beta (β) and gamma (γ) radiation. Cobalt- 60 (^{60}Co) and Cesium-137 (^{137}Cs) are both examples of beta and gamma emitting radionuclides that are routinely released from nuclear power plants and nuclear reprocessing plants (Adam-Guillermin et al., 2012).

1.4 Effects of ionizing radiation on biota

The effects of exposure to ionizing radiation depend primarily on the energy transferred into the tissue, defined as the absorbed dose, or Gray (J/kg). In turn, the amount of damage is also influenced by the rate of energy transfer per unit of distance (Linear Energy Transfer, LET, measured as $keV \cdot mm^{-1}$). While alpha particles and neutrons have a high rate of energy transfer (High-LET), gamma radiation, electrons (Beta particles) and X-rays are characterized by low-LET. Since high-LET particles deposit their energy

in a smaller volume than low-LET ionizing radiation type, about 90% of the energy deposited induces clustered damage sites, such as DNA Double Strand Breaks (DSBs) (Hall and Giaccia, 2006). In addition to a higher density, the complexity of the clusters, reflecting the amount of lesions caused, also increases with the LET of the radiation (Lomax et al., 2013). However, low-LET radiation, such as external exposure to gamma radiation of the whole body of an organism, can induce ionization of molecules in a more homogeneous way at the cell and tissue level. Gamma rays are high energy electromagnetic waves, which can penetrate matter over a longer distance compared to α and β particles (Choppin et al., 2002). About 70% of the energy deposited by low-LET radiation induces isolated lesions, which contributes to the overall oxidative burden of a cell. However, 30% of the energy deposited by high-energy photons will cause clustered damage sites, having different structural and chemical complexity (Nikjoo et al., 1999).

Internal exposure to alpha and beta particles can be highly harmful, but gamma and X-rays are more penetrating, meaning that environmental exposure to gamma rays induces a greater degree of biological damage than external exposure to alpha or beta particles. This study therefore adopted external gamma irradiation experiments in order to elucidate the cellular, molecular and phenotypical mechanisms induced by chronic exposure to this environmental stressor.

Ionization and excitation of atoms and molecules is the primary event leading to cellular effects caused by exposure to ionizing radiation (Reisz et al., 2014) (Fig. 1.a). However, there is a wide range of responses to radiation, which are determined by a multitude of factors, including the type and energy of the radiation source, dosage, length of exposure and the genetic and epigenetic background of the organism exposed (Adam-Guillermin et al., 2018, Horemans et al., 2019). The biological response to ionizing radiation may differ between chronic and acute exposure, both in the quality and intensity of effects (Schwartz et al., 2000). While acute irradiation means exposing an organism to high doses of radiation for a short period of time, chronic exposure to lower doses is defined as the continuous exposure of at least 10% of the duration of a species lifespan (Newman, 2009).

The effects of acute exposure have been assessed on a wide range of organisms, including human and non-human species, however, the consequences of a chronic

irradiation is less studied, especially in terms of understanding the mechanisms of toxicity of long-term effects (Garnier-Laplace et al., 2013, Hinton et al., 2013).

The Chernobyl and Fukushima accidents have raised the awareness and concerns regarding the consequences of chronic exposure to gamma radiation in the environment and the relative lack of knowledge of the potential harmful effects on non-human species (Hinton et al., 2013). In the past decade, studies on a multitude of plants and aquatic species, including crustaceans and fish, have provided more information on the toxicological mechanisms, the causes of direct phenotypical effects and the potential consequences of long-term hereditary effects (Vandenhove et al., 2010, Pereira et al., 2011, Gomes et al., 2017, Hurem et al., 2017a, Gomes et al., 2018, Xie et al., 2019). Knowledge on soil organisms, however, is largely restricted to earthworms and nematodes (Hertel-Aas et al., 2007, Lecomte-Pradines et al., 2017, Lecomte-Pradines et al., 2014). Although the nematode *C. elegans* is considered to be among the most radioresistant species, chronic exposure to gamma radiation has been shown to cause reprotoxic effects (Buisset-Goussen et al., 2014) accompanied by changes to the proteomic profiles (Dubois et al., 2018). Nevertheless, there still remains a considerable knowledge gap with respect to molecular responses and mechanisms of defence in radioresistant species, since knowledge is predominantly restricted to acute exposure scenarios (Krisko and Radman, 2010, Krisko et al., 2012a, Sakashita et al., 2010). Hence studies of the effects of chronic exposure at the cellular and molecular level in radioresistant organisms, not only contributes to improving our knowledge on the toxicological mechanisms but can also help us to understand similarities with more radiosensitive species and serve as an important tool to improve risk assessment.

1.5 Cellular and molecular effects of ionizing radiation

The biological response to ionizing radiation exposure can result either from the direct deposition of energy into biomolecules, including proteins, lipids and DNA, or indirectly, via the interaction between these biomolecules and free radicals produced by the dissociation of water molecules (water radiolysis) (Fig. 1.a) (Lomax et al., 2013). The major categories of DNA damage inflicted by exposure to ionizing radiation include deleterious alterations of bases and sugars, cross-link formation, single and double

strand breaks and DNA clustering (Duncan Lyngdoh and Schaefer III, 2009, Thompson, 2012).

For many years, the central dogma of radiation biology considered the direct interaction of ionizing radiation with DNA in the cell nucleus as the main mechanism responsible for the radiation-induced genotoxic insult (Hutchinson, 1966, Blok and Loman, 1973). It is now widely accepted that indirect effects of exposure to ionizing radiation can be a major contributor to genotoxic effects, especially at low dose and dose-rates (Sutherland et al., 2000)(Fig. 1.b). Most of the indirect insult to nucleic acids results from the hydroxyl radical ·OH, which represents the most abundant and destructive of the products of water radiolysis towards these macromolecules (Reisz et al., 2014). Specifically, the interaction of the ·OH radicals with nucleic acids generates a variety of products, including the 8-hydroxypurines. Among these, 8-oxodG is the most common product and considered to be the hallmark for radiation-induced oxidative DNA damage (Svoboda and Harms-Ringdahl, 2005). The persistence of oxidative DNA damage, however, does not only depend on the direct interaction of free radicals with nucleic acids. The overall amount of ROS generated from primary ionization events is further propagated via the perturbation of endogenous ROS-producing systems, such as the mitochondrial electron transport chain (Choi et al., 2007, Kam and Banati, 2013) (Fig. 1.b). In biological systems, organic radicals are also formed; these usually react rapidly with O_2 to form peroxyl radicals ($RO^{\cdot}_2$), which are stronger oxidizing agents than the ones primarily formed (Spitz et al., 2004). The highly reactive peroxyl radicals can interact with other molecules to abstract the H· and form hydroperoxides (ROOH), which is a known reaction involved in lipid peroxidation. Thus, the resulting oxidative damage of cells and tissues is further propagated due to the interaction between ROS and other biomolecules, such as lipids and proteins (Fig. 1.b). Lipid peroxidation is one of the radiation-induced oxidative damage responses; this leads to harmful biological consequences, such as increase in membrane permeability, disruption of ion gradients and altered activity of membrane-associated proteins (Wong-Ekkabut et al., 2007, Corre et al., 2010).

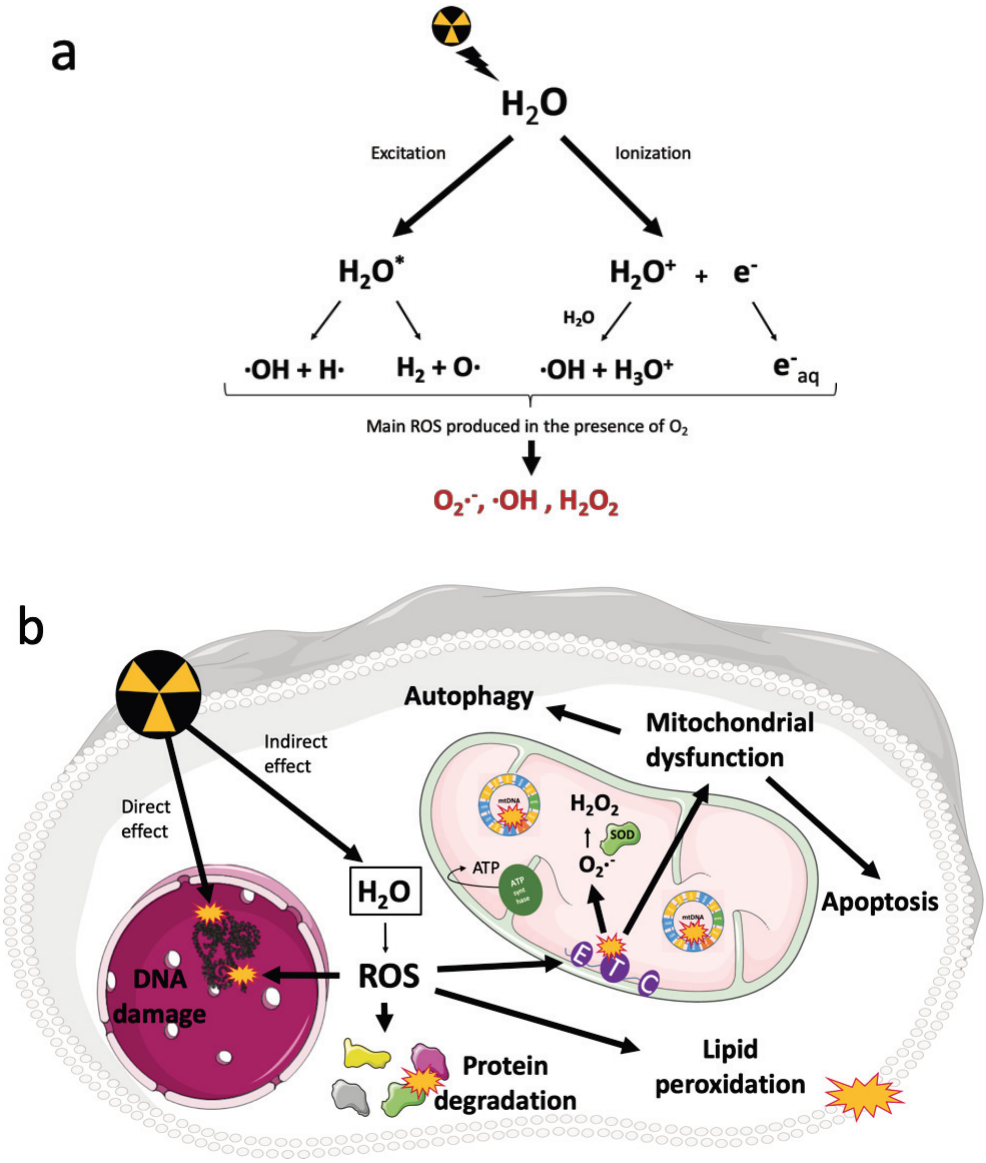

Figure 1. a) Interaction between ionizing radiation and water molecules leads to ionization and excitation reactions producing reactive oxygen species (ROS). **b)** Main cellular and molecular processes induced by direct or indirect effect from exposure to ionizing radiation.

In recent years, experimental evidence has converged on the conclusion that also proteins comprise a primary target of ionizing radiation, and that their impaired function promotes the manifestation of DNA damage to both mammalian and prokaryotic cells (Du and Gebicki, 2004, Krisko and Radman, 2010, Daly, 2012). These studies support the hypothesis that the survival of many organisms depends on the level of oxidative protein-damage following exposure to ionizing radiation, because such damage affects the efficiency and functionality of enzymes, including those involved in DNA repair and replication (Daly et al., 2007, Daly, 2012).

Furthermore, the excess of ROS produced by ionization events in cells and tissues can alter the physiological redox balance, not only by inducing direct oxidative damage onto biomolecules, but also by interfering with the redox signalling molecules, responsible for the regulation of a great number of cellular and molecular processes (Droge, 2002, Sarsour et al., 2009). Tight control of the redox environment is a vital requirement for homeostatic cellular function. For instance, at physiological levels, ROS are responsible for the regulation of specific genes (Allen and Tresini, 2000), for the modulation of ion channels activity, and can also be involved in signal transduction processes as second messengers (Schulze-Osthoff et al., 1997).

If the antioxidant defences cannot restore redox balance, or fail to ameliorate oxidative stress, the accumulation of oxidative damaged biomolecules will lead to tissue injury, including DNA mutagenesis, carcinogenesis, accelerated cell senescence, or cell death (Minafra and Bravatà, 2014, Li and Chen, 2018). At a molecular level this is induced by a variety of cell damage responses, including cell cycle arrest, altered cell proliferation, membrane rupture, distorted signalling networks and mitochondrial dysfunctions (Fig. 1.b) (Spitz et al., 2004, Azzam et al., 2012).

To conclude, the investigation of cellular and molecular mechanisms behind the phenotypical effects observed after chronic exposure to ionizing radiation are important for the prediction of potential adverse effects at an individual and population level.

1.6 *Caenorhabditis elegans* and radiation research

In 1897, a French zoologist and botanist, Emile Maupas, described *Caenorhabditis elegans* as a species of nematode dwelling in rich humus, in which "[he] came twice across…in the surroundings of Algiers" (Maupas 1900). Much has changed in the way biologists look at this nematode, since this organism was firstly observed, and its anatomy described. In the early '70s, Sydney Brenner was the first one to realize the great potential of this tiny nematode as a model organism. Later, Sulston and Horvitz (1977) investigated the cell and tissue differentiation during embryogenesis and post-embryonic development, describing the nematode entire cell lineage and providing invaluable information for the forward and reverse genetics studies performed later on this organism.

For all these reasons, as more recently described by Corsi et al. (2015), biologists see in *C. elegans* a lot more than a nematode dwelling the rich humus, it actually represents a "transparent window into biology".

In the field of radiation biology, the first study of radiation effects on *C. elegans* was performed by Herman (1976), who described the chromosomal rearrangement following X-ray exposure. Later on, the discovery of *C. elegans* radioresistance, by performing acute irradiation studies, was obtained by Hartman (1982) who identified radiation-sensitive mutants. Pre-treatment with 90% of oxygen, to induce oxidative stress, was later shown to induce hyper-resistance, in terms of increased survivals, in wild-type nematodes exposed to 400 Gy of X-rays (Yanase et al., 1999). Over time, research into radiation-induced mutations continued, until the interest shifted towards the molecular mechanisms behind the resistant and sensitive phenotypes (Sakashita et al., 2010). This research includes a multitude of functional genetic studies, which comprise life-span studies, the use of mutant and reporter strains, gene expression analysis, genome-wide or single-gene RNAi (Rosenbluth et al., 1985, Hartman et al., 1988, Takanami et al., 2000, Gartner, 2000, Nelson et al., 2002, Boulton et al., 2002, van Haaften et al., 2006, Sakashita et al., 2010, Ermolaeva et al., 2013). For instance, in the early 2000's, research into DNA damage response and gene functions was performed by Gartner (2000), who made use of *C. elegans* and ionizing radiation to unravel the mechanisms behind cell-cycle arrest and the activation of the core apoptotic machinery

following genotoxic stress. Later on, 45 genes within conserved pathways of DNA-damage response were shown to protect *C. elegans* from effects of acute ionizing radiation (van Haaften et al., 2006). Functional analysis of the *rad-51* gene demonstrated a vital role of this *recA* homolog in meiosis, fertility and organism resistance during development to acute doses of gamma radiation (20 Gy, 4 Gy·min^{-1}) (Rinaldo et al., 2002).

Notably, all these studies rely on acute doses (20 to 1000 Gy) of ionizing radiation, which are not environmentally realistic. Exposure to low doses or low dose-rates represents a more relevant scenario for the assessment of risks related to exposure in the environment, because critical developmental stages or the entire life cycle can be subjected to such stress (Hinton et al., 2013). Hence, performing chronic irradiation experiments on this radioresistant model organism to sub-lethal doses of exposure can improve the knowledge on radiosensitive processes and mechanisms of toxicity for other animal species. For all these reasons, *C. elegans* represents a suitable biological model system and was therefore adopted in this PhD study to investigate the phenotypical effects, as well as the cellular and molecular mechanisms induced by chronic exposure to ionizing radiation.

1.7 *C. elegans* as a model organism

C. elegans is a free-living nematode, about 1 mm long and transparent, that survives by feeding on microbes, primarily bacterial cells. Although often considered a soil nematode, it is mostly isolated from rotting vegetable matter, which represents a rich source of bacteria. In the laboratory, *C. elegans* can be cultivated on agar plates, seeded with a thin lawn of *Escherichia coli*, as well as in swirling liquid cultures (Lewis and Fleming, 1995). Its life cycle is characterized by four moulting stages (L1 to L4) before it reaches sexual maturity (Fig. 2). At room temperature, this cycle is complete in 3 days, thus allowing for rapid studies. Embryogenesis takes approximately 16 hours at 20 °C and embryos hatch at the 558 cell-stage into the first stage of development (L1). After each larval stage, a period of inactivity follows and cell proliferation arrests. Particularly, under food depravation, hatched embryos arrest in L1 stage. In this period of inactivity, L1 larvae can survive for up to 6-10 days, without feeding, and when food becomes

available they can resume metabolism and normal moulting development (Johnson et al., 1984). After alkaline hypochlorite treatment of gravid hermaphrodites, embryos can be isolated and this first stage of inactivity (at L1 stage) can be induced by starvation, allowing for synchronization of the population, which represents a very convenient feature for laboratory experiments (Porta-de-la-Riva et al., 2012). Once its development is completed, cell proliferation is restricted to the germline, while the number of somatic cells remains a constant 959 (Fig. 2). Because of this invariant number of somatic cells, over the years, researchers have been able to track the fate of every cell from the fertilization stage until the adulthood, generating a complete cell lineage map (Sulston and Horvitz, 1977, Kimble and Hirsh, 1979). Furthermore, the possibility to see inside the organism is not only useful for observing cellular events such as mitosis or cytokinesis in real-time, but it also allows the use of fluorescent reporter genes such as green fluorescent protein (GFP) to mark cells, label proteins or monitor gene expression in live animals (Chalfie et al., 1994). Normally, a population consists mostly (99%) of self-fertilizing hermaphrodites, producing both oocytes and spermatocytes (Fig. 2). This represents a valuable feature in genetics for many reasons: it permits the maintenance of homozygous mutation without the need for mating, the offspring of an unmated hermaphrodite are isogenic and due to the production of large number of offspring (~ 300 per adult unmated hermaphrodite), it is also suitable for studying effects over multiple generations.

Males do arise, although at a very low frequency (0.2%), introducing genetic variation and increasing the number of produced offspring (up to ~1000). This is beneficial to the population under stress conditions, such as starvation or heat stress, since it potentially enhances the chances to survive the environmental changes (Morran et al., 2009).

To summarize, this transparent worm is one of the most well studied biological systems for which complete cell lineage (Sulston and Horvitz, 1977), neuronal networks (White et al., 1986) and genome sequence have been established (The *C. elegans* Sequencing Consortium, 1998). Moreover, *C. elegans* research has broad implications because many cellular and molecular processes that control animal development are evolutionary conserved.

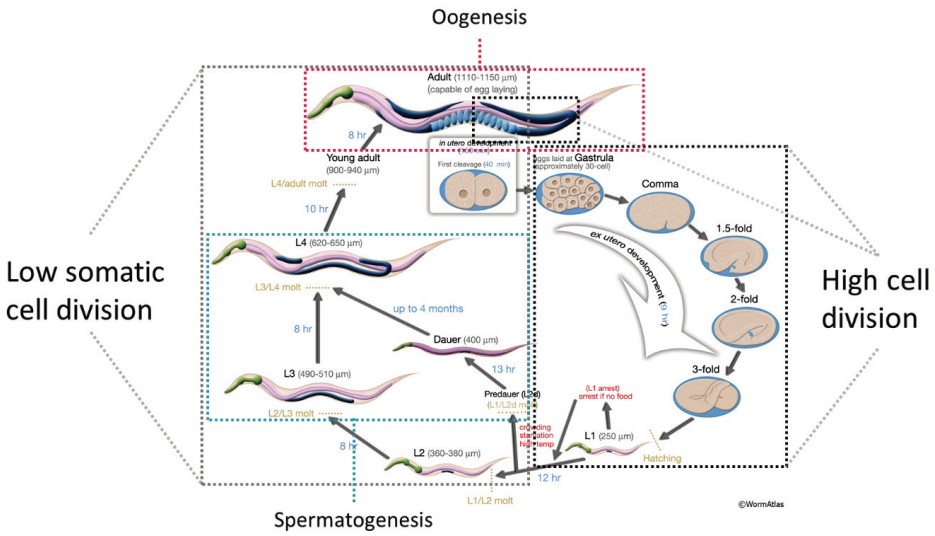

Figure 2. Life cycle of the nematode *Caenorhabditis elegans* adapted from wormatlas.com.

1.8 The reproductive system in *C. elegans*

Already in the 1970s, the reproductive system of the nematode *C. elegans* was adopted as a model system for reproductive studies. Wild-type *C. elegans* presents sexual dimorphism, with self-fertilizing hermaphrodites and males. The hermaphrodites present an ovotestis able to produce haploid amoeboid sperm, stored in the spermatheca from the L4 stage, when the germ line switches function to produce oocytes (Fig. 3.b). Particularly, an adult hermaphrodite possesses two U-shaped gonadal arms, one for each body extremity, which are joined at a common uterus and where the germline resides (Fig. 3.a). Germ cells at different stages of differentiation are contained in each gonadal arm. These develop sequentially from the proliferative germ cells, located near the somatic distal tip cell (DTC), through meiotic prophase I in the distal gonad and across the loop, finally culminating in the proximal gonad where fully formed oocytes are ready to migrate through the spermatheca, get fertilized and enter inside the uterus (Fig. 3.c).

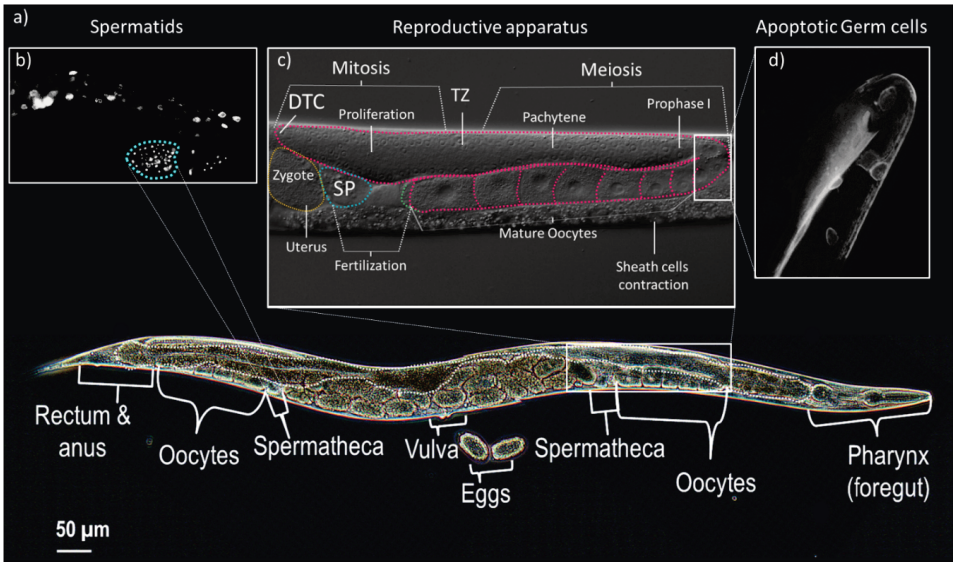

Figure 3. Anatomy and reproductive apparatus physiology of the nematode *C. elegans.* **a**) Phase-contrast micrograph of an adult hermaphrodite (72 hours from L1 stage) during the reproductive stage of its lifecycle. **b**) DAPI stained spermatids stored in the spermathecal compartment (blue region) of the gonadal arm. **c**) DIC (differential interference contrast) micrograph of the nematode reproductive apparatus, including the gonadal arm (pink region) where mature oocytes are produced through proliferative stage and Meiosis I and II, until fertilization and zygote formation (yellow circle) (DTC: distal tip cell; TZ: transition zone; SP: spermatheca). **d**) Micrograph of the apoptotic germ cell corpses emitting fluorescent signal (512 nm emission and 40X objective), from the loop region of the gonadal arm in the *C. elegans* reporter strain *CED1::GFP.* (Photo: E. Maremonti)

The reproductive tract differentiates during the post-embryonic development, from two primordial germ cells (Z2 and Z3) positioned between the two somatic precursor cells (Z1 and Z4). Already in L1 stage, the precursors Z2 and Z3 start to proliferate in order to generate the germ cells inside the gonadal arms, while the somatic gonad primordium is formed within the second molt and it is composed of twelve cells in total, including the two DTCs, one for each gonad. In the hermaphrodite, male germ cells are specified in the L3 stage and will differentiate into mature sperm in the L3/L4 stage, when spermatogenesis is completed. Female germ cells specify from L4 stage, and germ cell proliferation to produce oocytes continues for the entire duration of the nematode life. An adult hermaphrodite is able to use all of the stored spermatids in order to produce up to ~300 self-progeny (Singson, 2001). If mated with a male, the number of progeny

can reach up to ~1000. The number of stored spermatids thus comprises the primary limiting factor for the number of offspring by self-fertilization (Rinaldo et al., 2002).

Under chronic or acute exposure to ionizing radiation, gonad development and gametogenesis have been shown to be delicate processes (Sowmithra et al., 2015, Hertel-Aas et al., 2011a, UNSCEAR, 2008, UNSCEAR, 1996), therefore irradiation experiments, performed during the post-embryonic and larval development of the nematodes, can serve to identify potential radiosensitive developmental stages and biological processes.

1.9 Germ line apoptosis and the effect of DNA damage

The gonad germ cells represent a unique tissue, where cells are pluripotent and "immortal", and thus can differentiate in all cell types in the next generation (Kimble and Hirsh, 1979). In the adult nematode, the germline represents the only tissue that contains stem cells, with the ability to replenish the cell population. An important feature of the gonads is the capacity to ensure a quality control of the produced cells, through the intrinsic mechanism of germ cell apoptosis (Fig. 3.d). This is a physiological event and an important surveillance mechanism, where half of the potential oocytes are removed, in order to ensure a healthy cell population of the germline (Gumienny et al., 1999). Germline apoptosis only occurs during oocyte production and it is restricted to the gonadal loop region (Fig. 3.d), where the oocytes complete the meiotic prophase I in the pachytene region prior to transition into the diplotene stage (Fig. 3.c). The physiological germline programmed cell death occurs in the absence of any external stress, by the activation of the core apoptotic machinery, involving CED-9, CED-3 and CED-4 (Ellis and Horvitz, 1986, Lettre and Hengartner, 2006) (Fig. 4).

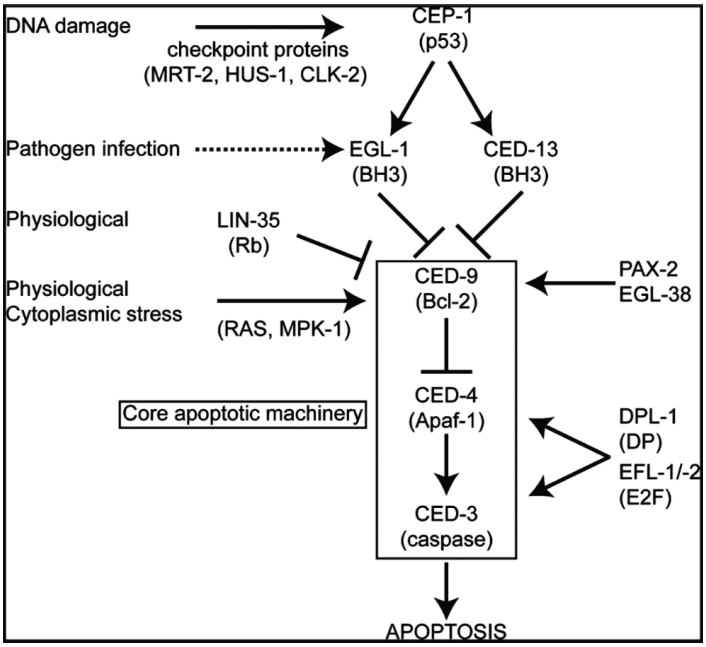

Figure 4. Main pathway and genes involved in physiological and DNA damage-induced germ cell apoptosis in the nematode *C. elegans*. Adopted from Gartner et al. (2005).

A clear distinction has been identified between the physiological and the CEP-1-dependent germline apoptosis. The latter is induced by DNA damage or effects on chromosomal integrity and, depending on the type of damage, specific upstream sensor proteins are triggered, including HUS-1, CLK-2, CES-2 and EGL-1 (Lettre and Hengartner, 2006) (Fig. 4). In particular, a study by Gartner (2000) showed that acute exposure to high doses (3.9 $Gy \cdot min^{-1}$, total dose ≥60 Gy) of gamma radiation, in L4 nematodes, induced a 10-fold increase in the number of apoptotic germ cells, 24 hours after the exposure, and the arrest of germ stem cells proliferation. Damage to reproductive tissues can have negative consequences in terms of fertility, but it can also induce mutations and heritable effects. Therefore, investigating adverse effects on germ cells proliferation and maturation after chronic exposure to gamma radiation can help us understand the mechanisms behind the radiation-induced reprotoxic effects seen in *C. elegans* (Buisset-Goussen et al., 2014).

1.10 Spermatogenesis

In both hermaphrodites and male germ cells of *C. elegans*, the molecular events driving the early stages of meiotic development include chromosome pairing, synapsis and recombination, and they occur in a similar way. However, unlike developing oocytes, where meiotic divisions lead to one single gamete, after the meiotic prophase, spermatocytes divide symmetrically, resulting in four equally sized gametes (Fig. 5)(Chu et al., 2006, Chu and Shakes, 2013). The progression of spermatids formation from the division zone starts with the formation of mature fibrous body (FB) and membranous organelle (MO) complexes, which are essential for the assembly and envelopment of the Major Sperm Proteins (MSP) (Fig. 5, 1). After this process, budding, maturation and sperm activation are the three key events leading to the production of mature spermatozoa (Fig. 5) (Chu and Shakes, 2013).

During the first of these events, (Fig. 5, 2) the late-stage budding spermatid is fully polarized, with FB-MOs and chromatin masses partitioned to the extremities and the spindle microtubules positioned in the central residual body. This division leads to the early maturing spermatid (Fig. 5, 3), where the MO retracts and the FBs are released into the cytoplasm where they begin to disassemble and release the MSPs (Fig. 5, 4).

At this stage (Fig. 5, 4), the late-stage quiescent spermatid is externally activated (Fig. 5, 5) to form microspikes from the fusion of the MOs with the plasma membrane. The maturation is finally accomplished when the spermatozoon is motile (Fig. 5, 6) and presents a distinct cell body containing fused MOs and a pseudopod enclosing the MSPs.

Thanks to several genome-wide expression studies, essential regulatory genes involved in *C. elegans* spermatogenesis have also been identified (Reinke et al., 2000, Ortiz et al., 2014). These results have demonstrated that chromosome IV is enriched in spermatogenesis specific genes, such as the MSP encoding genes, which have distinct temporal expression profiles (Chu and Shakes, 2013).

In contrast to the oogenesis program, spermatogenesis presents a faster rate of progression through meiotic prophase. While in oocytes checkpoint for DNA damage and meiotic recombination errors lead to removal of damaged cells by programmed cell death (Gartner, 2000), no apoptosis occurs in male germ cells (Jaramillo-Lambert et al., 2010). However, as in many other species, during meiosis I of spermatogenesis, the

chromatin is reorganized into a compact form by sperm chromatin enriched proteins (SPCH) and a sperm –specific histone 2 variant (HTAS-1), ensuring DNA protection and successful fertilization (Chu et al., 2006, Ellis and Stanfield, 2014).

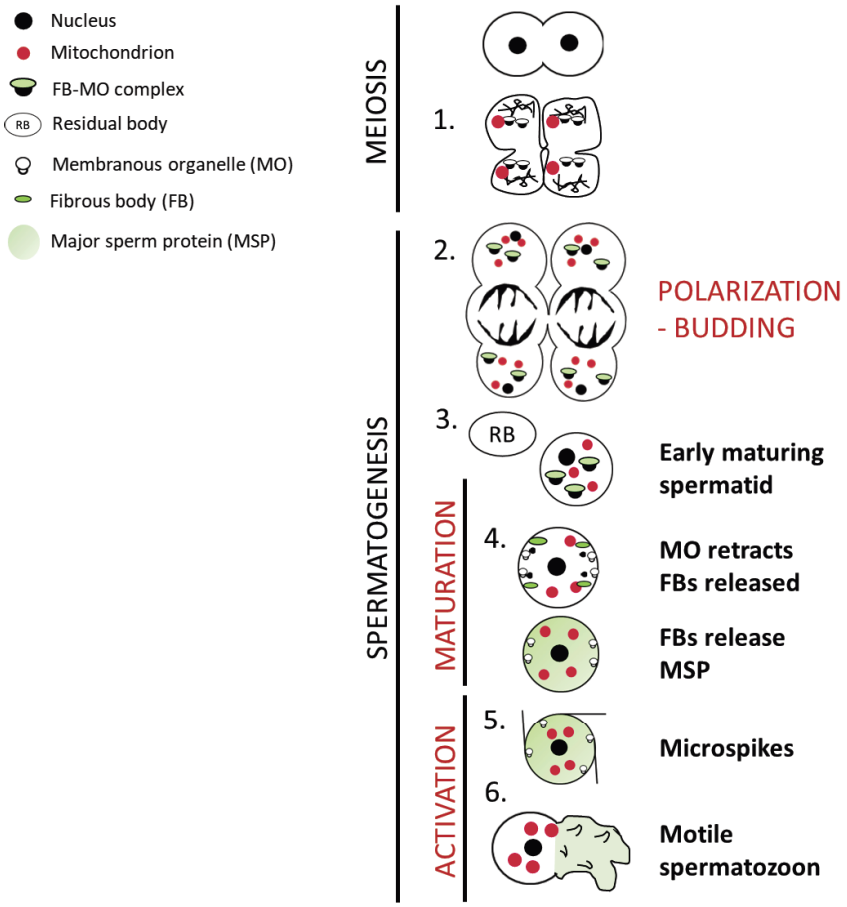

Figure 5. The progression of spermatid formation and pseudopod assembly to produce motile spermatozoa in *C. elegans*.

1.11 Ionizing radiation-induced DNA damage and repair

Genomic integrity is essential to the health of the individual as well as to the reproductive success of a species (Kermi et al., 2019). For this reason, organisms are equipped with faithful replication and repair mechanisms to prevent accumulation of damage and the transmission of altered genetic information. Nucleic acids are vulnerable to the effects of ionizing radiation whereby induced DNA damage range from simple single strand lesions or oxidized nucleobases, to complex clustered double strand breaks (Hall and Giaccia, 2006, Cadet et al., 2003, Brown and Rzucidlo, 2011). Single non-synonymous base mutations may ultimately lead to cancerous phenotype cells. Severe complex DNA damage, like chromosomal aberrations, will induce DDR (DNA damage response) and cell cycle arrest, where the consequences to the cell are highly dependent on the efficacy of the DNA repair machinery (Li and Chen, 2018). Irreparable damage may lead to apoptosis, senescence or necrosis (Wang et al., 2018). Even if cells are rescued, they may still inherit genomic instability, which means that latent damage may produce long-term effects.

In *C. elegans*, many DNA damage checkpoints and repair functions have been identified, and the majority of these mechanisms play essential roles during DNA replication, cell-cycle control, development, mitosis and meiosis (Boulton et al., 2002). The first class of genes encoding for DNA repair mechanisms was identified by Hartman (1982), who isolated radiosensitive mutants (*rad-1* to *rad-9*) after exposure to acute doses of UV radiation and ionizing radiation. Canonical DNA repair pathways and their related genes, such as nucleotide excision repair (NER), mismatch repair, non-homologous end joining (NHEJ), and homologous recombination (HR) were identified in *rad* mutants and functionally investigated in detail by RNAi, protein-protein interaction mapping, as well as phenotypical analysis (Hartman et al., 1988, Schumacher, 2001, Chin and Villeneuve, 2001, Boulton et al., 2002, Clejan et al., 2006, Lans and Vermeulen, 2015).

Besides the canonical DNA repair pathways, a tissue-specific DNA damage response has been identified and characterized by Lans and Vermeulen (2015). Particularly, non-proliferating somatic cells in larvae or adult worms have shown to be much more resistant to ionizing radiation than germ cells, presumably due to transcriptional repression of checkpoint signalling proteins (Vermezovic et al., 2012). However, in

response to different types of genotoxic insults, proliferating germ cells of *C. elegans* present a strong activation of cell cycle checkpoints and multiple, partially redundant, repair pathways, facilitating robust and efficient maintenance of the genome integrity (Lans and Vermeulen, 2015, Andux and Ellis, 2008). Most of the DNA damage that occurs in somatic proliferating cells is sensed by checkpoint mechanisms and repaired during S-phase by delaying the progression into mitosis. In contrast, early embryonic cells are characterized by rapid progression through the cell cycle and lack of Gap phases, for these reasons the mechanisms are activated by endogenous, developmentally programmed cues (Lans and Vermeulen, 2015, Brauchle et al., 2003, Encalada et al., 2000). When unscheduled signals occur, such as replication problems due to DNA damage, checkpoint asynchrony is reduced, the germ line fails to develop, and the nematode is rendered sterile (Brauchle et al., 2003, Kalogeropoulos et al., 2004). Although the rapid cell progression and lack of Gap phases could potentially lead to a higher sensitivity to DNA damage during early embryogenesis, paradoxically, embryos show a higher tolerance due to active checkpoint silencing during DNA damage response, which ensure cell cycle progression and provides an improved possibility of survival (Holway et al., 2006).

Overall and despite the tissue-specificity of DNA damage response, *C. elegans* presents a robust DNA repair system, which investigations often involve genotoxic stress by acute exposure to high doses of ionizing radiation. Nevertheless, there is a lack of information with respect to DNA damage response induced by chronic exposure at low dose-rate ionizing radiation. Such information could be extremely important because it may unravel the mechanisms of toxicity behind the reproduction impairment from chronic exposure to ionizing radiation.

1.12 Mitochondrial functions and mitochondrial DNA

Mitochondria represent a vulnerable target of ionizing radiation for several reasons. They occupy a substantial fraction (4-25%) of the cell volume (Kam and Banati, 2013). By their role in energy metabolism, they consume about 90% of the oxygen and thus they represent the main source of ROS in the organism (Leach et al., 2001). Importantly, the physiological and the radiolysis-dependent ROS production act synergistically, and

may eventually lead to malfunction of the mitochondrial electron transport chain (ETC) machinery (Leach et al., 2001). This constructs a self-propagating cycle which may cause redox imbalance, oxidative damage or ultimately mitochondrial dysfunction (Szumiel, 2015). Due to lack of histones, mitochondrial DNA (mtDNA) represents a vulnerable target of oxidative damage. Excess of ROS may therefore cause mutation and damage to mtDNA, which in turn may alter the production of proteins required for mitochondrial processes (Azzam et al., 2012). Thus, radiation-induced mitochondrial ROS has the potential to affect the mtDNA copy number (Malakhova et al., 2005), modulate the gene expression, induce autophagy, and apoptosis (Sidoti-de Fraisse et al., 1998). Mitochondrial stress response may also propagate to other compartments of the cell, including the nucleus, and thus damage nuclear DNA (Azzam et al., 2012). Mutations on the mtDNA and or nuclear DNA can persist and lead to heritable mitochondrial and cellular dysfunctions with serious consequences for the progeny of irradiated cells (Kim et al., 2006). For all these reasons, and due to lack of knowledge in this research area, it is important to investigate the potential adverse effects of chronic gamma irradiation on the mitochondrial gene expression and on the mtDNA.

1.13 The antioxidant defences in *C. elegans* and their potential role in tolerance to ionizing radiation

Due to aerobic metabolism, cells are continuously exposed to oxidative insult, with as many as 50000 lesions of DNA modifications per day (Swenberg et al., 2010). Organisms are therefore equipped with a series of antioxidant enzymes and molecules to maintain the physiological redox balance, and to prevent oxidative damage.

In most species, the antioxidant defence systems (AOD) are composed of a series of water soluble scavengers compounds, such as vitamin E, vitamin C and glutathione, and antioxidant enzymes, such as superoxide dismutases (SOD), catalases, glutathione-S-transferases and glutathione peroxidases (GPx), which enable the detoxification of reactive oxygen species (ROS) and reactive nitrous species (RNS) (Davies, 2000). *C. elegans* is well equipped to handle oxidative stress and inherits a robust and elaborate AOD system (Fig. 6), which is comprehensively reviewed by Braeckman et al. (2017).

In the nematode *C. elegans* the biology of SOD and catalases is unusual. While most organisms possess a single isoform of SOD per each compartment of the cell, *C. elegans* possesses two isoforms per each compartment (Doonan et al., 2008). The cytosolic *sod-1* and mitochondrial *sod-2* represent the major isoforms, expressed during reproductive development, whereas *sod-3* and *sod-5* are mostly expressed in the dauer stage. Another dissimilarity is related to the incorporation of copper to mature Cu/Zn SODs, which in *C. elegans* relies on an unidentified glutathione-dependent pathway in contrast to the copper chaperone of SOD (CCS) required for the rest of the eukaryotes (Giglio et al., 1994). Moreover, this nematode possesses three catalase encoding genes in its genome, in contrast with other metazoans where only a single catalase is present (Gems and Doonan, 2008). The glutathione-S-transferases (GSTs) together with GSH are major cellular detoxification enzymes. Seven species-independent and additional species-specific classes of GSTs have been identified and described (Board et al., 2000). In *C. elegans*, the genome contains over 50 putative GSTs, most of which are classified as nematode-specific (Campbell et al., 2001). One specific member of these GSTs classes, *Ce-GST-p24*, has been shown to induce oxidative stress-resistance, when RNAi was performed under exposure of nematodes to different ROS inducer compounds (Leiers et al., 2003).

Furthermore, ROS can serve as important signalling molecules, in particular $O_2^{\bullet-}$ and H_2O_2 can bind redox-sensitive switches, for instance the cysteine residues on the active sites to form disulphides, thus modulating protein conformation and activity. Because of this important role in activating redox-sensitive proteins, the cellular redox state and thus the levels of superoxide/H_2O_2 must be maintained within a narrow range. This does not only ensure the constitutive signals resulting from the homeostatic redox state, but also allows for meaningful thresholds, where a change in the redox state can be used to signal a change in metabolism, environment or stress (Johnston and Ebert, 2012)

Following irradiation, cells and tissues appear to respond by increasing the expression of cellular antioxidant defences (Okunieff et al., 2008). This increased antioxidant capacity has been hypothesized to be at least partially responsible for radiation-induced adaptive responses (Spitz et al., 2004). The ability of an organism to tolerate ionizing radiation is dependent on the efficiency of its DNA repair mechanisms (Cox and Battista, 2005, Zahradka et al., 2006), but also on the robust antioxidant defence system to

scavenge ROS and prevent oxidative damage to essential biomolecules (Daly et al., 2007, Daly, 2012, Krisko et al., 2012a). For these reasons and due to its highly specialized redox control system (Braeckman et al., 2017), the nematode *Caenorhabditis elegans* represents an optimal model to investigate whether ROS accumulation and AODs activation would induce a stress condition or an adaptive response under chronic exposure to ionizing gamma radiation.

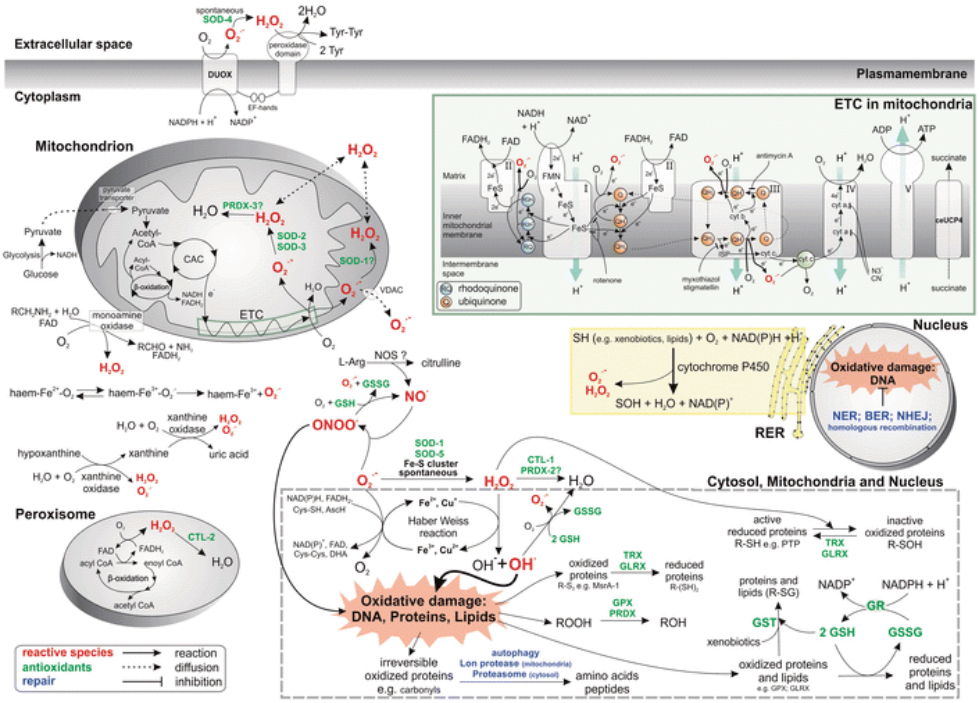

Figure 6. Schematic representation of ROS formation and Antioxidant defence systems in different compartments of the cell in the nematode *C. elegans*. Adopted from Braeckman et al. (2017).

1.14 Specific objectives of the study

The overall purpose of this PhD study was to improve knowledge on molecular mechanisms of toxicity and tolerance induced by chronic exposure to ionizing radiation in the nematode *Caenorhabditis elegans*.

Therefore, specific objectives were to:

1. Characterize toxic effects of chronic exposure to ionizing radiation on survival, growth and reproduction.
2. Investigate life stage-dependent radiosensitivity.
3. Investigate radiosensitivity of specific tissues and cells.
4. Investigate organism, tissue and cell specific ROS production, AODs response and oxidative stress effects in nematodes subjected to chronic gamma radiation.
5. Assess whole genome transcriptomic changes induced by exposure to gamma radiation.
6. Assess effects of chronic gamma radiation on mitochondrial functions including transcription and mtDNA copy number variation.

2. Methodology

2.1 Experimental design

During this PhD research, three main exposure regimes were employed: chronic, life-stage specific and acute. The chronic exposure of embryos/L1 nematodes, followed the same experimental design for every experiment performed, using three biological replicates combined with a fixed set of dose-rates of gamma radiation (0 – 0.4 – 1 – 10 – 40 – 100 – 1000 mGy·h^{-1}). In addition, an acute exposure of L4/Young adult nematodes was performed at dose-rates ranging from 1410.6 to 1490 mGy·h^{-1} (Paper I). The duration of each exposure was chosen according to the aim of the study, as presented in Fig. 7.

The aim of the first study (Paper I) was to identify differences between effects induced by acute or chronic exposures, as well as potential radiosensitive developmental stages. Therefore, effects on the reproductive capacity of nematodes were assessed after exposure during different stages of development, following four different designed scenarios. Each scenario covered early or late stages of development, as well as the nematode entire life cycle (Fig. 7). Since reprotoxic effects were observed following chronic exposure of early developmental stages, effects on the nematode germline proliferation were assessed with respect to germ cell apoptosis and spermatids production. Moreover, a transcriptome analysis was performed on nematodes exposed to 100 mGy·h^{-1} during this radiosensitive stage, in order to identify potential molecular mechanisms underlying the observed reprotoxic effects. Adverse effects on parentally exposed embryos (F1) were assessed, in the same study (Paper I), by measuring DNA damage effects on embryonic cells with the Comet assay, as well as phenotypical effects with respect to reproductive capacity and somatic growth (Fig. 7).

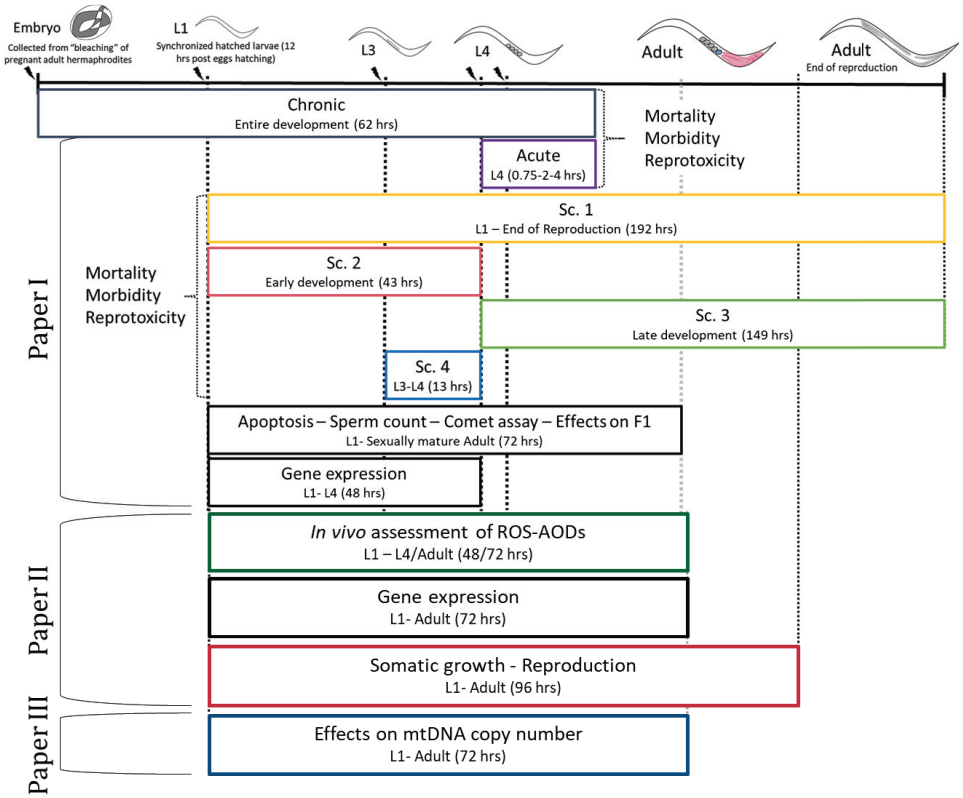

Figure 7. Experimental design employed for studying effects of chronic gamma irradiation in the nematode *C. elegans*. From L1 stage, the nematode development takes ~72 hours to reach sexual maturation, while it takes ~8 days (192 hours) to the end of reproduction at 20 °C. In Paper I, reprotoxic effects were assessed in two independent experiments, using different scenarios of exposure (i.e. Acute vs Chronic, or different stages of development: Sc. 1-4). This resulted in the identification of L1-L4 as radiosensitive larval stages. Therefore, irradiation during these phases of development was adopted to assess effects on spermatogenesis, germ cell apoptosis, genotoxicity, ROS production/AODs activation, gene expression and effects on mtDNA copy number. In parenthesis the duration of each exposure in hours.

In Paper II, nematodes were irradiated during the radiosensitive stage of development (L1- L4/Young adult, 48- or 72-hours development), identified in Paper I, in order to measure the accumulation of ROS and the activation of AODs *in vivo*, by using the *C. elegans* reporter strain *sod1::gfp* and the ratiometric biosensors *HyPer* and *Grx1- roGFP2*. The wild-type N2 was also used in this study for the assessment of somatic growth and reproduction as phenotypical endpoints, as well as for the analysis of differential gene expression through RNA-sequencing, following similar exposure

conditions (Fig. 7). In Paper III, attention was focused on the mitochondrial DNA (mtDNA), which is known to be a vulnerable target of ionizing radiation and ionizing radiation-induced oxidative stress. Specifically, effects on the mtDNA copy number were evaluated through the development of a new method, using digital Polymerase Chain Reaction (PCR) analysis. For this purpose, irradiation was performed using low (0 – 0.4 – 1 – 10 – 40 – 100 mGy·h^{-1}) as well as high (~1000 mGy·h^{-1}) dose-rates of exposure over the entire nematode larval development (from L1, L2/3 or L4 stage to sexually mature adult, 72 hours development) (Fig. 7).

2.2 Gamma irradiation and dosimetry

All the irradiation experiments carried out in this study were performed at the Figaro Experimental Radiation Facility (NMBU) (Lind et al., 2019). The 400 GBq ^{60}Co source provides a near cone-shaped radiation field where the area for irradiation increases as doses decrease (Fig. 8). At maximum load (400 GBq), the dose-rates range from 3 Gy·h^{-1} (inside collimator) down to 0.4 mGy·h^{-1}, allowing for simultaneous, chronic exposure of organisms over the whole dose-rate field (Papers I – II – III) (Fig. 8, low-dose exposure). Exposure at the highest dose-rates (Papers I and III) was obtained for small samples by positioning NGM Petri dishes (Ø 3 or 6 cm) within the collimator during irradiation (Fig. 8, high-dose exposure). Control samples were placed in a section of the hall, outside the beam cone and shielded with two mobile lead (6 mm) walls resulting in air kerma rates 3-5 µGy·h^{-1} (Nanodots, Landauer) (Fig. 8). Moreover, technical equipment installed in the irradiation room allowed for the monitoring of light (darkness) and temperature (20°C) conditions providing high reproducibility over the different experimental studies (Lind et al., 2019).

For the studies conducted in Paper I and III, all the irradiation experiments were performed in triplicates in NGM Petri dishes vertically positioned facing the gamma source, this allowed for homogenous exposure over the entire experimental unit.

Irradiation experiments conducted in Paper II were performed in triplicates by using NGM Petri dishes as well as liquid cultures of nematodes placed in front rows of 24-well Petri dishes or in tissue-culture flasks (15 mL).

Field dosimetry (air kerma rates measured with an ionization chamber) was traceable to the Norwegian Secondary Standard Dosimetry Laboratory (Bjerke and Hetland, 2014). Air kerma rates were measured using an Optically Stimulated Luminescence (OSL) based nanoDots dosimetry (Landauer®) by positioning the dosimeters at the front and back of the experimental units. Dose-rates to water were calculated according to Hansen et al. (2019) and used as a proxy for dose-rates to the nematodes. Measured total doses, dose-rates and duration of the exposures, can be found in the Supporting Material for Paper I, II and III.

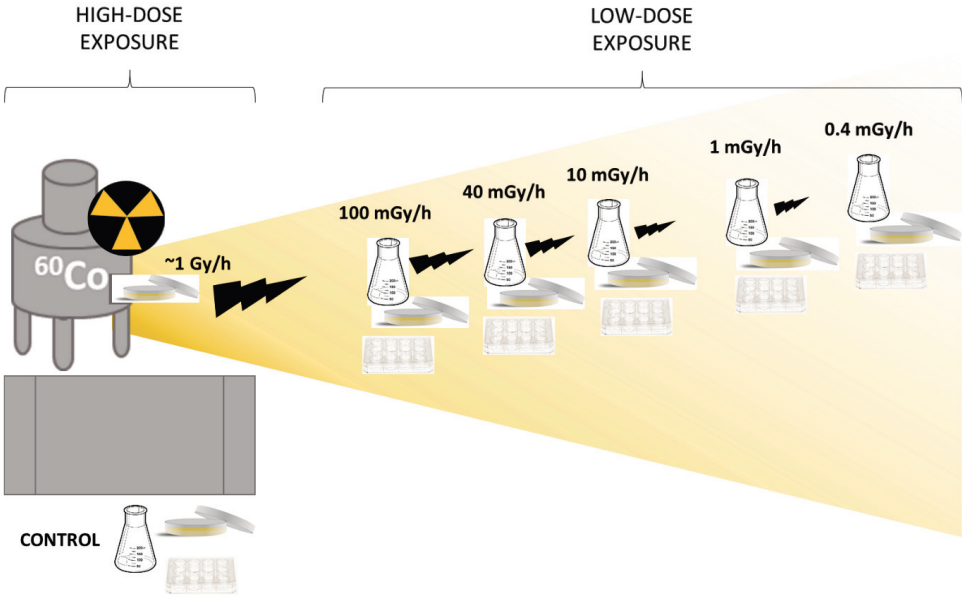

Figure 8. Irradiation set up, experimental units, and dose-rates of exposure adopted in this PhD study and performed at the Figaro Low dose-rate Experimental Irradiation Facility (NMBU).

2.3 C. elegans strains and culturing

The N2 Bristol strain was adopted in this study as the wild-type *C. elegans* background for all the irradiation experiments. Germ cell apoptosis was assessed by using the *C. elegans* reporter strain *bcIs39 [lim-7p::ced-1::GFP+lin-15(+)]*, which enables the quantification of apoptotic germ cells engulfment corpses as described by Zhou et al. (2001) (Paper I). The expression of superoxide dismutase 1 was measured *in vivo* by

using the reporter strain *sod-1::gfp* (Doonan et al., 2008), while the ratiometric biosensors *HyPer* and *Grx1-roGFP2* were adopted to measure H_2O_2 levels and glutathione redox changes (Back et al., 2012) (Paper II).

Before performing the experiments, worms were maintained for two months at 20 °C in swirling liquid cultures under dark conditions (Brenner, 1974), in order to obtain a healthy stock population. Synchronous populations of nematodes were obtained by alkaline hypochlorite treatment as described by Stiernagle (2006).

2.4 Developmental and morphological effects assessment

Morphology and effects on development were assessed on nematodes after exposure to ionizing gamma radiation by visual investigation under a semi-automated research light microscope (at 20X or 40X, phase-contrast optics) (Upright Microscope Leica DM6 B). Specifically, nematodes were observed at the end of each exposure in order to identify any visible morphological change or delay during the larval development (Paper I). For this purpose, at least 10 individuals per treatment were anesthetized using 30 mM of NaN_3, placed onto 2% agarose pads, and observed under the microscope.

Furthermore, adverse effects on nematode development were evaluated by measuring the total body length of individuals at different larval stages (Paper I) or after reaching sexual maturity (Paper I - II). This quantitative analysis was performed on nematodes stained with 1 ml Rose Bengal (0.3 $g \cdot L^{-1}$) at 80 °C for 10 min, according to ISO guideline (International Organization for Standardization, n. 10872, 2010). NGM plates or 24-well tissue culture plates were finally stored at 4 °C and worms were randomly imaged under a stereo microscope (Leica M205C, 10X magnification) coupled with a computer-connected camera. The body length was measured by using the Leica software, provided with an auto calibrated micrometre scale bar.

2.5 Effects on reproduction

In Paper I, reprotoxic effects were evaluated by measuring the cumulative number of larvae (hatched eggs and L1, “total brood size”) produced by five nematodes (3

biological replicates, n=15 nematodes per treatment) until they stopped reproducing. Specifically, from 48 hours onwards from L1 stage, the adult worms were transferred to fresh NGM plates every two days for a total of 8 days.

In Paper II, however, the criteria for standard 96 hours toxicity tests were followed (International Organization for Standardization, n. 10872, 2010) and the cumulative number of larvae (hatched eggs and L1) was measured only at 96 hours of irradiation from L1 stage.

At the end of each experiment, nematodes were stained by adding 0.5 mL of Rose Bengal (0.3 $g \cdot L^{-1}$) to the wells and placed for 10 minutes at 80 °C. Plates were stored at 4 °C until nematodes on all plates were measured using a stereo microscope (Leica M205C, 16X magnification) for total number of offspring per recovered adult (reproduction), and for the number of pregnant nematodes (fertility), using a hand-held tally counter.

2.6 Germline apoptosis

The effect on germ cell apoptosis was measured in Paper I by exposing the *C. elegans* reporter strain *CED1::GFP* for 72 hours from L1 stage to different dose-rates of gamma radiation. At the end of the exposure, ~100 worms per treatment (two biological replicates) were mounted onto 2% agarose pads, anesthetized with 30 mM NaN_3 in M9 buffer, and apoptotic germ cells identified as previously described by Lu et al. (2009). Images of one gonadal arm in each adult hermaphrodite (n = 60, per treatment), 16 hours post L4-molt, were captured as ~10 serial Z-sections of 1.0 µm interval using Nomarski optics in combination with fluorescence signal under a semi-automated research light microscope (Upright Microscope Leica DM6 B) equipped with a GFP ET filter system (512 nm emission and 40X objective). The frequency of *CED1::GFP* clustering around cell corpses was successively quantified as described by Zhou et al. (2001).

2.7 Spermatids quantification

Effects on spermatogenesis and sperm production were investigated in Paper I in order to examine the potential cause of the observed reprotoxic effects. For this purpose, a spermatid quantification was performed on dissected gonads from hermaphrodite nematodes irradiated for 72 hours from L1 stage (Fig. 3, Table S.3 in Supporting Material for Paper I).

After the exposure, nematodes were dissected using a 0.5x16 mm gouge needle in M9 buffer to expose the spermatheca, fixed with Paraformaldehyde (2%) and permeabilized by freeze cracking (Sadler and Shakes, 2000). A total of > 45 nematodes per each treatment were dissected (>15 per slide, in triplicate). Slides were then stained with 10 µl DAPI DNA staining (10 $\mu g \cdot mL^{-1}$) for 20 minutes, before proceeding with the spermatids count, under a semi-automated research light microscope (Upright Microscope Leica DM6 B) equipped with a DAPI filter system (461 nm emission and 40X objective). For each analysed spermatheca, images were captured as a ~20 serial Z-sections of ~5.0 µm interval.

2.8 Monitoring *in vivo* ROS production and AODs response to ionizing radiation in *C. elegans*

While conventional redox-sensitive fluorogenic probes are nonspecific, irreversible, and disruptive, genetically encoded fluorescent sensors can overcome such limitations (Gomes et al., 2005, Meyer and Dick, 2010). Therefore, in Paper II, ROS production and induction of Antioxidant defences (AODs) following chronic exposure to gamma radiation were assessed by using the *sod1::gfp* reporter strain and two ratiometric biosensors, *HyPer* and *Grx1-roGFP2* (Doonan et al., 2008, Cabreiro et al., 2011, Back et al., 2012). Specifically, the *sod1::gfp* reporter strain was implemented to measure the expression of the cytosolic superoxide dismutase 1, while the ratiometric biosensors *HyPer* and *Grx1-roGFP2* were adopted to measure the levels of H_2O_2 and the glutathione redox changes.

The *sod1::gfp* reporter strain, carrying a transgene of green fluorescent protein (gfp) driven by the superoxide dismutase 1 (*sod-1*) promoter, can reveal the capacity of this organism to dismutate the superoxide anion ($O_2^{\bullet -}$) in terms of expression of the gene *sod-1*, when the stressed nematodes are examined under a fluorescent microscope (Fig. 9) (Doonan et al., 2008). Therefore, this reporter strain was adopted for measuring the indirect production of the superoxide radical after chronic exposure to gamma radiation.

Figure 9. Phase-contrast (**a**) and epifluorescence (**b**) image (405 nm excitation and 535 nm emission filters for fluorescent intensity measurements) of *sod1::gfp* adopted for the quantification of Superoxide Dismutase 1 (SOD1) expression after chronic exposure to gamma radiation in Paper II. (Photo: E. Maremonti)

The spontaneous or catalytic breakdown of superoxide anions ($O_2^{\bullet -}$) is one of the most common biological sources of hydrogen peroxide, this is a potent ROS produced by the partial reduction of oxygen during aerobic respiration or due to the exposure of cells to a variety of physical, chemical, and biological agents (Veal et al., 2007). The production of H_2O_2 was monitored *in vivo* in *C. elegans* by using the biosensor *HyPer* (Fig. 10). *HyPer* (named after hydrogen peroxide) is a genetically encoded fluorescent H_2O_2 sensor. It consists of a *cpYFP* (circularly permuted yellow fluorescent protein) fused with the

regulatory domain of *OxyR-RD* and has a high affinity and selectivity for H_2O_2 (Belousov et al., 2006). These nematodes are therefore enable to emit fluorescence proportionally to the levels of H_2O_2 produced in response to stressors, and therefore were used to assess effects on cellular levels of H_2O_2 *in vivo* by epifluorescence microscopy (Back et al., 2012).

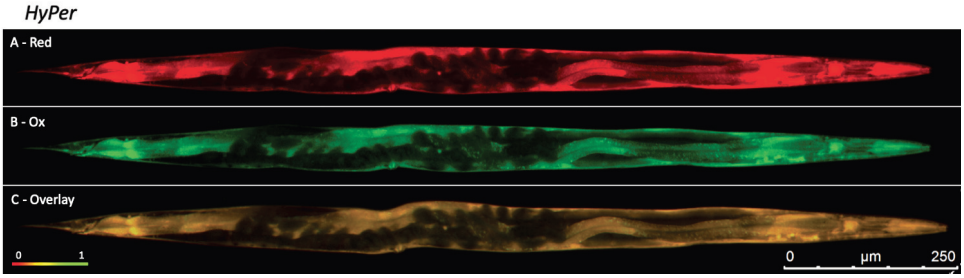

Figure 10. Epifluorescence images of *Hyper* ratiometric biosensor, taken with two different filter cubes (excitation 490 nm and emission 535 nm, reduced state (**a**), 405 nm excitation and 535 nm emission filters, oxidized state (**b**)) and as overlay (**c**) for the quantification of hydrogen peroxide levels as a measure of oxidized/reduced ratio (Back et al., 2012) after chronic exposure to gamma radiation (Paper II). (Photo: E. Maremonti)

The glutathione disulphide-glutathione couple [GSSG]/[2GSH] is considered to be the major thiol-disulphide redox buffer and the most abundant redox couple in a cell (Gilbert, 1990, Schafer and Buettner, 2001). *Grx1-roGFP2* (redox-sensitive green fluorescent protein 2) is a ratiometric biosensor, where the fusion of the human *Grx1* to the redox-sensitive *roGFP2* greatly enhances the response to glutathione redox changes (Fig. 11) (Gutscher et al., 2008, Back et al., 2012). The [GSSG]/[2GSH] equilibrium is an important indicator of cellular redox status, therefore, oxidized to reduced ratio [GSSG]/[2GSH] of *Grx1-roGFP2* was used as a proxy to assess the impact of chronic exposure to ionizing radiation on the redox potential and to visualize the relative oxidation pattern in the nematode *C. elegans* (Back et al., 2012).

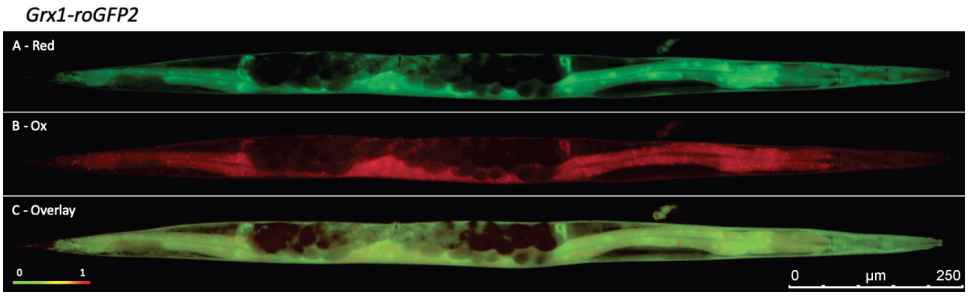

Figure 11. Epifluorescence images of *Grx1-roGFP2* ratiometric biosensor, taken with two different filter cubes (405 nm excitation and 535 nm emission filters, reduced state (**a**), excitation 490 nm and emission 535 nm, oxidized state (**b**)) and as overlay (**c**) for the quantification of glutathione redox changes measured as an oxidized/reduced ratio (Back et al., 2012) after chronic exposure to gamma radiation (Paper II). (Photo: E. Maremonti)

2.8.1 Epifluorescence microscopy

Genetically encoded fluorescent sensors *sod1::gfp, HyPer* and *Grx1-roGFP2* were irradiated for 48 and 72 hours from L1 stage. Immediately after the exposure, nematodes were transferred onto an agar pad (2 % agar) on a glass slide and immobilized with 30 mM of NaN_3 (NaAzide), then subsequently mounted and observed for the fluorescent signals.

Anatomical localization and intensity average of the fluorescent signal for *sod1::gfp* were assessed under a semi-automated research light microscope (Upright Microscope Leica DM6 B, 10X magnification) equipped with a 405 nm excitation and 535 nm emission filters for fluorescent intensity measurements (n= 10) (Fig. 9). For the ratio between the oxidized and reduced forms of either the *HyPer* (Fig. 10) or *Grx1-roGFP2* strains (Fig. 11) (n= 10), a second image, at excitation 490 nm and emission 535 nm, was taken. Intensity-normalized images of at least ten nematodes per treatment were taken within 30 minutes from the sampling and quantification of the fluorescence signals was performed on the Leica® LAS software. Further details of the method and method validation are available in *Sections 2.6* of Paper II and *S.M.2 - S.M.3* of Paper II *Supporting Material*.

2.9 Transcriptomic analysis through RNA sequencing

Total gene expression via RNA sequencing analysis has become a widely adopted tool to assess changes in the transcriptome profiles of organisms under certain environmental stressors, including gamma radiation (Hurem et al., 2017b). This method allows for the identification of differentially expressed genes (DEGs) by measuring global gene expression, in comparison to a control group. Thus, it provides with important information with respect to repression or activation of transcription of single genes, canonical pathways and molecular functions affected by the environmental/experimental conditions.

For this reason, in Paper I and II, RNA sequencing analysis was adopted in order to obtain the transcriptomic profiles of nematodes chronically exposed to different dose-rates of gamma radiation. Synchronized populations were irradiated in triplicates for 48 (Paper I) and 72 hours (Paper II) from L1 stage, in order to assess changes in the gene expression before and after reaching sexual maturation. After the irradiation, three selected exposure treatment were chosen (0.4, 10 and 100 $mGy \cdot h^{-1}$) and nematodes snap-frozen in liquid nitrogen until further analysis as described in the workflow diagram presented in Fig. 12.

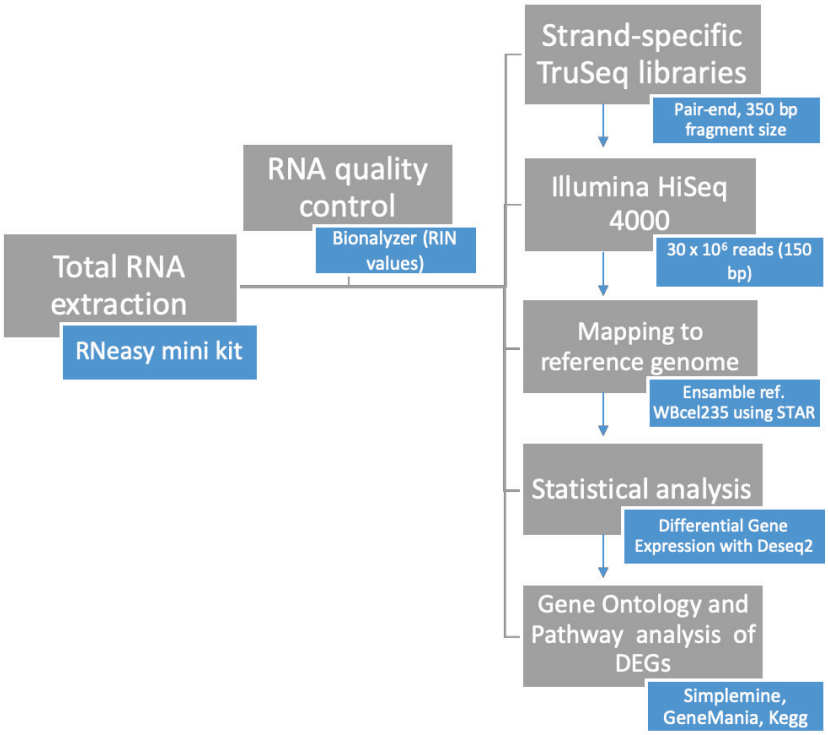

Figure 12. Workflow diagram of RNA sequencing analysis, from total RNA extraction to statistical analysis of differentially expressed genes (DEGs) (FDR <0.05, -0.3 ≥ log2FC ≥ 0.3), performed on the L1 stage *C. elegans* chronically exposed to gamma radiation for 48 and 72 hours.

2.10 Mitochondrial DNA copy number variation by droplet digital PCR analysis

The hither to most predominantly used techniques for measuring the presence and concentration of a DNA sequence has been by real-time quantitative Polymerase Chain Reaction (qRT-PCR or qPCR). In qPCR the target DNA is amplified until a certain level of fluorescent signal (cycle threshold, CT) is produced and detected. The number of DNA molecules is then calculated based on the number of amplification cycles needed to reach the CT threshold relative to a standard curve obtained by amplification from serial dilution of known concentrations of input target DNA.

Sykes et al. (1992) pioneered a major advance in the PCR technique by using the combination of limiting dilution, end-point PCR and Poisson distribution. This new strategy is now called digital PCR (dPCR), and it is based on dilution and partition of samples into hundreds or even millions of separate reaction "chambers", so each contains one (positive partition) or no copies (negative partition) of the sequence of interest (Baker, 2012). By simply counting the number of positive versus the number of negative partitions, it is possible to determine the absolute copy number of the selected DNA sequence (Basu, 2017). The advantage of this new technique is that by using the same primers and probes of qPCR it is possible to obtain the absolute quantification of nucleic acids in a more sensitive, precise and accurate way, which in turn allows researchers to explore complex genetic landscapes (Hindson et al., 2011).

In droplet digital PCR (ddPCR) an emulsion of oil, PCR reaction mix and stabilizing chemicals, obtained with a droplet generator instrument, is used to partition the total DNA samples into circa 20.000 nanoliter droplets representing the reaction chambers (Hindson et al., 2011)(Fig. 13). Dilution of the DNA followed by sonication or treatment with restriction enzymes is commonly applied in order to optimize template DNA partitioning, droplet formation and the ddPCR performance. The DNA amplification is performed in a standard thermal cycler instrument until it reaches the endpoint or plateau phase. Subsequently, the plate is transferred into a droplet reader, which functions like a flow cytometer where droplets are aspirated and streamed into the detector, where the injection of a spacer fluid separates and aligns them for single-file simultaneous two-color detection (Hindson et al., 2011). Based on fluorescence amplitude, a threshold assigns each droplet as PCR product positive or negative. The use of TaqMan assays provides specific duplexed detection of target and reference genes.

This type of assay is described in detail in Paper III and it was adopted in our study for the quantification of the absolute copy number of mitochondrial DNA (mtDNA), measured as ratio mt/nDNA (nuclear DNA). For this purpose, five mitochondrial targets and two reference nuclear genes were used in a duplex ddPCR format (Paper III). The mtDNA CNV (copy number variation) was assessed in response to chronic exposure to ionizing gamma radiation, as changes in the mitochondrial genome content have been shown in other model organisms after acute X-ray irradiation (Evdokimovsky et al., 2011).

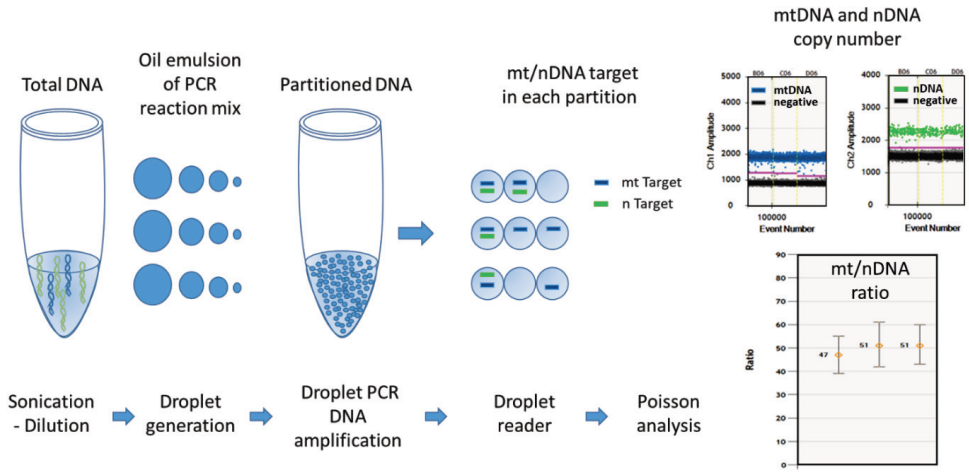

Figure 13. Experimental procedure applied for the quantification of mtDNA copy number variation as a measure of mt/nDNA ratio in *C. elegans* chronically exposed to ionizing radiation by using duplex droplet digital PCR assay.

2.11 Effects on parentally irradiated nematodes (F1): DNA damage, development and reproduction

The effects of chronic exposure to ionizing gamma radiation was evaluated on the progeny (F1) of F0 irradiated nematodes, in terms of embryonic DNA damage, development and reproduction (Fig. 14). For this purpose, and in order to avoid further damage induced by using alkaline hypochlorite treatment (bleaching), a method was optimized for the isolation of gastrula-stage embryos from reproducing adult hermaphrodites. This method is described in detail in Section 2.8 of Paper I and it was implemented with a cell isolation procedure in order to perform the Comet assay on homogeneous essentially undifferentiated embryonal cells.

Briefly, F0 nematodes were exposed for 72 hours from L1 stage to increasing dose-rates of ionizing gamma radiation (Section 2.2). At the end of the irradiation, embryos (F1) from exposed nematodes (F0) were isolated and filtered in order to remove the excess of *E. coli* cells. Synchronous populations of L1 stage nematodes (F1) were obtained from incubation overnight in non-seeded NGM plates of the *E. coli*-free embryos. These were

kept under control conditions and adopted for assessing effects on morphology, development and total brood size, as previously described in Section 2.4 and 2.5 for F0 nematodes.

For the DNA damage assessment, the collected and filtered F1 embryos were mechanically disrupted with a glass Dounce tissue homogenizer in order to isolate single cells, which were lysed and adopted in the Comet assay (Section 2.8.1 of Paper I). The method established by the current study provided high number of viable cells and low level of background DNA damage in control cell populations (2.2 - 5.8% of tail intensity), compared to previous methods (~30% of tail intensity) (Sobkowiak and Lesicki, 2009, Ng et al., 2019).

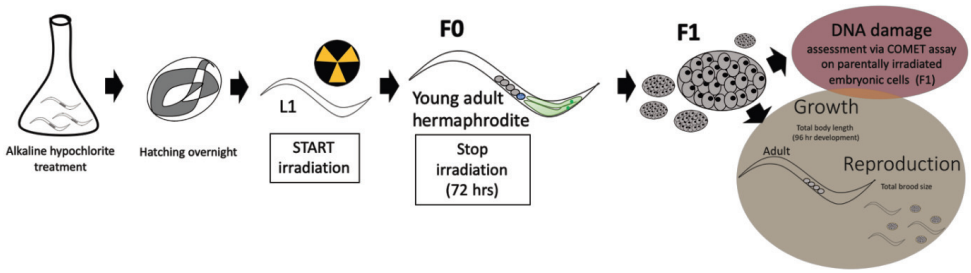

Figure 14. Experimental set up for assessing DNA damage and effects on development and reproduction on parentally exposed nematodes (F1) (Paper I).

2.12 Statistical analysis

Data analysis was performed on Minitab® 18 (Minitab Statistical Software (2010). [Computer software]. State College, PA:Minitab, Inc. (www.minitab.com)), JMP Pro v14 (SAS institute, Cary, NC, USA) and SigmaPlot 10.0 (Systat Software, San Jose, CA).

Difference between exposure groups were assessed using parametric or non-parametric test, based on normality distribution of data and homogeneity of variance (homoscedasticity). One-way Analysis of Variance (ANOVA) was adopted in the first case, followed by Tukey *post hoc* for multiple comparisons, whereas in case of non-normally distributed data, the Kruskal-Wallis test was adopted. Normality and

homoscedasticity assumption were assessed on residuals by using Anderson-Darling normality test and visually on residuals vs. fitted value plot, respectively. Statistical significance was considered when *p*-value was lower than 0.05, unless differently stated.

In Paper I, the Effective Dose-Rate estimations were obtained on 10 and 50% of the population (EDR10 and EDR50) for reproduction and DNA damage on embryonic cells, by using the free software RegTox developed by Eric Vindimian (http://www.normalesup.org/~vindimian/en_download.html). For this purpose, the Hill model was used with corresponding confidence intervals of 95%. Principal Component Analysis (PCA) was performed in order to evaluate correlation between selected endpoints.

In Paper II, simple linear regression analysis (SLR) (Montgomery et al., 2012) was applied in order to assess increase in the ROS levels with respect to dose-rate and time of exposure.

In Paper III, a linear model was adopted in order to evaluate the influence of the reference gene (multi-copy *act* or single-copy *gpi-1*) on the measure of mtDNA copy number variation in response to ionizing radiation exposure. When required, a log transformation of the dose-rates and the mt/nDNA ratios was applied and a regression analysis performed. The Logistic 4P Hill model was adopted to identify the effective dose inducing increase in the mtDNA copy number after chronic exposure to different doses of gamma radiation.

3. Results

3.1 Paper I

In Paper I, different scenarios of exposure to ionizing radiation were compared in order to identify the most radiosensitive larval stages of *C. elegans* and to assess whether similar total doses of chronic or acute exposure would induce equivalent adverse effects. The results from total brood size experiments demonstrated a clear reduction in the reproductive capacity (43%), when nematodes were subjected to chronic irradiation at doses ≥6.7 Gy during larval development. Conversely, acute exposure using similar doses during the post-mitotic stage in young adult nematodes did not induce any adverse effect. This result indicated that developing larvae were more sensitive to gamma radiation, and accordingly the L1- young L4 stages were identified as the most susceptible to reprotoxicity, since even lower doses (4.3 Gy, 100 mGy·h^{-1}) were able to induce a significant reduction in the number of produced offspring (35%).

In order to unravel the mechanisms of toxicity behind the observed impairment of the nematode reproductive capacity under chronic exposure to ionizing radiation, a systematic investigation of vulnerable larval developmental processes and molecular mechanisms was performed by measuring germ cell apoptosis, sperm production and total gene expression. This analysis revealed that doses of exposure down to ~2.8 Gy (40 mGy·h^{-1}) resulted in enhanced germ cell apoptosis and significantly reduced the number of spermatids. RNA sequencing analysis showed down-regulation of more than 140 genes related to reproduction, of which 101 down-regulated genes were specific to sperm production and maturation, including 28 Major Sperm Protein (MSP), sperm meiosis genes *smz-1* and *smz-2* and the sperm specific histone 2 variant (*htas-1*).

Differential regulation of genes related to cell cycle, programmed cell death, chromatin organization, DNA repair, spindle formation and embryonal development were also found, suggesting potential adverse effects on the progeny of irradiated nematodes. The enhanced DNA damage, demonstrated by Comet assay carried out on F1 parentally irradiated embryos, validated this hypothesis, and was accompanied by impairment of the nematode somatic growth. However, no significant effect was observed on F1 nematodes in terms of hatching, survival or loss in their reproductive capacity.

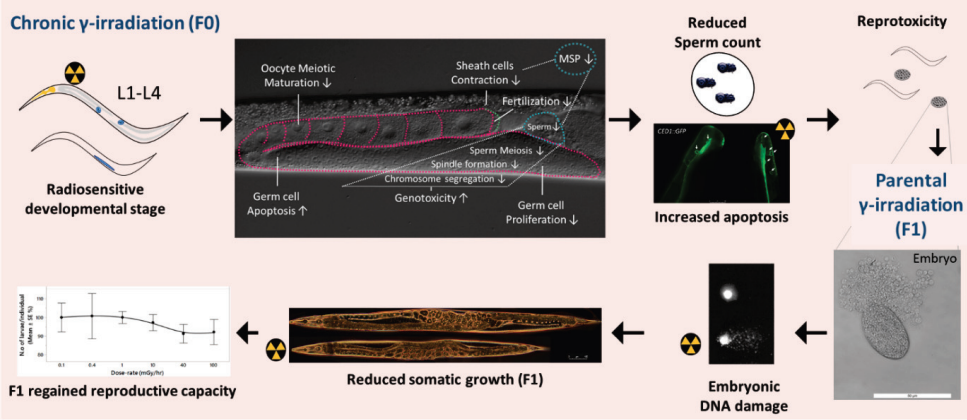

Figure 15. Graphical summary of main findings from Paper I.

3.2 Paper II

In this study, the ability of the nematode *C. elegans* to tolerate chronic ionizing radiation exposure was assessed by measuring ROS production and AODs activation, in combination with phenotypical adverse effects on somatic growth and reproductive capacity. For this purpose, spatiotemporal patterns of hydrogen peroxide (H_2O_2) were measured *in vivo* together with the expression of superoxide dismutase 1 (*sod-1*) and glutathione redox potential, by using a GFP reporter strain (*sod1::gfp*) and two ratiometric biosensors (*HyPer* and *Grx1-roGFP2*). Furthermore, a global gene expression analysis on young adult nematode, exposed for 72 hours from L1 stage, was performed in order to identify cellular and molecular mechanisms triggered by chronic gamma radiation exposure, by assessing changes in the nematode transcriptome profile.

In line with previous studies, results showed adverse effects on reproduction when nematodes were exposed to gamma radiation during the larval development at doses ≥3.9 Gy (dose-rate ≥40 mGy·h^{-1}), this result was also corroborated by differential regulation of more than 300 genes related to reproduction. The observed reprotoxic effect was accompanied by a dose-dependent and time dependent (48 and 72 hours) increase of H_2O_2 levels and AODs activation via higher expression of *sod-1*. Moreover, a temporary but significant redox imbalance was shown at 48 hours of exposure by increased oxidized/reduced ratio of *Grx1-roGFP2*. The data showed that at dose-rates ≤10 mGy·h^{-1} (total dose ~1 Gy) defence mechanisms were able to prevent the manifestation of oxidative stress response, whereas at dose-rates ≥40 mGy·h^{-1} (total dose 1.9 Gy) the continuous formation of radicals caused a redox shift, leading to oxidative stress transcriptomic response. This included changes in mitochondrial function, as indicated by the down-regulation of 10 of the twelve mtDNA encoded genes essential for the assembly of the mitochondrial electron transport chain (ETC), but also changes in functions related to protein degradation, lipid metabolism and collagen synthesis.

Moreover, genotoxic effects were among the most over-represented functions affected by chronic gamma irradiation, as indicated by differential regulation of genes involved in DNA damage, DNA repair, cell-cycle checkpoints, chromosome segregation and chromatin remodelling.

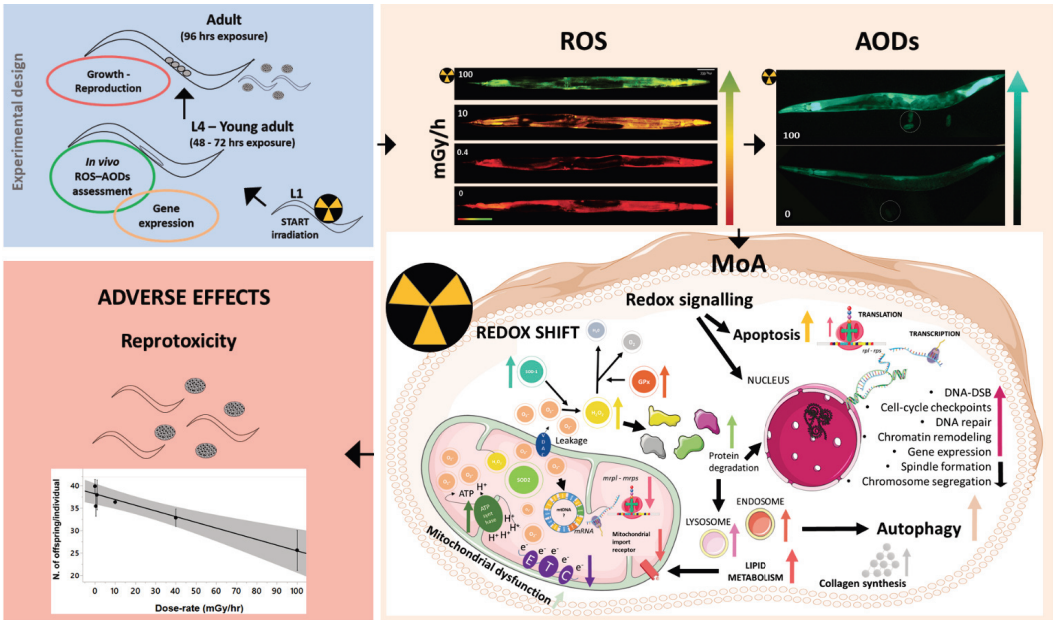

Figure 16. Graphical summary of assessed endpoints and main findings from Paper II.

3.3 Paper III

Following oxidative stress, mtDNA damage has been shown to be more extensive and persist longer than nuclear DNA damage, thus, mtDNA CNV (copy number variation) has been proposed as a marker for mitochondrial dysfunction following exposure to ionizing radiation (Malik and Czajka, 2013). The standard method used for quantification of mtDNA content relies on standard quantitative PCR, which provides a relative rather than an absolute quantification and presents some limitations.

In Paper III, a method based on droplet digital PCR (ddPCR) was developed in order to measure the absolute variation in the mtDNA copy number in *C. elegans*, following chronic exposure to gamma radiation. For this purpose, five mitochondrial target (COX1, COX3, ND5, s-rRNA and tRNA-val/ND6) and two nuclear reference genes (single-copy *gpi-1* and multi-copy *act*) were selected and amplified pairwise in duplex PCR format, in order to obtain an absolute quantification of the ratio mt/nDNA.

Results showed that the optimized ddPCR method represents a more simple and robust means of quantification, that can overcome the known uncertainties related to qPCR measurements. The method was used to investigate the effects of chronic gamma irradiation after low (up to 7.2 Gy, dose-rate ≤100 $mGy \cdot h^{-1}$) and high (24 to 72 Gy, dose-rate ~1 $Gy \cdot h^{-1}$) dose ranges of exposure. A significant difference (~1.6-fold increase) was observed in terms of mtDNA content after exposure to high doses compared to low doses and control treatments. This result showed a Hill type dose-dependent increase of the mtDNA copy number and a predicted dose threshold of effect at 10.3 ±1 Gy. Thus, nematodes subjected to low dose-range chronic exposure demonstrated the ability to maintain a stable mtDNA content. In contrast, exposure to high dose range appeared to induce mtDNA replication, which may suggest a compensatory response to counteract genotoxic effects or mitochondrial dysfunction.

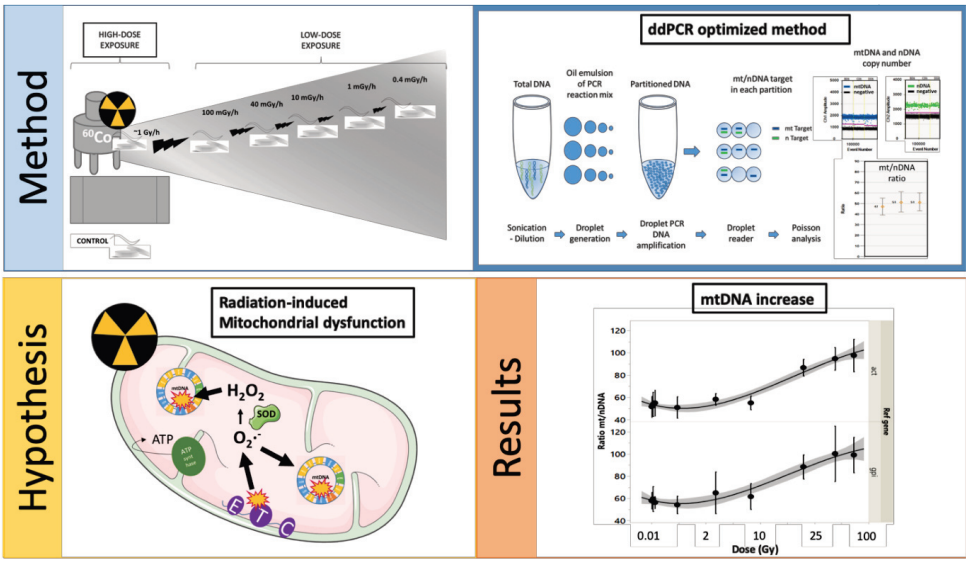

Figure 17. Graphical summary of method development and main findings from Paper III.

4. Discussion

The vast differences between radioresistant and radiosensitive species are well documented and have been known for decades (Harrison and Anderson, 1996, UNSCEAR, 2006, Garnier-Laplace et al., 2013), however, the underlying mechanisms represent a long standing scientific conundrum. A recent review lists several potential factors that might influence species radiosensitivity, including exposure scenario, stage of development, biology of the organisms and the evolved cellular and molecular defence systems (Adam-Guillermin et al., 2018). The lack of knowledge on vulnerability of developmental stages or different tissues to the effects of chronic ionizing radiation exposure in radioresistant species, underlines the importance of the current study. The research performed in this thesis addressed the effects of chronic exposure to ionizing radiation in the soil invertebrate *C. elegans*, to elucidate the mechanisms involved in sensitivity and tolerance of an important and hitherto presumed radioresistant model organism (Krisko et al., 2012b, Sugimoto et al., 2006, Guo et al., 2013, Vermezovic et al., 2012). For this purpose, a multitude of cellular and molecular biology techniques was applied after irradiation of nematodes to a range of low and high dose-rates of gamma radiation from a ^{60}Co source (0.4 to ~1 $Gy \cdot h^{-1}$). Moreover, this study required the development and optimization of new methods, including the gastrula-stage embryonal cells isolation in order to assess DNA damage via the Comet assay or the droplet digital PCR method, optimized to measure the mtDNA copy number variation. Furthermore, by comparing acute *versus* chronic gamma irradiation, and by performing exposure of different stages during nematode development, novel insights with respect to reprotoxic effects, sensitive larval stages and cell-specific sensitivity were obtained. Successively, this study addressed the interaction between ROS production, AODs responses, DNA damage and repair, and mitochondrial function. Finally, the results were compiled and integrated into a conceptual adverse outcome pathway (AOP) network on radiation induced reprotoxic effects in *C. elegans*.

4.1 Life stage-dependent radiosensitivity in C. elegans

A major aim of this PhD study was to investigate to what extent life history traits or certain stage(s) of *C. elegans* development showed higher sensitivity to ionizing radiation. The first major objective was thus to investigate the difference in sensitivity between post-mitotic adult hermaphrodites and developing larvae. In line with previous studies (Krisko et al., 2012a, Weidhaas et al., 2006, Dubois et al., 2018), results showed that acute or chronic exposure of post-mitotic adult hermaphrodites to ionizing radiation (at doses up to ~15 Gy) did not induce any adverse effect in terms of survival, somatic growth or reproductive capacity of nematodes (Paper I, Fig. 2 & 3). Whereas, results from three independent experiments on nematodes chronically exposed during larval development showed reprotoxic effects induced at doses ≥3.9 Gy (dose-rates ≥40 $mGy \cdot h^{-1}$), even when different culturing conditions were employed (NGM agar plates and swirling liquid culture, Papers I and II respectively). Specifically, impairment of the reproductive capacity was measured at similar doses of exposure (≥4.3 Gy in Paper I and ≥3.9 Gy in Paper II), even though the duration and dose-rates of exposure were different (100 $mGy \cdot h^{-1}$ for 43 and 62 hours, and 40 $mGy \cdot h^{-1}$ for 96 hours, respectively). Previous studies have shown negative effects on vulval development, fertility and reproduction following exposure throughout the larval development, but at significantly higher doses (>70 Gy) (Weidhaas et al., 2006, Bailly et al., 2010), compared to the highest dose (~19 Gy) adopted in the current study.

The reduced reproductive capacity shown in Papers I and II was in line with previous studies on other invertebrates, which have shown comparable reprotoxic effects at similar total doses following exposure during the development (Hertel-Aas et al., 2007, Parisot et al., 2015). Notably, the irradiation during the embryonal developmental stage of nematode unhatched eggs, performed in Paper I, did not enhance the reprotoxic effects compared to exposure of early larval stages (L1-Young L4).

To conclude, in support of the first hypothesis of the study, larval development was demonstrated to be a more sensitive stage compared to the post-mitotic stage of the nematode life cycle. Specifically, the L1 to young L4-molt was unequivocally shown to be the most sensitive, and probably represent the critical stages of development, being affected by gamma radiation, at doses ≥3.9 Gy (dose-rate ≥40 $mGy \cdot h^{-1}$). These

observations strongly suggested that the observed reprotoxic effects were linked to adverse effects on the gonadal development or on the production of gametes.

4.2 Vulnerable cell types and biological processes in irradiated nematodes

Reproduction is recognized to be one of the most radiosensitive endpoints, possibly because cells undergoing rapid division either for renewal (i.e. germ cells) or growth (i.e. embryonal development) are more vulnerable (UNSCEAR, 2006). With respect to this theory, one of the main objectives investigated in the current study was to assess tissue and cell-specific radiosensitivity. Thus, novel insights into the mechanisms underlying nematode reprotoxicity were discovered by studying the effects of chronic gamma irradiation on oogenesis and spermatogenesis (Paper I). The initial results from the present study indicated that sperm is the most vulnerable cell type, which was affected at doses ≥2.8 Gy (dose-rates ≥40 $mGy \cdot h^{-1}$) (Paper I), since a significantly reduced number of spermatids was observed after 72 hours of exposure. This is consistent with previous studies performed on several more radiosensitive species, including earthworms (Hertel-Aas et al., 2011b), fish (UNSCEAR, 1996, Kuwahara et al., 2002) and rodents (Haines et al., 2001, Liu et al., 2006), showing that sperms are vulnerable to ionizing radiation. Interestingly, this effect on sperm was not observed when a targeted exposure of the spermatogenesis process was performed in Paper I, possibly because the total dose of exposure was not sufficiently high (1.3 Gy, L3-L4 stage, 13 hours exposure to 100 $mGy \cdot h^{-1}$). Similarly, prolonged irradiation post-spermatogenesis to significantly higher doses (~15 Gy, Paper I) did not affect reproduction, suggesting that mature sperm were essentially tolerant to radiation. This is consistent with the fact that mature sperm are transcriptionally silent and have condensed chromatin (Ellis and Stanfield, 2014, Chu and Shakes, 2013). Together, these findings indicated that injury had to occur during the early gonadal development in order to manifest during the production of sperm germ cells. Consistent with this model, RNAseq analysis at 48 hours of 100 $mGy \cdot h^{-1}$ irradiation (~4.8 Gy), identified dysregulation of genes with essential role in the meiotic process during *C. elegans* spermatogenesis. A previous study showed that the perturbation of the S phase via RNAi

or exposure to 120 Gy resulted in arrest of the male germ line nuclei in the proliferative zone, which suggested that male as well as hermaphrodite germ cells are competent for checkpoint signalling (Jaramillo-Lambert et al., 2010). Furthermore, the male checkpoint machinery was shown to be more successful than the corresponding hermaphrodite mechanism at handling an asynapsed chromosome, thus improving the chromosome transmission (reproductive success). This implies that the male germ cells possess functional gamete quality control, despite absence of physiological or CED-3 caspase-activated apoptosis (Jaramillo-Lambert et al., 2010). This may indicate that the radiation induced reprotoxic effects in *C. elegans* may be gender specific.

In good accordance to this hypothesis, in Paper I, the spermatids reduction in hermaphrodites was correlated with significant down-regulation of genes essential for chromosome segregation during sperm meiosis (*smz-1* and *smz-2*) and chromatin condensation during sperm maturation (*htas-1*). Inhibition of these genes has previously been shown to induce the arrest of spermatocytes progression through meiotic division in males, with negative consequences for their fertility (Chu et al., 2006). The observed effects are in good accordance with immature spermatocyte formation being a vulnerable process, as suggested by Hasan et al. (1989). Moreover, this was further corroborated by the down-regulation of 28 sperm cytoskeletal structural proteins (MSP) (Paper I), required not only for sperm motility but also for the stimulation of oocyte meiotic maturation and ovulation (Miller et al., 2001) (Fig. 18). At 72 hours of exposure the *spr-5*-regulated *set-17* was significantly down-regulated (Paper I-II). *Set-17* is a lysin methyltransferase, which controls the expression of the MSP gene clusters (Engert et al., 2018), while *spr-5* is a histone H3K4 demethylase with a role in meiotic double-strand break repair (Nottke et al., 2011). *Spr- 5* mutants have shown perturbation of DSB repair, including increased *p53*-dependent germ cell apoptosis, increased levels of the DSB repair marker *RAD-51*, sensitivity toward DSB-inducing treatments (Nottke et al., 2011) and progressive sterility over many generations (Katz et al., 2009). In the same study by Katz et al. (2009), this sterility was correlated with the dysregulation of spermatogenesis-expressed genes and with the transgenerational accumulation of the demethylated histone H3 on lysine 4 (H3K4me2). This may imply that complex DNA damage such as DSB, may have affected the regulation of *spr-5* and *set-17*, thereby leading to impaired expression of the spermatogenesis gene

program (Fig. 18), as well as suggest potential adverse effects on the transmission of the epigenetic memory over multiple generations (Katz et al., 2009).

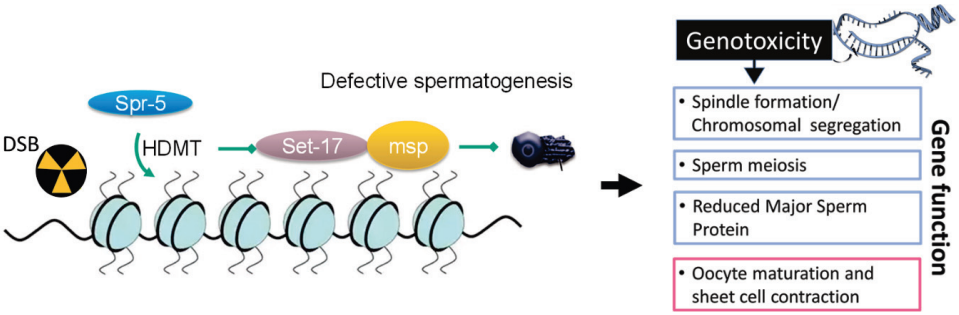

Figure 18. Proposed model for gamma radiation induced defective sperm meiosis in the *C. elegans* hermaphrodite. Repair of complex DNA damage such as DSB is initiated via histone demethylation by *spr-5*, which concomitantly represses *set-17* regulated genes including *msp*. DNA damage onto the gametes causes defective chromosomal segregation and spindle formation. The concerted effect leads to reduced number of mature sperms with the downstream feedback inhibition of oocyte maturation and sheet cell contraction signalling.

In addition to a differential regulation of spermatogenic genes, the degree of sperm reduction and the normal sperm reserve in the hermaphrodites (Singson, 2001) were demonstrated to comprise the main determining factor for the radiation induced impairment of reproductive capacity. However, exposure at ~2.8 Gy during larval development, including post-embryonic development, induced adverse effects on oocytes as well as on developing spermatids. Enhanced germ cell apoptosis, measured after 72 hours of irradiation, demonstrated that proliferating oocytes were also vulnerable to the effects of ionizing radiation at comparable doses of exposure (2.9 Gy). Germ cell apoptosis in *C. elegans* has previously been shown to act as a protective mechanism that removes damaged cells and reduces the probability of mis-repair at acute high doses (>30 Gy) of ionizing radiation (Bailly and Gartner, 2013). The current study demonstrates that apoptosis is a highly sensitive defence mechanism and can be activated at 10-fold lower doses (Paper I).

In line with the second hypothesis formulated in the study, the results demonstrated that the reproductive apparatus is a vulnerable target for chronic low-dose gamma

irradiation due to high cell proliferation in the gonadal tissues and specifically because of vulnerable cells undergoing meiosis.

These results are important because, in contrast to effects observed at high doses during acute exposure of *C. elegans* males (Jaramillo-Lambert et al., 2010), the current study demonstrates that developing spermatids of hermaphrodites are intrinsically more radiosensitive than oocytes, presumably due to lack of proper checkpoint mechanisms, absence of apoptosis, and no means for replenishment of non-functional cells. In contrast, the apoptotic machinery constitutes an efficient defence mechanism for excluding DNA damaged oocytes.

The observed effects on *C. elegans* spermatogenesis is a *bona fide* example of an important principle that even resistant species may inherit vulnerable cellular and molecular processes, which may have consequences to the population sustainability. This is in contrast with other soil organisms, such as earthworms, where radiation-induced sterility is reversible, and individuals showed full recovery of the reproductive capacity within two months after termination of the exposure (Hertel-Aas et al., 2011a).

In the *C. elegans* hermaphrodite spermatogenesis is restricted to a short stage during germline development prior the onset of oogenesis and cannot be resumed (L'Hernault, 2006). Hence, it is tempting to speculate that a chronic exposure scenario over multiple generation could potentially favour a higher incidence of males to compensate for the stress conditions. This could potentially ameliorate the reprotoxic effects caused by the reduced sperm production in the hermaphrodites.

This means that chronic radiation is likely to cause long-term transgenerational effects, thus, further investigation over multiple generations is necessary, to properly address adverse effects on the progeny of irradiated nematodes, as previously reported by Buisset-Goussen et al. (2014) and as suggested by the *spr-5* role in epigenetic and fertility (Katz et al., 2009, Kerr et al., 2014).

4.3 Effects on the progeny of irradiated nematodes

A remarkable capacity to repair radiation-induced DNA damaged has been previously shown in radiorestistant and desiccation-resistant species such as tardigrades, bdelloid

rotifers and the bacterium *D. radiodurans* (Zahradka et al., 2006, Gladyshev and Meselson, 2008b, Hashimoto et al., 2016). In contrast, in *C. elegans,* exposure to significantly lower doses (100 mGy·h^{-1}, total dose 4.8 and 7.2 Gy) provided during larval development (Papers I-II) affected the expression of genes related to reproductive system, meiotic chromosome segregation, aneuploidy, spindle formation and embryonic development, strongly indicating adverse effects on the DNA of cells under division. Moreover, the severe genotoxic effects shown in proliferating germ cells from chronically irradiated F0 nematodes (Paper I) suggested that potential adverse effects could be protracted to developing embryos in their progeny (F1).

For this reason, DNA damage analysis was performed on undifferentiated cells extracted from gastrula stage F1 embryos from irradiated parents (F0). In line with Bergonie's (1906) classic radiation biology hypothesis that proliferating cells would be a vulnerable target for ionizing radiation, this revealed that 100% of the cells carried significant DNA damage from doses to parents ≥2.9 Gy (dose-rate ≥40 mGy·h^{-1}) (Paper I). This was further corroborated by gene expression analysis, which identified 24 up-regulated genes related to 'Variant Sister Chromatid segregation defective in early embryo', and that also comprised the most significantly enriched phenotypical variant (3.1-fold enrichment) (Paper II).

Consistent with previous studies (Dubois et al., 2018, Bailly et al., 2010, Clejan et al., 2006), this severe genotoxic effect did not induce any deleterious consequence on hatchability and/or viability of the parentally irradiated embryos (Paper I). However, in order to study potential adverse effects on the nematode development, somatic growth and reproductive fitness were monitored by measuring total body length and total brood size on parentally irradiated F1 nematodes, under control conditions. Results from this analysis showed a significant reduced somatic growth, but no obvious effect on cell viability, or tissue formation. Surprisingly, despite the observed genotoxic effect, nematodes maintained their reproductive fitness, since no significant reduction was detected in the number of viable progenies. Thus, showing that nematodes irradiated during early embryogenesis can produce viable embryos, even when the majority of the proliferating embryonal cells carried a substantial damage on their DNA.

Interesting, significant effects on somatic growth were shown for all the parentally irradiated nematodes, including the lowest dose of exposure (0.03 Gy, dose-rate 0.4

mGy·h^{-1}, Paper I). This result is consistent with the gene expression GO-term analysis (Paper II) performed at 100 mGy·h^{-1}, showing down-regulation of multiple biological functions related to embryonic and post-embryonic development, while 'Pleiotropic severe defects in early embryo' was significantly up-regulated.

Checkpoint response to DNA damage has previously shown to be actively silenced in irradiated embryos of *C. elegans*, thus allowing their survival after exposure to DNA-damaging agents (Holway et al., 2006). Based on these findings, Holway et al. (2006) proposed that adherence to the schedule of cell division is evolutionary selected over error-free replication during early embryogenesis. In agreement with this model, the present study showed that despite the severe damage to DNA exerted by low-dose gamma irradiation, embryos were able to survive and reproduce, but at the cost of somatic growth.

The effects on nematode body size has been previously related to dysregulation of genes with autophagic functions, such as *unc-51*, encoding for a serine-threonine kinase (Megalou and Tavernarakis, 2009). Specifically, *unc-51* mutants have shown defects in autophagy, which resulted in significantly shorter mean body size but constant number of cells. Consistent with this study and with the reduced body size observed in parentally irradiated F1 nematodes, the transcriptomic analysis (paper II), showed significant up-regulation of *unc-51, atg-6* and *atg-9,* all genes involved in the autophagic process (Megalou and Tavernarakis, 2009). This might suggest that autophagy is important to the recovery of radiation-damaged embryos, however this hypothesis needs to be further investigated.

4.4 ROS production as a molecular initiating event of ionizing radiation effects

The radioresistance demonstrated for bdelloid rotifers, tardigrades and certain bacteria such as *D. radiodurans* has been associated to their remarkable ability to survive and resume reproduction or growth after desiccation (Welch et al., 2009, Fredrickson et al., 2008, Gladyshev and Meselson, 2008a). Specifically, they have evolved and adapted to survive enhanced damage to biomolecules caused by the production of ROS from the

disruption of the electron transport chain during the desiccation process (Leprince et al., 1994, França et al., 2007). The mechanisms involved in the adaptive response demonstrated after exposure to ionizing radiation include the protection of proteins from oxidative damage (i.e. potent antioxidant complexes consisting of Mn^{2+} - Pi, and small organic molecules specifically protect proteins from oxidation in *D. radiodurans*) (Daly, 2012), as well as an exceptional anti-oxidant capacity (Daly, 2012, Daly et al., 2007, Krisko et al., 2012a). For these reasons, one of the hypotheses formulated in this study, was that the anti-oxidant defence capacity of *C. elegans* (described in Section 1.13) (Braeckman et al., 2017) would ameliorate oxidative damage and thereby provide tolerance towards chronic exposure to ionizing radiation. This hypothesis was tested by investigating organism, tissue and cell-specific ROS production, AODs response and oxidative stress effects in nematodes subjected to chronic gamma radiation using reporter strains, ratiometric biosensors and transcriptomic analysis (Paper I-II).

The results in Paper II showed that chronic exposure to doses ≥3.9 Gy (40 $mGy \cdot h^{-1}$), induced reprotoxic effects, high levels of H_2O_2 and a temporary glutathione redox imbalance in young adult nematodes. Moreover, consistent with enhanced germ cell apoptosis, the gonads showed persistent redox imbalance in nematodes irradiated for 72 hours at 100 $mGy \cdot h^{-1}$ (~7.2 Gy). These adverse effects, however, were accompanied by enhanced activation of anti-oxidant defences, such as cytosolic superoxide dismutase, catalase and glutathione, as demonstrated *in vivo* as well as by gene expression analysis (Paper I-II). RNA sequencing revealed up-regulation of many genes involved in the oxidative stress response after 48 (i.e. *atg-9, ubc-3, ubc-8, ubh-4, epg-9, mak-1* and *jnk-1*) or 72 hours of exposure (i.e. *sod-1, ctl-1, glrx-10, gst-20, trx-2* and *trxr-2)* (Paper I-II). Moreover, and in line with the restored glutathione redox potential (Paper II) measured after 72 hours of exposure, genes required for the glutathione *de novo* synthesis were found up-regulated. However, evidence of the significant oxidation was found in the temporary redox imbalance measured at 48 hours and in the persistent high levels of H_2O_2 measured after 72 hours of exposure. This was further corroborated by 85 differentially regulated genes (DEGs) (72 hours of exposure) found in common with a study from Shin et al. (2011), where the oxidative stress transcriptomic response was analysed after exposure to ROS-inducing agents, such as the herbicide Paraquat. Most of these genes had functions related to mitochondrial ATP synthesis, mitochondrial ribosomal activity/assembly, collagen production, response to heat

stress, chromatin modification and ubiquitination, giving further evidence to the oxidative-stress response induced by chronic gamma irradiation. In line with these results, at high doses of acute exposure (>100 Gy) a previous study by Krisko et al., (2012a) demonstrated a 10-fold lower tolerance of *C. elegans* in comparison to the highly radioresistant rotifer *Adineta vaga.* Specifically, *C. elegans* showed higher levels of ionizing radiation-induced protein carbonylation, accompanied by similar adverse effects on fecundity.

Excess of ROS formed inside the mitochondria may trigger the downstream regulation of genes involved in apoptosis by the ROS-dependent signalling pathway (Sidoti-de Fraisse et al., 1998). However, no apoptosis or impaired viability on somatic cells was assessed in the current study, Paper I and II showed enhanced germ cell apoptosis, as well as differential expression of genes related to cell-cycle checkpoint, DNA double strand break, DNA repair and 87 genes involved in programmed cell death. These included the well-known markers for DNA damage-induced apoptosis *egl-1* and *hus-1* (Hofmann et al., 2002) and was consistent with the significant oxidation measured in the gonads of nematodes irradiated for 72 hours (Paper II), as well as with the meiotic impairment and thus the reprotoxic effects (Paper I-II).

Taken together these findings indicate that nematodes can maintain homeostasis at chronic exposure to dose-rates ≤10 $mGy \cdot h^{-1}$ (~1 Gy total dose). Since, despite the enhanced ROS levels, the activation of a multitude of defence mechanisms, aids the maintenance of somatic cell viability, growth, and normal biological functions, demonstrating its robust and efficient AOD and DNA repair systems. This is consistent with a previous study from Dubois et al., (2018) on protein carbonylation, showing that defence mechanisms, such as the 20S proteasome activity, was induced at similar doses (≥1 Gy) of chronic gamma-irradiation. However, exposure to 100 $mGy \cdot h^{-1}$ (~7.2 Gy) demonstrated enhanced oxidation in the gonadal arms, with adverse consequences for the nematode reproductive capacity. In contrast to the soma, germ cells under division in the reproductive tissue showed high vulnerability and specifically the developing sperm. In order to maintain high levels of defence, considerable energy expenditure might be required, and this could partially explain the impaired reproductive fitness observed at ≥40 $mGy \cdot h^{-1}$ (~3.9 Gy) in F0 nematodes and the reduced somatic growth observed in their progeny F1 (Paper I-II). It may thus appear that the nematode AODs

are capable of ameliorating ox-stress damage at doses ≤1 Gy. In contrast, the AODs were not able to counteract manifestation of ox-stress at doses ≥3.9 Gy, which indicates that tolerance to high level radiation in *C. elegans* requires the concerted action of multiple cellular mechanisms.

4.5 Effects of chronic ionizing radiation exposure on mitochondria

Processes associated with oxidative phosphorylation are known to be a susceptible target of radiation exposure, and consequent dysfunctions lead to further production of mitochondrial ROS due to alteration of the complexes involved in electron transport chain (ETC) and ATP synthase activity (Kam and Banati, 2013). This is consistent with the model where cells deficient in mitochondrial ETC (rho(o) cells) do not show radiation-induced ROS production (Leach et al., 2001), and in line with resistance to genotoxic stress shown in germ cells under reduced mitochondrial activity (Torgovnick et al., 2018). In Paper II, the significant down-regulation of fundamental genes required for the assembly of the complexes I, III, IV and V of the mitochondrial ETC, was accompanied with similar dysregulation of genes encoding for mitochondrial ribosomal proteins, all essential for the ETC proper assembly and function (Berg et al., 2006). This strongly suggested cellular redox imbalance as well as an early sign of mitochondrial dysfunction.

Mitochondrial DNA (mtDNA) is more vulnerable to oxidative stress conditions and inflicted damage persists longer than corresponding lesions onto nuclear DNA (Yakes and Van Houten, 1997). This might be due to its close proximity to the ETC, the lack of protective histones or fewer DNA repairing mechanisms (Mandavilli et al., 2002, Sawyer and Van Houten, 1999), which subsequently may render the mtDNA a more susceptible target to radiation-induced genotoxicity (Malakhova et al., 2005, Kam and Banati, 2013). Since increased levels of mtDNA have been reported in mammalian systems exposed to ionizing radiation (Nugent et al., 2010, Malakhova et al., 2005), mtDNA copy number variation (CNV) has been proposed as a measure for radiation-induced mitochondrial dysfunction (Malik and Czajka, 2013). For these reasons, one of the hypotheses formulated in this study was that mitochondria would present radiation-induced dysfunction and nematodes would counteract mtDNA damage by increasing the mtDNA

replication. For this purpose, in Paper III a new and accurate method for the quantification of mtDNA CNV was developed as a measure of mt/nDNA ratio, by using droplet digital PCR analysis (ddPCR).

This method revealed high accuracy and a simple and robust means of quantification that overcomes the known uncertainties related to qPCR measurements (Section 2.10 and Paper III) (Côté et al., 2011, Kam et al., 2013). Due to the high precision of ddPCR, it was possible to accurately detect significant changes in the mtDNA copy number by using both low and high dose ranges of chronic gamma radiation exposure. Specifically, a ~2-fold significant increase of mtDNA copies was observed, but this effect was only shown at doses of exposure ≥ 24 Gy (~1 $Gy \cdot h^{-1}$). Under low-dose range exposure (0.03 – 7.2 Gy, dose-rates ranging from 0.4 to 100 $mGy \cdot h^{-1}$), the number of mtDNA copies was similar to the control levels, thus indicating the ability of *C. elegans* to maintain a stable mtGenome content. However, by using a Logistic 4P Hill model, a threshold effect was measured at 10.3 ± 1 Gy, which is a dose ~2.4-fold higher than the one required for the manifestation of reprotoxic effects (Paper I-II).

Even though mtDNA damage was not an end-point assessed in the current study, this new method supports the hypothesis that nematodes would increase the mtDNA replication due to increased mitochondrial oxidative damage and genotoxic effects, as shown by the high levels of ROS, DNA damage and AODs measured in Paper I and II. Moreover, *C. elegans* post-mitotic cells show a remarkable ability to maintain viability even when subjected to high doses of ionizing radiation (≤19 Gy). It follows that mitochondrial functions maintain at a level that sustains cell viability. Thus, it is conceivable that the effects induced by chronic exposure to ionizing radiation trigger the activation of mtDNA replication as defence mechanisms. Hence, it is tempting to speculate that mitochondrial robustness contributes to the intrinsic radioresistance of *C. elegans*, however, this subject requires further investigation.

5. Conclusions

The results presented in this thesis provide important novel information about the mechanisms of toxicity and tolerance induced by chronic exposure to gamma radiation in a generally radioresistant organism. *C. elegans* has been reported to survive up to 3-5 kGy, while this study demonstrates that chronic irradiation to total dose ≥3.9 Gy (≥40 mGy·h^{-1}) may have devastating impact on reproduction, and hence population sustainability. Furthermore, reproduction is highly sensitive, particularly if vulnerable larval stages and proliferative germ cells experience chronic exposure to gamma radiation. These effects are directly related to impairment of spermatogenesis, where sperm meiosis and maturation were identified as the most radiosensitive processes. The findings from this research thus demonstrate that despite the activation of defence mechanisms to counteract radiation-induced damage, chronic exposure during larval development induces reprotoxic effects at approximately 13-fold lower total doses (~3.9 Gy), compared to previously published acute studies on post-mitotic adult larvae (~50 Gy) (Dubois et al., 2018). Notably, the current work did not detect any evidence of somatic cell death or failure in tissue development from the exposure conditions inducing reprotoxicity.

This study also showed that *C. elegans* do mount multiple defence responses, including DNA repair and AODs when subjected to chronic irradiation. Particularly, the enhanced AOD levels together with the oxidative-stress transcriptomic response suggest that these defences aid to counteract the radiation-induced excess ROS. Furthermore, the homeostatic maintenance of normal biological functions was observed at dose-rates ≤10 mGy·h^{-1}, whereas at dose-rates >40 mGy·h^{-1} a significant redox imbalance was shown particularly in the gonad. Enhanced germ cell apoptosis and impaired sperm meiosis at dose-rates ≥40 mGy·h^{-1} represent *bona fide* evidence of DNA damage response. These effects culminate in reduced reproductive capacity.

The down-regulation of essential mitochondrial ETC genes, suggested that mitochondria comprise a vulnerable target of chronic ionizing radiation. However, results showed stable mtDNA content after low-dose chronic exposure (≤7.2 Gy), implying the normal replication and integrity of the mitochondrial genome. In contrast,

high-doses of chronic exposure (≥24 Gy) induced significantly higher mtDNA copy number, indicating a compensatory mechanism.

Through the establishment of a new protocol for the quantification of DNA damage on embryonal cells via Comet assay, this study demonstrated that the progeny (F1) of irradiated F0 nematodes may suffer severe DNA damage. However, parentally irradiated nematodes were able to maintain normal cell and tissue functionality, as well as reproductive capacity at the expense of reduced somatic growth.

Finally, the main findings of this study were integrated into an Adverse Outcome Pathway (AOP) framework (Ankley et al., 2010) (Fig. 19). This AOP links the molecular initiating events by direct and indirect effects, to key events including oxidative stress, genotoxic and reprotoxic effects, which lead to adverse outcome on the population level.

Taken together these results provide new insight in the molecular and cellular mechanisms induced by chronic exposure to ionizing radiation in a radioresistant organism, which could be used for future multi-generational studies on the same model system, or for comparisons to both radiosensitive or more radioresistant species.

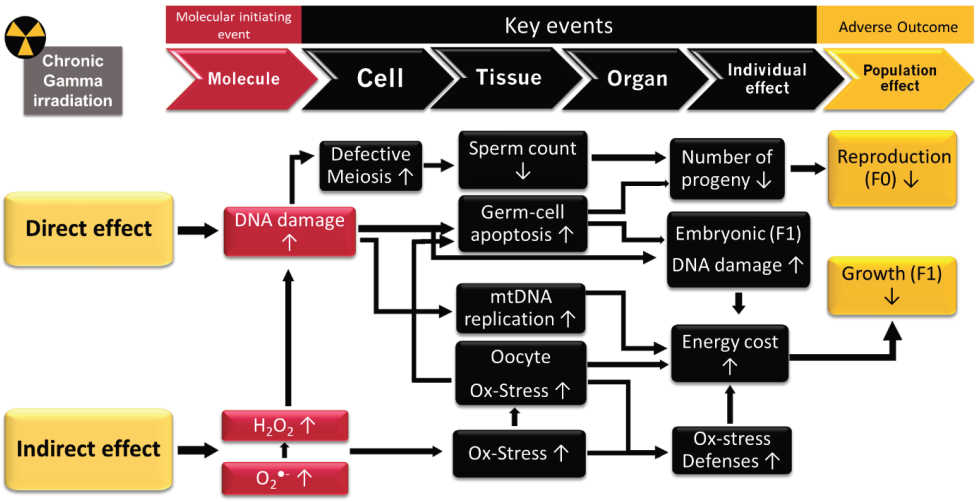

Figure 19. Conceptual AOP model of chronic exposure to ionizing radiation in the nematode *C. elegans*. Molecular initiating events include ROS formation and DNA damage. Key events include oxidative stress and genotoxic effects on proliferative germ cells, accompanied by activation of defense mechanisms, including AODs, DNA repair and mtDNA replication and increased energy cost. Reprotoxicity and reduced growth cause adverse outcome at the population level.

6. Limitations of the study and future prospective

The current study investigated mechanistic effects induced by chronic exposure to ionizing radiation, for this purpose higher doses than the ones considered environmentally relevant were employed. Environmental scenarios of exposure, such as those presented in the Chernobyl Exclusion Zone after more than 20 years from the accident, have shown negligible or no effect on nematode populations exposed to estimated total dose-rates of 200 $\mu Gy \cdot h^{-1}$ (Lecomte-Pradines et al., 2014). However, the doses and dose-rates adopted in the current study were intended to include a full dose-response for toxic effects assessment. The estimated dose-rates for the soil dwelling organisms (i.e. earthworms), five months after the Chernobyl nuclear accident, were above ~85 Gy (Krivolutzkii and Pokarzhevskii, 1992). Therefore, they might only represent relevant doses of exposure during a short period of time, directly after contamination from nuclear accidents. For these reasons, results presented in this work are primarily relevant at the mechanistic cellular and molecular level for comparison to other model organisms or to environmentally relevant scenarios of exposure.

Another limitation presented in the current study concerns the high inter-individual variability measured in terms of glutathione redox potential. This did not prevent proper assessment of oxidation effects after 72 hours of gamma irradiation. Therefore, in order to overcome the intrinsic variability, future analysis should employ a higher number of individuals per replicate, or further validation by using different methods.

The alteration of essential molecular and cellular mechanisms may over time exacerbate effects onto important biological functions and over multiple generations. For instance, mitochondrial dysfunction may lead to changes in metabolism due to defective energy production, which are adverse effects that could potentially represent a threat for the population dynamics in the environment. Development, longevity and reproductive fitness are essential for the population dynamics of a species, representing the most important ecological functions and the basis for the population survival. For these reasons, multigenerational studies should be performed in order to obtain a more reliable information with respect to radiosensitivity and population dynamics in response to chronic exposure to ionizing radiation. Such studies could monitor the male incidence over multiple generations, in order to investigate potential adaptive

responses induced by chronic ionizing radiation exposure. Particularly, further analysis on genotoxicity is necessary to elucidate DNA damage effects in vulnerable cell-types or vulnerable organelles, such as the developing sperm of hermaphrodites and the mitochondria. Analysis directed to spermatid morphology and viability, in combination with analysis on targeted spermatogenic genes could aid identifying the cause of the faulty sperm meiosis. Among these, functional analysis of the genes involved in the *set-17* and *spr-5* pathways also in other species could give a better understanding of the conserved nature and effects on the spermatogenic genes regulation and on its epigenetic consequence.

7. References

ABELLA, M. K. I. L., MOLINA, M. R., NIKOLIĆ-HUGHES, I., HUGHES, E. W. & RUDERMAN, M. A. 2019. Background gamma radiation and soil activity measurements in the northern Marshall Islands. *Proceedings of the National Academy of Sciences,* 116**,** 15425.

ADAM-GUILLERMIN, C., HERTAL-AAS, T., OUGHTON, D., BLANCHARD, L., ALONZO, F., ARMANT, O. & HOREMANS, N. 2018. Radiosensitivity and transgenerational effects in non-human species. *Annals of the ICRP***,** 0146645318756844.

ADAM-GUILLERMIN, C., PEREIRA, S., DELLA-VEDOVA, C., HINTON, T. & GARNIER-LAPLACE, J. 2012. Genotoxic and Reprotoxic Effects of Tritium and External Gamma Irradiation on Aquatic Animals. *In:* WHITACRE, D. M. (ed.) *Reviews of Environmental Contamination and Toxicology.* New York, NY: Springer New York.

ALLEN, R. & TRESINI, M. 2000. Oxidative stress and gene regulation. *Free Radical Biology Medicine,* 28**,** 463-499.

ANDERSSON, P., GARNIER-LAPLACE, J., BERESFORD, N. A., COPPLESTONE, D., HOWARD, B. J., HOWE, P., OUGHTON, D. & WHITEHOUSE, P. 2009. Protection of the environment from ionising radiation in a regulatory context (protect): proposed numerical benchmark values. *Journal of Environmental Radioactivity,* 100**,** 1100-1108.

ANDUX, S. & ELLIS, R. E. 2008. Apoptosis maintains oocyte quality in aging *Caenorhabditis elegans* females. *PLoS genetics,* 4**,** e1000295.

ANKLEY, G. T., BENNETT, R. S., ERICKSON, R. J., HOFF, D. J., HORNUNG, M. W., JOHNSON, R. D., MOUNT, D. R., NICHOLS, J. W., RUSSOM, C. L., SCHMIEDER, P. K., SERRRANO, J. A., TIETGE, J. E. & VILLENEUVE, D. L. 2010. Adverse outcome pathways: A conceptual framework to support ecotoxicology research and risk assessment. *Environmental Toxicology and Chemistry,* 29**,** 730-741.

AZZAM, E. I., JAY-GERIN, J.-P. & PAIN, D. 2012. Ionizing radiation-induced metabolic oxidative stress and prolonged cell injury. *Cancer letters,* 327**,** 48-60.

BACK, P., DE VOS, W. H., DEPUYDT, G. G., MATTHIJSSENS, F., VANFLETEREN, J. R. & BRAECKMAN, B. P. 2012. Exploring real-time in vivo redox biology of developing and aging Caenorhabditis elegans. *Free Radic Biol Med,* 52**,** 850-9.

BAILLY, A. & GARTNER, A. 2013. Germ Cell Apoptosis and DNA Damage Responses. *In:* SCHEDL, T. (ed.) *Germ Cell Development in C. elegans.* New York, NY: Springer New York.

BAILLY, A. P., FREEMAN, A., HALL, J., DECLAIS, A.-C., ALPI, A., LILLEY, D. M., AHMED, S. & GARTNER, A. 2010. The Caenorhabditis elegans homolog of Gen1/Yen1 resolvases links DNA damage signaling to DNA double-strand break repair. *PLoS genetics,* 6**,** e1001025.

BAKER, M. 2012. Digital PCR hits its stride. *Nature Methods,* 9**,** 541-544.

BASU, A. S. 2017. Digital assays part I: partitioning statistics and digital PCR. *SLAS TECHNOLOGY: Translating Life Sciences Innovation,* 22**,** 369-386.

BELOUSOV, V. V., FRADKOV, A. F., LUKYANOV, K. A., STAROVEROV, D. B., SHAKHBAZOV, K. S., TERSKIKH, A. V. & LUKYANOV, S. 2006. Genetically encoded fluorescent indicator for intracellular hydrogen peroxide. *Nature Methods,* 3**,** 281.

BERG, J. M., TYMOCZKO, J. L. & STRYER, L. 2006. *Biochemistry. 5th,* New York: , WH Freeman.

BERGONIE, J. 1906. Interpretation de quelques resultats de la radiotherapie et ssai de fixation d'une technique rationelle. *Compt Rend Acad Sci,* 143**,** 983-985.

BJERKE, H. & HETLAND, P. O. 2014. Dosimetri ved FIGARO gammaanlegget ved NMBU, ÅS. *Målerapport fra oppmåling av doseraten i strålefeltet fra kobolt-60. NRPA Technical Document Series,* 2.

BLOK, J. & LOMAN, H. 1973. The effects of gamma-radiation in DNA. *Current Topics in Radiation Research,* 9**,** 165-245.

BOARD, P. G., COGGAN, M., CHELVANAYAGAM, G., EASTEAL, S., JERMIIN, L. S., SCHULTE, G. K., DANLEY, D. E., HOTH, L. R., GRIFFOR, M. C. & KAMATH, A. V. 2000. Identification, characterization, and crystal structure of the Omega class glutathione transferases. *Journal of Biological Chemistry,* 275**,** 24798-24806.

BOULTON, S. J., GARTNER, A., REBOUL, J., VAGLIO, P., DYSON, N., HILL, D. E. & VIDAL, M. 2002. Combined functional genomic maps of the C. elegans DNA damage response. *Science,* 295**,** 127-131.

BRAECKMAN, B. P., BACK, P. & MATTHIJSSENS, F. 2017. Oxidative stress. *Ageing: Lessons from C. elegans.* Springer.

BRAUCHLE, M., BAUMER, K. & GÖNCZY, P. 2003. Differential Activation of the DNA Replication Checkpoint Contributes to Asynchrony of Cell Division in C. elegans Embryos. *Current Biology,* 13**,** 819-827.

BRENNER, S. 1974. The genetics of *Caenorhabditis elegans*. *Genetics,* 77**,** 71-94.

BROWN, K. R. & RZUCIDLO, E. 2011. Acute and chronic radiation injury. *Journal of Vascular Surgery,* 53**,** 15S-21S.

BUISSET-GOUSSEN, A., GOUSSEN, B., DELLA-VEDOVA, C., GALAS, S., ADAM-GUILLERMIN, C. & LECOMTE-PRADINES, C. 2014. Effects of chronic gamma irradiation: a multigenerational study using *Caenorhabditis elegans*. *J Environ Radioact,* 137**,** 190-7.

CABREIRO, F., ACKERMAN, D., DOONAN, R., ARAIZ, C., BACK, P., PAPP, D., BRAECKMAN, B. P. & GEMS, D. 2011. Increased life span from overexpression of superoxide dismutase in Caenorhabditis elegans is not caused by decreased oxidative damage. *Free Radical Biology and Medicine,* 51**,** 1575-1582.

CADET, J., DOUKI, T., GASPARUTTO, D. & RAVANAT, J.-L. 2003. Oxidative damage to DNA: formation, measurement and biochemical features. *Mutation Research/Fundamental and Molecular Mechanisms of Mutagenesis,* 531**,** 5-23.

CAMPBELL, A. M., TEESDALE-SPITTLE, P. H., BARRETT, J., LIEBAU, E., JEFFERIES, J. R. & BROPHY, P. M. 2001. A common class of nematode glutathione S-transferase (GST) revealed by the theoretical proteome of the model organism Caenorhabditis elegans. *Comparative Biochemistry Physiology Part B: Biochemistry Molecular biology of the cell,* 128**,** 701-708.

CHALFIE, M., TU, Y., EUSKIRCHEN, G., WARD, W. W. & PRASHER, D. C. 1994. Green fluorescent protein as a marker for gene expression. *Science,* 263**,** 802-805.

CHIN, G. M. & VILLENEUVE, A. M. 2001. C. elegans mre-11 is required for meiotic recombination and DNA repair but is dispensable for the meiotic G2 DNA damage checkpoint. *Genes & Development,* 15**,** 522-534.

CHOI, K.-M., KANG, C.-M., CHO, E. S., KANG, S. M., LEE, S. B. & UM, H.-D. 2007. Ionizing radiation-induced micronucleus formation is mediated by reactive oxygen species that are produced in a manner dependent on mitochondria, Nox1, and JNK. *Oncology reports,* 17**,** 1183-1188.

CHOPPIN, G., LILJENZIN, J.-O. & RYDBERG, J. 2002. *Radiochemistry and nuclear chemistry*, Butterworth-Heinemann.

CHU, D. S., LIU, H., NIX, P., WU, T. F., RALSTON, E. J., YATES III, J. R. & MEYER, B. J. 2006. Sperm chromatin proteomics identifies evolutionarily conserved fertility factors. *Nature,* 443**,** 101.

CHU, D. S. & SHAKES, D. C. 2013. Spermatogenesis. *Germ cell development in C. elegans.* Springer.

CLEJAN, I., BOERCKEL, J. & AHMED, S. 2006. Developmental Modulation of Nonhomologous End Joining in *Caenorhabditis elegans*. *Genetics,* 173**,** 1301-1317.

CONSORTIUM, T. C. E. S. 1998. Genome sequence of the nematode C. elegans: a platform for investigating biology. *Science***,** 2012-2018.

COPPLESTONE, D., BIELBY, S., JONES, S., PATTON, D., DANIEL, P. & GIZE, I. 2001. Impact Assesment of ionising Radiation on Wildlife.

CORRE, I., NIAUDET, C. & PARIS, F. 2010. Plasma membrane signaling induced by ionizing radiation. *Mutation Research/Reviews in Mutation Research,* 704**,** 61-67.

CORSI, A. K., WIGHTMAN, B. & CHALFIE, M. 2015. A transparent window into biology: a primer on Caenorhabditis elegans. *Genetics,* 200**,** 387-407.

CÔTÉ, H. C. F., GERSCHENSON, M., WALKER, U. A., MIRO, O., GARRABOU, G., HAMMOND, E., VILLARROYA, J., GIRALT, M., VILLARROYA, F., CINQUE, P., GARCIA-ARUMI, E., ANDREU, A. L., PINTI, M. & COSSARIZZA, A. 2011. Quality assessment of human mitochondrial DNA quantification: MITONAUTS, an international multicentre survey. *Mitochondrion,* 11**,** 520-527.

COX, M. M. & BATTISTA, J. R. 2005. Deinococcus radiodurans — the consummate survivor. *Nature Reviews Microbiology,* 3**,** 882-892.

DALY, M. J. 2009. A new perspective on radiation resistance based on Deinococcus radiodurans. *Nature Reviews Microbiology,* 7**,** 237.

DALY, M. J. 2012. Death by protein damage in irradiated cells. *DNA Repair (Amst),* 11**,** 12-21.

DALY, M. J., GAIDAMAKOVA, E. K., MATROSOVA, V. Y., VASILENKO, A., ZHAI, M., LEAPMAN, R. D., LAI, B., RAVEL, B., LI, S.-M. W. & KEMNER, K. M. 2007. Protein oxidation implicated as the primary determinant of bacterial radioresistance. *PLoS biology,* 5**,** e92.

DALY, M. J., OUYANG, L., FUCHS, P. & MINTON, K. W. 1994. In vivo damage and recA-dependent repair of plasmid and chromosomal DNA in the radiation-resistant bacterium Deinococcus radiodurans. *Journal of bacteriology,* 176**,** 3508-3517.

DAVIES, K. J. 2000. Oxidative stress, antioxidant defenses, and damage removal, repair, and replacement systems. *IUBMB life,* 50**,** 279-289.

DOONAN, R., MCELWEE, J. J., MATTHIJSSENS, F., WALKER, G. A., HOUTHOOFD, K., BACK, P., MATSCHESKI, A., VANFLETEREN, J. R. & GEMS, D. 2008. Against the oxidative damage theory of aging: superoxide dismutases protect against oxidative stress but have little or no effect on life span in Caenorhabditis elegans. *Genes Dev,* 22**,** 3236-41.

DROGE, W. 2002. Free radicals in the physiological control of cell function. *Physiological reviews,* 82**,** 47-95.

DU, J. & GEBICKI, J. M. 2004. Proteins are major initial cell targets of hydroxyl free radicals. *Int J Biochem Cell Biol,* 36**,** 2334-43.

DUBOIS, C., LECOMTE, C., RUYS, S. P. D., KUZMIC, M., DELLA-VEDOVA, C., DUBOURG, N., GALAS, S. & FRELON, S. 2018. Precoce and opposite response of proteasome activity after acute or chronic exposure of C. elegans to γ-radiation. *Scientific Reports,* 8**,** 11349.

DUNCAN LYNGDOH, R. H. & SCHAEFER III, H. F. 2009. Elementary lesions in DNA subunits: electron, hydrogen atom, proton, and hydride transfers. *Accounts of chemical research,* 42**,** 563-572.

ELLIS, H. M. & HORVITZ, H. R. 1986. Genetic control of programmed cell death in the nematode C. elegans. *Cell,* 44**,** 817-829.

ELLIS, R. E. & STANFIELD, G. M. The regulation of spermatogenesis and sperm function in nematodes. Seminars in cell & developmental biology, 2014. Elsevier, 17-30.

ENCALADA, S. E., MARTIN, P. R., PHILLIPS, J. B., LYCZAK, R., HAMILL, D. R., SWAN, K. A. & BOWERMAN, B. 2000. DNA replication defects delay cell division and disrupt cell polarity in early Caenorhabditis elegans embryos. *Developmental biology,* 228**,** 225-238.

ENGERT, C. G., DROSTE, R., VAN OUDENAARDEN, A. & HORVITZ, H. R. 2018. A Caenorhabditis elegans protein with a PRDM9-like SET domain localizes to chromatin-associated foci and promotes spermatocyte gene expression, sperm production and fertility. *PLoS genetics,* 14**,** e1007295.

ERMOLAEVA, M. A., SEGREF, A., DAKHOVNIK, A., OU, H.-L., SCHNEIDER, J. I., UTERMÖHLEN, O., HOPPE, T. & SCHUMACHER, B. 2013. DNA damage in germ cells induces an innate immune response that triggers systemic stress resistance. *Nature,* 501**,** 416.

EVDOKIMOVSKY, E. V., USHAKOVA, T. E., KUDRIAVTCEV, A. A. & GAZIEV, A. I. 2011. Alteration of mtDNA copy number, mitochondrial gene expression and extracellular DNA content in mice after irradiation at lethal dose. *Radiation and Environmental Biophysics,* 50**,** 181-188.

FRANÇA, M., PANEK, A. & ELEUTHERIO, E. 2007. Oxidative stress and its effects during dehydration. *Comparative Biochemistry Physiology Part A: Molecular Integrative Physiology,* 146**,** 621-631.

FREDRICKSON, J. K., SHU-MEI, W. L., GAIDAMAKOVA, E. K., MATROSOVA, V. Y., ZHAI, M., SULLOWAY, H. M., SCHOLTEN, J. C., BROWN, M. G., BALKWILL, D. L. & DALY, M. J. 2008. Protein oxidation: key to bacterial desiccation resistance? *The ISME journal,* 2**,** 393.

GARNIER-LAPLACE, J., GERAS'KIN, S., DELLA-VEDOVA, C., BEAUGELIN-SEILLER, K., HINTON, T., REAL, A. & OUDALOVA, A. 2013. Are radiosensitivity data derived from natural field conditions consistent with data from controlled exposures? A case study of Chernobyl wildlife chronically exposed to low dose-rates. *Journal of environmental radioactivity,* 121**,** 12-21.

GARTNER, A., BOAG, P. R. & BLACKWELL, T. K. 2005. Germline survival and apoptosis. *WormBook: The Online Review of C. elegans Biology [Internet].* WormBook.

GARTNER, A., MILSTEIN, S., AHMED, S., HODGKIN, J., & HENGARTNER, M. O. 2000. A Conserved Checkpoint Pathway Mediates DNA Damage–Induced Apoptosis and Cell Cycle Arrest in C. elegans. *Molecular cell,* 5**,** 435-443.

GEMS, D. & DOONAN, R. 2008. Oxidative Stress and Aging in the NematodeCaenorhabditis elegans. *Oxidative Stress in Aging.* Springer.

GIGLIO, M.-P., HUNTER, T., BANNISTER, J. V., BANNISTER, W. H. & HUNTER, G. J. 1994. The manganese superoxide dismutase gene of Caenorhabditis elegans. *Biochemistry and molecular biology international,* 33**,** 37-40.

GILBERT, H. F. 1990. Molecular and cellular aspects of thiol–disulfide exchange. *Advances in enzymology and related areas of molecular biology,* 63**,** 69-172.

GLADYSHEV, E. & MESELSON, M. 2008a. Extreme resistance of bdelloid rotifers to ionizing radiation. *Proceedings of the National Academy of Sciences,* 105**,** 5139.

GLADYSHEV, E. & MESELSON, M. 2008b. Extreme resistance of bdelloid rotifers to ionizing radiation. *Proceedings of the National Academy of Sciences,* 105**,** 5139-5144.

GOMES, A., FERNANDES, E. & LIMA, J. L. 2005. Fluorescence probes used for detection of reactive oxygen species. *Journal of biochemical and biophysical methods,* 65**,** 45-80.

GOMES, T., SONG, Y., BREDE, D. A., XIE, L., GUTZKOW, K. B., SALBU, B. & TOLLEFSEN, K. E. 2018. Gamma radiation induces dose-dependent oxidative stress and transcriptional alterations in the freshwater crustacean Daphnia magna. *Science of The Total Environment,* 628**,** 206-216.

GOMES, T., XIE, L., BREDE, D., LIND, O.-C., SOLHAUG, K. A., SALBU, B. & TOLLEFSEN, K. E. 2017. Sensitivity of the green algae Chlamydomonas reinhardtii to gamma radiation: photosynthetic performance and ROS formation. *Aquatic toxicology,* 183**,** 1-10.

GUMIENNY, T. L., LAMBIE, E., HARTWIEG, E., HORVITZ, H. R. & HENGARTNER, M. O. 1999. Genetic control of programmed cell death in the Caenorhabditis elegans hermaphrodite germline. *Development,* 126**,** 1011-1022.

GUO, X., SUN, J., BIAN, P., CHEN, L., ZHAN, F., WANG, J., XU, A., WANG, Y., HEI, T. K. & WU, L. 2013. Radiation-induced bystander signaling from somatic cells to germ cells in Caenorhabditis elegans. *Radiat Res,* 180**,** 268-75.

GUTSCHER, M., PAULEAU, A.-L., MARTY, L., BRACH, T., WABNITZ, G. H., SAMSTAG, Y., MEYER, A. J. & DICK, T. P. 2008. Real-time imaging of the intracellular glutathione redox potential. *Nature Methods,* 5**,** 553.

HAINES, G. A., HENDRY, J. H., DANIEL, C. P. & MORRIS, I. D. 2001. Increased levels of comet-detected spermatozoa DNA damage following in vivo isotopic-or X-irradiation of spermatogonia. *Mutation Research/Genetic Toxicology Environmental Mutagenesis,* 495**,** 21-32.

HALL, E. J. & GIACCIA, A. J. 2006. *Radiobiology for the Radiologist*, Lippincott Williams & Wilkins.

HANSEN, E., LIND, O., OUGHTON, D. & SALBU, B. 2019. A framework for exposure characterization and gamma dosimetry at the NMBU FIGARO irradiation facility. *International journal of radiation biology,* 95**,** 82-89.

HARRISON, F. & ANDERSON, S. 1996. Taxonomic and developmental aspects of radiosensitivity. Lawrence Livermore National Lab., CA (United States).

HARTMAN, P. S., & HERMAN, R. K. 1982. Radiation-sensitive mutants of Caenorhabditis elegans. *Genetics,* 102**,** 159-178.

HARTMAN, P. S., SIMPSON, V. J., JOHNSON, T. & MITCHELL, D. 1988. Radiation sensitivity and DNA repair in Caenorhabditis elegans strains with different mean life spans. *Mutation Research Letters,* 208**,** 77-82.

HASAN, M., KHALEQUZZAMAN, M. & RAHMAN KHAN, A. J. E. E. E. A. 1989. Development of Tribolium anaphe irradiated as larvae of various ages with gamma rays. 53**,** 92-94.

HASHIMOTO, T., HORIKAWA, D. D., SAITO, Y., KUWAHARA, H., KOZUKA-HATA, H., SHIN-I, T., MINAKUCHI, Y., OHISHI, K., MOTOYAMA, A., AIZU, T., ENOMOTO, A., KONDO, K., TANAKA, S., HARA, Y., KOSHIKAWA, S., SAGARA, H., MIURA, T., YOKOBORI, S.-I., MIYAGAWA, K., SUZUKI, Y., KUBO, T., OYAMA, M., KOHARA, Y., FUJIYAMA, A., ARAKAWA, K., KATAYAMA, T., TOYODA, A. & KUNIEDA, T. 2016. Extremotolerant tardigrade genome and improved radiotolerance of human cultured cells by tardigrade-unique protein. *Nature Communications,* 7**,** 12808.

HERMAN, R. K., ALBERTSON, D. G., & BRENNER, S. 1976. Chromosome rearrangements in Caenorhabditis elegans. *Genetics,* 83**,** 91-105.

HERTEL-AAS, T., BRUNBORG, G., JAWORSKA, A., SALBU, B. & OUGHTON, D. H. 2011a. Effects of different gamma exposure regimes on reproduction in the earthworm Eisenia fetida (Oligochaeta). *Science of The Total Environment,* 412-413**,** 138-147.

HERTEL-AAS, T., OUGHTON, D. H., JAWORSKA, A., BJERKE, H., SALBU, B. & BRUNBORG, G. 2007. Effects of chronic gamma irradiation on reproduction in the earthworm Eisenia fetida (Oligochaeta). *Radiation research,* 168**,** 515-526.

HERTEL-AAS, T., OUGHTON, D. H., JAWORSKA, A. & BRUNBORG, G. 2011b. Induction and repair of DNA strand breaks and oxidised bases in somatic and spermatogenic cells from the earthworm Eisenia fetida after exposure to ionising radiation. *Mutagenesis,* 26**,** 783-793.

HINDSON, B. J., NESS, K. D., MASQUELIER, D. A., BELGRADER, P., HEREDIA, N. J., MAKAREWICZ, A. J., BRIGHT, I. J., LUCERO, M. Y., HIDDESSEN, A. L. & LEGLER, T. C. 2011. High-throughput droplet digital PCR system for absolute quantitation of DNA copy number. *Analytical chemistry,* 83**,** 8604-8610.

HINTON, T. G., GARNIER-LAPLACE, J., VANDENHOVE, H., DOWDALL, M., ADAM-GUILLERMIN, C., ALONZO, F., BARNETT, C., BEAUGELIN-SEILLER, K., BERESFORD, N. A., BRADSHAW, C., BROWN, J., EYROLLE, F., FEVRIER, L., GARIEL, J. C., GILBIN, R., HERTEL-AAS, T., HOREMANS, N., HOWARD, B. J., IKÄHEIMONEN, T., MORA, J. C., OUGHTON, D., REAL, A., SALBU, B., SIMON-CORNU, M., STEINER,

M., SWEECK, L. & VIVES I BATLLE, J. 2013. An invitation to contribute to a strategic research agenda in radioecology. *Journal of Environmental Radioactivity,* 115**,** 73-82.

HOFMANN, E. R., MILSTEIN, S., BOULTON, S. J., YE, M., HOFMANN, J. J., STERGIOU, L., GARTNER, A., VIDAL, M. & HENGARTNER, M. O. 2002. Caenorhabditis elegans HUS-1 Is a DNA Damage Checkpoint Protein Required for Genome Stability and EGL-1-Mediated Apoptosis. *Current Biology,* 12**,** 1908-1918.

HOLWAY, A. H., KIM, S.-H., LA VOLPE, A. & MICHAEL, W. M. 2006. Checkpoint silencing during the DNA damage response in Caenorhabditis elegans embryos. *J Cell Biol,* 172**,** 999-1008.

HOREMANS, N., SPURGEON, D. J., LECOMTE-PRADINES, C., SAENEN, E., BRADSHAW, C., OUGHTON, D., RASNACA, I., KAMSTRA, J. H. & ADAM-GUILLERMIN, C. 2019. Current evidence for a role of epigenetic mechanisms in response to ionizing radiation in an ecotoxicological context. *Environmental Pollution,* 251**,** 469-483.

HORIKAWA, D. D., SAKASHITA, T., KATAGIRI, C., WATANABE, M., KIKAWADA, T., NAKAHARA, Y., HAMADA, N., WADA, S., FUNAYAMA, T., HIGASHI, S., KOBAYASHI, Y., OKUDA, T. & KUWABARA, M. 2006. Radiation tolerance in the tardigrade Milnesium tardigradum. *International Journal of Radiation Biology,* 82**,** 843-848.

HUREM, S., GOMES, T., BREDE, D. A., LINDBO HANSEN, E., MUTOLOKI, S., FERNANDEZ, C., MOTHERSILL, C., SALBU, B., KASSAYE, Y. A., OLSEN, A.-K., OUGHTON, D., ALESTRÖM, P. & LYCHE, J. L. 2017a. Parental gamma irradiation induces reprotoxic effects accompanied by genomic instability in zebrafish (Danio rerio) embryos. *Environmental Research,* 159**,** 564-578.

HUREM, S., MARTÍN, L. M., BREDE, D. A., SKJERVE, E., NOURIZADEH-LILLABADI, R., LIND, O. C., CHRISTENSEN, T., BERG, V., TEIEN, H.-C., SALBU, B., OUGHTON, D. H., ALESTRÖM, P. & LYCHE, J. L. 2017b. Dose-dependent effects of gamma radiation on the early zebrafish development and gene expression. *PLOS ONE,* 12**,** e0179259.

HUTCHINSON, F. 1966. The molecular basis for radiation effects on cells. *Cancer research,* 26**,** 2045-2052.

INTERNATIONAL, O., FOR, STANDARDIZATION 2010. Water quality – Determination of the Toxic effect of Sediment and Soil Samples on Growth, Fertility and Reproduction of *Caenorhabditis elegans (Nematoda*). *ISO 10872:2010*.

JARAMILLO-LAMBERT, A., HARIGAYA, Y., VITT, J., VILLENEUVE, A. & ENGEBRECHT, J. 2010. Meiotic errors activate checkpoints that improve gamete quality without triggering apoptosis in male germ cells. *Current Biology,* 20**,** 2078-2089.

JOHNSON, T. E. & HARTMAN, P. S. 1988. Radiation Effects on Life Span in Caenorhabditis Elegans. *Journal of Gerontology,* 43**,** B137-B141.

JOHNSON, T. E., MITCHELL, D. H., KLINE, S., KEMAL, R. & FOY, J. 1984. Arresting development arrests aging in the nematode Caenorhabditis elegans. *Mechanisms of ageing development,* 28**,** 23-40.

JOHNSTON, A. D. & EBERT, P. R. 2012. The Redox System in C. elegans, a Phylogenetic Approach. *Journal of Toxicology,* 2012**,** 20.

KALOGEROPOULOS, N., CHRISTOFOROU, C., GREEN, A. J., GILL, S. & ASHCROFT, N. R. 2004. chk-1 is an essential gene and is required for an SM checkpoint during early embryogenesis. *Cell cycle,* 3**,** 1194-1198.

KAM, W., LAKE, V., BANOS, C., DAVIES, J. & BANATI, R. J. I. J. O. M. S. 2013. Apparent polyploidization after gamma irradiation: pitfalls in the use of quantitative polymerase chain reaction (qPCR) for the estimation of mitochondrial and nuclear DNA gene copy numbers. 14**,** 11544-11559.

KAM, W. W.-Y. & BANATI, R. B. 2013. Effects of ionizing radiation on mitochondria. *Free Radical Biology Medicine,* 65**,** 607-619.

KAMSTRA, J. H., HUREM, S., MARTIN, L. M., LINDEMAN, L. C., LEGLER, J., OUGHTON, D., SALBU, B., BREDE, D. A., LYCHE, J. L. & ALESTRÖM, P. 2018. Ionizing radiation induces transgenerational effects of DNA methylation in zebrafish. *Scientific Reports,* 8**,** 15373.

KATZ, D. J., EDWARDS, T. M., REINKE, V. & KELLY, W. G. 2009. A C. elegans LSD1 demethylase contributes to germline immortality by reprogramming epigenetic memory. *Cell,* 137**,** 308-320.

KERMI, C., AZE, A. & MAIORANO, D. 2019. Preserving Genome Integrity During the Early Embryonic DNA Replication Cycles. *Genes,* 10**,** 398.

KERR, S. C., RUPPERSBURG, C. C., FRANCIS, J. W. & KATZ, D. J. 2014. SPR-5 and MET-2 function cooperatively to reestablish an epigenetic ground state during passage through the germ line. *Proceedings of the National Academy of Sciences of the United States of America,* 111**,** 9509-9514.

KIM, G. J., FISKUM, G. M. & MORGAN, W. F. 2006. A role for mitochondrial dysfunction in perpetuating radiation-induced genomic instability. *Cancer research,* 66**,** 10377-10383.

KIMBLE, J. & HIRSH, D. 1979. The postembryonic cell lineages of the hermaphrodite and male gonads in Caenorhabditis elegans. *Developmental biology,* 70**,** 396-417.

KRISKO, A., LEROY, M., RADMAN, M. & MESELSON, M. 2012a. Extreme anti-oxidant protection against ionizing radiation in bdelloid rotifers. *Proc Natl Acad Sci U S A,* 109**,** 2354-7.

KRISKO, A., LEROY, M., RADMAN, M. & MESELSON, M. 2012b. Extreme anti-oxidant protection against ionizing radiation in bdelloid rotifers. *Proceedings of the National Academy of Sciences,* 109**,** 2354.

KRISKO, A. & RADMAN, M. 2010. Protein damage and death by radiation in *Escherichia coli* and *Deinococcus radiodurans*. *Proceedings of the National Academy of Sciences,* 107**,** 14373-14377.

KRIVOLUTZKII, D. & POKARZHEVSKII, A. 1992. Effects of radioactive fallout on soil animal populations in the 30 km zone of the Chernobyl atomic power station. *Science of the total environment,* 112**,** 69-77.

KUWAHARA, Y., SHIMADA, A., MITANI, H. & SHIMA, A. 2002. A critical stage in spermatogenesis for radiation-induced cell death in the medaka fish, Oryzias latipes. *Radiation research,* 157**,** 386-392.

L'HERNAULT, S. W. 2006. Spermatogenesis. *WormBook: The Online Review of C. elegans Biology [Internet].* WormBook.

LANS, H. & VERMEULEN, W. 2015. Tissue specific response to DNA damage: C. elegans as role model. *DNA Repair (Amst),* 32**,** 141-8.

LEACH, J. K., VAN TUYLE, G., LIN, P.-S., SCHMIDT-ULLRICH, R. & MIKKELSEN, R. B. 2001. Ionizing radiation-induced, mitochondria-dependent generation of reactive oxygen/nitrogen. *Cancer research,* 61**,** 3894-3901.

LECOMTE-PRADINES, C., BONZOM, J. M., DELLA-VEDOVA, C., BEAUGELIN-SEILLER, K., VILLENAVE, C., GASCHAK, S., COPPIN, F., DUBOURG, N., MAKSIMENKO, A., ADAM-GUILLERMIN, C. & GARNIER-LAPLACE, J. 2014. Soil nematode assemblages as bioindicators of radiation impact in the Chernobyl Exclusion Zone. *Science of The Total Environment,* 490**,** 161-170.

LECOMTE-PRADINES, C., HERTEL-AAS, T., COUTRIS, C., GILBIN, R., OUGHTON, D. & ALONZO, F. 2017. A dynamic energy-based model to analyze sublethal effects of chronic gamma irradiation in the nematode Caenorhabditis elegans. *J Toxicol Environ Health A,* 80**,** 830-844.

LEIERS, B., KAMPKÖTTER, A., GREVELDING, C. G., LINK, C. D., JOHNSON, T. E. & HENKLE-DÜHRSEN, K. 2003. A stress-responsive glutathione S-transferase confers resistance to oxidative stress in Caenorhabditis elegans. *Free Radical Biology and Medicine,* 34**,** 1405-1415.

LEPRINCE, O., ATHERTON, N. M., DELTOUR, R. & HENDRY, G. A. 1994. The involvement of respiration in free radical processes during loss of desiccation tolerance in germinating Zea mays L.(an electron paramagnetic resonance study). 104**,** 1333-1339.

LETTRE, G. & HENGARTNER, M. O. 2006. Developmental cell biology: developmental apoptosis in C. elegans: a complex CEDnario. *Nature Reviews Molecular Cell Biology,* 7**,** 97.

LEWIS, J. A. & FLEMING, J. T. 1995. Chapter 1 Basic Culture Methods. *In:* EPSTEIN, H. F. & SHAKES, D. C. (eds.) *Methods in Cell Biology.* Academic Press.

LI, T. & CHEN, Z. J. 2018. The cGAS–cGAMP–STING pathway connects DNA damage to inflammation, senescence, and cancer. *The Journal of Experimental Medicine,* 215**,** 1287.

LIND, O. C., OUGHTON, D. H. & SALBU, B. 2019. The NMBU FIGARO low dose irradiation facility. *International journal of radiation biology,* 95**,** 76-81.

LIU, G., GONG, P., ZHAO, H., WANG, Z., GONG, S. & CAI, L. 2006. Effect of low-level radiation on the death of male germ cells. *Radiation research,* 165**,** 379-389.

LOMAX, M. E., FOLKES, L. K. & O'NEILL, P. 2013. Biological Consequences of Radiation-induced DNA Damage: Relevance to Radiotherapy. *Clinical Oncology,* 25**,** 578-585.

LU, N., YU, X., HE, X. & ZHOU, Z. 2009. Detecting apoptotic cells and monitoring their clearance in the nematode Caenorhabditis elegans. *Methods Mol Biol,* 559**,** 357-70.

MALAKHOVA, L., BEZLEPKIN, V. G., ANTIPOVA, V., USHAKOVA, T., FOMENKO, L., SIROTA, N. & GAZIEV, A. I. 2005. The increase in mitochondrial DNA copy number in the tissues of γ-irradiated mice. *Cellular Molecular Biology Letters,* 10**,** 721.

MALIK, A. N. & CZAJKA, A. 2013. Is mitochondrial DNA content a potential biomarker of mitochondrial dysfunction? *Mitochondrion,* 13**,** 481-492.

MANDAVILLI, B. S., SANTOS, J. H. & VAN HOUTEN, B. 2002. Mitochondrial DNA repair and aging. *Mutation Research/Fundamental and Molecular Mechanisms of Mutagenesis,* 509**,** 127-151.

MEGALOU, E. V. & TAVERNARAKIS, N. 2009. Autophagy in Caenorhabditis elegans. *Biochimica et Biophysica Acta (BBA) - Molecular Cell Research,* 1793**,** 1444-1451.

MERRIFIELD, M. & KOVALCHUK, O. 2013. Epigenetics in radiation biology: a new research frontier. *Frontiers in genetics,* 4**,** 40.

MEYER, A. J. & DICK, T. P. 2010. Fluorescent protein-based redox probes. *Antioxidants & redox signaling,* 13**,** 621-650.

MILLER, M. A., NGUYEN, V. Q., LEE, M.-H., KOSINSKI, M., SCHEDL, T., CAPRIOLI, R. M. & GREENSTEIN, D. 2001. A sperm cytoskeletal protein that signals oocyte meiotic maturation and ovulation. *Science,* 291**,** 2144-2147.

MINAFRA, L. & BRAVATÀ, V. 2014. Cell and molecular response to IORT treatment. *Translational Cancer Research,* 3**,** 32-47.

MONTGOMERY, D. C., PECK, E. A. & VINING, G. G. 2012. *Introduction to linear regression analysis*, John Wiley & Sons.

MORRAN, L. T., CAPPY, B. J., ANDERSON, J. L. & PHILLIPS, P. C. 2009. Sexual partners for the stressed: facultative outcrossing in the self-fertilizing nematode Caenorhabditis elegans. *Evolution: International Journal of Organic Evolution,* 63**,** 1473-1482.

NELSON, G. A., JONES, T. A., CHESNUT, A. & SMITH, A. L. 2002. Radiation-induced Gene Expression in the Nematode Caenorhabditis elegans. *Journal of Radiation Research,* 43**,** S199-S203.

NEWMAN, M. C. 2009. *Fundamentals of ecotoxicology*, CRC press.

NG, L. F., NG, L. T., VAN BREUGEL, M., HALLIWELL, B. & GRUBER, J. 2019. Mitochondrial DNA damage does not determine *C. elegans* lifespan. *Frontiers in Genetics,* 10.

NIKJOO, H., O'NEILL, P., TERRISSOL, M. & GOODHEAD, D. T. 1999. Quantitative modelling of DNA damage using Monte Carlo track structure method. *Radiation and Environmental Biophysics,* 38**,** 31-38.

NOTTKE, A. C., BEESE-SIMS, S. E., PANTALENA, L. F., REINKE, V., SHI, Y. & COLAIÁCOVO, M. P. 2011. SPR-5 is a histone H3K4 demethylase with a role in meiotic double-strand break repair. *Proceedings of the National Academy of Sciences,* 108**,** 12805-12810.

NUGENT, S., MOTHERSILL, C. E., SEYMOUR, C., MCCLEAN, B., LYNG, F. M. & MURPHY, J. E. J. 2010. Altered mitochondrial function and genome frequency post exposure to γ-radiation and bystander factors. *International Journal of Radiation Biology,* 86**,** 829-841.

OKUNIEFF, P., SWARTS, S., KENG, P., SUN, W., WANG, W., KIM, J., YANG, S., ZHANG, H., LIU, C. & WILLIAMS, J. P. 2008. Antioxidants reduce consequences of radiation exposure. *Oxygen Transport to Tissue XXIX.* Springer.

ORTIZ, M. A., NOBLE, D., SOROKIN, E. P. & KIMBLE, J. 2014. A new dataset of spermatogenic vs. oogenic transcriptomes in the nematode Caenorhabditis elegans. *Genes, Genomes, Genetics,* 4**,** 1765-1772.

PARASHAR, V., FRANKEL, S., LURIE, A. G. & ROGINA, B. 2008. The effects of age on radiation resistance and oxidative stress in adult Drosophila melanogaster. *Radiation research,* 169**,** 707-711.

PARISOT, F., BOURDINEAUD, J.-P., PLAIRE, D., ADAM-GUILLERMIN, C. & ALONZO, F. 2015. DNA alterations and effects on growth and reproduction in Daphnia magna during chronic exposure to gamma radiation over three successive generations. *Aquatic Toxicology,* 163**,** 27-36.

PENTREATH, R. J., LOCHARD, J., LARSSON, C. M., COOL, D. A., STRAND, P., SIMMONDS, J., COPPLESTONE, D., OUGHTON, D. & LAZO, E. 2014. ICRP Publication 124: Protection of the Environment under Different Exposure Situations. *Annals of the ICRP,* 43**,** 1-58.

PEREIRA, S., BOURRACHOT, S., CAVALIE, I., PLAIRE, D., DUTILLEUL, M., GILBIN, R. & ADAM-GUILLERMIN, C. 2011. Genotoxicity of acute and chronic gamma-irradiation on zebrafish cells and consequences for embryo development. *Environmental toxicology and chemistry,* 30**,** 2831-2837.

PORTA-DE-LA-RIVA, M., FONTRODONA, L., VILLANUEVA, A. & CERON, J. 2012. Basic Caenorhabditis elegans methods: synchronization and observation. *J Vis Exp***,** e4019.

REINKE, V., SMITH, H. E., NANCE, J., WANG, J., VAN DOREN, C., BEGLEY, R., JONES, S. J. M., DAVIS, E. B., SCHERER, S., WARD, S. & KIM, S. K. 2000. A Global Profile of Germline Gene Expression in C. elegans. *Molecular Cell,* 6**,** 605-616.

REISZ, J. A., BANSAL, N., QIAN, J., ZHAO, W. & FURDUI, C. M. 2014. Effects of ionizing radiation on biological molecules—mechanisms of damage and emerging methods of detection. *Antioxidants & redox signaling,* 21**,** 260-292.

RINALDO, C., BAZZICALUPO, P., EDERLE, S., HILLIARD, M. & LA VOLPE, A. 2002. Roles for Caenorhabditis elegans rad-51 in Meiosis and in Resistance to Ionizing Radiation During Development. *Genetics,* 160**,** 471.

ROSENBLUTH, R. E., CUDDEFORD, C. & BAILLIE, D. L. 1985. Mutagenesis in Caenorhabditis elegans. II. A spectrum of mutational events induced with 1500 r of γ-radiation. *Genetics,* 109**,** 493-511.

SADLER, P. L. & SHAKES, D. C. 2000. Anucleate Caenorhabditis elegans sperm can crawl, fertilize oocytes and direct anterior-posterior polarization of the 1-cell embryo. *Development,* 127**,** 355-366.

SAKASHITA, T., TAKANAMI, T., YANASE, S., HAMADA, N., SUZUKI, M., KIMURA, T., KOBAYASHI, Y., ISHII, N. & HIGASHITANI, A. 2010. Radiation Biology of Caenorhabditis elegans: Germ Cell Response, Aging and Behavior. *Journal of Radiation Research,* 51**,** 107-121.

SALBU, B. 2008. Radioactive particles released from different nuclear sources: With focus on nuclear weapons tests. *Nuclear Risks in Central Asia.* Springer.

SALBU, B., KREKLING, T., OUGHTON, D., ØSTBY, G., KASHPAROV, V., BRAND, T. & DAY, J. 1994. Hot particles in accidental releases from Chernobyl and Windscale nuclear installations. *Analyst,* 119**,** 125-130.

SALBU, B. J. R. P. D. 2000. Source-related characteristics of radioactive particles: a review. 92**,** 49-54.

SARSOUR, E. H., KUMAR, M. G., CHAUDHURI, L., KALEN, A. L. & GOSWAMI, P. C. 2009. Redox control of the cell cycle in health and disease. *Antioxidants redox signaling,* 11**,** 2985-3011.

SAWYER, D. E. & VAN HOUTEN, B. 1999. Repair of DNA damage in mitochondria. *Mutation Research/DNA Repair,* 434**,** 161-176.

SCHAFER, F. Q. & BUETTNER, G. R. 2001. Redox environment of the cell as viewed through the redox state of the glutathione disulfide/glutathione couple. *Free Radical Biology and Medicine,* 30**,** 1191-1212.

SCHULZE-OSTHOFF, K., BAUER, M., VOGT, M., WESSELBORG, S. & BAEUERLE, P. A. 1997. Reactive oxygen intermediates as primary signals and second messengers in the activation of transcription factors. *Oxidative stress and signal transduction.* Springer.

SCHUMACHER, B., HOFMANN, K., BOULTON, S., & GARTNER, A. 2001. The C. elegans homolog of the p53 tumor suppressor is required for DNA damage-induced apoptosis. *Current biology,* 11**,** 1722-1727.

SCHWARTZ, J. L., JORDAN, R., SUN, J., MA, H. & HSIE, A. W. 2000. Dose-dependent changes in the spectrum of mutations induced by ionizing radiation. *Radiation Research,* 153**,** 312-317.

SHIN, H., LEE, H., FEJES, A. P., BAILLIE, D. L., KOO, H.-S. & JONES, S. J. 2011. Gene expression profiling of oxidative stress response of C. elegans aging defective AMPK mutants using massively parallel transcriptome sequencing. *BMC research notes,* 4**,** 34.

SIDOTI-DE FRAISSE, C., RINCHEVAL, V., RISLER, Y., MIGNOTTE, B. & VAYSSIÈRE, J.-L. 1998. TNF-α activates at least two apoptotic signaling cascades. *Oncogene,* 17**,** 1639.

SINGSON, A. 2001. Every sperm is sacred: fertilization in Caenorhabditis elegans. *Developmental biology,* 230**,** 101-109.

SOBKOWIAK, R. & LESICKI, A. 2009. Genotoxicity of nicotine in cell culture of Caenorhabditis elegans evaluated by the comet assay. *Drug and Chemical Toxicology,* 32**,** 252-257.

SOWMITHRA, K., SHETTY, N. J., HARINI, B. P., JHA, S. K. & CHAUBEY, R. C. 2015. Effects of acute gamma radiation on the reproductive ability of the earthworm Eisenia fetida. *Journal of Environmental Radioactivity,* 140**,** 11-15.

SPITZ, D. R., AZZAM, E. I., LI, J. J. & GIUS, D. 2004. Metabolic oxidation/reduction reactions and cellular responses to ionizing radiation: a unifying concept in stress response biology. *Cancer and Metastasis Reviews,* 23**,** 311-322.

STIERNAGLE, T. 2006. Maintenance of C. elegans. *WormBook***,** 1-11.

STOHL, A., SEIBERT, P., WOTAWA, G., ARNOLD, D., BURKHART, J. F., ECKHARDT, S., TAPIA, C., VARGAS, A., YASUNARI, T. J. J. A. C. & PHYSICS 2012. Xenon-133 and caesium-137 releases into the atmosphere from the Fukushima Dai-ichi nuclear power plant: determination of the source term, atmospheric dispersion, and deposition. 12**,** 2313-2343.

SUGIMOTO, T., DAZAI, K., SAKASHITA, T., FUNAYAMA, T., WADA, S., HAMADA, N., KAKIZAKI, T., KOBAYASHI, Y. & HIGASHITANI, A. 2006. Cell cycle arrest and apoptosis in Caenorhabditis elegans germline cells following heavy-ion microbeam irradiation. *Int J Radiat Biol,* 82**,** 31-8.

SULSTON, J. E. & HORVITZ, H. R. 1977. Post-embryonic cell lineages of the nematode, Caenorhabditis elegans. *Developmental biology,* 56**,** 110-156.

SUTHERLAND, B. M., BENNETT, P. V., SIDORKINA, O. & LAVAL, J. 2000. Clustered DNA damages induced in isolated DNA and in human cells by low doses of ionizing radiation. *Proceedings of the National Academy of Sciences,* 97**,** 103-108.

SVOBODA, P. & HARMS-RINGDAHL, M. 2005. Influence of chromatin structure and radical scavengers on yields of radiation-induced 8-oxo-dG and DNA strand breaks in cellular model systems. *Radiation research,* 164**,** 303-311.

SWENBERG, J. A., LU, K., MOELLER, B. C., GAO, L., UPTON, P. B., NAKAMURA, J. & STARR, T. B. 2010. Endogenous versus Exogenous DNA Adducts: Their Role in Carcinogenesis, Epidemiology, and Risk Assessment. *Toxicological Sciences,* 120**,** S130-S145.

SYKES, P., NEOH, S., BRISCO, M., HUGHES, E., CONDON, J. & MORLEY, A. 1992. Quantitation of targets for PCR by use of limiting dilution. *Biotechniques,* 13**,** 444-449.

SZUMIEL, I. 2015. Ionizing radiation-induced oxidative stress, epigenetic changes and genomic instability: the pivotal role of mitochondria. *Int J Radiat Biol,* 91**,** 1-12.

TAKANAMI, T., MORI, A., TAKAHASHI, H. & HIGASHITANI, A. 2000. Hyper-resistance of meiotic cells to radiation due to a strong expression of a single recA-like gene in Caenorhabditis elegans. *Nucleic Acids Research,* 28**,** 4232-4236.

THOMPSON, L. H. 2012. Recognition, signaling, and repair of DNA double-strand breaks produced by ionizing radiation in mammalian cells: the molecular choreography. *Mutation Research/Reviews in Mutation Research,* 751**,** 158-246.

TORGOVNICK, A., SCHIAVI, A., SHAIK, A., KASSAHUN, H., MAGLIONI, S., REA, S. L., JOHNSON, T. E., REINHARDT, H. C., HONNEN, S., SCHUMACHER, B., NILSEN, H. & VENTURA, N. 2018. BRCA1 and BARD1 mediate apoptotic resistance but not longevity upon mitochondrial stress in Caenorhabditis elegans. *EMBO reports,* 19**,** e45856.

UNSCEAR 1996. *Sources and effects of ionizing radiation: Report to the General Assembly, with Scientific Annexes*, United Nations Publications.

UNSCEAR 2000. *Sources and effects of ionizing radiation: sources*, United Nations Publications.

UNSCEAR 2006. Effects of ionizing radiation: UNSCEAR 2006 Report to the General Assembly, with scientific annexes. United Nations Publications.

UNSCEAR 2008. *Sources and Effects of Ionizing Radiation: United Nations Scientific Committee on the Effects of Atomic Radiation: UNSCEAR 2008 Report to the General Assembly, with Scientific Annexes*, United Nations.

VAN HAAFTEN, G., ROMEIJN, R., POTHOF, J., KOOLE, W., MULLENDERS, L. H. F., PASTINK, A., PLASTERK, R. H. A. & TIJSTERMAN, M. 2006. Identification of Conserved Pathways of DNA-Damage Response and Radiation Protection by Genome-Wide RNAi. *Current Biology,* 16**,** 1344-1350.

VANDENHOVE, H., VANHOUDT, N., CUYPERS, A., VAN HEES, M., WANNIJN, J., HOREMANS, N. J. P. P. & BIOCHEMISTRY 2010. Life-cycle chronic gamma exposure of Arabidopsis thaliana induces growth effects but no discernable effects on oxidative stress pathways. 48**,** 778-786.

VEAL, E. A., DAY, A. M. & MORGAN, B. A. 2007. Hydrogen peroxide sensing and signaling. *Molecular cell,* 26**,** 1-14.

VERMEZOVIC, J., STERGIOU, L., HENGARTNER, M. O. & D'ADDA DI FAGAGNA, F. 2012. Differential regulation of DNA damage response activation between somatic and germline cells in Caenorhabditis elegans. *Cell Death and Differentiation,* 19**,** 1847-1855.

WANG, J.-S., WANG, H.-J. & QIAN, H.-L. 2018. Biological effects of radiation on cancer cells. *Military Medical Research,* 5**,** 20.

WEIDHAAS, J., EISENMANN, D., HOLUB, J. & NALLUR, S. 2006. A Caenorhabditis elegans tissue model of radiation-induced reproductive cell death. *Proceedings of the National Academy of Sciences,* 103**,** 9946-9951.

WELCH, D. B. M., RICCI, C. & MESELSON, M. 2009. Bdelloid rotifers: progress in understanding the success of an evolutionary scandal. *Lost sex.* Springer.

WENDEL, C. C., FIFIELD, L. K., OUGHTON, D. H., LIND, O. C., SKIPPERUD, L., BARTNICKI, J., TIMS, S. G., HØIBRÅTEN, S. & SALBU, B. 2013. Long-range tropospheric transport of uranium and plutonium weapons fallout from Semipalatinsk nuclear test site to Norway. *Environment International,* 59**,** 92-102.

WHITE, J. G., SOUTHGATE, E., THOMSON, J. N. & BRENNER, S. 1986. The structure of the nervous system of the nematode Caenorhabditis elegans: the mind of a worm. *Phil. Trans. R. Soc. Lond,* 314**,** 1-340.

WONG-EKKABUT, J., XU, Z., TRIAMPO, W., TANG, I.-M., TIELEMAN, D. P. & MONTICELLI, L. 2007. Effect of lipid peroxidation on the properties of lipid bilayers: a molecular dynamics study. *Biophysical journal,* 93**,** 4225-4236.

XIE, L., SOLHAUG, K. A., SONG, Y., BREDE, D. A., LIND, O. C., SALBU, B. & TOLLEFSEN, K. E. 2019. Modes of action and adverse effects of gamma radiation in an aquatic macrophyte Lemna minor. *Science of The Total Environment,* 680**,** 23-34.

YAKES, F. M. & VAN HOUTEN, B. 1997. Mitochondrial DNA damage is more extensive and persists longer than nuclear DNA damage in human cells following oxidative stress. *Proceedings of the National Academy of Sciences,* 94**,** 514-519.

YANASE, S., HARTMAN, P. S., ITO, A. & ISHII, N. 1999. Oxidative stress pretreatment increases the X-radiation resistance of the nematode Caenorhabditis elegans. *Mutation Research/Fundamental and Molecular Mechanisms of Mutagenesis,* 426**,** 31-39.

YUSHKOVA, E. 2019. Effects of ionizing radiation at Drosophila melanogaster with differently active hobo transposons. *International Journal of Radiation Biology,* 95**,** 1564-1572.

ZAHRADKA, K., SLADE, D., BAILONE, A., SOMMER, S., AVERBECK, D., PETRANOVIC, M., LINDNER, A. B. & RADMAN, M. 2006. Reassembly of shattered chromosomes in Deinococcus radiodurans. *Nature,* 443**,** 569.

ZHOU, Z., HARTWIEG, E. & HORVITZ, H. R. 2001. CED-1 Is a Transmembrane Receptor that Mediates Cell Corpse Engulfment in C. elegans. *Cell,* 104**,** 43-56.

Errata

Thesis: Investigating sensitivity and tolerance to chronic gamma irradiation in the nematode *Caenorhabditis elegans*

Page number	**Paragraph**	**Line**	**Change from**	**Change to**
31	Capture Figure 4.	2	(Gartner et al. 2005)	Gartner et al. (2005)
41	Capture Figure 7.	3	(from L1 stage)	-
47	Figure 9.	8	Missing scalebar	Scalebar (250 µm)
51	2.10	1	Technique	Techniques
52	2.10	27	-	(nuclear DNA)
54	2.11	4	Lysate	Lysed
62	4.	11	Mechanism	Mechanisms

8. Scientific papers

Paper I

Science of the Total Environment 695 (2019) 133835

Contents lists available at ScienceDirect

Science of the Total Environment

journal homepage: www.elsevier.com/locate/scitotenv

Gamma radiation induces life stage-dependent reprotoxicity in *Caenorhabditis elegans via* impairment of spermatogenesis

Erica Maremonti [a,*], Dag M. Eide [a,b], Deborah H. Oughton [a], Brit Salbu [a], Fabian Grammes [c], Yetneberk A. Kassaye [a], Rémi Guédon [d], Catherine Lecomte-Pradines [d], Dag Anders Brede [a]

[a] Centre for Environmental Radioactivity (CERAD), Faculty of Environmental Sciences and Natural Resource Management (MINA), Norwegian University of Life Sciences (NMBU), 1432 Ås, Norway
[b] Norwegian Institute of Public Health, Lovisenberggata 8, 0456 Oslo, Norway
[c] Centre for Integrative Genetics (CIGENE), Faculty of Biosciences (BIOVIT), Norwegian University of Life Sciences (NMBU), 1432 Ås, Norway
[d] Institut de Radioprotection et de Sûreté Nucléaire (IRSN), PRP-ENV, SERIS, Laboratoire d'ECOtoxicologie des radionucléides (LECO), Cadarache, France

HIGHLIGHTS

- Radiosensitivity of *C. elegans* developmental stage L1-Young L4 was demonstrated following chronic gamma-irradiation.
- Reprotoxic effects were a consequence of sperm meiosis and spermatogenesis impairment.
- Genotoxicity persisted in offspring (F1) of irradiated nematodes and was associated with somatic growth impairment.
- A conceptual model for cellular and biological processes affected by gamma radiation in *C. elegans* was developed based on RNAseq analysis.

GRAPHICAL ABSTRACT

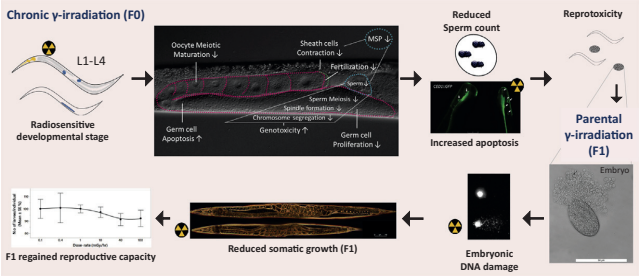

ARTICLE INFO

Article history:
Received 2 July 2019
Received in revised form 31 July 2019
Accepted 6 August 2019
Available online 09 August 2019

Editor: Henner Hollert

Keywords:
Caenorhabditis elegans
Ionizing gamma radiation
Reprotoxicity
Early life stages
Spermatogenesis

ABSTRACT

The current study investigated life stage, tissue and cell dependent sensitivity to ionizing radiation of the nematode *Caenorhabditis elegans*. Results showed that irradiation of post mitotic L4 stage larvae induced no significant effects with respect to mortality, morbidity or reproduction at either acute dose ≤6 Gy (1500 mGy·h^{-1}) or chronic exposure ≤15 Gy (≤100 mGy·h^{-1}). In contrast, chronic exposure from the embryo to the L4-young adult stage caused a dose and dose-rate dependent reprotoxicity with 43% reduction in total brood size at 6.7 Gy (108 mGy·h^{-1}). Systematic irradiation of the different developmental stages showed that the most sensitive life stage was L1 to young L4. Exposure during these stages was associated with dose-rate dependent genotoxic effects, resulting in a 1.8 to 2 fold increase in germ cell apoptosis in larvae subjected to 40 or 100 mGy·h^{-1}, respectively. This was accompanied by a dose-rate dependent reduction in the number of spermatids, which was positively correlated to the reprotoxic effect (0.99, PCC). RNAseq analysis of nematodes irradiated from L1 to L4 stage revealed a significant enrichment of differentially expressed genes related to both male and hermaphrodite reproductive processes. Gene network analysis revealed effects related to down-regulation of genes required for spindle formation and sperm meiosis/maturation, including *smz-1*, *smz-2* and *htas-1*. Furthermore, the expression of a subset of 28 *set-17* regulated Major Sperm Proteins (MSP) required for spermatid production was correlated (R^2 0.80) to the reduction in reproduction and the number of spermatids. Collectively these observations corroborate the impairment of spermatogenesis as the major cause of gamma radiation induced life-stage dependent reprotoxic effect.

* Corresponding author.
E-mail address: erica.maremonti@nmbu.no (E. Maremonti).

https://doi.org/10.1016/j.scitotenv.2019.133835

Furthermore, the progeny of irradiated nematodes showed significant embryonal DNA damage that was associated with persistent effect on somatic growth. Unexpectedly, these nematodes maintained much of their reproductive capacity in spite of the reduced growth.

1. Introduction

At the cellular level, ionizing radiation is known to inflict damage either indirectly *via* formation of free radicals or by direct interaction with essential molecules including proteins, lipids, RNA and DNA (Reisz et al., 2014), resulting in a complex mixture of adverse effects. While established genotoxic mechanisms include a combination of DSB, SSB (double strand break, single strand break) and oxidative lesions to DNA (Lomax et al., 2013), the adverse effects at an organism level can differ between individual species (Bréchignac et al., 2012; Garnier-Laplace et al., 2013; UNSCEAR, 2006). The biological response to ionizing radiation may also differ between chronic and acute exposure, both in the quality and intensity of effects (Kovalchuk et al., 2000; Pereira et al., 2011; Schwartz et al., 2000; Dubois et al., 2018). Chronic exposure is defined as an exposure of at least 10% of the duration of a species lifespan, and could consequently cover the entire developmental phase of an organism. In this sense, chronic exposure to low doses of ionizing radiation has the potential to produce long-term and hereditary effects. For any species, an assessment of the impacts of chronic radiation on survival, growth, developmental, reproductive and hereditary effects is essential to predict the consequences for a population's sustainability (Adam-Guillermin et al., 2018). Furthermore, certain life stages, tissues or cell types may inherently be more vulnerable to the effects of ionizing radiation, this influencing species radiosensitivity. Reproduction is known to be one of the most radiosensitive biological functions even in tolerant species, as well as being ecologically most relevant (UNSCEAR, 1996). Exposure to chronic ionizing radiation of invertebrates have demonstrated that doses corresponding to <10% of the lethal dose were harmful to reproductive performance, and that the negative effects persisted over multiple generations (Parisot et al., 2015; Hertel-Aas et al., 2011).

The nematode *Caenorhabditis elegans* tolerates acute doses of ionizing radiation >1 kGy without mortality (Johnson and Hartman et al., 1988). This tolerance has been linked to the ability of *C. elegans* to maintain genomic stability following radiation-induced DNA damage by activating checkpoints that induce cell-cycle arrest or apoptosis (Gartner et al., 2000). The majority of studies have been performed using acute high dose X-ray, proton beam or gamma irradiation of post mitotic stage young adult larvae (Gartner et al., 2000; van Haaften et al., 2006; Krisko et al., 2012; Guo et al., 2013; Min et al., 2017). However, in the last decade, more studies have focused on sub-lethal effects on multiple generations as well as on modelling approaches. These have shown that reproduction is a sensitive phenotypical change in nematodes, but there is still little mechanistic understanding of the factors influencing differences between chronic and acute exposures (Buisset-Goussen et al., 2014; Lecomte-Pradines et al., 2017).

The current study utilizes *C. elegans* to compare the effects of acute *versus* chronic gamma irradiation. This includes a systematic investigation of life stage, tissue and cell dependent radiosensitivity during the *C. elegans* development. A combined RNA-sequencing and phenotypic analysis was performed with the aim to elucidate the processes leading to reproduction impairment.

2. Materials and methods

2.1. C. elegans strains and culturing

The N2 Bristol strain was obtained from *Caenorhabditis* Genetic Centre, Minneapolis, MN and used in this study as the wild-type *C. elegans* background for all the irradiation experiments, with the exception of germ cell apoptosis assessment. The GFP (green fluorescent protein) reporter strain bcls39 [lim-7p::ced-1::GFP + lin-15(+)] was employed to quantify engulfment corpses of apoptotic germ cells as described by Zhou et al. (2001).

Before performing the experiments, worms were maintained for two months at 20 °C in swirling liquid cultures under dark conditions (Brenner, 1974), in order to obtain a healthy stock population. Synchronous populations of nematodes were obtained by alkaline hypochlorite treatment as described by Stiernagle (2006).

2.2. Nematode irradiation and dosimetry

Gamma radiation exposures were conducted at the FIGARO experimental facility at the Norwegian University of Life Sciences (NMBU, Ås, Norway) (Lind et al., 2019). For every experiment performed in this study (Fig. 1), synchronous cohorts of embryos or L1 nematodes were placed on NGM plates (Ø 3 or 6 cm) (1.7% agar, 2.5 mg·mL^{-1} peptone, 25 mM NaCl, 50 mM KH_2PO_4 pH 6.0, 5 μg·mL^{-1} cholesterol, 1 mM $CaCl_2$, 1 mM $MgSO_4$) with fresh *Escherichia coli* OP50 as a food source (cultured overnight at 37 °C in L-Broth medium, Lewis and Fleming (1995)). Experiments were conducted at 20 °C in the dark. For each experiment, three control NGM plates were placed behind lead shielding, and three plates per exposure position were placed at distances equivalent to dose rates from 0.4 to 1490 mGy·h^{-1} (Supporting material S.M. 1, Table S.1).

Field dosimetry (air kerma rates measured with an ionization chamber) was traceable to the Norwegian Secondary Standard Dosimetry Laboratory (Bjerke and Hetland, 2014). Air kerma rates were measured using an Optically Stimulated Luminescence (OSL) based nanoDots dosimetry (Landauer) or Radio Photo Luminescent dosimeters (RPL, GD-301 type, Chiyoda Technol Corporation, Japan) by positioning the dosimeters at the front and back of the plates. Dose rates to water were calculated according to Hansen et al. (2019) and used as a proxy for dose rates to the nematodes (S.M. 1, Table S.1).

2.3. Comparing effects on reproduction by acute and chronic exposure to gamma radiation

To assess the effects of acute irradiation on reproduction, synchronous L4 nematodes were irradiated at 1445 mGy·h^{-1} for 0.75, 2 and 4 h, and total brood size was measured. To assess the effects of chronic irradiation, synchronized nematodes were exposed to 6 dose-rates ranging from 0.9 to 227.9 mGy·h^{-1} from the unhatched embryonic stage until they reached sexual maturity, for a total of 62 h (Fig. 1 and Table S.1 for total doses). Effects on reproduction were assessed by measuring the total number of offspring per adult hermaphrodite (three biological replicates and 5 individuals per replicate).

2.4. Analysis of life stage dependent effects of gamma radiation

To assess life stage dependent adverse effects of ionizing radiation, triplicate samples of synchronized nematodes were irradiated using five dose rates from 0.4 to 100 mGy·h^{-1} plus a control treatment, during selected developmental stages. Four exposure scenarios were designed (see Fig. 1 and Tables S.1–2 for dosimetry) and effects on morphology, growth, fecundity, and total fertility were measured.

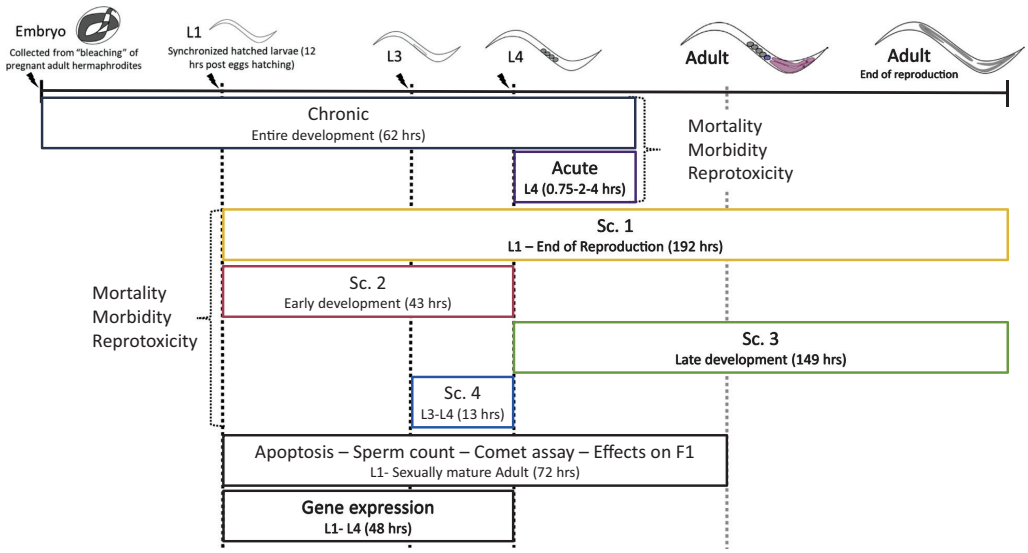

Fig. 1. Experimental design for the gamma irradiation exposures performed in the current study. The irradiation time (hours) is given in parenthesis for each scenario.

2.4.1. Reprotoxic effect assessment

Reproduction effects were evaluated by measuring the cumulative number of larvae (hatched eggs and L1) produced by five nematodes (3 biological replicates, $n = 15$ per treatment) (Table S.1 for dosimetry). From 48 h onwards from L1 stage, the adult worms were transferred to fresh NGM plates every two days for a total of 8 days, and offspring were stained with 1 mL Rose Bengal (0.3 g/L) in an oven at 80 °C for 10 min. NGM plates were then stored at 4 °C and the larvae counted, using a Leica stereo microscope (Leica M205C, 16× magnification).

2.5. Assessment of germline apoptosis

CED1::GFP nematodes were exposed in duplicates ($n = 100$) on NGM agar plates (Ø 3 cm) from L1 molt for 72 h (Fig. 1) to either 10.8, 40.8 or 99.9 mGy·h^{-1} of gamma radiation plus control (Table S.3 for dosimetry). After irradiation, ten worms per treatment were mounted onto 2% agarose pads, anesthetized with 30 mM NaN_3 in M9 buffer, and apoptotic germ cells identified as previously described by Lu et al. (2009). Images of one gonadal arm in each adult hermaphrodite ($n = 20$), 16 h post L4 molt, were captured as ~10 serial *Z*-sections of 1.0 μm interval using Nomarski optics in combination with fluorescence signal under a semi-automated research light microscope (Upright Microscope Leica DM6 B) equipped with a GFP ET filter system (512 nm emission and 40× objective). The frequency of *CED1::GFP* clustering around cell corpses was successively quantified as described by Zhou et al. (2001).

2.6. Spermatids quantification

After 72 h of irradiation (Fig. 1 and Table S.3 for dosimetry), worms were mounted on glass microscope slides pre-coated with Poly-Lysine (1 mg·mL^{-1}), dissected using a 0.5 × 16 mm gouge needle in M9 buffer to expose the spermatheca, fixed with Paraformaldehyde (2%) and permeabilized by freeze cracking (Sadler and Shakes, 2000). For this purpose, fifteen to twenty hermaphrodites per slide were dissected (three slides per treatment, $n > 45$) under a Leica stereo microscope (Leica M205C, 16× magnification). Slides were then stained with 10 μl DAPI DNA staining (10 μg·mL^{-1}) for 20 min, before proceeding with the spermatids count, under a semi-automated research light microscope (Upright Microscope Leica DM6 B) equipped with a DAPI filter system (461 nm emission and 40× objective).

For each analyzed spermatheca, images were captured as a ~20 serial *Z*-sections of ~5.0 μm interval.

2.7. Gene expression analysis

2.7.1. Transcriptomic analysis

RNA sequencing was performed in order to obtain gene expression profiles of triplicate nematode populations exposed to 10.8 or 99.9 mGy·h^{-1} compared to control nematodes (see Table S.3 for dosimetry). For this purpose, total RNA was extracted from samples snap-frozen immediately after 48 h of exposure from L1 stage on L4-young adult nematodes ($n = 1000$ per replicate) with Direct-zol Reagent (Nordic Biosite) and purified with RNeasy Mini Kit (Zymo Research) according to manufacture instruction. In brief, 100 μL of RNase-free Water and 600 μL of Direct-zol were added to each thawed sample, consisting of ~1000 nematodes, prior to homogenization with bead beating (0.1–0.5 mm Ø) using FastPrep (20 m/s per 10 s). The homogenate was transferred to a new Eppendorf tube, mixed with 700 μL of absolute ethanol (96% EtOH) and treated with DNase I and DNA digestion buffer on Zymo-spin mini Column, before further purification on column. RNA purity and yield (A260/A280 > 1.8, A260/A230 > 2, yield >100 ng/μL) was determined using NanoDrop-1000 Spectrophotometer (NanoDrop Technology, Wilmington, DE) and quality (RIN > 7) was assessed with Agilent 2100 Bioanalyzer (Agilent Technologies, Palo Alto, CA) using RNA Nano LabChip Kit (Agilent Technologies). Photometric parameters and RNA integrity number determined the quality of the RNA sequenced samples. Strand-specific TruSeq™ RNA-seq pair-end libraries with 350 bp fragment size were prepared for each treatment (three biological replicates). For each sample ca 30 × 10^6 reads (read length 150 bp) were sequenced using two lanes of Illumina HiSeq 4000 (Norwegian High Throughput Sequencing Centre in Oslo, Norway), and made available on ArrayExpress (accession E-MTAB-8004).

Sequenced reads were mapped to the Ensemble reference genome WBcel235 using STAR (Dobin et al., 2013). Statistical analysis for detection of differentially expressed genes (DEGs) was done in R using Deseq2 package (rlog, variance Stabilizing Transformation)

transformed data (Love et al., 2015), with FDR ≤0.05 and $0.3 \leq \log_2 fc \leq -0.3$ as cut off.

2.7.2. Gene ontology and gene set enrichment analysis

In order to obtain information about processes affected by gamma radiation with respect to anatomical, phenotypical and functional processes down to the single-cell level, the DEGs were subjected to gene ontology(GEA), tissue(TEA) and phenotype(PEA) enrichment analyses using the WormBase Enrichment tool (Angeles-Albores et al., 2016; Lee et al., 2017). Analysis was performed using hypergeometric probability distribution with Benjamini-Hochberg step-up algorithm FDR correction (Angeles-Albores et al., 2017).

2.7.3. Pathway and network analysis

For predicted pathway and biological function analyses of DEGs, SimpleMine (Lee et al., 2017), Reactome Knowledgbase (Fabregat et al., 2017) and KEGG Pathways (Kyoto Encyclopedia of Genes and Genomes) (Kanehisa et al., 2018) tools were used. The analysis was performed on the total number of DEGs for each of the exposure groups and the most significant categories found in each of the databases were compiled and subsequently manually curated in order to obtain annotations of the cellular and molecular processes affected by exposure to gamma radiation.

Gene interaction analysis was performed using GeneMANIA 3.5.1 (Warde-Farley et al., 2010; Franz et al., 2018) within Cytoscape 3.7.1 to identify predicted networks based on the total DEGs resulting from the 100 $mGy \cdot h^{-1}$ exposure.

2.8. Effects of parental irradiation on F1 nematodes

2.8.1. DNA damage analysis on nematode embryonic cells with comet assay

Triplicate samples of synchronous L1 stage larvae (>2500 per replicate) were irradiated for 72 h (Fig. 1) using dose rates from 0.43 to 99.9 $mGy \cdot h^{-1}$ (see Table S.3 for dosimetry). Embryos of irradiated parents were then sampled and DNA damage immediately assessed using the Comet assay. The method detects single strand breaks and alkali-labile DNA lesions using GelBond® films, for a high throughput single cell gel electrophoresis (Gutzkow et al., 2013) was adapted to the conditions of the present experiment. At the end of the irradiation, adult nematodes were removed from NGM plates with 3 × 2 mL of ice-cold Merchant's buffer (0.14 M NaCl, 0.00147 M KH_2PO_4, 0.0027 M KCl, 0.0081 M Na_2HPO_4, 0.01 M Na_2EDTA, pH 7.4). Embryos were gently dislodged from the agar surface by using the tip of a Pasteur pipette. The collected volume (6 mL), containing embryos was filtered using a cell-strainer (Ø 15 μm mesh) to remove the *E. coli* cells. Retained embryos were further rinsed with 6 mL of ice-cold Merchant's buffer. Nematodes embryos were then collected from the cell-strainer in 6 mL of ice-cold Merchant's buffer, and centrifuged at 3000*g* for 2 min.

Three biological replicates, each comprising >12,000 embryos, were placed in 0.5 mL ice-cold Merchant's buffer (pH 7.4) and cells extracted by mechanical dissociation using a 2 mL glass Dounce tissue grinder and piston B (Sigma-Aldrich®, Germany). After extraction, the resulting cell suspension was transferred into a new Eppendorf tube with 0.5 mL of ice-cold Merchant's buffer and settle by gravity on ice for 10 min. A volume of ~400 μL was then gently removed from the supernatant, and a sample from the suspension close to the pellet was taken in order to check for cell viability by using Trypan blue exclusion assay (10 $mg \cdot mL^{-1}$) (Sigma-Aldrich®, Germany) (Strober, 2015). The cell-suspension was adjusted to 1×10^6 $cells \cdot mL^{-1}$ and resuspended in 1:1 low melting point agarose (1.35%, LMP) at 37 °C. By using a multichannel pipette, four technical replicates (4 × 4 μL), from each biological replicate were immediately dispensed onto a cold GelBond® film. Cell lysis was performed overnight in lysis buffer at 4 °C (2.5 M NaCl, 0.1 M Na_2EDTA, 0.01 M Tris-base, 0.2 M NaOH, 0.034 M N-Laurylsarcosine, 10% DMSO, 1% Triton X-100, pH 10). The unwinding was performed by immersing the films in cold electrophoresis solution (0.3 M NaOH, 0.001 M Na_2EDTA, pH 13) for 40 min. Electrophoresis was performed in cold, freshly prepared electrophoresis solution for 20 min at 4 °C, 25 V and 0.8 V/cm, with circulation of the solution kept over time.

Immediately after the electrophoresis, the films were immersed in neutralization buffer (0.4 M Tris-HCL, pH 7.5) 2 × 5 min, fixed in ethanol (>90 min in 96% EtOH) and dried overnight.

SYBR®Gold Nucleic Acid Gel Stain (Life Technologies, Paisley, UK) in TE-buffer (1:10,000) (1 mM Na_2EDTA, 10 mM Tris–HCl, pH 8) was used to stain the nuclei before scoring of films, once the drying process was accomplished. Comets' scoring was performed at 40× magnification under an Olympus BX51microscope (light source: Olympus BH2-RFL-T3, Olympus Optical Co., Ltd.; camera: A312f-VIS, BASLER, Ahrensburg, Germany). Forty randomly chosen cells per replicate (160 cells per biological replicate, total of 480 cells per dose rate) were scored using the Comet IV analysis software (Perceptive Instruments Ltd., Bury St. Edmunds, UK). Tail intensity (% Tail DNA), defined as the percentage of DNA migrated from the head of the comet into the tail, was used as a measure of DNA damage induced by gamma radiation. Mean percentage (%) of DNA in the tail per exposure group was calculated using the median values of % Tail DNA from the 40 comets from each technical replicate (total of 12 median values per exposure group).

2.8.2. Developmental and reprotoxic effects assessment in progeny (F1) of exposed (F0) nematodes

The effect of ionizing radiation was evaluated on the progeny (F1) of nematodes (F0) exposed for 72 h from L1 stage to reproducing adult hermaphrodites (Fig. 1). Adults were washed off the NGM plates using 2 × 3 mL of M9-buffer. Subsequently, embryos were gently dislodged from the agar surface using the tip of a Pasteur pipette. M9 buffer was added to the plates and the collected volume (6 mL), containing embryos was filtered throughout a cell-strainer (Ø 15 μm mesh) in order to remove *E. coli* cells. Embryos were washed off the cell-strainer with 6 mL of M9 buffer, centrifuged at 3000*g* for 2 min, and incubated on non-seeded NGM plates overnight. The following day, synchronous L1 nematodes were transferred to seeded NGM plates (three biological replicates and 5 individuals per replicate) and kept under control conditions. Effects on morphology, growth, development and reproduction were assessed as previously described (Sections 2.4.1 and S.1).

2.9. Statistical analysis

Statistical analysis was performed using Minitab® 18 (Minitab Statistical Software (2010). [Computer software]. State College, PA: Minitab, Inc. (www.minitab.com)), JMP Pro v14 (SAS institute, Cary, NC, USA) and SigmaPlot 10.0 (Systat Software, San Jose, CA). Significant differences between different treatments were calculated using one-way analysis of variance (ANOVA) and, when significance was found, the Tukey pairwise comparisons method was applied. For ANOVA analysis, normality and homogeneity assumption were assessed on residuals by using Anderson-Darling normality test and visually on residuals *vs*. fitted value plot, respectively. Statistical significance was considered when *p*-value was lower than 0.05, unless differently stated.

The Effective Dose-Rate estimations were obtained on 10 and 50% of the population (EDR10 and EDR50) for reproduction and DNA damage on embryonic cells, by using the free software RegTox developed by Eric Vindimian (http://www.normalesup.org/~vindimian/en_download.html). For this purpose, the Hill model was used with corresponding confidence intervals of 95%.

Principal Component Analysis (PCA) was performed in order to find possible correlation between selected endpoints.

3. Results

3.1. Chronic exposure to ionizing radiation exacerbates reprotoxic effects compared to acute irradiation

In order to compare toxic effects of acute and chronic irradiation on nematodes, synchronous populations of *C. elegans* were exposed to similar total doses, but at different dose-rates of gamma radiation (S.1 Table for dosimetry). The chronic exposure from egg stage to young adult stage (62 h) was performed with dose-rates ranging from 0.9 to 227 mGy·h^{-1}, while acute exposure of young adult nematodes was conducted at 1445 mGy·h^{-1}. Neither exposure resulted in any mortality nor in any obvious morbid effects. However, while acute exposure did not induce any significant effect in terms of reproduction, the total number of hatched larvae per adult hermaphrodite was significantly affected in chronically exposed nematodes. The number of offspring was significantly reduced (Tukey *post hoc*, *p*-value <0.05) by 43% and 61%, when nematodes were chronically exposed from embryos to adult stage to 108 mGy·h^{-1} (total dose 6.7 Gy) and 228 mGy·h^{-1} (total dose of 14 Gy), respectively (Fig. 2). The calculated EDR50 (*i.e.*, the dose rate able to inflict a 50% effect on reproduction) was 160 mGy·h^{-1} (equivalent total dose 9.9 Gy), with the 95% confidence interval ranging from 134 to 192 mGy·h^{-1}. The corresponding EDR10 was estimated to 31.3 mGy·h^{-1} (95% CI 15.9 to 49.3 mGy·h^{-1}), with ED10 total dose of 1.9 Gy.

In contrast, the acute exposure of L4 nematodes (total dose up to 6.0 Gy) did not show any significant effect on reproduction (Tukey *post hoc*, *p*-value >0.05) (Fig. 2). This indicated that radiosensitivity of *C. elegans* could be linked to vulnerable life stage(s) or processes during larval development.

3.2. Exposure to gamma radiation during early larval development is detrimental to reproduction

Life-stage dependent radiosensitvitiy was assessed with respect to development, morbidity, fecundity and the cumulative number of hatched larvae per adult hermaphrodite by targeted irradiation of selected developmental stages (Fig. 1).

This revealed a significant contribution of life-stage dependent sensitivity with respect to reprotoxic effects (Fig. 3). As expected, no significant morbidity or effect on fecundity was seen, while a minor reduction of the total body length was measured (SM.1, Section S.1). A dose-rate dependent effect on reproduction was seen in nematodes exposed

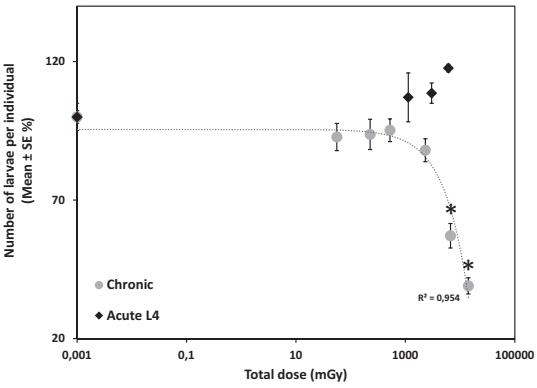

Fig. 2. Total number of offspring per adult hermaphrodite (Mean ± SE in %) measured after chronic or acute exposure to ionizing gamma radiation. Adults were placed on fresh plates every 24 h from onset of egg laying for a total of 6 days. Asterisk indicates significant difference from control treatment (*p*-value <0.05).

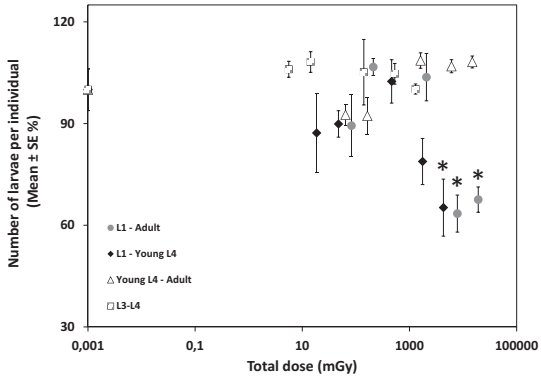

Fig. 3. Total number of offspring per adult hermaphrodite (Mean ± SE in %) measured after four different scenarios of exposure to chronic gamma radiation. Asterisk indicates significant difference from control treatment (*p*-value <0.05).

from the L1 stage throughout the reproductive period of adult hermaphrodite (192 h) as well as those exposed from L1 up to the Young L4 stage (43 h) (Fig. 3). At the two highest dose-rates of exposure (40.8 and 99.9 mGy·h^{-1}), nematodes irradiated from L1 molt to end of reproduction (total doses 7.8 and 19 Gy, respectively) showed a significant decrease in the cumulative number of hatched larvae (37% and 34% reduction respectively) compared to controls (Tukey *post hoc*, *p*-value < 0.05). Nematodes irradiated at 99.9 mGy·h^{-1} from L1 to young L4 molt (total dose 4.3 Gy) showed a 35% reduction (Tukey *post hoc*, *p*-value < 0.05), while no significant decrease, compared to controls, was seen at 40.8 mGy·h^{-1} (total dose 1.8 Gy) (Tukey *post hoc*, *p*-value > 0.05). This demonstrates that despite the differences in exposure times and total dose, the detrimental effects on reproduction were similar when these two scenarios were compared.

In contrast, neither nematodes irradiated from L4 molt throughout the reproductive period (143 h), nor the nematodes exposed from L3 to early L4 molt showed any significant reprotoxic effect (Tukey *post hoc*, *p*-value > 0.05), even when the total dose reached 14.9 Gy.

3.3. Enhanced germ cell apoptosis in chronically irradiated young adult nematodes

Assessment of apoptosis after 72 h of exposure to gamma radiation revealed a dose-rate dependent increase in the number of germ cell corpses in the *C. elegans* reporter strain *CED1*::*GFP* (MD701) (Fig. 4a–c). A significantly increased number of apoptotic germ cells was found when nematodes were exposed to the two highest dose-rates (40.8 and 99.9 mGy·h^{-1}) compared to control nematodes (Tukey *post hoc*, *p*-value < 0.05). At these dose-rates we observed an average of 3.1 and 3.4 apoptotic germ cells per gonadal arm respectively (Fig. 4a,b). This corresponds to a 2-fold increase in apoptosis compared to the control treatment (1.7 apoptotic germ cells per gonadal arm). We also noted a slight (1.6-fold higher), but not significant effect on germ cell apoptosis in nematodes exposed to 10.8 mGy·h^{-1} (Tukey *post hoc*, *p*-value > 0.05).

3.4. Chronic irradiation reduces the number of spermatids

In order to identify the cause of the reprotoxicity shown after irradiation during the early development, effects induced by chronic gamma irradiation on spermatogenesis were assessed in adult hermaphrodites at 72 h of exposure from L1 stage (Fig. 5). Nematodes exposed to total doses equal or >2.8 Gy showed a significant reduction in the number of spermatids compared to control nematodes, with dose-rates of 38.9

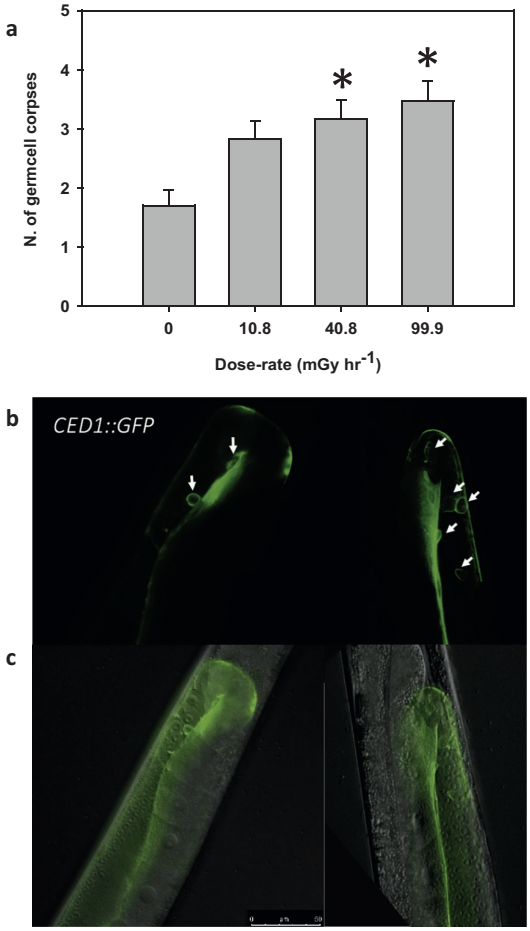

Fig. 4. a) Effect of chronic exposure to gamma radiation (72 h) on germ-cell apoptosis (number of germ cell corpses ± CI) pr gonadal arm in young adult *CED1::GFP* hermaphrodites ($n = 20$). Asterisks indicate significant difference compared to control treatment (p-value <0.05). b) Epifluorescence photomicrographs of gonadal arms in control hermaphrodite (left) and hermaphrodite irradiated at 100 mGy·h^{-1} (right). White arrows indicate apoptotic germ cells expressing the *CED1::GFP*. Scale bar: 50 μm. c) Nomarski and epifluorescence photomicrographs of gonadal arms from the same nematodes shown in Fig. 5b. Scale bar: 50 μm.

and 101 mGy·h^{-1} showing a 34% and 23% of reduction, respectively (Tukey *post hoc*, p-value < 0.05).

3.5. Gene expression analysis

In order to identify changes in the gene expression profiles during critical stages of gonadal development, a transcriptome analysis was performed on nematodes exposed to 10 and 100 mGy·h^{-1} for 48 h from L1 stage (S.M. 1). A total number of 1.75×10^3 genes was expressed in all samples, while the number of differentially expressed genes (DEGs) was 359 at the highest dose-rate of exposure (100 mGy·h^{-1}) compared to 540 resulting from the 10 mGy·h^{-1} exposure group (FDR < 0.05, log2FC ≤ −0.3 or ≥0.3) (Figs. S.2a-b and S.3a).

Among the DEGs a group of 54 genes was found to be in common between nematodes exposed to 10 and 100 mGy·h^{-1} (Fig. S.3b).

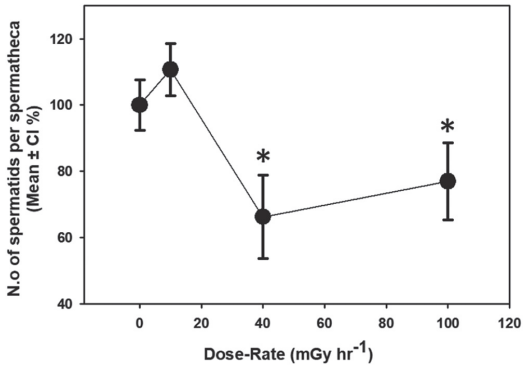

Fig. 5. Effect of chronic gamma irradiation on the number of spermatids per spermatheca (Mean % relative to control ± Confidence Interval, n = 20) counted in young adult hermaphrodites (72 h from L1 stage). Asterisk indicates significant difference compared to control treatment (p-value <0.05).

3.5.1. Functional enrichment analysis of DEGs

Gene function analysis of DEGs assessed by Gene Ontology (GOTERM) enrichment showed distinct differences in functionally enriched categories between the 10 and 100 mGy·h^{-1} exposures.

A total of 21 significantly over-represented Biological Functions were identified for the 10 mGy·h^{-1} group (Fig. S.4). Integrated pathway analysis combining the outputs from Simplemine, Reactome and KEGG databases corroborated the enrichment analysis from the 10 mGy·h^{-1} exposed group with respect to cuticle-collagen, protein and lipid metabolism (Table S.4). In addition, we found 10 genes with functions related to biological oxidation and Glutathione metabolism and 45 genes related to Immune system, Signal transduction, Peroxisome and Response to pathogens.

A total of 18 GOTERMs were significantly over-represented among the down-regulated genes in the 100 mGy·h^{-1} exposure group (Fig. 6a), while no significant GOTERM resulted from the list of up-regulated genes. The GOTERMs were related to cellular components such as organelle, cytoplasm, nucleus, nucleolus, cytoskeleton, mitochondrion, and structural constituent of ribosome. Biological and molecular functions included multicellular organism reproductive process, rRNA metabolic process, RNA splicing, peptide biosynthetic process and macromolecule biosynthetic process (Fig. 6 and Table S.5). From the 100 mGy·h^{-1} group 159 of 174 down-regulated genes had an annotation in the Tissue Enrichment Analysis tool (TEA, Fig. 6b). The significantly enriched terms were mostly related to reproduction, and included Reproductive system, Male, Spermatheca, Oocyte and Amphid sheath cell. The Phenotype Enrichment Analysis (PEA, Fig. 6c) showed that the Linker-cell migration variant, Cytoplasmic processing body (P-granule) variant, and Spindle position variant were the most significant terms. Pathway analysis identified 7 biological functions related to reproduction (Table S.5). These comprised exclusively down-regulated genes (101) related to spermatogenesis, 28 of them being Major Sperm Proteins, 3 genes related to sperm meiosis and maturation. Fifteen of these genes also participate in germline proliferation, spindle formation and oogenesis.

In addition, a significant effect was identified on Cell-cycle, Programmed cell death, Chromatin organization and DNA repair, Cellular stress response, Immune system modulation, and Signal transduction. A further 24 DEGs were related to Protein Metabolism, Macroautophagy and Peroxisome. Among these, we found up-regulation of stress-activated protein kinases (*jnk-1* and *mak-1*) (Kawasaki et al., 1999), a target of ERK kinase MPK-1 (*toe-4*) (Miller and Chin-Sang, 2012), ferritin (*ftn-1*) (Kim et al., 2004), Ubiquitin conjugating enzymes (*ubc-3* and

ubc-8) (Dove et al., 2017; Jones et al., 2001) and Ubiquitin carboxyl-terminal hydrolase (*ubh-4*), which are hallmarks of cell response to damage to proteins, mitochondria and lipids.

3.5.2. Network analysis

In order to identify operational gene interactions, a Genemania (Franz et al., 2018) network analysis was performed on the complete list of DEGs resulting from the 100 mGy·h^{-1} exposure group. Out of 359 genes, 331 clustered into three distinct groups, connected by co-expression, shared protein domain and physical or predicted interaction (Fig. S.5). One of these clusters corresponded to the genes involved in reproduction identified by Tissue Enrichment and Pathway analysis. Within this cluster, we identified a common attribute in the Cytosolic Motility Protein (Fig. S.5). This included a total of 71 genes, 64 of these were spermatogenic (assigned according to Ortiz et al. (2014)), including *ssp-10*, *ssp-35* and *sss-1* as well as 28 MSP class genes. In addition, nearest neighbors included *htas-1* (sperm specific histone H2A) *smz-1* and *smz-2* (involved in spermatid meiosis chromosome segregation) (Samson et al., 2014; Chu et al., 2006).

The second cluster was defined by 11 Serine/Threonine protein kinase genes (Figs. S.5, S.6) related to stress response, cell-cycle control and meiosis. Among these genes, *mak-1*, *jnk-1* and *air-1* were identified by the first neighbor analysis as main inter-nodes connecting 157 genes. Specifically, the Aurora/Ipl1 Related kinase *air-1* represented a major node, showing co-expression with two subsets of genes (Fig. S.6), one interconnecting two of the major clusters and containing 8 genes with protein kinase activity (*W02B12.12*, *Y38H8A.3*, *C39H7.1*, *T05A7.6*, *mak-1*, *T07F12.4*, *F32B6.10* and *ZC123.4*). In addition, *air-1*, which is required for the assembly/stabilization of female meiotic spindle microtubules (Sumiyoshi et al., 2015), physically interacts with *spd-5* and *ran-1* (Boxem et al., 2008), also involved in spindle formation (Hamill et al., 2002; Cheng et al., 2008).

The third cluster comprised genes related to gene regulation and chromatin remodeling, such as *cec-5* gene, predicted to have methylated histone binding activity, *rpb-5*, *Y54H5A.1* and *ruvb-2* with DNA binding activity (Poulin et al., 2005) and the major sperm protein *vpr-1*, which is required for proper distal tip cell migration during somatic gonad development (Cottee et al., 2017). The latter was also identified as a major node, sharing the same protein domain with 30 spermatogenic genes and co-expression with 9 non-spermatogenic genes. The *cec-5 and let-418* genes, involved in the negative regulation of germline transcription and vulva development (Käser-Pébernard et al., 2014; Turcotte et al., 2018), were connected to 26 genes, including *air-1* and *vpr-1* (targets of *cec-5*). Furthermore *let-418* targets were *ima-3* involved in meiosis I (Weber and Brangwynne, 2015), *emb-4* required for regulation of the transcription in the germ line (Tyc et al., 2017), and *his-24* involved in epigenetic regulation of heterochromatin (Jedrusik-Bode, 2013).

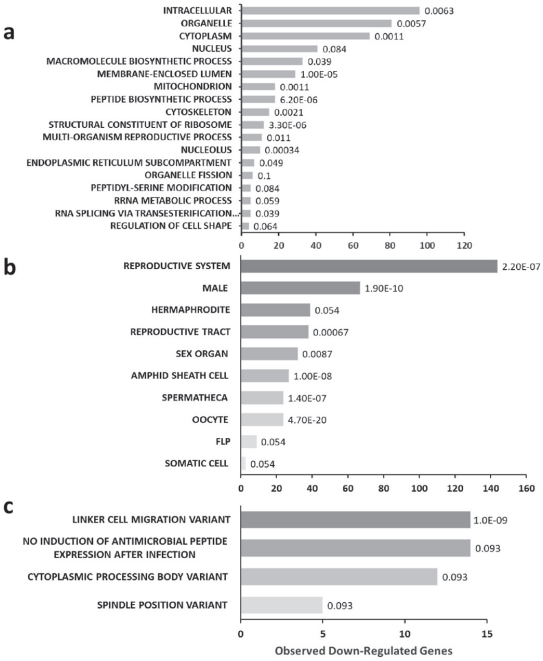

Fig. 6. a) Functional categories of over-represented Gene Ontology (GO) terms, b) Tissue Enrichment Analysis (TEA) and c) Phenotype Enrichment Analysis (PEA) of down regulated genes resulting from *C. elegans* exposed for 48 h to 100 mGy·h^{-1} of gamma radiation. Hypergeometric probability distribution was adopted to calculate the enrichment of down-regulated genes observed in each specific function. (Data labels indicate *q*-values).

3.6. Adverse effects on the progeny (F1) of irradiated nematodes

3.6.1. Radiation induced DNA damage in C. elegans embryonic cells

In order to assess DNA damage on the progeny of irradiated parents, a protocol for performing Comet Assay on *C. elegans* embryonic cells was developed (see Section 2.8.1). The Comet assay was performed using embryos to extract homogeneous essentially undifferentiated cell populations that were mitotically active (Fig. 7a) (Ehrenstein and Schierenberg, 1980; Wood, 1988). The established protocol produced high numbers of viable cells (assessed using trypan blue staining), with low level background comet tail in control cell populations (2.2–5.8%) compared to a previous study done by Ng et al. (2019).

Comet assay on embryonic cells showed a tendency of increased DNA damage (Mean % tail intensity and frequency of cells with significant DNA damage) after exposure of parents to dose-rates ranging from 0.43 to 10.8 mGy·h^{-1} although this was not statistically significant (Tukey *post hoc*, $p > 0.05$) (see Figs. 7c and S.7). However, exposure to dose-rates of 40.8 and 99.9 mGy·h^{-1} caused significant DNA damage, with a 3.9 and 4.4 fold increase of tail intensity, compared to non-irradiated embryonic cells (Tukey *post hoc*, $p < 0.05$, Fig. 7b,c).

The EDR50 value calculated for the DNA damage was 38.4 mGy·h^{-1}, with the 95% confidence interval ranging from 13.9 to 39.2 mGy·h^{-1}.

Moreover, the proportion of damaged cells increased in a dose rate dependent manner, where all cells from the 40.8 and 99.9 mGy·h^{-1} (2.94 and 7.19 Gy total dose) treatments showed DNA damage significantly higher than control level (6% tail intensity) (Fig. S.7).

3.6.2. Significant size reduction accompanied by low reprotoxic effects on parentally irradiated F1 nematodes

To investigate the late effects on the parentally irradiated (F1) embryos, the F1 generation was followed during development and effects were measured with respect to mortality, morphology, growth, and reproduction.

No effect was observed with respect to mortality, but a clear dose/dose rate-dependent reduction on the total body length was measured at 96 h post L1 molt (see Fig. 8a–c). This reduction was statistically significant already at the lowest dose-rate of exposure 0.43 mGy·h^{-1} (Tukey *post hoc*, *p*-value < 0.05). The reduction in body length was not associated with other visible anatomical morbid changes as formation of pharynx, gastrointestinal tract, and reproductive systems appeared intact, but were smaller in size (Fig. 9c). We also observed a trend towards reduced total brood size for the parentally irradiated F1 nematodes, (Fig. 8b), but the effect was not significant compared to control nematodes (Tukey *post hoc*, *p*-value > 0.05).

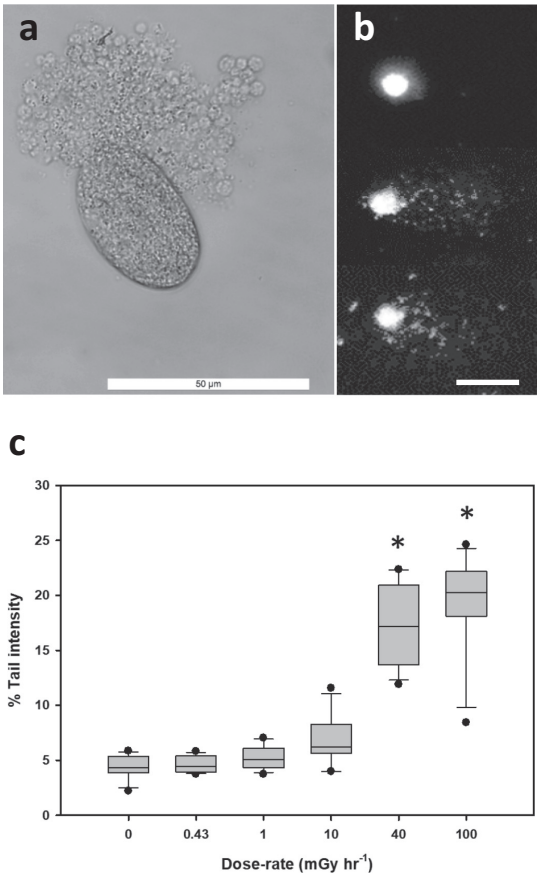

Fig. 7. a) Undifferentiated mitotically active embryonic cells harvested by mechanical disruption of gastrula stage embryos of irradiated parents. Micrograph from a semi-automated research light microscope at 40×, bright field optics. Scale bar: 50 µm. b) Comet micrographs taken at 40× magnification under an Olympus BX51 microscope (light source: Olympus BH2-RFL-T3, Olympus Optical Co.). From Top to Bottom: Control, 40 and 100 mGy·h^{-1}. Scale bar: 10 µm. c) DNA damage (Mean of Tail intensity in %) assessed on embryonal cells from parentally irradiated embryos, using the Comet assay. Asterisks indicate significant difference from control treatment (p-value <0.05).

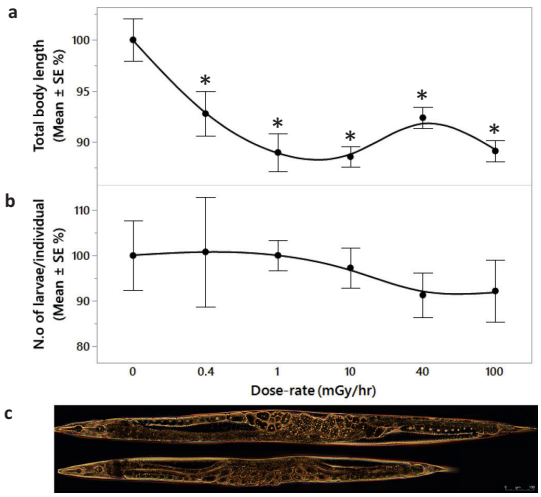

Fig. 8. Effects on somatic growth in offspring of nematodes exposed to gamma radiation. a) Total body length relative to control ± SE in % measured at 96 h of development using a stereo microscope (Leica M205C, 10× magnification) coupled with a computer-connected camera. Asterisks indicate significant difference compared to control treatment (p-value <0.05). b) Total number of offspring per adult hermaphrodite (Mean % relative to control nematodes ± SE), produced by nematodes parentally exposed to chronic gamma radiation. Adults were placed on fresh plates every 48 h from onset of egg laying for a total of 6 days. c) Physiological appearance of F1 adult hermaphrodites (96 h post L1), resulting from parental (F0) exposure to chronic gamma radiation (UP: Control, Bottom: 100 mGy·h^{-1}). Micrographs from a semi-automated research light microscope at 10×, phase-contrast optics, Scale bar: 100 µm.

4. Discussion

4.1. Chronic irradiation induces life-stage dependent reprotoxic effects in C. elegans

Caenorhabditis elegans is considered among the most radioresistant of organisms, tolerating >1 kGy dose of ionizing gamma radiation (Hartman and Herman, 1982, Hartman et al., 1988, Johnson and Hartman, 1988, Gartner et al., 2000, Bailly and Gartner, 2013, Guo et al., 2013). In contrast, recent studies have revealed that chronic exposure may cause adverse cellular and reproductive effects at much lower doses (Hartman and Herman, 1982; Hartman et al., 1988; Johnson and Hartman, 1988; Gartner et al., 2000; Bailly and Gartner, 2013; Guo et al., 2013; Buisset-Goussen et al., 2014; Lecomte-Pradines et al., 2017; Dubois et al., 2018). We therefore hypothesized that the apparent differences in effect may either be caused by different efficacy of acute *versus* chronic irradiation. Alternatively, the discrepancy in effects may be related to radiosensitivity of individual life stages, cell types or molecular functions in *C. elegans*.

In the present study, exposure of L4 young adults *C. elegans* to acute and chronic gamma irradiation (~6 Gy) did not cause any significant effect with respect to mortality, morbidity, or any of the reproductive endpoints, confirming that nematodes can tolerate high acute doses of radiation without mortality (Hartman and Herman, 1982; Krisko et al., 2012) (Fig. 2). Results are also consistent with previous studies where significant effects on hatchability and fecundity appeared only at doses >50 Gy (Krisko et al., 2012 and Dubois et al., 2018). In comparison, subjecting nematodes during development (embryos to L4 young adults) to chronic irradiation at a similar cumulative dose (>4 Gy), did not affect mortality or morbidity, but caused significant reprotoxic effects (Figs. 2 and 3). This demonstrates that the pre-L4 young adult stage is more sensitive to ionizing gamma radiation compared to the post mitotic stage. However, it was not evident whether the observed reprotoxic effects were related to a specific developmental stage, tissue or vulnerable cell type.

The results from the four exposure scenarios further support the differences in radiosensitivity between early and late larval development in this nematode. A dose-dependent reprotoxic effect was observed when larvae were exposed during their early development (L1-Young L4), while no effects were seen when adult stages were irradiated (Fig. 3). Furthermore, our results showed that extending the irradiation to include the embryonal stage did not enhance the reprotoxic effect compared to exposure during larval stage only. In *C. elegans* DNA repair is particularly robust during early embryogenesis (Clejan et al., 2006), and somatic cells in larvae are more tolerant to DNA damage than germ cells (Vermezovic et al., 2012; Lans and Vermeulen, 2015). Based on the observed reprotoxic effects (Figs. 2 and 3), it appears that the post-embryonic development is the phase where the critical damage occurred. During this phase, cell proliferation resumes and

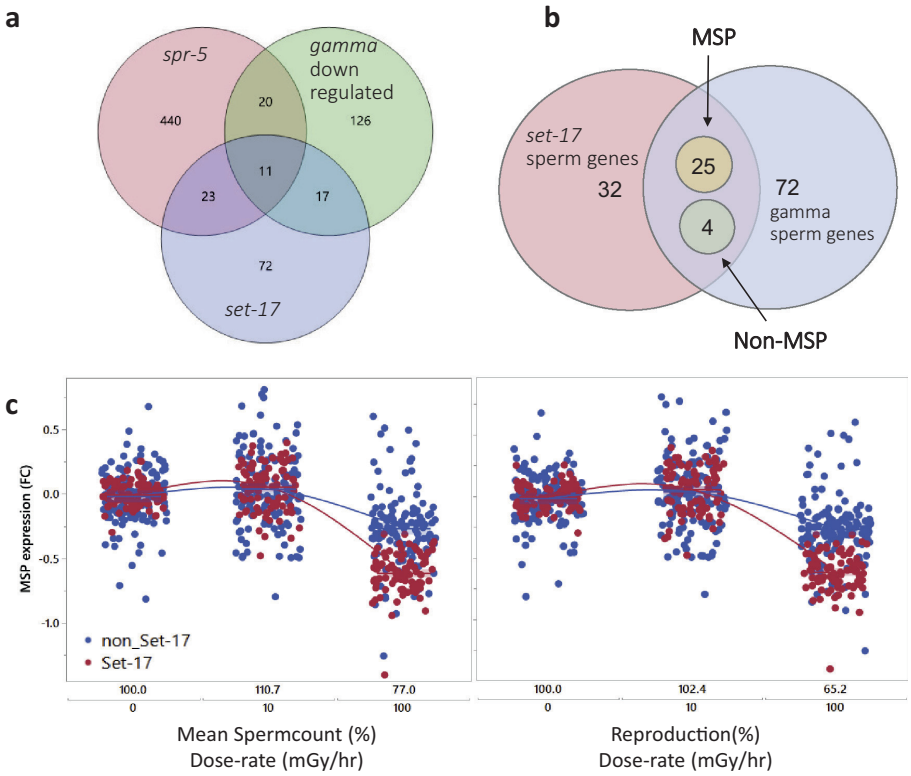

Fig. 9. a) Venn diagram of down-regulated genes resulting after chronic exposure to gamma radiation (4.8 Gy) or regulated by *spr-5* or *set-17* (gene expression data from Katz et al. (2009) and Engert et al. (2018), respectively). b) Venn diagram of spermatogenic genes regulated by chronic exposure to 4.8 Gy of gamma radiation and by *set-17* (Engert et al., 2018). c) MSP expression (Fold Change) plotted as a function of fertility (No. offspring/individual %), No. of spermatids (%) and dose-rate of exposure ($mGy \cdot h^{-1}$) to gamma radiation ($R^2 = 0.8$). In red 25 MSP genes found significantly down-regulated (FDR <0.05) after chronic exposure to 4.8 Gy of gamma radiation and in common with *set-17* regulated spermatogenic genes found by Engert et al. (2018). In blue MSP genes not regulated by *set-17*. Spermatogenic genes were assigned according to Ortiz et al. (2014).

the reproductive tract is generated, with the establishment of Z1-Z4 gonad (Pazdernik and Schedl, 2013) and Z2 and Z3 germline precursor cells to initiate gonadogenesis (Kimble and Hirsh, 1979).

The reduction in number of hatched larvae per adult caused by irradiation of L1- Young L4 to a total dose of 4.3 Gy was similar to that following irradiation of the L1 to the end of reproduction to a total dose of 7.8 Gy. Furthermore, since no effects were seen when the L4-adults were irradiated to total doses of up to 15 Gy, it would appear that the L1 to the young L4 stage are the most critical radiosensitive stages with respect to reprotoxicity (Figs. 2 and 3). The results thus suggest that post L4 stage larvae are able to effectively ameliorate genotoxic effects, at least up to doses of 15 Gy.

4.2. Effect of ionizing radiation on the C. elegans germline: Enhanced apoptosis and impaired sperm production

In order to investigate the mechanisms behind the observed reprotoxicity we assessed adverse effects on the germline of irradiated nematodes with respect to DNA damage, by measuring the number of apoptotic cells and the number of produced spermatids. The apoptosis assessment was carried out using a reporter strain (*CED1*::*GFP*), while the N2 Bristol strain was used for the spermatid measurement. In both cases, irradiation covered the radiosensitive L1-L4 developmental stage.

Germ cell death in *C. elegans* is known to be a natural physiological event, where half of the potential oocytes are removed (Gumienny et al., 1999; Lettre and Hengartner, 2006). Apoptosis is as an important surveillance mechanisms that ensures quality control in the germline (Bailly and Gartner, 2013), which may be enhanced by genotoxic insult like high doses of ionizing radiation *via* a series of DNA damage response mechanisms including cell-cycle arrest and programmed cell death (Gartner et al., 2000).

Strikingly, our results showed that, in comparison to the reprotoxic effects and to previous studies where germ cell apoptosis was only identified after acute doses of exposure, exerted on L4 nematodes, (>60 Gy) (Schumacher et al., 2001; Schumacher et al., 2005), already a dose as low as 2.9 Gy during L1 to L4 stages effectively enhanced the number of apoptotic germ cells (Fig. 4a). Thus showing that proliferating oocytes are very vulnerable to the effects of ionizing radiation, but also that germ cell apoptosis in *C. elegans* is a highly responsive protective mechanism that removes damaged cells and reduces the probability of misrepair at such low doses. The enhanced germ cell apoptosis observed in the present study may therefore be considered as a defense mechanism activated to obtain an efficient removal of non-salvageable oocytes (Andux and Ellis, 2008), preserving the embryos genome integrity (Lans and Vermeulen, 2015) and viability of the progeny (Bailly and Gartner, 2013).

While oocytes are continuously produced and can be replenished, each hermaphrodite produces a limited amount (~300) of spermatocytes during the L3/L4 stage (Chu and Shakes, 2013). The internal fertilization of *C. elegans* is extremely efficient. An unmated hermaphrodite

will use all of its sperm to produce offspring (Singson, 2001). Spermatogenesis has been reported to be affected by chronic irradiation in other invertebrate species (Hertel-Aas et al., 2011). We therefore hypothesized that spermatogenesis might also be a vulnerable process in *C. elegans*. Accordingly, we found a significant reduction on the number of spermatids at 2.8 Gy (Fig. 5), which is similar to the dose causing enhanced germ cell apoptosis (Fig. 4). In terms of the dose rates, in both cases dose-rates of 8–10 $mGy \cdot h^{-1}$ showed non-significant effects from controls, while significant changes were seen at higher dose-rates such as 40 and 100 $mGy \cdot h^{-1}$. The Pearson correlation analysis identified a positive correlation between the reduction in spermatids and the observed reprotoxic effect (PCC: 0.99 for L1-End of reproduction, PCC: 0.86 for L1-Young L4 exposure) (Figs. 2–4, S.8). Consistently, the limiting factor for self-fertility in *C. elegans* is not the number of oocytes, but rather the amount of self-sperm produced by the hermaphrodite (Hodgkin and Barnes, 1991).

Our results therefore suggest that the defective spermatogenesis induced by chronic exposure to ionizing radiation is the most plausible cause of the life stage-dependent reprotoxic effects in *C. elegans*.

4.3. Chronic exposure to gamma radiation impairs expression of genes required for spermatogenesis, oogenesis and embryogenesis

Ionizing gamma radiation is able to exert adverse effects on genes and proteins directly, through DNA damage (single and double strand breaks as well as DNA oxidation), or indirectly *via* formation of free radicals, recombination and induction of ROS (National Research Council, 2006). Consistent with these known effects, the transcriptomic analysis revealed that chronic exposure to gamma radiation induced differential regulation of genes involved in Cell-cycle control, Programmed cell death, Chromatin organization, DNA repair, Biological oxidation and Cellular stress response (Table S.5). The transcriptomic data also reflected significant differences between exposure to 10 $mGy \cdot h^{-1}$ and 100 $mGy \cdot h^{-1}$ (0.4 and 4.8 Gy total dose) with respect to toxic effects, including reproduction, apoptosis and spermatid production. It is known that the set of genes involved in apoptotic cell clearance in *C. elegans*, also mediates the removal of residual bodies during spermatogenesis. Defective clearance of residual bodies has been proven to reduce the number of spermatids in both males and hermaphrodites, possibly by decreasing sperm transfer efficiency (Huang et al., 2012; Ellis and Stanfield, 2014). Notably, physiological germ-cell death has not been reported in male gonads, and apoptosis appears to be restricted to oogenesis in hermaphrodites (Lettre and Hengartner, 2006).

We therefore hypothesized that other *hitherto* unknown mechanisms could be involved in the impaired spermatogenesis.

In line with the observed adverse phenotypic effects, the gene expression analysis at L4-stage showed that central molecular and cellular processes related to reproduction, and in particular to spermatogenesis, were negatively affected at 100 $mGy \cdot h^{-1}$ (total dose >4 Gy) (Fig. 6a–c, Table S.5). Consistent with the reduction of spermatids (Fig. 5), we found significant down-regulation of genes related to chromosome segregation in sperm meiosis (*smz-1* and *smz-2*) (Chu et al., 2006) and chromatin condensation during sperm maturation (*htas-1*) (Samson et al., 2014). Throughout spermatogenesis, the processes of meiosis, sperm differentiation, and chromatin remodeling are intimately intertwined, RNA inhibition of the gene *smz-1* or *smz-2* has shown to induce the arrest of spermatocytes progression through meiotic division thus affecting male fertility (Chu et al., 2006).

Moreover, down regulation of 28 sperm cytoskeletal structural protein genes (MSP) and 3 sperm-specific genes also suggested a severe defect in spermatogenesis (Table S.5). This family of proteins accounts for >40% of the cytosolic protein in *C. elegans* sperm (Smith, 2006). Several gamete-signaling events are required for high levels of oocyte maturation and ovulation and major sperm proteins (MSPs) play a central role not only in pseudopod motility, but also in promoting oocyte meiotic maturation, sheath contraction and ovulation of the oocyte in the spermatheca (Miller et al., 2001). When we performed a more thorough investigation on the 101 down-regulated genes spermatogenic (assigned according to Ortiz et al. (2014)), a significant correspondence (29 genes) with a previous study from Engert et al. (2018) was found (Fig. 9a,b). In the study from Engert and co-authors, a 50% reduction in terms of fertility was due to down-regulation of 28 MSP genes as a result of the mutation in the gene *set-17*(*n5017*). Furthermore, *let-418*, which was down-regulated in our transcriptomic analysis, interacts physically and genetically with *spr-5* to promote the normal development of germline stem cells (Käser-Pébernard et al., 2014). *Spr-5* is a histone H3K4 demethylase with a role in meiotic double-strand break repair (Nottke et al., 2011). Loss of *spr-5* and *let-418* has shown to induce immediate sterility and aberrant gonad development, demonstrating a collaborative role of these two genes in promoting fertility (Käser-Pébernard et al., 2014). Our network analysis showed interactions *via* co-expression between chromo-domain genes *let-418* and *cec-5* with 26 genes involved in gonad development, regulation of transcription in the germ line and meiosis (Fig. S.5).

This may imply that DNA double-strand breaks, resulting from exposure to ionizing radiation, may play a role in the regulation of *spr-5* and *set-17* and thereby inducing defective meiosis, which is consistent with the down-regulation of *smz-1* and *smz-2*, reduction of spermatocytes, fertility and consequently the down-stream regulation of 28 MSP genes (Fig. 9a–c).

We also identified a potential downstream effect of the impaired spermatocyte/MSP expression by the down-regulation of *spd-5* and *air-1*, two genes essential for the centrosome maturation and spindle assembly during the first mitotic division of the *C. elegans* zygote (Hamill et al., 2002). Consistent with this result, *air-1* was also a target of the major sperm protein *vpr-1* in our network analysis (Fig. S.6). This is an essential gene which shares the protein domain with the *MSP*s and whose expression is crucial in neuron and germ cells to induce gonadogenesis (Cottee et al., 2017), suggesting that in *C. elegans* exposure of early life stages to ionizing radiation may also impair this signaling mechanism required for the development of sexual organs. Moreover, prior to fertilization, the major sperm proteins have shown to promote oocyte microtubule reorganization (Harris et al., 2006). This suggests that the down-regulation of Aurora A kinase/AIR-1, shown in our transcriptomic analysis, may play a central role not only for the impairment during the formation of the spindle microtubules in female meiosis, but also for the regulation of mitotic cell cycle, as shown by the physical interaction with the gene *spd-5*. This notion was further supported by the down regulation of 23 genes related to germline proliferation, spindle assembly, oogenesis and embryonic development (Table S.5). In sum these observations substantiate that chronic exposure to ionizing radiation (>4 Gy total dose) in early stage nematodes has a profound effect on the entire *C. elegans* reproductive system (Fig. 10).

4.4. Embryonic DNA damage leads to a significant impairment on somatic growth but minimal effects on reproduction in the progeny (F1) of irradiated nematodes

Although DNA damage like DSB may cause replication problems (Bailly and Gartner, 2013), particularly when cell division rate is high *e.g.* during early embryogenesis, a previous study showed that *C. elegans* embryos are relatively tolerant to high doses of UV or other genotoxic agents (Holway et al., 2006). However, little was known about parental exposure to low doses of the germline and the later effects on the surviving embryos. Therefore, in this study we have investigated the embryonic DNA damage exerted by parental exposure to low doses of ionizing gamma radiation in combination with somatic growth impairment and reprotoxic effects on the F1 progeny. The focus of these experiments was therefore to examine the radiosensitivity in nematodes exposed during the proliferation stage, corresponding to cell divisions from a single cell (prior fertilization) to 558 essentially undifferentiated

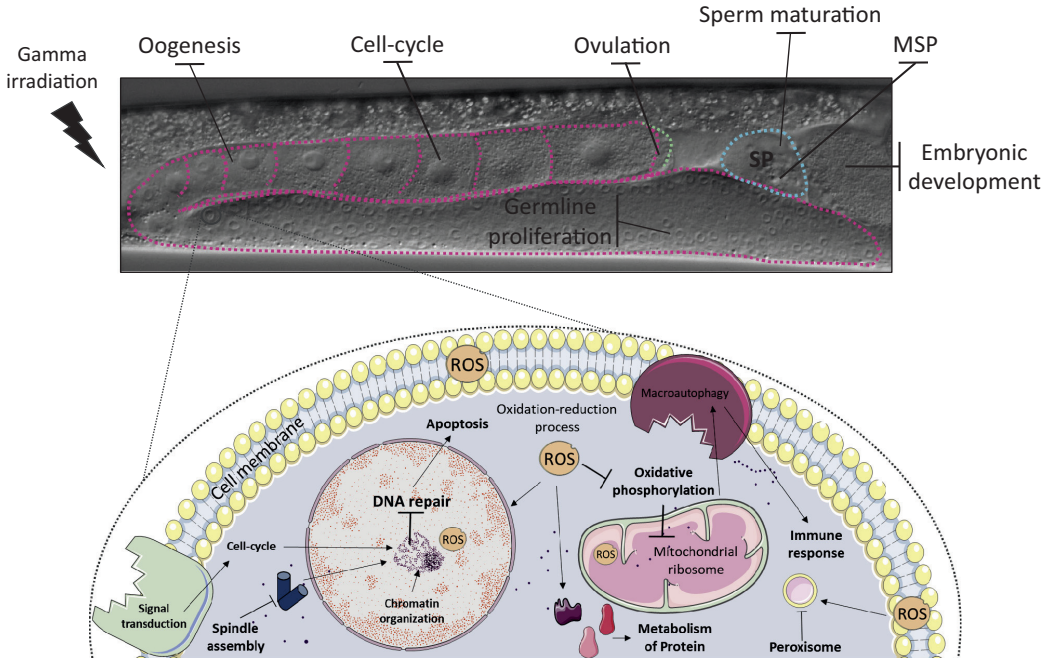

Fig. 10. Conceptual model of cellular and molecular processes induced (↑) or inhibited (T) after chronic exposure to gamma radiation (100 mGy·h^{-1}) in the nematode *C. elegans*.

cells by the end of "16 E stage" (Ehrenstein and Schierenberg, 1980; Wood, 1988). Our results demonstrated a dose-dependent sensitivity of embryonic cells in terms of DNA damage. Specifically, at accumulated doses higher than 2.9 Gy we observed an increased frequency of damaged cells (Fig. S.7) and a significantly higher damage compared to background levels (control treatment) (Fig. 7b,c).

Despite the significant damage seen in these embryonic cells and consistent with Dubois et al. (2018), we could not observe any deleterious effect on hatching and or lethality on embryos parentally exposed at doses up to 7.2 Gy. In a previous study, an acute dose of 50 Gy during early embryonal development was required to induce almost complete embryonic lethality for wild type. This effect was considered to be a consequence of cell proliferation (Clejan et al., 2006). In the same study, no embryonic lethality was observed when late-stage embryos, composed of non-cycling cells, were irradiated with doses up to 140 Gy, even in NHEJ (non-homologous end joining) or HR (homologous recombination) deficient mutant strains. Consistent with these results, we did not observe any lethality or significant effect on the nematodes fertility at much lower doses of exposure, since the total number of offspring showed only a minor and non-significant decrease at doses higher than 2.9 Gy (dose-rate of 40 mGy·h^{-1}) (Fig. 8b). This result showed that nematodes parentally exposed were either able to ameliorate the observed genotoxic effect, or that the doses adopted in our study were not sufficient to induce any impairment during the development of the somatic gonads.

In contrast, parental irradiation was able to induce a clear dose-dependent reduction in terms of somatic growth of the offspring (Fig. 8a), with nematodes being significantly smaller already at the lowest dose of exposure (0.03 Gy, dose-rate of 0.4 mGy·h^{-1}). Although we did not assess DNA damage in somatic cells any further during the nematodes' development, the combination of somatic growth impairment with the high levels of genotoxicity seen in embryonic cells (Figs. 7b,c, S.7) demonstrates the remarkable tolerance of these embryos, but implies a considerable related cost to repair this damage. HR is known to provide error free DSB repair, but this repair mechanism is only active when the sister chromatid template is available, *i.e.* in proliferating somatic cells and germ cells at all embryonic stages (Clejan et al., 2006). In contrast, non-proliferating somatic cells arrest in G1 and perform NHEJ, which is the major pathway for repair of radiation-induced DNA damage in quiescent somatic cells of *C. elegans* embryos, but is an error prone mechanism. Indeed, a mis-segregation of chromosome fragments was found by Clejan et al. (2006) to be the likely trigger for the somatic developmental abnormalities displayed in irradiated late-stage NHEJ mutant embryos.

Thus, parental irradiation of nematodes impairs the somatic growth of embryos significantly, while the negative effects on reproductive performance are less severe. This is probably a result of the different activity of these DNA repair pathways on a mixed population of replicating and quiescent cells that rely on HR and NHEJ.

5. Conclusions

Sensitivity to ionizing gamma radiation in *C. elegans* is highly dependent on life stage. The post-mitotic adult nematodes tolerate both acute and high dose chronic irradiation without adverse effects. In contrast, L1-L4 developmental stages are highly sensitive to gamma radiation induced reprotoxic effects. At the mechanistic level, gamma irradiation induced genotoxic insult, germ cell apoptosis and reduced spermatids production. The decrease in spermatids production was identified as the major cause of the reduced fertility. Parental exposure leads to DNA damage in developing embryos. Surprisingly, these progeny were able to maintain a high reproductive capacity, despite reduced somatic growth.

Supplementary data to this article can be found online at https://doi.org/10.1016/j.scitotenv.2019.133835.

CRediT authorship contribution statement

Erica Maremonti: Conceptualization, Data curation, Formal analysis, Investigation, Methodology, Software, Validation, Visualization, Writing - original draft, Writing - review & editing. **Dag M. Eide:** Data curation, Formal analysis. **Deborah H. Oughton:** Conceptualization. **Brit Salbu:** Resources. **Fabian Grammes:** Data curation. **Yetneberk A. Kassaye:** Methodology. **Rémi Guédon:** Methodology, Data curation. **Catherine Lecomte-Pradine:** Methodology. **Dag Anders Brede:** Conceptualization, Funding acquisition, Investigation, Methodology, Project administration, Resources, Supervision, Validation, Visualization, Writing - original draft, Writing - review & editing.

Declaration of Competing Interest

The authors declare that they have no known competing financial interests or personal relationships that could have appeared to influence the work reported in this paper.

Acknowledgment

We thank Nicolas Dubourg for assistance with RPL-dosimetry. We kindly thank Lisa Rossbach, Kristine Bjerve Gützkow and Ann-Karin Olsen for their help with the experiments.

Funding

This work was supported by the Norwegian University of Life Sciences (NMBU) through a PhD scholarship and by the Research Council of Norway through its Centre of Excellence (CoE) "Centre for Environmental Radioactivity" (CERAD, project No. 223268). RG was supported by PNREST Anses, Cancer ITMO AVESIAN, 2015/1/212 project.

References

Adam-Guillermin, C., Hertal-Aas, T., Oughton, D., Blanchard, L., Alonzo, F., Armant, O., Horemans, N., 2018. Radiosensitivity and transgenerational effects in non-human species. Ann. ICRP 47 (3–4), 327–341 (0146645318756844).

Andux, S., Ellis, R.E., 2008. Apoptosis maintains oocyte quality in aging *Caenorhabditis elegans* females. PLoS Genet. 4, e1000295.

Angeles-Albores, D., Lee, R.Y., Chan, J., Sternberg, P.W., 2016. Tissue enrichment analysis for *C. elegans* genomics. BMC Bioinf. 17, 366.

Angeles-Albores, D., Leighton, D.H., Tsou, T., Khaw, T.H., Antoshechkin, I., Sternberg, P.W., 2017. The *Caenorhabditis elegans* female-like state: decoupling the transcriptomic effects of aging and sperm status. G3: Genes, Genomes, Genetics 7, 2969–2977.

Bailly, A., Gartner, A., 2013. Germ cell apoptosis and DNA damage responses. In: Schedl, T. (Ed.), Germ Cell Development in *C. elegans*. Springer New York, New York, NY.

Bjerke, H., Hetland, P.O., 2014. Dosimetri ved FIGARO gammaanlegget ved NMBU, ÅS. Målerapport fra oppmåling av doseraten i strålefeltet fra kobolt-60. NRPA Technical Document Series p. 2.

Boxem, M., Maliga, Z., Klitgord, N., Li, N., Lemmens, I., Mana, M., De Lichtervelde, L., Mul, J.D., Van De Peut, D., Devos, M., Simonis, N., Yildirim, M.A., Cokol, M., Kao, H.-L., De Smet, A.-S., Wang, H., Schlaitz, A.-L., Hao, T., Milstein, S., Fan, C., Tipsword, M., Drew, K., Galli, M., Rhrissorrakrai, K., Drechsel, D., Koller, D., Roth, F.P., Iakoucheva, L.M., Dunker, A.K., Bonneau, R., Gunsalus, K.C., Hill, D.E., Piano, F., Tavernier, J., Van Den Heuvel, S., Hyman, A.A., Vidal, M., 2008. A protein domain-based interactome network for *C. elegans* early embryogenesis. Cell 134, 534–545.

Bréchignac, F., Bradshaw, C., Carroll, S., Fuma, S., Håkanson, L., Jaworska, A., ... Sazykina, T., 2012. Towards an ecosystem approach for environment protection with emphasis on radiological hazards. *IUR*, Report 7.

Brenner, S., 1974. The genetics of *Caenorhabditis elegans*. Genetics 77, 71–94.

Buisset-Goussen, A., Goussen, B., Della-Vedova, C., Galas, S., Adam-Guillermin, C., Lecomte-Pradines, C., 2014. Effects of chronic gamma irradiation: a multigenerational study using *Caenorhabditis elegans*. J. Environ. Radioact. 137, 190–197.

Cheng, H., Govindan, J.A., Greenstein, D., 2008. Regulated trafficking of the MSP/Eph receptor during oocyte meiotic maturation in *C. elegans*. Curr. Biol. 18, 705–714.

Chu, D.S., Shakes, D.C., 2013. Spermatogenesis. Germ Cell Development in *C. elegans*. Springer.

Chu, D.S., Liu, H., Nix, P., Wu, T.F., Ralston, E.J., Yates III, J.R., Meyer, B.J., 2006. Sperm chromatin proteomics identifies evolutionarily conserved fertility factors. Nature 443, 101.

Clejan, I., Boerckel, J., Ahmed, S., 2006. Developmental modulation of nonhomologous end joining in *Caenorhabditis elegans*. Genetics 173, 1301–1317.

Cottee, P.A., Cole, T., Schultz, J., Hoang, H.D., Vibbert, J., Han, S.M., Miller, M.A., 2017. The C. elegans VAPB homolog VPR-1 is a permissive signal for gonad development. Development 144, 2187–2199.

Dobin, A., Davis, C.A., Schlesinger, F., Drenkow, J., Zaleski, C., Jha, S., Batut, P., Chaisson, M., Gingeras, T.R., 2013. STAR: ultrafast universal RNA-seq aligner. Bioinformatics 29, 15–21.

Dove, K.K., Kemp, H.A., Di Bona, K.R., Reiter, K.H., Milburn, L.J., Camacho, D., Fay, D.S., Miller, D.L., Klevit, R.E., 2017. Two functionally distinct E2/E3 pairs coordinate sequential ubiquitination of a common substrate in *Caenorhabditis elegans* development. Proc. Natl. Acad. Sci. 114, E6576–E6584.

Dubois, C., Lecomte, C., Ruys, S.P.D., Kuzmic, M., Della-Vedova, C., Dubourg, N., Galas, S., Frelon, S., 2018. Precoce and opposite response of proteasome activity after acute or chronic exposure of *C. elegans* to γ-radiation. Sci. Rep. 8, 11349.

Ehrenstein, G.V., Schierenberg, E., 1980. Cell lineages and development of *Caenorhabditis elegans* and other nematodes. Cell Lineages and Development of Caenorhabditis elegans and Other Nematodes, pp. 1–71.

Ellis, R.E., Stanfield, G.M., 2014. The regulation of spermatogenesis and sperm function in nematodes. Semin. Cell Dev. Biol. 17–30 Elsevier.

Engert, C.G., Droste, R., Van Oudenaarden, A., Horvitz, H.R., 2018. A *Caenorhabditis elegans* protein with a PRDM9-like SET domain localizes to chromatin-associated foci and promotes spermatocyte gene expression, sperm production and fertility. PLoS Genet. 14, e1007295.

Fabregat, A., Jupe, S., Matthews, L., Sidiropoulos, K., Gillespie, M., Garapati, P., Haw, R., Jassal, B., Korninger, F., May, B., 2017. The reactome pathway knowledgebase. Nucleic Acids Res. 46, D649–D655.

Franz, M., Rodriguez, H., Lopes, C., Zuberi, K., Montojo, J., Bader, G.D., Morris, Q., 2018. GeneMANIA update 2018. Nucleic Acids Res. 46, W60–W64.

Garnier-Laplace, J., Geras'kin, S., Della-Vedova, C., Beaugelin-Seiller, K., Hinton, T., Real, A., Oudalova, A., 2013. Are radiosensitivity data derived from natural field conditions consistent with data from controlled exposures? A case study of Chernobyl wildlife chronically exposed to low dose rates. J. Environ. Radioact. 121, 12–21.

Gartner, A., Milstein, S., Ahmed, S., Hodgkin, J., Hengartner, M.O., 2000. A conserved checkpoint pathway mediates DNA damage–induced apoptosis and cell cycle arrest in *C. elegans*. Mol. Cell 5, 435–443.

Gumienny, T.L., Lambie, E., Hartwieg, E., Horvitz, H.R., Hengartner, M.O., 1999. Genetic control of programmed cell death in the *Caenorhabditis elegans* hermaphrodite germline. Development 126, 1011–1022.

Guo, X., Sun, J., Bian, P., Chen, L., Zhan, F., Wang, J., Xu, A., Wang, Y., Hei, T.K., Wu, L., 2013. Radiation-induced bystander signaling from somatic cells to germ cells in *Caenorhabditis elegans*. Radiat. Res. 180, 268–275.

Gutzkow, K.B., Langleite, T.M., Meier, S., Graupner, A., Collins, A.R., Brunborg, G., 2013. High-throughput comet assay using 96 minigels. Mutagenesis 28, 333–340.

Hamill, D.R., Severson, A.F., Carter, J.C., Bowerman, B., 2002. Centrosome maturation and mitotic spindle assembly in *C. elegans* require SPD-5, a protein with multiple coiled-coil domains. Dev. Cell 3, 673–684.

Hansen, E., Lind, O., Oughton, D., Salbu, B., 2019. A framework for exposure characterization and gamma dosimetry at the NMBU FIGARO irradiation facility. Int. J. Radiat. Biol. 95, 82–89.

Harris, J.E., Govindan, J.A., Yamamoto, I., Schwartz, J., Kaverina, I., Greenstein, D., 2006. Major sperm protein signaling promotes oocyte microtubule reorganization prior to fertilization in *Caenorhabditis elegans*. Dev. Biol. 299, 105–121.

Hartman, P.S., Herman, R.K., 1982. Radiation-sensitive mutants of *Caenorhabditis elegans*. Genetics 102, 159–178.

Hartman, P.S., Simpson, V.J., Johnson, T., Mitchell, D., 1988. Radiation sensitivity and DNA repair in *Caenorhabditis elegans* strains with different mean life spans. Mutat. Res. Lett. 208, 77–82.

Hertel-Aas, T., Brunborg, G., Jaworska, A., Salbu, B., Oughton, D.H., 2011. Effects of different gamma exposure regimes on reproduction in the earthworm *Eisenia fetida* (*Oligochaeta*). Sci. Total Environ. 412-413, 138–147.

Hodgkin, J., Barnes, T.M., 1991. More is not better: brood size and population growth in a self-fertilizing nematode. Proc. R. Soc. Lond. B 246, 19–24.

Holway, A.H., Kim, S.-H., La Volpe, A., Michael, W.M., 2006. Checkpoint silencing during the DNA damage response in *Caenorhabditis elegans* embryos. J. Cell Biol. 172, 999–1008.

Huang, J., Wang, H., Chen, Y., Wang, X., Zhang, H., 2012. Residual body removal during spermatogenesis in *C. elegans* requires genes that mediate cell corpse clearance. Development 139, 4613–4622.

Jedrusik-Bode, M., 2013. Histone H1 and heterochromatin protein 1 (HP1) regulate specific gene expression and not global transcription. Worm 2, e23703.

Johnson, T.E., Hartman, P.S., 1988. Radiation effects on life span in *Caenorhabditis elegans*. J. Gerontol. 43, B137–B141.

Jones, D., Crowe, E., Stevens, T.A., Candido, E.P.M., 2001. Functional and phylogenetic analysis of the ubiquitylation system in *Caenorhabditis elegans*: ubiquitin-conjugating enzymes, ubiquitin-activating enzymes, and ubiquitin-like proteins. Genome Biol. 3, 1 research0002.

Kanehisa, M., Sato, Y., Furumichi, M., Morishima, K., Tanabe, M., 2018. New approach for understanding genome variations in KEGG. Nucleic Acids Res. 47, D590–D595.

Käser-Pébernard, S., Müller, F., Wicky, C.J.S.C.R., 2014. LET-418/Mi2 and SPR-5/LSD1 cooperatively prevent somatic reprogramming of *C. elegans* germline stem cells. 2, 547–559.

Katz, D.J., Edwards, T.M., Reinke, V., Kelly, W.G., 2009. A C. elegans LSD1 demethylase contributes to germline immortality by reprogramming epigenetic memory. Cell 137 (2), 308–320.

Kawasaki, M., Hisamoto, N., Iino, Y., Yamamoto, M., Ninomiya-Tsuji, J., Matsumoto, K., 1999. A *Caenorhabditis elegans* JNK signal transduction pathway regulates

coordinated movement via type-D GABAergic motor neurons. EMBO J. 18, 3604–3615.
Kim, Y.-I., Cho, J.H., Yoo, O.J., Ahnn, J., 2004. Transcriptional regulation and life-span modulation of cytosolic aconitase and ferritin genes in *C. elegans*. J. Mol. Biol. 342, 421–433.
Kimble, J., Hirsh, D., 1979. The postembryonic cell lineages of the hermaphrodite and male gonads in *Caenorhabditis elegans*. Dev. Biol. 70, 396–417.
Kovalchuk, O., Dubrova, Y.E., Arkhipov, A., Hohn, B., Kovalchuk, I., 2000. Germline DNA: wheat mutation rate after Chernobyl. Nature 407, 583.
Krisko, A., Leroy, M., Radman, M., Meselson, M., 2012. Extreme anti-oxidant protection against ionizing radiation in bdelloid rotifers. Proc. Natl. Acad. Sci. U. S. A. 109, 2354–2357.
Lans, H., Vermeulen, W., 2015. Tissue specific response to DNA damage: *C. elegans* as role model. DNA Repair (Amst) 32, 141–148.
Lecomte-Pradines, C., Hertel-Aas, T., Coutris, C., Gilbin, R., Oughton, D., Alonzo, F., 2017. A dynamic energy-based model to analyze sublethal effects of chronic gamma irradiation in the nematode *Caenorhabditis elegans*. J. Toxic. Environ. Health A 80, 830–844.
Lee, R.Y.N., Howe, K.L., Harris, T.W., Arnaboldi, V., Cain, S., Chan, J., Chen, W.J., Davis, P., Gao, S., Grove, C., Kishore, R., Muller, H.-M., Nakamura, C., Nuin, P., Paulini, M., Raciti, D., Rodgers, F., Russell, M., Schindelman, G., Tuli, M.A., Van Auken, K., Wang, Q., Williams, G., Wright, A., Yook, K., Berriman, M., Kersey, P., Schedl, T., Stein, L., Sternberg, P.W., 2017. WormBase 2017: molting into a new stage. Nucleic Acids Res. 46, D869–D874.
Lettre, G., Hengartner, M.O., 2006. Developmental cell biology: developmental apoptosis in *C. elegans*: a complex CEDnario. Nat. Rev. Mol. Cell Biol. 7, 97.
Lewis, J.A., Fleming, J.T., 1995. Chapter 1 basic culture methods. In: Epstein, H.F., Shakes, D.C. (Eds.), Methods in Cell Biology. Academic Press.
Lind, O.C., Helen Oughton, D., Salbu, B., 2019. The NMBU FIGARO low dose irradiation facility. Int. J. Radiat. Biol. 95, 76–81.
Lomax, M.E., Folkes, L.K., O'neill, P., 2013. Biological consequences of radiation-induced DNA damage: relevance to radiotherapy. Clin. Oncol. 25, 578–585.
Love, M.I., Anders, S., Kim, V., Huber, W., 2015. RNA-Seq workflow: gene-level exploratory analysis and differential expression. FResearch 4.
Lu, N., Yu, X., He, X., Zhou, Z., 2009. Detecting apoptotic cells and monitoring their clearance in the nematode *Caenorhabditis elegans*. Methods Mol. Biol. 559, 357–370.
Miller, M.A., Chin-Sang, I.D., 2012. Eph receptor signaling in C. elegans. *WormBook: The Online Review of C. elegans* Biology, p. 1.
Miller, M.A., Nguyen, V.Q., Lee, M.-H., Kosinski, M., Schedl, T., Caprioli, R.M., Greenstein, D., 2001. A sperm cytoskeletal protein that signals oocyte meiotic maturation and ovulation. Science 291, 2144–2147.
Min, H., Sung, M., Son, M., Kawasaki, I., Shim, Y.-H., 2017. Transgenerational effects of proton beam irradiation on *Caenorhabditis elegans* germline apoptosis. Biochem. Biophys. Res. Commun. 490, 608–615.
National, Research, Council, 2006. Health Risks From Exposure to Low Levels of Ionizing Radiation: BEIR VII Phase 2. National Academies Press.
Ng, L.F., Ng, L.T., Van Breugel, M., Halliwell, B., Gruber, J., 2019. Mitochondrial DNA damage does not determine *C. elegans* lifespan. Front. Genet. 10.
Nottke, A.C., Beese-Sims, S.E., Pantalena, L.F., Reinke, V., Shi, Y., Colaiácovo, M.P., 2011. SPR-5 is a histone H3K4 demethylase with a role in meiotic double-strand break repair. Proc. Natl. Acad. Sci. 108, 12805–12810.
Ortiz, M.A., Noble, D., Sorokin, E.P., Kimble, J., 2014. A new dataset of spermatogenic vs. oogenic transcriptomes in the nematode *Caenorhabditis elegans*. Genes, Genomes, Genetics 4, 1765–1772.
Parisot, F., Bourdineaud, J.-P., Plaire, D., Adam-Guillermin, C., Alonzo, F., 2015. DNA alterations and effects on growth and reproduction in *Daphnia magna* during chronic exposure to gamma radiation over three successive generations. Aquat. Toxicol. 163, 27–36.
Pazdernik, N., Schedl, T., 2013. Introduction to Germ Cell Development in *Caenorhabditis elegans*. *Germ Cell Development in C. elegans*. Springer.
Pereira, S., Bourrachot, S., Cavalie, I., Plaire, D., Dutilleul, M., Gilbin, R., Adam-Guillermin, C., 2011. Genotoxicity of acute and chronic gamma-irradiation on zebrafish cells and consequences for embryo development. Environ. Toxicol. Chem. 30, 2831–2837.
Poulin, G., Dong, Y., Fraser, A.G., Hopper, N.A., Ahringer, J., 2005. Chromatin regulation and sumoylation in the inhibition of Ras-induced vulval development in *Caenorhabditis elegans*. EMBO J. 24, 2613–2623.
Reisz, J.A., Bansal, N., Qian, J., Zhao, W., Furdui, C.M., 2014. Effects of ionizing radiation on biological molecules—mechanisms of damage and emerging methods of detection. Antioxid. Redox Signal. 21, 260–292.
Sadler, P.L., Shakes, D.C., 2000. Anucleate *Caenorhabditis elegans* sperm can crawl, fertilize oocytes and direct anterior-posterior polarization of the 1-cell embryo. Development 127, 355–366.
Samson, M., Jow, M.M., Wong, C.C., Fitzpatrick, C., Aslanian, A., Saucedo, I., Estrada, R., Ito, T., Park, S.-K.R., Yates III, J.R., 2014. The specification and global reprogramming of histone epigenetic marks during gamete formation and early embryo development in *C. elegans*. PLoS Genet. 10, e1004588.
Schumacher, B., Hofmann, K., Boulton, S., Gartner, A., 2001. The *C. elegans* homolog of the p53 tumor suppressor is required for DNA damage-induced apoptosis. Curr. Biol. 11, 1722–1727.
Schumacher, B., Schertel, C., Wittenburg, N., Tuck, S., Mitani, S., Gartner, A., Conradt, B., Shaham, S., 2005. *C. elegans* ced-13 can promote apoptosis and is induced in response to DNA damage. Cell Death Differ. 12, 153.
Schwartz, J.L., Jordan, R., Sun, J., Ma, H., Hsie, A.W., 2000. Dose-dependent changes in the spectrum of mutations induced by ionizing radiation. Radiat. Res. 153, 312–317.
Singson, A., 2001. Every sperm is sacred: fertilization in *Caenorhabditis elegans*. Dev. Biol. 230, 101–109.
Smith, H., 2006. Sperm motility and MSP. WormBook 2006, 1–8.
Stiernagle, T., 2006. Maintenance of *C. elegans* (February 11, 2006). In: Wormbook (Ed.), The *C. elegans* Research Community. WormBook https://doi.org/10.1895/wormbook (1.101. 1).
Strober, W., 2015. Trypan blue exclusion test of cell viability. Curr. Protoc. Immunol. 111, A3. B. 1–A3. B. 3.
Sumiyoshi, E., Fukata, Y., Namai, S., Sugimoto, A., 2015. *Caenorhabditis elegans* Aurora A kinase is required for the formation of spindle microtubules in female meiosis. Mol. Biol. Cell 26, 4187–4196.
Turcotte, C.A., Sloat, S.A., Rigothi, J.A., Rosenkranse, E., Northrup, A.L., Andrews, N.P., Checchi, P.M., 2018. Maintenance of genome integrity by Mi2 homologs CHD-3 and LET-418 in *Caenorhabditis elegans*. Genetics 208, 991–1007.
Tyc, K.M., Nabih, A., Wu, M.Z., Wedeles, C.J., Sobotka, J.A., Claycomb, J.M., 2017. The conserved intron binding protein EMB-4 plays differential roles in germline small RNA pathways of *C. elegans*. Dev. Cell 42 (e6), 256–270.
UNSCEAR, 1996. Sources and Effects of Ionizing Radiation: Report to the General Assembly, With Scientific Annexes. United Nations Publications.
UNSCEAR, 2006. Effects of Ionizing Radiation: UNSCEAR 2006 Report to the General Assembly, With Scientific Annexes. United Nations Publications.
Van Haaften, G., Romeijn, R., Pothof, J., Koole, W., Mullenders, L.H.F., Pastink, A., Plasterk, R.H.A., Tijsterman, M., 2006. Identification of conserved pathways of DNA-damage response and radiation protection by genome-wide RNAi. Curr. Biol. 16, 1344–1350.
Vermezovic, J., Stergiou, L., Hengartner, M.O., D'adda Di Fagagna, F., 2012. Differential regulation of DNA damage response activation between somatic and germline cells in *Caenorhabditis elegans*. Cell Death Differ. 19, 1847–1855.
Warde-Farley, D., Donaldson, S.L., Comes, O., Zuberi, K., Badrawi, R., Chao, P., Franz, M., Grouios, C., Kazi, F., Lopes, C.T., 2010. The GeneMANIA prediction server: biological network integration for gene prioritization and predicting gene function. Nucleic Acids Res. 38, W214–W220.
Weber, Stephanie C., Brangwynne, Clifford P., 2015. Inverse size scaling of the nucleolus by a concentration-dependent phase transition. Curr. Biol. 25, 641–646.
Wood, W.B., 1988. In: Wood, W.B. (Ed.), Embryology in the Nematode *C. elegans*. Cold Spring Harbor Laboratory Press, pp. 215–241 Chapter 8.
Zhou, Z., Hartwieg, E., Horvitz, H.R., 2001. CED-1 is a transmembrane receptor that mediates cell corpse engulfment in *C. elegans*. Cell 104, 43–56.

Supporting Material 1.

Gamma radiation induces Life stage-dependent reprotoxicity in *Caenorhabditis elegans* via impairment of spermatogenesis

Erica Maremonti [1], Dag M. Eide [1,2], Deborah H. Oughton [1], Brit Salbu [1], Fabian Grammes [3], Yetneberk A. Kassaye [1], Rémi Guédon [4], Catherine Lecomte-Pradine [4], Dag Anders Brede [1]

[1] Centre for Environmental Radioactivity (CERAD), Faculty of Environmental Sciences and Natural Resource Management (MINA) Norwegian University of Life Sciences (NMBU), 1432 Ås, Norway

[2] Norwegian Institute of Public Health, Lovisenberggata 8, 0456 Oslo, Norway

[3] Centre for Integrative Genetics (CIGENE), Faculty of Biosciences (BIOVIT), Norwegian University of Life Sciences (NMBU), 1432, Ås, Akershus, Norway.

[4] Institut de Radioprotection et de Sûreté Nucléaire (IRSN), PRP-ENV, SERIS, Laboratoire d'ECOtoxicologie des radionucléides (LECO), Cadarache, France

*Corresponding author: erica.maremonti@nmbu.no

S. 1. Assessment of morphological and developmental effects

To examine radiation-induced morphological changes, at 72 hours of development from L1 stage, treated animals (n=10 per treatment) were anesthetized using 30 mM of NaN_3, placed onto 2% agarose pads, and observed using a semi-automated research light microscope (at 20X or 40X, phase-contrast optics) (Upright Microscope Leica DM6 B).

Adverse effects on the nematodes development were further evaluated by measuring the total body length of ten individuals per treatment every 24 hours from L1 stage and until 96 hours of exposure (**Table S.2** for dosimetry). For this purpose, treated nematodes were stained with 1 ml Rose Bengal (0.3 $g \cdot L^{-1}$) at 80 °C for 10 min, according to ISO guideline (International Organization for Standardization, n. 10872, 2010) . NGM plates were finally stored at 4 °C and worms (n=10 per each treatment) were randomly imaged under a stereo microscope (Leica M205C, 10X magnification) coupled with a computer-connected camera. The body length was measured by using the Leica software, provided with an auto calibrated micrometer scale bar.

Chronic exposure to Gamma radiation induces minor dose rate-dependent effects on growth and development

In order to investigate toxicological and adverse phenotypic effects, synchronized L1 stage larvae were subjected to chronic gamma radiation exposure at dose rates ranging from 0.43 to 99.9 mGy·hr^{-1} (**Table S.2**).

After 72 hours of irradiation from L1 stage, when nematodes were scored for morbid phenotypes, no obvious morphological alteration was detected in any of the exposed nematodes (**Fig. S.1.a**). However, analysis of nematodes irradiated at 99.9 mGy·hr^{-1} for 96 hours, and for some individuals we observed vacuole-like structures occupying the space where the vulva cells should be (see **Fig S.1.a**, vulva), consistent with previously observations by Weidhaas et al. (2006).

Effects on growth were assessed in continuously exposed nematodes during development, by monitoring the body size every 24 hours from L1 molt to adult stage (96 hours). After 24 hours of irradiation the total body length of nematodes exposed to 99.9 mGy·hr^{-1} showed to be significantly lower (9% reduction, Tukey *post hoc, p*-value < 0.05) in comparison to control nematodes (**Fig. 2**). A significant increase (9 and 11%) of the total body length was recorded at 0.43 and 1.1 mGy·hr^{-1}, respectively (Tukey *post hoc, p*-value < 0.05). These significant differences on the total body size were no longer observed at 48, 72 and 96 hours of exposure (p-value > 0.05), in comparison with non-irradiated nematodes when Tukey *post hoc test* was performed. Nevertheless, after 96 hours of irradiation there was a tendency towards reduced size, as nematodes exposed to 40.8 or 99.9 mGy·hr^{-1} showed a reduction of 8% on their total body length, compared to control nematodes (Tukey *post hoc, p*-value < 0.1)(**Fig. S.1.b**).

No significant effects were found in nematodes exposed for a shorter period and at lower cumulative doses, when different stages of development were targeted (data not shown).

Table S.1. Dose-rates and total doses of exposure used for assessing mortality, morbidity and reprotoxic effects under different scenarios of exposure.

Total dose (Gy)							
Mortality - Morbidity - Reproduction experiments							
Dose rate ($mGy \cdot hr^{-1}$)	62 hrs	0.75-2-4 hrs	Dose rate ($mGy \cdot hr^{-1}$)	192 hrs	43 hrs	143 hrs	13 hrs
	Chronic	Acute		Sc.1	Sc.2	Sc.3	Sc.4
0	0	0	**0**	0	0	0	0
0.9	0.06	-	**0.43**	0.08	0.02	0.06	0.01
3.6	0.23	-	**1.1**	0.21	0.05	0.16	0.01
8.4	0.52	-	**10.8**	2.07	0.46	1.61	0.14
37.4	2.32	-	**40.8**	7.83	1.75	6.08	0.53
107.6	6.67	-	**99.9**	19.18	4.30	14.89	1.30
227.9	14.13	-					
1410.6		1.06					
1435.3		2.87					
1490		5.96					

Table S.2. Dose-rates and total doses of exposure used for assessing effects on somatic growth under different scenarios of exposure.

	Total dose (Gy)			
Dose rate ($mGy \cdot hr^{-1}$)	Irradiation time during somatic growth experiment (hrs)			
	24	**48**	**72**	**96**
0	0.00	0.00	0.00	0.00
0.43	0.01	0.02	0.03	0.04
1.1	0.03	0.05	0.08	0.11
10.8	0.26	0.52	0.78	1.04
40.8	0.98	1.96	2.94	3.92
99.9	2.40	4.80	7.19	9.59

Table S.3. Dose-rates and total doses of exposure used for assessing germ-cell apoptosis, embryonic DNA-damage and effects on the progeny (F1) of irradiated nematodes, number of spermatids and gene expression in L4/young adult hermaphrodites.

Apoptosis - Comet assay - Effects on F1 nematodes		Sperm count		Gene expression	
Dose rate ($mGy \cdot hr^{-1}$)	Total dose after 72 hrs (Gy)	Dose rate ($mGy \cdot hr^{-1}$)	Total dose after 72 hrs (Gy)	Dose rate ($mGy \cdot hr^{-1}$)	Total dose after 48 hrs (Gy)
0	0.00	**0**	0	**0**	0
0.43	0.03	-	-	-	-
1.1	0.08	-	-	-	-
10.8	0.78	**8**	0.58	**8**	0.38
40.8	2.94	**38.9**	2.81	-	-
99.9	7.19	**100.9**	7.26	**100.9**	4.84

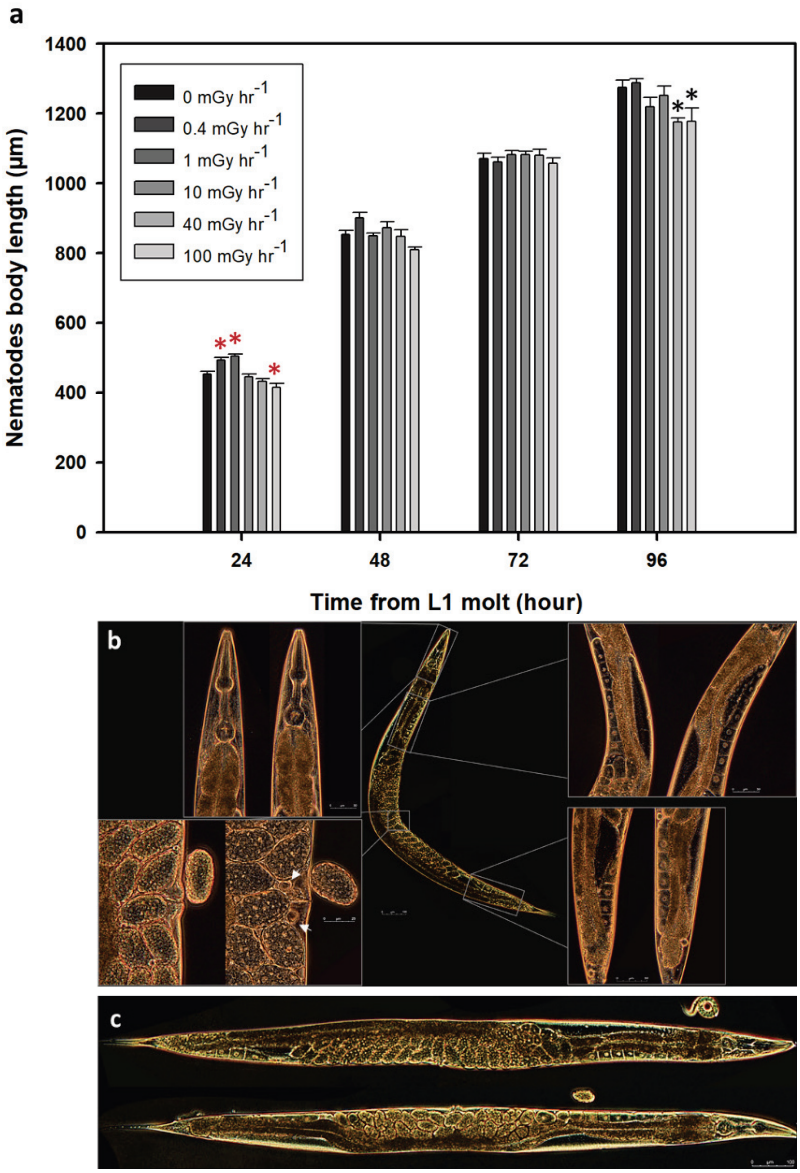

Figure S.1. a) Effects on somatic growth (total body length in µm) measured on nematodes exposed to chronic doses of ionizing radiation every 24 hours from L1 stage using a stereo microscope (Leica M205C) coupled with a computer-connected camera. Red and black asterisks indicate significant difference compared to control treatment at p-values <0.05 or <0.1 respectively. **b)** Morphological and developmental effects assessed in young adult hermaphrodites (middle) after 72 hours of exposure from L1 stage to chronic doses of ionizing radiation (Left: Control, Right: 100 mGy·hr-1) using a semi-automated research light microscope (from top-left: pharynx, anterior-posterior gonads and vulva, at 10X, 20X or 40X, phase-contrast optics, Scale bar 25, 50 or 100 µm). From Up-left micrographs of Pharynx, Anterior gonads, Posterior gonads and Vulva with laid embryo. White arrows

radiation (**UP**: Control, **Bottom**: 100 mGy·hr-1) using a semi-automated research light microscope (10X, phase-contrast optics, Scale bar 100 μm).

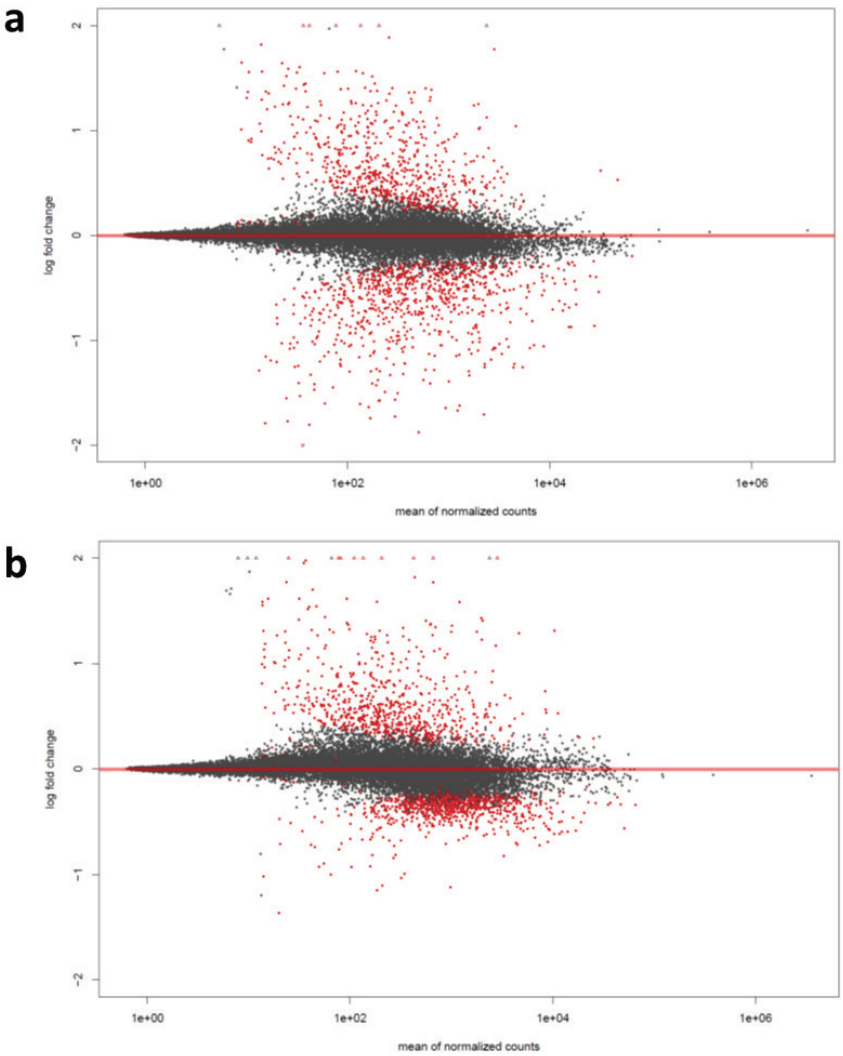

Fig. S.2. MA plot of the total number of 1.75×10^3 genes resulting from 10 **(a)** and 100 mGy·hr^{-1} **(b)** exposure groups compared to control. An average of 55 ± 12 million pair-end reads were mapped from both irradiated and non-irradiated groups. Red dots represent differentially expressed genes (DEGs) (FDR <0.05).

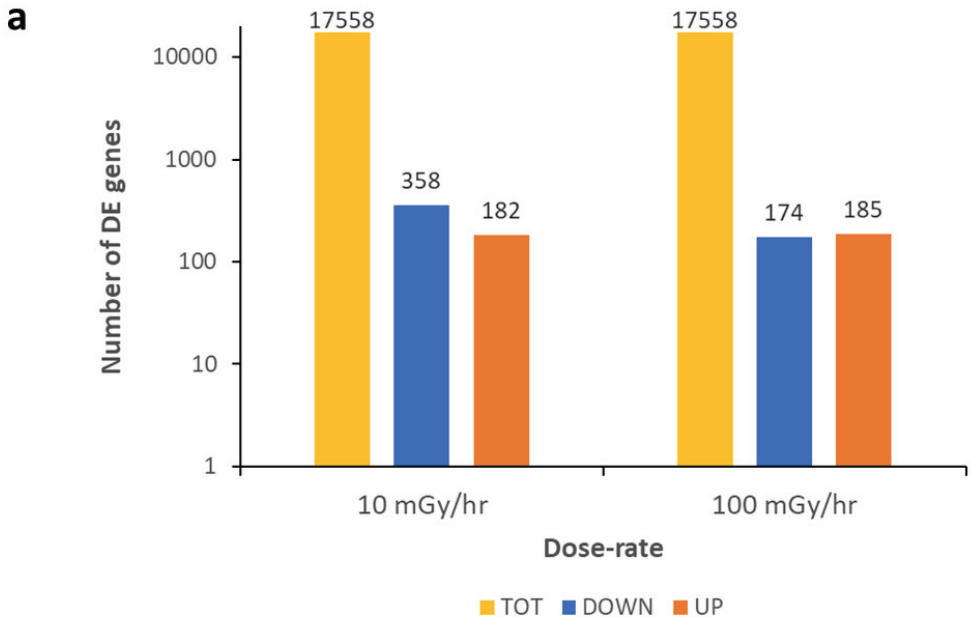

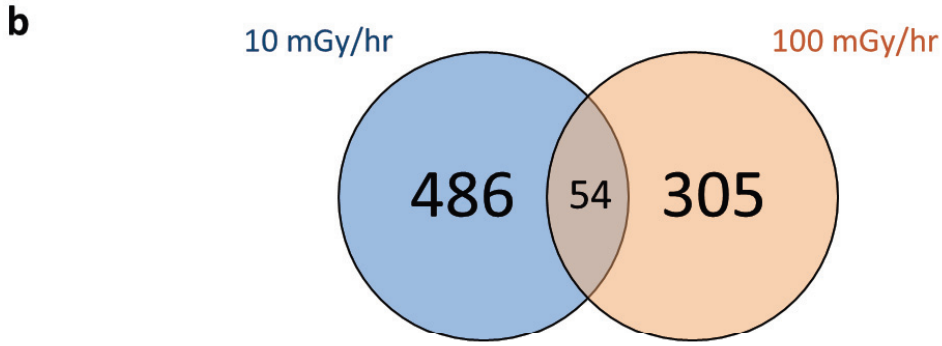

Figure S.3. a) Expressed and differentially expressed (DE) genes after 48 hours of exposure to 10 and 100 mGy·hr^{-1}. Threshold set to FC ± 1.2 and False Discovery Rate (FDR) <0.05. Total number of expressed genes (yellow), down-regulated genes (blue) and up-regulated genes (red). **b)** Venn diagram of common and unique sets of DEGs between two exposure treatments (10 and 100 mGy·hr^{-1} in blue and orange respectively).

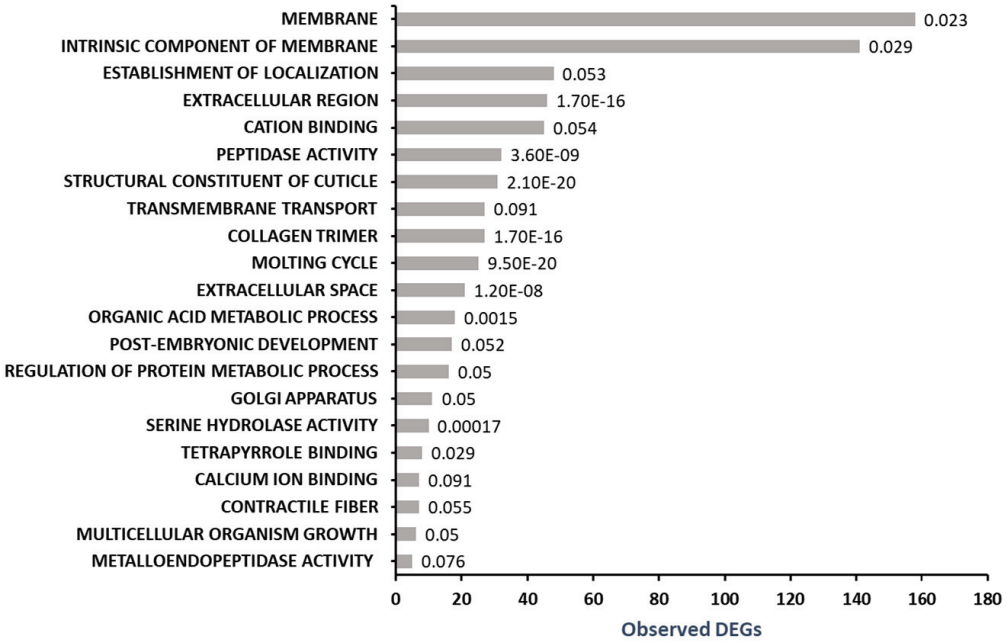

Figure S.4. Functional categories of over-represented Gene Ontology (GO) biological processes that were down regulated in *C. elegans* after 48 hours of exposure to 10 mGy·hr^{-1} of gamma radiation. Hypergeometric probability distribution is adopted to measure the number of enriched terms (observed number of DEGs in each specific function).
(Data labels indicate *q*-values).

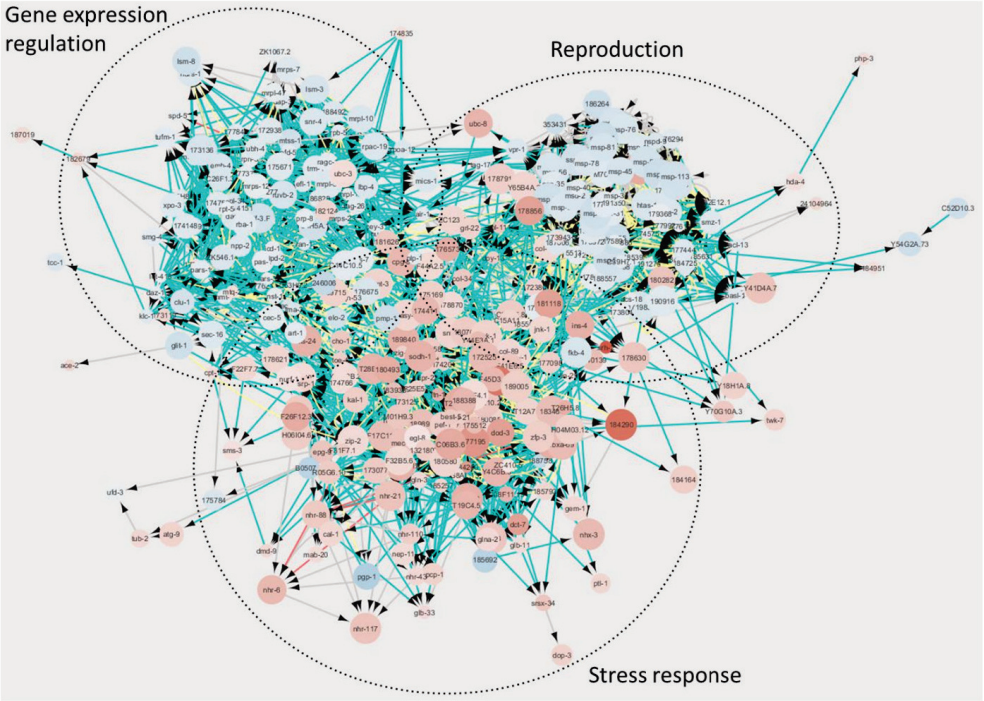
Gene expression regulation
Reproduction
Stress response

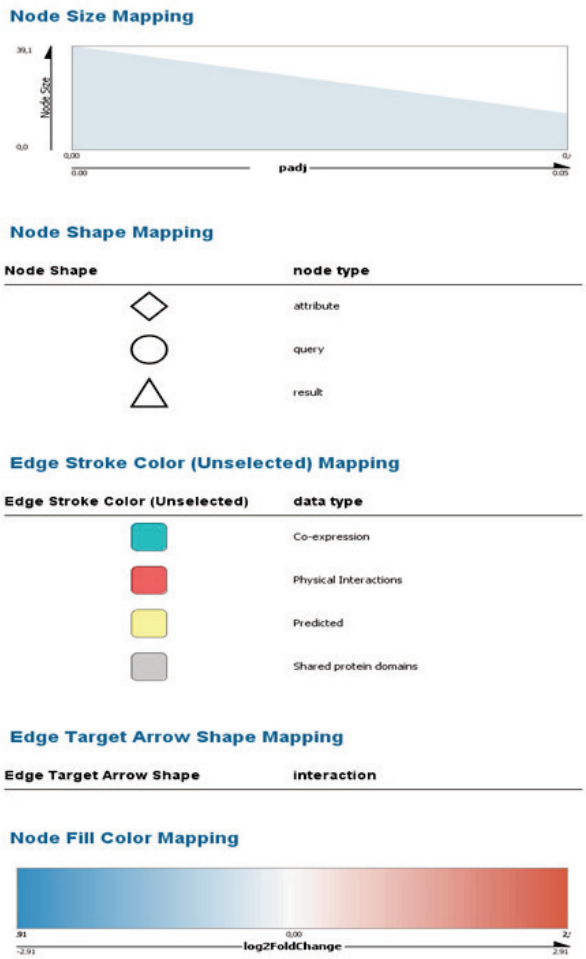

Figure S.5. Network analysis of 331 DEGs resulting from exposure to 100 mGy·hr^{-1} of gamma radiation. Dotted line circles indicate separation into the three main subset gene networks identified by Genemania plug-in within the software Cytoscape.

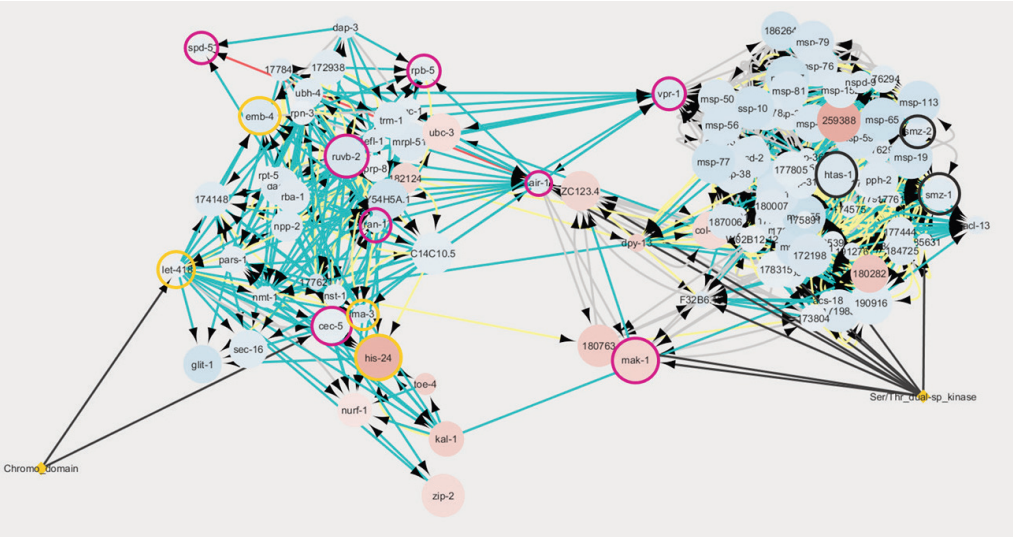

Node Size Mapping

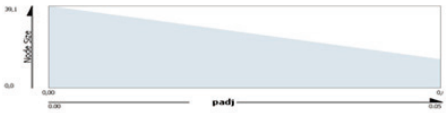

Node Shape Mapping

Node Shape	node type
◇	attribute
○	query
△	result

Edge Stroke Color (Unselected) Mapping

Edge Stroke Color (Unselected)	data type
	Co-expression
	Physical Interactions
	Predicted
	Shared protein domains

Edge Target Arrow Shape Mapping

Edge Target Arrow Shape	interaction

Node Fill Color Mapping

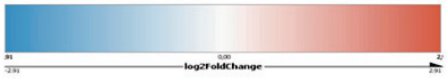

Figure S.6. Network analysis of genes involved in chromatin remodeling (yellow circles), spindle formation, gonad development (pink circles) and sperm meiosis/maturation (black circles) resulting from exposure to 100 mGy·hr^{-1} of gamma radiation.

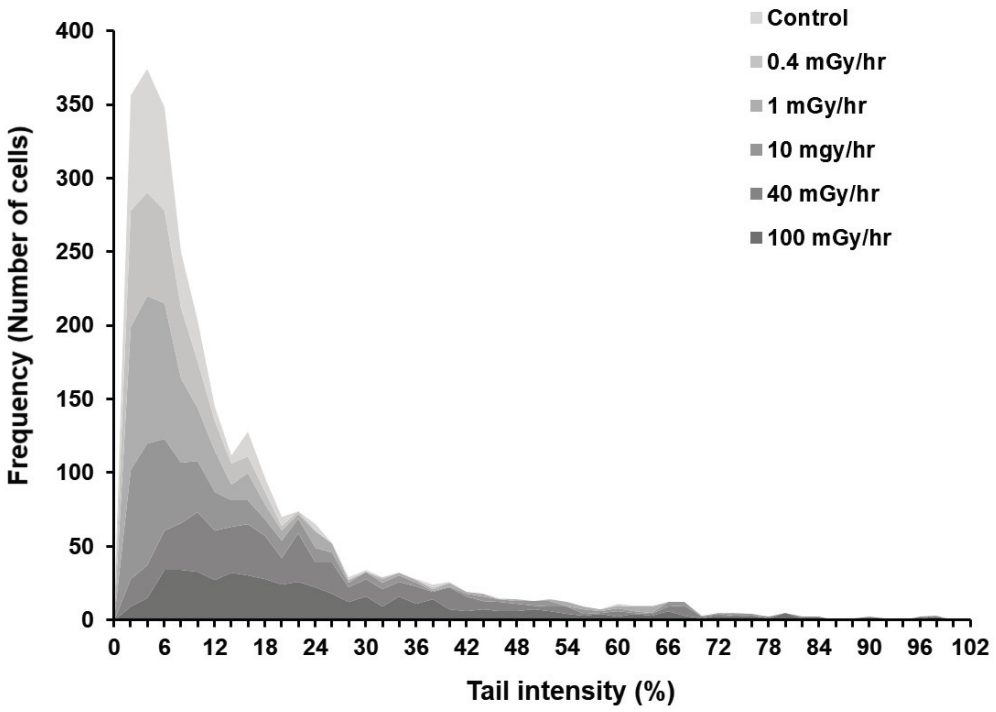

Figure S.7. Frequency of cell tail intensity distribution assessed via Comet assay in *C. elegans* embryos parentally irradiated to chronic doses of ionizing radiation.

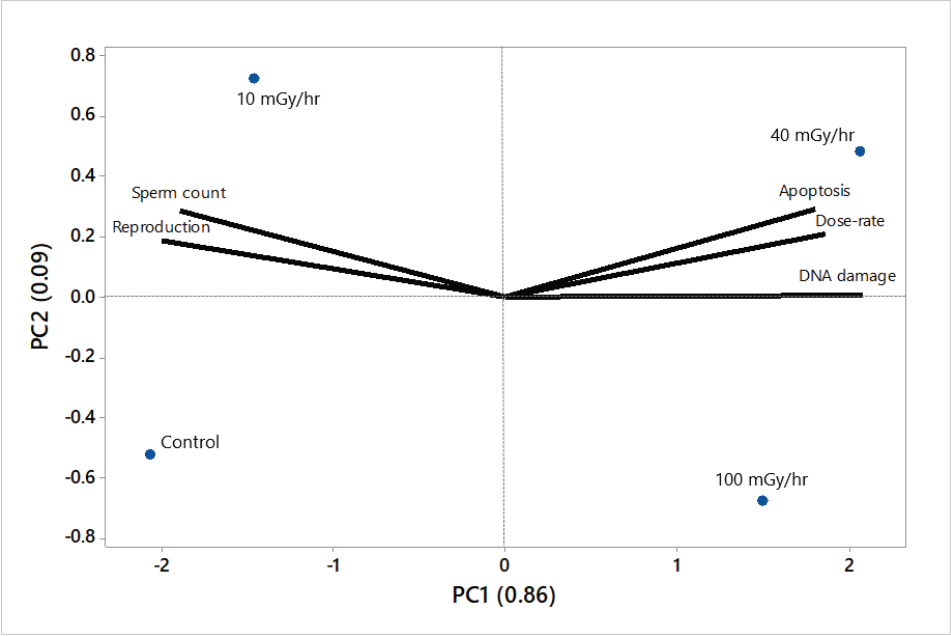

Figure S.8. Principal Component Analysis of selected endpoints assessed after chronic exposure to gamma radiation in the nematode *C. elegans*, showing negative correlation between Reproduction/Sperm count, Apoptosis, Dose-rate and DNA damage and positive correlation between Reproduction and Sperm count.

Table S. 6. Total number of offspring per adult hermaphrodite (Mean ± SE) measured after chronic or acute exposure to ionizing gamma radiation. Asterisk indicates significant difference from control treatment (*p*-value < 0.05).

Condition of irradiation	No. of larvae/individual (Mean ± SE)									
	0 mGy/hr	0.9 mGy/hr	3.6 mGy/hr	8.4 mGy/hr	37.4 mGy/hr	107.6 mGy/hr	227.9 mGy/hr	1410.6 mGy/hr	1435.3 mGy/hr	1490 mGy/hr
Chronic	224.8 ± 9	208 ± 19	211 ± 13	214 ± 16	198 ± 16	128 ± 17*	88 ± 11*	-	-	-
Acute	182 ± 19							195 ± 34	198 ± 14	214 ± 5

Table S. 7. Total number of offspring per adult hermaphrodite (Mean ± SE) measured after four different scenarios of exposure to chronic doses of ionizing radiation. Asterisk indicates significant difference from control treatment (*p*-value < 0.05).

Condition of irradiation	No. of larvae/individual (Mean ± SE)					
	0 mGy/hr	0.43 mGy/hr	1.1 mGy/hr	10.8 mGy/hr	40.8 mGy/hr	99.9 mGy/hr
L1 - Adult	269 ± 16.6	240 ± 24	287 ± 7	279 ± 19	171 ± 15*	182 ± 10*
L1 - Young L4	270 ± 16.6	234 ± 31	242 ± 10	275 ± 17	212 ± 18	175 ± 23*
Young L4 - Adult	271 ± 16.6	249 ± 8	248 ± 15	292 ± 6	287 ± 5	291 ± 5
L3 - Young L4	272 ± 16.6	285 ± 6	291 ± 8	283 ± 26	281 ± 8	269 ± 4

Table S. 8. Number of spermatids per spermatheca (Mean) in young adult hermaphrodites (72 hours from L1 stage). Asterisk indicates significant difference compared to control treatment (*p*-value <0.05).

Dose-rate (mGy/hr)	Total dose (mGy)	No. of spermatids/spermatheca (Mean)	CI (95%)
0	0	60.95	4.68
8	0.58	67.47	5.27
38.9	2.81	40.38*	5.1
100.9	7.26	46.93*	5.46

Table S. 9. Total number of offspring per adult hermaphrodite (Mean ± SE) and total body length (Mean ± SE), measured in F1 nematodes parentally irradiated to different dose-rate of ionizing gamma radiation. Asterisk indicates significant difference from control treatment (*p*-value < 0.05).

Dose-rate (mGy/hr)	No. of larvae/individual (Mean)	SE	Total body length (mm)	SE
0	295.6	22.6	1.462	0.03
0.43	298.0	35.8	1.357*	0.03
1.1	295.7	9.7	1.3015*	0.03
10.8	287.6	12.9	1.2955*	0.01
40.8	269.9	14.5	1.3512*	0.01
99.9	272.6	19.9	1.3037*	0.02

References

International Organization for Standardization *(ISO)* 2010. Water quality—Determination of the toxic effect of sediment and soil samples on growth, fertility and reproduction of *Caenorhabditis elegans(Nematoda) 10872:2010*.

WEIDHAAS, J., EISENMANN, D., HOLUB, J. & NALLUR, S. 2006. A *Caenorhabditis elegans* tissue model of radiation-induced reproductive cell death. *Proceedings of the National Academy of Sciences,* 103**,** 9946-9951.

Pathway analysis	Ensamble ID	Gene name	Annotation	q-value	log_2FC
Cuticle-Collagen					
	WBGene00000749	col-176	COLlagen	0.029421212	-1.356262716
	WBGene00000606	col-17	COLlagen	1.60E-05	-1.049929221
	WBGene00000649	col-73	COLlagen	0.000462723	-0.842774792
	WBGene00000683	col-109	COLlagen	0.000114273	-0.83545642
	WBGene00000639	col-63	COLlagen	0.005213502	-0.83070014
	WBGene00000684	col-110	COLlagen	0.029162398	-0.807077269
	WBGene00000625	col-48	COLlagen	0.000785287	-0.702528432
	WBGene00000672	col-97	COLlagen	0.010997706	-0.69997479
	WBGene00000711	col-138	COLlagen	0.019832004	-0.698848506
	WBGene00000626	col-49	COLlagen	2.49E-05	-0.667666949
	WBGene00000755	col-182	COLlagen	0.022920046	-0.60784418
	WBGene00000748	col-175	COLlagen	0.009758625	-0.594351121
	WBGene00000742	col-169	COLlagen	0.049574492	-0.571543661
	WBGene00000615	col-38	COLlagen	0.039723735	-0.501625924
	WBGene00022591	cuti-1	CUTicle and epithelial Integrity	0.026426498	-1.030034295
	WBGene00005018	sqt-3	Cuticle collagen 1	3.10E-05	-1.232519516
	WBGene00000599	col-10	Cuticle collagen 10	0.030827384	-0.512417659
	WBGene00004398	rol-8	Cuticle collagen 6	0.000271573	-1.217906086
	WBGene00000251	bli-1	Cuticle collagen bli-1	7.57E-05	-1.661494223
	WBGene00001064	dpy-2	Cuticle collagen dpy-2	0.004967922	-1.549680081
	WBGene00001067	dpy-5	Cuticle collagen dpy-5	0.000867492	-0.679075962
	WBGene00001069	dpy-7	Cuticle collagen dpy-7	0.013422442	-1.328328985
	WBGene00003057	lon-3	Cuticle collagen lon-3	5.42E-11	-1.718550619
	WBGene00005016	sqt-1	Cuticle collagen sqt-1	1.54E-06	-1.253553104
	WBGene00013960	cutl-8	CUTiclin-Like	0.005686441	-0.8094778
	WBGene00011888	cutl-15	CUTiclin-Like	3.63E-05	-0.70548195
	WBGene00017351	cutl-5	CUTiclin-Like	0.024305783	-0.546270686
	WBGene00001065	dpy-3	DumPY: shorter than wild-type	0.001622128	-1.602607707
	WBGene00001073	dpy-11	DumPY: shorter than wild-type	0.001408533	-0.966704484
Energy Metabolism					
	WBGene00000928	dao-2	Dauer or Aging adult Overexpression	6.66E-05	-1.649412217
	WBGene00000930	dao-4	Dauer or Aging adult Overexpression	6.65E-05	-1.045818187
	WBGene00000929	dao-3	Dauer or Aging adult Overexpression	0.000841848	-0.595404862
	WBGene00003254	mig-23	Nucleoside-diphosphatase mig-23	0.023420205	-0.389694104
	WBGene00003731	nhx-3	Probable Na(+)/H(+) antiporter nhx-3	0.000367636	0.85194663
	WBGene00007848	cytb-5.1	Cytochrome B	0.047499527	-0.411655567
	WBGene00007942	idh-2	Isocitrate dehydrogenase [NADP]	0.007187994	-0.504615694
	WBGene00018682	aagr-4	Acid Alpha Glucosidase Relate	3.59E-05	-1.003473152
	WBGene00020307	T07D3.4	Orthologous to the human gene, Fukutin	0.017679645	-0.650920054
	WBGene00020491	T13G4.4	Predicted to have metal ion binding activity and methyltransferase activity	0.02603419	-0.451192387
	WBGene00007964	cyp-25A2	CYtochrome P450 family	1.99E-05	-1.180958277
	WBGene00008564	acox-1.1	Acyl-coenzyme A oxidase	0.013989087	-0.696593952
	WBGene00008732	F13B12.4	Putative pyridoxal-phosphate dependent protein F13B12.4	0.001302026	-0.693569176
	WBGene00010924	M153.1	Predicted to have pyrroline-5-carboxylate reductase activity	0.017381287	-0.512893305
	WBGene00013585	cyp-42A1	CYtochrome P450 family	0.017473063	-0.98009234
	WBGene00015894	acdh-2	Acyl CoA DeHydrogenase	0.005328346	1.099522227
	WBGene00019967	cyp-33C8	CYtochrome P450 family	0.003703653	0.797419283
	WBGene00020107	R151.2	Orthologous to the human gene PHOSPHORIBOSYL PYROPHOSPHATE SYNTHETASE 1	0.043796666	-0.486110034
	WBGene00020215	T04G9.4	Orthologous to the human gene, Fukutin	0.003056057	-0.649231368
	WBGene00077701	poml-3	PON (paraoxonase) and MEC-6 Like	0.041533638	0.532087931
Metabolism of proteins					
	WBGene00004270	rab-6.2	Ras-related protein Rab-6.2	0.008007338	-0.4692537
	WBGene00015734	copd-1	Probable coatomer subunit delta	0.026207217	-0.427236613
	WBGene00009674	nucb-1	NUCleoBindin homolog	0.009189867	-0.452734267
	WBGene00007507	C10C5.3	Aminoacylase	0.026847049	0.866689785
	WBGene00004025	phy-2	Prolyl 4-hydroxylase subunit alpha-2	0.010208732	-0.765982128
	WBGene00008435	glna-2	Putative glutaminase 2	0.042993653	0.457614431
	WBGene00009177	F26H9.5	Probable phosphoserine aminotransferase	1.40E-05	-0.68167274
	WBGene00011938	alh-13	Glutamate 5-kinase	7.44E-05	-1.080973304
	WBGene00016201	tdo-2	Tryptophan 2.3-dioxygenase	1.22E-05	-0.86595332
	WBGene00022176	Y71H2AM.11	Predicted to have dipeptidase activity and metal ion binding activity	0.042279569	-0.425409751
	WBGene00002065	iff-2	Eukaryotic translation initiation factor 5A-2	0.000874492	-0.735218489
	WBGene00008547	F07A11.4	Ubiquitin carboxyl-terminal hydrolase	0.040431999	-0.441478504
	WBGene00003497	mup-4	Transmembrane matrix receptor MUP-4	0.01732802	-0.460011681
	WBGene00007703	gbf-1	Ortholog of human GBF1; is predicted to have ARF guanyl-nucleotide exchange factor activity	0.035761966	-0.382349522
	WBGene00003963	pdi-2	Protein disulfide-isomerase 2	0.019606875	-0.678982858
	WBGene00001169	eef-1A.2	Elongation factor 1-alpha	0.048610242	-0.758994378
	WBGene00001646	gna-1	Glucosamine 6-phosphate N-acetyltransferase	0.000256973	-0.880123832
	WBGene00000039	acn-1	Inactive angiotensin-converting enzyme-related protein	0.000902991	-0.839263639
	WBGene00018533	F47B7.2	Sulfhydryl oxidase	0.002156267	-0.638213739
	WBGene00018853	sec-22	Yeast SEC homolog	0.005903339	-0.688659607
	WBGene00015168	pdi-6	Protein disulfide-isomerase A6 homolog	0.025089958	-0.509474836
Metabolism of lipids					
	WBGene00016934	mboa-3	Membrane Bound O-Acyl transferase. MBOAT	0.029615679	-0.511462334
	WBGene00007210	agmo-1	Alkylglycerol monooxygenase	6.66E-05	-0.579081913
	WBGene00000198	art-1	Probable very-long-chain enoyl-CoA reductase art-1	0.022227467	-0.324921045
	WBGene00004259	pyr-1	Glutamine-dependent carbamoyl-phosphate synthase	0.010762796	-0.667966923
	WBGene00077701	poml-3	PON (paraoxonase) and MEC-6 Like	0.041533638	0.532087931
	WBGene00008564	acox-1.1	Acyl-coenzyme A oxidase	0.013989087	-0.696593952
	WBGene00008607	F09B12.3	Putative phospholipase B-like 2	0.027361574	-0.683799095
	WBGene00007964	cyp-25A2	Cytochrome P450 family	1.99E-05	-1.180958277
	WBGene00013197	ttm-5	Putative sphingolipid delta(4)-desaturase/C4-monooxygenase	0.027041389	-0.377943661
	WBGene00044623	bus-8	Involved in morphogenesis of an epithelium and phosphatidylinositol metabolic process	0.000490395	-1.027167249
	WBGene00044631	bus-18	Involved in morphogenesis of an epithelium and phosphatidylinositol metabolic process	3.02E-06	-1.477097361

	WBGene00000198	art-1	Probable very-long-chain enoyl-CoA reductase art-1	0.022227467	-0.324921045
Biological oxidation					
	WBGene00001775	gst-27	Glutathione S-Transferase	0.019860851	-0.49934459
	WBGene00019967	cyp-33C8	CYtochrome P450 family	0.003703653	0.797419283
	WBGene00013585	cyp-42A1	CYtochrome P450 family	0.017473063	-0.98009234
	WBGene00001790	gst-42	Probable maleylacetoacetate isomerase	0.005935935	-0.579469882
	WBGene00007964	cyp-25A2	Cytochrome P450 family	1.99E-05	-1.180958277
	WBGene00007507	C10C5.3	Aminoacylase	0.026847049	0.866689785
	WBGene00013263	txdc-12.1	ThioredoXin Domain Containing protein homolog	8.34E-05	-1.044322973
	WBGene00018656	txdc-12.2	ThioredoXin Domain Containing protein homolog	0.002596175	-1.010094036
	WBGene00007848	cytb-5.1	Cytochrome B	0.047499527	-0.411655567
	WBGene00022176	Y71H2AM.11	Predicted to have dipeptidase activity and metal ion binding activity	0.042279569	-0.425409751
Glutathione metabolism					
	WBGene00012416	Y7A9A.1	Predicted to have glutathione hydrolase activity	0.029506123	-0.660250459
	WBGene00001775	gst-27	Glutathione S-Transferase	0.019860851	-0.49934459
	WBGene00001790	gst-42	Probable maleylacetoacetate isomerase	0.005935935	-0.579469882
	WBGene00007942	idh-2	Isocitrate dehydrogenase [NADP]	0.007187994	-0.504615694
	WBGene00013263	txdc-12.1	ThioredoXin Domain Containing protein homolog	8.34E-05	-1.044322973
Arginine and Proline metabolism					
	WBGene00004025	phy-2	Prolyl 4-hydroxylase subunit alpha-2	0.010208732	-0.765982128
	WBGene00010924	M153.1	Predicted to have pyrroline-5-carboxylate reductase activity	0.017381287	-0.512893305
	WBGene00011938	alh-13	Glutamate 5-kinase	7.44E-05	-1.080973304
	WBGene00022076	daao-1	D-amino-acid oxidase	3.07E-05	1.221635327
Endocytosis					
	WBGene00007703	gbf-1	Ortholog of human GBF1; is predicted to have ARF guanyl-nucleotide exchange factor activity	0.035761966	-0.382349522
	WBGene00000157	aps-2	AP complex subunit sigma	0.047092712	-0.37633588
	WBGene00000161	apa-2	AP-2 complex subunit alpha	0.006097248	-0.459154019
Homeostasis					
	WBGene00011102	R07E3.1	Predicted to have cysteine-type peptidase activity	0.011928966	-0.579331727
	WBGene00000778	cpn-2	Transgelin	3.10E-05	-0.908390631
	WBGene00018533	F47B7.2	Sulfhydryl oxidase	0.002156267	-0.638213739
	WBGene00003930	pat-3	Integrin beta pat-3	0.033692884	-0.333806379
Immune system					
	WBGene00004270	rab-6.2	Ras-related protein Rab-6.2	0.008007338	-0.4692537
	WBGene00011112	R07E5.4	Predicted to have Gamma interferon inducible lysosomal thiol reductase GILT domain	0.014467427	-0.328449654
	WBGene00010681	mak-1	MAP kinase-activated protein kinase mak-1	0.001210994	0.568135885
	WBGene00011000	R03G8.6	Aminopeptidase	0.020735016	0.51371417
	WBGene00008284	C53D6.7	Galectin	0.033724619	0.563490853
	WBGene00005078	src-2	Tyrosine protein-kinase src-2	0.004028965	-0.709847836
	WBGene00020465	T12E12.6	Predicted to have metallopeptidase activity and zinc ion binding activity	0.019021401	-1.51757324
	WBGene00003930	pat-3	Integrin beta pat-3	0.033692884	-0.333806379
	WBGene00001169	eef-1A.2	Elongation factor 1-alpha	0.048610242	-0.758994378
	WBGene00000778	cpn-2	Transgelin	3.10E-05	-0.908390631
	WBGene00007605	hrg-7	Heme Responsive Gene	0.016015628	-0.758188683
	WBGene00007529	C11H1.3	Predicted to have ubiquitin-protein transferase activity	0.009761102	-0.539626701
	WBGene00014053	ZK669.3	GILT-like protein ZK669.3	9.19E-05	1.065458083
	WBGene00018533	F47B7.2	Sulfhydryl oxidase	0.002156267	-0.638213739
	WBGene00013197	ttm-5	Putative sphingolipid delta(4)-desaturase/C4-monooxygenase	0.027041389	-0.377943661
Signal transduction					
	WBGene00000116	alh-10	ALdehyde deHydrogenase	0.040595576	-0.477796164
	WBGene00010681	mak-1	MAP kinase-activated protein kinase mak-1	0.001210994	0.568135885
	WBGene00009059	chw-1	CHp/Wrch Rho-like protein homolog	0.02339794	-0.492526261
	WBGene00012186	mlt-11	Predicted to have serine-type endopeptidase inhibitor activity	0.022227467	-1.105389286
	WBGene00000161	apa-2	AP-2 complex subunit alpha	0.006097248	-0.459154019
	WBGene00006367	sym-2	RNA-binding protein sym-2	0.037774881	-0.393475323
	WBGene00004210	ptc-3	Protein patched homolog 3	1.10E-05	-0.98922291
	WBGene00005078	src-2	Tyrosine protein-kinase src-2	0.004028965	-0.709847836
	WBGene00013585	cyp-42A1	Cytochrome P450 family	0.017473063	-0.98009234
	WBGene00003930	pat-3	Integrin beta pat-3	0.033692884	-0.333806379
	WBGene00018547	clec-78	C-type LECtin	0.038658657	-0.725883807
	WBGene00000157	aps-2	AP complex subunit sigma	0.047092712	-0.37633588
Peroxisome					
	WBGene00007942	idh-2	Isocitrate dehydrogenase [NADP]	0.007187994	-0.504615694
	WBGene00008564	acox-1.1	Acyl-coenzyme A oxidase	0.013989087	-0.696593952
	WBGene00022076	daao-1	D-amino-acid oxidase	3.07E-05	1.221635327
Response to pathogens					
	WBGene00009096	fipr-1	FIP (Fungus-Induced Protein) Related	0.009761102	0.97620127
	WBGene00008245	fipr-10	FIP (Fungus-Induced Protein) Related	0.004335349	1.319133771
	WBGene00010183	fipr-13	FIP (Fungus-Induced Protein) Related	0.04680313	0.870697563
	WBGene00009097	fipr-2	FIP (Fungus-Induced Protein) Related	0.001132101	1.0981755
	WBGene00007989	fipr-22	FIP (Fungus-Induced Protein) Related	0.035761966	0.806967999
	WBGene00009090	fipr-3	FIP (Fungus-Induced Protein) Related	0.012842431	0.982508393
	WBGene00007541	fipr-4	FIP (Fungus-Induced Protein) Related	0.00412602	1.31346106
	WBGene00044174	fipr-5	FIP (Fungus-Induced Protein) Related	9.65E-05	1.234043356
	WBGene00007544	fipr-6	FIP (Fungus-Induced Protein) Related	0.041533638	0.993062156
	WBGene00007543	fipr-7	FIP (Fungus-Induced Protein) Related	0.049750793	0.820568788
	WBGene00007537	fipr-8	FIP (Fungus-Induced Protein) Related	0.024613984	0.879130513
	WBGene00044175	fipr-9	FIP (Fungus-Induced Protein) Related	0.008007338	1.177600384

Pathway analysis	Ensamble ID	Gene name	Annotation	q-value	$\log_2$FC
Sperm Cytoskeletal structural proteins					
	WBGene00007714	C25D7,1	Major sperm protein	0.0173359	-0.42462
	WBGene00018840	F58A6.9	Major sperm protein	0.0087362	-0.656501
	WBGene00009682	msd-2	Major Sperm protein Domain containing	0.0035314	-0.533681
	WBGene00003468	msp-113	Major sperm protein 19/31/40/45/50/51/53/59/61/65/81/113/142	0.0010018	-0.609851
	WBGene00003470	msp-152	Major sperm protein 152	0.0131545	-0.43782
	WBGene00003426	msp-19	Major sperm protein 19/31/40/45/50/51/53/59/61/65/81/113/142	0.0002551	-0.591407
	WBGene00003429	msp-31	Major sperm protein 19/31/40/45/50/51/53/59/61/65/81/113/142	0.0159394	-0.402922
	WBGene00003431	msp-33	Major sperm protein 33	0.0188356	-0.425153
	WBGene00003432	msp-36	Major sperm protein 10/36/56/76	0.0457516	-0.382608
	WBGene00003434	msp-38	Major sperm protein 38	0.0061242	-0.491728
	WBGene00003435	msp-40	Major sperm protein 19/31/40/45/50/51/53/59/61/65/81/113/142	0.0387605	-0.355356
	WBGene00003438	msp-45	Major sperm protein 19/31/40/45/50/51/53/59/61/65/81/113/142	0.0091287	-0.545714
	WBGene00003442	msp-49	Major sperm protein 49	0.0217256	-0.490838
	WBGene00003443	msp-50	Major sperm protein 19/31/40/45/50/51/53/59/61/65/81/113/142	0.0089973	-0.497006
	WBGene00003444	msp-51	Major sperm protein 19/31/40/45/50/51/53/59/61/65/81/113/142	0.0006118	-0.606367
	WBGene00003446	msp-53	Major sperm protein 19/31/40/45/50/51/53/59/61/65/81/113/142	4.72E-06	-0.679686
	WBGene00003448	msp-55	Major sperm protein 55/57	1.90E-06	-0.71107
	WBGene00003449	msp-56	Major sperm protein 10/36/56/76	0.0056099	-0.545225
	WBGene00003450	msp-57	Major sperm protein 55/57	2.70E-05	-0.704053
	WBGene00003452	msp-59	Major sperm protein 19/31/40/45/50/51/53/59/61/65/81/113/142	0.0002551	-0.589088
	WBGene00003458	msp-65	Major sperm protein 19/31/40/45/50/51/53/59/61/65/81/113/142	0.0002912	-0.692043
	WBGene00003463	msp-76	Major sperm protein 10/36/56/76	0.0030554	-0.502776
	WBGene00003464	msp-77	Major sperm protein 77/79	0.0001117	-0.651888
	WBGene00003465	msp-78	Major sperm protein 78	0.0148364	-0.463393
	WBGene00003466	msp-79	Major sperm protein 77/79	0.0020472	-0.568785
	WBGene00003467	msp-81	Major Sperm Protein	0.0077619	-0.552907
	WBGene00006039	ssp-10	Sperm-specific class P protein 10	0.0002003	-0.607729
	WBGene00010091	ssp-35	Sperm Specific family, class P	0.0151902	-0.40244
	WBGene00006056	sss-1	Sperm-Specific family, class S	8.80E-05	-0.546967
	WBGene00018008	vpr-1	Major sperm protein	0.0249191	-0.449149
	WBGene00022002	Y59E9AR.7	Major sperm protein	0.0359681	-0.733635
Sperm meiosis and Chromosome segragation					
	WBGene00000098	air-1	Aurora/Ipl1 Related kinase	0.0417025	-0.389565
	WBGene00002074	ima-3	Importin subunit alpha-3	0.044438	-0.45933
	WBGene00007733	smz-1	Sperm Meiosis PDZ domain containing proteins	0.0184597	-0.398857
	WBGene00020661	smz-2	Sperm Meiosis PDZ domain containing proteins	0.0326802	-0.423683
Sperm maturation					
	WBGene00014240	htas-1	Histone H2A	0.000189	-0.502406
	WBGene00002074	ima-3	Importin subunit alpha-3	0.044438	-0.45933
Germline proliferation					
	WBGene00000098	air-1	Aurora/Ipl1 Related kinase	0.0417025	-0.389565
	WBGene00000933	dap-3	Mammalian cell Death Associated Protein related	0.0372581	-0.427359
	WBGene00000935	daz-1	DAZ protein 1	0.0448321	-0.34584
	WBGene00001258	emb-4	Intron-binding spliceosomal'Aquarius' protein with a helicase-like domain	0.0173359	-0.464885
	WBGene00002001	hars-1	Histidine--tRNA ligase	0.0132773	-0.463158
	WBGene00014240	htas-1	Histone H2A	0.000189	-0.502406
	WBGene00002074	ima-3	Importin subunit alpha-3	0.044438	-0.45933
	WBGene00003821	nst-1	Guanine nucleotide-binding protein-like 3 homolog	0.0360204	-0.331753
	WBGene00020112	pfd-5	Probable prefoldin subunit 5	0.0374243	-0.372319
	WBGene00004302	ran-1	GTP-binding nuclear protein ran-1	0.0461447	-0.44538
	WBGene00020687	ruvb-2	RuvB-like 2	0.0077619	-0.512348
	WBGene00007733	smz-1	Sperm Meiosis PDZ domain containing proteins	0.0184597	-0.398857
	WBGene00020661	smz-2	Sperm Meiosis PDZ domain containing proteins	0.0326802	-0.423683
	WBGene00004955	spd-5	Spindle-defective protein 5	0.045081	-0.319305
Spindle assembly					
	WBGene00000098	air-1	Aurora/Ipl1 Related kinase	0.0417025	-0.389565
	WBGene00002214	klc-1	Kinesin Light Chain	0.0415699	-0.381073
	WBGene00004302	ran-1	GTP-binding nuclear protein ran-1	0.0461447	-0.44538
	WBGene00004955	spd-5	Spindle-defective protein 5	0.045081	-0.319305
Oogenesis					
	WBGene00000098	air-1	Aurora/Ipl1 Related kinase	0.0417025	-0.389565
	WBGene00000933	dap-3	Mammalian cell Death Associated Protein related	0.0372581	-0.427359
	WBGene00000935	daz-1	DAZ protein 1	0.0448321	-0.34584
	WBGene00002074	ima-3	Importin subunit alpha-3	0.044438	-0.45933
	WBGene00020112	pfd-5	Probable prefoldin subunit 5	0.0374243	-0.372319
	WBGene00004302	ran-1	GTP-binding nuclear protein ran-1	0.0461447	-0.44538
	WBGene00020687	ruvb-2	RuvB-like 2	0.0077619	-0.512348
	WBGene00004955	spd-5	Spindle-defective protein 5	0.045081	-0.319305

Embryonic development					
	WBGene00000098	air-1	Aurora/Ipl1 Related kinase	0.0417025	-0.389565
	WBGene00016907	C53H9.2	Predicted GTP binding activity	0.0462789	-0.405555
	WBGene00000474	cey-3	C. elegans Y-box	0.044754	-0.334389
	WBGene00001161	efl-1	E2F-like (mammalian transcription factor)	0.0358504	-0.42145
	WBGene00001258	emb-4	Intron-binding spliceosomal'Aquarius' protein with a helicase-like domain	0.0173359	-0.464885
	WBGene00002045	icd-1	Transcription factor BTF3 homolog	0.0387183	-0.308287
	WBGene00002074	ima-3	Importin subunit alpha-3	0.044438	-0.45933
	WBGene00002214	klc-1	Kinesin Light Chain	0.0415699	-0.381073
	WBGene00003821	nst-1	Guanine nucleotide-binding protein-like 3 homolog	0.0360204	-0.331753
	WBGene00004189	pars-1	Prolyl Amino-acyl tRNA Synthetase	0.0298758	-0.344551
	WBGene00020112	pfd-5	Probable prefoldin subunit 5	0.0374243	-0.372319
	WBGene00004046	plp-1	Pur alpha Like Protein	0.0436353	-0.397802
	WBGene00004302	ran-1	GTP-binding nuclear protein ran-1	0.0461447	-0.44538
	WBGene00013985	sec-16	Protein transport protein Sec16	0.0091723	-0.415352
Cell-cycle					
	WBGene00001161	efl-1	E2F-like (mammalian transcription factor)	0.0358504	-0.42145
	WBGene00001258	emb-4	Intron-binding spliceosomal'Aquarius' protein with a helicase-like domain	0.0173359	-0.464885
	WBGene00014240	htas-1	Histone H2A	0.000189	-0.502406
	WBGene00019246	rpb-5	DNA-directed RNA polymerases I, II, and III subunit RPABC1	0.0386856	-0.363268
	WBGene00022852	ZK1127.5	Probable RNA 3'-terminal phosphate cyclase-like protein	0.044754	-0.377192
Programmed cell death					
	WBGene00000098	air-1	Aurora/Ipl1 Related kinase	0.0417025	-0.389565
	WBGene00000474	cey-3	C. elegans Y-box	0.044754	-0.334389
	WBGene00000933	dap-3	Mammalian cell Death Associated Protein related	0.0372581	-0.427359
	WBGene00017488	dct-7	DAF-16/FOXO Controlled, germline Tumor affecting	0.0244993	1.5798059
	WBGene00001161	efl-1	E2F-like (mammalian transcription factor)	0.0358504	-0.42145
	WBGene00002045	icd-1	Transcription factor BTF3 homolog	0.0387183	-0.308287
	WBGene00003059	lpd-2	Lipid Depleted	0.0370568	-0.435521
	WBGene00012556	mrps-10	Probable 28S ribosomal protein S10, mitochondrial	0.0358504	-0.428449
	WBGene00020549	nmt-1	Glycylpeptide N-tetradecanoyltransferase	0.0392083	-0.353408
	WBGene00003821	nst-1	Guanine nucleotide-binding protein-like 3 homolog	0.0360204	-0.331753
	WBGene00004189	pars-1	Prolyl Amino-acyl tRNA Synthetase	0.0298758	-0.344551
	WBGene00004302	ran-1	GTP-binding nuclear protein ran-1	0.0461447	-0.44538
	WBGene00004312	rba-1	Probable histone-binding protein rba-1	0.0162808	-0.393418
	WBGene00004476	rps-7	40S ribosomal protein S7	0.0128192	-0.332022
	WBGene00004917	snr-4	Probable small nuclear ribonucleoprotein Sm D2	0.0091287	-0.433281
	WBGene00004955	spd-5	Spindle-defective protein 5	0.045081	-0.319305
Chromatin organization					
	WBGene00017993	cec-5	C. elegans Chromodomain protein	0.0148364	-0.319612
	WBGene00002637	let-418	Protein let-418	0.0469882	-0.274547
	WBGene00001837	hda-4	Histone deacetylase 4	0.0326786	0.4134539
	WBGene00001898	his-24	Histone H1,1	0.00118	1.258294
	WBGene00014240	htas-1	Histone H2A	0.000189	-0.502406
	WBGene00004312	rba-1	Probable histone-binding protein rba-1	0.0162808	-0.393418
DNA repair					
	WBGene00001258	emb-4	Intron-binding spliceosomal'Aquarius' protein with a helicase-like domain	0.0173359	-0.464885
	WBGene00019246	rpb-5	DNA-directed RNA polymerases I, II, and III subunit RPABC1	0.0386856	-0.363268
Immune System					
	WBGene00001500	ftn-1	Ferritin	0.044754	1.2811676
	WBGene00019185	H10E21,5	Zinc finger, RING-type and Zinc finger, RING/FYVE/PHD-type	0.0068583	0.6844981
	WBGene00002178	jnk-1	Stress-activated protein kinase jnk-1	0.0120895	0.5705376
	WBGene00010681	mak-1	MAP kinase-activated protein kinase mak-1	0.0003041	0.6535781
	WBGene00019782	M60.7	Ankyrin repeat-containing domain, SOCS box-like domain superfamily	0.0058122	2.3561592
	WBGene00012194	toe-4	Target Of ERK kinase MPK-1	0.0383117	0.7084691
	WBGene00006702	ubc-3	UBiquitin Conjugating enzyme	0.0091287	0.4699845
	WBGene00006705	ubc-8	UBiquitin Conjugating enzyme	0.0071042	1.2213064
	WBGene00014848	VM106R,1	Ortholog of human KCTD12, KCTD16, and KCTD8	0.0455031	0.5624022
	WBGene00022026	Y65B4A,2	Predicted to have cysteine-type peptidase activity	0.0009935	0.6092627
Metabolism of protein					
	WBGene00001229	eif-3,F	Eukaryotic translation initiation factor 3 subunit F	0.003598	-0.599724
	WBGene00019782	M60.7	Ankyrin repeat-containing domain, SOCS box-like domain superfamily	0.0058122	2.3561592
	WBGene00004312	rba-1	Probable histone-binding protein rba-1	0.0162808	-0.393418
	WBGene00018853	sec-22	Yeast SEC homolog	0.0457516	-0.51436
	WBGene00006702	ubc-3	UBiquitin Conjugating enzyme	0.0091287	0.4699845
	WBGene00006705	ubc-8	UBiquitin Conjugating enzyme	0.0071042	1.2213064
	WBGene00006724	ubh-4	Ubiquitin carboxyl-terminal hydrolase ubh-4	0.0244993	-0.398408
Signal Transduction					
	WBGene00012907	cpt-1	Carnitine Palmitoyl Transferase	0.044754	0.483742
	WBGene00020506	dop-3	Dopamine receptor 3	0.025045	0.6919784
	WBGene00002178	jnk-1	Stress-activated protein kinase jnk-1	0.0120895	0.5705376
	WBGene00002181	kal-1	Human KALlmann syndrome homolog	0.0148364	0.7481636
	WBGene00010681	mak-1	MAP kinase-activated protein kinase mak-1	0.0003041	0.6535781
	WBGene00003605	nhr-6	Nuclear hormone receptor family member nhr-6	0.0059894	1.1434303
	WBGene00019902	R05G6,10	Predicted to have guanyl-nucleotide exchange factor activity	0.0195877	0.7973768

Macroautophagy - Cellular responses to stress					
	WBGene00020706	atg-9	Autophagy-related protein 9	0.0173359	0.6569137
	WBGene00022078	epg-9	Ectopic P Granules	0.0197544	0.8996206
	WBGene00010681	mak-1	MAP kinase-activated protein kinase mak-1	0.0003041	0.6535781
	WBGene00002178	jnk-1	Stress-activated protein kinase jnk-1	0.0120895	0.5705376
Peroxisome					
	WBGene00004058	pmp-1	Peroxisomal Membrane Protein related	0.01287255	-0.682045
	WBGene00011173	acs-18	Fatty Acid CoA Synthetase family	0.0454965	-0.330259
	WBGene00013999	ZK550.5	Uncharacterized protein	0.0249191	-0.36666
Structural constituent of mitochondrial ribosome					
	WBGene00010458	mrpl-10	Mitochondrial Ribosomal Protein, Large	0.009422	-0.458634
	WBGene00007712	mrpl-34	Mitochondrial Ribosomal Protein, Large	0.0378533	-0.544118
	WBGene00015092	mrpl-47	Mitochondrial Ribosomal Protein, Large	0.0303043	-0.331319
	WBGene00011740	mrpl-51	39S ribosomal protein L51, mitochondrial	0.0091723	-0.443039
	WBGene00012556	mrps-10	Probable 28S ribosomal protein S10, mitochondrial	0.0358504	-0.428449
	WBGene00011391	mrps-12	Mitochondrial Ribosomal Protein, Small	0.0150873	-0.333963
	WBGene00020499	mrps-18,C	Mitochondrial Ribosomal Protein, Small	0.0230003	-0.44792
	WBGene00014224	mrps-23	Probable 28S ribosomal protein S23, mitochondrial	0.0392729	-0.513658
	WBGene00023487	mrps-24	28S ribosomal protein S24, mitochondrial	0.0003041	-0.460069
	WBGene00013324	mrps-7	28S ribosomal protein S7, mitochondrial	0.0148364	-0.425498
Methabolic pathways - Oxidative phosphorylation					
	WBGene00011173	acs-18	Fatty Acid CoA Synthetase family	0.0454965	-0.330259
	WBGene00000198	art-1	Probable very-long-chain enoyl-CoA reductase art-1	0.0240548	-0.334617
	WBGene00015467	basl-1	BAS-Like	0.0402681	-0.394027
	WBGene00006519	cox-6A	Cytochrome c oxidase subunit 6A, mitochondrial	0.0405776	-0.344619
	WBGene00012166	nuo-6	NADH Ubiquinone Oxidoreductase	0.0439367	-0.381868

Paper II

In vivo assessment of reactive oxygen species production and oxidative stress effects induced by chronic exposure to gamma radiation in *Caenorhabditis elegans*

*Erica Maremonti [1, 3], Dag M. Eide [2, 3], Lisa M. Rossbach [1], Ole Christian Lind [1, 3], Brit Salbu [1, 3], Dag Anders Brede [1, 3]

[1] Faculty of Environmental Sciences and Natural Resource Management (MINA) Norwegian University of Life Sciences (NMBU), 1432 Ås, Norway

[2] Norwegian Institute of Public Health, Lovisenberggata 8, 0456 Oslo, Norway

[3] Centre for Environmental Radioactivity (CERAD)

*Corresponding author

23

Graphical abstract

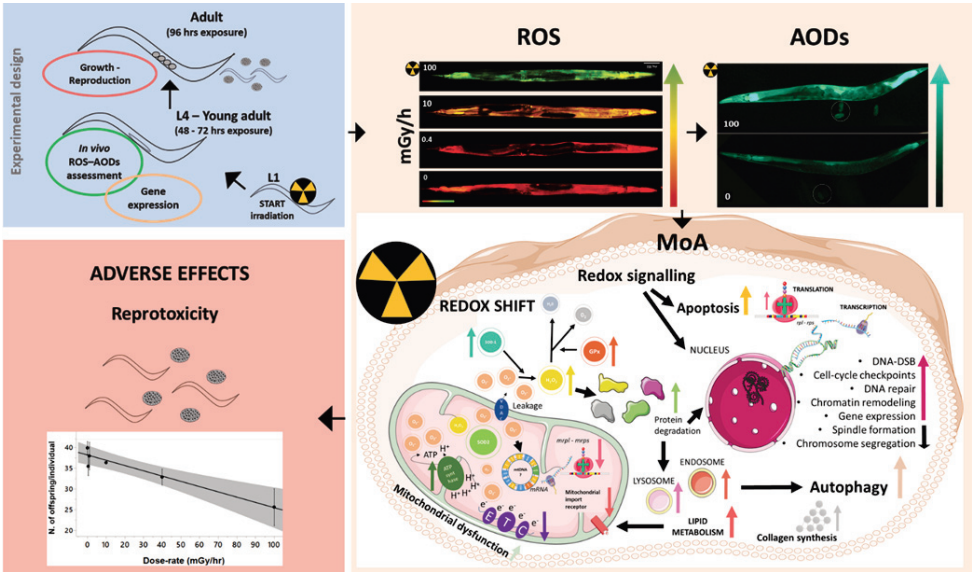

Highlights

- Chronic exposure to gamma radiation causes increased cellular ROS and induces Antioxidant defences in the nematode *Caenorhabditis elegans*
- Oxidative stress transcriptomic response is induced by chronic gamma irradiation
- Mitochondrial functions are negatively affected by chronic gamma irradiation
- Gamma radiation-induced reproductive impairment is associated with dysregulation of meiotic cell-cycle checkpoints, spindle formation and chromosome segregation

Abstract

In the current study, effects of chronic exposure to ionizing gamma radiation were assessed in the radioresistant nematode *Caenorhabditis elegans* in order to understand whether antioxidant defences (AODs) could ameliorate radical formation, or if increased ROS levels would cause oxidative damage. This analysis was accompanied by phenotypical as well as molecular investigations, via assessment of reproductive capacity, somatic growth and RNA-seq analysis.

The use of a fluorescent reporter strain (*sod1::gfp*) and two ratiometric biosensors (*HyPer* and *Grx1-roGFP2*) demonstrated increased ROS production (H_2O_2) and activation of AODs (SOD1 and Grx) *in vivo.* The data showed that at dose-rates ≤10 mGy·h^{-1} defence mechanisms were able to prevent the manifestation of oxidative stress. In contrast, at dose-rates ≥40 mGy·h^{-1} the continuous formation of radicals caused a redox shift, which lead to oxidative stress transcriptomic responses, including changes in mitochondrial functions, protein degradation, lipid metabolism and collagen synthesis. Moreover, genotoxic effects were among the most over-represented functions affected by chronic gamma irradiation, as indicated by differential regulation of genes involved in DNA damage, DNA repair, cell-cycle checkpoints, chromosome segregation and chromatin remodelling. Ultimately, the exposure to gamma radiation caused reprotoxic effects, with >20% reduction in the number of offspring per adult hermaphrodite at dose-rates ≥40 mGy·h^{-1}, accompanied by the down-regulation of more than 300 genes related to reproductive system, apoptosis, meiotic functions and gamete development and fertilization.

Keywords: Ionizing gamma radiation; *Caenorhabditis elegans*; *in vivo* Redox sensors; reactive oxygen species; mitochondrial dysfunction

1. Introduction

Exposure to ionizing radiation can cause harmful toxic effects either by direct energy deposition onto biomolecules or by indirect damage through the production of free radicals (Reisz et al., 2014). The indirect effects proceed through a chain of physical and chemical events which leads to the production of free-radicals due to dissociation of water molecules, and thus to a dose-dependent formation of reactive oxygen species (ROS), such as superoxide ($O_2^{\cdot -}$), hydroxyl radicals ($HO^{\cdot}$), hydrogen radicals ($H^{\cdot}$) and hydrogen peroxide (H_2O_2) (Yamamori et al., 2012, Riley, 1994, Smith et al., 2012). These radicals are continuously produced in the cells of organisms during exposure to ionizing radiation, and increased ROS levels have been measured in a wide range of species, including the green algae *Chlamydomonas reinhardtii*, the aquatic macrophyte *Lemna minor* and zebrafish (Xie et al., 2019, Gomes et al., 2017, Hurem et al., 2017). Despite a short (nanoseconds) half-life (Bergendi et al., 1999), the formation of ionizing radiation-induced radicals has shown to increase persistently in the cells during prolonged exposures (Tateishi et al., 2008, Chen et al., 2003). This may result in changes of the cellular redox balance, which can lead to the perturbation of essential biochemical processes including metabolism (Finkel and Holbrook, 2000). For instance, radiation may cause mitochondrial dysfunction, by compromising the electron transport chain (ETC), which exacerbates endogenous ROS production and the formation of oxidative stress condition (Reisz et al., 2014). Increased generation of mitochondrial ROS following low-dose irradiation plays multiple roles in signalling cascades and mediates apoptosis, thus may contribute significantly to cell survival (Azzam et al., 2012). Accordingly, oxidative damage to essential biomolecules,

including DNA, lipids and proteins are important contributors to the late effects following exposure to ionizing radiation (Spitz et al., 2004, Azzam et al., 2012, Dubois et al., 2018, Hertel-Aas et al., 2011, Gomes et al., 2018). Therefore, it is becoming increasingly evident that not only the indirect effects during the exposure itself, but even the subsequent production of free radicals plays a significant role to the overall biological effects of this stressor. Hence, detailed investigations into the role of ROS and the changes in the redox status produced following the exposure to ionizing radiation is of high importance.

At the species level, radiosensitivity ranges over several orders of magnitude (UNSCEAR, 1996). It has been postulated that the ability of an organism to tolerate ionizing radiation is dependent on the efficiency of DNA repair mechanisms, and robust antioxidant defences to mitigate ROS and prevent oxidative stress (Daly, 2012).

The nematode *Caenorhabditis elegans* is amongst the most radioresistant organisms and is frequently used in radiation biology studies, particularly the post-mitotic stage can tolerate high doses of both X-ray and gamma radiation (Hartman et al., 1988, Buisset-Goussen et al., 2014, Guo et al., 2013, Krisko et al., 2012). Interestingly, *C. elegans* possesses a wider range of antioxidant defences (AODs), compared to most organisms (Gems and Doonan, 2008, Doonan et al., 2008). Among these, the glutathione peroxidases (GPx) play an important role in oxidative stress defence, through ROS scavenging. Glutathione (GSH) is therefore central to the maintenance of cellular redox homeostasis (Wu et al., 2004, Back et al., 2012). Measurement of the ratio between the oxidized to reduced [GSSG]/[2GSH] form of GSH has been shown to be a reliable proxy for oxidative stress manifestation (Braeckman et al., 2016, Braeckman et al., 2017, Storey, 1996). Due to its highly specialized ROS and redox control system (Braeckman et al., 2016), *C. elegans* presents a suitable model for studying

radiation induced ROS production, besides being a well-defined model organism for genetics and cell biology (Honnen, 2017).

Therefore, in the current study, we investigate the effects of chronic exposure to gamma radiation on the accumulation of free radicals and the subsequent antioxidant responses in relation to apical reproductive and developmental effects in the nematode *C. elegans*. Furthermore, we examined the changes on the transcriptome upon irradiation during the entire larval development, in order to identify cellular and molecular functions related to the observed adverse effects and mechanisms mediating tolerance to ionising radiation.

2. Material and methods

2.1 Culture and maintenance of nematodes

Synchronised cohorts of nematodes were maintained in continuously shaking liquid cultures at 20 °C in the dark (Lewis and Fleming, 1995). The following strains were used: N2, wild type (Bristol) (*Caenorhabditis Genetic Centre*, Minneapolis, USA); *sod1::gfp* transgene, (GA508 wuIs54[pPD95.77 sod-1::GFP, rol-6(su1006)] (Institute of Healthy Ageing Genetics, University College London) (Doonan et al., 2008); H_2O_2 biosensor (HyPer) *(jrIs1[Prpl-17::HyPer];* [GSSG]/[2GSH] biosensor (*jrIs2[Prpl-17::Grx1-roGFP2])* (Back et al., 2012).

Synchronization of nematodes was performed prior exposure to gamma radiation by alkaline hypochlorite treatment (Porta-de-la-Riva et al., 2012). To facilitate hatching, eggs were suspended in 1 ml M9 buffer and placed on NGM-Petri dishes overnight.

Viability and hatching of L1 stage nematodes was assessed prior the start of the exposure.

2.3 Exposure to gamma radiation

The external gamma radiation exposure was conducted at the FIGARO ^{60}Co irradiation facility (maximum permissible activity 400 GBq) at the Norwegian University of Life Sciences (NMBU) (Lind et al., 2019). Nematodes were exposed, in triplicate, in liquid media (15 ml tissue-culture flasks or front row 24-well cell culture plates) or on NGM-Petri dishes (Ø 6 cm) (Porta-de-la-Riva et al., 2012) containing 15 or 0.5 ml of fresh *Escherichia coli OP50* (cultured overnight at 37 °C in L-Broth medium, (Lewis and Fleming, 1995)), respectively, re-suspended in moderately hard reconstituted water (MHRW) plus cholesterol (United States Environmental Protection Agency, 2002) at pH 7.5 (Khanna et al., 1997).

During exposure, controls were placed, in triplicate, behind lead shielding, while exposure containers were placed at distances corresponding to a calculated average absorbed dose-rates to water of 0.43 – 1.1 – 10.8 – 40.8 and 99.9 mGy·h^{-1} (**Table S.8** for dose-rates and respective total doses). Field dosimetry (air kerma rates measured with an ionization chamber) was traceable to the Norwegian Secondary Standard Dosimetry Laboratory (Norwegian Radiation Protection Authority, DSA, Oslo, Norway) (Bjerke and Hetland, 2014). Air kerma rates were measured using an Optically Stimulated Luminescence (OSL)

based nanoDots dosimetry system (Landauer®) by positioning the dosimeters at the front and back of the experimental units. Dose rates to water, calculated according to Lindbo Hansen E. (2017), were used as a proxy for dose rates to the nematodes.

2.4 Effects on somatic growth and reproduction

N2 nematodes were used to assess phenotypic endpoints (growth, fertility and reproduction) by performing standard 96 hours toxicity tests in 24-well cell culture plates, carried out at 20 °C in the dark (International Organization of Standardization, 2010). Organisms (n = 12 ±5 per well) were exposed to gamma radiation from L1 stage in triplicates.

For sampling, nematodes were stained with 0.5 mL of Rose Bengal (0.3 g/L) and placed for 10 minutes at 80°C. Plates were stored at 4 °C until nematodes on all plates were measured using a stereo microscope (Leica M205C, 16X magnification) for total body length (size), total number of offspring per recovered adult (reproduction), and for the number of pregnant nematodes (fertility), using a hand-held tally counter (International Organization of Standardization, 2010).

2.5 Monitoring *in vivo* ROS production response to ionizing radiation in *C. elegans*

187 While conventional redox-sensitive fluorogenic probes are nonspecific, irreversible, and
188 disruptive, genetically encoded fluorescent sensors can overcome such limitations (Gomes
189 et al., 2005, Meyer and Dick, 2010). Therefore, in the current study the *sod1::gfp* reporter
190 strain and two ratiometric biosensors, *HyPer* and *Grx1-roGFP2*, were employed as *in vivo*
191 proxies for ROS production following chronic exposure to gamma radiation (Doonan et al.,
192 2008, Cabreiro et al., 2011). Specifically, the *sod1::gfp* reporter strain was implemented to
193 measure the expression of the cytosolic Superoxide dismutase 1, while the ratiometric
194 biosensors *HyPer* and *Grx1-roGFP2* were adopted to measure the levels of H_2O_2 and the
195 glutathione redox changes.
196 Treatments with Paraquat or H_2O_2 were used as positive controls for method validation for
197 the *sod1::gfp* reporter strain and the *Grx1-roGFP2* ratiometric biosensor, respectively
198 (Supporting material, Section S.M. 2-3.).
199
200
201 ## 2.6 Epifluorescence microscopy
202
203 To analyse for changes in expression patterns following the exposure to ionizing gamma
204 radiation, nematodes, exposed for 48 and 72 hours from L1 stage, were transferred
205 immediately onto an agar pad (2 % agar) on a glass slide, immobilized with 30 mM of
206 Sodium Azide (NaAzide), mounted and observed for the fluorescent signals.
207 Anatomical localization and intensity average of the fluorescent signal for *sod1::gfp* were
208 assessed under a semi-automated research light microscope (Upright Microscope Leica
209 DM6 B, 10X magnification) equipped with a 405 nm excitation and 535 nm emission filters

210 for fluorescent intensity measurements (n= 10). For the ratio between the oxidized and
211 reduced forms of either the *HyPer* or *Grx1-roGFP2* strains (n= 10), a second image, at
212 excitation 490 nm and emission 535 nm, was taken. For each experiment, gain and
213 exposure settings were kept unvaried between different treatments, in order to ensure
214 comparable and unbiased measurements of the fluorescent signal. Intensity-normalized
215 images of at least ten nematodes per treatment were taken within 30 minutes from the
216 sampling and quantification of the fluorescence signals was performed on the Leica® LAS
217 software. A method validation with ROS inducer compounds (Paraquat and H_2O_2) was
218 performed for the quantification of the fluorescent signal in *sod1::gfp* and *Grx1-roGFP2*
219 (Supporting Material, sections S.M.2 and S.M.3). Gamma irradiation over 48 or 72 hours
220 induced decrease in *sod1::gfp* worm size in relation to controls, therefore fluorescence
221 signals were normalized to the worms' total body length. Oxidized/reduced *HyPer* and
222 *Grx1-roGFP2* ratios were calculated as described by Back et al. (2012).
223
224

225 2.7 Gene expression analysis

226 2.7.1 Transcriptomic analysis

227
228 RNA sequencing was performed in order to obtain gene expression profiles of nematodes
229 exposed to 0.4, 10.8 or 99.9 $mGy \cdot h^{-1}$ compared to control nematodes. For this purpose, after
230 72 hours of exposure from L1 stage to young adult stage (n=1000 per replicate, three
231 biological replicates per treatment), nematodes were washed and snap-frozen in LIN

232 (liquid nitrogen) and stored at -80 °C until used. Total RNA was extracted using Direct-zol
233 Reagent (Nordic Biosite) and purified with RNeasy Mini Kit (Zymo Research) according to
234 manufacture instruction. RNA purity and yield (A260/A280 > 1.8, A260/A230 > 2, yield >
235 100 ng/µl) was determined using NanoDrop-1000 Spectrophotometer (Thermo Scientific,
236 Wilmington, DE) and quality (RIN > 7) was assessed with Agilent 2100 Bioanalyzer (Agilent
237 Technologies, Palo Alto, CA) using RNA Nano LabChip Kit (Agilent Technologies).
238 Photometric parameters and RNA integrity number determined the quality of the RNA
239 sequenced samples. Strand-specific TruSeq™ RNA-seq pair-end libraries with 350 bp
240 fragment size were prepared for each treatment (three biological replicates). For each
241 sample ca $30x10^6$ reads (read length 150 bp) were sequenced using two lanes of Illumina
242 HiSeq 4000 (Norwegian High Throughput Sequencing Centre, UiO Oslo, Norway), and made
243 available on ArrayExpress with E-MTAB-8284.
244 Sequenced reads were mapped to the Ensemble reference genome WBcel235 using STAR
245 (Dobin et al., 2013). Statistical analysis for detection of differentially expressed genes
246 (DEGs) was done using Deseq2 package in the R software (rlog, variance Stabilizing
247 Transformation) for transformed data (Love et al., 2015), with FDR ≤0.05 and 0.3 ≤ log2fc
248 ≤ -0.3 as cut off.
249
250
251 ### 2.7.2 Gene set enrichment analysis and phenotypical analysis
252
253 In order to obtain information about processes affected by gamma radiation with respect
254 to anatomical, phenotypical and functional processes down to the single-cell level, the DEGs

were subjected to gene ontology (GEA), tissue (TEA) and phenotype (PEA) Enrichment Analyses using the WormBase Enrichment tool (BioRxiv: https://doi.org/10.1101/106369) (Angeles-Albores et al., 2016, Lee et al., 2017). Analysis were performed using HyPergeometric probability distribution with Benjamini-Hochberg step-up algorithm FDR correction (Angeles-Albores et al., 2017).

Moreover, a phenotypical analysis was performed by comparing the list of DEGs from the 100 $mGy \cdot h^{-1}$ exposure group with selected phenotypical variants using the public knowledge resource WormBase (Lee et al., 2017).

2.8 Statistical analysis

Results from somatic growth and reproduction assessment were analysed using the One-way Analysis of Variance (ANOVA) and when significance was found the Tukey *post hoc* test was adopted for comparison with the control group. Normality and homogeneity assumption were assessed on residuals by using Anderson-Darling normality test and visually on residuals vs. fitted value plot, respectively.

Fluorometric ratios from *HyPer* and *Grx1-roGFP2* and fluorescence intensity from *sod1::gfp* were used to measure levels of ROS in irradiated nematodes. Linear trends were estimated using Simple Linear Regression analysis (SLR) (Montgomery et al., 2012), while ANOVA and Tukey *post hoc* analysis were adopted for multiple comparisons with control treatment. Statistical analysis were performed using JMP Pro v14 (SAS institute, Cary, NC, USA) and SigmaPlot 10.0 (Systat Software, San Jose, CA).

3. Results

3.1 Chronic Gamma irradiation induced dose rate-dependent reprotoxic effect in *C. elegans* and no significant effects on somatic growth

In the nematode *Caenorhabditis elegans*, chronic exposure to gamma radiation did not induce any significant effect on lethality, morbidity, hatchability, or reproductive capacity at dose-rates ≤10 mGy·h^{-1} (total dose ≤1.4 Gy, **Fig. 1.b**). Furthermore, non-significant effects on size/total body length were found in any of the wild-type irradiated groups compared to control nematodes (**Fig. 1.a**).

However, after 96 hours of exposure, a significant linear dose-dependent reduction (SLR, *p*-value <0.001) in the number of offspring was shown with reproduction reduced by 20 and 40% (Tukey *post hoc*, *p*-value <0.05) following exposure to 40 and 100 mGy·h^{-1}, respectively (total doses ~3.9 and 9.6 Gy, **Fig. 1.b**).

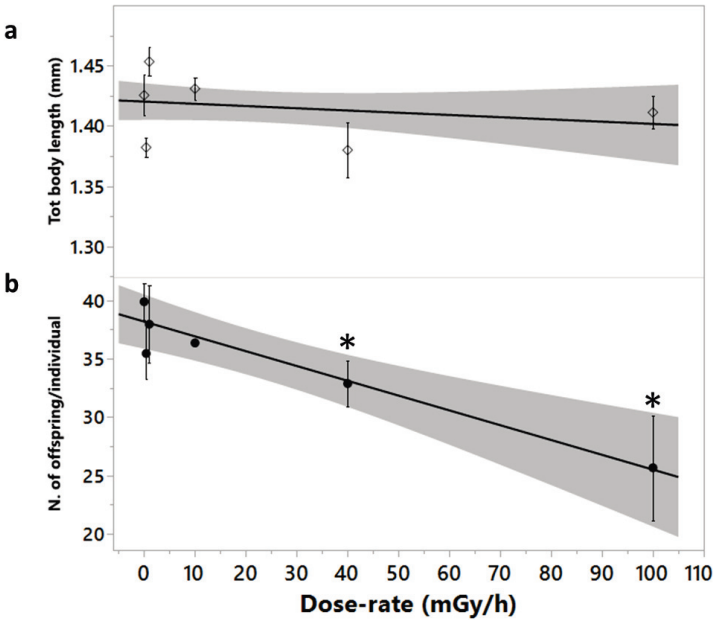

Figure 1. Effects on **a)** Somatic growth and **b)** reproduction on wild-type *C. elegans* exposed to gamma radiation (mGy·h^{-1}, total doses in **Table S.8**) for 96 hours, in front row of 24-well plates containing MHRW/*E. coli* OP50 suspension. Data represents Mean ± SE (n = 15). Asterisks indicate significant difference to control treatment (Tukey post hoc, p-value < 0.05).

3.1.1 Linear increase of *sod-1* expression following chronic gamma irradiation

The effect of external whole body gamma irradiation on superoxide anion ($O_2^{\cdot-}$) metabolism was assessed *in vivo* using the superoxide dismutase *sod1::gfp* reporter strain (Doonan et

307 al., 2008). In contrast to N2 strain, a minor but significant dose-dependent effect on somatic
308 growth was shown when the *sod1::gfp* reporter strain was irradiated (SLR, *p*-value <0.05),
309 with a 10% reduction of the body length following 100 mGy·h^{-1} of gamma irradiation (total
310 dose ~7.2 Gy, Tukey *post hoc*, *p*-value <0.05) (**Fig. S.1**).
311 Total body *sod-1* expression at 48 hours of irradiation (≥1 mGy·h^{-1}) increased significantly
312 in a dose-rate dependent manner (SLR, *p*-value <0.0001) (**Fig. 2.a**). The expression of *sod-*
313 *1* also showed a time-dependent increase, since gamma radiation induced a significantly
314 higher expression at 72 hours of exposure in all treatments compared to 48 hours and to
315 non-irradiated nematodes (SLR, *p*-value <0.0001). Moreover, One-Way ANOVA and Tukey
316 *post hoc* tests showed a significant threshold-effect between 0.4 and 1 mGy·h^{-1} (total dose
317 between 0.02 and 0.05 Gy), with all exposure groups having a significantly higher
318 expression of SOD1 compared to the control and 0.4 mGy·h^{-1} treatments at both 48 or 72
319 hours of exposure (*p*-value <0.001 and <0.0001) (**Fig. 2.a**). The highest dose-rates of
320 exposure in particular (40 and 100 mGy·h^{-1}), showed a 2-fold increase compared to the
321 control group (Tukey *post hoc*, *p*-value <0.0001) (**Fig. 2.a**). Visually, this mark increase was
322 seen in nematodes' images, as shown in **Fig. 2. b-c**. Consistent with a previous study
323 conducted by Doonan et al. (2008), the signal from non-irradiated or low-dose exposed
324 nematodes was primarily evident in the anterior and posterior part of the intestine, while
325 at the highest dose-rate, the expression pattern was visible across the entire intestinal
326 length for all the nematodes imaged after 48 or 72 hours of exposure (**Fig. 2.b-c**).
327 Additionally, at 100 mGy·h^{-1} (total dose ~7.2 Gy) in 40% of the assessed nematodes the
328 fertilized embryos, both inside the uterus (in particular those in close proximity of the
329 vulva) and the laid embryos exhibited enhanced fluorescent signal, while control embryos

330 did not show any expression (**Fig. 3.b-d**). Similarly, the vulva muscles along the body wall,
331 together with the pharyngeal epithelium and muscles, the anterior/posterior intestine and
332 the anus revealed a higher expression at 100 mGy·h^{-1} (total dose ~7.2 Gy) in 50% of the
333 imaged nematodes (n = 10, **Fig. 3.a-b-c**). The profound increase in *sod-1* expression in most
334 parts of the nematodes' body is consistent with a model where the energy depositions and
335 radical formation occurs uniformly in all irradiated cells, while the *sod-1:gfp* reporter is not
336 equally effectively expressed in all tissues (Doonan et al., 2008). The fact that *sod-1*
337 expression inevitably leads to H_2O_2 formation implied that further downstream effects on
338 ROS metabolism might result from the irradiation.
339

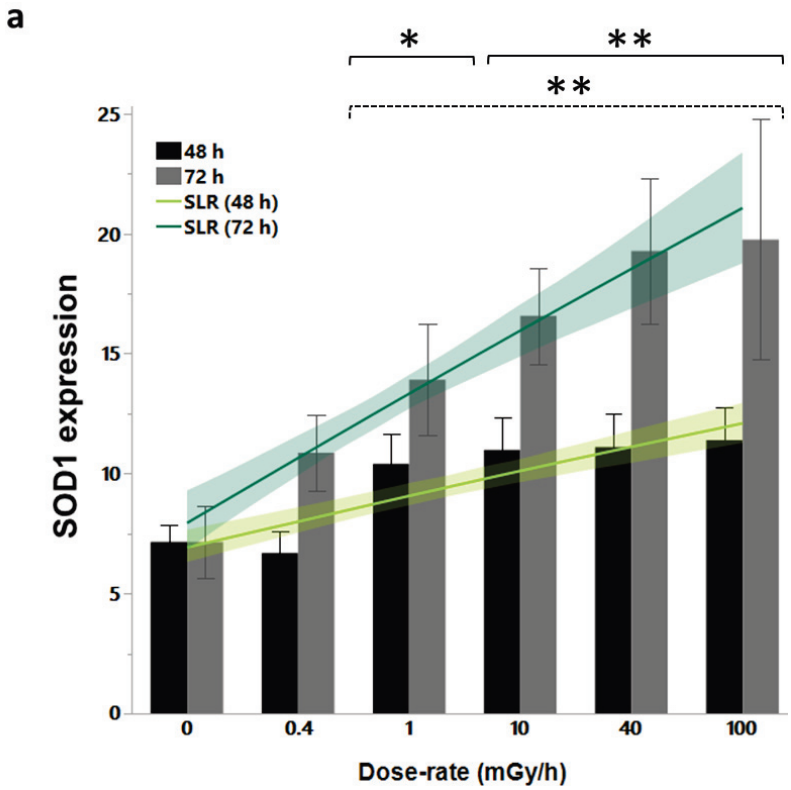
a
*
**
**
48 h
72 h
SLR (48 h)
SLR (72 h)
SOD1 expression
25
20
15
10
5
0
0
0.4
1
10
40
100
Dose-rate (mGy/h)

340

341

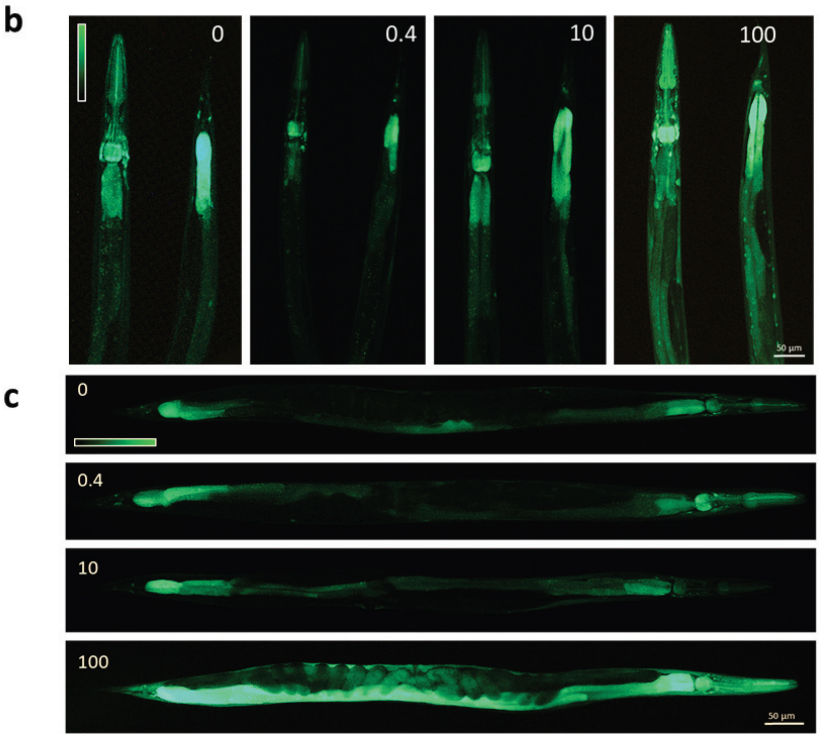

Figure 2. a) Sod-1 expression assessed *in vivo* in *C. elegans* reporter strain *sod1::gfp*, after 48 and 72 hours of exposure to increasing dose-rates of gamma radiation (mGy·h^{-1}, total doses in **Table S.8**), in MHRW containing OP50. Data represent Mean ± 95% CI (n = 10), values are normalized to somatic growth. Dashed or continuous line with asterisk indicates significant difference to control treatment at 48 and 72 hours, respectively (Tukey *post hoc*, *p*-value < 0.001 and < 0.0001). Projected on top of the bar chart are the regression lines for the SOD-1 expression on the $\log_{10}$(dose rate) values. **b**) Relative epifluorescence images of the expression pattern at different dose-rates of exposure (mGy·h^{-1}) after 48 (head and tail, respectively) and (**c**) 72 hours of irradiation (tail to head orientation). Scale bar: 50 µm.

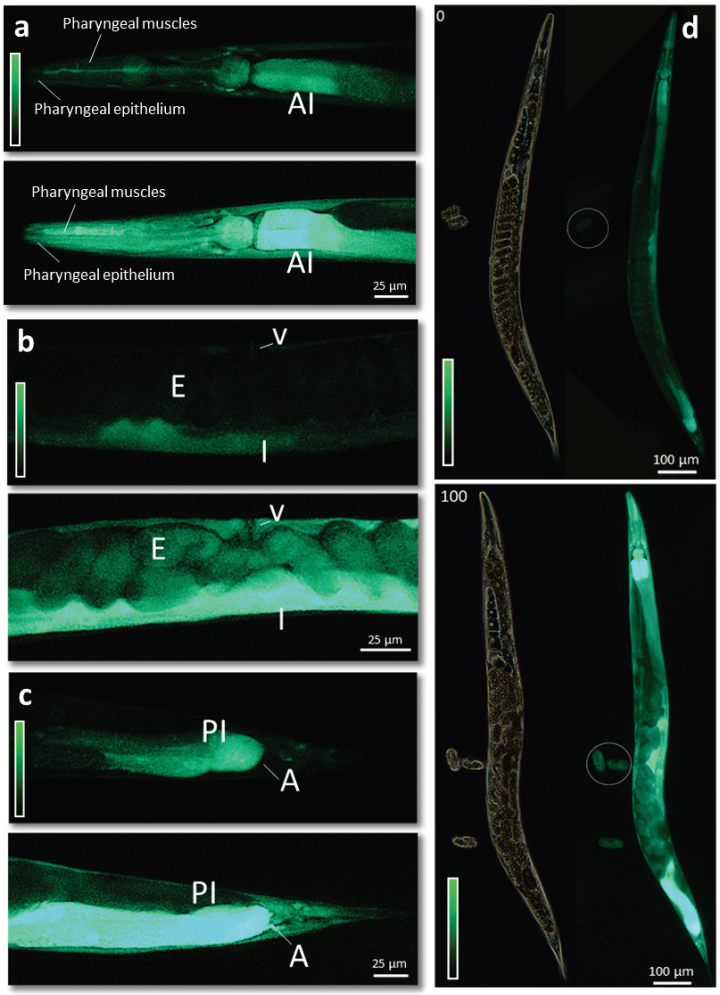

Figure 3. Epifluorescence images of the expression pattern assessed *in vivo* in (**a**) pharynx (AI: anterior intestine); **b**) mid-body (E: embryos, V: vulva, I: intestine), and (**c**) tail (PI: posterior intestine, A: anus) of *C. elegans* reporter strain *sod1::gfp* after 72 hours of irradiation to 0 (control) (**Top**) or 100 mGy·h^{-1} (total dose ~7.2 Gy, **Bottom**). **d**) Phase-Contrast optics and epifluorescence images of control (**Top**) nematodes or nematodes exposed to 100 mGy·h^{-1} (**Bottom**) for 72 hours from L1 stage, white circle indicates laid embryos (from top to bottom, head to tail orientation). Scale bar: 25 or 100 µm.

3.1.2 Dose-rate dependent increase in H_2O_2 production

The primary source of cellular H_2O_2 is via catalytic dismutation of $O_2^{\cdot-}$ by antioxidant enzymes including SOD1 (Back et al., 2012). The effects of gamma radiation on peroxide metabolism were investigated *in vivo* by using the *HyPer* biosensor (Back et al., 2012). At 48 hours of exposure, analysis of the entire body of the nematodes showed that H_2O_2 levels increased linearly with dose-rate (SLR, *p*-value <0.001) (**Fig. 4.a**). At 100 mGy·h^{-1} (total dose ~4.8 Gy) the H_2O_2 levels were visibly increased (**Fig. 4.b**), however, due to high inter-variability between organisms within the same treatment, this was not significant (Tukey *post hoc*, *p*-value > 0.05). Nonetheless, it was clear that the H_2O_2 levels increased with exposure time. At 72 hours of irradiation, a significant dose-dependent increase (SLR, *p*-value <0.0001) in the oxidized/reduced *HyPer* ratios was measured from doses ≥1 mGy·h^{-1} (Tukey *post hoc*, *p*-value < 0.001), as shown in **Fig. 4.a**. Consistent with the *sod-1* expression, the highest dose-rate (100 mGy·h^{-1}, total dose ~7.2 Gy) induced the highest levels of H_2O_2, either at 48 or 72 hours (Tukey *post hoc*, *p*-value < 0.0001). This shows that gamma radiation at these dose-rates caused a significant peroxide production that surpassed the nematodes capacity to sequester H_2O_2. In contrast, both the control and 0.4 mGy·h^{-1} groups showed a decreased H_2O_2-level between 48 and 72 hours of exposure.

Accordingly, when assessing the accumulation of hydrogen peroxide in different tissues at 48 hours, it was evident that no visible oxidation pattern was identified with no evident change observed in the fluorescence ratio below 100 mGy·h^{-1} (total dose <7.2 Gy, **Fig. 4.b**), while after 72 hours of exposure, at ≥10 mGy·h^{-1} the nematodes showed a significant

383 enhanced level of oxidation (**Fig. 4.c**). Moreover, the *HyPer* oxidation pattern showed a
384 visible dose-dependent increase, from a reduced signal observed in the control and 0.4
385 mGy·h^{-1} groups, to an oxidized signal in the 10 and 100 mGy·h^{-1} groups (**Fig. 4.c**, total doses
386 in **Table S.8**). In order to investigate whether there were differences between certain
387 tissues or cell types, the *HyPer* ratios were quantified in the Pharynx posterior bulb and in
388 the Posterior intestine after exposure to 100 mGy·h^{-1} compared to non-irradiated
389 nematodes (**Fig. 5.a-b-c**). Consistent with the whole-body measurements (**Fig. 4.a** and **5.a**),
390 the 100 mGy·h^{-1} exposure (total dose ~7.2 Gy) showed a significant difference in the
391 oxidation signal (green fluorescent signal) compared to controls, specifically in the pharynx
392 and along the posterior part of the intestine (Student's t-test, p-value <0.0001) (**Fig. 5**). The
393 results did however not reveal any difference between different tissues or cell types
394 (Student's t-test, p-value >0.05).
395
396

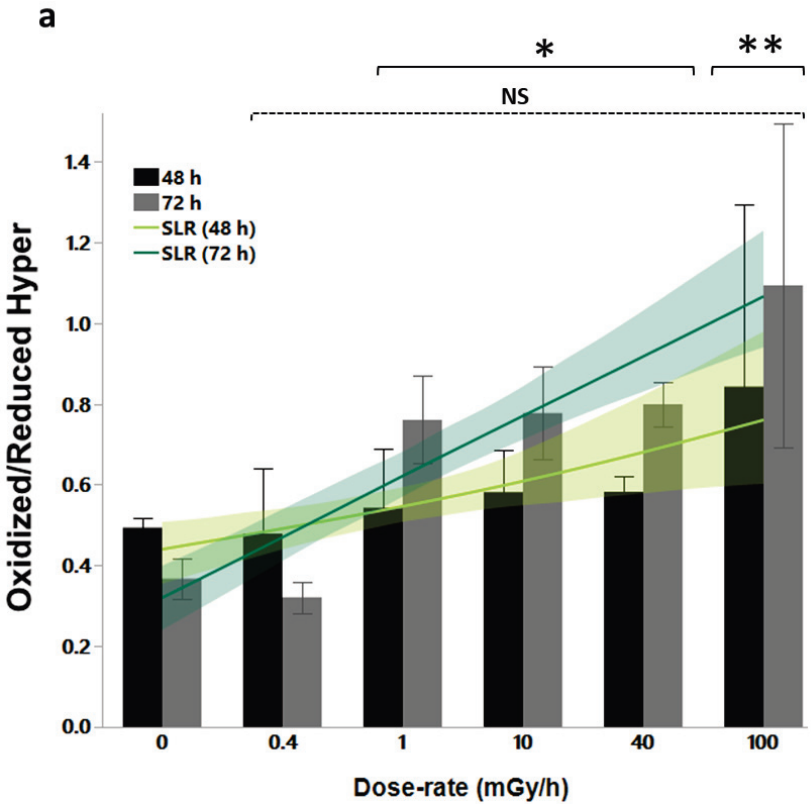
a
*
**
NS
48 h
72 h
SLR (48 h)
SLR (72 h)
Oxidized/Reduced Hyper
1.4
1.2
1.0
0.8
0.6
0.4
0.2
0.0
0
0.4
1
10
40
100
Dose-rate (mGy/h)

397

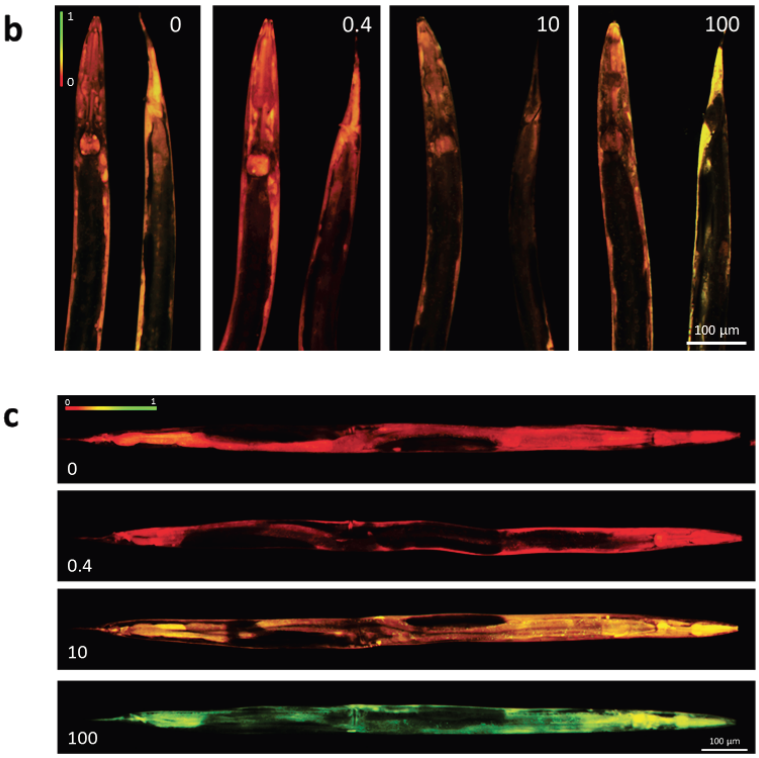

Figure 4. a) H_2O_2 level assessed *in vivo,* in *C. elegans* ratiometric biosensor *HyPer,* after 48 and 72 hours of exposure to gamma radiation (total doses in **Table S.8**), in front row 24-well plates containing MHRW/OP50. Data represent Mean ± 95% CI (n = 10). Dashed or continuous line with asterisk indicates non-significant (NS) or significant difference to control treatment at 48 and 72 hours, respectively (Tukey *post hoc*, *p*-value < 0.001 and < 0.0001). Projected on top of the bar chart are the regression lines for the H_2O_2 levels on the $\log_{10}$(dose rate) values. (**b**) Relative epifluorescence images of the H_2O_2 oxidation pattern at different dose-rates of exposure (mGy·h^{-1}) after (**b**) 48 (head and tail respectively) and (**c**) 72 hours of irradiation (from left to right, tail to head orientation). Scale bar: 100 µm.

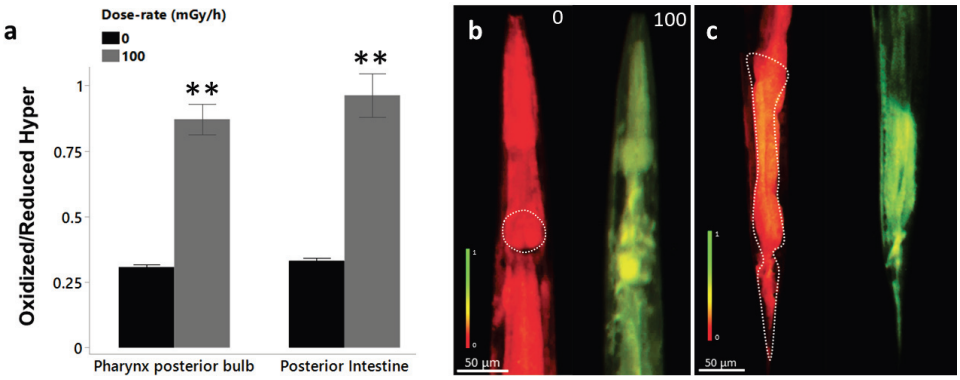

Figure 5. a) H_2O_2 level assessed *in vivo* in specific tissues of *C. elegans* ratiometric biosensor *HyPer,* after 72 hours of exposure to 0 and 100 mGy·h^{-1} (total dose ~7.2 Gy) of gamma radiation. Asterisk indicates significant difference to control treatment (Student's t test, *p*-value < 0.0001). (**b**) Epifluorescence images of the relative expression pattern assessed *in vivo* in (**b**) the pharynx posterior bulb and (**c**) posterior intestine of *C. elegans* biosensor *HyPer* after 72 hours of irradiation to 0 (control) or 100 mGy·h^{-1}. Scale bar: 50 µm.

3.1.3 Glutathione redox changes

The glutathione disulphide-glutathione couple [GSSG]/[2GSH] serves as the cell's primary mediator for the maintenance of redox homeostasis (Back et al., 2012). Therefore, the oxidized to reduced ratio [GSSG]/[2GSH] of *Grx1-roGFP2* (Back et al., 2012) was used as a proxy to assess the impact of chronic exposure to ionizing radiation *in vivo* on the redox potential and to visualize the relative oxidation pattern in the nematode *C. elegans*. At 48

426 hours from L1 stage, at dose-rates as low as 0.4 mGy·h^{-1} (total dose ~0.02 Gy), a significant
427 imbalance between oxidized to reduced signal was measured on the irradiated *Grx1-*
428 *roGFP2* compared to control nematodes (Tukey *post hoc*, *p*-value < 0.001) (**Fig. 6.a**). This
429 significant oxidative imbalance was shown for all measured dose-rates (Tukey *post hoc*, *p*-
430 value <0.001). Despite the statistically significant imbalance detected on the whole-body
431 measurements after 48 hours of exposure, in all the irradiated groups, we found no
432 evidence of tissue-specific effect compared to control nematodes (**Fig. 6.b**).
433 In contrast, at 72 hours of exposure, assessment of oxidative effects on whole body was
434 hampered by excessively large variation between individuals (S.M.4, **Fig. S.4.a-b**).
435 However, previous reports have demonstrated large differences between tissues (Back et
436 al., 2012). At this time-point, the only dose-rate inducing a higher but not statistically
437 significant oxidation of the [GSSG]/[2GSH] couple was 100 mGy·h^{-1} (total dose ~7.2 Gy)
438 (Tukey *post hoc*, *p*-value > 0.05) (**Fig. 6.a**), we therefore, investigated effects on different
439 tissues and cell types in this exposure group compared to control nematodes. This analysis
440 showed a significant oxidation in the gonads compared to the control (Student's t-test, *p*-
441 value <0.001) (**Fig. 7.b-c**), while the signal measured in the spermatheca showed no
442 difference between these two groups (Student's t-test, *p*-value > 0.05) (**Fig. 7.c-d**).
443
444
445

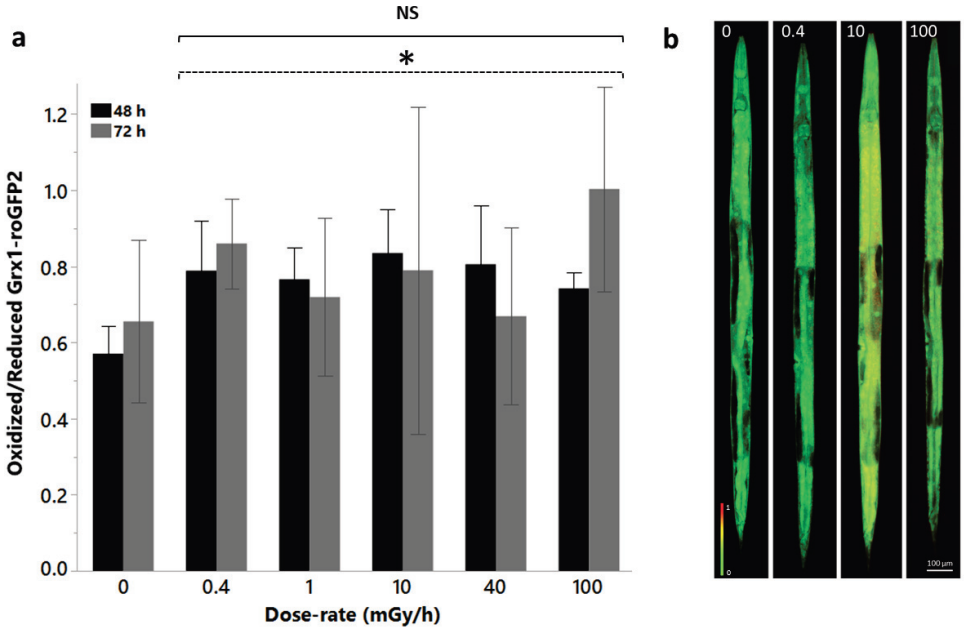

Figure 6. a) *In vivo* measurement of oxidized to reduced ratio of the *C. elegans* ratiometric biosensor *Grx1-roGFP2,* assessed after 48 and 72 hours of exposure to gamma radiation (total doses in **Table S.8**), in front row 24-well plates containing MHRW/OP50. Data represent Mean ± 95% CI (n = 10). Dashed or continuous line indicates non-significant (NS) or significant difference (asterisk) to control treatment at 48 and 72 hours, respectively (Tukey *post hoc*, *p*-value < 0.001). (**b**) Relative epifluorescence images of the oxidation pattern in *Grx1-roGFP2* at different dose-rates of exposure (mGy·h^{-1}) after 48 hours of irradiation (from top to bottom, head to tail orientation). Scale bar: 100 µm.

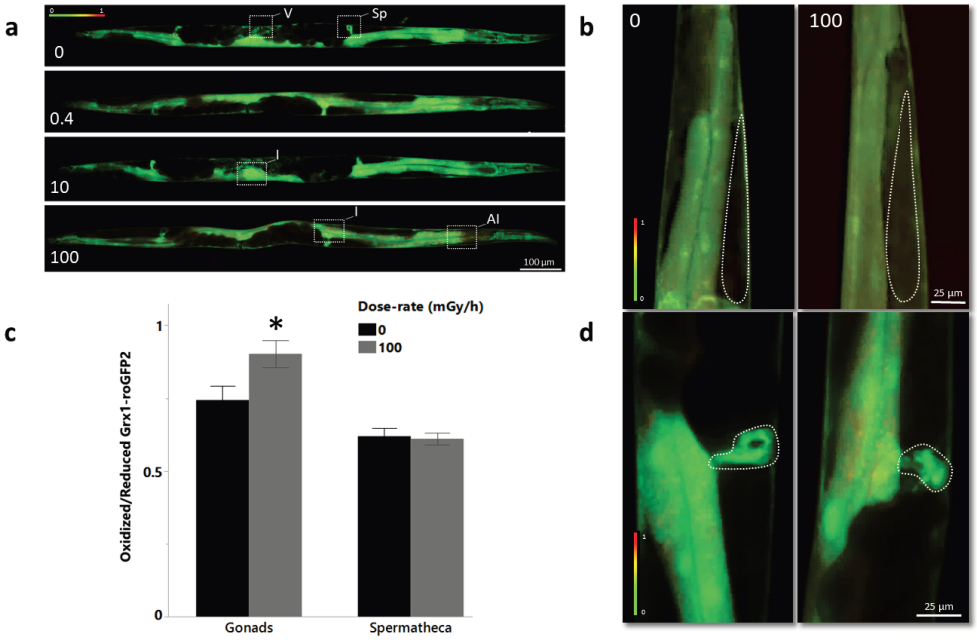

Figure 7. a) Epifluorescence images of the oxidation pattern in *Grx1-roGFP2* after 72 hours of gamma irradiation to different dose-rates of exposure (mGy·h^{-1}, total doses in **Table S.8**) in the entire body (V: vulva, Sp: spermatheca, I: intestine, AI: Anterior Intestine) (from left to right, tail to head orientation) or in selected tissues **b**) gonad and **d**) spermatheca. (**c**) Relative measurement of the GSSG/2GSH ratio in gonad and spermatheca after exposure to 0 (control) or 100 mGy·h^{-1} of gamma radiation. Asterisk indicates significant difference to control treatment (Student's t test, p-value < 0.001). Scale bar: 25 or 100 µm.

3.2 Chronic exposure to gamma radiation induces dose-rate dependent effects on *C. elegans* transcriptome

472 A gene expression analysis was performed after 72 hours of exposure to gamma radiation
473 from L1 stage in order to identify potential changes in the nematode's transcriptional
474 program. The RNA-seq analysis revealed a clear dose-dependent increase in the number of
475 differentially expressed genes (DEGs) (**Fig. S.5.a**). No significant differences in the gene
476 expression profile were found in nematodes exposed to 0.4 mGy·h^{-1} compared to the
477 control group, while the 10 and 100 mGy·h^{-1} groups (total doses ~0.8 and 7.2 Gy) showed a
478 total of 62 and 1317 DEGs, respectively, with 15 DEGs in common between these two
479 treatments (**Fig. S.5.b** and **Table S.1**). The complete list of DEGs resulting from 10 and 100
480 mGy·h^{-1} exposure groups can be found in **Supplementary Tables S.2 and S.3,** respectively.
481
482
483 ### 3.2.1 Functional enrichment analysis of DEGs
484
485 A gene set enrichment analysis was performed on the DEGs resulting from 10 and 100
486 mGy·h^{-1} exposure groups in order to identify functions significantly affected by exposure to
487 gamma radiation with respect to tissue, phenotype and gene ontology (**Fig. S.6-7, Table 1-**
488 **2, Table S.6**). A clear distinction between the expression profiles was found in the DEGs
489 resulting from the two exposure groups (**Fig. S.5**). The exposure to 10 mGy·h^{-1} (total dose
490 ~0.8) indicated overall effects on functions related to intestine, immune, reproductive and
491 nervous systems (**Fig. S.6.a-b-c**).
492
493 When the same analysis was performed on 100 mGy·h^{-1} DEGs, several functions and
494 categories related to reproduction and effects on progeny were significantly enriched

among down-regulated genes. Specifically, the reproductive system, embryonic development, meiotic chromosome segregation and cell cycle, spindle defective in early embryo, aneuploidy and embryonic cell physiology were among the most over-represented functions and variants observed (**Fig. S.7.a-b-c, Table S.4**). The TEA tool identified more than 300 down-regulated genes related to the reproductive system and more than 100 genes related to the muscular system (**Fig. S.7.c, Table S.4**). From the muscular system category, 19 genes had mitochondrial functions, including mitochondrial ribosomal proteins (*mrpl* and *mrps*), genes involved in mitochondrial membrane and genome maintenance (*pgs-1, R04F11.5, tomm-7, C27H6.9* and *rpap-3*) and mitochondrial dysfunction or disease (F39H2.3, nuaf-1 and pgs-1) (**Table S.4**). The Embryonic development variant identified by the PEA tool, on the other hand, included 94 down-regulated genes, among these, genes required for meiotic and mitotic chromosome segregation (*mut-2, dnc-2, him-10, nmat-2, cec-3, syp-3, rsa-1, unc-59, cids-1, him-8, nos-2, hpo-9* and *hus-1*), apoptosis and DNA repair (*rad-54, ced-12, pch-2, tyms-1, uri-1*), gamete development and fertilization (*trcs-1, nos-2, unc-59, pgs-1, uri-1, spd-3, hus-1 and mdt-6*) (**Table S.4**). The genes *mut-2, hus-1, nos-2, him-10, cids-1, syp-3, rsa-1* and *him-8* are all related to adverse 'variant Aneuploidy', 'Chromosome segregation', 'Meiotic cell-cycle functions' and the 'Reproductive system' (**Table S.4**).

Similarly, the up-regulated genes resulting from the same exposure group showed that important functions with respect to cellular development, post-embryonic development, cuticle and collagen synthesis, sex organ, protein interaction and cytokinesis were affected (**Table 1, 2, Table S.6**). The GEA tool identified multiple molecular functions related to the

518 modulation of gene expression via transcriptional initiation, post-transcriptional
519 modification and RNA transport and processing (**Table 1, Table S.5**). Also chromatin
520 remodelling appeared to be affected as evidenced by 'Protein heterodimerization activity'
521 category, which included 31 core histones (**Table 1**, **Table S.5**). The most significantly
522 enriched PEA category comprised 24 up-regulated genes related to 'Variant Sister
523 Chromatid segregation defective in early embryo' (q-value < 0.00001) (**Table 2, Table S.5)**.
524 Further indication of effects related to cell division and reproduction were seen by 19
525 histones and ribosomal subunits encoding genes associated to 'Diplotene absent during
526 oogenesis' phenotype. Another 19 up-regulated genes were related to 'Apoptosis fails to
527 occur'. These included activator of the programmed cell-death pathway, *egl-1*, regulator of
528 asymmetric cell division, *ces-2*, regulator of cell fate during post-embryonic development,
529 *mab-5, mcd-1,* which promotes the developmentally programmed progression of cells
530 through apoptosis and 7 genes encoding for large and small ribosomal subunits (*rpl* and
531 *rps*) (**Table S.5**). Collectively, a large proportion of the DEGs were related to cell cycle
532 impairments and responses to genotoxic effects.
533
534
535
536
537
538
539
540

541 **Table 1.** Over-represented biological processes, molecular functions and cellular components functional
542 categories, from Gene Ontology (GO), which were up-regulated in *C. elegans* after 72 hours of exposure to 100
543 mGy·h^{-1} of gamma radiation. HyPergeometric probability distribution is adopted to measure the number of
544 enriched terms (Observed number of DEGs in each specific function).

Term (GEA)	Observed	Enrichment Fold Change	P value	Q value
Intracellular GO:0005622	466	1.1	0.0053	0.023
Organelle GO:0043226	401	1.1	0.0019	0.011
Cytoplasm GO:0005737	295	1.1	0.016	0.061
Cellular developmental process GO:0048869	92	1.7	5.90E-07	9.40E-06
Regulation of nucleobase-containing compound metabolic process GO:0019219	91	1.2	0.015	0.061
Membrane-enclosed lumen GO:0031974	86	1.3	0.0026	0.013
Supramolecular complex GO:0099080	61	2.7	1.90E-13	6.10E-12
Cytoskeleton GO:0005856	60	1.8	6.50E-06	6.90E-05
Hydrolase activity acting on acid anhydrides GO:0016817	57	1.3	0.027	0.087
Structural constituent of cuticle GO:0042302	53	4.4	1.10E-21	1.50E-19
Post-embryonic development GO:0009791	53	1.5	0.0015	0.0093
Collagen trimer GO:0005581	49	4	3.20E-18	2.10E-16
Peptide biosynthetic process GO:0043043	48	1.8	2.00E-05	0.0002
Neurogenesis GO:0022008	44	2.3	1.10E-07	2.40E-06
Neuron development GO:0048666	39	2.5	2.50E-08	6.30E-07
Cell projection organization GO:0030030	39	1.8	8.10E-05	0.00074
Protein heterodimerization activity GO:0046982	35	4.6	9.40E-16	4.00E-14
Nucleoplasm GO:0005654	33	1.6	0.0024	0.013
Actin filament-based process GO:0030029	31	2.7	1.30E-07	2.40E-06
Cell part morphogenesis GO:0032990	30	2.5	7.40E-07	1.10E-05
Nucleoside phosphate metabolic process GO:0006753	30	1.4	0.02	0.07
Ribose phosphate metabolic process GO:0019693	29	1.7	0.0012	0.0083
Cell morphogenesis involved in differentiation GO:0000904	28	2.5	3.10E-06	3.60E-05
Purine nucleotide metabolic process GO:0006163	28	1.8	0.00066	0.0048
Neuron projection guidance GO:0097485	24	2.8	8.00E-07	1.10E-05
Regulatory region nucleic acid binding GO:0001067	24	1.8	0.0014	0.0093
Post-embryonic animal organ development GO:0048569	22	1.7	0.0041	0.019
Negative regulation of RNA metabolic process GO:0051253	22	1.5	0.018	0.063
Purine nucleoside monophosphate metabolic process GO:0000976	21	2.3	8.40E-05	0.00074
Structural constituent of ribosome GO:0003735	21	2.1	0.00043	0.0035
Transcription regulatory region sequence-specific DNA binding GO:0000976	20	1.9	0.0018	0.011
RNA splicing via transesterification reactions GO:0000375	18	2.2	0.00064	0.0048
RNA polymerase II regulatory region DNA binding GO:0001012	17	1.8	0.0066	0.028
Reproductive system development GO:0061458	17	1.8	0.0071	0.029
Development of primary sexual characteristics GO:0045137	16	2	0.0028	0.014
Regulation of cellular amide metabolic process GO:0034248	16	2	0.0031	0.015
Molting cycle GO:0042303	14	1.7	0.016	0.061
Negative regulation of transcription by RNA polymerase II GO:0000122	14	1.7	0.017	0.063
Small ATPase binding GO:0031267	13	1.7	0.025	0.083
Ribonucleoprotein granule GO:0035770	12	1.7	0.024	0.082

545
546
547
548
549
550
551

552 **Table 2.** Functional over-represented variants from Phenotype Enrichment analysis (PEA) that were up-
553 regulated in *C. elegans* after 72 hours of exposure to 100 mGy·h^{-1} of gamma radiation (total doses ~7.2 Gy).
554 Hypergeometric probability distribution is adopted to measure the number of enriched terms (Observed
555 number of DEGs in each specific function).

Term (PEA)	Observed	Enrichment Fold Change	P value	Q value
Protein interaction variant WBPhenotype:0001369	71	1.3	0.0053	0.09
Avoids bacterial lawn WBPhenotype:0000402	65	1.6	4.20E-05	0.0046
Cytokinesis variant WBPhenotype:0002408	48	1.7	6.40E-05	0.0047
Endosome morphology variant WBPhenotype:0002090	45	1.5	0.0028	0.055
Lysosome-related organelle morphology variant WBPhenotype:0002095	42	1.5	0.0024	0.054
Neuronal outgrowth variant WBPhenotype:0000572	38	1.7	0.00051	0.023
Sluggish WBPhenotype:0000646	34	1.6	0.0015	0.049
Endosome localization variant WBPhenotype:0002100	34	1.7	0.00088	0.032
Sister chromatid segregation defective early emb WBPhenotype:0000772	26	3.1	2.40E-08	5.20E-06
Pleiotropic defects severe early emb WBPhenotype:0000270	22	2	0.00037	0.02
Diplotene absent during oogenesis WBPhenotype:0001954	19	1.9	0.0016	0.049
Apoptosis fails to occur WBPhenotype:0000184	16	1.9	0.0035	0.063
Gonad small WBPhenotype:0001957	15	2.1	0.0022	0.053

556

557

558 ### 3.2.2 Over-represented categories modulated by ionizing radiation-induced
559 oxidative damage

560

561 The transcriptome analysis, at 100 mGy·h^{-1}, identified several genes involved in oxidation-
562 reduction processes and AOD (antioxidant defences) system, within the cytosol or in the
563 mitochondrion *(ctl-1, COX1, COX2, COX3, cox-4, cox-5B, cox-6C, cox-7C, CYTB, hpo-19, sdhd-1,*
564 *ucr-2.1, gst-20, egl-1, egl-18, trx-2, trxr-2, sod-1* and *rad-8)*. Moreover, we found significant
565 up-regulation of genes involved in the glutathione *de novo* synthesis, such as F22F7.7 and
566 gln-3. Therefore, in order to identify specific transcriptional responses related to the
567 increased generation of ROS and evidence of oxidative damage effects on cell physiology

568 and metabolism, we performed an in depth manual assignment of the DEGs from
569 nematodes exposed to 100 mGy·h^{-1} into relevant categories assigned from the curated
570 WormBase phenotype (Lee et al., 2017) and transcriptomic analysis of oxidative stress
571 (Shin et al., 2011) (**Fig. 8, Table S.7**). As expected, a number of genes within Oxidative
572 stress response, PCD (Programmed Cell Death), DNA damage and response to ionizing
573 radiation were found (**Fig. 8**). Within the first most over-represented category
574 (Programmed cell death), we found genes related to general response to stress, such as
575 Autophagy (*atg-3, atg-9, ces-2* and *rab-7*), but also Cell cycle and Cell division (*pch-2, egl-1,*
576 *hus-1, ced-12, dapk-1, ces-2, chk-1, mcd-1, tads-1, pcn-1, car-1, set-17*), Ribosomal proteins
577 (*rpl-12, rpl-13, rpl-18, rpl-19, rpl-20, rpl-26, rps-10, rps-20, rps-26, rps-3, rps-6, rps-9*),
578 Proteasome (*pbs-1, pbs-1, pbs-5*) and Histones (*his-24, his-68, his-3, his-7, his-61, his-47*)
579 (**Table S.7**). Phenotypes directly related to exposure to ionizing radiation were also found
580 with respect to organismal and germline response, these included genes related to cell cycle
581 and DNA repair (*rad-54*, *chk-1, hus-1, umps-1 and rpa-2*), innate immune response (*elt-2*),
582 chromosome segregation and apoptosis (*hus-1, rad-54, ing-3, lin-40* and *car-1*).
583 From the total DEGs resulting after exposure to 100 mGy·h^{-1} we found 40 genes involved in
584 mitochondrial functions, among them, genes related to mitochondrial membrane,
585 mitochondrial ribosomal proteins, mitochondrial metabolism and mitochondrial
586 respiratory chain. Among the selected phenotypes, mitochondrial metabolism included
587 mostly up-regulated genes, while mitochondrial respiratory chain was the only phenotype
588 significantly down-regulated, comprising 10 (*COX1, COX2, COX3, ND1, ND2, ND3, ND4, ND5,*
589 *CYTB* and *ATP6*) of the 12 genes which encode for the oxidative phosphorylation system
590 (Chomyn and Attardi, 2014) (**Table S.7**).

591 The second most represented category (**Fig. 8**) included 85 genes found in common with
592 RNA sequencing analysis performed on oxidative stressed wild-type N2 (499 DEGs in total)
593 after exposure to Paraquat from a previous study by Shin et al. (2011). Among these DEGs
594 found in common, 80 genes showed significant up-regulation and were mostly related to
595 Collagen (*col-104, col-107, col-109, col-130, col-155, col-166, col-167, col-48, col-77, col-81,*
596 *col-95, let-2*), Mitochondrion (*sdhd-1, tomm-7, F58F12.1*), Histones (*his*) and Ribosomal
597 proteins (*rpl, rps*), the list also included the heat-shock protein *hsp-3* and the *daf-2* regulated
598 gene *dao-2*.
599 Consistent with the effects induced by oxidative damage (Shin et al., 2011), lipid
600 metabolism, cuticle morphology, protein degradation and energy expenditure were also
601 among the most over-represented phenotypes, comprising mostly up-regulated genes
602 (**Table S.7**).
603

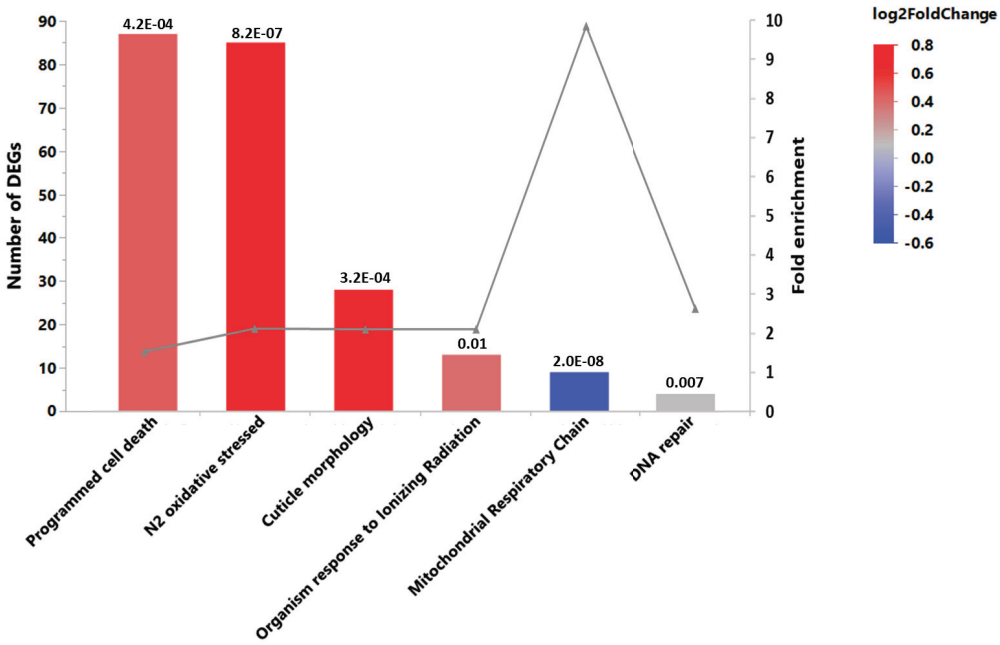

Figure 8. Over-represented categories modulated by ionizing radiation-induced oxidative damage resulting from 72 hours exposure to 100 mGy·h^{-1} of gamma radiation (total doses ~ 7.2 Gy) in the nematode *C. elegans.* (Data labels indicate Fisher's exact test *p*-values).

4. Discussion

The oxidative damage exerted on cellular molecules and macromolecules accounts for the total indirect effect following exposure to ionizing radiation (Azzam et al., 2012, Reisz et al., 2014). Therefore, the assessment of ROS/AOD levels and the subsequent oxidative damage response represents a fundamental parameter to understand and monitor the

616 changes in the homeostasis of an organism. To the best of our knowledge, this is the first
617 study to demonstrate *in vivo* ROS formation, antioxidant response and oxidative stress
618 effects to the cellular redox homeostasis in a radiation tolerant organism subjected to
619 chronic gamma irradiation. Furthermore, we connect molecular initiating events related to
620 ROS production and redox imbalance to phenotypical effects by performing a deep gene
621 expression analysis. Consistent with previous studies (Buisset-Goussen et al., 2014,
622 Maremonti et al., 2019), only dose-rates ≥40 mGy·h^{-1} (total doses ≥3.9 Gy) were able to
623 inflict a reprotoxic effect (**Fig. 1**). In line with studies performed on other aquatic and soil
624 organisms (Gomes et al., 2018, Gomes et al., 2017, Xie et al., 2019), our study suggests that
625 ROS production plays an important role in the induction of molecular, cellular and
626 organismal adverse effects also in *C. elegans*, with reproduction being the most
627 radiosensitive endpoint compared to somatic growth, fertility and mortality (Hertel-Aas et
628 al., 2007, Adam-Guillermin et al., 2012, Hurem et al., 2017, Parisot et al., 2015). No
629 significant effects with respect to somatic growth or somatic cell viability could be detected
630 even for nematodes that received 100 mGy·h^{-1} (total doses ~9.6 Gy) during their entire
631 larval development. This demonstrates that *C. elegans* has a relatively high tolerance
632 towards the effects of gamma radiation at the organismal level, but the mechanisms
633 involved remained to be elucidated. By using ROS reporter strain we were able to
634 investigate whether ionizing radiation affected cellular metabolism in *C. elegans in vivo*, but
635 also to address whether tolerance to ionizing radiation is mediated by high anti-oxidant
636 capacity.
637
638

4.1 ROS production and scavenging in *C. elegans* exposed to chronic gamma radiation

External gamma irradiation causes ionizations homogenously in the whole body of an organism like *C. elegans*. We therefore hypothesised that ROS formation would be dose-rate dependent and uniform within all cells and tissues of the nematode. To investigate the effect of gamma radiation on ROS formation in *C. elegans* we first assessed the effect on *sod-1* gene expression as a proxy for $O_2^{\cdot-}$ production. The results confirmed an overall linear correlation between dose-rate and *sod-1* expression (**Fig. 2**). The response was uniform throughout the entire nematode body, including embryos (**Fig. 2.c and 3.d**). Any discrepancies could be ascribed to tissue specific constraints *of sod-1::gfp* expression (Doonan et al., 2008). The fact that *sod-1* expression increased with time implies continuous formation and accumulation of $O_2^{\cdot-}$ during the exposure. These observations are consistent with the LET-model for radiolysis radical formation (Smith et al., 2012). Notably, the $O_2^{\cdot-}$ formation by gamma radiation appears to be quite high considering that the *sod-1* response was about 3-fold higher compared to Paraquat exposure (**Fig. S.2**). This indicated a considerable potential for other effects of ROS and oxidative damage.

In other species (i.e. bdelloid rotifers) the enhanced capacity for scavenging reactive molecular species generated by ionizing radiation has been addressed as one of the major contributors to radiation resistance (Krisko et al., 2012). Therefore, in the current study, we have assessed the redox status after chronic irradiation, in order to verify whether the unusually high abundance of AODs in *C. elegans* compared to other organisms plays a key role in its tolerance towards ionizing radiation.

662 Consistent with results from other organisms expressing high radioresistance (Krisko et al.,
663 2012), we measured higher levels of AODs in nematodes exposed to much lower dose-rates
664 of gamma radiation. In particular, after 48 hours of exposure and from dose-rates higher
665 than 1 mGy·h^{-1} (total doses ≥0.05 Gy), we measured a linear dose-rate dependent increase
666 of cytosolic superoxide dismutase and a significant imbalance in the oxidation of the
667 [GSSG]/[2GSH] couple (**Fig 2. a** and **6. a**). On the other hand, at this time-point, H_2O_2 levels
668 did not show a significant change in any of the irradiated groups, even though a linear dose-
669 dependent increase was detected (SLR) (**Fig 4. a**). A time-dependent increase in the levels
670 of SOD1 and H_2O_2 was measured after 72 hours of irradiation, with SOD1 and H_2O_2 levels
671 being significantly increased already at dose-rates ≥1 mGy·h^{-1} (total doses ≥0.08 Gy). At this
672 time-point, as should be expected, the highest dose-rate of exposure (100 mGy·h^{-1}, total
673 dose ~7.2 Gy) showed the most elevated levels of ROS and AODs (**Fig 2. a**, **4. a, 6. a**).
674 Under 'normal' aerobic conditions, during mitochondrial respiration, approximately 2 – 3%
675 of oxygen is incompletely reduced and leads to the production of a small amount of
676 superoxide radical anion ($O_2^{\cdot-}$) through the mitochondrial electron transport chain (ETC)
677 (Turrens, 2003). This free radical is transformed into hydrogen peroxide (H_2O_2), which is
678 also a potent oxidizing agent, by the mitochondrial isoforms SOD2 and SOD3 (manganese
679 superoxide dismutase) (Brady, 2006, Brand, 2010, Daiber, 2010, Dröse and Brandt, 2012).
680 Nevertheless, $O_2^{\cdot-}$ may also leak into the cytosol through the voltage-dependent anion
681 channels (Han et al., 2003) to become the substrate for the cytosolic Cu, Zn-SOD (SOD1).
682 Upon cell exposure to ionizing radiation, the physiological production of ROS in the
683 different compartments of the cell are joined by ROS produced by water radiolysis (Szumiel,
684 2015). Moreover, perturbation in the redox balance can be further affected when

685 mitochondrial dysfunction occurs in irradiated cell, leading to ulterior production of
686 mitochondrial ROS in addition to the radicals resulting from the water radiolysis (Azzam et
687 al., 2012).
688 Therefore, we suggest that chronic exposure to gamma radiation may induce the
689 accumulation of $O_2^{\cdot-}$ inside the mitochondria, which due to the increased leakage of $O_2^{\cdot-}$ in
690 the cytosol contributed to the increased *sod-1* expression (**Fig. 2.a**). Moreover, the
691 dismutation of $O_2^{\cdot-}$ and the consequently increased production of H_2O_2 (**Fig. 4.a**) and other
692 ROS, over time, culminated in the observed effect on the redox status (**Fig. 6.a, 7.b**).
693 Maintenance of the proper [GSSG]/[2GSH] ratio ensures redox homeostasis, whereas
694 changes to this ratio provides effective means to adjust the redox state between as well as
695 within cellular compartments under different physiological conditions (Johnston and Ebert,
696 2012). The significant changes in the ratio of reduced glutathione to glutathione disulphide
697 in the different tissues and cell compartments (**Fig. 6** and **7.b-c**) indicated that ROS were
698 produced at higher rates than *C. elegans* was able to sequester. Furthermore, the increased
699 ROS production did significantly affect the overall cellular redox balance at 48 hours of
700 exposure (**Fig. 6.a**). It appears that at 72 hours of exposure the nematodes mobilized AOD
701 systems were capable of counteracting the redox imbalance in most tissues (**Fig 7.a**)
702 despite the increased ROS levels (**Fig. 2.a** and **Fig. 4.a**).
703 Glutathione plays an essential role in the antioxidant defence system, as a source of
704 electrons for antioxidant enzymes such as glutaredoxins and peroxidases (Pompella et al.,
705 2003). Two possible events can explain the partial restored balance of glutathione,
706 observed after 72 hours of exposure: i) the high concentrations (1-11 mM) of glutathione
707 in the cell, which ensure an abundance of electrons for these antioxidant systems and thus

a robust buffer against oxidative shifts in the redox state (Schafer and Buettner, 2001); ii) the induced glutathione *de novo* synthesis, as indicated by the up-regulation of gamma-glutamylcyclotransferase (*F22F7.7*) and glutamine synthetase *(gln-3*) (Lu, 2009), resulting from RNA-seq analysis on nematodes exposed to 100 mGy·h^{-1} (total dose ~7.2 Gy) (**Table S.3**).

However, changing the redox balance can alter the physiological homeostasis of an organism not only because ROS are harmful for proteins, lipids and nucleic acids, but also because they represent important signalling molecules in a biological system, and even a minor change can result in a substantial alteration for example in terms of metabolism, cell proliferation and host defence (Finkel and Holbrook, 2000). Despite the partially restored redox balance, observed after 72 hours with the *Grx1-roGFP2* strain, the increased expression of SOD1 and the high H_2O_2 levels measured, together with the glutathione redox imbalanced, observed after 48 hours of chronic gamma irradiation and in the gonads of 72 hours irradiated nematodes, implied that the changes of the redox status of the nematodes could cause significant oxidative damages and affect molecular, cellular and physiological processes of the organism.

4.2 Ionizing radiation-induced oxidative stress effects lead to differential regulation of genes required for cuticle morphology, protein degradation, lipid metabolism and gene expression

730 In the current study, the overall redox balance of nematodes exposed to chronic gamma
731 radiation was shown to be shifted towards a more oxidized status, since increased levels of
732 ROS and a temporary but significant imbalance in the ratio of reduced glutathione to
733 glutathione disulphide were measured. Within the "redox hypothesis" paradigm (Jones,
734 2008), much of the toxicity of oxidative stress could result from an oxidative shift in redox
735 state within one or more cellular compartments. This shift might transiently disrupt redox
736 signalling as well as perturb the regular function of redox regulated proteins within these
737 compartments. The result could still be pathological oxidative damage to cellular
738 components, even though the cause could be indirect. Therefore, we anticipated a
739 significant change in the transcriptome profile of irradiated nematodes, as a response to
740 the observed increased levels of ROS and AODs.
741 As hypothesised, the transcriptome analysis performed on nematodes exposed to 100
742 $mGy \cdot h^{-1}$ revealed differential modulation of genes involved in oxidation-reduction
743 processes and accordingly a significant enhancement of functions related to stress
744 response (Sections 3.2.1-3.2.2).
745 In line with the results from the *sod1::gfp* reporter strain and the two ratiometric
746 biosensors adopted in our study, RNA sequencing revealed dysregulation of genes involved
747 in AOD system such as *sod-1, ctl-1, glrx-10, gst-20, trx-2* and *trxr-2.* Moreover, changes in the
748 redox balance affected glutathione metabolism, by up-regulation of glutathione *de novo*
749 synthesis (Section 3.2.2).
750 Oxidative stress response was the most up-regulated phenotypical variant gene category
751 observed, followed by lipid metabolism, cuticle morphology and protein degradation (**Fig.**
752 **8, Table S.7**), all functions that have been previously correlated to oxidative damage in *C.*

753 *elegans* (Shin et al., 2011), which corroborates that chronic gamma radiation does cause an
754 oxidative stress type transcriptional response.
755 Chronic exposure to 100 mGy·h^{-1} of ionizing gamma radiation (total dose ~7.2 Gy) induced
756 up-regulation of 53 genes related to structural constituent of cuticle, collagen trimmer and
757 moulting cycle. As suggested by Shin and co-authors (2011), this significant enrichment
758 may indicate the involvement of collagens in the adaptive mechanism response against the
759 ionizing radiation-induced oxidative stress. In this organism, the cuticle represents the
760 barrier between the animal and the external environment, therefore it may have a direct
761 protective function towards environmental perturbations as well as being indirectly
762 regulated in response to ROS production and oxidative damage. Moreover, accumulation or
763 excess of collagen has been shown to cause radiation-induced fibrosis, as well as to be a
764 response to loss of redox-sensitive control during the inflammatory or proliferative stage
765 (Sarsour et al., 2009).
766 Proteins segregation and degradation has also been addressed as a major target of ionizing
767 radiation-induced oxidative damage, particularly, the carbonylation damage is
768 unrepairable and when this impairs the activity of key proteins, such as those needed to
769 repair and replicate the DNA, cell survival is endangered (Nyström, 2005, Daly, 2012).
770 Consistently, the differential regulation of 12 genes involved in protein ubiquitination
771 activity (*C17H11.6, mib-1, plr-1, rle-1, siah-1, skr-16, smo-1, ubc-15, ubc-20, ubc-3, ubl-1, urm-*
772 *1*), together with 6 genes encoding for proteasome subunits and protease activity (*asp-1,*
773 *pbs-1, pbs-2, pbs-5, psmd-9, try-10*) gave indication of protein damage effects under
774 exposure to chronic gamma radiation. This result was further validated by 17 DEGs

775 identified in the over-represented category "Protein degradation variant" resulting from
776 the oxidative-stress induced phenotype analysis (**Table S.7**).
777 Excessive ROS formation can also affect lipids, in particular the oxidative deterioration of
778 polyunsaturated fatty acids present in cellular membranes can lead to membrane
779 destabilization and therefore further oxidative damage to biomolecules (Halliwell and
780 Gutteridge, 2015). Consistent with the increased levels of H_2O_2 measured with the *HyPer*
781 biosensor, we observed effects on lipids through the identification of more than 50 DEGs
782 involved in lipid metabolism (**Table S.7**), the up-regulation of 86 genes involved in
783 membrane-enclosed lumen, 45 and 42 genes involved in endosome and lysosome-related
784 morphology, respectively (**Table 1, 2, Table S.5**). These results suggest that under chronic
785 exposure to ionizing gamma radiation, the modulation of processes involved in
786 maintenance, biosynthesis and accumulation of lipids is a further response to ROS
787 production, as well as associated to effects on cell and organelle's membrane.
788 To further validate the hypothesis that the increased ROS levels was among the molecular
789 initiating events responsible for the observed redox imbalance and the modulation of the
790 nematode's transcription profile, we found 85 genes in common with wild-type oxidative
791 stressed after exposure to Paraquat from Shin and co-authors (2011) ("N2 oxidative
792 stressed" category, **Fig. 8** and **Table S.7**). These genes were mostly involved in collagen
793 production, mitochondrial functions, ATP synthesis, chromatin modification (histones and
794 methyltransferase activity), ribosomal functions, response to heat stress and
795 ubiquitination; giving further evidence of the specific mode of action of ionizing gamma
796 radiation in terms of oxidative damage on a molecular and cellular level.
797

Furthermore, as a consequence of changes in the physiological process of cellular signalling, we observed a significant enrichment in molecular functions required for the modulation of the gene expression (Section 3.2.1), including chromatin remodelling and transcriptional regulation. Molecular functions related to chromatin domains, transcription, post-transcriptional modifications, RNA transport and processing were significantly over-represented (**Table 1**, **Fig. 9**), giving indication of changes in the gene expression profile of nematodes under exposure to chronic gamma radiation.

These findings demonstrate that a tolerant organism, like the nematode *C. elegans*, is able to effectively respond to a persistent stress condition, such as a chronic irradiation during the entire larval development, by modulating its biological, cellular and molecular functions (**Fig. 9**), in order to maintain the organism homeostasis, however this comes to the cost of energy expenditure and reproductive fitness (**Fig. 1**).

4.3 Transcriptomic analysis reveals mitochondrial functions and ATP synthesis as targets of ionizing gamma radiation in *C. elegans*

Exposure to ionizing radiation is associated with the manifestation of mitochondrial dysfunction (Azzam et al., 2012). Oxidative phosphorylation is susceptible to this stressor, due to the alteration of the complexes involved in the Electron Transport Chain (ETC) and the ATP synthase activity (Kam and Banati, 2013). As a response to oxidative stress, the mtDNA copy number increases (Hori et al., 2008) and in order to ensure stable levels of ATP also the mitochondrial mass increases (Dayal et al., 2009). Dysfunctions in the ETC

leads to further production of mitochondrial ROS, and conversely, cells deficient in mitochondrial ETC (rho$^{(0)}$ cells) do not show radiation-induced ROS production (Leach et al., 2001). Consistently, we observe compelling down-regulation of all ten protein encoding genes out of the 12 genes required for the assembly of the Mitochondrial respiratory chain (*COX1, COX2, COX3, ND1, ND2, ND3, ND4, ND5, CYTB* and *ATP6*) (**Fig. 8**, **Table S.7**). Furthermore, we identified down-regulation of 10 genes encoding for small and large mitochondrial ribosomal proteins (mrpl-10, mrpl-18, mrpl-28, mrpl-36, mrpl-41, mrpl-49, mrpl-50, mrps-17, mrps-21, mrps-23), which are required for the proper assembly and function of ETC mediated energy production (Berg et al., 2006). We also observed differential regulation of genes involved in Mitochondrial metabolism (*immt-1, let-2, ril-1, cox-4, sdha-1, madd-2, unc-52, rict-1, pgs-1, bcs-1, mics-1, mspn-1, mttu-1, nuaf-1, rad-8, ZK1128.1*), genome maintenance (*C27H6.9*), protein import (*tomm-22, tomm-7, ddp-1*), Energy expenditure (*sdha-1, cox-5B, rict-1, sdhd-1, T02H6.11*) (**Table S.7**) and ATP synthesis (*asb-2, asg-2, atp-1, atp-4, atp-5, catp-1,* vha-3 and *F58F12.1*) (**Fig. 9**). Differential regulation of the mitochondrial cytochrome b and its subunits (*CYTB, hpo-19, sdhd-1, ucr-2.1*) was also observed, specifically the inhibition of cytochrome b5 reductase (*hpo-19*) has previously shown to induce decreased levels of poly-unsaturated fatty acids (PUFAs), which leads to decreased fat accumulation, reduced brood size and impaired development (Zhang et al., 2016).

Mitochondrial dysfunctions in irradiated cells can significantly contribute to perturbation in the physiological redox reactions and signalling (Kam and Banati, 2013). Such perturbation can lead to signalling cascades which can induce a multitude of other non-targeted responses such as apoptosis, autophagy, nuclear DNA damage, genomic instability

844 and other degenerative conditions (Sidoti-de Fraisse et al., 1998, Lomonaco et al., 2009,
845 Choi et al., 2007, Sarsour et al., 2009). Thus, consistent with the induced AODs and ROS
846 production, measured in the current study, the changes observed in the nematode's
847 transcriptome profile, with respect to mitochondrial functions and ATP production, were a
848 clear evidence of the mitochondrial vulnerability under exposure to ionizing radiation and
849 a signal for late consequences on other cellular, molecular and biological functions.
850
851

852 4.4 Ionizing radiation-induced DNA damage leads to histones up-regulation 853 and methylation, defective chromosome segregation, programmed cell 854 death, and impairment of nervous system and embryonic development

855
856 Upon severe stress condition, survival is dependent on the ability of the cell to adapt or
857 resist the stress, by for instance repairing or replacing the damaged molecules (Finkel and
858 Holbrook, 2000). Beyond the well-known DNA repair mechanisms of homologous
859 recombination (HR) and non-homologous end-joining (NHEJ), emerging evidence indicates
860 that also epigenetic changes can enable adaptation responses in the surviving cells
861 (Szumiel, 2015, Wei et al., 2018). Consistent with this hypothesis, we identified a significant
862 up-regulation of 20 core histone encoding genes (H3, H4), which might represent a
863 response to DNA damage and, in this sense, a protective mechanism via the promotion of
864 chromatin condensation (Takata et al., 2013). Furthermore, methylation of lysine residues
865 on histones can play an important role in determining the repair pathway upon double-
866 strand breaks (DSBs)(Wei et al., 2018). In good accordance, we identified a significant up-

867 regulation of *dot-1.1, set-9, set-16* and *set-26*, which encode for histone-lysine N-
868 methyltransferases. The genes *set-9* and *set-26* are also required for longevity, germline
869 development and heat stress response, giving further evidence of the connection between
870 oxidative damage and adverse effects exerted by chronic irradiation on the reproductive
871 system.
872 Consistent with our previous study (Maremonti et al., 2019), we found further indication of
873 adverse effects exerted by chronic gamma irradiation on chromosome segregation, mitotic
874 and meiotic cell-cycle, spindle formation and embryonic development (**Fig. S.7; Tables 1,**
875 **2, Table S.6**). In both studies, these effects were accompanied by impairment of the
876 nematodes reproductive capacity (**Fig. 1.b**), which was further supported, in the current
877 study, by the down-regulation of more than 300 genes related to the reproductive system
878 (**Fig. S. 7.c**). Specifically, we found a differential regulation of cellular and molecular
879 functions related to reproduction, such as gamete development and fertilization,
880 cytokinesis, sister chromatid segregation defective in early embryo, diplotene absent
881 during oogenesis, gonad small, reproductive system development, meiotic chromosome
882 segregation, spindle position and orientation and aneuploidy. As already shown in our
883 previous study, where enhanced germ cell apoptosis and impaired spermatogenesis lead to
884 reprotoxicity (Maremonti et al., 2019), all these over-represented categories gave further
885 evidence of the persistent adverse effects induced by chronic gamma irradiation on the
886 meiotic process, which subsequently leads to loss of the reproductive fitness.
887
888 Oxidative metabolic processes that produce ROS are important for the regulation of the cell-
889 cycle functions, proliferation and differentiation (Sarsour et al., 2009). Hence, metabolic

890 defects that disrupt signalling function of ROS could be detrimental to a multitude of
891 cellular processes. In line with our previous research (Maremonti et al., 2019), in the
892 current study, chronic gamma irradiation showed effects on the cell-cycle via induction of
893 genomic instability and DNA damage through the differential expression of genes involved
894 in DNA double strand break (*dsb-3*), cell-cycle checkpoint (*hus-1*, *cdc-25.2, cdc-37, cdc-48.3,*
895 *chk-1, cki-1*) and DNA repair (*rad-54*, *chd-7, laf-1, pif-1, snrp-200, ssl-1*, *pms-2*, *nth-1, polk-1,*
896 *rpa-2* and *unc-51*). A cell damaged beyond repair will be destined to apoptosis; increased
897 levels of ROS formed inside the mitochondrion have the potential to induce downstream
898 regulation of genes required for apoptosis by the early ROS-dependent signalling pathway
899 (Sidoti-de Fraisse et al., 1998). Consistently, we found 87 differentially expressed genes
900 involved in programmed cell death (**Fig. 8**, **Table S.7**), among them *egl-1* and *hus-1*, which
901 are clear markers of DNA damage-induced apoptosis (Hofmann et al., 2002).
902 On the other hand, proliferative disorders due to differential regulation of the cell-cycle
903 under redox cycle control, are addressed as the cause of many dysfunctions as well as
904 diseases, including cancer and neurodegenerative disorders (Sarsour et al., 2009).
905 Consistently, a significant modulation of genes related to nervous system functions was
906 identified in our gene expression analysis, through the up-regulation of genes involved in
907 neurogenesis, neuronal development, neuron projection guidance and neuronal outgrowth
908 (**Table 1, 2, Table S.6**). These results suggest an effect exerted by ionizing radiation on
909 somatic cells. Specifically, and in contrast to the germline, adverse effects on somatic cells
910 might induce a savage beyond repair as indicated by the categories apoptosis fails to occur,
911 defective locomotion (sluggish), endosome and lysosome-related morphology variants
912 (**Table 2**) and autophagy related genes (*unc-51*, *atg-3, atg-9, ces-2* and *rab-7*). In particular,

913 the lysosome-mediated self-degradation process of autophagy can be used to supply the
914 cells with energy or provide building block for the synthesis of macromolecules, under
915 stress condition (Erdélyi et al., 2011). This mechanism is known to be specific for terminally
916 differentiated cells, where it is required for the effective elimination of damaged, non-
917 functional macromolecules and organelles, in order to avoid this cellular toxins to interfere
918 with cellular functions (Vellai et al., 2009). Moreover, the over-activation of autophagy in
919 cells of the nervous system has been suggested as the cause of "physiological" death
920 (Takács-Vellai et al., 2006). Autophagy and apoptosis are two intertwined processes
921 required redundantly for viability and normal development in *C. elegans* (Erdélyi et al.,
922 2011). In line with the significantly enhanced embryonic DNA damage and reduced somatic
923 growth, observed in parentally irradiated nematodes from our previous study (Maremonti
924 et al., 2019), the differential regulation of genes related to autophagy, programmed cell
925 death, embryonic and post-embryonic development (**Fig. S.7**, **Fig. 8**, **Table 1**), strongly
926 suggests that the effects of chronic gamma irradiation persist on the progeny of irradiated
927 nematodes.
928 Taken together these results demonstrate the ability of *C. elegans* to activate its wide range
929 of AODs and protective mechanisms against increased levels of ROS following chronic
930 gamma irradiation throughout its life cycle. This did however present a stress condition
931 able to induce changes in the physiological oxidants levels, which lead to a comprehensive
932 modulation of cellular and molecular functions (**Fig. 9**), leading up to adverse effects on
933 energy production/expenditure and reproductive capacity as well as persistent damage on
934 the parentally irradiated offspring (Maremonti et al., 2019).
935

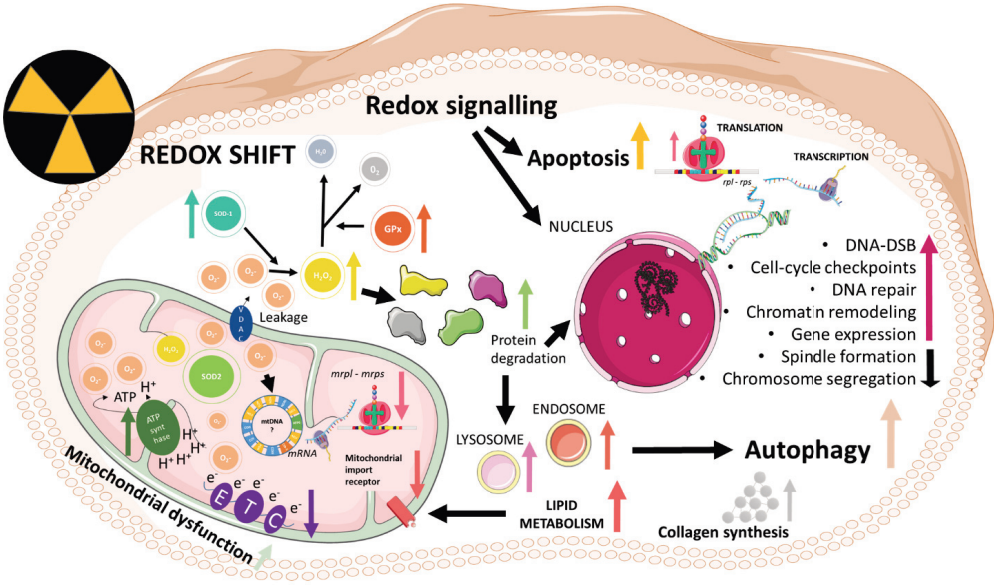

Figure 9. Conceptual model of cellular and molecular processes induced (↑) or inhibited (↓) after 72 hours of chronic exposure to gamma radiation (100 mGy·h^{-1}) in the nematode *C. elegans.*

ETC: Electron Transport Chain. VDAC: Voltage-Dependent Anion Channel. SOD: Superoxide Dismutase. *mrpl – mrps*: Mitochondrial Ribosomal Protein Large – Small subunit. mtDNA: mitochondrial DNA. GPx: Glutathione Peroxidases. *rpl – rps*: Ribosomal Protein Large – Small subunit. DNA-DSB: DNA Double Strand Break.

Conclusion

In the radioresistant nematode *C. elegans,* chronic exposure to ionizing gamma radiation, during larval development, significantly enhances the levels of ROS and induces activation of AODs. At doses ≤10 mGy·h^{-1} (total doses ≤0.8 Gy)nematodes demonstrate to tolerate chronic gamma irradiation, while at doses ≥40 mGy·h^{-1} (total doses ≥2.9 Gy) , the observed

redox shift in the cell induces oxidative damage and changes in the redox signalling functions, modulating a cascade of molecular and cellular processes in the entire organism with adverse consequences for its reproductive system. Specifically, oxidative damage of proteins, lipids and DNA is suggested as the cause of mitochondrial dysfunctions, impaired energy production, autophagy induction, enhanced programmed cell death and defective meiosis, which leads to impairment of the reproductive fitness and potential adverse effects on the progeny. Findings from the current study provide detailed information of the consequences of chronic exposure to ionizing radiation, as well as the important role of redox balance and signalling for the cellular homeostasis, particularly in the gonads. Future research should be focused on the effects of this imbalance at the mitochondrial level, with emphasis on the potential adverse effects of ROS on the ATP production and the mitochondrial genome.

Funding

This work was supported by the Norwegian University of Life Sciences (NMBU) through a PhD scholarship and by the Research Council of Norway through its Centre of Excellence (CoE) “Centre for Environmental Radioactivity” (CERAD, project No. 223268).

Acknowledgments

We are grateful to Dr. Marina Ezcurra and Prof. David Gems from the Institute of Healthy Ageing Genetics (University College London) for providing the *C. elegans* reporter strain *sod-1::gfp* (GA508 wuls54[pPD95.77 sod-1::GFP, rol-6(su1006)]) and Dr. Braeckman from the Laboratory for Ageing Physiology and Molecular Evolution (University of Ghent, Belgium) for providing the *C. elegans* biosensors *Grx1-roGFP2* and *HyPer*. We also thank Fabian Grammes for bioinformatics assistance and Simen Gylterud Owe, YeonKyeong Lee, Hilde Raanaas Kolstad and Lene Cecilie Hermansen for kind assistance and help during the microscopy analysis.

References

ADAM-GUILLERMIN, C., PEREIRA, S., DELLA-VEDOVA, C., HINTON, T. & GARNIER-LAPLACE, J. 2012. Genotoxic and Reprotoxic Effects of Tritium and External Gamma Irradiation on Aquatic Animals. *In:* WHITACRE, D. M. (ed.) *Reviews of Environmental Contamination and Toxicology.* New York, NY: Springer New York.

ANGELES-ALBORES, D., LEE, R. Y., CHAN, J. & STERNBERG, P. W. 2016. Tissue enrichment analysis for *C. elegans* genomics. *BMC bioinformatics,* 17**,** 366.

ANGELES-ALBORES, D., LEE, R. Y., CHAN, J. & STERNBERG, P. W. 2017. Phenotype and gene ontology enrichment as guides for disease modeling in C. elegans. *BioRxiv***,** 106369.

AZZAM, E. I., JAY-GERIN, J.-P. & PAIN, D. 2012. Ionizing radiation-induced metabolic oxidative stress and prolonged cell injury. *Cancer letters,* 327**,** 48-60.

BACK, P., DE VOS, W. H., DEPUYDT, G. G., MATTHIJSSENS, F., VANFLETEREN, J. R. & BRAECKMAN, B. P. 2012. Exploring real-time in vivo redox biology of developing and aging Caenorhabditis elegans. *Free Radic Biol Med,* 52**,** 850-9.

BERG, J. M., TYMOCZKO, J. L. & STRYER, L. 2006. *Biochemistry. 5th,* New York: , WH Freeman.

BERGENDI, L., BENEŠ, L., ĎURAČKOVÁ, Z. & FERENČIK, M. 1999. Chemistry, physiology and pathology of free radicals. *Life Sciences,* 65**,** 1865-1874.

BJERKE, H. & HETLAND, P. O. 2014. Dosimetri ved FIGARO gammaanlegget ved NMBU, ÅS. *Målerapport fra oppmåling av doseraten i strålefeltet fra kobolt-60. NRPA Technical Document Series,* 2.

1017 BRADY, N. R., HAMACHER-BRADY, A., WESTERHOFF, H. V., & GOTTLIEB, R. A. 2006. A wave
1018 of reactive oxygen species (ROS)-induced ROS release in a sea of excitable
1019 mitochondria. *Antioxidants & redox signaling,* 8**,** 1651-1665.
1020 BRAECKMAN, B., BACK, P. U., MATTHIJSSENS, F. G. E., OLSEN, A. E. & GILL, M. S. E. 2017.
1021 Oxidative Stress. *In:* RATTAN, S. I. S. (ed.) *Healthy Ageing and Longevity.* Springer.
1022 BRAECKMAN, B. P., SMOLDERS, A., BACK, P. & DE HENAU, S. 2016. In Vivo Detection of
1023 Reactive Oxygen Species and Redox Status in Caenorhabditis elegans. *Antioxidants*
1024 *& Redox Signaling,* 25**,** 577-592.
1025 BRAND, M. D. 2010. The sites and topology of mitochondrial superoxide production.
1026 *Experimental gerontology,* 45**,** 466-472.
1027 BUISSET-GOUSSEN, A., GOUSSEN, B., DELLA-VEDOVA, C., GALAS, S., ADAM-GUILLERMIN, C.
1028 & LECOMTE-PRADINES, C. 2014. Effects of chronic gamma irradiation: a
1029 multigenerational study using *Caenorhabditis elegans*. *J Environ Radioact,* 137**,** 190-
1030 7.
1031 CABREIRO, F., ACKERMAN, D., DOONAN, R., ARAIZ, C., BACK, P., PAPP, D., BRAECKMAN, B.
1032 P. & GEMS, D. 2011. Increased life span from overexpression of superoxide
1033 dismutase in Caenorhabditis elegans is not caused by decreased oxidative damage.
1034 *Free Radical Biology and Medicine,* 51**,** 1575-1582.
1035 CHEN, Q., CHAI, Y. C., MAZUMDER, S., JIANG, C., MACKLIS, R. M., CHISOLM, G. M. & ALMASAN,
1036 A. 2003. The late increase in intracellular free radical oxygen species during
1037 apoptosis is associated with cytochrome c release, caspase activation, and
1038 mitochondrial dysfunction. *Cell Death Differ,* 10**,** 323-34.

1039 CHOI, K.-M., KANG, C.-M., CHO, E. S., KANG, S. M., LEE, S. B. & UM, H.-D. 2007. Ionizing
1040 radiation-induced micronucleus formation is mediated by reactive oxygen species
1041 that are produced in a manner dependent on mitochondria, Nox1, and JNK. *Oncology*
1042 *reports,* 17**,** 1183-1188.
1043 CHOMYN, A. & ATTARDI, G. 2014. Mitochondrial gene products. *Current Topics in*
1044 *Bioenergetics: Structure, Biogenesis, and Assembly of Energy Transducing Enzyme*
1045 *Systems,* 15**,** 295.
1046 DAIBER, A. 2010. Redox signaling (cross-talk) from and to mitochondria involves
1047 mitochondrial pores and reactive oxygen species. *Biochim Biophys Acta,* 1797**,** 897-
1048 906.
1049 DALY, M. J. 2012. Death by protein damage in irradiated cells. *DNA Repair (Amst),* 11**,** 12-
1050 21.
1051 DAYAL, D., MARTIN, S. M., OWENS, K. M., AYKIN-BURNS, N., ZHU, Y., BOOMINATHAN, A.,
1052 PAIN, D., LIMOLI, C. L., GOSWAMI, P. C., DOMANN, F. E. & SPITZ, D. R. 2009.
1053 Mitochondrial Complex II Dysfunction Can Contribute Significantly to Genomic
1054 Instability after Exposure to Ionizing Radiation. *Radiation Research,* 172**,** 737-745,
1055 9.
1056 DOBIN, A., DAVIS, C. A., SCHLESINGER, F., DRENKOW, J., ZALESKI, C., JHA, S., BATUT, P.,
1057 CHAISSON, M. & GINGERAS, T. R. 2013. STAR: ultrafast universal RNA-seq aligner.
1058 *Bioinformatics,* 29**,** 15-21.
1059 DOONAN, R., MCELWEE, J. J., MATTHIJSSENS, F., WALKER, G. A., HOUTHOOFD, K., BACK, P.,
1060 MATSCHESKI, A., VANFLETEREN, J. R. & GEMS, D. 2008. Against the oxidative
1061 damage theory of aging: superoxide dismutases protect against oxidative stress but

have little or no effect on life span in Caenorhabditis elegans. *Genes Dev,* 22**,** 3236-41.

DRÖSE, S. & BRANDT, U. 2012. Molecular mechanisms of superoxide production by the mitochondrial respiratory chain. *Mitochondrial Oxidative Phosphorylation.* Springer.

DUBOIS, C., LECOMTE, C., RUYS, S. P. D., KUZMIC, M., DELLA-VEDOVA, C., DUBOURG, N., GALAS, S. & FRELON, S. 2018. Precoce and opposite response of proteasome activity after acute or chronic exposure of C. elegans to γ-radiation. *Scientific Reports,* 8**,** 11349.

ERDÉLYI, P., BORSOS, É., TAKÁCS-VELLAI, K., KOVÁCS, T., KOVÁCS, A. L., SIGMOND, T., HARGITAI, B., PÁSZTOR, L., SENGUPTA, T., DENGG, M., PÉCSI, I., TÓTH, J., NILSEN, H., VÉRTESSY, B. G. & VELLAI, T. 2011. Shared developmental roles and transcriptional control of autophagy and apoptosis in *Caenorhabditis elegans*. *Journal of Cell Science,* 124**,** 1510-1518.

FINKEL, T. & HOLBROOK, N. J. 2000. Oxidants, oxidative stress and the biology of ageing. *Nature,* 408**,** 239.

GEMS, D. & DOONAN, R. 2008. Oxidative Stress and Aging in the NematodeCaenorhabditis elegans. *Oxidative Stress in Aging.* Springer.

GOMES, A., FERNANDES, E. & LIMA, J. L. 2005. Fluorescence probes used for detection of reactive oxygen species. *Journal of biochemical and biophysical methods,* 65**,** 45-80.

GOMES, T., SONG, Y., BREDE, D. A., XIE, L., GUTZKOW, K. B., SALBU, B. & TOLLEFSEN, K. E. 2018. Gamma radiation induces dose-dependent oxidative stress and transcriptional alterations in the freshwater crustacean Daphnia magna. *Science of The Total Environment,* 628**,** 206-216.

1085 GOMES, T., XIE, L., BREDE, D., LIND, O.-C., SOLHAUG, K. A., SALBU, B. & TOLLEFSEN, K. E.
1086 2017. Sensitivity of the green algae Chlamydomonas reinhardtii to gamma radiation:
1087 photosynthetic performance and ROS formation. *Aquatic toxicology,* 183**,** 1-10.
1088 GUO, X., SUN, J., BIAN, P., CHEN, L., ZHAN, F., WANG, J., XU, A., WANG, Y., HEI, T. K. & WU, L.
1089 2013. Radiation-induced bystander signaling from somatic cells to germ cells in
1090 Caenorhabditis elegans. *Radiat Res,* 180**,** 268-75.
1091 HALLIWELL, B. & GUTTERIDGE, J. M. 2015. *Free radicals in biology and medicine*, Oxford
1092 University Press, USA.
1093 HAN, D., ANTUNES, F., CANALI, R., RETTORI, D. & CADENAS, E. 2003. Voltage-dependent
1094 anion channels control the release of the superoxide anion from mitochondria to
1095 cytosol. *Journal of Biological Chemistry,* 278**,** 5557-5563.
1096 HARTMAN, P. S., SIMPSON, V. J., JOHNSON, T. & MITCHELL, D. 1988. Radiation sensitivity
1097 and DNA repair in Caenorhabditis elegans strains with different mean life spans.
1098 *Mutation Research Letters,* 208**,** 77-82.
1099 HERTEL-AAS, T., BRUNBORG, G., JAWORSKA, A., SALBU, B. & OUGHTON, D. H. 2011. Effects
1100 of different gamma exposure regimes on reproduction in the earthworm Eisenia
1101 fetida (Oligochaeta). *Science of The Total Environment,* 412-413**,** 138-147.
1102 HERTEL-AAS, T., OUGHTON, D. H., JAWORSKA, A., BJERKE, H., SALBU, B. & BRUNBORG, G.
1103 2007. Effects of chronic gamma irradiation on reproduction in the earthworm
1104 Eisenia fetida (Oligochaeta). *Radiation research,* 168**,** 515-526.
1105 HOFMANN, E. R., MILSTEIN, S., BOULTON, S. J., YE, M., HOFMANN, J. J., STERGIOU, L.,
1106 GARTNER, A., VIDAL, M. & HENGARTNER, M. O. 2002. *Caenorhabditis elegans* HUS-1

1107 Is a DNA Damage Checkpoint Protein Required for Genome Stability and EGL-1-
1108 Mediated Apoptosis. *Current Biology,* 12**,** 1908-1918.
1109 HONNEN, S. 2017. Caenorhabditis elegans as a powerful alternative model organism to
1110 promote research in genetic toxicology and biomedicine. *Archives of Toxicology,* 91**,**
1111 2029-2044.
1112 HORI, A., YOSHIDA, M., SHIBATA, T. & LING, F. 2008. Reactive oxygen species regulate DNA
1113 copy number in isolated yeast mitochondria by triggering recombination-mediated
1114 replication. *Nucleic Acids Research,* 37**,** 749-761.
1115 HUREM, S., GOMES, T., BREDE, D. A., LINDBO HANSEN, E., MUTOLOKI, S., FERNANDEZ, C.,
1116 MOTHERSILL, C., SALBU, B., KASSAYE, Y. A., OLSEN, A.-K., OUGHTON, D., ALESTRÖM,
1117 P. & LYCHE, J. L. 2017. Parental gamma irradiation induces reprotoxic effects
1118 accompanied by genomic instability in zebrafish (Danio rerio) embryos.
1119 *Environmental Research,* 159**,** 564-578.
1120 INTERNATIONAL, O., FOR, STANDARDIZATION 2010. Water quality—Determination of the
1121 toxic effect of sediment and soil samples on growth, fertility and reproduction of
1122 *Caenorhabditis elegans(Nematoda)*
1123 *International Organization for Standardization (ISO) 10872:2010*.
1124 JOHNSTON, A. D. & EBERT, P. R. 2012. The Redox System in C. elegans, a Phylogenetic
1125 Approach. *Journal of Toxicology,* 2012**,** 20.
1126 JONES, D. P. 2008. Radical-free biology of oxidative stress. *American Journal of Physiology-*
1127 *Cell Physiology,* 295**,** C849-C868.
1128 KAM, W. W.-Y. & BANATI, R. B. 2013. Effects of ionizing radiation on mitochondria. *Free*
1129 *Radical Biology Medicine,* 65**,** 607-619.

KHANNA, N., CRESSMAN III, C., TATARA, C. & WILLIAMS, P. 1997. Tolerance of the nematode Caenorhabditis elegans to pH, salinity, and hardness in aquatic media. *Archives of Environmental Contamination and Toxicology,* 32**,** 110-114.

KRISKO, A., LEROY, M., RADMAN, M. & MESELSON, M. 2012. Extreme anti-oxidant protection against ionizing radiation in bdelloid rotifers. *Proc Natl Acad Sci U S A,* 109**,** 2354-7.

LEACH, J. K., VAN TUYLE, G., LIN, P.-S., SCHMIDT-ULLRICH, R. & MIKKELSEN, R. B. 2001. Ionizing radiation-induced, mitochondria-dependent generation of reactive oxygen/nitrogen. *Cancer research,* 61**,** 3894-3901.

LEE, R. Y. N., HOWE, K. L., HARRIS, T. W., ARNABOLDI, V., CAIN, S., CHAN, J., CHEN, W. J., DAVIS, P., GAO, S. & GROVE, C. 2017. WormBase 2017: molting into a new stage. *Nucleic acids research,* 46**,** D869-D874.

LEWIS, J. A. & FLEMING, J. T. 1995. Chapter 1 Basic Culture Methods. *In:* EPSTEIN, H. F. & SHAKES, D. C. (eds.) *Methods in Cell Biology.* Academic Press.

LIND, O. C., OUGHTON, D. H. & SALBU, B. 2019. The NMBU FIGARO low dose irradiation facility. *International journal of radiation biology,* 95**,** 76-81.

LINDBO HANSEN E. , P. O. H. Ø. 2017. Air kerma measurements with Landauer nanoDots in Cs-137 and Co-60 beams. Teknisk dokument nr. 8. *Norwegian Radiation Protection Authority*.

LOMONACO, S. L., FINNISS, S., XIANG, C., DECARVALHO, A., UMANSKY, F., KALKANIS, S. N., MIKKELSEN, T. & BRODIE, C. 2009. The induction of autophagy by γ-radiation contributes to the radioresistance of glioma stem cells. *International journal of cancer,* 125**,** 717-722.

LOVE, M. I., ANDERS, S., KIM, V. & HUBER, W. 2015. RNA-Seq workflow: gene-level exploratory analysis and differential expression. *FResearch,* 4.

LU, S. C. 2009. Regulation of glutathione synthesis. *Molecular Aspects of Medicine,* 30**,** 42-59.

MAREMONTI, E., EIDE, D. M., OUGHTON, D. H., SALBU, B., GRAMMES, F., KASSAYE, Y. A., GUÉDON, R., LECOMTE-PRADINE, C. & BREDE, D. A. 2019. Gamma radiation induces life stage-dependent reprotoxicity in Caenorhabditis elegans via impairment of spermatogenesis. *Science of The Total Environment***,** 133835.

MEYER, A. J. & DICK, T. P. 2010. Fluorescent protein-based redox probes. *Antioxidants & redox signaling,* 13**,** 621-650.

MONTGOMERY, D. C., PECK, E. A. & VINING, G. G. 2012. *Introduction to linear regression analysis*, John Wiley & Sons.

NYSTRÖM, T. 2005. Role of oxidative carbonylation in protein quality control and senescence. *The EMBO journal,* 24**,** 1311-1317.

PARISOT, F., BOURDINEAUD, J.-P., PLAIRE, D., ADAM-GUILLERMIN, C. & ALONZO, F. 2015. DNA alterations and effects on growth and reproduction in Daphnia magna during chronic exposure to gamma radiation over three successive generations. *Aquatic Toxicology,* 163**,** 27-36.

POMPELLA, A., VISVIKIS, A., PAOLICCHI, A., TATA, V. D. & CASINI, A. F. 2003. The changing faces of glutathione, a cellular protagonist. *Biochemical Pharmacology,* 66**,** 1499-1503.

PORTA-DE-LA-RIVA, M., FONTRODONA, L., VILLANUEVA, A. & CERON, J. 2012. Basic Caenorhabditis elegans methods: synchronization and observation. *J Vis Exp***,** e4019.

1175 REISZ, J. A., BANSAL, N., QIAN, J., ZHAO, W. & FURDUI, C. M. 2014. Effects of ionizing
1176 radiation on biological molecules—mechanisms of damage and emerging methods
1177 of detection. *Antioxidants & redox signaling,* 21**,** 260-292.
1178 RILEY, P. A. 1994. Free radicals in biology: oxidative stress and the effects of ionizing
1179 radiation. *Int J Radiat Biol,* 65**,** 27-33.
1180 SARSOUR, E. H., KUMAR, M. G., CHAUDHURI, L., KALEN, A. L. & GOSWAMI, P. C. 2009. Redox
1181 control of the cell cycle in health and disease. *Antioxidants*
1182 *redox signaling,* 11**,** 2985-3011.
1183 SCHAFER, F. Q. & BUETTNER, G. R. 2001. Redox environment of the cell as viewed through
1184 the redox state of the glutathione disulfide/glutathione couple. *Free Radical Biology*
1185 *and Medicine,* 30**,** 1191-1212.
1186 SHIN, H., LEE, H., FEJES, A. P., BAILLIE, D. L., KOO, H.-S. & JONES, S. J. 2011. Gene expression
1187 profiling of oxidative stress response of C. elegans aging defective AMPK mutants
1188 using massively parallel transcriptome sequencing. *BMC research notes,* 4**,** 34.
1189 SIDOTI-DE FRAISSE, C., RINCHEVAL, V., RISLER, Y., MIGNOTTE, B. & VAYSSIÈRE, J.-L. 1998.
1190 TNF-α activates at least two apoptotic signaling cascades. *Oncogene,* 17**,** 1639.
1191 SMITH, J. T., WILLEY, N. J. & HANCOCK, J. T. 2012. Low dose ionizing radiation produces too
1192 few reactive oxygen species to directly affect antioxidant concentrations in cells. *Biol*
1193 *Lett,* 8**,** 594-7.
1194 SPITZ, D. R., AZZAM, E. I., LI, J. J. & GIUS, D. 2004. Metabolic oxidation/reduction reactions
1195 and cellular responses to ionizing radiation: a unifying concept in stress response
1196 biology. *Cancer and Metastasis Reviews,* 23**,** 311-322.

STOREY, K. B. 1996. Oxidative stress: animal adaptations in nature. *Braz J Med Biol Res,* 29**,** 1715-33.

SZUMIEL, I. 2015. Ionizing radiation-induced oxidative stress, epigenetic changes and genomic instability: the pivotal role of mitochondria. *Int J Radiat Biol,* 91**,** 1-12.

TAKÁCS-VELLAI, K., BAYCI, A. & VELLAI, T. 2006. Autophagy in neuronal cell loss: a road to death. *Bioessays,* 28**,** 1126-1131.

TAKATA, H., HANAFUSA, T., MORI, T., SHIMURA, M., IIDA, Y., ISHIKAWA, K., YOSHIKAWA, K., YOSHIKAWA, Y. & MAESHIMA, K. 2013. Chromatin Compaction Protects Genomic DNA from Radiation Damage. *PLOS ONE,* 8**,** e75622.

TATEISHI, Y., SASABE, E., UETA, E. & YAMAMOTO, T. 2008. Ionizing irradiation induces apoptotic damage of salivary gland acinar cells via NADPH oxidase 1-dependent superoxide generation. *Biochem Biophys Res Commun,* 366**,** 301-7.

TURRENS, J. F. 2003. Mitochondrial formation of reactive oxygen species. *J Physiol,* 552**,** 335-44.

UNITED STATES ENVIRONMENTAL PROTECTION AGENCY, U. E. 2002. Methods for Measuring the Acute Toxicity of Effluents and Receiving Waters to Freshwater and Marine Organisms. . *5th ed. EPA-821-R-02-012*.

UNSCEAR 1996. *Sources and effects of ionizing radiation: Report to the General Assembly, with Scientific Annexes*, United Nations Publications.

VELLAI, T., TAKÁCS-VELLAI, K., SASS, M. & KLIONSKY, D. 2009. The regulation of aging: does autophagy underlie longevity? *Trends in cell biology,* 19**,** 487-494.

WEI, S., LI, C., YIN, Z., WEN, J., MENG, H., XUE, L. & WANG, J. 2018. Histone methylation in DNA repair and clinical practice: new findings during the past 5-years. *Journal of Cancer,* 9**,** 2072-2081.

WU, G., FANG, Y.-Z., YANG, S., LUPTON, J. R. & TURNER, N. D. 2004. Glutathione Metabolism and Its Implications for Health. *The Journal of Nutrition,* 134**,** 489-492.

XIE, L., SOLHAUG, K. A., SONG, Y., BREDE, D. A., LIND, O. C., SALBU, B. & TOLLEFSEN, K. E. 2019. Modes of action and adverse effects of gamma radiation in an aquatic macrophyte Lemna minor. *Science of The Total Environment,* 680**,** 23-34.

YAMAMORI, T., YASUI, H., YAMAZUMI, M., WADA, Y., NAKAMURA, Y., NAKAMURA, H. & INANAMI, O. 2012. Ionizing radiation induces mitochondrial reactive oxygen species production accompanied by upregulation of mitochondrial electron transport chain function and mitochondrial content under control of the cell cycle checkpoint. *Free Radic Biol Med,* 53**,** 260-70.

ZHANG, Y., WANG, H., ZHANG, J., HU, Y., ZHANG, L., WU, X., SU, X., LI, T., ZOU, X. & LIANG, B. 2016. The cytochrome b5 reductase HPO-19 is required for biosynthesis of polyunsaturated fatty acids in Caenorhabditis elegans. *Biochimica et Biophysica Acta (BBA) - Molecular and Cell Biology of Lipids,* 1861**,** 310-319.

The word file **Supporting Material** provides method validation for microscopy analysis and fluorescence measurements, additional gene expression and gene set enrichment analysis data.

Supporting material Paper II

In vivo assessment of ROS production and oxidative stress effects induced by chronic exposure to gamma radiation in *Caenorhabditis elegans*

Erica Maremonti *[1, 3], Dag M. Eide [2, 3], Lisa M. Rossbach [1], Ole Christian Lind [1, 3], Brit Salbu [1, 3], Dag Anders Brede [1, 3]

[1] Faculty of Environmental Sciences and Natural Resource Management (MINA) Norwegian University of Life Sciences (NMBU), 1432 Ås, Norway

[2] Norwegian Institute of Public Health, Lovisenberggata 8, 0456 Oslo, Norway

[3] Centre for Environmental Radioactivity (CERAD)

*Corresponding author

S.M.1. Effects of chronic exposure to ionizing gamma radiation on the somatic growth of *sod-1::gfp C. elegans* reporter strain

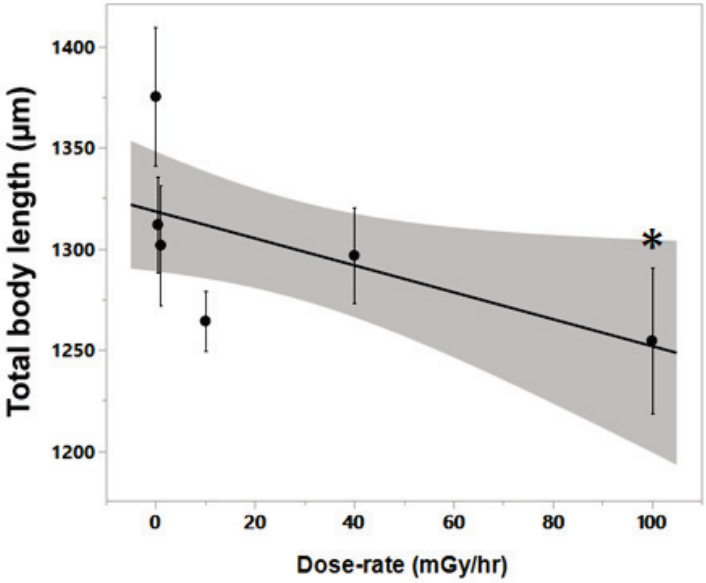

Figure S.1. Effects on somatic growth in *C. elegans* reporter strain *sod1::gfp* exposed to gamma radiation for 96 hours, in 24-well plates containing OP50 re-suspended in MHRW. Data represents Mean ± SE (n = 10). Asterisks indicate significant difference to control treatment (Tukey *post hoc*, *p*-value < 0.01).

S.M.2. Effect of 24 hours exposure to different concentrations of Paraquat on the SOD1 expression in *sod1::gfp C. elegans* reporter strain: validation of microscopy analysis and fluorescence measurements

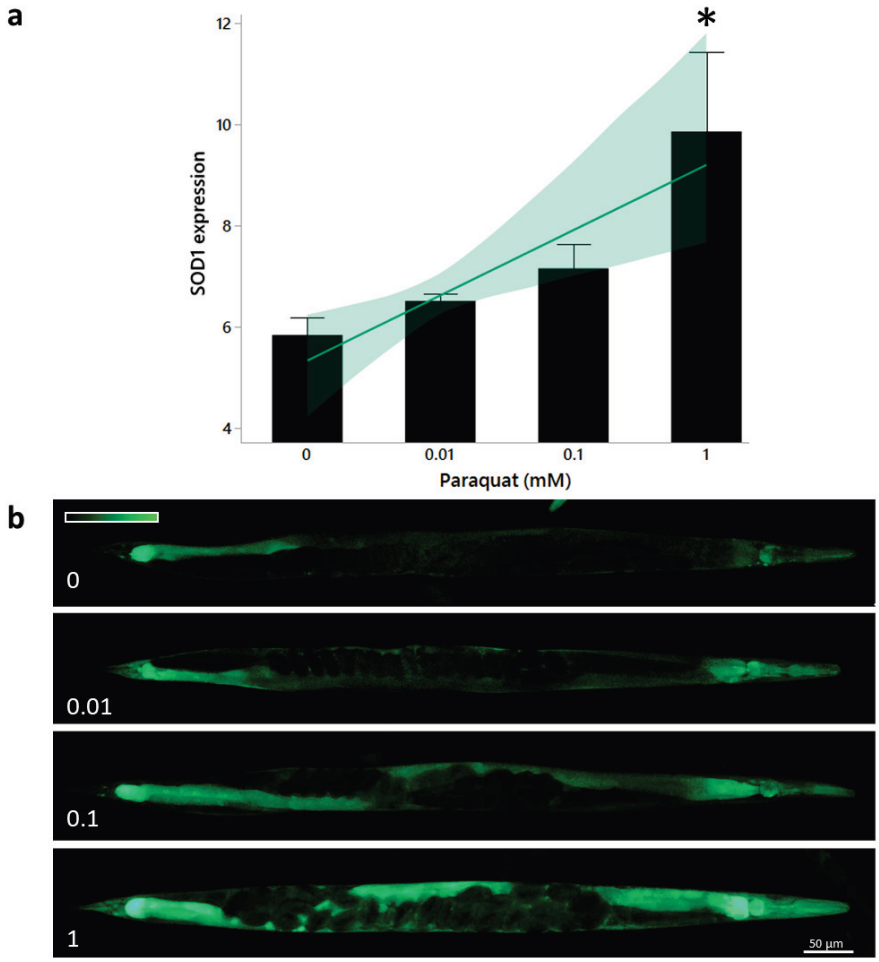

Figure S.2. a) *Sod-1* expression assessed *in vivo* (at 72 hours of development from L1 stage), in *C. elegans* reporter strain *sod1::gfp,* after 24 hours of exposure to Paraquat (mM), in MHRW containing OP50. Data represent Mean ± SE (n = 10) (Doonan et al., 2008). Asterisk indicates significant difference to control treatment (Tukey *post hoc*, *p*-value < 0.01). Expression was normalized to size of individual nematodes.

(**b**) Epifluorescence images of the relative expression pattern at different concentrations of exposure (mM) (from left to right, tail to head orientation). Scale bar: 50 µm.

S.M.3. Effects of the exposure to different concentrations of H_2O_2 on the *Grx1-roGFP2 C. elegans* ratiometric biosensor: positive validation of microscopy analysis and fluorescence measurements

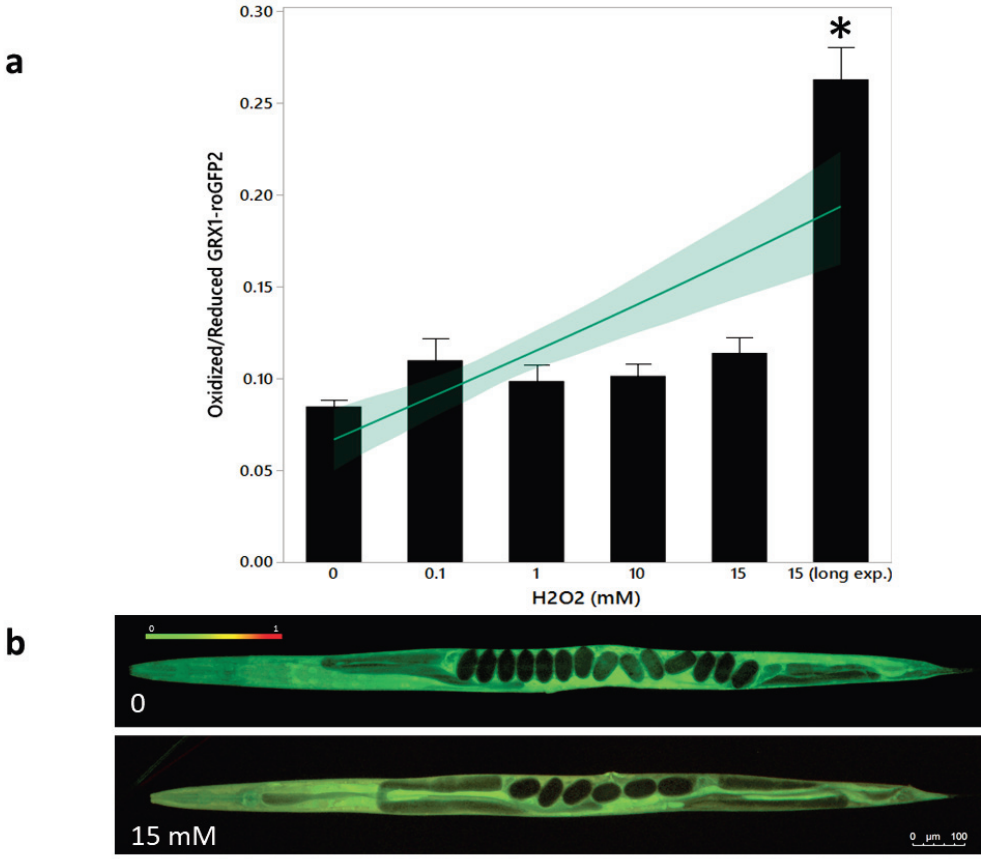

Figure S.3. a) Oxidized/reduced ratio assessed *in vivo,* in the *C. elegans* ratiometric biosensor *GRx1-roGFP2* (Back et al., 2012) *(*72 hours of development from L1), after exposure to increasing concentrations of H_2O_2 (mM), for 5 or 15 minutes (long exp.) in MHRW containing OP50. Data represent Mean ± SE (n =

10). Asterisk indicates significant difference to control treatment (Tukey *post hoc*, *p*-value < 0.01) (15 (long exp.) indicates 15 minutes exposure). (**b**) Epifluorescence images of the relative oxidation pattern at different concentrations of exposure (mM) (Bottom image is from nematode exposed to 15 mM, long exposure: 15 minutes) (from left to right, head to tail orientation). Scale bar: 50 µm.

S.M.4. High inter-variability of the oxidation pattern in the ratiometric biosensor *Grx1-roGFP2* exposed to 100 mGy·h^{-1} of ionizing gamma radiation

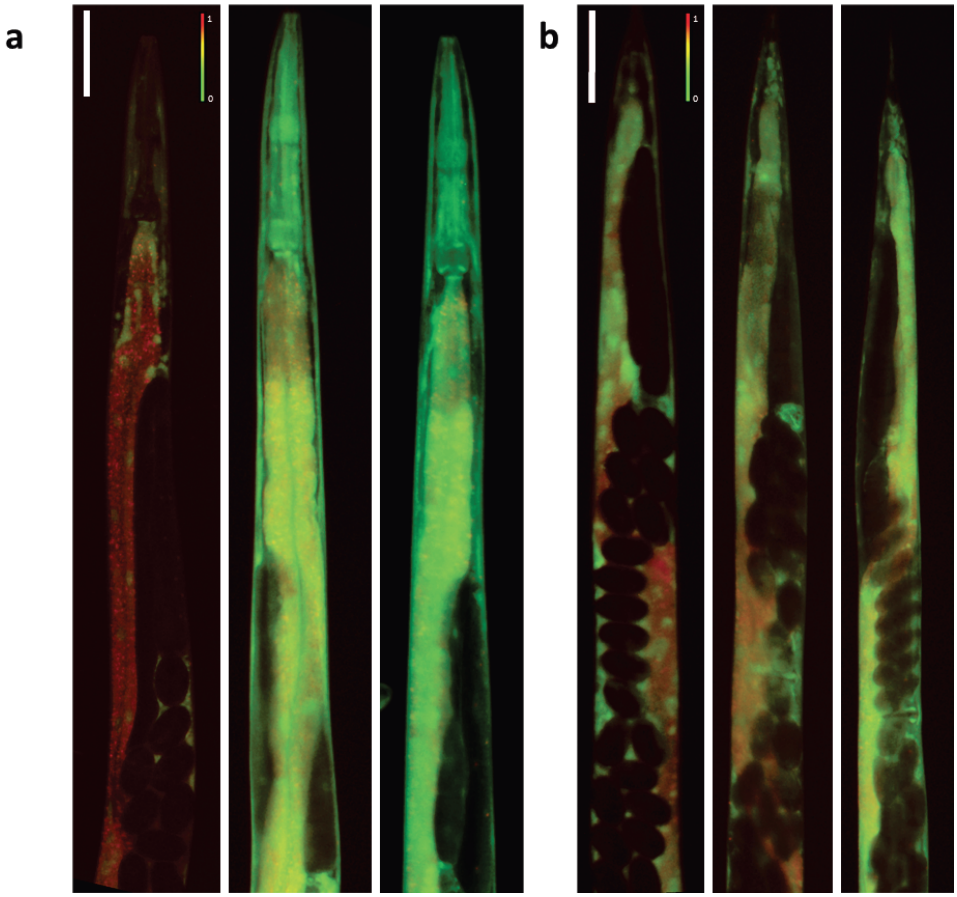

Figure S.4. **a**) Anterior and **b**) Posterior body of *C. elegans Grx1-roGFP2* strain showing high inter-variability between individuals exposed for 72 hours from L1 stage to 100 mGy·h^{-1} of gamma radiation. Scale bar: 100 µm.

S.M.5. Gene expression analysis performed on nematodes irradiated for 72 hours to increasing dose-rates of ionizing gamma radiation

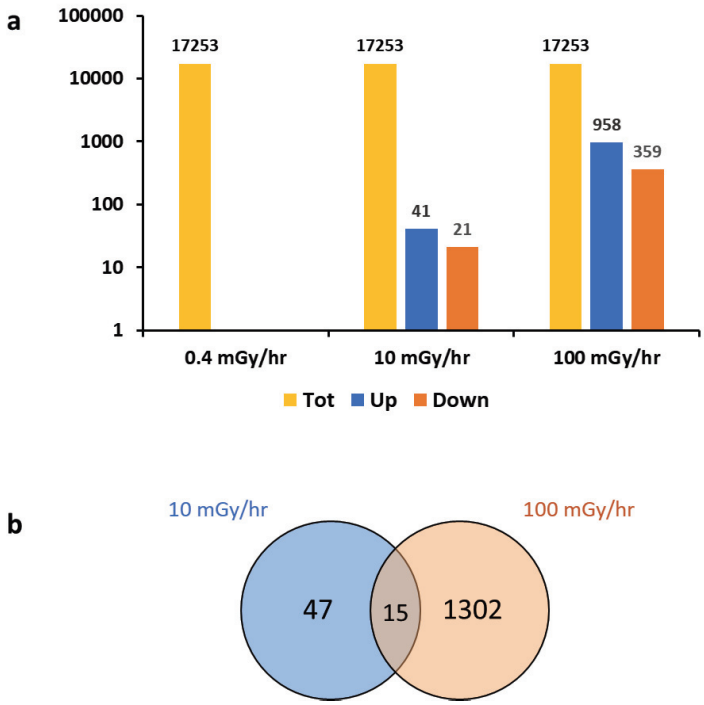

Figure S.5. a) Expressed and differentially expressed (DE) genes after 72 hours of exposure to 0.4, 10 and 100 mGy·h^{-1}. Threshold set to FC ± 1.2 and False Discovery Rate (FDR) <0.05. Total number of expressed genes (yellow), up-regulated genes (blue) and down-regulated genes (orange). **b**) Venn diagram of common and unique sets of DEGs between two exposure treatments (10 and 100 mGy·h^{-1} in blue and orange respectively).

Table S.1. Significantly up or down-regulated genes, found in common between 10 and 100 mGy·h^{-1} exposure groups compared to Control group.

Shared DEGs			10 mGy/hr		100 mGy/hr	
Ensamble ID	Gene name	Annotation	log2FC	FDR	log2FC	FDR
WBGene00012953	fbxa-216	F-box A protein	0.468072867	2.45E-02	0.345287744	1.71E-02
WBGene00009957	F53B2.8	hypothetical protein	0.833717544	2.67E-04	0.368170583	3.09E-02
WBGene00008577	F08G2.5	hypothetical protein	1.249817566	6.33E-03	1.041943411	2.46E-03
WBGene00016942	C55B7.3	Tyrosine-protein phosphatase	1.227866744	1.08E-13	0.68843637	4.51E-05
WBGene00019564	K09D9.1	hypothetical protein	2.167652542	2.41E-13	0.677561002	1.12E-02
WBGene00018725	kreg-1	Protein kreg-1	2.257878476	3.45E-10	0.668460874	2.31E-02
WBGene00009349	F32H5.3	hypothetical protein	0.751678447	1.23E-02	0.558969603	8.88E-03
WBGene00020188	T03F1.6	hypothetical protein	0.758306039	4.40E-04	0.553824844	1.98E-03
WBGene00008944	F19B2.5	hypothetical protein	0.753568331	2.29E-08	0.533228228	5.11E-05
WBGene00019300	swt-1	Sugar transporter SWEET1	-0.593285466	2.63E-03	-0.704903581	2.94E-05
WBGene00009724	F45D3.4	hypothetical protein	-0.473218912	6.78E-05	-0.574599837	1.79E-07
WBGene00017488	dct-7	DAF-16/FOXO Controlled, germline Tumor affecting	-1.192527634	3.52E-02	-0.520429229	4.05E-02
WBGene00003093	lys-4	LYSozyme	-0.441889856	3.70E-04	-0.433754268	6.54E-05
WBGene00020891	T28C12.4	Carboxylic ester hydrolase	-0.502730788	5.33E-03	-0.41011037	3.34E-03
WBGene00009785	F46C5.10	hypothetical protein	-0.430737642	1.62E-02	-0.377481597	4.68E-03

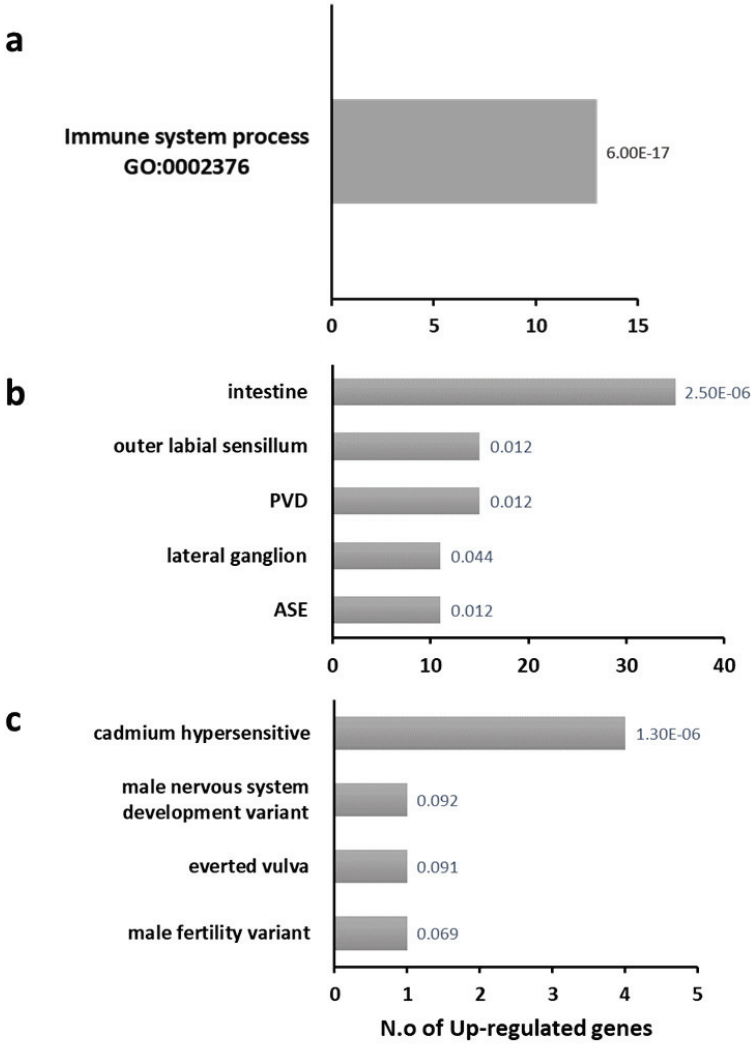

Figure S.6. Functional categories over-represented terms of Up-regulated (n=41) DEGs (n=62) from *C. elegans* subjected to 10 mGy·h^{-1} gamma radiation for 72 hours. (**a**) Gene Ontology (GO), (**b**) Phenotype, and (**c**) Tissue Enrichment analysis. Hypergeometric probability distribution is adopted to measure the number of enriched terms (observed number of DEGs in each specific function). Data labels indicate *q*-values.

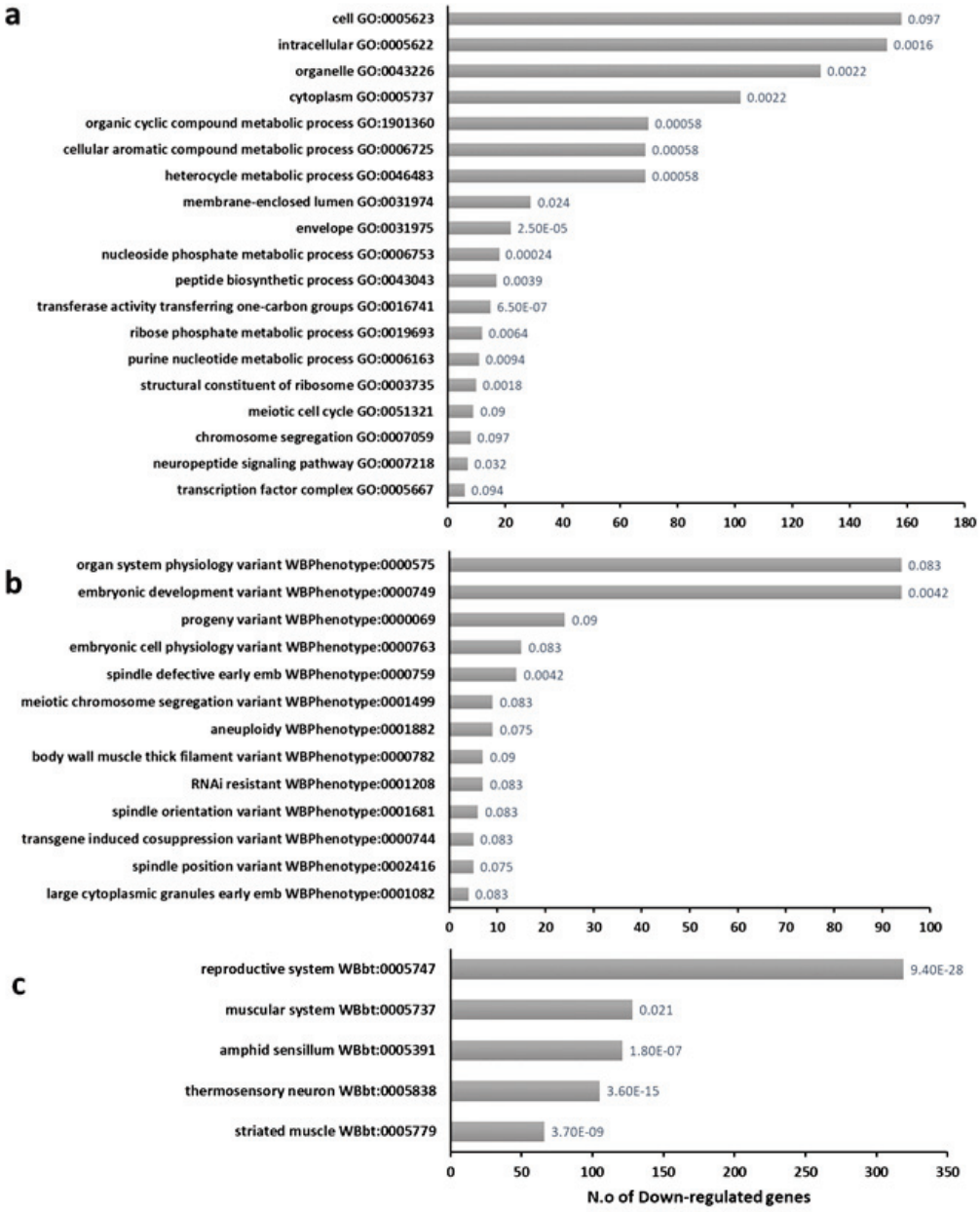

Figure S.7. Over-represented biological processes, molecular functions and cellular components functional categories and variants, from (**a**) Gene Ontology (GO), (**b**) Phenotype and (**c**) Tissue Enrichment analysis that were down-regulated in *C. elegans* after 72 hours of exposure to 100 mGy·h^{-1} of

gamma radiation. Hypergeometric probability distribution is adopted to measure the number of enriched terms (observed number of DEGs in each specific function). Data labels indicate *q*-values.

Table S.6. Functional over-represented categories from Tissue Enrichment analysis (TEA) that were up-regulated in *C. elegans* after 72 hours of exposure to 100 mGy·h^{-1} of gamma radiation. Hypergeometric probability distribution is adopted to measure the number of enriched terms.

Term (TEA)	Observed	Enrichment Fold Change	P value	Q value
Pharynx WBbt:0003681	427	1.1	0.0094	0.074
PVD WBbt:0006831	251	1.2	0.0042	0.059
Outer labial sensillum WBbt:0005501	250	1.2	0.01	0.074
Corpus WBbt:0003733	214	1.4	1.90E-06	0.00054
Hermaphrodite WBbt:0007849	214	1.2	0.0032	0.05
Sex organ WBbt:0008422	170	1.4	1.00E-05	0.0015
Nerve ring WBbt:0006749	86	1.3	0.0057	0.067
Midbody WBbt:0005740	84	1.5	0.00025	0.014
Dorsal nerve cord WBbt:0006750	60	1.3	0.0092	0.074
Anal depressor muscle WBbt:0004292	59	1.7	2.40E-05	0.0023
Somatic gonad WBbt:0005785	56	1.4	0.004	0.059
Lateral nerve cord WBbt:0006769	45	1.5	0.004	0.059
Psub1 WBbt:0006874	31	1.8	0.00064	0.022
Intestinal muscle WBbt:0005796	29	2	0.00019	0.014
Anal sphincter muscle WBbt:0005798	21	2.2	0.00028	0.014
Uterine muscle WBbt:0005342	19	1.9	0.0021	0.039
Anchor cell WBbt:0004522	13	2.4	0.00072	0.022
P11 WBbt:0004410	11	2.6	0.00096	0.022
P8.p WBbt:0006896	11	2.3	0.0027	0.044
P6.p WBbt:0006894	11	2.1	0.0063	0.067
P7.p WBbt:0006895	11	2	0.0071	0.069
Body wall WBbt:0005742	10	2.7	0.0011	0.023
P4.p WBbt:0006892	10	2.1	0.0069	0.069
P3.p WBbt:0006891	10	2.1	0.0069	0.069
P5.p WBbt:0006893	10	1.9	0.016	0.078
ABpraappa WBbt:0006035	9	2.9	0.0008	0.022
MSapa WBbt:0005898	8	3.3	0.0005	0.02
MSapp WBbt:0006036	8	3.2	0.00063	0.022
ABpraappp WBbt:0006270	8	2.8	0.0018	0.037
P12 WBbt:0004409	8	2.3	0.0079	0.069
Somatic cell WBbt:0008378	8	2	0.015	0.078
ABprpaapa WBbt:0006047	7	2.9	0.0023	0.041
MSpapp WBbt:0006201	7	2.6	0.0041	0.059
ABarpaapa WBbt:0005844	7	2.6	0.0041	0.059
ABplppap WBbt:0006028	7	2.5	0.0059	0.067
ABplpppp WBbt:0006647	7	2.5	0.0059	0.067
ABplpappp WBbt:0006390	7	2.4	0.0069	0.069
ABalaaaa WBbt:0006427	7	2.4	0.0069	0.069
P10 WBbt:0006779	7	2.4	0.0081	0.069
Anal region WBbt:0006919	7	2.3	0.0094	0.074
ABprappp WBbt:0006702	7	2.2	0.013	0.075
ABarpaaa WBbt:0006398	7	2.1	0.016	0.078
ABpraapp WBbt:0006335	6	2.5	0.0093	0.074
ABprapaap WBbt:0006624	6	2.5	0.0093	0.074
ABplpaapa WBbt:0006115	6	2.5	0.0093	0.074
P8 WBbt:0006777	6	2.5	0.0093	0.074
ABalaapp WBbt:0006553	6	2.5	0.0093	0.074
ABalappa WBbt:0006157	6	2.4	0.011	0.074
ABalaapa WBbt:0006130	6	2.4	0.011	0.074
ABarpppap WBbt:0006251	6	2.4	0.011	0.074
ABprpppp WBbt:0005983	6	2.3	0.013	0.076
ABplapapp WBbt:0006413	6	2.3	0.013	0.076
ABprappaa WBbt:0006350	6	2.3	0.013	0.076
P7 WBbt:0006776	6	2.3	0.013	0.076
ABprapapp WBbt:0006290	6	2.3	0.013	0.076
P9 WBbt:0006778	6	2.3	0.013	0.076
MSaapp WBbt:0006425	6	2.3	0.015	0.078
ABplappap WBbt:0006067	6	2.3	0.015	0.078
ABplpaaa WBbt:0006315	6	2.3	0.015	0.078
ABplpppap WBbt:0006665	6	2.3	0.015	0.078
ABprpapaa WBbt:0006446	6	2.3	0.015	0.078
ABprappap WBbt:0006220	6	2.3	0.015	0.078
ABprapapa WBbt:0006510	6	2.3	0.015	0.078
ABplpaap WBbt:0006077	6	2.3	0.015	0.078
Caaaa WBbt:0005899	6	2.2	0.017	0.078
ABalaaap WBbt:0005982	6	2.2	0.017	0.078
ABplpappa WBbt:0006232	6	2.2	0.017	0.078
ABplpppa WBbt:0006423	6	2.2	0.017	0.078
ABplppaa WBbt:0006170	6	2.1	0.02	0.081
ABprpappa WBbt:0006088	6	2.1	0.02	0.081
ABprpppaa WBbt:0006552	6	2.1	0.02	0.081
ABpraaaa WBbt:0006442	6	2.1	0.023	0.089
ABpraapa WBbt:0006302	6	2.1	0.023	0.089

Table S.8. Dose-rates (mGy·h^{-1}) of exposure and relative total absorbed doses (Gy) calculated based on total exposure time (h).

Total Dose (Gy)			
	Exposure time (hours)		
Dose-rate (mGy/hr)	48	72	96
0	0	0	0
0.43	0.02	0.03	0.04
1.1	0.05	0.08	0.11
10.8	0.52	0.78	1.04
40.8	1.96	2.94	3.92
99.9	4.80	7.19	9.59

References

BACK, P., DE VOS, W. H., DEPUYDT, G. G., MATTHIJSSENS, F., VANFLETEREN, J. R. & BRAECKMAN, B. P. 2012. Exploring real-time in vivo redox biology of developing and aging *Caenorhabditis elegans*. *Free Radic Biol Med,* 52**,** 850-9.

DOONAN, R., MCELWEE, J. J., MATTHIJSSENS, F., WALKER, G. A., HOUTHOOFD, K., BACK, P., MATSCHESKI, A., VANFLETEREN, J. R. & GEMS, D. 2008. Against the oxidative damage theory of aging: superoxide dismutases protect against oxidative stress but have little or no effect on life span in *Caenorhabditis elegans*. *Genes Dev,* 22**,** 3236-41.

148 **Table S.2.** List of differentially expressed genes (DEGs) resulting from nematodes
149 exposed to 10 mGy·h^{-1} of ionizing gamma radiation for 72 hours from L1 stage.
150
151 **Table S.3.** List of differentially expressed genes (DEGs) resulting from nematodes
152 exposed to 100 mGy·h^{-1} of ionizing gamma radiation for 72 hours from L1 stage.
153
154 **Table S.4.** Over-represented categories with relative DEGs resulting from Gene
155 Ontology, Tissue and Phenotype Enrichment analysis performed on DEGs resulting from
156 nematodes exposed to 10 mGy·h^{-1} of ionizing gamma radiation for 72 hours from L1
157 stage.
158
159 **Table S.5.** Over-represented categories with relative DEGs resulting from Gene
160 Ontology, Tissue and Phenotype Enrichment analysis performed on DEGs resulting from
161 nematodes exposed to 100 mGy·h^{-1} of ionizing gamma radiation for 72 hours from L1
162 stage.
163
164 **Table S.7.** Over-represented categories with relative DEGs related to Oxidative stress
165 response resulting from Phenotype Enrichment analysis performed on DEGs resulting
166 from nematodes exposed to 100 mGy·h^{-1} of ionizing gamma radiation for 72 hours from
167 L1 stage.
168
169
170 N.B: The large excel-files for Tables S.4 an S.5 will be available on the official publication
171 by the journal *Free Radical Biology and Medicine,* but can also be provided upon request
172 to the corresponding author.

	ENSEMBLE GeneID	SYMBOL	GENENAME	log2FoldChange	lfcSE	pvalue	padj	baseMean
1	WBGene00019667	spe-49	hypothetical protein	5.835011028	1.356479717	5.58E-07	0.000294	7.104863298
2	WBGene00016502	C37C3.10	hypothetical protein	4.192110805	0.83036642	7.16E-08	5.39E-05	8.629470792
3	WBGene00005448	srh-241	Serpentine Receptor, class H	4.015699705	1.349875233	0.000229	0.049448	4.698697594
4	WBGene00005657	srr-6	Serpentine Receptor, class R	2.463204765	0.46663219	5.68E-09	5.28E-06	16.25545662
5	WBGene00045457	F33H12.7	hypothetical protein	2.365274255	0.475340101	2.67E-08	2.22E-05	20.71585297
6	WBGene00018725	kreg-1	Protein kreg-1	2.257878476	0.319670129	1.09E-13	3.45E-10	28.77794178
7	WBGene00016785	C49G7.7	hypothetical protein	2.183186964	0.454943442	8.04E-08	5.77E-05	18.41118282
8	WBGene00019564	K09D9.1	hypothetical protein	2.167652542	0.268306378	4.57E-17	2.41E-13	68.59505449
9	WBGene00008602	oac-14	O-ACyltransferase homolog	1.991905241	0.333281902	9.31E-11	1.06E-07	52.99411438
10	WBGene00012101	zip-10	Transcription factor zip-10	1.725571325	0.271896949	9.10E-12	1.60E-08	80.2077153
11	WBGene00003092	lys-3	Lysozyme-like protein 3	1.714447705	0.500110883	2.31E-05	0.007588	19.66319043
12	WBGene00011672	cyp-13A5	Putative cytochrome P450 CYP13A5	1.585070831	0.1901651	3.55E-18	5.60E-14	158.573594
13	WBGene00017093	E02C12.8	hypothetical protein	1.451888093	0.195203434	4.83E-15	1.91E-11	129.276103
14	WBGene00006628	tsp-2	TetraSPanin family	1.443629676	0.494931598	0.000122	0.028026	29.44890233
15	WBGene00019660	K11H12.4	hypothetical protein	1.395680992	0.218954257	8.89E-12	1.60E-08	79.37156273
16	WBGene00011957	T23F11.6	hypothetical protein	1.294445351	0.383364208	2.55E-05	0.00788	26.99600907
17	WBGene00018707	oac-31	O-ACyltransferase homolog	1.26762398	0.376540174	2.51E-05	0.00788	27.83332322
18	WBGene00008577	F08G2.5	hypothetical protein	1.249817566	0.361503534	1.88E-05	0.006331	33.24005044
19	WBGene00016942	C55B7.3	Tyrosine-protein phosphatase	1.227866744	0.15006983	1.36E-17	1.08E-13	174.36698
20	WBGene00020760	T24C4.4	hypothetical protein	1.198892515	0.256600758	1.22E-07	8.01E-05	47.89305532
21	WBGene00007833	oac-6	O-ACyltransferase homolog	1.170372183	0.177226956	1.72E-12	4.53E-09	100.8800663
22	WBGene00010658	K08D8.4	hypothetical protein	1.063474872	0.169050711	1.54E-11	2.20E-08	180.4371305
23	WBGene00001770	gst-22	Glutathione S-Transferase	1.003958654	0.178945098	8.76E-10	9.22E-07	143.8145744
24	WBGene00015932	C17H12.6	hypothetical protein	0.901128868	0.303604307	0.000102	0.024534	37.53738214
25	WBGene00016788	C49G7.10	hypothetical protein	0.891317341	0.148525197	9.43E-11	1.06E-07	153.3377331
26	WBGene00002274	lec-11	Galectin	0.886722738	0.14043446	1.20E-11	1.89E-08	211.1858047
27	WBGene00012494	nhr-232	Nuclear Hormone Receptor family	0.848343007	0.213323988	2.57E-06	0.001129	112.51913
28	WBGene00009957	F53B2.8	hypothetical protein	0.833717544	0.190605293	4.90E-07	0.000267	239.5829128
29	WBGene00008255	C51E3.10	hypothetical protein	0.816063291	0.146796628	1.20E-09	1.19E-06	158.7550853
30	WBGene00010749	K10D11.5	hypothetical protein	0.775312368	0.173409032	3.04E-07	0.000178	147.1542355
31	WBGene00020188	T03F1.6	hypothetical protein	0.758306039	0.179141069	8.92E-07	0.00044	238.8234312
32	WBGene00008944	F19B2.5	hypothetical protein	0.753568331	0.120358035	1.74E-11	2.29E-08	444.0647034
33	WBGene00003995	pgp-1	Multidrug resistance protein pgp-1	0.75342572	0.16531086	2.12E-07	0.000134	308.7975379
34	WBGene00009349	F32H5.3	hypothetical protein	0.751678447	0.233562975	4.52E-05	0.01231	75.11060785
35	WBGene00021204	fbxb-77	F-box B protein	0.740497735	0.224552131	3.39E-05	0.010004	63.71281014
36	WBGene00003480	klf-3	Kruppel-Like Factor (zinc finger protein)	0.684190806	0.211256458	4.13E-05	0.011428	113.5870144
37	WBGene00008486	ugt-44	UDP-GlucuronosylTransferase	0.652914566	0.102407003	8.67E-12	1.60E-08	580.9166744
38	WBGene00002058	ifd-2	Intermediate filament protein ifd-2	0.522717621	0.131247413	2.56E-06	0.001129	280.7445392
39	WBGene00012953	fbxa-216	F-box A protein	0.468072867	0.157961149	0.000103	0.024534	187.2262341
40	WBGene00003613	nhr-14	Nuclear hormone receptor family member nhr-14	0.4501657	0.134472599	3.03E-05	0.00921	235.211134
41	WBGene00017964	F31F7.1	hypothetical protein	0.317737756	0.11815816	0.000232	0.049499	966.5830111
42	WBGene00000781	cpr-1	Gut-specific cysteine proteinase	-0.346217983	0.105055607	3.42E-05	0.010004	4788.749729
43	WBGene00003093	lys-4	LYSozyme	-0.441889856	0.103037708	7.26E-07	0.00037	2880.365065
44	WBGene00003163	mdl-1	MAD-Like	-0.456923254	0.115024366	3.11E-06	0.001328	347.4871568
45	WBGene00003511	mxl-3	MaX-Like	-0.36631772	0.124870366	0.000126	0.028351	626.8109522
46	WBGene00008038	C40H1.2	hypothetical protein	-0.569446497	0.187672822	8.77E-05	0.021647	87.43566117
47	WBGene00008341	ttr-44	TransThyretin-Related family domain	-0.409926079	0.097710035	1.11E-06	0.000532	419.3991215
48	WBGene00009724	F45D3.4	hypothetical protein	-0.473218912	0.10023116	9.87E-08	6.78E-05	483.5247348
49	WBGene00009785	F46C5.10	hypothetical protein	-0.430737642	0.13804584	6.45E-05	0.016164	221.3207507
50	WBGene00009895	scl-2	SCP-Like extracellular protein	-0.462111977	0.14744487	6.18E-05	0.015745	254.1703789
51	WBGene00010204	F57F5.1	hypothetical protein	-0.357942693	0.081311397	4.45E-07	0.000251	23371.7932
52	WBGene00010793	LLC1.2	hypothetical protein	-0.310377407	0.095760458	5.16E-05	0.013806	1891.065613
53	WBGene00012251	clec-49	C-type LECtin	-0.411954042	0.129443197	5.32E-05	0.014008	455.5392515
54	WBGene00013996	ZK550.2	hypothetical protein	-0.459452288	0.146551784	6.06E-05	0.01569	195.9956877
55	WBGene00017488	dct-7	DAF-16/FOXO Controlled, germline Tumor affecting	-1.192527634	0.420186048	0.000158	0.035229	29.72237633
56	WBGene00017565	ddo-2	D-aspartate oxidase 2	-0.302302751	0.09242679	3.98E-05	0.011221	1108.776985
57	WBGene00017969	F32A5.3	Uncharacterized serine carboxypeptidase F32A5.3	-0.374105296	0.105980707	1.51E-05	0.005329	567.3321485
58	WBGene00019164	H06H21.8	hypothetical protein	-0.469118144	0.089504604	6.51E-09	5.71E-06	555.4993048
59	WBGene00019300	swt-1	Sugar transporter SWEET1	-0.593285466	0.158838169	7.00E-06	0.002633	148.9499398
60	WBGene00020453	fbxa-55	F-box A protein	-0.72388904	0.149734743	5.83E-08	4.60E-05	154.7174557
61	WBGene00020891	T28C12.4	Carboxylic ester hydrolase	-0.502730788	0.142628755	1.54E-05	0.005329	244.293457
62	WBGene00022643	ZK6.8	hypothetical protein	-0.679695826	0.186272234	1.01E-05	0.003707	108.8850367

	ENSEMBLE GeneID	SYMBOL	GENENAME	log2FoldChange	lfcSE	pvalue	padj	baseMean
1	WBGene00003124	mai-1	ATPase inhibitor mai-1, mitochondrial	0.384035309	0.199038	0.004338	0.023711	129.1903092
2	WBGene00012928	aakb-2	AMP-Activated Kinase Beta subunit	0.704067441	0.160277	7.13E-07	3.48E-05	525.8503672
3	WBGene00021927	abhd-14	ABHydrolase Domain containing homolog	0.904012272	0.469141	0.001637	0.011428	40.81840548
4	WBGene00016507	abhd-5.2	Abhydrolase domain-containing protein abhd-5.2	-0.385250492	0.11802	0.000123	0.001576	316.37267
5	WBGene00000033	abu-10	Activated in Blocked Unfolded protein response	0.992118465	0.934096	0.004538	0.024512	24.10569073
6	WBGene00000034	abu-11	Activated in Blocked Unfolded protein response	1.463216475	0.475275	8.14E-05	0.001166	29.01330834
7	WBGene00020366	acdh-10	Probable medium-chain specific acyl-CoA dehydrogenase 10, mitochondrial	0.333466049	0.096595	8.04E-05	0.00116	1656.969774
8	WBGene00020812	acdh-7	Acyl CoA DeHydrogenase	0.734684536	0.198222	1.17E-05	0.000273	987.5483089
9	WBGene00011543	acl-2	ACyLtransferase-like	-0.325932704	0.09893	0.000148	0.001804	1536.551905
10	WBGene00016995	acly-1	Probable ATP-citrate synthase	0.323491327	0.076889	4.34E-06	0.000131	2176.307437
11	WBGene00008565	acox-1.2	Acyl-coenzyme A oxidase	0.355092148	0.087969	7.23E-06	0.000193	449.1193248
12	WBGene00022037	acs-13	fatty Acid CoA Synthetase family	0.542693195	0.158237	4.36E-05	0.000756	6766.72062
13	WBGene00000066	act-4	Actin-4	0.716588298	0.18996	9.45E-06	0.000238	13620.48055
14	WBGene00000067	act-5	ACTin	0.606783569	0.13932	9.25E-07	4.19E-05	2133.991095
15	WBGene00016509	adss-1	Adenylosuccinate synthetase	0.368879115	0.160223	0.002109	0.013706	3783.351885
16	WBGene00021009	afd-1	AFaDin (actin filament binding protein) homolog	0.845487334	0.140896	1.18E-10	4.59E-08	649.9574212
17	WBGene00019322	ahcy-1	Adenosylhomocysteinase	0.312881415	0.145416	0.004093	0.02266	19161.69995
18	WBGene00015547	ain-1	ALG-1 INteracting protein	0.433179041	0.098123	1.05E-06	4.66E-05	1972.480252
19	WBGene00000100	ajm-1	Apical junction molecule	0.491217988	0.184897	0.000566	0.005062	1172.020081
20	WBGene00011474	aldo-1	Fructose-bisphosphate aldolase 1	1.011023307	0.264336	6.24E-06	0.000172	696.9996209
21	WBGene00000106	alg-2	Protein argonaute	0.344356241	0.135399	0.001318	0.009695	1647.333901
22	WBGene00011193	algn-13	Asparagine Linked Glycosylation (ALG) homolog, Nematode	-0.428517056	0.073949	7.59E-10	1.83E-07	827.8141613
23	WBGene00000112	alh-6	ALdehyde deHydrogenase	0.499957391	0.163898	0.000169	0.002012	960.8827981
24	WBGene00000113	alh-7	ALdehyde deHydrogenase	0.933995953	0.165033	8.66E-10	1.91E-07	336.8998634
25	WBGene00000114	alh-8	ALdehyde deHydrogenase	0.494885649	0.193251	0.000726	0.006143	9997.664884
26	WBGene00000123	ama-1	DNA-directed RNA polymerase II subunit RPB1	0.339749104	0.093857	4.23E-05	0.000741	2077.224042
27	WBGene00011573	anmt-3	Amine N-MethylTransferase	0.343928429	0.14446	0.001997	0.013187	383.9559638
28	WBGene00000144	apc-10	Anaphase-promoting complex subunit 10	-0.408763507	0.080473	4.38E-08	4.53E-06	749.1095626
29	WBGene00000149	apl-1	Amyloid-beta-like protein	0.41887973	0.121707	5.82E-05	0.000938	1977.587268
30	WBGene00000170	aqp-2	AQuaPorin or aquaglyceroporin related	0.931834793	0.205455	3.06E-07	2.01E-05	2434.690998
31	WBGene00044689	arid-1	ARID (AT-rich Interactive Domain-containing protein) homolog	0.347678836	0.103268	9.94E-05	0.001347	2390.741908
32	WBGene00010268	arrd-10	ARRestin Domain protein	0.527612055	0.2641	0.002342	0.014808	72.33478501
33	WBGene00011055	arrd-14	ARRestin Domain protein	0.322669395	0.18433	0.00832	0.03895	102.804032
34	WBGene00000207	asb-2	ATP Synthase B homolog	0.350570716	0.153325	0.002417	0.015157	2647.297355
35	WBGene00016019	ascc-1	activating signal cointegrator 1 complex subunit 1 homolog	-0.3111703	0.078204	1.19E-05	0.000277	945.3955379
36	WBGene00000210	asg-2	Probable ATP synthase subunit g 2, mitochondrial	0.361556566	0.174047	0.003646	0.020692	1525.081601
37	WBGene00000214	asp-1	ASpartyl Protease	0.633421947	0.374941	0.003433	0.019734	7572.537787
38	WBGene00007100	asps-1	ASPScr1 (ASPSCR1) homolog	-0.355639313	0.068592	2.73E-08	3.16E-06	2364.525515
39	WBGene00021922	atg-3	Autophagy-related protein 3	0.692818768	0.236332	0.000174	0.002046	625.7441249
40	WBGene00020706	atg-9	Autophagy-related protein 9	0.474106118	0.180674	0.000631	0.0055	815.2125202
41	WBGene00010419	atp-1	ATP synthase subunit alpha, mitochondrial	0.518834935	0.188139	0.000393	0.003775	19304.94776
42	WBGene00020275	atp-4	ATP synthase subunit	0.360239329	0.246731	0.009967	0.044719	4853.569454
43	WBGene00007385	atp-5	ATP synthase subunit	0.317425921	0.13193	0.00221	0.014179	7053.972054
44	WBGene00010960	ATP6	ATP synthase F0 subunit 6	-0.432902342	0.127605	6.49E-05	0.001	38953.46577
45	WBGene00018794	attf-3	AT hook Transcription Factor family	0.361705062	0.148016	0.001563	0.011046	758.7584988
46	WBGene00000231	atx-2	Ataxin-2 homolog	0.30452198	0.184885	0.011162	0.048699	2458.389091
47	WBGene00206362	B0041.11	hypothetical protein	0.548828666	0.190113	0.000253	0.002701	839.3297747
48	WBGene00015011	B0041.8	hypothetical protein	-0.331712248	0.060193	6.35E-09	9.26E-07	4137.034427
49	WBGene00015023	B0205.9	hypothetical protein	-0.305029574	0.063863	3.29E-07	2.08E-05	2257.193144
50	WBGene00007133	B0284.3	hypothetical protein	0.682615868	0.226987	0.000137	0.001716	69.38823803
51	WBGene00007144	B0334.4	hypothetical protein	-0.303459196	0.063192	2.92E-07	1.96E-05	2956.233142
52	WBGene00015155	B0353.1	hypothetical protein	0.403805413	0.201454	0.003468	0.019869	113.7458496
53	WBGene00015156	B0361.2	CWF19-like protein 2 homolog	-0.362814874	0.062239	1.22E-09	2.61E-07	2026.921364
54	WBGene00015160	B0361.6	Putative methyltransferase B0361.6	-0.351507909	0.068486	4.23E-08	4.52E-06	1339.422154
55	WBGene00015189	B0432.8	hypothetical protein	-0.336189021	0.126085	0.000968	0.007644	733.2526594
56	WBGene00007188	B0464.9	Probable protein phosphatase methylesterase 1	-0.457744007	0.079105	7.33E-10	1.81E-07	1272.038772
57	WBGene00015220	B0507.3	hypothetical protein	0.411108792	0.253116	0.006554	0.032422	66.3700256
58	WBGene00000236	bag-1	BAG family molecular chaperone regulator 1	0.377272654	0.061592	1.24E-10	4.68E-08	1815.918669
59	WBGene00017450	bath-27	BTB and MATH domain containing	-0.386391464	0.09277	3.90E-06	0.000123	676.5047756
60	WBGene00019141	bath-5	BTB and MATH domain containing	-0.374429992	0.092639	6.68E-06	0.000182	579.3820232
61	WBGene00012713	bckd-1A	2-oxoisovalerate dehydrogenase subunit alpha	0.418074938	0.151814	0.000535	0.004851	1263.043443
62	WBGene00010042	bcs-1	BCS1 (mitochondrial chaperone) homolog	-0.342691426	0.075111	7.55E-07	3.61E-05	1372.187158
63	WBGene00012943	bed-2	BED-type zinc finger putative transcription factor	0.740729449	0.157605	1.58E-07	1.21E-05	721.8537487
64	WBGene00011872	blos-1	Biogenesis of lysosome-related organelles complex 1 subunit 1	-0.317096061	0.084245	2.67E-05	0.000519	653.3032103
65	WBGene00020783	blos-4	Biogenesis of lysosome-related organelles complex 1 subunit 4	-0.390850345	0.125285	0.000193	0.002199	743.0014987
66	WBGene00021376	blos-7	BLOC (Biogenesis of Lysosome-related Organelles Complex) and Related complexes subunit homolog	0.428689243	0.283779	0.006966	0.03399	501.5860345
67	WBGene00000273	brp-1	Bypass of Response to Pheromone in yeast	0.317656187	0.130849	0.002093	0.013641	3305.263967
68	WBGene00007216	C01A2.4	hypothetical protein	-0.363352906	0.090459	7.85E-06	0.000206	937.6444709
69	WBGene00015291	C01B12.8	hypothetical protein	-0.409319381	0.093482	1.39E-06	5.76E-05	1037.072593
70	WBGene00015339	C02E7.6	hypothetical protein	2.365851201	0.60735	3.77E-06	0.000121	148.7810905
71	WBGene00015340	C02E7.7	hypothetical protein	1.935079736	0.615973	6.43E-05	0.001	29.65703455
72	WBGene00015353	C02F5.13	TM2 domain-containing protein C02F5.13	-0.361437954	0.077593	4.36E-07	2.52E-05	817.3864113
73	WBGene00015456	C04G6.6	hypothetical protein	0.41346283	0.209912	0.003553	0.020264	128.0819417
74	WBGene00015472	C05D9.3	Uncharacterized integrin beta-like protein C05D9.3	0.440704921	0.111664	7.60E-06	0.000201	393.8767
75	WBGene00015505	C06A5.8	hypothetical protein	-0.312260348	0.082488	2.59E-05	0.000511	768.0020407
76	WBGene00007365	C06B3.6	hypothetical protein	-0.543249034	0.080039	1.00E-12	1.60E-09	824.1004526
77	WBGene00007372	C06B8.7	hypothetical protein	0.37156502	0.154517	0.001661	0.011528	253.9726101
78	WBGene00015529	C06E2.5	hypothetical protein	0.361922963	0.217982	0.007718	0.036697	311.7847012
79	WBGene00015561	C07A12.7	hypothetical protein	0.757449998	0.123716	6.06E-11	2.68E-08	280.4275788
80	WBGene00015565	C07D8.6	hypothetical protein	0.636064855	0.188843	4.56E-05	0.000785	3000.132772
81	WBGene00044773	C08A9.10	hypothetical protein	-0.499429348	0.212979	0.001212	0.009057	397.882895
82	WBGene00007435	C08B11.8	Probable dolichyl pyrophosphate Man9GlcNAc2 alpha-1,3-glucosyltransferase	-0.385199504	0.081338	2.71E-07	1.85E-05	1249.218482
83	WBGene00015613	C08F1.10	hypothetical protein	0.310486368	0.121471	0.001542	0.01093	568.7392558
84	WBGene00007449	C08F8.9	hypothetical protein	0.950080739	0.511148	0.001796	0.012176	83.34835906
85	WBGene00044418	C08G5.7	hypothetical protein	1.124077204	0.30899	1.19E-05	0.000278	37.75783917
86	WBGene00007479	C09F9.2	hypothetical protein	1.02078016	0.327404	7.86E-05	0.001141	132.1654168
87	WBGene00007486	C09G1.4	hypothetical protein	0.472313528	0.269847	0.004358	0.023781	59.84374194
88	WBGene00015662	C10A4.1	hypothetical protein	-0.439069077	0.422077	0.010449	0.04638	31.32022127
89	WBGene00007507	C10C5.3	Aminoacylase	-0.340381791	0.176641	0.005482	0.028279	116.4087486
90	WBGene00007515	C10C6.7	hypothetical protein	-0.588623384	0.250427	0.001	0.007829	78.49045266
91	WBGene00015710	C12D5.9	hypothetical protein	-0.501675245	0.211543	0.001138	0.008638	81.68729189
92	WBGene00015744	C13F10.5	hypothetical protein	-0.363159224	0.099245	3.24E-05	0.000603	947.495071
93	WBGene00015745	C13F10.6	hypothetical protein	-0.362827423	0.069166	2.12E-08	2.64E-06	2707.66877
94	WBGene00184990	C14B1.12	hypothetical protein	-0.387276548	0.089503	1.84E-06	7.06E-05	869.7251206
95	WBGene00007585	C14C10.2	hypothetical protein	-0.304620946	0.127423	0.002401	0.01508	286.6762585
96	WBGene00015766	C14C11.2	hypothetical protein	-0.301528666	0.069101	2.50E-06	8.84E-05	987.7036907
97	WBGene00007602	C15C6.3	hypothetical protein	0.386701107	0.216244	0.005536	0.028487	1329.218192
98	WBGene00015807	C16A3.2	hypothetical protein	-0.354803687	0.106839	0.000115	0.0015	693.1969499
99	WBGene00015843	C16C8.5	hypothetical protein	-0.443387217	0.124993	3.59E-05	0.000651	469.5631263
100	WBGene00044236	C17E4.11	hypothetical protein	-0.301497799	0.112268	0.001117	0.008519	321.3903372
101	WBGene00015899	C17E7.4	hypothetical protein	0.411206659	0.163756	0.001063	0.008197	738.4876936
102	WBGene00270322	C17G10.13	hypothetical protein	-0.414400045	0.082605	5.86E-08	5.41E-06	729.1723066
103	WBGene00015926	C17H11.6	RBR-type E3 ubiquitin transferase	0.496247947	0.09948	5.35E-08	5.19E-06	367.8959318
104	WBGene00007679	C18D11.1	hypothetical protein	0.575671194	0.166733	3.67E-05	0.000662	193.2983175
105	WBGene00016021	C23H3.5	hypothetical protein	-0.331455796	0.070581	4.29E-07	2.49E-05	1204.963334
106	WBGene00016048	C24B9.3	hypothetical protein	0.468097088	0.215847	0.001951	0.012926	1429.854585
107	WBGene00007720	C25D7.10	hypothetical protein	-0.322433932	0.114995	0.00072	0.006113	932.4195275
108	WBGene00016146	C26F1.1	hypothetical protein	0.763866761	0.28772	0.000353	0.003469	101.1147038
109	WBGene00016148	C26F1.3	hypothetical protein	-0.380729936	0.064038	3.72E-10	1.08E-07	1630.37246
110	WBGene00007766	C27C7.1	hypothetical protein	0.895315732	0.272874	4.75E-05	0.000803	700.3181563
111	WBGene00016169	C27F2.7	Uncharacterized F-box protein C27F2.7	-0.30608652	0.085546	6.00E-05	0.000956	785.4884401
112	WBGene00043156	C27F2.9	hypothetical protein	-0.327598454	0.06166	1.73E-08	2.22E-06	1546.663146

	ENSEMBLE GeneID	SYMBOL	GENENAME	log2FoldChange	lfcSE	pvalue	padj	baseMean
113	WBGene00077500	C27H6.9	Mitochondrial genome maintenance exonuclease 1	-0.307362624	0.064744	3.73E-07	2.26E-05	1126.352741
114	WBGene00016274	C30G12.2	hypothetical protein	0.982717359	0.131815	5.24E-15	2.24E-11	435.6991649
115	WBGene00007825	C30H6.8	hypothetical protein	-0.38108676	0.084449	8.25E-07	3.85E-05	758.1460322
116	WBGene00007836	C31C9.2	hypothetical protein	1.075383326	0.240719	3.87E-07	2.31E-05	459.0161555
117	WBGene00007878	C33A11.2	hypothetical protein	0.504707049	0.227181	0.001557	0.011013	181.5744866
118	WBGene00016353	C33F10.4	hypothetical protein	-0.460901668	0.077569	2.95E-10	9.45E-08	759.6138665
119	WBGene00007934	C34E7.4	hypothetical protein	0.481107323	0.169293	0.000335	0.003341	635.3120377
120	WBGene00016442	C35D10.5	hypothetical protein	-0.308269679	0.088922	8.83E-05	0.001237	808.5949463
121	WBGene00016443	C35D10.6	hypothetical protein	-0.361771237	0.085947	3.44E-06	0.000113	1536.678153
122	WBGene00044614	C36B1.14	hypothetical protein	-0.358287442	0.103493	6.84E-05	0.001035	978.6213228
123	WBGene00016493	C37A2.7	60S acidic ribosomal protein P2	1.142912694	0.576296	0.001328	0.009749	5354.416738
124	WBGene00016494	C37A2.8	hypothetical protein	-0.436475052	0.091124	1.73E-07	1.28E-05	1999.008937
125	WBGene00016511	C37H5.13	hypothetical protein	0.434043393	0.117891	2.25E-05	0.000455	422.4138569
126	WBGene00008010	C38D9.2	hypothetical protein	0.617589509	0.813621	0.007485	0.035895	21.16305781
127	WBGene00008019	C38H2.2	Glycoprotein-N-acetylgalactosamine 3-beta-galactosyltransferase 1	0.339189575	0.12094	0.000648	0.005626	339.7621669
128	WBGene00016540	C39F7.5	hypothetical protein	0.398631623	0.185179	0.0027	0.016447	170.7652934
129	WBGene00016547	C40A11.4	hypothetical protein	0.424020638	0.209017	0.00305	0.018059	94.29929312
130	WBGene00016573	C41H7.3	hypothetical protein	0.795974518	0.184251	8.68E-07	4.00E-05	465.910465
131	WBGene00016574	C41H7.4	hypothetical protein	0.430316182	0.217444	0.003242	0.018856	253.9131662
132	WBGene00016575	C41H7.5	hypothetical protein	0.489727913	0.226572	0.001861	0.012543	226.9119289
133	WBGene00016576	C41H7.6	hypothetical protein	0.709471585	0.239849	0.000158	0.001898	659.5677034
134	WBGene00016590	C42C1.12	hypothetical protein	-0.537738009	0.088393	1.01E-10	4.06E-08	640.4850314
135	WBGene00016616	C43H6.3	hypothetical protein	0.534035987	0.205422	0.000576	0.00513	239.9838618
136	WBGene00016674	C45G9.2	Uncharacterized tRNA-dihydrouridine synthase-like protein C45G9.2	-0.375722828	0.081249	4.98E-07	2.74E-05	975.8389093
137	WBGene00016706	C46C11.3	hypothetical protein	0.684976007	0.234024	0.000178	0.002085	74.18210504
138	WBGene00016767	C49C8.3	hypothetical protein	-0.377929553	0.157537	0.001601	0.011259	187.1502137
139	WBGene00016791	C49H3.4	hypothetical protein	-0.349314324	0.091174	1.77E-05	0.000379	535.4718593
140	WBGene00008220	C50B6.7	Alpha-amylase	-0.475583898	0.165939	0.000316	0.003195	146.4065173
141	WBGene00016809	C50D2.6	hypothetical protein	0.388217953	0.23689	0.007032	0.034233	83.99641349
142	WBGene00016816	C50E3.5	hypothetical protein	-0.361410322	0.099683	3.73E-05	0.000669	1315.200752
143	WBGene00016877	C52D10.3	hypothetical protein	0.484281089	0.166209	0.000266	0.002801	123.7876274
144	WBGene00194706	C53A5.16	hypothetical protein	-0.36288997	0.094729	1.66E-05	0.00036	748.6997535
145	WBGene00016906	C53D5.5	hypothetical protein	0.327185822	0.134567	0.001916	0.012766	292.8220624
146	WBGene00008281	C53D6.4	hypothetical protein	-0.320417014	0.060769	2.36E-08	2.83E-06	1682.222247
147	WBGene00008318	C54G4.9	hypothetical protein	-0.321622246	0.09395	9.66E-05	0.00132	991.0583066
148	WBGene00016942	C55B7.3	Tyrosine-protein phosphatase	0.68843637	0.15921	1.00E-06	4.51E-05	174.36698
149	WBGene00008343	C56A3.4	hypothetical protein	-0.335410399	0.082598	7.29E-06	0.000194	982.5399109
150	WBGene00008344	C56A3.5	hypothetical protein	-0.311132886	0.073545	3.94E-06	0.000123	1441.313665
151	WBGene00008346	C56A3.8	hypothetical protein	-0.339151781	0.085047	9.88E-06	0.000247	602.2305294
152	WBGene00016965	C56C10.9	hypothetical protein	-0.310164412	0.069539	1.45E-06	5.92E-05	1258.710831
153	WBGene00000281	cah-3	Putative carbonic anhydrase 3	0.337051249	0.144906	0.002373	0.014959	579.824899
154	WBGene00012484	car-1	Cytokinesis, Apoptosis, RNA-associated	0.326062253	0.168141	0.00619	0.031116	24233.54208
155	WBGene00000294	cas-1	Adenylyl cyclase-associated protein	0.338707468	0.102069	0.000132	0.001661	1025.41326
156	WBGene00013672	catp-1	Cation transporting ATPase	0.312310005	0.15449	0.00537	0.027835	157.2208188
157	WBGene00016987	CC8.2	Protein phosphatase 1 regulatory subunit	0.397762466	0.189729	0.003017	0.017938	332.1962583
158	WBGene00000368	ccb-1	Calcium Channel, Beta subunit	0.5508618	0.179557	0.000141	0.001741	165.2814755
159	WBGene00012277	ccch-3	CCCH-type zinc finger putative transcription factor	-0.349555555	0.067868	3.93E-08	4.31E-06	1319.931584
160	WBGene00002391	cct-7	Chaperonin Containing TCP-1	0.619496598	0.171189	2.00E-05	0.000416	4452.115806
161	WBGene00000387	cdc-25.2	M-phase inducer phosphatase cdc-25.2	0.413095038	0.125377	0.000102	0.001376	1822.454346
162	WBGene00021097	cdc-37	Probable Hsp90 co-chaperone cdc37	0.615910009	0.449761	0.005069	0.026682	1472.205855
163	WBGene00010562	cdc-48.3	Cell Division Cycle related	-0.310032391	0.096331	0.000211	0.002357	987.8948227
164	WBGene00019994	cdh-1	CaDHerin family	0.940446667	0.221359	1.11E-06	4.82E-05	131.7268309
165	WBGene00016997	cebp-1	C/EBP (CCAAT/enhancer-binding protein) homolog	0.938234581	0.278948	3.55E-05	0.000647	58.13622429
166	WBGene00011636	cec-3	Chromo domain-containing protein cec-3	-0.422790474	0.062864	2.09E-12	2.97E-09	2481.177921
167	WBGene00000426	ced-12	Cell death abnormality protein 12	-0.318630367	0.067569	4.22E-07	2.47E-05	2016.364156
168	WBGene00000444	ceh-21	Homeobox protein ceh-21	0.403235787	0.205175	0.003763	0.021199	450.8272117
169	WBGene00000453	ceh-32	Homeobox protein ceh-32	0.314734938	0.169396	0.007204	0.034898	432.2716061
170	WBGene00000455	ceh-34	Homeobox protein ceh-34	0.556967819	0.318989	0.003633	0.020642	96.12910097
171	WBGene00000457	ceh-36	Homeobox protein ceh-36	0.491074485	0.297479	0.004615	0.024809	85.0434434
172	WBGene00013583	ceh-51	C. Elegans Homeobox	0.556811478	0.253515	0.001465	0.010522	59.67944982
173	WBGene00011069	ceh-62	Homeobox protein ceh-62	0.460076743	0.331652	0.007234	0.034983	48.05270718
174	WBGene00000469	ces-2	Cell death specification protein 2	0.456395534	0.241469	0.003545	0.020229	190.6976003
175	WBGene00000472	cey-1	C. Elegans Y-box	0.430481728	0.119673	2.71E-05	0.000527	6001.04723
176	WBGene00000475	cey-4	C. Elegans Y-box	0.863667658	0.307646	0.000217	0.00241	4289.502424
177	WBGene00000478	cfz-2	Frizzled-2	0.304432386	0.139921	0.00411	0.022728	251.0022981
178	WBGene00007053	chd-7	Chromodomain and Helicase Domain protein	0.454319302	0.121994	1.82E-05	0.000386	1305.378971
179	WBGene00018051	che-10	Rootletin	0.397965657	0.16848	0.001647	0.01148	244.0423673
180	WBGene00000498	chk-1	Serine/threonine-protein kinase chk-1	0.647028743	0.186807	3.21E-05	0.000603	1059.5555
181	WBGene00015347	cids-1	CID domain-containing protein 1	-0.338431606	0.081581	5.04E-06	0.000147	1887.141909
182	WBGene00000509	cka-1	Choline Kinase A	-0.339362522	0.077518	1.85E-06	7.08E-05	1519.227765
183	WBGene00000516	cki-1	Cyclin-dependent kinase inhibitor 1	0.748803253	0.177878	1.47E-06	5.94E-05	225.2997585
184	WBGene00009394	clec-63	C-type LECtin	0.361925459	0.213583	0.007386	0.035554	4498.350371
185	WBGene00018547	clec-78	C-type LECtin	0.711300783	0.537812	0.004621	0.024808	129.4310237
186	WBGene00019606	clec-88	C-type lectin domain-containing protein 88	-0.32270681	0.061308	2.23E-08	2.73E-06	15468.51165
187	WBGene00020808	clik-1	CaLponIn-liKe proteins	0.482142018	0.12866	1.54E-05	0.000339	3948.022375
188	WBGene00000553	cmk-1	Calcium/calmodulin-dependent protein kinase type 1	0.45031814	0.366972	0.008907	0.041145	91.67373133
189	WBGene00016564	cmt-1	Protein cmt-1	-0.327133279	0.063915	5.06E-08	5.07E-06	2285.773318
190	WBGene00000584	cog-1	hypothetical protein	1.348103084	0.390167	2.17E-05	0.000445	27.71168102
191	WBGene00000675	col-101	COLlagen	0.368454989	0.140346	0.001051	0.00813	12746.80197
192	WBGene00000677	col-103	COLlagen	0.49630734	0.598349	0.009054	0.041714	6170.099399
193	WBGene00000678	col-104	COLlagen	1.167653644	0.449995	0.000334	0.003337	95.13876544
194	WBGene00000680	col-106	COLlagen	1.535971329	0.488922	5.67E-05	0.000921	3882.132694
195	WBGene00000681	col-107	COLlagen	1.279468021	1.394916	0.004096	0.02266	89.02223157
196	WBGene00000683	col-109	COLlagen	0.857804454	0.749963	0.004674	0.025023	46.67669861
197	WBGene00000691	col-117	COLlagen	1.801621387	0.313287	4.93E-10	1.38E-07	35.83819185
198	WBGene00000594	col-117	COLlagen	1.061249334	0.370141	0.000167	0.001987	28.27791841
199	WBGene00000692	col-118	COLlagen	0.303047741	0.13874	0.004019	0.022331	284.5391785
200	WBGene00000693	col-119	COLlagen	0.745140994	0.374568	0.001685	0.011644	19306.97071
201	WBGene00000696	col-122	COLlagen	0.873256531	0.522357	0.002563	0.015831	6986.380957
202	WBGene00000698	col-124	COLlagen	0.964927702	0.308223	8.10E-05	0.001165	6802.638809
203	WBGene00000699	col-125	COLlagen	1.205242415	0.833513	0.00287	0.017272	157.9803024
204	WBGene00000703	col-129	COLlagen	0.950941432	0.315772	0.000109	0.001438	170.8023807
205	WBGene00000704	col-130	COLlagen	1.389667138	0.503541	0.000206	0.00231	53.23511431
206	WBGene00000712	col-139	COLlagen	0.899597028	0.274	4.58E-05	0.000785	118.5752913
207	WBGene00000713	col-140	COLlagen	0.466987657	0.350608	0.00773	0.036737	14012.51945
208	WBGene00000715	col-142	COLlagen	1.035015817	0.270484	5.97E-06	0.000167	234.7480811
209	WBGene00000716	col-143	COLlagen	0.670948954	0.324801	0.001629	0.011386	6068.181448
210	WBGene00000722	col-149	COLlagen	0.779562323	0.352731	0.001057	0.008163	55.27589681
211	WBGene00000723	col-150	COLlagen	0.365594104	0.219136	0.007418	0.035665	73.16122539
212	WBGene00000728	col-155	Putative cuticle collagen 155	0.745088271	0.242187	0.000104	0.001398	330.5545479
213	WBGene00000733	col-160	COLlagen	0.658617713	0.404268	0.003536	0.020187	2880.677951
214	WBGene00000739	col-166	COLlagen	1.304997162	0.268327	5.94E-08	5.41E-06	237.1458558
215	WBGene00000740	col-167	COLlagen	1.200948359	0.936511	0.003423	0.019686	96.17996588
216	WBGene00000754	col-181	COLlagen	0.593767873	0.193418	0.000138	0.001723	12626.39877
217	WBGene00000757	col-184	COLlagen	0.770748117	0.306048	0.000512	0.004687	6479.822759
218	WBGene00000608	col-19	Cuticle collagen 19	0.633057464	0.211459	0.000171	0.002017	6957.136344
219	WBGene00000609	col-20	COLlagen	0.398482885	0.202053	0.003794	0.021318	15066.36762
220	WBGene00000611	col-34	Cuticle collagen 34	1.11191962	0.330421	3.25E-05	0.000603	39.39375096
221	WBGene00000616	col-39	Cuticle collagen 39	1.431443142	0.376326	6.28E-06	0.000173	39.27183281
222	WBGene00013489	col-42	COLlagen	1.39099474	0.648904	0.00085	0.006953	1392.281734
223	WBGene00000620	col-43	COLlagen	0.730254834	0.582288	0.00483	0.025678	34.43615715
224	WBGene00000625	col-48	COLlagen	1.365118076	0.361158	6.74E-06	0.000183	83.98191616
225	WBGene00000641	col-65	COLlagen	1.830899913	0.696614	0.000265	0.002797	86.76095194

	ENSEMBLE GeneID	SYMBOL	GENENAME	log2FoldChange	lfcSE	pvalue	padj	baseMean
226	WBGene00000653	col-77	COLlagen	1.003842472	0.417679	0.00058	0.005155	135.6910123
227	WBGene00000656	col-80	Putative cuticle collagen 80	0.802776789	0.423711	0.001942	0.012882	5696.97044
228	WBGene00000657	col-81	COLlagen	1.035489211	0.398111	0.000335	0.003341	50.69038652
229	WBGene00000664	col-89	COLlagen	0.984752827	0.601403	0.002556	0.015808	24.474175
230	WBGene00000667	col-92	COLlagen	0.705560228	0.330238	0.001322	0.009718	44.62640166
231	WBGene00000668	col-93	COLlagen	0.55360609	0.482854	0.006917	0.033804	5029.591915
232	WBGene00000669	col-94	COLlagen	1.033231828	0.312898	4.18E-05	0.000734	178.274793
233	WBGene00000670	col-95	COLlagen	0.400486733	0.240654	0.006414	0.031965	2120.853845
234	WBGene00000671	col-96	COLlagen	0.902252237	0.298701	0.00011	0.001449	56.777721
235	WBGene00000672	col-97	COLlagen	1.062048817	0.575516	0.001787	0.012135	62.59057482
236	WBGene00000673	col-98	COLlagen	0.867272025	0.398106	0.000939	0.007474	1677.234115
237	WBGene00000674	col-99	Putative cuticle collagen 99	1.083883039	0.300464	1.36E-05	0.000308	124.0229179
238	WBGene00021292	copb-1	Coatomer subunit beta	0.301536632	0.08998	0.00014	0.001738	2611.737761
239	WBGene00000768	cor-1	Coronin-like protein cor-1	0.517583172	0.153787	5.90E-05	0.000948	192.6181867
240	WBGene00010964	COX1	cytochrome c oxidase subunit I	-0.564287741	0.098621	7.97E-10	1.86E-07	58242.78892
241	WBGene00010965	COX2	cytochrome c oxidase subunit II	-0.591370434	0.109198	4.22E-09	6.72E-07	44059.44091
242	WBGene00010962	COX3	cytochrome c oxidase subunit III	-0.392635368	0.097161	6.17E-06	0.000171	37155.27909
243	WBGene00012354	cox-4	Cytochrome OXidase assembly protein	0.514435837	0.226738	0.001373	0.010003	3236.810037
244	WBGene00000371	cox-5B	Cytochrome OXidase assembly protein	0.426891424	0.215976	0.003349	0.019342	3095.73987
245	WBGene00017926	cox-6C	Cytochrome OXidase assembly protein	0.507203885	0.513828	0.008296	0.038869	906.2387741
246	WBGene00009161	cox-7C	Cytochrome OXidase assembly protein	0.881349024	0.62131	0.003559	0.02029	1601.862585
247	WBGene00010723	cpg-7	Chondroitin proteoglycan 7	0.592513718	0.239657	0.000734	0.006195	80.93737424
248	WBGene00019357	cpg-8	Chondroitin proteoglycan 8	0.984170332	0.370312	0.000299	0.003073	1285.206594
249	WBGene00000776	cpl-1	CathePsin L family	0.623346133	0.181316	4.11E-05	0.000723	16843.94328
250	WBGene00000779	cpn-3	CalPoNin	0.353024187	0.153533	0.002525	0.015671	5421.222641
251	WBGene00000785	cpr-5	Cathepsin B-like cysteine proteinase 5	0.318244509	0.192491	0.010597	0.04696	1534.508484
252	WBGene00017313	cpsf-2	Probable cleavage and polyadenylation specificity factor subunit 2	-0.324428114	0.062203	4.53E-08	4.65E-06	2109.863889
253	WBGene00022271	cpx-1	Putative complexin-1	0.577701209	0.18559	0.000113	0.001479	124.329749
254	WBGene00000792	crb-1	Drosophila CRumBs homolog	0.406321519	0.163886	0.001156	0.008736	246.3631919
255	WBGene00000793	crh-1	CREB Homolog	0.50417349	0.172501	0.00025	0.002677	744.4578926
256	WBGene00010303	cri-3	Conserved regulator of innate immunity protein 3	0.399523988	0.153572	0.000874	0.007098	2898.314186
257	WBGene00000804	csc-1	Chromosome segregation and cytokinesis defective protein 1	0.457270093	0.257587	0.004294	0.023508	847.1209514
258	WBGene00011915	ctf-8	Chromosome Transmission Fidelity factor homolog	-0.335832096	0.09492	5.73E-05	0.000926	635.9026971
259	WBGene00000830	ctl-1	Catalase-2	0.521888802	0.200937	0.000571	0.005097	105.0615445
260	WBGene00000832	ctn-1	alpha-CaTuliN (catenin/vinculin related)	0.642277573	0.150024	1.21E-06	5.13E-05	270.8970327
261	WBGene00013093	cup-14	hypothetical protein	0.426637035	0.105155	5.17E-06	0.00015	1052.454314
262	WBGene00009983	cut-2	Cuticlin-2	1.909315682	0.762525	0.000352	0.003469	165.5095001
263	WBGene00013180	cutl-10	CUTiclin-Like	1.071035954	0.298738	1.60E-05	0.000349	58.12406397
264	WBGene00017421	cutl-29	CUTiclin-Like	0.577746424	0.587655	0.007323	0.035342	34.83347155
265	WBGene00000870	cyd-1	G1/S-specific cyclin-D	0.54267436	0.120032	4.77E-07	2.65E-05	369.5619037
266	WBGene00000886	cyn-10	Peptidyl-prolyl cis-trans isomerase 10	-0.398831579	0.082601	1.66E-07	1.23E-05	1268.553319
267	WBGene00000881	cyn-5	Peptidyl-prolyl cis-trans isomerase 5	0.458717347	0.138679	8.21E-05	0.001169	7566.990776
268	WBGene00000882	cyn-6	Peptidyl-prolyl cis-trans isomerase 6	0.412959768	0.119575	5.61E-05	0.000914	815.843537
269	WBGene00019962	cysl-3	Cysteine synthase 3	0.3020016	0.168033	0.008827	0.040845	396.3050181
270	WBGene00000829	CYTB	cytochrome b	-0.403706952	0.100424	6.54E-06	0.000179	44701.13399
271	WBGene00017002	D1007.4	hypothetical protein	-0.334154334	0.111038	0.000349	0.003444	615.0532444
272	WBGene00017005	D1007.8	hypothetical protein	-0.312343627	0.096206	0.000187	0.002158	807.6793058
273	WBGene00000820	D2030.11	hypothetical protein	-0.424177163	0.103042	4.07E-06	0.000126	596.5629727
274	WBGene00008413	D2030.3	hypothetical protein	-0.30518993	0.0722	4.30E-06	0.000131	1664.337609
275	WBGene00008417	D2030.7	hypothetical protein	-0.338067443	0.090547	2.77E-05	0.000535	2150.472721
276	WBGene00017068	D2092.8	hypothetical protein	0.872083678	0.904505	0.005345	0.027748	20.75851353
277	WBGene00017073	D2096.6	hypothetical protein	0.815046287	0.490149	0.002772	0.016791	51.1754689
278	WBGene00017074	D2096.7	hypothetical protein	-0.434242293	0.069944	5.80E-11	2.65E-08	1141.277714
279	WBGene00018976	daam-1	DAAM (Disheveled-Associated Activator of Morphogenesis) homolog	0.509745546	0.379429	0.006548	0.032418	81.99077258
280	WBGene00000901	daf-5	hypothetical protein	0.592706516	0.136542	1.01E-06	4.53E-05	429.0788323
281	WBGene00015939	damt-1	DNA N6-methyl methyltransferase	-0.356507063	0.104596	8.40E-05	0.001187	631.2855733
282	WBGene00000928	dao-2	Dauer or Aging adult Overexpression	0.608670964	0.239313	0.000581	0.005159	695.3420457
283	WBGene00003400	dapk-1	Death-associated protein kinase dapk-1	0.590438009	0.124944	1.66E-07	1.23E-05	239.7794544
284	WBGene00010664	dbn-1	DreBrIN 1/DreBrIN-like (where Drebrin is from Developmentally REgulated BRaIN protein) family homolog	0.58066874	0.244442	0.000927	0.007399	1419.364132
285	WBGene00000940	dcs-1	m7GpppX diphosphatase	-0.344287343	0.091225	2.38E-05	0.000475	1182.848614
286	WBGene00017488	dct-7	DAF-16/FOXO Controlled, germline Tumor affecting	-0.520429229	0.59198	0.008716	0.040451	29.72237633
287	WBGene00013000	ddl-2	Daf-16-Dependent Longevity (WT but not daf-16 lifespan increased)	0.782895355	0.171052	2.68E-07	1.84E-05	226.4404934
288	WBGene00000941	ddp-1	Mitochondrial import inner membrane translocase subunit Tim8	0.692232561	0.628842	0.005602	0.028767	435.1533882
289	WBGene00010296	dgat-2	acyl-CoA:DiacylGlycerol AcylTransferase	0.415769818	0.197634	0.002666	0.016325	155.4523853
290	WBGene00000958	dgk-1	Diacylglycerol kinase	0.378505255	0.254626	0.00896	0.041316	97.05478173
291	WBGene00007974	dhfr-1	Putative dihydrofolate reductase	-0.345491409	0.073337	3.56E-07	2.18E-05	2516.662741
292	WBGene00000976	dhs-13	DeHydrogenases, Short chain	0.690064915	0.179085	6.96E-06	0.000188	1793.435592
293	WBGene00000988	dhs-25	DeHydrogenases, Short chain	0.423014908	0.185561	0.001785	0.012135	2070.77665
294	WBGene00017735	did-2	Doa4-Independent Degradation, homologous to yeast Did2	0.428841107	0.201922	0.002551	0.015789	1671.089343
295	WBGene00000998	dig-1	Mesocentin	0.323052872	0.194332	0.009616	0.043539	702.0531889
296	WBGene00001000	dim-1	Disorganized muscle protein 1	0.454243506	0.098135	3.62E-07	2.21E-05	2873.01521
297	WBGene00008549	din-1	Daf-12-interacting protein 1	0.315527612	0.114691	0.000887	0.007174	1285.328532
298	WBGene00001008	dlk-1	Mitogen-activated protein kinase kinase kinase dlk-1	0.633463896	0.125444	3.14E-08	3.59E-06	374.532254
299	WBGene00022060	dmd-9	DM (Doublesex/MAB-3) Domain family	0.624574556	0.141485	7.16E-07	3.48E-05	187.974246
300	WBGene00001018	dnc-2	Probable dynactin subunit 2	-0.32686747	0.058689	4.29E-09	6.72E-07	2431.832314
301	WBGene00021149	dnc-3	DyNactin Complex component	-0.333814348	0.07255	6.68E-07	3.32E-05	1015.785503
302	WBGene00001036	dnj-18	DNaJ domain (prokaryotic heat shock protein)	-0.331850931	0.07137	5.32E-07	2.87E-05	1052.212194
303	WBGene00001042	dnj-24	DNaJ domain (prokaryotic heat shock protein)	0.364810691	0.145357	0.001297	0.009587	192.5304463
304	WBGene00001044	dnj-26	DNaJ domain (prokaryotic heat shock protein)	-0.502525038	0.090338	2.42E-09	4.44E-07	565.6870706
305	WBGene00001048	dnj-30	DNaJ domain (prokaryotic heat shock protein)	-0.31107777	0.066082	4.52E-07	2.57E-05	1506.139474
306	WBGene00008316	dod-18	Downstream Of DAF-16 (regulated by DAF-16)	-0.418922328	0.089071	2.85E-07	1.92E-05	564.0509053
307	WBGene00021474	dot-1.1	Histone-lysine N-methyltransferase, H3 lysine-79 specific	0.444451011	0.181623	0.001105	0.008457	1373.15027
308	WBGene00001076	dpy-17	DumPY: shorter than wild-type	1.227347056	0.398103	8.07E-05	0.001161	2028.490773
309	WBGene00001077	dpy-18	Prolyl 4-hydroxylase subunit alpha-1	0.325474514	0.079781	7.06E-06	0.00019	681.8905017
310	WBGene00001081	dpy-22	Mediator of RNA polymerase II transcription subunit 12	0.394207846	0.278463	0.009093	0.041808	850.789052
311	WBGene00001065	dpy-3	DumPY: shorter than wild-type	2.068235176	0.35695	3.25E-10	1.02E-07	80.49004021
312	WBGene00001088	dpy-30	Dosage compensation protein dpy-30	0.46728693	0.185499	0.000872	0.007089	1982.501892
313	WBGene00001069	dpy-7	Cuticle collagen dpy-7	1.111370763	0.368165	0.000102	0.001372	191.4957557
314	WBGene00016701	dsb-3	Double-Strand Break factor	-0.313180459	0.081811	2.14E-05	0.00044	729.5904238
315	WBGene00001105	dsl-3	Delta-like protein	0.385974496	0.176886	0.002593	0.015983	218.4381938
316	WBGene00001113	dur-1	Dauer Up-Regulated	0.360129802	0.145053	0.001418	0.010229	243.3664255
317	WBGene00001131	dys-1	Dystrophin-1	0.599969778	0.162184	1.44E-05	0.000321	460.353147
318	WBGene00017153	E_BE45912.2	hypothetical protein	-0.322125714	0.123089	0.0012	0.008976	311.2686912
319	WBGene00008442	E01B7.2	hypothetical protein	-0.354307952	0.080249	1.46E-06	5.94E-05	754.2900434
320	WBGene00008447	E01G4.5	hypothetical protein	0.374965552	0.148296	0.00116	0.008755	246.042104
321	WBGene00008455	E02H1.1	Probable dimethyladenosine transferase	-0.306115241	0.084413	4.89E-05	0.000817	700.0361225
322	WBGene00017105	E02H9.7	hypothetical protein	-0.321965777	0.141557	0.002909	0.01744	373.3821347
323	WBGene00020770	eat-17	hypothetical protein	0.30980892	0.118595	0.001325	0.009728	743.737699
324	WBGene00001148	eat-20	Abnormal pharyngeal pumping eat-20	0.327822187	0.117552	0.000073	0.006169	651.568937
325	WBGene00001156	ech-7	Enoyl-CoA Hydratase	0.32526438	0.125471	0.001306	0.009639	1005.189101
326	WBGene00017142	EEED8.14	hypothetical protein	-0.417101276	0.090159	4.20E-07	2.47E-05	767.8649915
327	WBGene00017134	EEED8.3	hypothetical protein	-0.382105803	0.045799	9.86E-18	1.26E-13	6481.341488
328	WBGene00001168	eef-1A.1	Elongation factor 1-alpha	0.362980287	0.205612	0.00651	0.032319	133514.328
329	WBGene00001169	eef-1A.2	Elongation factor 1-alpha	0.869397617	0.142867	6.97E-11	2.98E-08	3247.090459
330	WBGene00018846	eef-1B.1	Probable elongation factor 1-beta/1-delta 1	0.773973615	0.335946	0.000794	0.006602	10163.98276
331	WBGene00012768	eef-1B.2	Probable elongation factor 1-beta/1-delta 2	0.430991285	0.185862	0.001594	0.011247	7361.331325
332	WBGene00001162	efl-2	E2F-like (mammalian transcription factor)	0.30010619	0.097165	0.00034	0.003379	708.1233605
333	WBGene00001170	egl-1	Programmed cell death activator egl-1	1.372562445	0.220915	2.56E-11	1.64E-08	61.84897162
334	WBGene00001186	egl-18	hypothetical protein	0.470112338	0.142802	8.25E-05	0.001172	810.1734568
335	WBGene00001196	egl-30	hypothetical protein	0.304911046	0.107789	0.000787	0.00656	2647.996666
336	WBGene00001215	ego-2	Enhancer of Glp-One (glp-1)	0.476444685	0.205806	0.001358	0.009926	1041.63647
337	WBGene00001232	eif-3.I	Eukaryotic translation initiation factor 3 subunit I	0.445179671	0.164176	0.000541	0.004889	3220.729848
338	WBGene00012738	eif-3.J	Eukaryotic Initiation Factor	0.401145736	0.248368	0.006798	0.033373	1066.435163

	ENSEMBLE GeneID	SYMBOL	GENENAME	log2FoldChange	lfcSE	pvalue	padj	baseMean
339	WBGene00001234	eif-6	Eukaryotic translation initiation factor 6	0.561601839	0.417898	0.005688	0.029142	1058.691067
340	WBGene00001235	elb-1	ELongin B	0.836479786	0.29208	0.000187	0.002155	290.7457649
341	WBGene00001236	elc-1	ELongin C	0.860968489	0.178313	7.61E-08	6.68E-06	1415.369361
342	WBGene00016029	elf-1	ETS-Like transcription Factor homolog	0.3167723	0.164679	0.006387	0.031854	168.7513766
343	WBGene00018330	elks-1	mammalian ELKS/CAST/ERC/Rab6 interacting protein homolog	0.409722663	0.19559	0.002814	0.017007	371.222816
344	WBGene00001247	elo-9	Elongation of very long chain fatty acids protein	0.303734703	0.162462	0.007698	0.036629	208.026527
345	WBGene00001250	elt-2	Transcription factor elt-2	0.378992143	0.162925	0.001919	0.012774	160.3932188
346	WBGene00001251	elt-3	Erythroid-Like Transcription factor family	0.385698544	0.145328	0.000812	0.00672	284.1153922
347	WBGene00001253	elt-6	Erythroid-Like Transcription factor family	0.498529235	0.339117	0.005859	0.029767	82.01856089
348	WBGene00001309	emr-1	Emerin homolog 1	0.360582638	0.170953	0.003374	0.019455	1457.614985
349	WBGene00017164	eng-1	Endo-b-N-acetylGlucosaminidase	-0.36086456	0.08875	6.41E-06	0.000176	642.6204401
350	WBGene00010362	enu-3.1	ENhancer of Uncoordination	0.328861468	0.201753	0.009685	0.043744	272.5834594
351	WBGene00008003	enu-3.2	ENhancer of Uncoordination	0.833944051	0.305067	0.000272	0.002853	368.1217641
352	WBGene00021015	enu-3.3	ENhancer of Uncoordination	0.652141605	0.232095	0.000262	0.002775	220.8518007
353	WBGene00021034	enu-3.4	ENhancer of Uncoordination	0.76140544	0.343818	0.001063	0.008197	51.39457856
354	WBGene00010477	enu-3.6	ENhancer of Uncoordination	0.650676501	0.380008	0.003003	0.017883	70.09255611
355	WBGene00019487	ephx-1	EPHeXin (Eph-interacting GEF) homolog	0.382874101	0.119806	0.000157	0.001898	348.2906989
356	WBGene00001330	eps-8	EPS (human endocytosis) related	0.514475375	0.174669	0.000227	0.002488	694.8908111
357	WBGene00007589	erg-28	Probable ergosterol biosynthetic protein 28 homolog	-0.325435194	0.117554	0.000756	0.006357	299.4755549
358	WBGene00001340	etr-1	ELAV-Type RNA binding-protein family	0.316415315	0.125255	0.00162	0.011345	1320.615113
359	WBGene00001371	exl-1	Chloride intracellular channel exl-1	-0.328000163	0.082408	1.09E-05	0.000262	676.6476665
360	WBGene00010325	exos-3	EXOSome (multiexonuclease complex) component	-0.317099004	0.070288	1.10E-06	4.80E-05	1643.129285
361	WBGene00001377	eya-1	Eyes absent homolog 1	0.652554362	0.120554	4.29E-09	6.72E-07	209.2535325
362	WBGene00008488	F01D4.5	hypothetical protein	-0.319030513	0.081887	1.61E-05	0.00035	1106.667042
363	WBGene00008536	F02H6.3	hypothetical protein	-0.342117039	0.078573	1.99E-06	7.42E-05	1500.270536
364	WBGene00017210	F07E5.5	hypothetical protein	0.349050052	0.18479	0.005693	0.029151	706.4765561
365	WBGene00008561	F07H5.10	hypothetical protein	-0.320194628	0.062388	4.59E-08	4.68E-06	1813.783716
366	WBGene00017238	F08B4.7	U1 small nuclear ribonucleoprotein C	0.30672894	0.171273	0.008639	0.040167	1939.803453
367	WBGene00017263	F08F3.6	hypothetical protein	-0.321312228	0.092751	8.19E-05	0.001169	1768.804426
368	WBGene00008577	F08G2.5	hypothetical protein	1.0419434111	0.378636	0.000223	0.002457	33.24005044
369	WBGene00008578	F08G2.7	hypothetical protein	0.779294044	0.242938	6.71E-05	0.001024	114.3084481
370	WBGene00008610	F09C3.2	hypothetical protein	0.642751781	0.278261	0.000954	0.007562	50.59095136
371	WBGene00008622	F09C8.2	hypothetical protein	0.442221317	0.133564	8.47E-05	0.001193	843.5719222
372	WBGene00017289	F09E5.11	hypothetical protein	-0.38473593	0.069949	5.01E-09	7.65E-07	1287.485769
373	WBGene00017286	F09E5.8	Pyridoxal phosphate homeostasis protein	-0.312841824	0.081363	2.04E-05	0.000422	898.1454614
374	WBGene00017302	F09F7.5	hypothetical protein	0.349368243	0.164345	0.00353	0.020161	197.1296336
375	WBGene00008639	F10B5.2	Protein AAR2 homolog	-0.312792222	0.085689	4.34E-05	0.000755	926.698562
376	WBGene00017344	F10E7.2	hypothetical protein	0.681487389	0.264184	0.000474	0.00442	357.2596004
377	WBGene00017360	F10E9.11	hypothetical protein	-0.311021511	0.12483	0.001842	0.012428	1537.706828
378	WBGene00017358	F10E9.7	hypothetical protein	-0.390161766	0.074744	2.24E-08	2.73E-06	1627.4909
379	WBGene00008667	F10G8.9	hypothetical protein	-0.346035711	0.092271	2.47E-05	0.00049	445.5590116
380	WBGene00008707	F11E6.3	hypothetical protein	0.85576429	0.610892	0.00366	0.020758	1645.214164
381	WBGene00017413	F13A2.4	hypothetical protein	0.532992119	0.270641	0.002437	0.015254	96.81952635
382	WBGene00017416	F13B6.1	hypothetical protein	0.537554892	0.579039	0.008511	0.039713	19.96731639
383	WBGene00017423	F13C5.2	hypothetical protein	0.461925051	0.120616	1.16E-05	0.000273	1009.347917
384	WBGene00008742	F13D12.8	hypothetical protein	0.427293483	0.25969	0.005804	0.029545	60.45643097
385	WBGene00008743	F13D12.9	hypothetical protein	0.568674176	0.366718	0.004566	0.024634	46.35534491
386	WBGene00008760	F13E9.11	hypothetical protein	0.421633759	0.339921	0.009662	0.04366	416.3601245
387	WBGene00017459	F14D2.11	hypothetical protein	-0.418223485	0.178893	0.001628	0.011385	119.9180156
388	WBGene00017484	F15E6.3	hypothetical protein	0.389444588	0.176646	0.00246	0.015355	429.9206926
389	WBGene00008865	F15G9.1	hypothetical protein	0.37705444	0.19291	0.004285	0.023473	310.8399761
390	WBGene00008944	F19B2.5	hypothetical protein	0.533228228	0.123033	1.20E-06	5.11E-05	444.0647034
391	WBGene00017621	F20A1.10	hypothetical protein	0.602364512	0.280194	0.001475	0.01057	358.220546
392	WBGene00017632	F20B6.9	hypothetical protein	1.449518279	0.426007	2.77E-05	0.000535	25.1397763
393	WBGene00008973	F20D1.1	hypothetical protein	0.659805063	0.167951	5.35E-06	0.000154	1037.098968
394	WBGene00017708	F22E5.9	hypothetical protein	0.512674615	0.106296	1.18E-07	9.40E-06	420.1319888
395	WBGene00017724	F22F7.7	Gamma-glutamylcyclotransferase	0.361557517	0.163303	0.002692	0.016429	228.9162831
396	WBGene00009064	F22G12.4	hypothetical protein	0.742750206	0.130754	8.48E-10	1.91E-07	700.7437429
397	WBGene00017734	F23C8.5	hypothetical protein	0.746040925	0.384663	0.001842	0.012428	1309.264363
398	WBGene00017736	F23C8.7	Tyrosine-protein kinase	0.417509667	0.385161	0.010914	0.047962	32.42380735
399	WBGene00009123	F25H2.12	hypothetical protein	-0.371405761	0.094286	1.02E-05	0.000253	645.4965083
400	WBGene00009220	F28D9.4	hypothetical protein	0.635041921	0.152985	2.17E-06	7.94E-05	270.9630882
401	WBGene00009262	F30A10.3	Kinase	-0.303282246	0.06351	3.32E-07	2.09E-05	2130.744737
402	WBGene00009270	F30F8.1	hypothetical protein	-0.339843709	0.078204	2.09E-06	7.70E-05	3166.880386
403	WBGene00017939	F31A3.5	hypothetical protein	0.420074253	0.140914	0.000263	0.00278	537.9591193
404	WBGene00009305	F32A7.4	hypothetical protein	-0.356416653	0.0836	2.80E-06	9.53E-05	1698.078221
405	WBGene00009314	F32B4.4	hypothetical protein	0.759406338	0.192976	4.62E-06	0.000138	564.5563483
406	WBGene00017984	F32D1.5	GMP reductase	0.397116442	0.142011	0.000513	0.004693	7712.052337
407	WBGene00017986	F32D1.7	hypothetical protein	0.618732382	0.390072	0.003832	0.021495	1359.650697
408	WBGene00017992	F32E10.5	hypothetical protein	-0.311697036	0.073606	3.87E-06	0.000123	1259.73592
409	WBGene00009346	F32H2.10	hypothetical protein	-0.352334984	0.078685	1.07E-06	4.71E-05	1029.002587
410	WBGene00009349	F32H5.3	hypothetical protein	0.558969603	0.244356	0.001185	0.008879	75.11060785
411	WBGene00009361	F33E2.5	hypothetical protein	0.495931035	0.174758	0.000324	0.00327	402.7726617
412	WBGene00044666	F33G12.7	hypothetical protein	-0.382452563	0.163223	0.001815	0.012294	368.0982818
413	WBGene00018145	F37C4.5	Protein F37C4.5	1.122809016	0.398579	0.000165	0.001966	1098.296596
414	WBGene00009533	F38B7.2	hypothetical protein	-0.437298979	0.287191	0.006592	0.032597	135.0638681
415	WBGene00009563	F39H2.3	hypothetical protein	-0.351190849	0.060559	1.00E-09	2.18E-07	2032.757493
416	WBGene00009574	F40E10.6	hypothetical protein	0.477673261	0.136817	4.02E-05	0.000711	965.709574
417	WBGene00009575	F40F8.1	UMP-CMP kinase	-0.316570246	0.071371	1.47E-06	5.94E-05	1895.163151
418	WBGene00009606	F40G12.11	hypothetical protein	-0.347035829	0.084075	5.31E-06	0.000153	1510.002237
419	WBGene00077531	F40G9.15	hypothetical protein	0.375313026	0.222167	0.006912	0.033789	98.20122085
420	WBGene00185078	F40G9.17	hypothetical protein	0.306213867	0.16387	0.007557	0.036157	854.326581
421	WBGene00018252	F40H3.6	hypothetical protein	0.542493558	0.225258	0.000919	0.007342	341.1339832
422	WBGene00018268	F41C3.2	hypothetical protein	-0.864935869	0.442235	0.001751	0.011976	28.83977611
423	WBGene00018297	F41F3.3	hypothetical protein	2.359045431	0.305878	5.89E-16	3.78E-12	263.4582079
424	WBGene00018337	F42A9.8	hypothetical protein	-0.346880803	0.128635	0.000853	0.006965	584.4381534
425	WBGene00009644	F42G4.7	hypothetical protein	0.560558725	0.250972	0.001309	0.009648	125.7947419
426	WBGene00018373	F43B10.1	hypothetical protein	0.333748317	0.182227	0.006896	0.033733	227.5001402
427	WBGene00009657	F43G6.4	hypothetical protein	0.520198588	0.229394	0.00133	0.009757	141.8427992
428	WBGene00009659	F43G6.7	hypothetical protein	1.525170003	0.428606	1.45E-05	0.000322	101.3662397
429	WBGene00018399	F43H9.3	hypothetical protein	-0.325783698	0.082178	1.16E-05	0.000272	890.0541675
430	WBGene00018405	F44A2.5	hypothetical protein	0.353971151	0.204626	0.007329	0.035357	201.6477339
431	WBGene00018408	F44B9.5	Ancient ubiquitous protein 1 homolog	-0.325387325	0.078267	5.28E-06	0.000152	1180.112126
432	WBGene00009688	F44E5.1	hypothetical protein	0.727707334	0.552806	0.004587	0.024703	1762.087623
433	WBGene00009713	F44G4.3	hypothetical protein	-0.400914119	0.109492	2.75E-05	0.000532	643.661926
434	WBGene00009724	F45D3.4	hypothetical protein	-0.574599837	0.099963	7.01E-10	1.79E-07	483.5247348
435	WBGene00009740	F45H10.3	hypothetical protein	0.871960144	0.381522	0.000811	0.006716	1102.037229
436	WBGene00009785	F46C5.10	hypothetical protein	-0.377481597	0.133706	0.00051	0.004681	221.3207507
437	WBGene00018489	F46E10.2	hypothetical protein	1.53626587	0.252874	5.79E-11	2.65E-08	136.0202353
438	WBGene00009787	F46F2.3	hypothetical protein	0.580293544	0.47238	0.006339	0.031666	1142.042251
439	WBGene00018519	F46H5.3	Probable arginine kinase F46H5.3	0.413222459	0.13431	0.000219	0.00242	12952.91793
440	WBGene00009825	F47G4.4	hypothetical protein	1.10761056	0.190881	3.58E-10	1.07E-07	181.5152125
441	WBGene00018710	F52G3.1	hypothetical protein	0.493917285	0.195788	0.000793	0.0066	778.8861906
442	WBGene00018717	F52H2.5	hypothetical protein	-0.335104409	0.110782	0.000331	0.003324	303.676383
443	WBGene00018734	F53A10.2	hypothetical protein	0.610052205	0.146635	2.15E-06	7.88E-05	241.4926918
444	WBGene00009957	F53B2.8	hypothetical protein	0.368170583	0.204861	0.006127	0.030871	239.5829128
445	WBGene00018762	F53E10.6	RRP15-like protein	0.451732985	0.186988	0.001169	0.008806	1178.62547
446	WBGene00009982	F53F1.4	hypothetical protein	1.205855838	0.232655	1.06E-08	1.42E-06	238.2579633
447	WBGene00044423	F53F10.8	hypothetical protein	-0.329404297	0.103215	0.000206	0.002303	525.1974725
448	WBGene00009994	F53F4.12	hypothetical protein	-0.367493585	0.098173	2.33E-05	0.00047	832.13353
449	WBGene00010002	F53F8.5	hypothetical protein	0.305321123	0.117438	0.001419	0.010231	1514.398711
450	WBGene00018772	F53G12.4	hypothetical protein	0.476662974	0.774851	0.009742	0.043911	24.45777682
451	WBGene00018778	F53H1.4	hypothetical protein	0.352396558	0.089644	1.17E-05	0.000273	3194.645001

	ENSEMBLE GeneID	SYMBOL	GENENAME	log2FoldChange	lfcSE	pvalue	padj	baseMean
452	WBGene00010065	F54F7.3	hypothetical protein	-0.411606586	0.220123	0.004279	0.023458	446.195733
453	WBGene00010081	F55A11.8	hypothetical protein	-0.301652518	0.072155	5.35E-06	0.000154	809.132057
454	WBGene00010141	F56A8.5	hypothetical protein	-0.474222486	0.084388	1.89E-09	3.66E-07	726.8378229
455	WBGene00018975	F56E10.1	hypothetical protein	0.453398117	0.138792	9.54E-05	0.001309	1037.893179
456	WBGene00010185	F57A10.4	hypothetical protein	-0.554780543	0.095776	5.52E-10	1.45E-07	459.7334142
457	WBGene00010229	F58A4.6	hypothetical protein	-0.307241599	0.091843	0.000135	0.001702	527.9143774
458	WBGene00010236	F58B4.3	hypothetical protein	0.368836704	0.246072	0.009315	0.042513	88.57931776
459	WBGene00019061	F58F12.1	ATP synthase subunit delta, mitochondrial	0.489714951	0.476122	0.008527	0.039776	2162.667432
460	WBGene00138720	F58H1.8	hypothetical protein	-0.344473998	0.108111	0.000196	0.002227	546.9681369
461	WBGene00045272	F59C12.4	hypothetical protein	1.135728684	0.290909	4.29E-06	0.000131	345.0264778
462	WBGene00044251	F59C6.12	UPF0598 protein F59C6.12	-0.454508716	0.147911	0.000182	0.00211	162.743333
463	WBGene00010337	F59F4.2	hypothetical protein	0.582247845	0.399338	0.005021	0.026475	1265.047448
464	WBGene00019068	faah-3	Fatty Acid Amide Hydrolase homolog	0.430228292	0.142108	0.000225	0.002469	225.244542
465	WBGene00012626	famh-161	Protein fam-161	0.599237049	0.406275	0.004745	0.025309	37.11191017
466	WBGene00001385	far-1	Fatty-acid and retinol-binding protein 1	0.3788917	0.164638	0.00221	0.014179	12595.76248
467	WBGene00001386	far-2	Fatty-acid and retinol-binding protein 2	0.529761983	0.209586	0.000709	0.006055	48825.17872
468	WBGene00001391	far-7	Fatty Acid/Retinol binding protein	-0.386744944	0.305999	0.011177	0.048715	50.82706619
469	WBGene00001397	fat-5	Delta(9)-fatty-acid desaturase fat-5	0.71441255	0.16093	5.39E-07	2.88E-05	276.7607997
470	WBGene00022816	fbn-1	FiBrilliN homolog	0.341665608	0.207624	0.008881	0.041061	485.3410641
471	WBGene00008569	fbxa-101	F-box A protein	-0.376846834	0.080401	3.63E-07	2.21E-05	886.1336708
472	WBGene00012879	fbxa-215	F-box A protein	-0.321704768	0.062463	4.34E-08	4.53E-06	7791.359966
473	WBGene00012953	fbxa-216	F-box A protein	0.345287744	0.154533	0.00284	0.017136	187.2262341
474	WBGene00021576	fbxc-51	F-box C protein	0.303031301	0.115919	0.001388	0.010077	772.9079684
475	WBGene00019207	fgt-1	Facilitated glucose transporter protein 1	0.374377906	0.1239	0.000301	0.003085	1775.633219
476	WBGene00001423	fib-1	rRNA 2'-O-methyltransferase fibrillarin	0.572167905	0.156965	1.97E-05	0.000411	10473.81015
477	WBGene00001427	fkb-2	Peptidylprolyl isomerase	0.641441675	0.406739	0.003776	0.021248	6579.717033
478	WBGene00001430	fkb-5	Peptidylprolyl isomerase	0.388162624	0.122698	0.00017	0.002013	738.0059897
479	WBGene00011271	flad-1	FAD synthase	-0.307113974	0.066247	6.45E-07	3.27E-05	1650.20018
480	WBGene00016006	fln-2	FiLamiN (actin binding protein) homolog	0.376586439	0.164453	0.00213	0.013818	660.4902702
481	WBGene00001444	flp-1	SQPNFLRF-amide	-0.328691626	0.103583	0.000211	0.002358	420.716818
482	WBGene00001459	flp-16	GQTFVRF-amide	-0.302947812	0.142909	0.004621	0.024809	216.6153592
483	WBGene00001460	flp-17	FMRF-Like Peptide	-0.376965751	0.16128	0.001879	0.012618	240.697886
484	WBGene00044686	flp-28	FMRF-Like Peptide	0.454287445	0.27235	0.005111	0.026838	261.9473933
485	WBGene00010982	flp-32	FMRF-Like Peptide	0.849106536	0.352615	0.000617	0.005417	32.4542265
486	WBGene00001451	flp-8	FMRF-Like Peptide	-0.329001496	0.164808	0.005159	0.027013	141.4357466
487	WBGene00001482	fog-2	Feminization Of Germline	-0.346049301	0.070974	1.61E-07	1.22E-05	1114.510305
488	WBGene00001484	fox-1	Sex determination protein fox-1	0.368495927	0.100002	2.90E-05	0.000553	435.20757
489	WBGene00021698	frl-1	FRL (Formin Related gene in Leukocytes) homolog	0.518208943	0.130174	5.60E-06	0.000159	423.5636722
490	WBGene00001492	frm-5.1	FERM domain (protein4.1-ezrin-radixin-moesin) family	0.915624822	0.376838	0.000555	0.00498	29.8631589
491	WBGene00001502	ftt-2	14-3-3-like protein 2	1.008642407	0.184526	2.51E-09	4.48E-07	2576.154855
492	WBGene00016489	fubl-3	FUBp (FUBP) Like	0.488494187	0.170047	0.000299	0.003069	514.649843
493	WBGene00016173	fust-1	FUS/TLS RNA binding protein homolog	1.129774391	0.33251	2.88E-05	0.000551	2504.983908
494	WBGene00007703	gbf-1	hypothetical protein	0.422709852	0.108475	1.07E-05	0.000259	1167.780021
495	WBGene00021697	gcn-1	GCN (yeast General Control Nondrepressible) homolog	0.472838373	0.101902	3.42E-07	2.13E-05	1564.885572
496	WBGene00001581	gfi-1	GEI-4 (Four) Interacting protein	0.332677586	0.176923	0.006258	0.031346	618.4068968
497	WBGene00001604	gln-3	Glutamine synthetase	0.780082853	0.209583	1.06E-05	0.000259	798.7125609
498	WBGene00021331	glrx-10	GLutaRedoXin	0.62217439	0.303086	0.001786	0.012135	452.9406773
499	WBGene00020146	got-1.2	Probable aspartate aminotransferase, cytoplasmic	0.323514433	0.133311	0.001995	0.013178	752.2760882
500	WBGene00001683	gpd-1	Glyceraldehyde-3-phosphate dehydrogenase 1	0.388976632	0.172581	0.002243	0.014325	7249.967927
501	WBGene00001686	gpd-4	Glyceraldehyde-3-phosphate dehydrogenase 4	0.326700846	0.152705	0.003878	0.021723	4493.950206
502	WBGene00001692	grd-3	GRounDhog (hedgehog-like family)	0.452958489	0.282681	0.005665	0.029056	871.84362
503	WBGene00013082	grdn-1	Girdin homolog	0.539606046	0.245085	0.001499	0.010711	200.5774186
504	WBGene00001707	grh-1	GRainyHead (Drosophila transcription factor) homolog	0.51561556	0.496014	0.008152	0.03836	115.5862461
505	WBGene00001725	grl-16	GRound-Like (grd related)	1.42038032	0.352444	2.55E-06	8.93E-05	65.81812892
506	WBGene00001713	grl-4	GRound-Like (grd related)	0.686393356	0.147561	2.02E-07	1.44E-05	359.2413739
507	WBGene00001714	grl-5	GRound-Like (grd related)	0.851767021	0.846245	0.005129	0.02691	43.42407787
508	WBGene00012840	grsp-1	Glycine Rich Secreted Protein	1.413427036	0.40917	2.15E-05	0.000442	79.69173045
509	WBGene00012118	grsp-2	Glycine Rich Secreted Protein	0.524148673	0.638504	0.008445	0.039435	893.9009573
510	WBGene00016403	grsp-3	Glycine Rich Secreted Protein	1.024871055	0.386279	0.000305	0.003105	56.1012502
511	WBGene00001745	gsa-1	G protein, Subunit Alpha	0.464242468	0.304908	0.006148	0.030951	90.80847968
512	WBGene00001768	gst-20	Glutathione S-Transferase	0.619246674	0.164052	1.04E-05	0.000256	186.2106605
513	WBGene00006863	gyg-1	Glycogenin-1	0.324914944	0.09675	0.000119	0.001538	504.3937106
514	WBGene00010364	H04D03.3	hypothetical protein	0.386627597	0.206008	0.004753	0.02534	144.5492338
515	WBGene00019157	H05C05.1	hypothetical protein	0.322635319	0.106991	0.000374	0.003626	2666.916667
516	WBGene00019170	H06I04.6	hypothetical protein	0.443535888	0.263538	0.005201	0.0272	137.4048797
517	WBGene00019188	H11E01.3	hypothetical protein	0.32985766	0.140979	0.002393	0.015063	200.4860297
518	WBGene00019189	H11L12.1	hypothetical protein	1.384923086	0.344433	2.41E-06	8.57E-05	79.15444061
519	WBGene00019197	H14A12.5	hypothetical protein	-0.304171046	0.16788	0.008504	0.039698	173.3501771
520	WBGene00019240	H24K24.3	Alcohol dehydrogenase class-3	0.534926588	0.173409	0.00014	0.001735	1668.467897
521	WBGene00019250	H28G03.2	hypothetical protein	0.458182354	0.141281	0.000101	0.001367	571.5420089
522	WBGene00045261	H29C22.1	hypothetical protein	-0.468215365	0.138539	6.08E-05	0.000963	581.2891765
523	WBGene00044200	H37A05.4	hypothetical protein	0.698338272	0.218714	7.55E-05	0.00111	636.6218663
524	WBGene00010814	haf-4	HAIF transporter (PGP related)	0.348036774	0.1242	0.00062	0.005432	291.9909285
525	WBGene00001820	ham-1	hypothetical protein	0.597383994	0.145398	2.75E-06	9.40E-05	323.3984688
526	WBGene00001823	hap-1	Inosine triphosphate pyrophosphatase	-0.358987315	0.090716	1.04E-05	0.000256	623.6548683
527	WBGene00001828	hch-1	Zinc metalloproteinase nas-34	0.609392439	0.305827	0.002012	0.013249	311.2100818
528	WBGene00021209	hgap-1	Heterodimeric GTPase Activating Protein subunit	0.657315275	0.143712	3.25E-07	2.08E-05	650.3226243
529	WBGene00001853	hil-2	Histone H1.2	1.06224306	0.337493	6.88E-05	0.001039	1942.983839
530	WBGene00001854	hil-3	Histone H1.3	1.061780683	0.229404	1.97E-07	1.42E-05	1271.519488
531	WBGene00001858	hil-7	HIstone H1 Like	0.465712522	0.96313	0.009427	0.042926	900.7639719
532	WBGene00001869	him-10	Kinetochore protein Nuf2 homolog	-0.316200283	0.063128	9.71E-08	7.83E-06	2486.419636
533	WBGene00001867	him-8	High Incidence of Males (increased X chromosome loss)	-0.36375949	0.079613	6.67E-07	3.32E-05	1584.790306
534	WBGene00011735	hip-1	Hsp-70 Interacting Protein homolog	0.955683021	0.193768	4.34E-08	4.53E-06	2887.247446
535	WBGene00001876	his-2	Histone H3	2.186575927	0.523281	1.10E-06	4.80E-05	59.50179886
536	WBGene00001898	his-24	Histone H1.1	1.272969384	0.457265	0.000191	0.002182	1116.93018
537	WBGene00001906	his-32	Histone H3	2.37124202	0.417719	5.52E-10	1.45E-07	79.99398076
538	WBGene00001909	his-35	Histone H2A	0.733687471	0.15951	2.55E-07	1.76E-05	595.5359754
539	WBGene00001878	his-4	Histone H2B 2	1.011720451	0.37185	0.000247	0.002655	140.5037511
540	WBGene00001919	his-45	Histone H3	1.188114742	0.371708	5.69E-05	0.000923	32.12236596
541	WBGene00001929	his-45	Histone H3	1.120030041	0.564095	0.001321	0.009716	39.99478618
542	WBGene00001922	his-48	Probable histone H2B 4	1.007813834	0.457517	0.000885	0.007167	457.4657758
543	WBGene00001891	his-59	Histone H3	2.311917051	0.397273	2.52E-10	8.49E-08	33.93077529
544	WBGene00001880	his-59	Histone H3	1.926372454	0.469405	1.58E-06	6.21E-05	75.95577362
545	WBGene00001933	his-59	Histone H3	1.708607789	0.480481	1.43E-05	0.00032	402.5217313
546	WBGene00001914	his-59	Histone H3	1.063997725	0.630732	0.002203	0.014151	66.23134018
547	WBGene00001905	his-60	Histone H4	0.457249392	1.175641	0.009214	0.04224	57.37632318
548	WBGene00001892	his-60	Histone H4	2.101477324	0.360285	2.27E-10	7.88E-08	137.6033847
549	WBGene00001879	his-60	Histone H4	1.718955411	0.559993	7.32E-05	0.001081	131.4211357
550	WBGene00001875	his-60	Histone H4	1.345132408	0.598634	0.000705	0.006032	176.3101676
551	WBGene00001930	his-60	Histone H4	1.308032218	0.858183	0.002487	0.015481	30.79888568
552	WBGene00001938	his-60	Histone H4	1.215782385	0.655479	0.001599	0.011251	656.1239463
553	WBGene00001912	his-60	Histone H4	0.97838801	0.374193	0.000332	0.003325	117.3569919
554	WBGene00001934	his-60	Histone H4	0.849931804	0.437136	0.001679	0.011608	707.9241595
555	WBGene00001941	his-60	Histone H4	0.734607153	0.283242	0.00043	0.004059	441.334655
556	WBGene00001936	his-62	Probable histone H2B 4	1.445491611	0.457665	5.90E-05	0.000948	636.9837214
557	WBGene00001937	his-63	Histone H3	1.516896363	0.52666	0.00013	0.001648	423.1303977
558	WBGene00001942	his-68	Histone H2A	0.4043148	0.267996	0.008151	0.03836	504.1742987
559	WBGene00001877	his-68	Histone H2A	1.671209005	0.406322	1.58E-06	6.21E-05	119.6834323
560	WBGene00001881	his-68	Histone H2A	1.370385549	0.400729	2.39E-05	0.000476	98.04443843
561	WBGene00001935	his-68	Histone H2A	1.228924648	0.293716	1.27E-06	5.31E-05	447.8563937
562	WBGene00001921	his-68	Histone H2A	1.208132037	0.775525	0.002536	0.015726	23.27933898
563	WBGene00001945	his-71	Histone H3.3 type 1	1.015920741	0.186776	2.88E-09	4.99E-07	220.3554982
564	WBGene00001946	his-72	Histone H3.3 type 2	0.863826962	0.427741	0.001424	0.010267	2538.853859

	ENSEMBLE GeneID	SYMBOL	GENENAME	log2FoldChange	lfcSE	pvalue	padj	baseMean
565	WBGene00001882	his-8	Histone H2B 2	0.753682683	0.415853	0.002214	0.014185	87.50734179
566	WBGene00001948	hlh-1	Myoblast determination protein 1 homolog	0.592543464	0.185075	8.44E-05	0.001192	158.3639145
567	WBGene00001971	hmg-1.1	HMG	0.590068481	0.197604	0.000172	0.002033	6425.606494
568	WBGene00001976	hmg-11	HMG	1.56314097	0.270123	3.45E-10	1.05E-07	512.4131572
569	WBGene00001977	hmg-12	HMG	0.494798536	0.497529	0.008741	0.040554	2137.880076
570	WBGene00022277	homt-1	Alpha N-terminal protein methyltransferase 1	0.314405905	0.115588	0.000964	0.007629	360.8371899
571	WBGene00020268	hpo-19	NADH-cytochrome b5 reductase	-0.303860842	0.051647	7.73E-10	1.83E-07	4653.062115
572	WBGene00022447	hpo-20	Phosphatidylinositol-glycan biosynthesis class W protein	0.477408979	0.188987	0.000815	0.006742	214.6450362
573	WBGene00012550	hpo-21	Probable signal peptidase complex subunit 2	0.725005685	0.238916	0.000123	0.001577	2967.95621
574	WBGene00015463	hpo-9	hypothetical protein	-0.309950153	0.079706	1.78E-05	0.00038	2598.976661
575	WBGene00001999	hrp-1	Heterogeneous nuclear ribonucleoprotein A1	0.716803928	0.163538	7.61E-07	3.62E-05	10951.3256
576	WBGene00002000	hrp-2	human HnRNP A1 homolog	0.445298839	0.116093	1.11E-05	0.000265	8422.172267
577	WBGene00002011	hsp-12.2	Heat shock protein Hsp-12.2	0.470770762	0.148194	0.000121	0.001555	562.9461228
578	WBGene00002007	hsp-3	Heat shock 70 kDa protein C	0.407981414	0.109537	1.73E-05	0.000372	11568.79452
579	WBGene00002040	hum-7	Heavy chain, Unconventional Myosin	0.507599876	0.157567	9.72E-05	0.001324	195.8158399
580	WBGene00002042	hus-1	human HUS1 related	-0.469388317	0.075314	4.57E-11	2.25E-08	720.1290469
581	WBGene00010416	hxk-2	Phosphotransferase	0.32420015	0.114496	0.000666	0.005758	1109.855975
582	WBGene00001564	icl-1	Malate synthase	0.43980481	0.126881	4.51E-05	0.000778	4071.228663
583	WBGene00002055	ifc-1	Intermediate filament protein ifc-1	0.498064927	0.15641	0.000108	0.001433	289.7058582
584	WBGene00002065	iff-2	Eukaryotic translation initiation factor 5A-2	0.724049881	0.16703	9.03E-07	4.12E-05	1602.868119
585	WBGene00020160	igcm-3	ImmunoGlobulin-like Cell adhesion Molecule family	0.338163663	0.097092	7.12E-05	0.001063	1518.487898
586	WBGene00020511	immt-1	MICOS complex subunit MIC60-1	0.375589245	0.118135	0.000179	0.002094	924.4998928
587	WBGene00013095	ing-3	Inhibitor of growth protein	0.337792918	0.118168	0.00056	0.005022	1425.718005
588	WBGene00012148	inos-1	INOsitol-3-phosphate Synthase	0.839229395	0.219607	7.05E-06	0.00019	838.6414089
589	WBGene00016871	inso-1	INSOmniac (Drosophila sleep affecting) homolog	0.447355396	0.157001	0.00036	0.00351	219.7751871
590	WBGene00002123	inx-1	Innexin	0.45745174	0.265674	0.004714	0.025163	237.9531909
591	WBGene00002175	jac-1	Juxtamembrane domain-associated catenin	0.643270409	0.132981	8.99E-08	7.45E-06	334.1999492
592	WBGene00012982	jmjd-2	Lysine-specific demethylase 4	0.351561771	0.177145	0.004619	0.024809	845.7685603
593	WBGene00002179	jph-1	JunctoPHilin	0.469818039	0.157962	0.000233	0.002536	547.3431788
594	WBGene00010483	K01G12.3	hypothetical protein	-0.310462388	0.10331	0.00041	0.003903	335.1387488
595	WBGene00010498	K02B12.5	hypothetical protein	-0.340000087	0.10934	0.000251	0.002686	1380.521224
596	WBGene00010491	K02B7.3	hypothetical protein	0.411308727	0.168301	0.00123	0.009165	477.8997691
597	WBGene00019354	K03B4.2	hypothetical protein	0.450436196	0.171643	0.000705	0.006034	1279.795412
598	WBGene00019355	K03B4.4	hypothetical protein	0.825960658	0.365219	0.000888	0.007177	36.01915002
599	WBGene00019458	K06H7.7	hypothetical protein	-0.308477448	0.089208	9.23E-05	0.001279	680.0241472
600	WBGene00010608	K07A1.1	hypothetical protein	-0.351146371	0.075303	4.45E-07	2.56E-05	1390.955088
601	WBGene00010619	K07A1.15	hypothetical protein	-0.357534361	0.181034	0.004545	0.024529	217.6928766
602	WBGene00019511	K08A2.1	hypothetical protein	0.801878471	0.252664	7.30E-05	0.00108	560.7966643
603	WBGene00019538	K08D12.4	hypothetical protein	0.546927641	0.536109	0.007657	0.03654	32.45634515
604	WBGene00010666	K08E4.2	hypothetical protein	-0.313001641	0.115863	0.001021	0.00793	536.6837202
605	WBGene00010667	K08E4.3	hypothetical protein	-0.349232388	0.093039	2.38E-05	0.000475	583.6023486
606	WBGene00010703	K09A9.6	hypothetical protein	0.322015546	0.140858	0.002845	0.017157	263.8687412
607	WBGene00019564	K09D9.1	hypothetical protein	0.677561002	0.325606	0.001597	0.011249	68.59505449
608	WBGene00010721	K09E4.3	hypothetical protein	0.54156627	0.146087	1.51E-05	0.000334	312.8647986
609	WBGene00044143	K09E9.4	hypothetical protein	0.417083122	0.277109	0.007395	0.03558	63.23560041
610	WBGene00045265	K10C2.8	hypothetical protein	-0.33478588	0.214063	0.010288	0.045854	163.8804653
611	WBGene00010738	K10D3.4	hypothetical protein	1.001458037	0.143933	1.95E-13	5.01E-10	748.4049839
612	WBGene00019651	K11D12.12	hypothetical protein	-0.386067332	0.11198	6.41E-05	0.000998	368.7237742
613	WBGene00010770	K11D2.4	hypothetical protein	0.728635589	0.275865	0.000376	0.003644	278.0910121
614	WBGene00019673	K12C11.1	hypothetical protein	0.501141312	0.200221	0.000809	0.006712	808.48774
615	WBGene00019677	K12H4.2	hypothetical protein	-0.341885284	0.079959	2.55E-06	8.93E-05	682.7708464
616	WBGene00002181	kal-1	human KALmann syndrome homolog	0.6825156	0.159633	1.20E-06	5.11E-05	201.6323074
617	WBGene00020064	kbp-1	KNL (kinetochore null) Binding Protein	-0.39023818	0.061015	1.83E-11	1.23E-08	2155.750724
618	WBGene00002184	kel-1	KELch-repeat containing protein	0.48264592	0.256817	0.003312	0.019191	62.72303364
619	WBGene00020952	kel-8	Kelch-like protein 8	0.614725167	0.187374	6.22E-05	0.000975	251.7955346
620	WBGene00004130	ketn-1	KETtiN (Drosophila actin-binding) homolog	0.507661815	0.123275	3.23E-06	0.000107	2114.915983
621	WBGene00002214	klc-1	Kinesin Light Chain	-0.312327644	0.055454	3.19E-09	5.39E-07	5147.875693
622	WBGene00002222	klp-11	Kinesin-like protein	-0.427326494	0.304903	0.008185	0.038452	196.8294273
623	WBGene00002226	klp-16	Kinesin-like protein	0.343699035	0.154132	0.002696	0.016433	2318.977132
624	WBGene00002219	klp-7	Kinesin-like protein	0.469222776	0.442873	0.009076	0.041757	1301.829984
625	WBGene00020392	knl-3	Kinetochore NuLI	0.412677588	0.174124	0.001514	0.010779	1040.12149
626	WBGene00018725	kreg-1	Protein kreg-1	0.668460874	0.442627	0.004184	0.023075	28.77794178
627	WBGene00002243	lad-2	L1 CAM ADhesion molecule homolog	0.438397252	0.39575	0.009971	0.044723	64.04492899
628	WBGene00002244	laf-1	ATP-dependent RNA helicase laf-1	0.328135918	0.076204	2.66E-06	9.27E-05	4206.37906
629	WBGene00002261	ldb-1	LIM Domain Binding protein	0.44293684	0.13978	0.000141	0.001741	727.9256707
630	WBGene00002262	ldh-1	L-lactate dehydrogenase	0.498400032	0.150296	7.34E-05	0.001082	1225.124117
631	WBGene00002264	lec-1	32 kDa beta-galactoside-binding lectin	1.053465896	0.317118	3.89E-05	0.000692	3136.342337
632	WBGene00002275	lem-2	LEM protein 2	0.680654323	0.202824	4.57E-05	0.000785	1368.76973
633	WBGene00021945	lem-4	Ankyrin repeat and LEM domain-containing protein 2 homolog	0.51053362	0.166674	0.000157	0.001891	515.3425141
634	WBGene00002280	let-2	Collagen alpha-2(IV) chain	0.66279107	0.186415	2.24E-05	0.000454	4974.115108
635	WBGene00002915	let-805	hypothetical protein	0.818328433	0.203242	3.04E-06	0.000102	712.4854049
636	WBGene00002977	lev-10	hypothetical protein	0.467643019	0.148528	0.000135	0.001696	255.4608513
637	WBGene00002978	lev-11	Tropomyosin	0.695674207	0.174249	5.79E-06	0.000164	7508.128453
638	WBGene00022500	lfi-1	Lin-5 (Five) Interacting protein	0.391162332	0.097119	6.61E-06	0.000181	1255.256683
639	WBGene00009799	lgc-47	Ligand-Gated ion Channel	0.480727484	0.381212	0.007898	0.03744	53.3448871
640	WBGene00002990	lin-1	hypothetical protein	0.648274911	0.208869	0.00011	0.00145	119.4634263
641	WBGene00003006	lin-17	hypothetical protein	0.665394123	0.167566	4.34E-06	0.000131	199.7566416
642	WBGene00002991	lin-2	Protein lin-2	0.367464891	0.130218	0.00054	0.004888	242.560528
643	WBGene00003025	lin-40	hypothetical protein	1.01466607	0.208575	5.93E-08	5.41E-06	768.1533133
644	WBGene00018572	lin-42	Period protein homolog lin-42	0.7474291	0.226614	5.05E-05	0.00084	140.6997943
645	WBGene00003038	lin-56	Protein lin-56	-0.418643309	0.074746	2.47E-09	4.46E-07	808.3820576
646	WBGene00001562	lin-66	hypothetical protein	0.310860326	0.0815	2.34E-05	0.00047	3155.954719
647	WBGene00002997	lin-8	Protein lin-8	0.609017462	0.161572	1.06E-05	0.000259	282.0241746
648	WBGene00022642	lipl-5	Lipase	0.357195708	0.142105	0.001333	0.009764	2967.827288
649	WBGene00003064	lpd-8	LiPid Depleted	-0.319336261	0.063153	7.09E-08	6.32E-06	2349.519821
650	WBGene00015779	lrch-1	Leucine-rich Repeats (LRR) and Calponin Homology (CH) domain homolog	0.332179016	0.178433	0.006553	0.032422	212.0645896
651	WBGene00022129	lron-11	eLRR (extracellular Leucine-Rich Repeat) ONly	0.798849524	0.164107	6.50E-08	5.83E-06	249.5755708
652	WBGene00022610	ltah-1.2	LeukoTriene A4 Hydrolase homolog	0.385876168	0.117848	0.000118	0.001529	731.4454779
653	WBGene00003093	lys-4	LYSozyme	-0.433754268	0.100709	1.68E-06	6.54E-05	2880.365065
654	WBGene00044690	M02B7.7	hypothetical protein	0.761352483	0.498542	0.003491	0.019986	48.28844813
655	WBGene00010913	M110.3	hypothetical protein	-0.388839038	0.095516	5.46E-06	0.000156	1053.206074
656	WBGene00044253	M117.6	hypothetical protein	-0.438435234	0.219066	0.003035	0.018007	154.6640937
657	WBGene00010922	M142.5	hypothetical protein	0.308298554	0.129501	0.002509	0.015587	765.752167
658	WBGene00010889	M18.3	hypothetical protein	-0.305304787	0.068065	1.37E-06	5.68E-05	1099.095516
659	WBGene00003111	mab-20	Semaphorin-2A	0.395443571	0.118853	9.45E-05	0.001302	763.0281372
660	WBGene00003102	mab-5	Homeobox protein mab-5	0.686321291	0.286407	0.000752	0.006328	46.40389576
661	WBGene00003119	mac-1	Protein mac-1	0.791460194	0.18436	1.02E-06	4.53E-05	525.136848
662	WBGene00016539	madd-2	hypothetical protein	0.426998303	0.160868	0.000682	0.005865	263.6752373
663	WBGene00008118	madf-8	MADF domain transcription factor	-0.32687866	0.087049	2.65E-05	0.000517	835.0119713
664	WBGene00021888	manf-1	Mesencephalic astrocyte-derived neurotrophic factor homolog	0.310188339	0.131816	0.002629	0.016175	2884.657504
665	WBGene00003129	map-1	Methionine aminopeptidase	0.470482714	0.216416	0.001929	0.012828	521.0009561
666	WBGene00009306	maph-1.1	Microtubule-associated protein homolog maph-1.1	0.770301052	0.163817	1.55E-07	1.20E-05	313.6154324
667	WBGene00009113	maph-1.2	Microtubule-Associated Protein Homolog	0.384520699	0.216891	0.005791	0.029515	1921.343369
668	WBGene00007966	maph-1.3	Microtubule-Associated Protein Homolog	0.591172343	0.196808	0.000162	0.001936	1085.756835
669	WBGene00013096	mcd-1	Modifier of cell death	0.567337655	0.213109	0.000474	0.00442	1069.87068
670	WBGene00003156	mcm-4	DNA replication licensing factor mcm-4	0.396521982	0.177367	0.002189	0.0141	3514.601162
671	WBGene00015273	mct-2	MonoCarboxylate Transporter family	0.863464608	0.383683	0.00085	0.006953	56.29575985
672	WBGene00003162	mdh-2	Probable malate dehydrogenase, mitochondrial	0.327320396	0.138773	0.00235	0.014835	8747.875937
673	WBGene00007026	mdt-31	Mediator of RNA polymerase II transcription subunit 31	-0.401642483	0.097389	4.00E-06	0.000124	500.5895181
674	WBGene00003164	mdt-6	Mediator of RNA polymerase II transcription subunit 6	-0.305877337	0.075211	8.62E-06	0.000222	2492.920469
675	WBGene00003175	mec-12	Detyrosinated tubulin alpha-3 chain	0.36626935	0.216616	0.007275	0.035165	259.8254778
676	WBGene00003172	mec-8	hypothetical protein	0.350895987	0.098335	4.83E-05	0.000809	902.7942472
677	WBGene00019757	memb-2	Golgi SNAP receptor complex member 2	-0.499895755	0.077604	1.10E-11	8.89E-09	1390.314671

	ENSEMBLE GeneID	SYMBOL	GENENAME	log2FoldChange	lfcSE	pvalue	padj	baseMean
678	WBGene00003229	mex-3	Muscle EXcess	0.409667114	0.155064	0.000756	0.006357	7764.492059
679	WBGene00012933	mib-1	MIB (MIndBomb) ubiquitin ligase homolog	0.465210204	0.13526	4.89E-05	0.000817	295.8547402
680	WBGene00011890	mics-1	Mitochondrial scaffolding protein 1	-0.317657769	0.044959	2.97E-13	6.36E-10	3007.95049
681	WBGene00003238	mig-1	hypothetical protein	0.47695818	0.181308	0.000616	0.005416	191.0711127
682	WBGene00003245	mig-13	Abnormal cell migration protein 13	0.661160691	0.158709	1.87E-06	7.11E-05	171.8658706
683	WBGene00003242	mig-6	Papilin	0.608807877	0.130594	2.29E-07	1.62E-05	2069.525124
684	WBGene00003369	mlc-1	Myosin regulatory light chain 1	0.406685659	0.088861	5.53E-07	2.93E-05	5574.28502
685	WBGene00003371	mlc-3	Myosin, essential light chain	0.824024247	0.193763	1.19E-06	5.09E-05	4823.181965
686	WBGene00003375	mlp-1	MLP/CRP family (Muscle LIM Protein/Cysteine-rich Protein)	0.352183362	0.146353	0.001787	0.012135	484.7223005
687	WBGene00015646	mlt-10	hypothetical protein	0.533646855	0.206137	0.0006	0.005286	217.7462936
688	WBGene00012186	mlt-11	hypothetical protein	0.620688373	0.522284	0.005841	0.029697	660.75569
689	WBGene00007139	mnp-1	Matrix non-peptidase homolog 1	0.340636006	0.108686	0.000239	0.002589	586.1465275
690	WBGene00021348	moag-4	MOdifier of protein AGgregation	0.523451434	0.212491	0.00081	0.006716	2065.761194
691	WBGene00009551	mob-1	Mps One Binder (Mats/MOB1) homolog	-0.42812246	0.065743	8.07E-12	8.19E-09	1016.204461
692	WBGene00008601	mob-2	Mps One Binder (Mats/MOB1) homolog	0.43789466	0.129899	7.07E-05	0.001058	544.8927997
693	WBGene00020858	mop-25.3	MO25-like protein 3	-0.363343324	0.079445	6.55E-07	3.30E-05	785.856668
694	WBGene00019282	mps-2	MiRP K channel accessory Subunit	0.31935535	0.19875	0.010736	0.047392	467.3154981
695	WBGene00010458	mrpl-10	Mitochondrial Ribosomal Protein, Large	-0.336901069	0.084996	1.06E-05	0.000259	1172.224674
696	WBGene00012361	mrpl-12	Mitochondrial Ribosomal Protein, Large	0.39636145	0.199282	0.003697	0.020929	778.6261534
697	WBGene00017044	mrpl-18	39S ribosomal protein L18, mitochondrial	-0.335548633	0.073371	7.20E-07	3.48E-05	1130.098712
698	WBGene00020796	mrpl-28	Mitochondrial Ribosomal Protein, Large	-0.329615384	0.077962	3.76E-06	0.000121	1143.35806
699	WBGene00010783	mrpl-36	Ribosomal protein	-0.306545672	0.152262	0.005701	0.029182	694.4778028
700	WBGene00015185	mrpl-41	39S ribosomal protein L41, mitochondrial	-0.303691217	0.086721	8.02E-05	0.001158	919.0462423
701	WBGene00011247	mrpl-49	Probable 39S ribosomal protein L49, mitochondrial	-0.303531705	0.083873	5.09E-05	0.000845	627.2468188
702	WBGene00011883	mrpl-50	Mitochondrial Ribosomal Protein, Large	-0.348456078	0.069855	9.42E-08	7.68E-06	1092.490199
703	WBGene00015487	mrps-17	28S ribosomal protein S17, mitochondrial	-0.389033089	0.078982	8.97E-08	7.45E-06	1306.632131
704	WBGene00017924	mrps-21	Mitochondrial Ribosomal Protein, Small	-0.320396674	0.095815	0.000124	0.001586	694.6987177
705	WBGene00014224	mrps-23	Probable 28S ribosomal protein S23, mitochondrial	-0.315698359	0.114185	0.000828	0.006821	1036.091564
706	WBGene00012830	mrps-28	Mitochondrial Ribosomal Protein, Small	0.632567842	0.292155	0.001362	0.009946	228.7248305
707	WBGene00045237	mrt-1	MoRTal germline	-0.311345644	0.078606	1.07E-05	0.00026	1200.14323
708	WBGene00010557	mspn-1	Mitochondrial sorting homolog	-0.310235144	0.073425	4.18E-06	0.000128	1867.748422
709	WBGene00003471	mtct-1	Mec-3 (Three) Dependent expression	0.419290262	0.509783	0.011186	0.048737	28.59291439
710	WBGene00007114	mttu-1	Probable mitochondrial tRNA-specific 2-thiouridylase 1	-0.353920278	0.117332	0.000313	0.003173	262.618374
711	WBGene00022516	mtx-2	Metaxin-2 homolog	-0.329419077	0.071156	5.90E-07	3.05E-05	1705.190012
712	WBGene00003495	mup-2	Troponin T	1.124220966	0.207376	3.02E-09	5.17E-07	1791.9566
713	WBGene00003499	mut-2	MUTator	-0.32132807	0.075932	3.67E-06	0.000119	2154.548424
714	WBGene00016404	mutd-1	Biogenesis of lysosome-related organelles complex 1 subunit 5	-0.318576654	0.079976	1.12E-05	0.000265	1214.441057
715	WBGene00002348	myo-1	Myosin-1	0.309710833	0.115965	0.00117	0.008806	1130.552943
716	WBGene00003514	myo-2	Myosin-2	0.572414393	0.211723	0.000406	0.003873	619.7084168
717	WBGene00003515	myo-3	Myosin-3	0.332304713	0.142387	0.002408	0.015109	1330.974765
718	WBGene00003530	nas-11	Zinc metalloproteinase nas-11	-0.310875474	0.089599	8.57E-05	0.001202	653.330381
719	WBGene00022453	ncap-1	NeCAP (NECAP) endocytosis associated protein homolog	0.553153227	0.234738	0.001022	0.00793	288.642461
720	WBGene00010959	ND1	NADH dehydrogenase subunit 1	-0.390223041	0.115503	0.000114	0.001489	19482.6872
721	WBGene00010961	ND2	NADH dehydrogenase subunit 2	-0.5554557	0.19943	0.000325	0.003276	10764.73205
722	WBGene00010966	ND3	NADH dehydrogenase subunit 3	-0.670390104	0.22552	0.000155	0.00188	10809.31926
723	WBGene00010963	ND4	NADH dehydrogenase subunit 4	-0.412938897	0.15141	0.000547	0.004935	9822.611924
724	WBGene00010967	ND5	NADH dehydrogenase subunit 5	-0.445125282	0.191195	0.001466	0.010527	20681.97514
725	WBGene00009119	ndk-1	Nucleoside diphosphate kinase	0.614163409	0.323328	0.00301	0.017904	21778.88743
726	WBGene00010070	nep-17	NEPrilysin metallopeptidase family	0.41915255	0.118148	4.00E-05	0.000708	2040.111031
727	WBGene00020230	nep-2	Neprilysin-2	0.356974211	0.217948	0.008186	0.038452	178.6420577
728	WBGene00003588	nex-1	Annexin	0.561220173	0.178627	0.000113	0.001475	1730.403217
729	WBGene00003589	nex-2	Annexin	0.376062347	0.141471	0.000825	0.006802	463.0095643
730	WBGene00007877	nfki-1	Nuclear Factor of Kappa light polypeptide gene enhancer in b(B)-cells Inhibitor, delta and zeta related	0.317514846	0.117563	0.001005	0.007857	252.7781379
731	WBGene00003595	ngn-1	NeuroGeNin	0.591146435	0.216788	0.000357	0.003496	70.96741511
732	WBGene00003597	nhl-1	RING finger protein nhl-1	0.329042014	0.158932	0.004419	0.02402	220.9827651
733	WBGene00003599	nhl-3	NHL (ring finger b-box coiled coil) domain containing	0.399796954	0.132203	0.00025	0.002677	214.4171446
734	WBGene00003704	nhr-114	Nuclear Hormone Receptor family	0.397977206	0.172195	0.001699	0.011714	2255.665372
735	WBGene00003709	nhr-119	Nuclear Hormone Receptor family	0.740893917	0.256238	0.000184	0.002133	98.98713472
736	WBGene00003618	nhr-19	Nuclear hormone receptor family member nhr-19	-0.304161945	0.172364	0.00939	0.042788	126.6869416
737	WBGene00003623	nhr-25	Nuclear hormone receptor family member nhr-25	0.444516087	0.146061	0.000205	0.002303	287.7910244
738	WBGene00003651	nhr-61	Nuclear hormone receptor family member nhr-61	0.553634785	0.192117	0.000237	0.002573	152.37296
739	WBGene00015497	nhr-76	Nuclear Hormone Receptor family	0.302398778	0.160975	0.007666	0.036567	156.1853777
740	WBGene00003749	nlp-11	Neuropeptide-like peptide 11	-0.432273295	0.160988	0.000597	0.005272	175.8390425
741	WBGene00003750	nlp-12	Neuropeptide-Like Protein	1.058044817	0.436069	0.000505	0.004647	33.63462302
742	WBGene00003762	nlp-24	Neuropeptide-Like Protein	0.663431677	0.243793	0.000331	0.003324	583.056377
743	WBGene00003764	nlp-26	Neuropeptide-Like Protein	0.695695775	0.325601	0.001304	0.009628	107.0674027
744	WBGene00011227	nlp-67	Neuropeptide-Like Protein	0.479351832	0.480493	0.009388	0.042788	24.44910517
745	WBGene00003746	nlp-8	Neuropeptide-Like Protein	-0.371012768	0.15604	0.001781	0.012135	135.2516969
746	WBGene00011428	nlp-80	Neuropeptide-Like Protein	-0.365503948	0.150303	0.001614	0.011315	205.5228104
747	WBGene00022063	nlp-81	Neuropeptide-Like Protein	0.766901191	0.3781	0.001556	0.01101	26.50684407
748	WBGene00009176	nmat-2	Nicotinamide/nicotinic acid mononucleotide adenylyltransferase 2	-0.302789978	0.118027	0.001555	0.011008	474.2725142
749	WBGene00017437	nmgp-1	Neuronal Membrane GlycoProtein	0.404994668	0.250377	0.006756	0.033203	75.29819024
750	WBGene00017778	nono-1	NONO (conserved nuclear protein, aka PSF) homolog	0.748209858	0.164674	3.29E-07	2.08E-05	1990.389883
751	WBGene00003784	nos-2	NanOS related	-0.43935931	0.085544	3.61E-08	4.03E-06	4664.979691
752	WBGene00013347	nova-1	NOVA kh (KH) homology domain homolog	0.332908423	0.122061	0.000847	0.006946	4788.844551
753	WBGene00003788	npp-2	Nuclear Pore complex Protein	-0.341390655	0.052101	8.94E-12	8.19E-09	4121.106014
754	WBGene00007493	npp-23	Nuclear Pore complex Protein	-0.300864034	0.068085	1.81E-06	6.96E-05	2105.876795
755	WBGene00012555	npp-25	Transmembrane protein 33 homolog	0.382354851	0.12221	0.000199	0.002254	1103.369047
756	WBGene00007651	nra-3	Nicotinic Receptor Associated	0.351861791	0.170486	0.003944	0.022017	733.1663609
757	WBGene00021415	nsy-4	Neuronal SYmmetry	0.481883261	0.384186	0.007671	0.036568	178.4086364
758	WBGene00011201	nth-1	Endonuclease III homolog	-0.36061458	0.105637	8.06E-05	0.001161	537.6995502
759	WBGene00003825	ntl-2	NOT-Like (yeast CCR4/NOT complex component)	0.39027511	0.139657	0.00053	0.004819	1858.890171
760	WBGene00003826	ntl-3	NOT-Like (yeast CCR4/NOT complex component)	0.371877033	0.123075	0.000286	0.002975	2537.215337
761	WBGene00008225	nuaf-1	Probable complex I intermediate-associated protein 30, mitochondrial	-0.426539137	0.093601	5.63E-07	2.96E-05	820.0318172
762	WBGene00021562	nuo-5	NADH Ubiquinone Oxidoreductase	0.931749555	0.164399	8.64E-10	1.91E-07	1597.475297
763	WBGene00009180	nurf-1	Nucleosome-remodeling factor subunit NURF301-like	0.458118814	0.120477	1.36E-05	0.000308	4300.840708
764	WBGene00018636	oef-1	Oocyte Excluded Factor	-0.30722045	0.059385	4.32E-08	4.53E-06	2647.242405
765	WBGene00003893	ost-1	SPARC	0.460955034	0.09562	1.41E-07	1.10E-05	5102.148927
766	WBGene00045483	oxy-5	hypothetical protein	-0.453460627	0.06901	7.26E-12	8.19E-09	3338.555353
767	WBGene00003902	pab-1	Polyadenylate-binding protein	0.403279048	0.158084	0.001249	0.009292	16966.43661
768	WBGene00003903	pab-2	Polyadenylate-binding protein	0.344520045	0.130529	0.000983	0.007735	1289.493453
769	WBGene00003917	par-2	hypothetical protein	0.326163047	0.169873	0.006019	0.030421	1496.115872
770	WBGene00003936	pat-12	Protein pat-12	0.611542769	0.113434	6.21E-09	9.15E-07	736.3749
771	WBGene00003931	pat-4	Integrin-linked protein kinase homolog pat-4	0.333291408	0.115482	0.000529	0.004812	316.602585
772	WBGene00003933	pat-9	Paralysed Arrest at Two-fold	0.520428631	0.177378	0.00023	0.00251	223.3265828
773	WBGene00003947	pbs-1	Proteasome subunit beta type	0.616289295	0.238922	0.000524	0.004778	2175.10778
774	WBGene00003948	pbs-2	Proteasome subunit beta type	0.528384252	0.244559	0.001726	0.011866	2675.731837
775	WBGene00003951	pbs-5	Proteasome subunit pbs-5	0.600722619	0.229973	0.000491	0.004545	4163.00484
776	WBGene00008641	pch-2	Putative pachytene checkpoint protein 2	-0.369836912	0.067594	6.19E-09	9.15E-07	2464.258912
777	WBGene00021043	pck-1	PhosphoenolpyruvateCarboxyKinase	0.748141144	0.149598	3.45E-08	3.91E-06	1332.600793
778	WBGene00003955	pcn-1	Proliferating cell nuclear antigen	0.60735647	0.192108	9.53E-05	0.001309	7912.411635
779	WBGene00022389	pde-6	Phosphodiesterase	0.896453717	0.193467	1.98E-07	1.42E-05	120.8068303
780	WBGene00003963	pdi-2	Protein disulfide-isomerase 2	0.697408245	0.174469	3.76E-06	0.000121	9312.403973
781	WBGene00003975	pen-2	Gamma-secretase subunit pen-2	-0.301130935	0.081999	4.23E-05	0.000741	686.2686361
782	WBGene00016636	perm-2	PERMeable eggshell	1.156685876	0.466796	0.000434	0.004094	6584.826702
783	WBGene00016638	perm-4	PERMeable eggshell	0.567337285	0.355428	0.004213	0.023208	13116.09324
784	WBGene00003978	pes-4	Patterned Expression Site	0.730671119	0.223592	5.73E-05	0.000926	226.5064982
785	WBGene00003980	pes-7	Patterned Expression Site	0.318763352	0.140895	0.003075	0.018134	190.9004805
786	WBGene00011936	pgrn-1	ProGRaNulin homolog	0.70214527	0.189883	1.26E-05	0.00029	412.581061
787	WBGene00021677	pgs-1	CDP-diacylglycerol--glycerol-3-phosphate 3-phosphatidyltransferase	-0.364817651	0.085796	2.86E-06	9.71E-05	1026.813462
788	WBGene00004013	pha-4	Defective pharyngeal development protein 4	0.368272564	0.178908	0.00374	0.021098	406.035978
789	WBGene00020237	phat-4	PHAryngeal gland Toxin-related	0.807196008	0.370038	0.001077	0.0083	72.61818459
790	WBGene00022181	pho-9	intestinal acid PHOsphatase	-0.390324162	0.16642	0.00174	0.011927	179.9443509

	ENSEMBLE GeneID	SYMBOL	GENENAME	log2FoldChange	lfcSE	pvalue	padj	baseMean
791	WBGene00017549	pid-1	21U-RNA biogenesis factor pid-1	-0.407842478	0.077727	1.85E-08	2.35E-06	888.8339782
792	WBGene00004028	pif-1	ATP-dependent DNA helicase	0.324768726	0.163322	0.005458	0.028209	754.511683
793	WBGene00022448	pinn-1	Peptidyl-prolyl cis-trans isomerase	0.609788958	0.15748	7.14E-06	0.000191	1101.011441
794	WBGene00011967	pir-1	RNA/RNP complex-1-interacting phosphatase homolog	-0.326785477	0.057125	1.78E-09	3.56E-07	1713.027681
795	WBGene00012897	pisy-1	CDP-diacylglycerol--inositol 3-phosphatidyltransferase	0.806846118	0.236464	3.23E-05	0.000603	586.1128561
796	WBGene00008976	plp-2	Pur alpha Like Protein	0.763345572	0.695417	0.005447	0.028163	26.8769029
797	WBGene00023404	plr-1	Probable E3 ubiquitin-protein ligase plr-1	0.521058466	0.129768	4.77E-06	0.000141	205.4618831
798	WBGene00004064	pms-2	PMS (Post Meiotic Segregation) family	-0.31222215	0.088254	6.55E-05	0.001008	1388.284025
799	WBGene00004075	pod-1	hypothetical protein	0.676934959	0.18984	2.73E-05	0.00053	4196.611403
800	WBGene00004076	pod-2	hypothetical protein	0.660141809	0.138413	1.32E-07	1.03E-05	2906.896356
801	WBGene00017696	polk-1	DNA polymerase kappa	-0.350690825	0.066833	2.31E-08	2.80E-06	3151.967603
802	WBGene00004128	pqn-41	Polyglutamine-repeat protein pqn-41	0.825936443	0.27001	0.000107	0.001424	368.4977198
803	WBGene00004129	pqn-42	Prion-like-(Q/N-rich)-domain-bearing protein	1.131866993	0.415123	0.000248	0.002658	28.08245206
804	WBGene00004153	pqn-71	Prion-like-(Q/N-rich)-domain-bearing protein	0.755256338	0.882452	0.006005	0.030361	39.4034007
805	WBGene00004154	pqn-72	Prion-like-(Q/N-rich)-domain-bearing protein	0.768111316	0.307748	0.000537	0.004868	52.6567456
806	WBGene00004156	pqn-74	Prion-like-(Q/N-rich)-domain-bearing protein	0.762582836	0.444151	0.00265	0.016266	135.3884347
807	WBGene00004167	pqn-87	Prion-like-(Q/N-rich)-domain-bearing protein	0.364324038	0.107197	8.48E-05	0.001193	5227.521133
808	WBGene00004202	pry-1	Axin-like protein pry-1	0.550213157	0.204761	0.000445	0.004183	166.3370644
809	WBGene00016623	psmd-9	Probable 26S proteasome non-ATPase regulatory subunit 9	-0.413312963	0.067811	1.31E-10	4.82E-08	1195.229545
810	WBGene00004205	psr-1	Bifunctional arginine demethylase and lysyl-hydroxylase psr-1	-0.358245204	0.085204	3.56E-06	0.000116	1649.14662
811	WBGene00004210	ptc-3	Protein patched homolog 3	0.501808091	0.227325	0.001649	0.01148	229.5625001
812	WBGene00004212	ptl-1	Microtubule-associated protein	0.46604353	0.320468	0.006688	0.032923	97.30525021
813	WBGene00004235	ptr-21	PaTched Related family	0.304982951	0.089782	0.000114	0.001485	678.8843274
814	WBGene00017499	pud-1.2	Protein Up-regulated in Daf-2(gf)	0.628866608	0.556153	0.006088	0.030689	128.5590818
815	WBGene00020696	pygl-1	Alpha-1,4 glucan phosphorylase	0.466567275	0.161213	0.000299	0.003069	11486.29475
816	WBGene00019825	R02D3.8	hypothetical protein	-0.361525346	0.071211	5.44E-08	5.22E-06	920.7479404
817	WBGene00010976	R02D5.1	hypothetical protein	0.305261705	0.142881	0.004437	0.02409	216.2062547
818	WBGene00019831	R02F2.1	hypothetical protein	0.417543181	0.167432	0.001088	0.008356	3260.149941
819	WBGene00019838	R02F2.9	hypothetical protein	-0.367729138	0.089014	4.74E-06	0.00014	1051.235037
820	WBGene00010987	R03C1.1	hypothetical protein	1.219597272	0.633854	0.001491	0.010656	28.05990507
821	WBGene00010989	R03D7.2	hypothetical protein	0.377982398	0.206317	0.005349	0.02776	305.35087
822	WBGene00019855	R03H10.2	hypothetical protein	0.583386504	0.267042	0.001451	0.010428	135.2953955
823	WBGene00019872	R04E5.9	hypothetical protein	0.71819316	0.184416	5.61E-06	0.000159	96.0370508
824	WBGene00011017	R04F11.5	hypothetical protein	-0.333519593	0.074725	1.29E-06	5.38E-05	1044.479712
825	WBGene00011040	R05H5.5	hypothetical protein	-0.384978843	0.071778	1.05E-08	1.42E-06	970.4201845
826	WBGene00011056	R06B9.5	hypothetical protein	2.168677971	0.396415	1.86E-09	3.66E-07	37.62886605
827	WBGene00011059	R06C1.4	hypothetical protein	0.756334354	0.178432	1.33E-06	5.54E-05	1560.526053
828	WBGene00011103	R07E3.2	hypothetical protein	0.833354038	0.452964	0.00211	0.013709	34.21532728
829	WBGene00019965	R08F11.1	Non-lysosomal glucosylceramidase	0.336802231	0.157194	0.00359	0.020448	302.4781703
830	WBGene00011289	R102.2	hypothetical protein	0.632039703	0.275927	0.001031	0.007985	180.1898443
831	WBGene00020090	R119.5	hypothetical protein	0.495454634	0.15449	0.000103	0.001382	226.5461832
832	WBGene00011253	R11H6.5	hypothetical protein	-0.40670309	0.080734	5.53E-08	5.22E-06	1835.343146
833	WBGene00020027	R12C12.7	hypothetical protein	-0.36687297	0.058187	4.14E-11	2.24E-08	1719.447283
834	WBGene00020039	R12E2.14	hypothetical protein	2.19144136	0.564855	4.31E-06	0.000131	21.09872237
835	WBGene00020040	R12E2.15	hypothetical protein	2.116138119	0.476514	4.23E-07	2.47E-05	33.55723694
836	WBGene00020033	R12E2.7	hypothetical protein	2.362399563	0.630002	7.64E-06	0.000202	19.54078065
837	WBGene00020043	R13A1.5	hypothetical protein	-0.487180118	0.504994	0.009753	0.043944	29.7823715
838	WBGene00014826	R13H4.2	hypothetical protein	0.374283957	0.10289	3.35E-05	0.000618	1790.959027
839	WBGene00020104	R148.5	hypothetical protein	0.577546987	0.134937	1.41E-06	5.80E-05	365.1477892
840	WBGene00004277	rab-18	Ras-related protein Rab-18	0.420797343	0.10425	5.91E-06	0.000166	4099.117378
841	WBGene00004271	rab-7	RAB family	0.310503908	0.151746	0.005222	0.027295	2183.935575
842	WBGene00004298	rad-54	hypothetical protein	-0.328706982	0.078892	3.83E-06	0.000121	1315.919193
843	WBGene00044305	rad-8	Reticulon-4-interacting protein 1, mitochondrial	-0.316062552	0.061802	5.58E-08	5.22E-06	1615.299068
844	WBGene00004300	ram-2	hypothetical protein	1.369637269	0.720188	0.001401	0.010153	180.0870317
845	WBGene00004680	rars-2	arginyl(R) Amino-acyl tRNA Synthetase	-0.351974365	0.069362	5.58E-08	5.22E-06	1468.692213
846	WBGene00004310	ras-1	R-RAS related	0.312589108	0.165581	0.00704	0.034247	171.2976872
847	WBGene00011156	rbm-3.2	RNA Binding Motif protein homolog	1.122866732	0.602213	0.001661	0.011528	4661.210267
848	WBGene00004326	rde-4	hypothetical protein	-0.32248154	0.054217	4.57E-10	1.30E-07	3882.238935
849	WBGene00007270	rei-1	Guanine nucleotide exchange factor rei-1	-0.308266085	0.049485	8.86E-11	3.66E-08	2844.662131
850	WBGene00004339	rfc-3	RFC (DNA replication factor) family	-0.339205998	0.053659	4.15E-11	2.24E-08	4990.183104
851	WBGene00022286	rga-4	Rho GTPase Activating protein	0.654421957	0.167741	6.04E-06	0.000169	1339.698574
852	WBGene00007064	rga-9	Rho GTPase Activating protein	0.61541611	0.231882	0.000428	0.004048	193.5319651
853	WBGene00004349	rgs-6	Regulator of G-protein signaling rgs-6	0.634429776	0.420884	0.004308	0.02358	56.64985749
854	WBGene00009245	rict-1	hypothetical protein	0.352634524	0.092407	1.88E-05	0.000396	1330.293187
855	WBGene00008262	ril-1	RNAi-Induced Longevity	0.50881635	0.205308	0.000853	0.006965	4658.408382
856	WBGene00006513	rimb-1	RIM Binding protein	1.019597417	0.465902	0.000942	0.007488	26.20982507
857	WBGene00004409	rla-1	60S acidic ribosomal protein P1	1.02660027	0.44726	0.000726	0.006143	5539.570201
858	WBGene00010923	rle-1	Regulation of longevity by E3 ubiquitin-protein ligase	0.316099119	0.089819	6.99E-05	0.001052	1859.283562
859	WBGene00004387	rnp-4	RNA-binding protein 8A	0.362085964	0.195732	0.005709	0.029214	3875.146861
860	WBGene00004388	rnp-5	RNP (RRM RNA binding domain) containing	0.621240457	0.263718	0.000904	0.007268	565.9203933
861	WBGene00018819	rog-1	Ras activating factor in development Of Germline	0.312511426	0.174366	0.008335	0.039007	1790.460378
862	WBGene00019767	rpa-2	Replication Protein A homolog	0.345458087	0.171521	0.004511	0.024387	5078.367974
863	WBGene00016375	rpap-3	Rna (RNA) Polymerase II Associated Protein homolog	-0.366055679	0.091833	8.74E-06	0.000225	755.3230597
864	WBGene00021845	rpb-7	RNA Polymerase II (B) subunit	0.842437022	0.20148	1.54E-06	6.11E-05	749.4263964
865	WBGene00004423	rpl-11.2	60S ribosomal protein L11-2	1.096601648	0.346719	6.49E-05	0.001	1529.336133
866	WBGene00004424	rpl-12	60S ribosomal protein L12	0.36665943	0.210828	0.00666	0.032834	26381.71101
867	WBGene00004425	rpl-13	60S ribosomal protein L13	0.815882076	0.494971	0.002786	0.016855	15205.18726
868	WBGene00004430	rpl-18	60S ribosomal protein L18	0.875926254	0.727253	0.004458	0.024169	5535.909084
869	WBGene00004431	rpl-19	60S ribosomal protein L19	0.517314248	0.382562	0.006353	0.031724	18818.45731
870	WBGene00004432	rpl-20	60S ribosomal protein L18a	0.395424077	0.18595	0.003647	0.020692	9674.034899
871	WBGene00004436	rpl-24.1	60S ribosomal protein L24	0.349578827	0.16652	0.003705	0.020953	22954.08863
872	WBGene00004440	rpl-26	60S ribosomal protein L26	1.188202017	0.508284	0.00071	0.006055	6738.213031
873	WBGene00004442	rpl-28	60S ribosomal protein L28	0.815362796	0.441746	0.002037	0.013353	5925.68183
874	WBGene00004419	rpl-7A	60S ribosomal protein L7a	0.414067374	0.398656	0.011169	0.048699	11836.02586
875	WBGene00012999	rpoa-1	DNA-directed RNA polymerase subunit	0.547586065	0.124536	8.44E-07	3.91E-05	881.49439
876	WBGene00004479	rps-10	Ribosomal Protein, Small subunit	0.367326615	0.199863	0.005466	0.028237	20944.78886
877	WBGene00004481	rps-12	40S ribosomal protein S12	0.988589689	0.569581	0.002158	0.013955	5551.931565
878	WBGene00004487	rps-18	Ribosomal Protein, Small subunit	0.631675799	0.515944	0.005641	0.028947	12499.25432
879	WBGene00004489	rps-20	Ribosomal Protein, Small subunit	0.762972918	0.317391	0.000675	0.005823	11639.49752
880	WBGene00004495	rps-26	40S ribosomal protein S26	0.871550327	0.407708	0.00112	0.00853	7139.850588
881	WBGene00004472	rps-3	40S ribosomal protein S3	0.343782316	0.228381	0.008776	0.040663	23961.47081
882	WBGene00004499	rps-30	40S ribosomal protein S30	0.343944573	0.233742	0.011088	0.048475	15240.41321
883	WBGene00004475	rps-6	40S ribosomal protein S6	0.610424505	0.519981	0.006078	0.030646	9496.671774
884	WBGene00004478	rps-9	40S ribosomal protein S9	0.798247224	0.380588	0.001293	0.009564	16106.3906
885	WBGene00020296	rrp-8	Ribosomal RNA-processing protein 8	-0.309194686	0.060862	7.55E-08	6.68E-06	1922.693309
886	WBGene00007710	rsa-1	Serine/threonine-protein phosphatase 2A regulatory subunit rsa-1	-0.320179909	0.071879	1.41E-06	5.80E-05	4545.576124
887	WBGene00011531	rsbp-1	R-Seven Binding Protein (R7BP) homolog	0.381888107	0.154516	0.001336	0.009784	402.022192
888	WBGene00004698	rsp-1	Probable splicing factor, arginine/serine-rich 1	0.502118421	0.174015	0.000295	0.003045	1638.143276
889	WBGene00004700	rsp-3	Probable splicing factor, arginine/serine-rich 3	0.391335523	0.222436	0.005717	0.02923	3127.792288
890	WBGene00004702	rsp-5	Probable splicing factor, arginine/serine-rich 5	0.646736074	0.220196	0.000181	0.00211	1464.609354
891	WBGene00004703	rsp-6	Probable splicing factor, arginine/serine-rich 6	0.49335337	0.231435	0.002042	0.013368	3242.791299
892	WBGene00004705	rsp-8	SR Protein (splicing factor)	0.909936828	0.33133	0.00025	0.00268	4270.040308
893	WBGene00013260	rsr-2	SR protein related	0.372273634	0.094575	1.05E-05	0.000258	1295.462068
894	WBGene00013177	rsy-1	Regulator of SYnapse formation	0.568357598	0.218704	0.00052	0.004748	558.1339585
895	WBGene00012990	sam-10	Single-stranded DNA-binding protein homolog sam-10	0.410329428	0.194751	0.002746	0.016672	1156.848369
896	WBGene00021870	samt-1	SAM (S-Adenosyl Methionine) Transporter	0.372659041	0.157014	0.001678	0.011607	138.2239954
897	WBGene00004739	scd-1	Suppressor of Constitutive Dauer formation	0.434344795	0.152422	0.000382	0.003687	791.7097559
898	WBGene00011935	scrm-1	Phospholipid scramblase	0.45706567	0.174645	0.000651	0.005638	171.1777219
899	WBGene00015391	sdha-1	Succinate dehydrogenase [ubiquinone] flavoprotein subunit, mitochondrial	0.371626372	0.11696	0.000181	0.00211	1247.041048
900	WBGene00009353	sdhd-1	Putative succinate dehydrogenase [ubiquinone] cytochrome b small subunit, mitochondrial	0.302278216	0.173638	0.009856	0.044281	2014.260663
901	WBGene00004751	sea-2	Signal Element on Autosome	0.525290796	0.157467	6.23E-05	0.000976	492.0989779
902	WBGene00008379	secs-1	O-phosphoseryl-tRNA(Sec) selenium transferase	-0.32432728	0.085291	2.27E-05	0.000459	622.8499513
903	WBGene00021046	sedl-1	Probable trafficking protein particle complex subunit 2	0.608603276	0.51442	0.005982	0.030283	97.07075595

	ENSEMBLE GeneID	SYMBOL	GENENAME	log2FoldChange	lfcSE	pvalue	padj	baseMean
904	WBGene00011411	sel-13	Suppressor/Enhancer of Lin-12	-0.316818038	0.073515	2.74E-06	9.40E-05	1524.36756
905	WBGene00011729	set-16	Histone-lysine N-methyltransferase	0.54483976	0.155385	3.25E-05	0.000603	1177.458699
906	WBGene00011887	set-17	SET (trithorax/polycomb) domain containing	-0.329240024	0.083317	1.20E-05	0.000278	3111.475231
907	WBGene00012527	set-22	SET (trithorax/polycomb) domain containing	-0.326028871	0.075477	2.53E-06	8.92E-05	1185.265725
908	WBGene00013106	set-26	Histone-lysine N-methyltransferase set-26	1.183138776	0.258829	2.33E-07	1.64E-05	996.3234103
909	WBGene00007403	set-3	SET domain-containing protein 3	-0.301173217	0.068826	2.27E-06	8.20E-05	1364.944975
910	WBGene00017482	set-9	Histone-lysine N-methyltransferase set-9	0.567555567	0.244453	0.001005	0.007855	1101.603052
911	WBGene00004783	seu-1	Suppressor of Ectopic Unc-5	0.309073799	0.139841	0.004278	0.023458	2431.530705
912	WBGene00013808	sfa-1	Splicing FActor	0.487623423	0.10462	3.01E-07	2.01E-05	1667.124777
913	WBGene00020867	shc-2	SHC (Src Homology domain C-terminal) adaptor homolog	0.405861942	0.118582	6.45E-05	0.001	265.5423828
914	WBGene00006444	shn-1	Protein shank	0.42472865	0.313831	0.008562	0.039897	207.2554937
915	WBGene00021369	siah-1	E3 ubiquitin-protein ligase siah-1	1.001959249	0.182945	2.30E-09	4.40E-07	376.6288672
916	WBGene00002207	sid-3	Tyrosine-protein kinase sid-3	0.318411156	0.158263	0.005293	0.027556	543.6685013
917	WBGene00004803	sir-2.4	NAD-dependent protein deacetylase sir-2.4	-0.374273824	0.085924	1.65E-06	6.47E-05	688.7668145
918	WBGene00013725	ska-1	Spindle and kinetochore-associated protein 1	-0.360871235	0.066155	7.04E-09	1.01E-06	1527.651596
919	WBGene00004822	skr-16	SKp1 Related (ubiquitin ligase complex component)	-0.307547779	0.128133	0.002345	0.014815	324.9427983
920	WBGene00004830	slo-1	Calcium-activated potassium channel slo-1	0.518080303	0.375735	0.006236	0.031271	77.60536935
921	WBGene00004875	smd-1	S-adenosylmethionine decarboxylase beta chain	0.663133407	0.149174	5.72E-07	2.98E-05	1400.222112
922	WBGene00004885	smg-7	Suppressor with Morphological effect on Genitalia	-0.34055069	0.07681	1.41E-06	5.80E-05	848.104342
923	WBGene00004888	smo-1	Small ubiquitin-related modifier	0.539949384	0.465039	0.007417	0.035665	4948.776019
924	WBGene00004891	smr-1	SMN (Survival of Motor Neuron protein) Related	0.445338649	0.221191	0.0029	0.017411	1102.458915
925	WBGene00017265	snpc-1.3	SNAPc (Small Nuclear RNA Activating Complex) homolog	-0.429034748	0.247205	0.005145	0.026959	60.86990908
926	WBGene00015098	snpc-3.1	SNAPc (Small Nuclear RNA Activating Complex) homolog	0.585196595	0.224365	0.000505	0.004644	171.1386285
927	WBGene00021667	snpc-3.2	SNAPc (Small Nuclear RNA Activating Complex) homolog	0.579343078	0.248736	0.001027	0.007963	110.4667741
928	WBGene00011367	snpc-3.4	SNAPc (Small Nuclear RNA Activating Complex) homolog	-0.309110152	0.09094	0.000113	0.001475	1237.743659
929	WBGene00004915	snr-2	Probable small nuclear ribonucleoprotein-associated protein B	0.398678764	0.161579	0.001018	0.007925	5153.814791
930	WBGene00012896	snrp-200	Putative U5 small nuclear ribonucleoprotein 200 kDa helicase	0.451662759	0.114377	7.35E-06	0.000195	2673.52931
931	WBGene00015974	snrp-40.2	Small Nuclear RibonucleoProtein homolog	-0.333725944	0.086649	1.76E-05	0.000378	920.7056907
932	WBGene00004927	snx-1	Sorting NeXin	0.743688461	0.162972	3.07E-07	2.01E-05	638.9186785
933	WBGene00013011	snx-14	Sorting NeXin	0.617974495	0.194611	8.91E-05	0.001246	660.9321302
934	WBGene00004930	sod-1	Superoxide dismutase [Cu-Zn]	0.32510875	0.124007	0.001109	0.008474	3853.289703
935	WBGene00013603	soem-1	Protein soem-1	0.379055173	0.170883	0.002483	0.015462	223.6116283
936	WBGene00004947	sos-1	Son of sevenless homolog	0.312789463	0.126317	0.00189	0.012644	629.8999936
937	WBGene00020496	spat-3	Suppressor of PAr-Two defect	0.614034579	0.140352	8.37E-07	3.89E-05	918.2430162
938	WBGene00004952	spd-1	hypothetical protein	0.460204197	0.187264	0.000995	0.007801	1046.421302
939	WBGene00004954	spd-3	hypothetical protein	-0.453339547	0.082845	4.49E-09	6.93E-07	624.1318824
940	WBGene00012909	spds-1	SPermiDine Synthase	0.562553801	0.146952	9.41E-06	0.000238	251.2688823
941	WBGene00021335	spp-23	SaPosin-like Protein family	1.570349759	0.366142	7.54E-07	3.61E-05	63.69586004
942	WBGene00005018	sqt-3	Cuticle collagen 1	1.271241572	0.564977	0.000711	0.006063	1120.822618
943	WBGene00011522	srap-1	Serine Rich Adhesion Protein-like	0.453316692	0.126722	3.31E-05	0.000612	359.0736331
944	WBGene00005078	src-2	Tyrosine protein-kinase src-2	0.542898352	0.357435	0.005055	0.026622	62.03799427
945	WBGene00005648	srp-7	SeRPin	-0.321072317	0.054267	5.38E-10	1.45E-07	4344.91401
946	WBGene00017245	srpa-72	Signal recognition particle subunit SRP72	0.379036922	0.156911	0.001567	0.011074	1186.05165
947	WBGene00005832	srw-85	Serpentine Receptor, class W	0.449260849	0.627817	0.010854	0.047811	35.5221571
948	WBGene00007027	ssl-1	Helicase ssl-1	0.773825598	0.124592	3.37E-11	2.06E-08	1698.846714
949	WBGene00020480	ssup-72	SSU (yeast Suppressor of SUa7) Protein homolog	-0.40388007	0.071712	2.39E-09	4.44E-07	934.3850633
950	WBGene00019983	sti-1	Stress-induced-phosphoprotein 1	0.582660008	0.17533	5.70E-05	0.000923	2465.138872
951	WBGene00006063	sto-1	Stomatin-1	0.420039715	0.10865	1.13E-05	0.000267	711.2180108
952	WBGene00006066	sto-4	Stomatin-4	0.360308811	0.09442	1.80E-05	0.000382	531.409298
953	WBGene00007350	sucl-1	Succinate--CoA ligase [ADP/GDP-forming] subunit alpha, mitochondrial	0.441862832	0.156385	0.000399	0.003818	1355.599357
954	WBGene00006331	sup-26	SUPpressor	0.326383606	0.113758	0.000576	0.00513	2943.400979
955	WBGene00007985	swah-1	SoWAH (Drosophila) homolog	-0.437094056	0.099864	1.23E-06	5.17E-05	831.3944945
956	WBGene00016373	swd-2.1	Set1 WD40 repeat protein	-0.317540632	0.088845	5.51E-05	0.0009	1458.051624
957	WBGene00004203	swsn-1	SWI/SNF nucleosome remodeling complex component	0.360851403	0.191373	0.005424	0.028078	1947.73088
958	WBGene00019300	swt-1	Sugar transporter SWEET1	-0.704903581	0.15873	5.58E-07	2.94E-05	148.9499398
959	WBGene00044068	syd-9	hypothetical protein	0.491693949	0.25747	0.003132	0.018361	346.165246
960	WBGene00021473	sydn-1	hypothetical protein	1.188696379	0.321192	8.96E-06	0.000228	57.49835228
961	WBGene00007750	syg-2	Synaptogenesis protein syg-2	0.34435859	0.235113	0.011307	0.049071	218.400564
962	WBGene00012104	sygl-1	hypothetical protein	0.495176096	0.474342	0.008571	0.039923	1984.071052
963	WBGene00006366	sym-1	hypothetical protein	0.473844291	0.202375	0.001275	0.009461	754.9950698
964	WBGene00006377	syp-3	hypothetical protein	-0.3354636	0.069154	1.92E-07	1.39E-05	929.4353976
965	WBGene00006374	syx-4	Putative syntaxin-4	0.442658938	0.176715	0.000953	0.007553	497.8555604
966	WBGene00011310	T01B4.3	hypothetical protein	0.332949155	0.124918	0.000917	0.007333	316.9962963
967	WBGene00011375	T02E1.2	hypothetical protein	-0.318654808	0.065011	1.65E-07	1.23E-05	1924.10595
968	WBGene00011383	T02E9.5	hypothetical protein	0.405479977	0.24119	0.006066	0.030607	878.8870619
969	WBGene00020181	T02H6.11	hypothetical protein	0.60407595	0.20896	0.000219	0.002424	1748.837458
970	WBGene00020188	T03F1.6	hypothetical protein	0.553824844	0.18383	0.000166	0.001977	238.8234312
971	WBGene00011435	T04D3.8	hypothetical protein	-0.364596872	0.146095	0.001332	0.009764	181.5175584
972	WBGene00020229	T05A8.3	hypothetical protein	0.488134302	0.251265	0.002908	0.01744	171.0180648
973	WBGene00045249	T07A9.15	hypothetical protein	-0.634823077	0.142843	5.86E-07	3.04E-05	398.0445979
974	WBGene00045407	T07D4.5	hypothetical protein	-0.376967883	0.087799	2.24E-06	8.11E-05	1435.922536
975	WBGene00011606	T08D2.1	hypothetical protein	0.736096124	0.303446	0.000655	0.005663	61.79780036
976	WBGene00011613	T08D2.8	hypothetical protein	0.972746203	0.290542	3.81E-05	0.000681	61.37440624
977	WBGene00011631	T08G11.4	hypothetical protein	-0.33090379	0.072912	9.43E-07	4.26E-05	1588.704349
978	WBGene00020379	T09B4.5	hypothetical protein	0.47250837	0.11215	2.31E-06	8.31E-05	2081.023679
979	WBGene00020402	T10B11.6	hypothetical protein	-0.332776824	0.072321	6.71E-07	3.32E-05	1108.721688
980	WBGene00020396	T10B5.10	hypothetical protein	0.882886579	0.381048	0.000758	0.006363	29.39447727
981	WBGene00020390	T10B5.4	hypothetical protein	0.332521203	0.18238	0.006994	0.034115	137.3884607
982	WBGene00011688	T10C6.6	hypothetical protein	0.769574762	0.20399	8.88E-06	0.000227	796.6713114
983	WBGene00020411	T10E9.1	hypothetical protein	-0.380434816	0.074372	4.12E-08	4.44E-06	1315.817039
984	WBGene00044604	T10F2.5	hypothetical protein	-0.452340956	0.092065	8.92E-08	7.45E-06	678.4906654
985	WBGene00020433	T11F8.1	hypothetical protein	-0.475088341	0.088334	7.22E-09	1.03E-06	887.4813669
986	WBGene00020446	T12B3.3	hypothetical protein	-0.351652168	0.110963	0.000197	0.002237	334.6041101
987	WBGene00011804	T16G12.3	hypothetical protein	0.747923692	0.217628	3.19E-05	0.000599	724.7329656
988	WBGene00020588	T19H12.2	Acidic leucine-rich nuclear phosphoprotein 32-related protein 2	0.630498196	0.193351	6.75E-05	0.001028	5628.370737
989	WBGene00011880	T21B6.3	hypothetical protein	0.590656564	0.179398	6.31E-05	0.000986	456.9396324
990	WBGene00011898	T21C9.13	hypothetical protein	-0.380458022	0.058642	1.18E-11	8.89E-09	3941.033396
991	WBGene00020662	T21H3.1	hypothetical protein	0.44799943	0.499629	0.010399	0.046236	2668.24181
992	WBGene00020678	T22B11.4	hypothetical protein	0.469248728	0.094054	5.89E-08	5.41E-06	607.9748775
993	WBGene00020674	T22B7.7	hypothetical protein	1.350568713	0.19986	6.44E-13	1.18E-09	171.3854221
994	WBGene00020709	T23B3.1	hypothetical protein	-0.308044112	0.070523	2.24E-06	8.11E-05	2533.958225
995	WBGene00011941	T23B5.4	hypothetical protein	-0.494279342	0.100683	8.20E-08	7.01E-06	561.9631957
996	WBGene00020732	T23E7.2	hypothetical protein	0.378741223	0.134092	0.000512	0.004687	1271.474475
997	WBGene00011976	T24B8.2	hypothetical protein	-0.312745134	0.062123	8.79E-08	7.45E-06	2118.854812
998	WBGene00044149	T24D5.6	hypothetical protein	0.516007831	0.220776	0.001173	0.008813	223.75522
999	WBGene00012002	T24H10.4	hypothetical protein	-0.341980855	0.086495	1.12E-05	0.000265	1596.608962
1000	WBGene00020801	T25D10.4	hypothetical protein	0.323542468	0.145177	0.003178	0.018546	193.1783926
1001	WBGene00020831	T26C12.1	Acetolactate synthase-like protein	0.398908774	0.122427	0.000119	0.001538	1584.560878
1002	WBGene00020854	T27C4.1	hypothetical protein	0.901117595	0.223041	2.74E-06	9.40E-05	140.7683299
1003	WBGene00012085	T27D12.1	hypothetical protein	0.470384868	0.137949	5.39E-05	0.000882	359.7176906
1004	WBGene00012106	T27F6.7	hypothetical protein	0.501342529	0.248957	0.002444	0.01529	199.2189543
1005	WBGene00012109	T28A8.3	hypothetical protein	-0.33659565	0.070973	3.27E-07	2.08E-05	1600.037217
1006	WBGene00020891	T28C12.4	Carboxylic ester hydrolase	-0.41011037	0.140399	0.000334	0.003337	244.293457
1007	WBGene00012123	T28D6.3	hypothetical protein	0.795997354	0.288502	0.000257	0.002735	485.0286232
1008	WBGene00012124	T28D6.4	hypothetical protein	0.72196596	0.269994	0.000354	0.003478	61.04062468
1009	WBGene00012125	T28D6.5	hypothetical protein	0.525710266	0.157481	6.20E-05	0.000975	147.8137993
1010	WBGene00020894	T28D9.1	hypothetical protein	0.538726228	0.226483	0.001008	0.007873	3969.169409
1011	WBGene00006381	tac-1	Transforming acid coiled-coil-containing protein 1	0.568377229	0.314885	0.003047	0.018054	471.0401984
1012	WBGene00007217	tads-1	Temporal Asymmetry between Division of Sister cells	-0.347020823	0.053263	1.11E-11	8.89E-09	2268.938856
1013	WBGene00006383	taf-2	Transcription initiation factor TFIID subunit 2	0.560562144	0.167133	5.66E-05	0.000921	768.6320213
1014	WBGene00006384	taf-3	TAF (TBP-associated transcription factor) family	0.325112632	0.200231	0.010031	0.044945	855.9091429
1015	WBGene00006385	taf-4	TAF (TBP-associated transcription factor) family	0.372686497	0.153283	0.00153	0.010879	827.4368202
1016	WBGene00006386	taf-5	TAF (TBP-associated transcription factor) family	-0.322873215	0.075388	2.93E-06	9.88E-05	2181.091759

	ENSEMBLE GeneID	SYMBOL	GENENAME	log2FoldChange	lfcSE	pvalue	padj	baseMean
1017	WBGene00006387	taf-6.1	TAF (TBP-associated transcription factor) family	0.426629427	0.186036	0.001705	0.011744	409.4010312
1018	WBGene00021363	taf-6.2	TAF (TBP-associated transcription factor) family	0.43349103	0.145664	0.000261	0.002759	829.6465935
1019	WBGene00006390	taf-8	TAF (TBP-associated transcription factor) family	-0.361474359	0.06674	8.64E-09	1.19E-06	1724.705299
1020	WBGene00006466	tag-115	hypothetical protein	-0.313969739	0.084304	3.40E-05	0.000625	1562.831872
1021	WBGene00044326	tag-322	hypothetical protein	-0.394777033	0.080935	1.31E-07	1.03E-05	1871.456076
1022	WBGene00006523	tam-1	Tandem Array expression Modifier	0.343982214	0.119285	0.000512	0.004687	2825.613947
1023	WBGene00006529	tba-2	Tubulin alpha-2 chain	0.64655408	0.359662	0.002691	0.016429	17119.62819
1024	WBGene00006537	tbb-2	Tubulin beta-2 chain	0.461581352	0.177483	0.000714	0.006082	24037.9474
1025	WBGene00012894	tbc-17	TBC (Tre-2/Bub2/Cdc16) domain family	0.551206703	0.129337	1.55E-06	6.14E-05	638.5199218
1026	WBGene00013196	tbc-20	TBC (Tre-2/Bub2/Cdc16) domain family	0.324021784	0.131024	0.001775	0.01211	1647.426403
1027	WBGene00019503	tbce-1	TuBulin folding Cofactor E homolog	-0.336210036	0.076822	1.94E-06	7.26E-05	1811.775659
1028	WBGene00006555	tbx-36	Putative T-box protein 36	-0.350041584	0.089131	1.20E-05	0.000278	668.8388148
1029	WBGene00006565	tfg-1	human TFG related	1.107064641	0.384589	0.000153	0.001855	538.0345403
1030	WBGene00014114	tfic-3	Transcription Factor ThreeC subunit (GTF3C homolog)	-0.312442049	0.096743	0.000198	0.002242	3002.013107
1031	WBGene00009341	thoc-3	THO Complex (transcription factor/nuclear export) subunit	-0.358195766	0.062576	1.51E-09	3.12E-07	1628.67893
1032	WBGene00012904	tiar-2	TIA-1/TIAL RNA binding protein homolog	0.376206245	0.122106	0.000233	0.002537	919.9838854
1033	WBGene00006771	tln-1	TaLiN	0.995249273	0.154294	6.23E-12	7.99E-09	898.4445248
1034	WBGene00006580	tlp-1	T lineage defect, LePtoderan tail	0.337549955	0.101885	0.000131	0.001654	516.6606123
1035	WBGene00006585	tni-3	Troponin I 3	0.705100139	0.174663	3.21E-06	0.000107	483.5052908
1036	WBGene00006586	tni-4	Troponin I 4	0.578603543	0.130259	6.70E-07	3.32E-05	589.741488
1037	WBGene00006587	tnt-2	TropoNin T	0.539477773	0.388311	0.005873	0.029813	4766.027404
1038	WBGene00006588	tnt-3	TropoNin T	0.47168447	0.149489	0.000137	0.00172	1320.094277
1039	WBGene00006589	tnt-4	TropoNin T	1.112670475	0.229731	6.36E-08	5.75E-06	378.467086
1040	WBGene00017298	toca-1	Transducer of Cdc42-dependent actin assembly protein 1 homolog	0.319558084	0.131813	0.002137	0.013851	501.1402904
1041	WBGene00012194	toe-4	Target Of ERK kinase MPK-1	0.77568584	0.261389	0.000142	0.001749	283.5644204
1042	WBGene00007785	tofu-1	Twenty One u-rna (21U-RNA) biogenesis Fouled Up	-0.300785166	0.070602	3.82E-06	0.000121	1722.389553
1043	WBGene00017620	tofu-2	Twenty One u-rna (21U-RNA) biogenesis Fouled Up	-0.356262054	0.089791	9.45E-06	0.000238	1612.607362
1044	WBGene00012167	tofu-5	Twenty One u-rna (21U-RNA) biogenesis Fouled Up	-0.338059302	0.075239	1.07E-06	4.72E-05	2202.696092
1045	WBGene00021133	tomm-22	Mitochondrial import receptor subunit TOM22 homolog	-0.310698415	0.085523	4.67E-05	0.000797	1553.251138
1046	WBGene00022783	tomm-7	Mitochondrial import receptor subunit TOM7 homolog	-0.429544654	0.18415	0.001486	0.010624	1173.438161
1047	WBGene00019466	tos-1	Target Of Splicing	0.368308859	0.056294	8.64E-12	8.19E-09	5170.323521
1048	WBGene00016321	tppp-1	Tubulin polymerization-promoting protein homolog	0.324062978	0.156436	0.004533	0.024494	1105.341134
1049	WBGene00022122	trap-1	TRanslocon-Associated Protein	0.64953203	0.183972	2.60E-05	0.000511	5724.835114
1050	WBGene00020216	trap-2	Translocon-associated protein subunit beta	0.583203373	0.1855	0.00011	0.001449	3608.537396
1051	WBGene00013238	trap-4	TRanslocon-Associated Protein	0.491456366	0.187157	0.000605	0.005322	5241.288019
1052	WBGene00009186	trcs-1	TRansport of membrane to Cell Surface	-0.338754534	0.083073	6.68E-06	0.000182	12857.10125
1053	WBGene00013255	tric-1B.1	Trimeric intracellular cation channel type 1B.1	0.75073818	0.173009	8.12E-07	3.83E-05	346.0975232
1054	WBGene00013268	tric-1B.2	Trimeric intracellular cation channel type 1B.2	0.322875073	0.115585	0.000776	0.006489	1151.914077
1055	WBGene00013259	trpp-5	Trafficking protein particle complex subunit 5	-0.346759118	0.099803	6.99E-05	0.001052	536.6531779
1056	WBGene00006618	trt-1	Telomerase Reverse Transcriptase	-0.396246727	0.072084	4.26E-09	6.72E-07	1486.233439
1057	WBGene00007099	trx-2	Probable thioredoxin-2	-0.332690419	0.065103	4.82E-08	4.87E-06	1014.942564
1058	WBGene00014028	trxr-2	Probable glutathione reductase 2	-0.30833009	0.128751	0.002304	0.014605	244.4908992
1059	WBGene00008849	try-10	TRYpsin-like protease	-0.515061731	0.265103	0.002558	0.01581	174.4475681
1060	WBGene00006640	tsp-14	Tetraspanin-14	0.520742174	0.237245	0.001616	0.011324	113.6338206
1061	WBGene00006647	tsr-1	Transporter of SR proteins	0.330366509	0.16397	0.004902	0.025997	504.661901
1062	WBGene00006648	ttb-1	Transcription initiation factor IIB	0.436622465	0.187279	0.001508	0.010742	943.7237739
1063	WBGene00015916	ttc-4	TeTratriCopeptide repeat domain protein related	-0.308052258	0.085433	5.35E-05	0.000878	1188.860446
1064	WBGene00021444	ttc-7	TeTratriCopeptide repeat domain protein related	-0.334553696	0.088485	2.34E-05	0.00047	1171.174612
1065	WBGene00006436	ttn-1	Titin homolog	0.483249059	0.148281	9.02E-05	0.001259	878.5099192
1066	WBGene00013079	ttr-26	TransThyretin-Related family domain	-0.337059541	0.176873	0.00588	0.029836	171.6799016
1067	WBGene00022139	tub-2	TUBby-related	0.973528207	0.158496	4.41E-11	2.25E-08	407.0172126
1068	WBGene00009256	tut-2	Cytoplasmic tRNA 2-thiolation protein 2	-0.342355507	0.073414	4.70E-07	2.62E-05	989.4380072
1069	WBGene00018187	twf-2	TWinFilin actin binding protein homolog	0.627486063	0.150707	2.09E-06	7.70E-05	521.9367938
1070	WBGene00006657	twk-2	TWiK family of potassium channels	0.694696199	0.353239	0.001898	0.012682	43.96849466
1071	WBGene00022455	tyms-1	Thymidylate synthase	-0.346333062	0.053623	1.66E-11	1.18E-08	2272.040687
1072	WBGene00006710	ubc-15	UBiquitin Conjugating enzyme	0.350896453	0.096445	3.72E-05	0.000669	748.6014967
1073	WBGene00006715	ubc-20	UBiquitin Conjugating enzyme	0.37373648	0.15855	0.001885	0.012618	2294.931768
1074	WBGene00006702	ubc-3	UBiquitin Conjugating enzyme	0.301209231	0.126788	0.002482	0.015462	2872.047397
1075	WBGene00006725	ubl-1	Ubiquitin-like protein 1	0.801769512	0.502805	0.003039	0.018025	9080.448452
1076	WBGene00012158	ucr-2.1	Ubiquinol-Cytochrome c oxidoReductase complex	0.573939653	0.177113	7.73E-05	0.001129	1041.042321
1077	WBGene00011564	ugt-50	Putative UDP-glucuronosyltransferase ugt-50	0.35168862	0.150108	0.002118	0.013753	541.2567201
1078	WBGene00019234	ugt-8	UDP-GlucuronosylTransferase	-0.395258352	0.276885	0.008936	0.041246	85.16745208
1079	WBGene00011559	umps-1	Orotidine 5'-phosphate decarboxylase	0.388000408	0.202848	0.004428	0.024047	1168.61057
1080	WBGene00006750	unc-10	Rab-3-interacting molecule unc-10	0.422360942	0.252269	0.005797	0.02953	95.01800933
1081	WBGene00006839	unc-115	hypothetical protein	0.365888677	0.110511	0.000115	0.001491	1109.511416
1082	WBGene00006853	unc-130	hypothetical protein	0.301384394	0.164813	0.008415	0.03931	151.5227201
1083	WBGene00006754	unc-15	Paramyosin	0.548774481	0.170556	9.43E-05	0.0013	5945.76466
1084	WBGene00006742	unc-2	hypothetical protein	0.755356573	0.234921	6.62E-05	0.001017	136.8942292
1085	WBGene00006764	unc-27	Troponin I 2	0.427308242	0.153524	0.00049	0.004537	6741.868312
1086	WBGene00006766	unc-30	Homeobox protein unc-30	0.573798602	0.297488	0.002396	0.015063	53.12007466
1087	WBGene00006769	unc-33	Protein unc-33	0.535307998	0.172201	0.000129	0.001626	1447.75461
1088	WBGene00006770	unc-34	hypothetical protein	0.367902319	0.09199	8.18E-06	0.000214	1239.594889
1089	WBGene00006780	unc-44	hypothetical protein	0.387438361	0.107895	3.84E-05	0.000686	2572.752298
1090	WBGene00006786	unc-51	Serine/threonine-protein kinase unc-51	0.736863794	0.160324	2.52E-07	1.75E-05	310.9814005
1091	WBGene00006787	unc-52	Basement membrane proteoglycan	0.63287148	0.127988	5.53E-08	5.22E-06	1485.673694
1092	WBGene00006789	unc-54	Myosin-4	0.992504488	0.313622	6.67E-05	0.001022	6891.479735
1093	WBGene00006793	unc-59	hypothetical protein	-0.300058639	0.055426	1.15E-08	1.52E-06	4295.99468
1094	WBGene00006796	unc-62	Homeobox protein unc-62	0.501547291	0.129196	8.47E-06	0.00022	569.6881199
1095	WBGene00006803	unc-70	Spectrin beta chain	0.32025118	0.102164	0.000261	0.002759	2536.845879
1096	WBGene00006807	unc-75	hypothetical protein	1.276708579	0.582038	0.000853	0.006965	33.03340205
1097	WBGene00006824	unc-95	hypothetical protein	1.29615279	0.25	1.06E-08	1.42E-06	106.8372432
1098	WBGene00016944	uri-1	URI (Unconventional prefoldin RPB5 Interactor) homolog	-0.309233741	0.055914	5.24E-09	7.91E-07	2421.958832
1099	WBGene00185048	urm-1	Ubiquitin-related modifier 1 homolog	-0.411536475	0.118784	5.34E-05	0.000877	322.5724046
1100	WBGene00006876	vab-10	hypothetical protein	0.542297719	0.122014	6.92E-07	3.39E-05	2824.406293
1101	WBGene00006882	vab-19	hypothetical protein	0.88902325	0.219385	2.64E-06	9.24E-05	114.067293
1102	WBGene00006869	vab-2	hypothetical protein	0.321389762	0.134457	0.002231	0.014271	179.3555325
1103	WBGene00015216	valv-1	hypothetical protein	0.367750763	0.18791	0.004572	0.024646	125.7140735
1104	WBGene00012151	VH15N14R.1	hypothetical protein	0.836438404	0.290938	0.000183	0.002117	182.4579354
1105	WBGene00006912	vha-3	V-type proton ATPase 16 kDa proteolipid subunit 2/3	0.385599258	0.131669	0.000355	0.00348	4663.148757
1106	WBGene00006924	vig-1	VIG (Drosophila Vasa Intronic Gene) ortholog	0.468191105	0.169322	0.000464	0.004349	1508.139859
1107	WBGene00012903	vps-2	related to yeast Vacuolar Protein Sorting factor	0.488455813	0.189119	0.000669	0.005776	1323.406182
1108	WBGene00018290	vps-60	related to yeast Vacuolar Protein Sorting factor	-0.320143988	0.058624	8.18E-09	1.15E-06	2710.670824
1109	WBGene00012188	W01G7.4	hypothetical protein	0.860073078	0.274157	7.80E-05	0.001135	418.2513255
1110	WBGene00012198	W02B8.2	hypothetical protein	0.318300627	0.115682	0.000861	0.007016	618.7605162
1111	WBGene00020941	W02D7.5	hypothetical protein	-0.544379141	0.165299	7.16E-05	0.001067	140.4791927
1112	WBGene00012216	W02D9.10	hypothetical protein	1.028685333	0.327505	6.85E-05	0.001035	67.48710553
1113	WBGene00012210	W02D9.4	hypothetical protein	-0.440236289	0.121399	2.66E-05	0.000519	288.3854454
1114	WBGene00020957	W02H5.2	hypothetical protein	0.419722871	0.146626	0.000386	0.003721	644.6558726
1115	WBGene00020962	W02H5.8	hypothetical protein	0.833985806	0.21193	4.24E-06	0.00013	188.2928551
1116	WBGene00021002	W03F9.4	hypothetical protein	0.453101975	0.213271	0.002267	0.014457	250.9176292
1117	WBGene00012226	W03G11.4	hypothetical protein	0.447254853	0.228411	0.003328	0.019263	289.7025763
1118	WBGene00044431	W03G9.8	hypothetical protein	-0.328878933	0.124526	0.001097	0.008412	965.6299343
1119	WBGene00012239	W04A8.4	hypothetical protein	0.378808635	0.223042	0.006685	0.03292	931.885156
1120	WBGene00021019	W04B5.2	hypothetical protein	0.392594674	0.209936	0.004624	0.024809	101.5123151
1121	WBGene00021020	W04B5.3	Galectin	0.431556298	0.234523	0.00427	0.023442	274.317419
1122	WBGene00012274	W05B5.1	hypothetical protein	0.357164529	0.168118	0.003238	0.018849	391.6100172
1123	WBGene00021035	W05F2.3	hypothetical protein	0.765336188	0.370347	0.001417	0.010229	6164.230108
1124	WBGene00021036	W05F2.4	hypothetical protein	0.515490614	0.139725	1.75E-05	0.000375	296.0371989
1125	WBGene00021044	W05H7.1	hypothetical protein	0.704110884	0.265067	0.00037	0.0036	94.42575443
1126	WBGene00012306	W06F12.2	hypothetical protein	0.749463714	0.272053	0.00028	0.00293	404.6010278
1127	WBGene00021066	W06H8.2	hypothetical protein	-0.427981161	0.27045	0.006675	0.032893	59.38513815
1128	WBGene00021080	W08A12.3	hypothetical protein	0.533627467	0.210039	0.000687	0.005902	78.08734261
1129	WBGene00012343	W08E3.2	hypothetical protein	0.504242496	0.158047	0.000106	0.001418	832.6983874

	ENSEMBLE GeneID	SYMBOL	GENENAME	log2FoldChange	lfcSE	pvalue	padj	baseMean
1130	WBGene00021101	W08F4.12	hypothetical protein	0.457215883	0.293496	0.00606	0.030594	53.78010213
1131	WBGene00021093	W08F4.3	hypothetical protein	0.54259217	0.180108	0.000176	0.002062	2459.310741
1132	WBGene00012359	W09D10.1	hypothetical protein	0.303079957	0.164782	0.008173	0.038418	933.6120648
1133	WBGene00012358	W09D6.5	hypothetical protein	0.743014007	0.264357	0.000234	0.002545	348.7016499
1134	WBGene00021123	W09G12.9	hypothetical protein	0.604044603	0.384649	0.004074	0.022578	102.1726232
1135	WBGene00012369	W09G3.6	hypothetical protein	0.346854391	0.120677	0.000527	0.004799	1231.446356
1136	WBGene00021128	W10C8.5	hypothetical protein	0.3857996	0.176253	0.002557	0.015808	786.6192709
1137	WBGene00021135	W10G11.2	hypothetical protein	-0.594301946	0.314561	0.002546	0.015762	55.01208747
1138	WBGene00006958	wve-1	WAVE (actin cytoskeleton modulator) homolog	0.309279993	0.141814	0.00392	0.021901	1584.358079
1139	WBGene00006959	xbp-1	X-box Binding Protein homolog	0.31333804	0.151549	0.005241	0.02735	3746.984842
1140	WBGene00002079	xpo-2	eXPOrtin (nuclear export receptor)	0.306000317	0.114723	0.001175	0.008823	3301.132351
1141	WBGene00012730	xrn-1	5'-3' exoribonuclease 1	0.580522929	0.163633	2.62E-05	0.000513	779.6245794
1142	WBGene00006964	xrn-2	5'-3' exoribonuclease 2 homolog	0.769039566	0.179341	1.06E-06	4.69E-05	1839.046366
1143	WBGene00013666	Y105E8A.1	hypothetical protein	0.397719136	0.262461	0.007901	0.037441	200.4549105
1144	WBGene00013699	Y106G6D.2	hypothetical protein	-0.35388737	0.106348	0.000108	0.001426	379.4160752
1145	WBGene00013702	Y106G6D.6	hypothetical protein	-0.366582356	0.180721	0.00395	0.022033	129.4034886
1146	WBGene00013726	Y106G6H.16	hypothetical protein	-0.342416552	0.120969	0.00059	0.005225	426.6513925
1147	WBGene00013741	Y111B2A.21	hypothetical protein	0.738821153	0.492098	0.003706	0.020953	33.86962711
1148	WBGene00013790	Y116A8C.10	hypothetical protein	0.399033353	0.151913	0.000817	0.006746	330.9996494
1149	WBGene00013792	Y116A8C.13	hypothetical protein	0.455190548	0.167799	0.000532	0.004832	540.2672999
1150	WBGene00013819	Y116F11A.6	hypothetical protein	0.434952308	0.419563	0.010441	0.046374	39.3954211
1151	WBGene00022489	Y119D3B.12	hypothetical protein	0.309281928	0.190888	0.011201	0.048775	1001.254719
1152	WBGene00022490	Y119D3B.13	hypothetical protein	0.634738482	0.28433	0.001161	0.008761	207.2238633
1153	WBGene00022491	Y119D3B.14	hypothetical protein	0.321243463	0.176821	0.007532	0.036063	650.6102909
1154	WBGene00012431	Y11D7A.7	hypothetical protein	-0.341895188	0.069508	1.32E-07	1.03E-05	1123.635703
1155	WBGene00021189	Y13C8A.2	hypothetical protein	1.395275938	0.373539	7.74E-06	0.000203	70.53808141
1156	WBGene00021208	Y18H1A.2	hypothetical protein	1.323138917	0.293978	3.07E-07	2.01E-05	235.9468584
1157	WBGene00021210	Y18H1A.4	hypothetical protein	0.871054978	0.219472	3.73E-06	0.00012	370.1151899
1158	WBGene00021248	Y22D7AL.10	hypothetical protein	0.589147729	0.340591	0.003385	0.0195	2885.975761
1159	WBGene00021269	Y23H5A.2	hypothetical protein	1.247190218	0.411651	9.07E-05	0.001263	46.62617349
1160	WBGene00021296	Y25C1A.13	hypothetical protein	0.315863222	0.11645	0.000972	0.007664	345.5571272
1161	WBGene00021333	Y34D9A.8	hypothetical protein	1.309777065	0.297244	5.09E-07	2.77E-05	44.00448358
1162	WBGene00021377	Y37E11B.5	tRNA-dihydrouridine(47) synthase [NAD(P)(+)]	0.323728381	0.145907	0.003242	0.018856	447.9366031
1163	WBGene00235158	Y37E3.30	hypothetical protein	0.743586817	0.258706	0.000187	0.002158	76.1095121
1164	WBGene00021430	Y38F2AR.12	hypothetical protein	0.330588556	0.146127	0.00285	0.017174	233.3553089
1165	WBGene00021427	Y38F2AR.9	Protein transport protein Sec61 subunit beta	1.083338922	0.289979	8.32E-06	0.000217	300.1537962
1166	WBGene00012664	Y39B6A.1	hypothetical protein	0.954976186	0.815044	0.004325	0.023653	1294.638111
1167	WBGene00012700	Y39E6A.42	hypothetical protein	1.184834162	0.410309	0.000149	0.001819	439.4838733
1168	WBGene00012717	Y39E4B.6	hypothetical protein	0.756011787	0.186309	2.72E-06	9.40E-05	368.2584564
1169	WBGene00021469	Y39G10AR.11	hypothetical protein	0.455890998	0.148439	0.00018	0.002101	1263.060882
1170	WBGene00012722	Y39G8B.1	hypothetical protein	0.714856356	0.243327	0.000164	0.00196	332.5471677
1171	WBGene00021482	Y39H10A.6	hypothetical protein	0.542168857	0.140977	8.89E-06	0.000227	343.376062
1172	WBGene00021502	Y40D12A.1	hypothetical protein	-0.305166815	0.091176	0.000138	0.001723	861.8929647
1173	WBGene00021533	Y42G9A.3	hypothetical protein	-0.451613928	0.107514	2.53E-06	8.92E-05	310.3092244
1174	WBGene00021544	Y43B11AR.3	hypothetical protein	-0.315881666	0.139215	0.003086	0.018162	208.4614787
1175	WBGene00044922	Y43C5A.7	hypothetical protein	0.654956159	0.30085	0.001276	0.009465	321.7901758
1176	WBGene00012812	Y43F8B.1	hypothetical protein	0.783552598	0.227442	2.99E-05	0.000568	604.2555701
1177	WBGene00012813	Y43F8B.2	hypothetical protein	0.471559816	0.212815	0.001728	0.011871	441.6676311
1178	WBGene00012819	Y43F8B.9	hypothetical protein	0.827761401	0.476126	0.002536	0.015726	23.66242433
1179	WBGene00012825	Y43F8C.3	hypothetical protein	0.509280621	0.332813	0.005307	0.027605	143.5128497
1180	WBGene00012875	Y45F10B.13	hypothetical protein	0.35766325	0.117916	0.000297	0.003066	437.2377191
1181	WBGene00021563	Y45G12B.2	Zinc finger protein-like 1 homolog	0.504627309	0.183179	0.000405	0.003867	491.3431986
1182	WBGene00021559	Y45G5AM.7	hypothetical protein	-0.371684329	0.064691	1.26E-09	2.64E-07	2614.553256
1183	WBGene00012908	Y46G5A.18	hypothetical protein	0.807434278	0.177792	3.20E-07	2.08E-05	486.9653784
1184	WBGene00012899	Y46G5A.7	hypothetical protein	0.320752094	0.117779	0.000911	0.007307	332.398317
1185	WBGene00021605	Y46H3C.5	hypothetical protein	0.955782078	0.527164	0.00201	0.013249	1111.621377
1186	WBGene00021607	Y46H3C.7	hypothetical protein	0.456303322	0.408043	0.009218	0.042247	1719.086562
1187	WBGene00021625	Y47D7A.13	hypothetical protein	2.521477928	0.360958	1.42E-13	4.54E-10	88.53369816
1188	WBGene00021649	Y47G6A.25	hypothetical protein	-0.339291836	0.072798	4.86E-07	2.69E-05	1158.202179
1189	WBGene00012964	Y48A6B.3	Putative H/ACA ribonucleoprotein complex subunit 2-like protein	1.172148283	0.245944	9.05E-08	7.45E-06	668.3271211
1190	WBGene00012968	Y48A6B.7	hypothetical protein	0.583521585	0.243194	0.000864	0.007036	175.5745678
1191	WBGene00012970	Y48A6B.9	Enoyl-[acyl-carrier-protein] reductase, mitochondrial	0.492711407	0.163425	0.00019	0.002173	126.8228229
1192	WBGene00012978	Y48B6A.1	Ribosome biogenesis protein BOP1 homolog	0.450976894	0.124913	2.79E-05	0.000538	1142.039106
1193	WBGene00012994	Y48C3A.12	hypothetical protein	0.555583603	0.170093	7.05E-05	0.001055	955.4685145
1194	WBGene00012989	Y48C3A.5	hypothetical protein	1.001296132	0.364561	0.000256	0.002727	41.22175663
1195	WBGene00013001	Y48E1B.2	hypothetical protein	0.458656293	0.135044	5.94E-05	0.000949	943.6878162
1196	WBGene00013007	Y48E1B.8	hypothetical protein	0.491612269	0.209893	0.001215	0.009072	235.0060101
1197	WBGene00013014	Y48E1C.1	hypothetical protein	0.638062143	0.195269	6.52E-05	0.001004	518.9632283
1198	WBGene00021658	Y48G1A.2	hypothetical protein	0.816871526	0.240504	3.42E-05	0.000627	879.4360339
1199	WBGene00021675	Y48G1BR.1	hypothetical protein	0.694895932	0.174235	3.92E-06	0.000123	228.9267046
1200	WBGene00021691	Y48G8AL.13	hypothetical protein	0.430960002	0.219531	0.003366	0.019414	1072.502365
1201	WBGene00013026	Y49A3A.3	hypothetical protein	-0.394461539	0.102306	1.31E-05	0.000298	495.6408347
1202	WBGene00013030	Y49E10.4	hypothetical protein	-0.36873252	0.065586	2.64E-09	4.63E-07	1389.326699
1203	WBGene00021153	Y4C6A.3	hypothetical protein	-0.413120687	0.069259	2.90E-10	9.45E-08	2085.194228
1204	WBGene00195169	Y50D4A.6	hypothetical protein	1.047143765	0.308241	3.26E-05	0.000604	33.12812896
1205	WBGene00021749	Y50D4C.5	hypothetical protein	0.360896548	0.183807	0.004576	0.024653	644.9107011
1206	WBGene00021758	Y50D7A.10	hypothetical protein	-0.314444802	0.103724	0.000373	0.003625	700.6109443
1207	WBGene00021763	Y51F10.2	hypothetical protein	0.494567586	0.358737	0.007013	0.03418	3822.066678
1208	WBGene00021764	Y51F10.3	hypothetical protein	0.57065099	0.12816	6.31E-07	3.23E-05	873.3085742
1209	WBGene00013094	Y51H1A.3	hypothetical protein	1.259816771	0.421247	0.000104	0.001398	518.1037915
1210	WBGene00044439	Y51H7C.15	hypothetical protein	0.749803146	0.471616	0.003209	0.018715	62.14586955
1211	WBGene00013124	Y52B11A.4	hypothetical protein	0.677011474	0.472048	0.004419	0.02402	40.53366472
1212	WBGene00013127	Y52B11A.8	Phospholipase A2-like protein Y52B11A.8	0.661161835	0.432101	0.003946	0.022017	958.2321562
1213	WBGene00175030	Y53C12A.10	hypothetical protein	-0.31575255	0.090056	7.33E-05	0.001082	989.3537487
1214	WBGene00013169	Y53F4B.23	hypothetical protein	0.937300555	0.606446	0.002984	0.017799	18.46299484
1215	WBGene00013150	Y53F4B.3	hypothetical protein	0.556657364	0.271372	0.001989	0.013146	495.0159803
1216	WBGene00013156	Y53F4B.9	hypothetical protein	0.360869006	0.154881	0.002102	0.013668	1444.258833
1217	WBGene00021813	Y53G8AR.6	hypothetical protein	0.324951538	0.175343	0.00689	0.03372	1662.774672
1218	WBGene00021816	Y53G8AR.9	hypothetical protein	0.487373318	0.12103	4.87E-06	0.000143	2002.669522
1219	WBGene00013189	Y54E2A.4	hypothetical protein	0.388500659	0.11264	6.38E-05	0.000995	1204.117933
1220	WBGene00021853	Y54F10AM.11	hypothetical protein	0.643351345	0.214708	0.000152	0.001845	406.8418634
1221	WBGene00021855	Y54F10AR.2	hypothetical protein	-0.300842547	0.097956	0.000353	0.003469	688.7886382
1222	WBGene00013221	Y54G11A.14	hypothetical protein	1.387562179	0.310506	3.47E-07	2.14E-05	67.12320046
1223	WBGene00021876	Y54G2A.11	hypothetical protein	0.499889905	0.169862	0.000238	0.002589	377.5877748
1224	WBGene00021883	Y54G2A.18	hypothetical protein	0.842891382	0.424221	0.001592	0.011237	1215.688445
1225	WBGene00021884	Y54G2A.19	hypothetical protein	0.681822767	0.30055	0.001004	0.007854	114.1977872
1226	WBGene00021890	Y54G2A.26	hypothetical protein	0.413094281	0.141876	0.000342	0.003397	1695.256254
1227	WBGene00021909	Y55B1BL.1	hypothetical protein	0.409895228	0.156684	0.000808	0.006709	199.492498
1228	WBGene00021912	Y55B1BR.2	hypothetical protein	0.334811497	0.19015	0.007572	0.036211	206.8725555
1229	WBGene00021915	Y55D5A.1	hypothetical protein	0.692549418	0.254782	0.000319	0.003222	74.32596002
1230	WBGene00021928	Y55F3AM.11	hypothetical protein	-1.472354457	0.239096	4.20E-11	2.24E-08	73.85044639
1231	WBGene00021933	Y55F3AR.2	hypothetical protein	0.957364548	0.195716	5.20E-08	5.13E-06	333.6829292
1232	WBGene00021939	Y55F3BR.2	hypothetical protein	0.534463015	0.178164	0.000184	0.002131	161.2302321
1233	WBGene00013244	Y56A3A.33	hypothetical protein	0.593172078	0.201396	0.000192	0.002196	91.06512294
1234	WBGene00013227	Y56A3A.6	hypothetical protein	0.626512328	0.255839	0.00072	0.006113	94.38579987
1235	WBGene00013228	Y56A3A.7	hypothetical protein	0.355190945	0.119912	0.000378	0.003657	522.8509871
1236	WBGene00013266	Y57A10A.26	hypothetical protein	0.905783821	0.179508	2.43E-08	2.89E-06	309.5411367
1237	WBGene00013253	Y57A10A.8	hypothetical protein	-0.303893291	0.075832	1.12E-05	0.000265	788.9926691
1238	WBGene00044258	Y57G11C.51	hypothetical protein	0.480483536	0.164815	0.000268	0.002824	379.5379052
1239	WBGene00012385	Y5F2A.4	hypothetical protein	-0.313266799	0.070238	1.45E-06	5.91E-05	1734.159726
1240	WBGene00013406	Y63D3A.7	hypothetical protein	0.423264967	0.244635	0.005227	0.027302	879.2664417
1241	WBGene00013418	Y65A5A.1	hypothetical protein	0.566458185	0.163261	3.58E-05	0.000651	212.2357775
1242	WBGene00022029	Y65B4A.6	hypothetical protein	0.40581847	0.196746	0.00306	0.018083	2660.03026

	ENSEMBLE GeneID	SYMBOL	GENENAME	log2FoldChange	lfcSE	pvalue	padj	baseMean
1243	WBGene00022031	Y65B4A.8	hypothetical protein	0.599878229	0.196608	0.000136	0.001709	431.0124137
1244	WBGene00022033	Y65B4BL.1	hypothetical protein	0.899477292	0.676756	0.003765	0.021203	172.3710077
1245	WBGene00013422	Y66A7A.2	Ribonuclease P/MRP protein subunit POP5	-0.348958509	0.105305	0.000122	0.001568	465.2322634
1246	WBGene00013445	Y66D12A.19	hypothetical protein	0.690955639	0.14208	7.77E-08	6.73E-06	436.6582765
1247	WBGene00013448	Y66D12A.24	hypothetical protein	0.420427063	0.170507	0.001154	0.00873	126.9572679
1248	WBGene00013433	Y66D12A.7	Glutamyl-tRNA(Gln) amidotransferase subunit C, mitochondrial	0.335848745	0.214888	0.010348	0.046057	140.8335319
1249	WBGene00022046	Y66H1A.4	Probable H/ACA ribonucleoprotein complex subunit 1-like protein	0.382246986	0.174968	0.002629	0.016175	2230.892543
1250	WBGene00022075	Y69A2AR.3	hypothetical protein	0.425478136	0.70042	0.01086	0.047821	845.1509828
1251	WBGene00022100	Y69A2AR.31	hypothetical protein	0.817027218	0.224371	1.45E-05	0.000322	67.01264319
1252	WBGene00013481	Y69H2.3	hypothetical protein	0.540165858	0.263936	0.002077	0.013556	983.7019089
1253	WBGene00044894	Y71F9AR.4	hypothetical protein	0.430402044	0.216851	0.003232	0.01882	149.6016441
1254	WBGene00022125	Y71F9B.1	hypothetical protein	0.602837083	0.2169	0.000298	0.003069	114.551759
1255	WBGene00022155	Y71G12B.17	hypothetical protein	0.468867433	0.645049	0.010027	0.044941	19.57219202
1256	WBGene00022158	Y71G12B.23	hypothetical protein	0.422758409	0.201658	0.002681	0.016394	96.6363896
1257	WBGene00022180	Y71H2AM.15	hypothetical protein	0.502226812	0.571424	0.008956	0.041316	98.86277876
1258	WBGene00022203	Y73B3A.1	hypothetical protein	0.383996873	0.287271	0.010225	0.045644	991.4046486
1259	WBGene00022250	Y73B6BL.29	tRNA pseudouridine synthase	-0.328854258	0.094636	7.70E-05	0.001128	446.9453653
1260	WBGene00022274	Y73E7A.8	hypothetical protein	0.829870166	0.64643	0.004353	0.023762	47.94461434
1261	WBGene00013550	Y75B8A.14	hypothetical protein	-0.32074293	0.072204	1.65E-06	6.47E-05	1059.552159
1262	WBGene00013543	Y75B8A.6	hypothetical protein	0.775622454	0.231033	4.04E-05	0.000713	200.3528735
1263	WBGene00013544	Y75B8A.7	U3 small nucleolar ribonucleoprotein protein MPP10	0.353215966	0.156664	0.002577	0.015901	813.5833002
1264	WBGene00022298	Y76B12C.4	hypothetical protein	0.598475709	0.32825	0.002776	0.016806	52.32263367
1265	WBGene00022307	Y77E11A.2	hypothetical protein	0.547450453	0.206847	0.000482	0.004475	218.4128713
1266	WBGene00013580	Y79H2A.3	hypothetical protein	0.571110651	0.179242	9.38E-05	0.001297	683.2907024
1267	WBGene00012420	Y7A9D.1	hypothetical protein	0.984625174	0.245663	2.92E-06	9.88E-05	242.2635593
1268	WBGene00022348	Y82E9BR.16	hypothetical protein	0.533426027	0.138138	8.62E-06	0.000222	925.3911574
1269	WBGene00022349	Y82E9BR.17	hypothetical protein	0.318408085	0.110012	0.000572	0.005105	646.5498804
1270	WBGene00022367	Y92H12BM.1	hypothetical protein	0.434408773	0.150245	0.000334	0.003337	198.0994562
1271	WBGene00022376	Y94H6A.3	hypothetical protein	0.457810387	0.228218	0.0029	0.017411	737.4058829
1272	WBGene00022379	Y94H6A.7	hypothetical protein	0.346697529	0.229231	0.010304	0.045909	221.0706988
1273	WBGene00022383	Y95B8A.2	hypothetical protein	0.984348103	0.410981	0.000591	0.005231	68.28453363
1274	WBGene00045434	Y95D11A.3	hypothetical protein	-0.374362347	0.072703	3.57E-08	4.02E-06	1529.191507
1275	WBGene00022398	Y97E10AR.3	hypothetical protein	-0.355288076	0.067037	1.73E-08	2.22E-06	1683.984249
1276	WBGene00022399	Y97E10AR.4	hypothetical protein	-0.416594791	0.098025	2.31E-06	8.31E-05	1043.168584
1277	WBGene00021186	Y9D1A.1	hypothetical protein	1.227005254	0.7385	0.002181	0.014059	780.6879203
1278	WBGene00021187	Y9D1A.2	pseudo	1.323038727	0.473506	0.000188	0.002162	26.25705503
1279	WBGene00022127	yop-1	Receptor expression-enhancing protein	0.41140838	0.188654	0.00234	0.014804	3225.359791
1280	WBGene00006970	zag-1	Zinc finger E-box-binding homeobox protein zag-1	1.102506227	0.31103	1.79E-05	0.00038	77.04184167
1281	WBGene00022519	ZC123.4	hypothetical protein	0.386808127	0.233637	0.00695	0.033923	89.41070146
1282	WBGene00022532	ZC155.4	hypothetical protein	-0.301635707	0.062906	3.06E-07	2.01E-05	3567.155467
1283	WBGene00013859	ZC247.1	hypothetical protein	0.313737011	0.109143	0.000589	0.005224	543.1008245
1284	WBGene00022586	ZC308.4	hypothetical protein	-0.30111651	0.064218	3.84E-07	2.30E-05	4764.699464
1285	WBGene00021047	zfp-3	Zinc Finger Protein	0.756167044	0.277622	0.000295	0.003045	310.4919343
1286	WBGene00021305	zig-11	2 (Zwei) IG domain protein	0.305163529	0.187563	0.011443	0.049561	1726.807674
1287	WBGene00006985	zig-8	Zwei Ig domain protein zig-8	0.423562964	0.401043	0.010834	0.047741	60.68322982
1288	WBGene00021082	zip-11	bZIP transcription factor family	0.359778908	0.248926	0.010373	0.046139	151.3319147
1289	WBGene00012330	zip-3	bZIP transcription factor family	0.311699196	0.159591	0.006214	0.031201	342.8737696
1290	WBGene00017755	zip-8	bZIP transcription factor 8	0.424753368	0.151607	0.000457	0.004292	1612.338291
1291	WBGene00006494	zipt-7.2	Zinc transporter zipt-7.2	0.468413259	0.103497	5.67E-07	2.97E-05	1214.313758
1292	WBGene00014205	ZK1058.5	Methyltransferase-like protein	-0.422939853	0.09138	4.00E-07	2.38E-05	630.6723417
1293	WBGene00014213	ZK1073.1	hypothetical protein	0.333199923	0.161577	0.004365	0.02381	557.3052602
1294	WBGene00014226	ZK1098.11	hypothetical protein	-0.408685625	0.166058	0.001189	0.008903	442.5409744
1295	WBGene00014227	ZK1128.1	Protein arginine methyltransferase NDUFAF7 homolog, mitochondrial	-0.368344075	0.071242	2.64E-08	3.07E-06	1085.453187
1296	WBGene00022881	ZK1248.11	hypothetical protein	-0.318509859	0.06683	3.28E-07	2.08E-05	1590.106054
1297	WBGene00022885	ZK1248.19	hypothetical protein	-0.420934166	0.101366	3.45E-06	0.000113	335.0433198
1298	WBGene00013934	ZK131.11	hypothetical protein	0.411749971	0.13905	0.000303	0.003097	233.1863485
1299	WBGene00022679	ZK180.5	hypothetical protein	1.91166451	0.5789	3.46E-05	0.000633	157.8361447
1300	WBGene00013967	ZK287.7	hypothetical protein	-0.317491314	0.075968	4.85E-06	0.000143	776.9359152
1301	WBGene00022704	ZK353.9	PITH domain-containing protein ZK353.9	-0.341790812	0.073182	4.60E-07	2.59E-05	1381.519884
1302	WBGene00022712	ZK355.2	hypothetical protein	0.671061492	0.219898	0.000123	0.001576	218.706083
1303	WBGene00014018	ZK632.11	hypothetical protein	-0.373041475	0.063917	7.12E-10	1.79E-07	2058.431712
1304	WBGene00014013	ZK632.4	Probable mannose-6-phosphate isomerase	-0.316418601	0.055101	1.53E-09	3.12E-07	3922.172236
1305	WBGene00044762	ZK688.11	hypothetical protein	-0.31302994	0.086213	4.74E-05	0.000802	932.0914454
1306	WBGene00022803	ZK688.9	TIP41-like protein	-0.324443158	0.066418	1.74E-07	1.28E-05	1185.529042
1307	WBGene00014074	ZK757.2	hypothetical protein	0.610577357	0.395325	0.004246	0.023327	36.3571044
1308	WBGene00014086	ZK809.3	hypothetical protein	0.32506192	0.151042	0.003621	0.020592	2856.625526
1309	WBGene00022649	ZK84.1	hypothetical protein	1.10898911	0.592512	0.001694	0.011692	35.88032026
1310	WBGene00014118	ZK858.5	TM2 domain-containing protein ZK858.5	-0.344214125	0.08709	1.10E-05	0.000264	817.4891885
1311	WBGene00014152	ZK930.2	hypothetical protein	-0.384775392	0.155898	0.001309	0.009648	207.4749117
1312	WBGene00022835	ZK973.9	hypothetical protein	0.527784337	0.177749	0.000204	0.002299	997.9640183
1313	WBGene00013683	zoo-1	ZO-1 (Zonula Occludens tight junctional protein) Ortholog	0.508545674	0.148578	4.80E-05	0.000809	410.8105224
1314	WBGene00012988	ztf-22	Zinc finger putative Transcription Factor family	0.501430961	0.209154	0.001054	0.008154	246.6398035
1315	WBGene00013438	ztf-29	Zinc finger putative Transcription Factor family	0.844408753	0.239495	2.09E-05	0.000431	355.7237603
1316	WBGene00013966	ztf-9	Zinc finger putative Transcription Factor family	-0.301479818	0.097035	0.00032	0.003236	472.8847577
1317	WBGene00006999	zyx-1	Zyxin	0.35866357	0.120281	0.000347	0.003436	1180.308149

WB variant	ENSEMBLE gene ID	SYMBOL	GENENAME	log2FoldChange	pvalue	padj
Cuticle morphology	WBGene00015547	ain-1	ALG-1 INteracting protein	0.433179041	1.05E-06	4.66E-05
Cuticle morphology	WBGene00000106	alg-2	Protein argonaute	0.344356241	0.001318	0.009695
Cuticle morphology	WBGene00021922	atg-3	Autophagy-related protein 3	0.692818768	0.000174	0.002046
Cuticle morphology	WBGene00000608	col-19	Cuticle collagen 19	0.633057464	0.000171	0.002017
Cuticle morphology	WBGene00000616	col-39	Cuticle collagen 39	1.431443142	6.28E-06	0.000173
Cuticle morphology	WBGene00000656	col-80	Putative cuticle collagen 80	0.802776789	0.001942	0.012882
Cuticle morphology	WBGene00003400	dapk-1	Death-associated protein kinase dapk-1	0.590438009	1.66E-07	1.23E-05
Cuticle morphology	WBGene00001076	dpy-17	DumPY: shorter than wild-type	1.227347056	8.07E-05	0.001161
Cuticle morphology	WBGene00001077	dpy-18	Prolyl 4-hydroxylase subunit alpha-1	0.325474514	7.06E-06	0.00019
Cuticle morphology	WBGene00001065	dpy-3	DumPY: shorter than wild-type	2.068235176	3.25E-10	1.02E-07
Cuticle morphology	WBGene00001069	dpy-7	Cuticle collagen dpy-7	1.111370763	0.000102	0.001372
Cuticle morphology	WBGene00001186	egl-18	hypothetical protein	0.470112338	8.25E-05	0.001172
Cuticle morphology	WBGene00001215	ego-2	Enhancer of Glp-One (glp-1)	0.476444685	0.001358	0.009926
Cuticle morphology	WBGene00001340	etr-1	ELAV-Type RNA binding-protein family	0.316415315	0.00162	0.011345
Cuticle morphology	WBGene00018772	F53G12.4	hypothetical protein	0.476662974	0.009742	0.043911
Cuticle morphology	WBGene00016173	fust-1	FUS/TLS RNA binding protein homolog	1.129774391	2.88E-05	0.000551
Cuticle morphology	WBGene00001707	grh-1	GRainyHead (Drosophila transcription factor) homolog	0.51561556	0.008152	0.03836
Cuticle morphology	WBGene00018572	lin-42	Period protein homolog lin-42	0.7474291	5.05E-05	0.00084
Cuticle morphology	WBGene00003242	mig-6	Papilin	0.608807877	2.29E-07	1.62E-05
Cuticle morphology	WBGene00015646	mlt-10	hypothetical protein	0.533646855	0.0006	0.005286
Cuticle morphology	WBGene00003623	nhr-25	Nuclear hormone receptor family member nhr-25	0.444516087	0.000205	0.002303
Cuticle morphology	WBGene00004751	sea-2	Signal Element on Autosome	0.525290796	6.23E-05	0.000976
Cuticle morphology	WBGene00004888	smo-1	Small ubiquitin-related modifier	0.539949384	0.007417	0.035665
Cuticle morphology	WBGene00004952	spd-1	hypothetical protein	0.460204197	0.000995	0.007801
Cuticle morphology	WBGene00005018	sqt-3	Cuticle collagen 1	1.271241572	0.000711	0.006063
Cuticle morphology	WBGene00006793	unc-59	hypothetical protein	-0.300058639	1.15E-08	1.52E-06
Cuticle morphology	WBGene00022046	Y66H1A.4	Probable H/ACA ribonucleoprotein complex subunit 1-like protein	0.382246986	0.002629	0.016175
Cuticle morphology	WBGene00006970	zag-1	Zinc finger E-box-binding homeobox protein zag-1	1.102506227	1.79E-05	0.00038
DNA repair	WBGene00011201	nth-1	Endonuclease III homolog	-0.36061458	8.06E-05	0.001161
DNA repair	WBGene00017696	polk-1	DNA polymerase kappa	-0.350690825	2.31E-08	2.8E-06
DNA repair	WBGene00019767	rpa-2	Replication Protein A homolog	0.345458087	0.004511	0.024387
DNA repair	WBGene00006786	unc-51	Serine/threonine-protein kinase unc-51	0.736863794	2.52E-07	1.75E-05
Energy expenditure	WBGene00000371	cox-5B	Cytochrome OXidase assembly protein	0.426891424	0.003349	0.019342
Energy expenditure	WBGene00009245	rict-1	hypothetical protein	0.352634524	1.88E-05	0.000396
Energy expenditure	WBGene00015391	sdha-1	Succinate dehydrogenase [ubiquinone] flavoprotein subunit, mitochondrial	0.371626372	0.000181	0.00211
Energy expenditure	WBGene00009353	sdhd-1	Putative succinate dehydrogenase [ubiquinone] cytochrome b small subunit, mitochondrial	0.302278216	0.009856	0.044281
Energy expenditure	WBGene00020181	T02H6.11	hypothetical protein	0.60407595	0.000219	0.002424
Genotoxicity induced apoptosis	WBGene00001170	egl-1	Programmed cell death activator egl-1	1.372562445	2.56E-11	1.64E-08
Genotoxicity induced apoptosis	WBGene00002042	hus-1	human HUS1 related	-0.469388317	4.57E-11	2.25E-08
Germcell response to Ionizing Radiation	WBGene00012484	car-1	Cytokinesis, Apoptosis, RNA-associated	0.326062253	0.00619	0.031116
Germcell response to Ionizing Radiation	WBGene00000498	chk-1	Serine/threonine-protein kinase chk-1	0.647028743	3.21E-05	0.000603
Germcell response to Ionizing Radiation	WBGene00010325	exos-3	EXOSome (multiexonuclease complex) component	-0.317099004	1.1E-06	4.8E-05
Germcell response to Ionizing Radiation	WBGene00013095	ing-3	Inhibitor of growth protein	0.337792918	0.00056	0.005022
Germcell response to Ionizing Radiation	WBGene00004298	rad-54	hypothetical protein	-0.328706982	3.83E-06	0.000121
Germcell response to Ionizing Radiation	WBGene00010923	rle-1	Regulation of longevity by E3 ubiquitin-protein ligase	0.316099119	6.99E-05	0.001052
Germcell response to Ionizing Radiation	WBGene00022046	Y66H1A.4	Probable H/ACA ribonucleoprotein complex subunit 1-like protein	0.382246986	0.002629	0.016175
Lipid metabolism	WBGene00016507	abhd-5.2	Abhydrolase domain-containing protein abhd-5.2	-0.385250492	0.000123	0.001576
Lipid metabolism	WBGene00020366	acdh-10	Probable medium-chain specific acyl-CoA dehydrogenase 10, mitochondrial	0.333466049	8.04E-05	0.00116
Lipid metabolism	WBGene00008565	acox-1.2	Acyl-coenzyme A oxidase	0.355092148	7.23E-06	0.000193
Lipid metabolism	WBGene00021922	atg-3	Autophagy-related protein 3	0.692818768	0.000174	0.002046
Lipid metabolism	WBGene00000231	atx-2	Ataxin-2 homolog	0.30452198	0.011162	0.048699
Lipid metabolism	WBGene00015011	B0041.8	hypothetical protein	-0.331712248	6.35E-09	9.26E-07
Lipid metabolism	WBGene00012713	bckd-1A	2-oxoisovalerate dehydrogenase subunit alpha	0.418074938	0.000535	0.004851
Lipid metabolism	WBGene00000691	col-117	COLlagen	1.801621387	4.93E-10	1.38E-07
Lipid metabolism	WBGene00000594	col-117	COLlagen	1.061249334	0.000167	0.001987
Lipid metabolism	WBGene00000693	col-119	COLlagen	0.745140994	0.001685	0.011644
Lipid metabolism	WBGene00000699	col-125	COLlagen	1.205242415	0.00287	0.017272
Lipid metabolism	WBGene00000371	cox-5B	Cytochrome OXidase assembly protein	0.426891424	0.003349	0.019342
Lipid metabolism	WBGene00009161	cox-7C	Cytochrome OXidase assembly protein	0.881349024	0.003559	0.02029
Lipid metabolism	WBGene00000830	ctl-1	Catalase-2	0.521888802	0.000571	0.005097
Lipid metabolism	WBGene00000901	daf-5	hypothetical protein	0.592706516	1.01E-06	4.53E-05
Lipid metabolism	WBGene00008549	din-1	Daf-12-interacting protein 1	0.315527612	0.000887	0.007174
Lipid metabolism	WBGene00001113	dur-1	Dauer Up-Regulated	0.360129802	0.001418	0.010229
Lipid metabolism	WBGene00012768	eef-1B.2	Probable elongation factor 1-beta/1-delta 2	0.430991285	0.001594	0.011247
Lipid metabolism	WBGene00008578	F08G2.7	hypothetical protein	0.779294044	6.71E-05	0.001024
Lipid metabolism	WBGene00017416	F13B6.1	hypothetical protein	0.537554892	0.008511	0.039713
Lipid metabolism	WBGene00008743	F13D12.9	hypothetical protein	0.568674176	0.004566	0.024634
Lipid metabolism	WBGene00001397	fat-5	Delta(9)-fatty-acid desaturase fat-5	0.71441255	5.39E-07	2.88E-05
Lipid metabolism	WBGene00019207	fgt-1	Facilitated glucose transporter protein 1	0.374377906	0.000301	0.003085
Lipid metabolism	WBGene00001460	flp-17	FMRF-Like Peptide	-0.376965751	0.001879	0.012618
Lipid metabolism	WBGene00020160	igcm-3	ImmunoGlobulin-like Cell adhesion Molecule family	0.338163663	7.12E-05	0.001063
Lipid metabolism	WBGene00012148	inos-1	INOsitol-3-phosphate Synthase	0.839229395	7.05E-06	0.00019
Lipid metabolism	WBGene00002184	kel-1	KELch-repeat containing protein	0.48264592	0.003312	0.019191
Lipid metabolism	WBGene00002977	lev-10	hypothetical protein	0.467643019	0.000135	0.001696
Lipid metabolism	WBGene00002990	lin-1	hypothetical protein	0.648274911	0.00011	0.00145
Lipid metabolism	WBGene00022642	lipl-5	Lipase	0.357195708	0.001333	0.009764
Lipid metabolism	WBGene00003064	lpd-8	LiPid Depleted	-0.319336261	7.09E-08	6.32E-06
Lipid metabolism	WBGene00022610	ltah-1.2	LeukoTriene A4 Hydrolase homolog	0.385876168	0.000118	0.001529
Lipid metabolism	WBGene00003119	mac-1	Protein mac-1	0.791460194	1.02E-06	4.53E-05
Lipid metabolism	WBGene00009306	maph-1.1	Microtubule-associated protein homolog maph-1.1	0.770301052	1.55E-07	1.2E-05
Lipid metabolism	WBGene00009113	maph-1.2	Microtubule-Associated Protein Homolog	0.384520699	0.005791	0.029515
Lipid metabolism	WBGene00007966	maph-1.3	Microtubule-Associated Protein Homolog	0.591172343	0.000162	0.001936
Lipid metabolism	WBGene00003623	nhr-25	Nuclear hormone receptor family member nhr-25	0.444516087	0.000205	0.002303
Lipid metabolism	WBGene00003749	nlp-11	Neuropeptide-like peptide 11	-0.432273295	0.000597	0.005272
Lipid metabolism	WBGene00003750	nlp-12	Neuropeptide-Like Protein	1.058044817	0.000505	0.004647
Lipid metabolism	WBGene00009176	nmat-2	Nicotinamide/nicotinic acid mononucleotide adenylyltransferase 2	-0.302789978	0.001555	0.011008
Lipid metabolism	WBGene00003825	ntl-2	NOT-Like (yeast CCR4/NOT complex component)	0.39027511	0.00053	0.004819
Lipid metabolism	WBGene00004013	pha-4	Defective pharyngeal development protein 4	0.368272564	0.00374	0.021098
Lipid metabolism	WBGene00004076	pod-2	hypothetical protein	0.660141809	1.32E-07	1.03E-05
Lipid metabolism	WBGene00004154	pqn-72	Prion-like-(Q/N-rich)-domain-bearing protein	0.768111316	0.000537	0.004868
Lipid metabolism	WBGene00011253	R11H6.5	hypothetical protein	-0.40670309	5.53E-08	5.22E-06
Lipid metabolism	WBGene00004271	rab-7	RAB family	0.310503908	0.005222	0.027295
Lipid metabolism	WBGene00009245	rict-1	hypothetical protein	0.352634524	1.88E-05	0.000396
Lipid metabolism	WBGene00004472	rps-3	40S ribosomal protein S3	0.343782316	0.008776	0.040663
Lipid metabolism	WBGene00015391	sdha-1	Succinate dehydrogenase [ubiquinone] flavoprotein subunit, mitochondrial	0.371626372	0.000181	0.00211
Lipid metabolism	WBGene00019300	swt-1	Sugar transporter SWEET1	-0.704903581	5.58E-07	2.94E-05
Lipid metabolism	WBGene00006588	tnt-3	TropoNin T	0.47168447	0.000137	0.00172

WB variant	ENSEMBLE gene ID	SYMBOL	GENENAME	log2FoldChange	pvalue	padj
Lipid metabolism	WBGene00022783	tomm-7	Mitochondrial import receptor subunit TOM7 homolog	-0.429544654	0.001486	0.010624
Lipid metabolism	WBGene00006796	unc-62	Homeobox protein unc-62	0.501547291	8.47E-06	0.00022
Lipid metabolism	WBGene00012369	W09G3.6	hypothetical protein	0.346854391	0.000527	0.004799
Mitochondrial content	WBGene00009245	rict-1	hypothetical protein	0.352634524	1.88E-05	0.000396
Mitochondrial content	WBGene00006786	unc-51	Serine/threonine-protein kinase unc-51	0.736863794	2.52E-07	1.75E-05
Mitochondrial metabolism	WBGene00012354	cox-4	Cytochrome OXidase assembly protein	0.514435837	0.001373	0.010003
Mitochondrial metabolism	WBGene00020511	immt-1	MICOS complex subunit MIC60-1	0.375589245	0.000179	0.002094
Mitochondrial metabolism	WBGene00002280	let-2	Collagen alpha-2(IV) chain	0.66279107	2.24E-05	0.000454
Mitochondrial metabolism	WBGene00016539	madd-2	hypothetical protein	0.426998303	0.000682	0.005865
Mitochondrial metabolism	WBGene00021677	pgs-1	CDP-diacylglycerol--glycerol-3-phosphate 3-phosphatidyltransferase	-0.364817651	2.86E-06	9.71E-05
Mitochondrial metabolism	WBGene00009245	rict-1	hypothetical protein	0.352634524	1.88E-05	0.000396
Mitochondrial metabolism	WBGene00008262	ril-1	RNAi-Induced Longevity	0.50881635	0.000853	0.006965
Mitochondrial metabolism	WBGene00015391	sdha-1	Succinate dehydrogenase [ubiquinone] flavoprotein subunit, mitochondrial	0.371626372	0.000181	0.00211
Mitochondrial metabolism	WBGene00006787	unc-52	Basement membrane proteoglycan	0.63287148	5.53E-08	5.22E-06
Mitochondrial respiratory chain subunit	WBGene00010960	ATP6	ATP synthase F0 subunit 6	-0.432902342	6.49E-05	0.001
Mitochondrial respiratory chain subunit	WBGene00010964	COX1	cytochrome c oxidase subunit I	-0.564287741	7.97E-10	1.86E-07
Mitochondrial respiratory chain subunit	WBGene00010965	COX2	cytochrome c oxidase subunit II	-0.591370434	4.22E-09	6.72E-07
Mitochondrial respiratory chain subunit	WBGene00010962	COX3	cytochrome c oxidase subunit III	-0.392635368	6.17E-06	0.000171
Mitochondrial respiratory chain subunit	WBGene00010959	ND1	NADH dehydrogenase subunit 1	-0.390223041	0.000114	0.001489
Mitochondrial respiratory chain subunit	WBGene00010961	ND2	NADH dehydrogenase subunit 2	-0.5554557	0.000325	0.003276
Mitochondrial respiratory chain subunit	WBGene00010966	ND3	NADH dehydrogenase subunit 3	-0.670390104	0.000155	0.00188
Mitochondrial respiratory chain subunit	WBGene00010963	ND4	NADH dehydrogenase subunit 4	-0.412938897	0.000547	0.004935
Mitochondrial respiratory chain subunit	WBGene00010967	ND5	NADH dehydrogenase subunit 5	-0.445125282	0.001466	0.010527
N2 oxidative stressed	WBGene00000149	apl-1	Amyloid-beta-like protein	0.41887973	5.82E-05	0.000938
N2 oxidative stressed	WBGene00000170	aqp-2	AQuaPorin or aquaglyceroporin related	0.931834793	3.06E-07	2.01E-05
N2 oxidative stressed	WBGene00020275	atp-4	ATP synthase subunit	0.360239329	0.009967	0.044719
N2 oxidative stressed	WBGene00007144	B0334.4	hypothetical protein	-0.303459196	2.92E-07	1.96E-05
N2 oxidative stressed	WBGene00007449	C08F8.9	hypothetical protein	0.950080739	0.001796	0.012176
N2 oxidative stressed	WBGene00016274	C30G12.2	hypothetical protein	0.982717359	5.24E-15	2.24E-11
N2 oxidative stressed	WBGene00016493	C37A2.7	60S acidic ribosomal protein P2	1.142912694	0.001328	0.009749
N2 oxidative stressed	WBGene00016494	C37A2.8	hypothetical protein	-0.436475052	1.73E-07	1.28E-05
N2 oxidative stressed	WBGene00020391	cct-7	Chaperonin Containing TCP-1	0.619496598	2E-05	0.000416
N2 oxidative stressed	WBGene00000472	cey-1	C. Elegans Y-box	0.430481728	2.71E-05	0.000527
N2 oxidative stressed	WBGene00000475	cey-4	C. Elegans Y-box	0.863667658	0.000217	0.00241
N2 oxidative stressed	WBGene00000678	col-104	COLlagen	1.167653644	0.000334	0.003337
N2 oxidative stressed	WBGene00000681	col-107	COLlagen	1.279468021	0.004096	0.02266
N2 oxidative stressed	WBGene00000683	col-109	COLlagen	0.857804454	0.004674	0.025023
N2 oxidative stressed	WBGene00000704	col-130	COLlagen	1.389667138	0.000206	0.00231
N2 oxidative stressed	WBGene00000728	col-155	Putative cuticle collagen 155	0.745088271	0.000104	0.001398
N2 oxidative stressed	WBGene00000739	col-166	COLlagen	1.304997162	5.94E-08	5.41E-06
N2 oxidative stressed	WBGene00000740	col-167	COLlagen	1.200948359	0.003423	0.019686
N2 oxidative stressed	WBGene00000625	col-48	COLlagen	1.365118076	6.74E-06	0.000183
N2 oxidative stressed	WBGene00000653	col-77	COLlagen	1.003842472	0.00058	0.005155
N2 oxidative stressed	WBGene00000657	col-81	COLlagen	1.035489211	0.000335	0.003341
N2 oxidative stressed	WBGene00000670	col-95	COLlagen	0.400486733	0.006414	0.031965
N2 oxidative stressed	WBGene00010723	cpg-7	Chondroitin proteoglycan 7	0.592513718	0.000734	0.006195
N2 oxidative stressed	WBGene00019357	cpg-8	Chondroitin proteoglycan 8	0.984170332	0.000299	0.003073
N2 oxidative stressed	WBGene00000776	cpl-1	CathePsin L family	0.623346133	4.11E-05	0.000723
N2 oxidative stressed	WBGene00000928	dao-2	Dauer or Aging adult Overexpression	0.608670964	0.000581	0.005159
N2 oxidative stressed	WBGene00000941	ddp-1	Mitochondrial import inner membrane translocase subunit Tim8	0.692232561	0.005602	0.028767
N2 oxidative stressed	WBGene00001000	dim-1	Disorganized muscle protein 1	0.454243506	3.62E-07	2.21E-05
N2 oxidative stressed	WBGene00001235	elb-1	ELongin B	0.836479786	0.000187	0.002155
N2 oxidative stressed	WBGene00001236	elc-1	ELongin C	0.860968489	7.61E-08	6.68E-06
N2 oxidative stressed	WBGene00008973	F20D1.1	hypothetical protein	0.659805063	5.35E-06	0.000154
N2 oxidative stressed	WBGene00044666	F33G12.7	hypothetical protein	-0.382452563	0.001815	0.012294
N2 oxidative stressed	WBGene00009659	F43G6.7	hypothetical protein	1.525170003	1.45E-05	0.000322
N2 oxidative stressed	WBGene00009688	F44E5.1	hypothetical protein	0.727707334	0.004587	0.024703
N2 oxidative stressed	WBGene00009982	F53F1.4	hypothetical protein	1.205855838	1.06E-08	1.42E-06
N2 oxidative stressed	WBGene00019061	F58F12.1	ATP synthase subunit delta, mitochondrial	0.489714951	0.008527	0.039776
N2 oxidative stressed	WBGene00001423	fib-1	rRNA 2'-O-methyltransferase fibrillarin	0.572167905	1.97E-05	0.000411
N2 oxidative stressed	WBGene00001430	fkb-5	Peptidylprolyl isomerase	0.388162624	0.00017	0.002013
N2 oxidative stressed	WBGene00001725	grl-16	GRound-Like (grd related)	1.42038032	2.55E-06	8.93E-05
N2 oxidative stressed	WBGene00001713	grl-4	GRound-Like (grd related)	0.686393356	2.02E-07	1.44E-05
N2 oxidative stressed	WBGene00001922	his-48	Probable histone H2B 4	1.007813834	0.000885	0.007167
N2 oxidative stressed	WBGene00001942	his-68	Histone H2A	0.4043148	0.008151	0.03836
N2 oxidative stressed	WBGene00001877	his-68	Histone H2A	1.671209005	1.58E-06	6.21E-05
N2 oxidative stressed	WBGene00001881	his-68	Histone H2A	1.370385549	2.39E-05	0.000476
N2 oxidative stressed	WBGene00001935	his-68	Histone H2A	1.228924648	1.27E-06	5.31E-05
N2 oxidative stressed	WBGene00001921	his-68	Histone H2A	1.208132037	0.002536	0.015726
N2 oxidative stressed	WBGene00002000	hrp-2	human HnRNP A1 homolog	0.445298839	1.11E-05	0.000265
N2 oxidative stressed	WBGene00002007	hsp-3	Heat shock 70 kDa protein C	0.407981414	1.73E-05	0.000372
N2 oxidative stressed	WBGene00002065	iff-2	Eukaryotic translation initiation factor 5A-2	0.724049881	9.03E-07	4.12E-05
N2 oxidative stressed	WBGene00002280	let-2	Collagen alpha-2(IV) chain	0.66279107	2.24E-05	0.000454
N2 oxidative stressed	WBGene00002978	lev-11	Tropomyosin	0.695674207	5.79E-06	0.000164
N2 oxidative stressed	WBGene00003025	lin-40	hypothetical protein	1.01466607	5.93E-08	5.41E-06
N2 oxidative stressed	WBGene00003893	ost-1	SPARC	0.460955034	1.41E-07	1.1E-05
N2 oxidative stressed	WBGene00011059	R06C1.4	hypothetical protein	0.756334354	1.33E-06	5.54E-05
N2 oxidative stressed	WBGene00011289	R102.2	hypothetical protein	0.632039703	0.001031	0.007985
N2 oxidative stressed	WBGene00004277	rab-18	Ras-related protein Rab-18	0.420797343	5.91E-06	0.000166
N2 oxidative stressed	WBGene00004300	ram-2	hypothetical protein	1.369637269	0.001401	0.010153
N2 oxidative stressed	WBGene00004432	rpl-20	60S ribosomal protein L18a	0.395424077	0.003647	0.020692
N2 oxidative stressed	WBGene00004440	rpl-26	60S ribosomal protein L26	1.188202017	0.00071	0.006055
N2 oxidative stressed	WBGene00004419	rpl-7A	60S ribosomal protein L7a	0.414067374	0.011169	0.048699
N2 oxidative stressed	WBGene00004481	rps-12	40S ribosomal protein S12	0.988589689	0.002158	0.013955
N2 oxidative stressed	WBGene00004495	rps-26	40S ribosomal protein S26	0.871550327	0.00112	0.00853
N2 oxidative stressed	WBGene00004499	rps-30	40S ribosomal protein S30	0.343944573	0.011088	0.048475
N2 oxidative stressed	WBGene00004700	rsp-3	Probable splicing factor, arginine/serine-rich 3	0.391335523	0.005717	0.02923
N2 oxidative stressed	WBGene00009353	sdhd-1	Putative succinate dehydrogenase [ubiquinone] cytochrome b small subunit, mitochondrial	0.302278216	0.009856	0.044281
N2 oxidative stressed	WBGene00021335	spp-23	SaPosin-like Protein family	1.570349759	7.54E-07	3.61E-05
N2 oxidative stressed	WBGene00006366	sym-1	hypothetical protein	0.473844291	0.001275	0.009461
N2 oxidative stressed	WBGene00020181	T02H6.11	hypothetical protein	0.60407595	0.000219	0.002424
N2 oxidative stressed	WBGene00006587	tnt-2	TropoNin T	0.539477773	0.005873	0.029813
N2 oxidative stressed	WBGene00022783	tomm-7	Mitochondrial import receptor subunit TOM7 homolog	-0.429544654	0.001486	0.010624
N2 oxidative stressed	WBGene00022122	trap-1	TRanslocon-Associated Protein	0.64953203	2.6E-05	0.000511
N2 oxidative stressed	WBGene00020216	trap-2	Translocon-associated protein subunit beta	0.583203373	0.00011	0.001449
N2 oxidative stressed	WBGene00006436	ttn-1	Titin homolog	0.483249059	9.02E-05	0.001259
N2 oxidative stressed	WBGene00006715	ubc-20	UBiquitin Conjugating enzyme	0.37373648	0.001885	0.012618

WB variant	ENSEMBLE gene ID	SYMBOL	GENENAME	log2FoldChange	pvalue	padj
N2 oxidative stressed	WBGene00006754	unc-15	Paramyosin	0.548774481	9.43E-05	0.0013
N2 oxidative stressed	WBGene00006789	unc-54	Myosin-4	0.992504488	6.67E-05	0.001022
N2 oxidative stressed	WBGene00006912	vha-3	V-type proton ATPase 16 kDa proteolipid subunit 2/3	0.385599258	0.000355	0.00348
N2 oxidative stressed	WBGene00006924	vig-1	VIG (Drosophila Vasa Intronic Gene) ortholog	0.466191105	0.000464	0.004349
N2 oxidative stressed	WBGene00044431	W03G9.8	hypothetical protein	-0.328878933	0.001097	0.008412
N2 oxidative stressed	WBGene00021883	Y54G2A.18	hypothetical protein	0.842891382	0.001592	0.011237
N2 oxidative stressed	WBGene00013406	Y63D3A.7	hypothetical protein	0.423264967	0.005227	0.027302
N2 oxidative stressed	WBGene00022029	Y65B4A.6	hypothetical protein	0.40581847	0.00306	0.018083
N2 oxidative stressed	WBGene00022075	Y69A2AR.3	hypothetical protein	0.425478136	0.01086	0.047821
N2 oxidative stressed	WBGene00013859	ZC247.1	hypothetical protein	0.313737011	0.000589	0.005224
N2 oxidative stressed	WBGene00022679	ZK180.5	hypothetical protein	1.91166451	3.46E-05	0.000633
Organism response to Ionizing Radiation	WBGene00000498	chk-1	Serine/threonine-protein kinase chk-1	0.647028743	3.21E-05	0.000603
Organism response to Ionizing Radiation	WBGene00001250	elt-2	Transcription factor elt-2	0.378992143	0.001919	0.012774
Organism response to Ionizing Radiation	WBGene00010325	exos-3	EXOSome (multiexonuclease complex) component	-0.317099004	1.1E-06	4.8E-05
Organism response to Ionizing Radiation	WBGene00017984	F32D1.5	GMP reductase	0.397116442	0.000513	0.004693
Organism response to Ionizing Radiation	WBGene00002042	hus-1	human HUS1 related	-0.469388317	4.57E-11	2.25E-08
Organism response to Ionizing Radiation	WBGene00013095	ing-3	Inhibitor of growth protein	0.337792918	0.00056	0.005022
Organism response to Ionizing Radiation	WBGene00003025	lin-40	hypothetical protein	1.01466607	5.93E-08	5.41E-06
Organism response to Ionizing Radiation	WBGene00003515	myo-3	Myosin-3	0.332304713	0.002408	0.015109
Organism response to Ionizing Radiation	WBGene00019767	rpa-2	Replication Protein A homolog	0.345458087	0.004511	0.024387
Organism response to Ionizing Radiation	WBGene00006587	tnt-2	TropoNin T	0.539477773	0.005873	0.029813
Organism response to Ionizing Radiation	WBGene00011559	umps-1	Orotidine 5'-phosphate decarboxylase	0.388000408	0.004428	0.024047
Organism response to Ionizing Radiation	WBGene00012964	Y48A6B.3	Putative H/ACA ribonucleoprotein complex subunit 2-like protein	1.172148283	9.05E-08	7.45E-06
Organism response to Ionizing Radiation	WBGene00022046	Y66H1A.4	Probable H/ACA ribonucleoprotein complex subunit 1-like protein	0.382246986	0.002629	0.016175
Oxidative stress	WBGene00012928	aakb-2	AMP-Activated Kinase Beta subunit	0.704067441	7.13E-07	3.48E-05
Oxidative stress	WBGene00000830	ctl-1	Catalase-2	0.521888802	0.000571	0.005097
Oxidative stress	WBGene00001768	gst-20	Glutathione S-Transferase	0.619246674	1.04E-05	0.000256
Oxidative stress	WBGene00004930	sod-1	Superoxide dismutase [Cu-Zn]	0.32510875	0.001109	0.008474
Oxidative stress	WBGene00014028	trxr-2	Probable glutathione reductase 2	-0.30833009	0.002304	0.014605
Oxidative stress	WBGene00007100	asps-1	ASPScr1 (ASPSCR1) homolog	-0.355639313	2.73E-08	3.16E-06
Oxidative stress	WBGene00017926	cox-6C	Cytochrome OXidase assembly protein	0.507203885	0.008296	0.038869
Oxidative stress	WBGene00000776	cpl-1	CathePsin L family	0.623346133	4.11E-05	0.000723
Oxidative stress	WBGene00001170	egl-1	Programmed cell death activator egl-1	1.372562445	2.56E-11	1.64E-08
Oxidative stress	WBGene00001186	egl-18	hypothetical protein	0.470112338	8.25E-05	0.001172
Oxidative stress	WBGene00001253	elt-6	Erythroid-Like Transcription factor family	0.498529235	0.005859	0.029767
Oxidative stress	WBGene00017416	F13B6.1	hypothetical protein	0.537554892	0.008511	0.039713
Oxidative stress	WBGene00003242	mig-6	Papilin	0.608807877	2.29E-07	1.62E-05
Oxidative stress	WBGene00012361	mrpl-12	Mitochondrial Ribosomal Protein, Large	0.39636145	0.003697	0.020929
Oxidative stress	WBGene00011201	nth-1	Endonuclease III homolog	-0.36061458	8.06E-05	0.001161
Oxidative stress	WBGene00003931	pat-4	Integrin-linked protein kinase homolog pat-4	0.333291408	0.000529	0.004812
Oxidative stress	WBGene00004013	pha-4	Defective pharyngeal development protein 4	0.368272564	0.00374	0.021098
Oxidative stress	WBGene00044305	rad-8	Reticulon-4-interacting protein 1, mitochondrial	-0.316062552	5.58E-08	5.22E-06
Oxidative stress	WBGene00012124	T28D6.4	hypothetical protein	0.72196596	0.000354	0.003478
Oxidative stress	WBGene00007099	trx-2	Probable thioredoxin-2	-0.332690419	4.82E-08	4.87E-06
Oxidative stress	WBGene00022180	Y71H2AM.15	hypothetical protein	0.502226812	0.008956	0.041316
Oxidative stress	WBGene00014086	ZK809.3	hypothetical protein	0.32506192	0.003621	0.020592
Programmed cell death	WBGene00000066	act-4	Actin-4	0.716588298	9.45E-06	0.000238
Programmed cell death	WBGene00000067	act-5	ACTin	0.606783569	9.25E-07	4.19E-05
Programmed cell death	WBGene00000123	ama-1	DNA-directed RNA polymerase II subunit RPB1	0.339749104	4.23E-05	0.000741
Programmed cell death	WBGene00021922	atg-3	Autophagy-related protein 3	0.692818768	0.000174	0.002046
Programmed cell death	WBGene00020706	atg-9	Autophagy-related protein 9	0.474106118	0.000631	0.0055
Programmed cell death	WBGene00010419	atp-1	ATP synthase subunit alpha, mitochondrial	0.518834935	0.000393	0.003775
Programmed cell death	WBGene00020275	atp-4	ATP synthase subunit	0.360239329	0.009967	0.044719
Programmed cell death	WBGene00015156	B0361.2	CWF19-like protein 2 homolog	-0.362814874	1.22E-09	2.61E-07
Programmed cell death	WBGene00008346	C56A3.8	hypothetical protein	-0.339151781	9.88E-06	0.000247
Programmed cell death	WBGene00012484	car-1	Cytokinesis, Apoptosis, RNA-associated	0.326062253	0.00619	0.031116
Programmed cell death	WBGene00020391	cct-7	Chaperonin Containing TCP-1	0.619496598	2E-05	0.000416
Programmed cell death	WBGene00000426	ced-12	Cell death abnormality protein 12	-0.318630367	4.22E-07	2.47E-05
Programmed cell death	WBGene00000455	ceh-34	Homeobox protein ceh-34	0.556967819	0.003633	0.020642
Programmed cell death	WBGene00000469	ces-2	Cell death specification protein 2	0.456395534	0.003545	0.020229
Programmed cell death	WBGene00000498	chk-1	Serine/threonine-protein kinase chk-1	0.647028743	3.21E-05	0.000603
Programmed cell death	WBGene00000776	cpl-1	CathePsin L family	0.623346133	4.11E-05	0.000723
Programmed cell death	WBGene00003400	dapk-1	Death-associated protein kinase dapk-1	0.590438009	1.66E-07	1.23E-05
Programmed cell death	WBGene00001168	eef-1A.1	Elongation factor 1-alpha	0.362980287	0.00651	0.032319
Programmed cell death	WBGene00001170	egl-1	Programmed cell death activator egl-1	1.372562445	2.56E-11	1.64E-08
Programmed cell death	WBGene00001232	eif-3.I	Eukaryotic translation initiation factor 3 subunit I	0.445179671	0.000541	0.004889
Programmed cell death	WBGene00001340	etr-1	ELAV-Type RNA binding-protein family	0.316415315	0.00162	0.011345
Programmed cell death	WBGene00010325	exos-3	EXOSome (multiexonuclease complex) component	-0.317099004	1.1E-06	4.8E-05
Programmed cell death	WBGene00001377	eya-1	Eyes absent homolog 1	0.652554362	4.29E-09	6.72E-07
Programmed cell death	WBGene00007703	gbf-1	hypothetical protein	0.422709852	1.07E-05	0.000259
Programmed cell death	WBGene00021697	gcn-1	GCN (yeast General Control Nondrepressible) homolog	0.472838373	3.42E-07	2.13E-05
Programmed cell death	WBGene00001867	him-8	High Incidence of Males (increased X chromosome loss)	-0.36375949	6.67E-07	3.32E-05
Programmed cell death	WBGene00001898	his-24	Histone H1.1	1.272969384	0.000191	0.002182
Programmed cell death	WBGene00001942	his-68	Histone H2A	0.4043148	0.008151	0.03836
Programmed cell death	WBGene00001877	his-3	Histone H2A	1.671209005	1.58E-06	6.21E-05
Programmed cell death	WBGene00001881	his-7	Histone H2A	1.370385549	2.39E-05	0.000476
Programmed cell death	WBGene00001935	his-61	Histone H2A	1.228924648	1.27E-06	5.31E-05
Programmed cell death	WBGene00001921	his-47	Histone H2A	1.208132037	0.002536	0.015726
Programmed cell death	WBGene00002000	hrp-2	human HnRNP A1 homolog	0.445298839	1.11E-05	0.000265
Programmed cell death	WBGene00002042	hus-1	human HUS1 related	-0.469388317	4.57E-11	2.25E-08
Programmed cell death	WBGene00013095	ing-3	Inhibitor of growth protein	0.337792918	0.00056	0.005022
Programmed cell death	WBGene00002179	jph-1	JunctoPHilin	0.469818039	0.000233	0.002536
Programmed cell death	WBGene00003102	mab-5	Homeobox protein mab-5	0.686321291	0.000752	0.006328
Programmed cell death	WBGene00013096	mcd-1	Modifier of cell death	0.567337655	0.000474	0.00442
Programmed cell death	WBGene00003156	mcm-4	DNA replication licensing factor mcm-4	0.396521982	0.002189	0.0141
Programmed cell death	WBGene00003588	nex-1	Annexin	0.561220173	0.000113	0.001475
Programmed cell death	WBGene00003589	nex-2	Annexin	0.376062347	0.000825	0.006802
Programmed cell death	WBGene00003597	nhl-1	RING finger protein nhl-1	0.329042014	0.004419	0.02402
Programmed cell death	WBGene00003623	nhr-25	Nuclear hormone receptor family member nhr-25	0.444516087	0.000205	0.002303
Programmed cell death	WBGene00018636	oef-1	Oocyte Excluded Factor	-0.30722045	4.32E-08	4.53E-06
Programmed cell death	WBGene00003947	pbs-1	Proteasome subunit beta type	0.616289295	0.000524	0.004778
Programmed cell death	WBGene00003948	pbs-2	Proteasome subunit beta type	0.528384252	0.001726	0.011866
Programmed cell death	WBGene00003951	pbs-5	Proteasome subunit pbs-5	0.600722619	0.000491	0.004545
Programmed cell death	WBGene00008641	pch-2	Putative pachytene checkpoint protein 2	-0.369836912	6.19E-09	9.15E-07
Programmed cell death	WBGene00003955	pcn-1	Proliferating cell nuclear antigen	0.60735647	9.53E-05	0.001309
Programmed cell death	WBGene00004075	pod-1	hypothetical protein	0.676934959	2.73E-05	0.00053
Programmed cell death	WBGene00004128	pqn-41	Polyglutamine-repeat protein pqn-41	0.825936443	0.000107	0.001424

Programmed cell death	WBGene00004271	rab-7	RAB family	0.310503908	0.005222	0.027295
WB variant	**ENSEMBLE gene ID**	**SYMBOL**	**GENENAME**	**log2FoldChange**	**pvalue**	**padj**
Programmed cell death	WBGene00004298	rad-54	hypothetical protein	-0.328706982	3.83E-06	0.000121
Programmed cell death	WBGene00004387	rnp-4	RNA-binding protein 8A	0.362085964	0.005709	0.029214
Programmed cell death	WBGene00018819	rog-1	Ras activating factor in development Of Germline	0.312511426	0.008335	0.039007
Programmed cell death	WBGene00021845	rpb-7	RNA Polymerase II (B) subunit	0.842437022	1.54E-06	6.11E-05
Programmed cell death	WBGene00004424	rpl-12	60S ribosomal protein L12	0.36665943	0.00666	0.032834
Programmed cell death	WBGene00004425	rpl-13	60S ribosomal protein L13	0.815882076	0.002786	0.016855
Programmed cell death	WBGene00004430	rpl-18	60S ribosomal protein L18	0.875926254	0.004458	0.024169
Programmed cell death	WBGene00004431	rpl-19	60S ribosomal protein L19	0.517314248	0.006353	0.031724
Programmed cell death	WBGene00004432	rpl-20	60S ribosomal protein L18a	0.395424077	0.003647	0.020692
Programmed cell death	WBGene00004440	rpl-26	60S ribosomal protein L26	1.188202017	0.00071	0.006055
Programmed cell death	WBGene00004479	rps-10	Ribosomal Protein, Small subunit	0.367326615	0.005466	0.028237
Programmed cell death	WBGene00004489	rps-20	Ribosomal Protein, Small subunit	0.762972918	0.000675	0.005823
Programmed cell death	WBGene00004495	rps-26	40S ribosomal protein S26	0.871550327	0.00112	0.00853
Programmed cell death	WBGene00004472	rps-3	40S ribosomal protein S3	0.343782316	0.008776	0.040663
Programmed cell death	WBGene00004475	rps-6	40S ribosomal protein S6	0.610424505	0.006078	0.030646
Programmed cell death	WBGene00004478	rps-9	40S ribosomal protein S9	0.798247224	0.001293	0.009564
Programmed cell death	WBGene00011935	scrm-1	Phospholipid scramblase	0.45706567	0.000651	0.005638
Programmed cell death	WBGene00011887	set-17	SET (trithorax/polycomb) domain containing	-0.329240024	1.2E-05	0.000278
Programmed cell death	WBGene00004927	snx-1	Sorting NeXin	0.743688461	3.07E-07	2.01E-05
Programmed cell death	WBGene00020181	T02H6.11	hypothetical protein	0.60407595	0.000219	0.002424
Programmed cell death	WBGene00007217	tads-1	Temporal Asymmetry between Division of Sister cells	-0.347020823	1.11E-11	8.89E-09
Programmed cell death	WBGene00006565	tfg-1	human TFG related	1.107064641	0.000153	0.001855
Programmed cell death	WBGene00009186	trcs-1	TRansport of membrane to Cell Surface	-0.338754534	6.68E-06	0.000182
Programmed cell death	WBGene00006725	ubl-1	Ubiquitin-like protein 1	0.801769512	0.003039	0.018025
Programmed cell death	WBGene00006786	unc-51	Serine/threonine-protein kinase unc-51	0.736863794	2.52E-07	1.75E-05
Programmed cell death	WBGene00006793	unc-59	hypothetical protein	-0.300058639	1.15E-08	1.52E-06
Programmed cell death	WBGene00006796	unc-62	Homeobox protein unc-62	0.501547291	8.47E-06	0.00022
Programmed cell death	WBGene00016944	uri-1	URI (Unconventional prefoldin RPB5 Interactor) homolog	-0.309233741	5.24E-09	7.91E-07
Programmed cell death	WBGene00006869	vab-2	hypothetical protein	0.321389762	0.002231	0.014271
Programmed cell death	WBGene00006959	xbp-1	X-box Binding Protein homolog	0.31333804	0.005241	0.02735
Programmed cell death	WBGene00021269	Y23H5A.2	hypothetical protein	1.247190218	9.07E-05	0.001263
Programmed cell death	WBGene00021912	Y55B1BR.2	hypothetical protein	0.334811497	0.007572	0.036211
Programmed cell death	WBGene00022046	Y66H1A.4	Probable H/ACA ribonucleoprotein complex subunit 1-like protein	0.382246986	0.002629	0.016175
Programmed cell death	WBGene00013859	ZC247.1	hypothetical protein	0.313737011	0.000589	0.005224
Programmed cell death	WBGene00014227	ZK1128.1	Protein arginine methyltransferase NDUFAF7 homolog, mitochondrial	-0.368344075	2.64E-08	3.07E-06
Protein degradation	WBGene00001148	eat-20	Abnormal pharyngeal pumping eat-20	0.327822187	0.00073	0.006169
Protein degradation	WBGene00001170	egl-1	Programmed cell death activator egl-1	1.372562445	2.56E-11	1.64E-08
Protein degradation	WBGene00001196	egl-30	hypothetical protein	0.304911046	0.000787	0.00656
Protein degradation	WBGene00002280	let-2	Collagen alpha-2(IV) chain	0.66279107	2.24E-05	0.000454
Protein degradation	WBGene00002977	lev-10	hypothetical protein	0.467643019	0.000135	0.001696
Protein degradation	WBGene00009306	maph-1.1	Microtubule-associated protein homolog maph-1.1	0.770301052	1.55E-07	1.2E-05
Protein degradation	WBGene00003495	mup-2	Troponin T	1.124220966	3.02E-09	5.17E-07
Protein degradation	WBGene00003931	pat-4	Integrin-linked protein kinase homolog pat-4	0.333291408	0.000529	0.004812
Protein degradation	WBGene00005018	sqt-3	Cuticle collagen 1	1.271241572	0.000711	0.006063
Protein degradation	WBGene00006771	tln-1	TaLiN	0.995249273	6.23E-12	7.99E-09
Protein degradation	WBGene00006786	unc-51	Serine/threonine-protein kinase unc-51	0.736863794	2.52E-07	1.75E-05
Protein degradation	WBGene00006787	unc-52	Basement membrane proteoglycan	0.63287148	5.53E-08	5.22E-06
Protein degradation	WBGene00006793	unc-59	hypothetical protein	-0.300058639	1.15E-08	1.52E-06
Protein degradation	WBGene00006796	unc-62	Homeobox protein unc-62	0.501547291	8.47E-06	0.00022
Protein degradation	WBGene00006876	vab-10	hypothetical protein	0.542297719	6.92E-07	3.39E-05
Protein degradation	WBGene00006959	xbp-1	X-box Binding Protein homolog	0.31333804	0.005241	0.02735
Protein degradation	WBGene00006999	zyx-1	Zyxin	0.35866357	0.000347	0.003436

Paper III

Development of droplet digital PCR method for the assessment of mitochondrial DNA copy number variation in response to ionizing radiation in the nematode *Caenorhabditis elegans*

Erica Maremonti [1*], Dag Anders Brede[1], Ann-Karin Olsen[1,2], Dag M. Eide[1,2], Einar S. Berg[2]

[1] Centre for Environmental Radioactivity (CERAD), Faculty of Environmental Sciences and Natural Resource Management (MINA) Norwegian University of Life Sciences (NMBU), 1432 Ås, Norway

[2] Norwegian Institute of Public Health, Division of Disease, Lovisenberggata 8, 0456 Oslo, Norway

*Corresponding author: erica.maremonti@nmbu.no

Abstract

The physiological generation of reactive oxygen species due to mitochondrial oxidative phosphorylation can be significantly enhanced under exposure to ionizing radiation, leading to oxidative stress and damage of biomolecules. Mitochondria are considered vulnerable targets to the effects of ionizing radiation and particularly mtDNA damage has shown to be more extensive and to persist longer than nuclear DNA damage. Mitochondrial DNA copy number variation has therefore been proposed as a marker for mitochondrial dysfunction following exposure to ionizing radiation. In the current study, we report the development of a duplex droplet digital PCR method for the accurate quantification of the mt/nDNA ratio in the model organism *Caenorhabditis elegans*. The effect of chronic exposure to gamma radiation was investigated at doses ranging from 0.03 to 72 Gy. For this purpose, five mitochondrial targets and two nuclear reference genes were amplified pairwise (one mitochondrial and one nuclear target per PCR reaction) in duplex PCR format by both ddPCR and standard qPCR. In all the duplex experiments performed, ddPCR but not qPCR, showed a significant (1.6 ± 0.1-fold) increase in the mtDNA copy number when nematodes were exposed to high doses (≥24 Gy) of ionizing gamma radiation. Thus ddPCR, by measuring absolute rather than relative copies of selected targets, provided with more precise measurements compared to qPCR and was a sensitive method with respect to copy number variation assessment. Results from the ddPCR assay also showed that chronic exposure of *C. elegans* to ionizing radiation affected the mtDNA copy number with a Hill type dose-dependent increase and predicted a dose threshold of effect at 10.3 ±1 Gy. This strongly suggests that chronic exposure to ionizing radiation affects mtDNA, by inducing genotoxic response and effects on mtDNA replication, with potential as marker for mitochondrial dysfunction.

1. Introduction

The direct deposition of high energy onto nucleic acids by high doses of ionizing radiation can induce a broad range of genetic alterations, from single base lesion/mutation, single-strand or double-strand breaks (SSB, DSB), to complex DNA lesions such as chromosomal damage/aberration and even chromosome loss (Lomax et al., 2013). In contrast, upon exposure to low doses of ionizing radiation, most of the genotoxicity is due to the indirect effect exerted by the production of Reactive Oxygen Species (ROS) and by the consequent oxidative insult to DNA (Azzam et al., 2012).

The mitochondrion represents, in a healthy cell, the primary source for endogenous ROS, since 1-5% of the oxygen, consumed via the mitochondrial Electron Transport Chain (ETC) for the production of ATP, via oxidation of NADH and FADH, inadvertently ends up as oxygen radicals (Cadenas and Davies, 2000). Following oxidative stress, damage to the mitochondrial DNA (mtDNA) has been shown to be more extensive and persists longer than nuclear DNA damage (Yakes and Van Houten, 1997). In addition to endogenous ROS production caused by the physiological electron leakage in the ETC, ionizing radiation exposure can induce excess of free radicals through water radiolysis which can cause improper assembly and functioning of ETC and ATP synthase machineries (Dayal et al., 2009, Spitz et al., 2004, Kam and Banati, 2013). Moreover, due to the close proximity to the ETC, the lack of DNA-protective histones (Mandavilli et al., 2002), the higher density of coding sequences (Evdokimovsky et al., 2011) and fewer DNA repair systems (Sawyer and Van Houten, 1999), the mitochondrial DNA (mtDNA) represents a more vulnerable target for low dose radiation-induced genotoxicity than its nuclear counterpart (Malakhova et al., 2005). However, the mitochondrial function may be unaffected even if some mitochondrial genome copies are damaged or truncated.

In such cases, the genotoxic damage may be compensated by the remaining intact mtDNAs, although adverse effects arise if the proportion of damaged genomes causes a deficiency of protein products required for proper oxidative phosphorylation and efficient ATP production (Bai and Wong, 2005, Montier et al., 2009). Mitochondrial DNA is therefore considered a susceptible target of ionizing radiation (Kam and Banati, 2013). The ratio of mtDNA to nDNA can be used as an estimate for the number of mitochondrial genomes per cell, or mtDNA copy number (Phillips et al., 2014). An increase in the mtDNA copy number has been reported both *in vitro* and *in vivo* after exposure to ionizing radiation of mammalian systems (Nugent et al., 2010, Malakhova et al., 2005, Kam and Banati, 2013). This increase is believed to be a compensatory mechanism (Okunieff et al., 2008) or an adaptive response of mitochondria to maintain function post-irradiation (Nugent et al., 2010, Rogounovitch et al., 2002). Changes in the mtDNA content may thus serve as a readout to measure radiation response for mitochondrial dysfunction (Malik and Czajka, 2013).

One widely adopted method for measuring the mt/nDNA ratio is based on a quantitative PCR (qPCR) assay (Bratic et al., 2010, Polyak et al., 2012, Haroon et al., 2018). This advantageously enables analysis over an extremely wide dynamic range from single molecule input copy number of target DNA, up to very high concentrations of DNA (Basu, 2017). The qPCR technique can provide measurement of mtDNA copy number based on the comparison between a standard curve and the amplification of a small mitochondrial and a small nuclear target (usually ≤200 bp). However, qPCR provides only semi-quantitative or relative quantification analysis, since the quantification is based on interpolation of a sample result against a standard curve (Evdokimovsky et al., 2011, Gahan et al., 2001, Côté et al., 2011). This method, although widely adopted and cost efficient, presents some limitations and the determination of mtDNA copy number

has shown to be influenced by DNA extraction procedures (Guo et al., 2009). Furthermore, erroneous results may also occur, in quantitative real-time PCR assays (Côté et al., 2011), due to preferential amplification of one of the selected targets, well-to-well variability and PCR inhibitors leading to different amplification efficiencies of the selected targets (Malik and Czajka, 2013). These limitations are bypassed in multiplex digital PCR (dPCR) assays, where target DNA molecules are fractionated into multiple partitions, each containing a PCR reaction, at a level where there are some partitions that have no DNA template and others that have one or more DNA template copies present (Baker, 2012). After amplification to the terminal plateau phase of PCR, reactions containing one or more DNA templates yield positive end-points, whereas those without DNA template remain negative (Hindson et al., 2011). Based on Poisson distribution, this technique allows for absolute quantification of number of target DNA molecules and thus represents an improved accurate method to quantify the mtDNA copy number (Memon et al., 2017, Basu, 2017).

Therefore, the aim of the current study was to optimize a method based on duplex droplet digital PCR (ddPCR) for the quantification of mtDNA copy number relative to nDNA. The established method was employed to evaluate the effects on mtDNA copy number variation (CNV) in response to genotoxic stress, by using *Caenorhabditis elegans* as a model organism chronically exposed to low and high doses of ionizing gamma radiation.

116 ## 2. Materials and methods

117 ### 2.1 Nematode culturing and irradiation

118

119 Wild-type *C. elegans* N2 (var. Bristol) were grown in 6 cm Ø Petri dishes under dark
120 conditions at 20 °C in nematode growth medium (NGM) and fed with *Escherichia coli*
121 strain OP50 according to a standard protocol (Lewis and Fleming, 1995). Age-
122 synchronous worm populations were initiated from eggs following alkaline
123 hypochlorite treatment of gravid adults as described by Stiernagle (1999).

124 For the low-dose exposure, synchronized L1 stage N2 cultures on NGM agar seeded with
125 OP50 were gamma irradiated with a ^{60}Co source (maximum permissible activity 400
126 GBq) at dose-rates ranging from 0.4 to 100 mGy·hr^{-1} at the Figaro facility (Norwegian
127 University of Life Sciences, Norway) (Lind et al., 2019) for 72 hours (**Table S.2**). Three
128 biological replicates per dose-rate (~1000 nematodes per replicate) were placed
129 vertically facing the gamma source, non-irradiated nematodes were placed in the
130 control zone, next to the source, in order to maintain the same exposure condition.

131 For the high-dose exposure, synchronized cultures (L1 stage, in triplicates, ~1000
132 nematodes per replicate) in NGM plus OP50 were irradiated at ~1 Gy·hr^{-1} for a total of
133 24, 48 or 72 hours (**Table S.2**) and all treatment were sampled after 72 hours of
134 development from L1 stage, when nematodes reached the adult stage.

135 After the irradiation, worm populations were sieved and rinsed by passing 3x 10 mL M9
136 solution through a cell-strainer (30 µm Ø mashes) in order to remove the bacterial cells.
137 Before snap-freezing the samples in liquid nitrogen, nematodes were treated with EDTA
138 (2 mM), in order to preserve the DNA integrity during storing conditions (-80 °C).

2.2 Total DNA extraction

Snap-frozen aliquots of nematodes (approximately 1000 individuals per sample) were thawed and disrupted by using ATL buffer (Qiagen, Germany) and beads beating (0.1-0.5 mm Ø) in a FastPrep homogenizer (MP Biomedicals, 20 m/s per 10 seconds). Isolation of total DNA was performed by using the DNeasy Blood and Tissue Kit (Qiagen, Germany), according to the manufacturer's instructions with some modifications. Briefly, prior to precipitate the DNA onto the columns, the nematodes' lysate was subjected to RNase A (10 µg/µl) treatment (1 hour at 37 °C) followed by incubation in water bath for 2 hours at 56 °C with Proteinase K (2 mg/ml).

DNA quantification and purity were assessed by using NanoDrop ND-1000 Micro-Volume UV-Vis Spectrophotometer (NanoDrop Technologies, Wilmington, DE, USA). DNA concentrations were further validated by using Qubit fluorometer measurements (Thermo Fisher scientific).

In order to optimize the droplet formation and the performance of ddPCR analysis (Basu, 2017), DNA samples were sonicated for 10 minutes in a water bath equipped with an ultrasonic probe (Sonic Vibra Cell Ultrasonic processor, VC 130, 130 W, Sonic & Materials Inc., Newton,CT, USA) and diluted to a final concentration of 0.5 ng/µl.

160 ## 2.3 PCR primers and TaqMan probes design

161

162 The *C. elegans* mtDNA NC_001328 was obtained from the National Centre for
163 Biotechnology Information (NCBI) and it was used as reference sequence for the design
164 of the five mitochondrial PCR targets. As nuclear PCR reference targets, we selected the
165 actin-4 (*act-4*) gene (NC_003284.9), which is a member of the multi-copy actin family,
166 together with the single-copy glucose-6-phosphate isomerase (*gpi-1*) gene
167 (NC_003279.8).

168 The PCR primers and TaqMan probes were designed by use of Oligo® Primer Analysis
169 Software (Rychlik, 1995). The *in silico* analysis of each set of mtDNA and nDNA primer
170 pairs with their corresponding TaqMan probes was first done in singleplex- and then in
171 duplex PCR format to select oligonucleotides with nearly the same thermodynamic
172 properties and without undesired DNA secondary structures, or dimer formation and in
173 order to achieve the most robust and sensitive duplex PCR amplification. The five-
174 mtDNA targets were distributed across the mitochondrial genome but did intentionally
175 not include the common deletion *uaDf5* (**Fig. 1**). Their corresponding genes encoded the
176 small subunit rRNA (s-rRNA), subunits I and III of cytochrome c oxidase (COX1 and
177 COX3), subunit 5 of NADH dehydrogenase (ND5), and the junction between tRNA for
178 valine and subunit 6 of NADH dehydrogenase (tRNA-Val/ND6). The sequences and
179 amplicon lengths for each selected PCR primer and TaqMan probe are listed in **Table 1**.

180 The specificity of the primers was also analyzed by the NCBI Primer-BLAST analysis (Ye
181 et al., 2012). Hereby, only the primers/probe set for the nDNA reference target *act-4*
182 seemed able to produce two additional positive amplicons, when limits for the number

183 of allowed primer and probe mismatches (less than 3) and for the amplicon length (less
184 than 0,5 kb) were taken into account.

185 The mtDNA TaqMan probes were synthesized with a 6FAM/BHQ-1 reporter/quencher
186 whereas the nDNA probes had HEX/BHQ-1 combination. All primers and probes were
187 obtained from Sigma-Aldrich (Oslo, Norway).

188

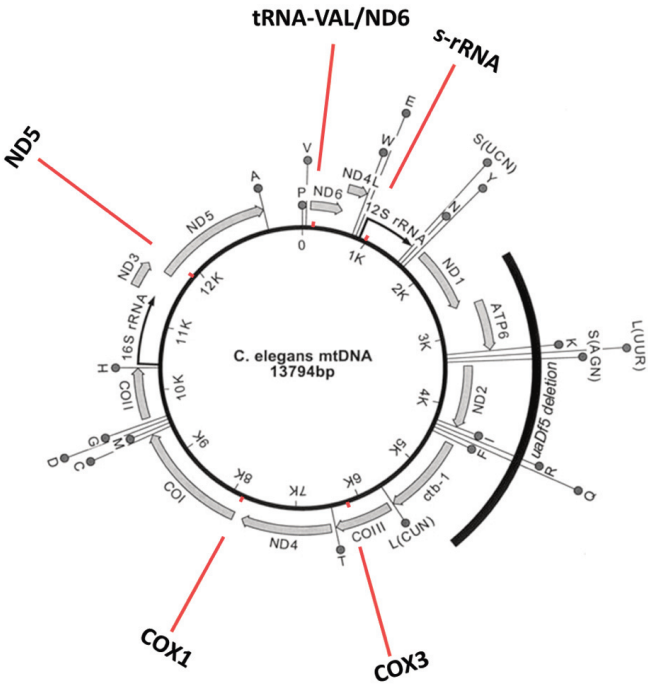

189

190 **Figure 1.** Gene map of the *C. elegans* mtDNA, comprising twelve proteins encoding genes (thick grey
191 arrows), two rRNAs genes (black arrows), and 22 tRNAs genes (circles labeled with one-letter amino acid
192 code). The positions of the putative uaDf5 deletion region is indicated by the thick black mark outside the
193 circle. Red marks denote positions of the five target amplicons used for the ddPCR and qPCR duplex assay
194 performed in this study. Figure is adapted from Lemire, B. Mitochondrial genetics (September 14,
195 2005), WormBook, ed. The *C. elegans* Research Community, WormBook,

196 doi/10.1895/wormbook.1.25.1, http://www.wormbook.org.

197

198 **Table 1.** Primers and TaqMan probes sequences for amplification of mitochondrial and nuclear target

199 genes selected for the quantification of the ratio mt/nDNA via duplex ddPCR and qPCR assays.

Name		Sequence 5' → 3'	Amplicon length (bp)	NCBI Ref. seq. NC_001328
Mitochondrial				
tRNA-Val/ND6	Up	CTTACAATGATGGGGTTT	105	87 - 192
	Low	AACTTCTTTTTATAGGGTCAA		
	TaqMan	TCCTACTTAAAACAGCTAAAACAAA		
s-rRNA	Up	TATCGCTTGTAAAATACTTGT	86	1008 - 1194
	Low	TTCTCTAACCAGGTACTAATC		
	TaqMan	TCCAGAATAATCGGCTAGACTTGTT		
COX3	Up	GCAGACGGAGTATTTGGAAGG	149	6224 - 6373
	Low	GCAAATTCCAACCCCAGATG		
	TaqMan	TGCTAAGAAGAAACCACCACACAAGACA		
COX1	Up	TGGCAGTTTGATTAGAGAG	184	7876 - 8060
	Low	AAAATAGCATGACGTGTAATAA		
	TaqMan	CTGAATTATACAACTGTCCATTCCT		
ND5	Up	TGTTAATTTTCGTAGGTAGA	169	11935 - 12104
	Low	CCTAGACGATTAGTTAATGC		
	TaqMan	TATTGCACCCCTACATCTATCTCA		
Genomic				
act	Up	GAAGCCCAGTCCAAGAGAG	107	
	Low	TTGTAGAAGGTGTGATGCCAG		
	TaqMan	TGAGCACGGAATCGTCACCAACT		
gpi-1	Up	GTAGTCTAATGAATTAAATTTACAG	75	
	Low	TCTTTCCTTTCATTAGTGCCTC		
	TaqMan	TCTCGCCAACTTCCTCGCTCAAA		

200

201 ## 2.4 Initial PCR optimization

202

203 The composition of the reaction mixture for ddPCR is very similar to a qPCR mixture

204 except that the water-oil emulsion with nL droplets requires additional stabilizing

205 chemicals (Baker, 2012). Accordingly, the DNA amplification and fluorescent signal

206 generation for both methods occur by the same principles. Under identical reaction
207 conditions, a head-to-head comparison of the two PCR formats could be enabled by
208 separating a fully assembled ddPCR reaction mixture into two ddPCR/qPCR aliquots
209 with subsequent amplification and signal detection in respective instrument platforms.

210 Initially, by using qPCR, different concentrations of each primer pair and relative
211 TaqMan probes were tested with a DNA sample obtained from nematodes at 72 hours
212 development from L1 stage (1 ng/25 µl reaction mixture) at different annealing
213 temperatures in reaction mixtures based on the 2x ddPCR Supermix for Probes (No
214 dUTP, Bio-Rad). The reaction conditions that gave the most efficient amplification in
215 singleplex format were also used in duplex qPCR with co-amplification of one nDNA and
216 one mtDNA target. The results of these experiments demonstrated a feasible
217 compromise between the individual primer/probe concentrations/annealing
218 temperature for universal reaction conditions.

219 In the optimized duplex qPCR and ddPCR assay, the concentration of each primer and
220 TaqMan probe was set to 200 nM and 50 nM, respectively. The COX1 was the only
221 exception with 100 nM of TaqMan probe. Moreover, the thermal cycling protocol used
222 for DNA amplification was performed as follows: initial activation of the enzyme at 95˚C
223 for 10 minutes, 40 cycles of a two-step protocol with DNA denaturation at 95˚C for 15
224 seconds followed by combined annealing/extension at 52˚C for 75 seconds. The
225 temperature ramp rate between the two cycling stages was adjusted slower for ddPCR
226 (2˚C per second) than qPCR, where it was applied the default rapid ramp rate for the
227 CFX qPCR instrument (Bio-Rad).

228

229

2.5 Droplet digital PCR

In the ddPCR assay, the fully assembled reaction mixture was dispersed into nL droplets in a water-oil emulsion by using a microfluidic cartridge and the QC200 Droplet Generator (Bio-Rad). The water-oil emulsion of the sample was then carefully transferred to a rigid PCR plate, sealed with pierceable foil in a PX1 PCR plate sealer (Bio-Rad), and subjected to thermal cycling in a PCR machine (Section 2.4, Eppendorf Mastercycler, Oslo, Norway). Subsequently, the PCR plate was transferred to the QX200 Droplet Reader (Bio-Rad) which automatically counts the mtDNA and nDNA positive/negative droplets. Analysis of ddPCR data with Poisson statistics was done by using the QuantSoft software from the QX200 system (Bio-Rad) (Hindson et al., 2011, Memon et al., 2017).

2.6 Real-time qPCR analysis

A 20-ul aliquot of the fully assembled PCR mixtures for each pair of mtDNA/nDNA assays were subjected to parallel qPCR testing in a CFX96 Touch Deep Well Real-Time PCR Detection System (Bio-Rad). After thermal cycling, the qPCR data were analyzed using the Bio-Rad CFX Manager software. Hereby, the default temperature ramp rate for the qPCR was adopted (no water/oil emulsion reduced heat transfer rate) and data acquisition occurred real-time, thus allowing to perform the qPCR assay as similarly as possible to ddPCR assay, in order to obtain comparable results.

2.7 Statistical analysis

Statistical analysis and graphs were performed using JMP Pro v14 (SAS institute, Cary, NC, USA). The linearity of the ddPCR and qPCR assays at different concentrations of DNA template was tested by linear regression analysis and R-square (R^2) was calculated for best fit. Normality and variance homogeneity assumptions, for the mtDNA levels, were tested on residuals by using Anderson-Darling normality test and visually on residuals *vs.* fitted value plot, respectively. MtDNA levels were normally distributed, therefore significant difference between different exposure groups were calculated using one-way analysis of variance (ANOVA). When significant, the Tukey pair-wise comparisons method was applied to identify differences between specific groups.

266 The ratios mt/nDNA for both reference genes were analysed with all replicates
267 simultaneously. A linear model was applied to study the influence of the reference gene
268 copy number (multi-copy *act* or single-copy *gpi-1*) on the mtDNA CNV at different
269 irradiation doses. A regression of ratio on log transformed doses was done separately
270 for the reference genes and split into high dose range (24 to 72 Gy) and low dose range
271 (0.03 to 7.2 Gy). The ratio of the intercept (*gpi-1)*/intercept (*act)* was used as correction
272 factor to multiply *act*-values at high and low doses. Substituting Ratio with Log10(Ratio)
273 revealed that log transformation of the dependent variable would reduce the high slopes
274 observed with higher ratios.

275 Because the whole dose range of exposure from zero to 72 Gy showed two distinct levels
276 of effect at 7.2 Gy and 24 Gy, a threshold model was estimated by curve fitting, where
277 the Akaike information criterion (AIC) was used to select between logistic models with
278 different parametrization. The Logistic 4P Hill model was adopted as it showed the best
279 fit, with similar values for slope and inflection point when the ratios were calculated
280 using both reference genes (*act* and *gpi-1*).

281

282

283 # 3. Results and discussion

284

285 The mitochondrial genomes encode genes with essential functions to central
286 metabolism (Anderson et al., 1981). It thus follows that loss or mutation of mtDNA
287 invariably affects energy production and leads to mitochondrial dysfunction, which can
288 be devastating to the organism (Haroon et al., 2018). It has been shown that

289 mitochondrial DNA is highly susceptible to genotoxic stress, including exposure to
290 ionizing radiation (Azzam et al., 2012, Kam and Banati, 2013). Radiation induced
291 mitochondrial dysfunction leads to excessive ROS formation, oxidative damage effects,
292 and induction of genomic instability (Spitz et al., 2004). Conventional long amplicon
293 qPCR based methods permit relative quantification of damage both in mitochondrial
294 and nuclear DNA, by using a small amplicon as reference for total copy number (Yakes
295 and Van Houten, 1997, Phillips et al., 2014). Moreover, by assuming that the damage in
296 the small reference amplicon is negligible, PCR product yield indicates changes in the
297 mtDNA copy number (Hunter et al., 2010). Changes in the ratio mt/nDNA have been
298 proposed as a potential biomarker for mitochondrial dysfunction (Malik and Czajka,
299 2013).

300 In the current study, we therefore aimed to investigate the effect of chronic exposure to
301 ionizing radiation on the mtDNA copy number in the model organism *C. elegans*. We
302 developed and validated a ddPCR based method to facilitate accurate and robust
303 determination of mtDNA copy number relative to nDNA reference genes.

304

305

306 3.1 Reference (nDNA) and target (mtDNA) genes

307

308 In order to assess variations of the mtDNA copy number, five mtDNA (COX1, COX3, ND5,
309 s-rRNA and tRNA-val/ND6) targets and two nDNA reference genes (*gpi-1, act*) were
310 selected (**Fig. 1**) and corresponding primer pairs and TaqMan probes were designed
311 (**Table 1**). The suitability of each amplicon was investigated by performing qPCR and

312 ddPCR simplex experiments with temperature gradient, primers and probes serial
313 dilutions (data not shown) and serial dilutions of template DNA (**Fig. 2**; ddPCR).

314 In order to exclude mitochondrial targets with potential duplicates on the nuclear
315 genome, and in order to ensure specificity of the selected targets, we performed a NCBI
316 nucleotide/primer BLAST® analysis on the *C. elegans* refseq genome (Ye et al., 2012).

317 The specificity of the primer pairs was validated by performing duplex assay
318 experiments with both the qPCR and ddPCR methods, using serial dilutions of DNA
319 template, extracted from nematodes at 72 hours development from L1 stage. The duplex
320 assay from ddPCR results showed linearity for all mitochondrial targets as well as for
321 the reference genomic target *gpi-1,* (Linear Regression Analysis, *p*-value <0.0001) (**Fig.**
322 **2**). The number of DNA copies, from each PCR amplicon, measured as a function of input
323 DNA (ng/µl) showed a high correlation (R^2=0.99). This demonstrates that the assay was
324 stable and exhibit a wide dynamic range for all five selected mitochondrial targets as
325 well as for the nDNA reference gene (*gpi-1*), and thus suitable for the mtDNA copy
326 number quantification.

327

328 When the same experiment was performed by using standard quantitative PCR duplex
329 assay, linearity (R^2 > 0.94) was also observed for all the mitochondrial targets and for
330 the reference gene *gpi-1* (**Fig. S.1**). However, variability between the selected target
331 genes was found in the amplification efficiency values E_x (%) (**Fig. S.2**, **Table S.1**). This
332 indicated lower performance of qPCR compared to ddPCR, likely due to competition
333 between primers in the amplification reactions, which resulted in different
334 amplification efficiency between the selected targets, as well as for the nDNA target,

335 when this was measured in a duplex assay with a mitochondrial target gene (**Fig. S.1,**

336 **S2**).

337

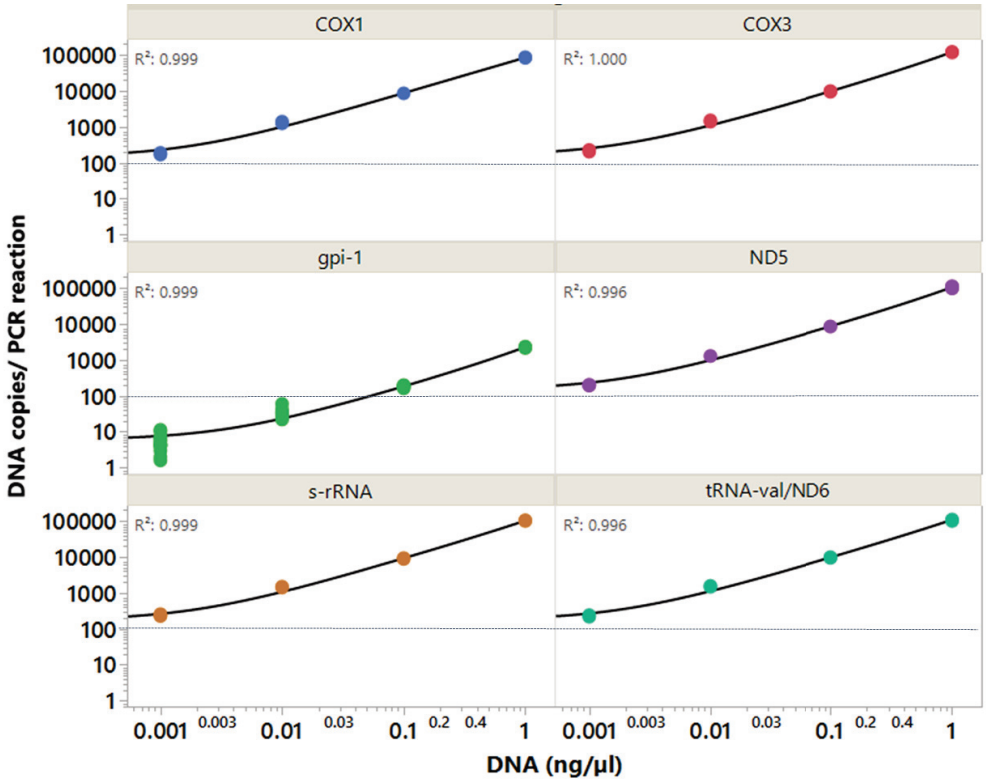

338

339 **Fig. 2.** DNA copies per PCR reaction (20 µl) measured at different concentrations of input DNA (ng/µl)

340 with ddPCR duplex assay, by using five mitochondrial targets (COX1, COX3, ND5, s-rRNA, tRNA-val/ND6)

341 and *gpi-1* as nDNA reference gene. Linear regression analysis shows equal correlation (R^2 ≥0.99) for all

342 mitochondrial targets and for the nDNA reference gene *gpi-1*. Horizontal lines indicate the 100 DNA

343 copies/PCR reaction cut off for the genomic target suggested for the optimal quantification of the ratio

344 mt/nDNA (Droplet Digital PCR Application guide).

345

346 ## 3.2 Optimization of DNA template concentration for measuring the ratio
347 mt/nDNA with ddPCR duplex assay
348

349 As previously reported by Malik et al. (2011), bias can be introduced into a qPCR
350 reaction due to suboptimal DNA concentrations. In ddPCR also, it is particularly
351 important to identify the optimal DNA concentration range for the assessment of ratio
352 mt/nDNA, considering that mtDNA copie number is known to be significantly higher
353 than the number of nDNA copies in the same sample, and that these numbers vary
354 between species or tissues (Memon et al., 2017). Therefore, quantification of the
355 mt/nDNA ratio with both qPCR and ddPCR methodologies was obtained from the serial
356 dilution experiments discussed in Section 3.1. The mean and 95% Confidence Interval
357 (CI) values showed that the ddPCR assay provided more consistent results with lower
358 variation (~46±4 mt/nDNA) compared to the conventional method based on qPCR,
359 even when the DNA concentration was as low as 0.01 ng/µl (**Fig. 3**, **Table 2, and Fig.**
360 **S.3**). However, in order to measure the Copy Number Variation (CNV) with ddPCR and
361 to optimize the ratio measurements, the manufacturer recommends a minimal
362 concentration of nuclear target of 100 copies per PCR reaction (Droplet Digital PCR
363 Application guide) (horizontal lines in **Fig. 2**). In line with this recommendation, the
364 statistical analysis showed a significantly higher variance for template concentrations
365 (<0.1 ng/µL) containing < 100 copies of nDNA. Therefore, based on this criterion and
366 on the low variation shown in the mt/nDNA ratios (95% Confidence Intervals in **Table**
367 **2**, **Fig. 3** and **Fig. S.3**), the optimal concentration of template DNA for reliable
368 quantification and optimal partitioning for both mt/nDNA targets was identified
369 between 0.1 and 1 ng/µl of DNA. For these reasons, 0.5 ng/µl was the concentration

370 adopted in this study to measure mtDNA CNV induced by exposure to ionizing gamma

371 radiation.

372

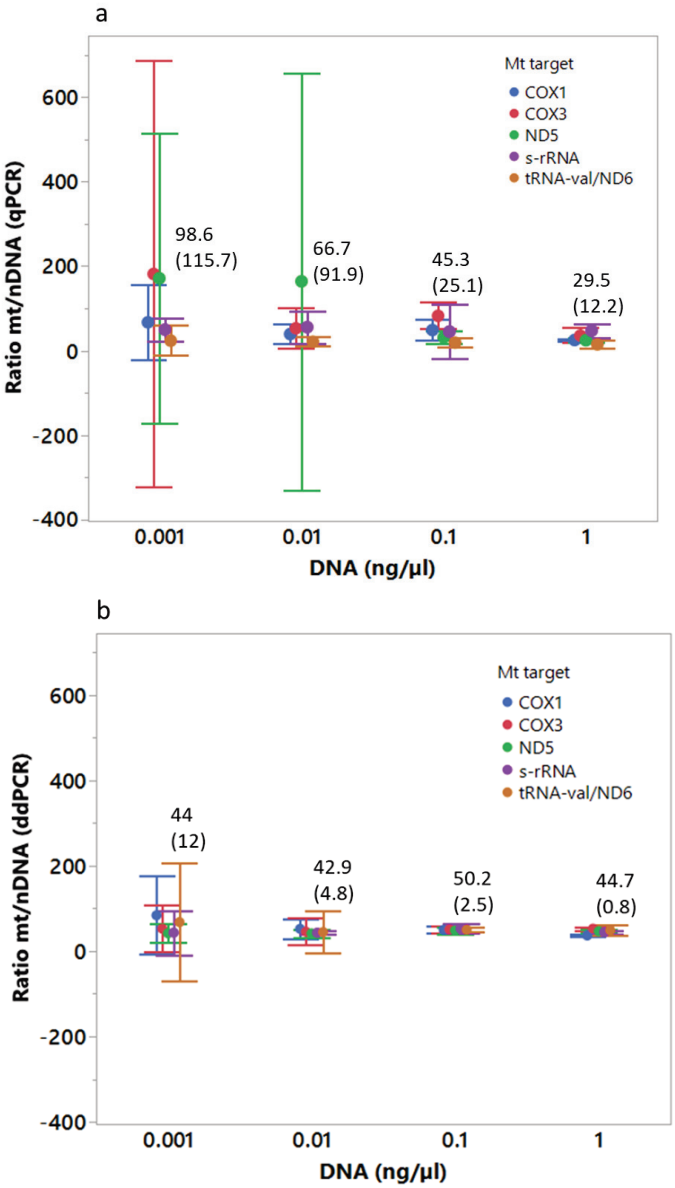

373 **Figure 3.** mt/nDNA ratios measured with (**a**) qPCR and (**b**) ddPCR assays, by using different
374 concentrations of DNA template (ng/µl) with five mitochondrial target genes and *gpi-1* as nDNA reference
375 gene. Error bars indicate the measurement range. Data labels indicate Mean and 95% Confidence Interval.

376

377 **Table 2.** Mt/nDNA ratios (Mean ± 95% CI) measured per each of the five mitochondrial target genes with
378 duplex ddPCR and qPCR assays performed simultaneously at different concentrations of DNA template
379 (ng/µl) by using *gpi-1* as nuclear reference gene.

mt/nDNA ratio					
Mitochondrial target	Method	DNA input (ng/µl)			
		0.001	**0.01**	**0.1**	**1**
s-rRNA	ddPCR	35 ± 21	43 ± 12	53 ± 5	44 ± 2
	qPCR	49.8 ± 10.9	55.6 ± 15.7	45.1 ± 25.9	47.4 ± 6.5
COX1	ddPCR	70 ± 60	52 ± 14	50 ± 5	37 ± 1.3
	qPCR	67 ± 35.7	39.2 ± 9.5	48.8 ± 9.9	25.1 ± 1.5
COX3	ddPCR	44 ± 29	43 ± 10	51 ± 5	53 ± 2
	qPCR	181.6 ± 203	52.9 ± 19.2	82.4 ± 12.7	35.8 ± 7.2
ND5	ddPCR	41 ± 26	41 ± 11	48 ± 5	46 ± 1.7
	qPCR	171.2 ± 138.4	164.1 ± 198.7	31.5 ± 6.3	24.5 ± 2.3
tRNA-val/ND6	ddPCR	44 ± 27	38 ± 8	50 ± 5	48 ± 1.7
	qPCR	23.7 ± 14.3	21.1 ± 4.5	18.9 ± 4.3	14.9 ± 3.4

380

381

382 ## 3.3 Comparison between nDNA reference genes *act* and *gpi-1*

383

384 Among the uncertainties related to the quantification of mt/nDNA ratio with the
385 methodology based on qPCR, the selection of proper genomic reference genes has
386 shown to be critical (Malik and Czajka, 2013). Therefore, in order to test the accuracy
387 of the ddPCR assay in this matter, and to assess whether the specificity of the nDNA

target would influence the quantification of the mtDNA CNV, we compared two nDNA reference genes. In particular, the *gpi-1* target was selected as single copy reference, while the *act* target was designed to amplify three individual targets. By using the NCBI primer BLAST®, we were able to design primer pairs and TaqMan probe that were specific to *act-4, act-3* and *act-1* genes. Particularly, this analysis in combination with the ddPCR results indicated that while *gpi-1* showed affinity only for one target on Chromosome I, both primers and the TaqMan probe for *act-4* showed affinity for *act-4* on Chromosome X and for two orthologue genes on Chromosome V (*act-1* and *act-3*). Where *act-4* showed 100% identity for both primers set and TaqMan probe (amplicon length 108 bp), while *act-1* and *act-3* showed 98% identity with two mismatches on the total PCR product and 1 mismatch contained in the TaqMan sequence (Supporting material).

As expected, when performing the ddPCR assay for the quantification of the mtDNA copy number, the mt/nDNA ratio was ~3 times lower for the nDNA reference target *act,* compared to the *gpi-1* target gene, as indicated by the slope value (=3) in the equation presented in **Fig. 4**. Furthermore, to check robustness and consistency between single versus multi copy nDNA amplicon, ddPCR analysis were performed in *C. elegans* populations subjected to a high-level genotoxic stress. This showed a significant linearity (R^2=0.83) and similar dose-dependent increases for both *gpi-1* and *act* targets, in the mt/nDNA ratio measured after chronic exposure to high doses of ionizing gamma radiation (>24 Gy) (**Fig. 4**).

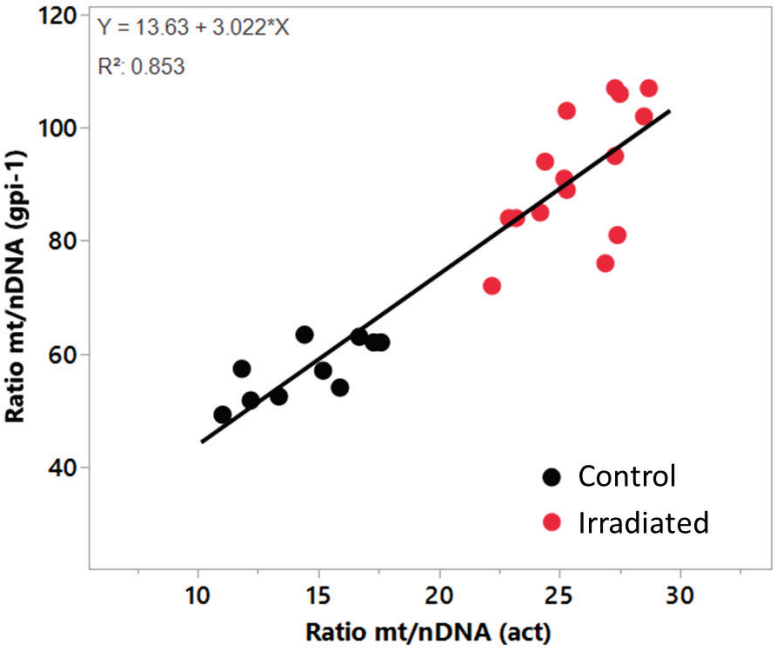

Figure 4. Linear correlation between mtDNA CNV assed by using the nuclear targets *gpi-1* and *act-4 (act)* as reference genes for the measurement of the mt/nDNA-ratio using the duplex ddPCR assay with five mitochondrial target genes. Dots indicate the average of three replicates from five mtTarget genes with both nDNA reference genes *act* (x-axis) or *gpi-1* (y-axis) measured in DNA extracted from nematodes chronically exposed to high doses (24, 48 and 72 Gy) of ionizing gamma radiation.

422 ## 3.4 ddPCR in comparison to qPCR methodology

423

424 In order to test the accuracy of the ddPCR method for the quantification of the mtDNA
425 copy number, we compared the optimized ddPCR assay with a standard qPCR method
426 analysis. For this purpose, we collected samples of total DNA extracted from nematodes
427 exposed to high dose ranges of ionizing gamma radiation (24, 48 and 72 Gy), plus a
428 control group of non-irradiated nematodes. The mt/nDNA ratio was measured by
429 performing two independent duplex experiments, one for each of the two nDNA
430 reference genes (*gpi-1* and *act*), which were measured with each of the five
431 mitochondrial target genes (Section 3.1, **Table 1**). The ddPCR and qPCR assays were
432 performed using aliquots of the same reaction mixtures to minimise variation not
433 associated with the two methods (Sections 2.3, 2.4).

434 In line with Memon et al. (2017), our results from the standard qPCR assay showed less
435 accuracy, as indicated by the large variation within the same exposure group compared
436 to results from the ddPCR assay (95% CI in brackets from the data labels, **Fig. 5.a-b**).
437 We observed a significant dose-dependent increase (ANOVA and Tuckey *post hoc*, *p*-
438 value < 0.05) in the mt/nDNA-ratio using the ddPCR assay with both nDNA reference
439 genes in all the irradiated groups compared to the control group (**Fig. 5.a-b**). In contrast,
440 under similar experimental conditions using qPCR, due to large intra-variability, no
441 significant differences were detected (ANOVA, *p*-value > 0.05).

442 Particularly, ~1.5±0.1 and ~1.6±0.1-fold increases in the mt/nDNA ratio was observed
443 in irradiated nematodes, with ddPCR analysis, when *gpi-1* and *act* were used as nuclear
444 reference genes respectively. This was accompanied by a consistent dose-response
445 increases of the mtDNA copy number, for both nDNA targets. Therefore, both *gpi-1* and

446 *act* were considered suitable reference nuclear genes for the quantification of mtDNA

447 copy number in the ddPCR assay.

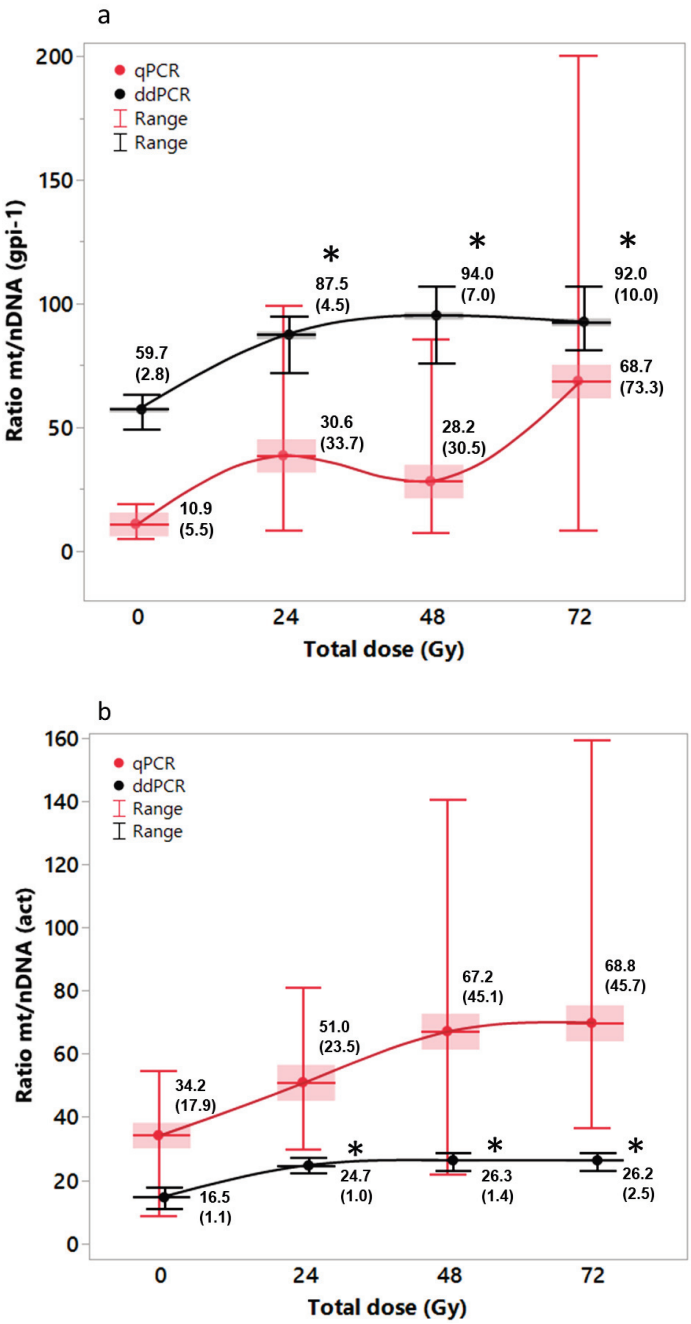

448 **Figure 5.** Comparison between duplex qPCR (red) and ddPCR (black) assay, for the quantification of
449 mt/nDNA-ratios, measured in DNA extracted from nematodes exposed to high dose ranges of ionizing
450 gamma radiation (24 to 72 Gy, dose-rate ~1 Gy·hr^{-1}). Results are from two independent experiments using
451 two different targets as nuclear reference genes, *gpi-1* (**a**) and *act* (**b**). Data labels indicate mean and 95%
452 Confidence Interval.

453

454

455 3.5 Evaluating the effects of chronic exposure to ionizing gamma
456 radiation on mtDNA copy number in *C. elegans*

457

458 Previously we have shown that chronic exposure to gamma radiation induced life stage-
459 dependent reprotoxicity via increased germ cell apoptosis, impaired sperm meiosis and
460 adverse effects on sperm production in the nematode *C. elegans* (Maremonti et al.,
461 2019a). These effects were accompanied by increased levels of ROS production that
462 affected cellular redox balance despite antioxidant defence response. Gene expression
463 analysis indicated a comprehensive effect related to mitochondrial functions, including
464 reduced expression of the mitochondrial ETC (Maremonti et al., 2019b).

465 This indicated that mitochondria have a prominent role in *C. elegans* response to chronic
466 ionizing radiation exposure. To investigate whether i) the observed effects were related
467 to compromised integrity of the mitochondrial genome, or ii) *C. elegans* would respond
468 to genotoxic stress by increasing the mtDNA copy number to maintain mitochondrial
469 function, we measured effects on the mtDNA copy number in nematodes exposed to

470 gamma radiation doses ranging from 0.03 to 72 Gy, administered chronically during
471 larval development.

472 The ddPCR based mitochondrial CNV analyses showed consistent, accurate and precise
473 results for all the mitochondrial and the nuclear targets adopted, including the multi-
474 copy reference gene *act* (Section 3.2, **Fig. 4**). We observed only a small variation
475 between the different mtTargets (1-4 copies for *act* and 5-10 copies for *gpi-1,* in control
476 groups), which may be attributed to the mtDNA-replication mode in *C. elegans* via
477 Rolling Circle Replication mechanism which generates concatemeric mtGenomes (Lewis
478 et al., 2015). Moreover, a consistent level of variation was detected in all the irradiated
479 groups, indicating that none of the selected targets were prone to hyper-variability or
480 were particularly susceptible to deletion.

481 The mt/nDNA-ratios increased in a dose-dependent manner (p-value < 0.0001, Logistic
482 4P Hill model) following gamma radiation (**Fig. 6.a-b**). However, a significant increase
483 of mtDNA copy number was only evident for dose-rates as high as ~1 $Gy \cdot hr^{-1}$ provided
484 for an extended period of time (24 to 72 hours). A threshold dose of effect was identified
485 by using the Logistic 4P Hill model at 10.3 ± 1Gy, which is a dose ~2.4-fold higher than
486 the one required for the manifestation of reprotoxic effects (Maremonti et al., 2019a).
487 Thus, despite the significant effect exerted on the regulation of mitochondrial genes
488 (Maremonti et al., 2019b), essential for the proper assembly of the oxidative
489 phosphorylation system, dose-rates of gamma radiation below 100 $mGy \cdot hr^{-1}$ did not
490 significantly affect mtDNA copy numbers. Moreover, this may be related to adaptive
491 response, where mtDNA disease can be rescued by multiple molecular mechanisms
492 (Haroon et al., 2018).

493 Changes in the mtDNA content have been previously adopted as a measure for radiation-
494 induced mitochondrial dysfunction (Malik and Czajka, 2013, Nugent et al., 2010,
495 Malakhova et al., 2005), which suggests that the *C. elegans* mitochondrial function is
496 significantly compromised at doses ≥ 24 Gy (~1 $Gy \cdot hr^{-1}$). Previous studies have
497 proposed that if depletion of mtDNA copies falls below a critical threshold, this will
498 trigger replication by up-regulating the mitochondrial replication machinery (Montier
499 et al., 2009). Conversely, according to the same model by Montier et al. (2009), if the
500 mtDNA copy number increases above a certain threshold this triggers mtDNA
501 degradation. Control of the mtDNA copy number is considered an important aspect of
502 mitochondrial genetics and biogenesis, therefore essential for normal cellular function.
503 For instance, reduction in the mtDNA copy number causes an imbalance in the number
504 of proteins derived from the nuclear and mitochondrial genome. This imbalance has
505 shown to induce further proteotoxic stress, by preventing proteins from finding their
506 natural binding partner inside the mitochondrion (Haroon et al., 2018). Based on the
507 threshold model and on aforementioned observations, in our study, nematodes exposed
508 to relatively low doses of ionizing gamma radiation (up to 7.2 Gy) showed the ability to
509 maintain a stable mtGenome content. In contrast, high-dose exposure led to induction
510 of a ~1.5-fold significant increase in mtDNA copy number, suggesting a compensatory
511 effect induced by mtDNA deletion due to excessive production of ROS and radiation-
512 induced DNA damage, as previously reported by Bai and Wong (2005).

513 This scenario is consistent with the *C. elegans* ability to tolerate 1 kGy without mortality
514 (Krisko et al., 2012), or loss of cell viability in post-mitotic tissues (Johnson and
515 Hartman, 1988). This may imply a remarkable ability to maintain mitochondrial
516 functions as well and could indicate that the increased copy number is part of the
517 intrinsic radioresistance of *C. elegans*.

a

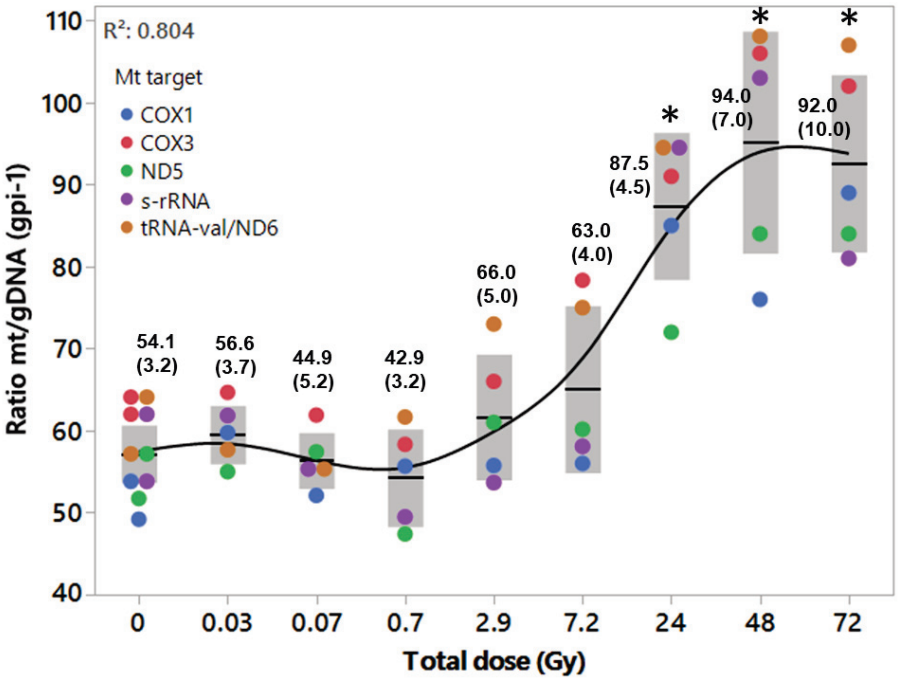
R²: 0.804
Mt target
COX1
COX3
ND5
s-rRNA
tRNA-val/ND6
Ratio mt/gDNA (gpi-1)
110
100
90
80
70
60
50
40
54.1 (3.2)
56.6 (3.7)
44.9 (5.2)
42.9 (3.2)
66.0 (5.0)
63.0 (4.0)
87.5 (4.5)
94.0 (7.0)
92.0 (10.0)
*
*
*
0
0.03
0.07
0.7
2.9
7.2
24
48
72
Total dose (Gy)

b

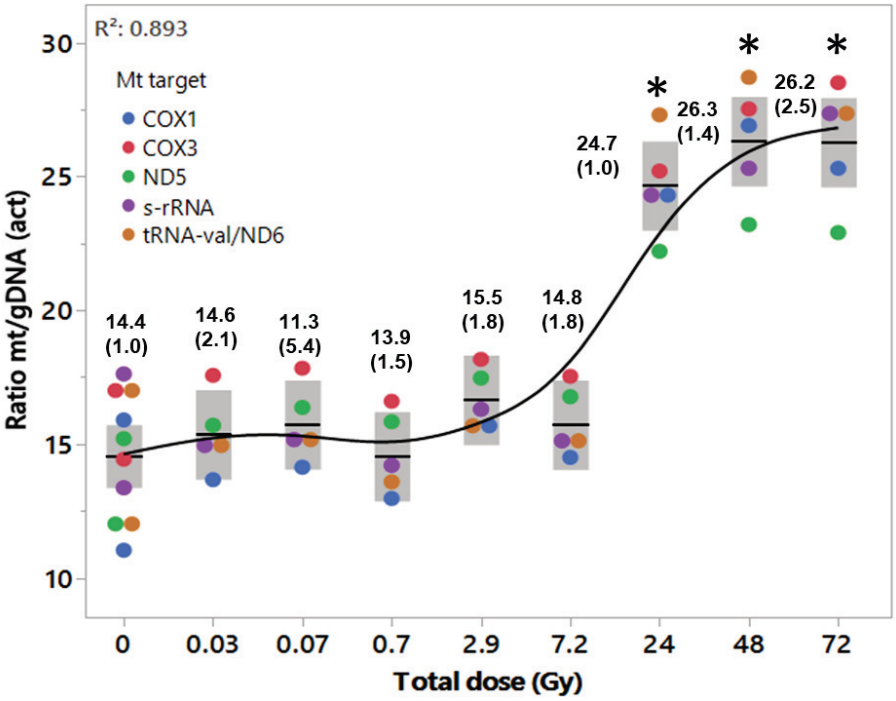
R²: 0.893
Mt target
COX1
COX3
ND5
s-rRNA
tRNA-val/ND6
Ratio mt/gDNA (act)
30
25
20
15
10
14.4 (1.0)
14.6 (2.1)
11.3 (5.4)
13.9 (1.5)
15.5 (1.8)
14.8 (1.8)
24.7 (1.0)
26.3 (1.4)
26.2 (2.5)
*
*
*
0
0.03
0.07
0.7
2.9
7.2
24
48
72
Total dose (Gy)

518

519 **Figure 6.** mt/nDNA ratio measured with duplex ddPCR assay on nematodes exposed to low and high
520 dose-rates of ionizing gamma radiation, ranging from 0.4 to 100 mGy·hr^{-1} (up to 7.2 Gy) or ~1 Gy·hr^{-1} (24
521 to 72 Gy), by using five mitochondrial targets and two nuclear (*gpi-1* and *act*) reference genes. Data labels
522 indicate Mean and 95% Confidence Interval.

523

524

525 # Conclusions

526

527 The current study presents a new ddPCR duplex method for the absolute quantification
528 of mtDNA copy number. Based on the mt/nDNA ratio, the ddPCR method facilitates a
529 simple and robust means of quantification that overcomes the known uncertainties
530 related to qPCR measurements. The results consistently showed increased mtDNA copy
531 number in response to chronic exposure to ionizing gamma radiation in the nematode
532 *C. elegans,* demonstrating the high accuracy and sensitivity of the ddPCR assay. This
533 method represents a novel tool for the assessment of effects on mitochondrial function,
534 and indicates that genotoxic stress triggers dose-dependent effects on mtDNA copy
535 number in *C. elegans*.

536

537

538

539

References

ANDERSON, S., BANKIER, A. T., BARRELL, B. G., DE BRUIJN, M. H., COULSON, A. R., DROUIN, J., EPERON, I. C., NIERLICH, D. P., ROE, B. A. & SANGER, F. J. N. 1981. Sequence and organization of the human mitochondrial genome. 290**,** 457.

AZZAM, E. I., JAY-GERIN, J.-P. & PAIN, D. 2012. Ionizing radiation-induced metabolic oxidative stress and prolonged cell injury. *Cancer letters,* 327**,** 48-60.

BAI, R.-K. & WONG, L.-J. C. 2005. Simultaneous detection and quantification of mitochondrial DNA deletion (s), depletion, and over-replication in patients with mitochondrial disease. *The Journal of Molecular Diagnostics,* 7**,** 613-622.

BAKER, M. 2012. Digital PCR hits its stride. *Nature Methods,* 9**,** 541-544.

BASU, A. S. 2017. Digital assays part I: partitioning statistics and digital PCR. *SLAS TECHNOLOGY: Translating Life Sciences Innovation,* 22**,** 369-386.

BRATIC, I., HENCH, J. & TRIFUNOVIC, A. 2010. Caenorhabditis elegans as a model system for mtDNA replication defects. *Methods,* 51**,** 437-443.

CADENAS, E. & DAVIES, K. J. A. 2000. Mitochondrial free radical generation, oxidative stress, and aging11This article is dedicated to the memory of our dear friend, colleague, and mentor Lars Ernster (1920–1998), in gratitude for all he gave to us. *Free Radical Biology and Medicine,* 29**,** 222-230.

CÔTÉ, H. C. F., GERSCHENSON, M., WALKER, U. A., MIRO, O., GARRABOU, G., HAMMOND, E., VILLARROYA, J., GIRALT, M., VILLARROYA, F., CINQUE, P., GARCIA-ARUMI, E., ANDREU, A. L., PINTI, M. & COSSARIZZA, A. 2011. Quality assessment of human mitochondrial DNA quantification: MITONAUTS, an international multicentre survey. *Mitochondrion,* 11**,** 520-527.

DAYAL, D., MARTIN, S. M., OWENS, K. M., AYKIN-BURNS, N., ZHU, Y., BOOMINATHAN, A., PAIN, D., LIMOLI, C. L., GOSWAMI, P. C., DOMANN, F. E. & SPITZ, D. R. 2009. Mitochondrial Complex II Dysfunction Can Contribute Significantly to Genomic Instability after Exposure to Ionizing Radiation. *Radiation Research,* 172**,** 737-745, 9.

EVDOKIMOVSKY, E. V., USHAKOVA, T. E., KUDRIAVTCEV, A. A. & GAZIEV, A. I. 2011. Alteration of mtDNA copy number, mitochondrial gene expression and extracellular DNA content in mice after irradiation at lethal dose. *Radiation and Environmental Biophysics,* 50**,** 181-188.

GAHAN, M. E., MILLER, F., LEWIN, S. R., CHERRY, C. L., HOY, J. F., MIJCH, A., ROSENFELDT, F. & WESSELINGH, S. L. 2001. Quantification of mitochondrial DNA in peripheral blood mononuclear cells and subcutaneous fat using real-time polymerase chain reaction. *Journal of Clinical Virology,* 22**,** 241-247.

GUO, W., JIANG, L., BHASIN, S., KHAN, S. M. & SWERDLOW, R. H. 2009. DNA extraction procedures meaningfully influence qPCR-based mtDNA copy number determination. *Mitochondrion,* 9**,** 261-265.

HAROON, S., LI, A., WEINERT, J. L., FRITSCH, C., ERICSON, N. G., ALEXANDER-FLOYD, J., BRAECKMAN, B. P., HAYNES, C. M., BIELAS, J. H., GIDALEVITZ, T. & VERMULST, M. 2018. Multiple Molecular Mechanisms Rescue mtDNA Disease in C. elegans. *Cell Reports,* 22**,** 3115-3125.

HINDSON, B. J., NESS, K. D., MASQUELIER, D. A., BELGRADER, P., HEREDIA, N. J., MAKAREWICZ, A. J., BRIGHT, I. J., LUCERO, M. Y., HIDDESSEN, A. L. & LEGLER, T. C. 2011. High-throughput droplet digital PCR system for absolute quantitation of DNA copy number. *Analytical chemistry,* 83**,** 8604-8610.

HUNTER, S. E., JUNG, D., DI GIULIO, R. T. & MEYER, J. N. 2010. The QPCR assay for analysis of mitochondrial DNA damage, repair, and relative copy number. *Methods,* 51**,** 444-451.

JOHNSON, T. E. & HARTMAN, P. S. 1988. Radiation Effects on Life Span in Caenorhabditis Elegans. *Journal of Gerontology,* 43**,** B137-B141.

KAM, W. W.-Y. & BANATI, R. B. 2013. Effects of ionizing radiation on mitochondria. *Free Radical Biology Medicine,* 65**,** 607-619.

590 KRISKO, A., LEROY, M., RADMAN, M. & MESELSON, M. 2012. Extreme anti-oxidant protection against
591 ionizing radiation in bdelloid rotifers. *Proc Natl Acad Sci U S A,* 109**,** 2354-7.
592 LEWIS, J. A. & FLEMING, J. T. 1995. Basic culture methods. *Methods in cell biology,* 48**,** 3-29.
593 LEWIS, S. C., JOERS, P., WILLCOX, S., GRIFFITH, J. D., JACOBS, H. T. & HYMAN, B. C. 2015. A Rolling
594 Circle Replication Mechanism Produces Multimeric Lariats of Mitochondrial DNA in
595 Caenorhabditis elegans. *PLOS Genetics,* 11**,** e1004985.
596 LIND, O. C., OUGHTON, D. H. & SALBU, B. 2019. The NMBU FIGARO low dose irradiation facility.
597 *International journal of radiation biology,* 95**,** 76-81.
598 LOMAX, M. E., FOLKES, L. K. & O'NEILL, P. 2013. Biological Consequences of Radiation-induced DNA
599 Damage: Relevance to Radiotherapy. *Clinical Oncology,* 25**,** 578-585.
600 MALAKHOVA, L., BEZLEPKIN, V. G., ANTIPOVA, V., USHAKOVA, T., FOMENKO, L., SIROTA, N. &
601 GAZIEV, A. I. 2005. The increase in mitochondrial DNA copy number in the tissues of γ-
602 irradiated mice. *Cellular Molecular Biology Letters,* 10**,** 721.
603 MALIK, A. N. & CZAJKA, A. 2013. Is mitochondrial DNA content a potential biomarker of mitochondrial
604 dysfunction? *Mitochondrion,* 13**,** 481-492.
605 MALIK, A. N., SHAHNI, R., RODRIGUEZ-DE-LEDESMA, A., LAFTAH, A. & CUNNINGHAM, P. 2011.
606 Mitochondrial DNA as a non-invasive biomarker: accurate quantification using real time
607 quantitative PCR without co-amplification of pseudogenes and dilution bias. *Biochemical and*
608 *biophysical research communications,* 412**,** 1-7.
609 MANDAVILLI, B. S., SANTOS, J. H. & VAN HOUTEN, B. 2002. Mitochondrial DNA repair and aging.
610 *Mutation Research/Fundamental and Molecular Mechanisms of Mutagenesis,* 509**,** 127-151.
611 MAREMONTI, E., EIDE, D. M., OUGHTON, D. H., SALBU, B., GRAMMES, F., KASSAYE, Y. A., GUÉDON,
612 R., LECOMTE-PRADINE, C. & BREDE, D. A. 2019a. Gamma radiation induces life stage-
613 dependent reprotoxicity in Caenorhabditis elegans via impairment of spermatogenesis.
614 *Science of The Total Environment***,** 133835.
615 MAREMONTI, E., EIDE, D. M., ROSSBACH, L., SALBU, B., LIND, O. C. & BREDE, D. A. 2019b. In vivo
616 assessment of ROS production and oxidative stress effects induced by chronic exposure to
617 gamma radiation in *C. elegans*. Submitted manuscript (September 2019).
618 MEMON, A. A., ZÖLLER, B., HEDELIUS, A., WANG, X., STENMAN, E., SUNDQUIST, J. & SUNDQUIST, K.
619 2017. Quantification of mitochondrial DNA copy number in suspected cancer patients by a
620 well optimized ddPCR method. *Biomolecular Detection and Quantification,* 13**,** 32-39.
621 MONTIER, L. L. C., DENG, J. J. & BAI, Y. 2009. Number matters: control of mammalian mitochondrial
622 DNA copy number. *Journal of genetics and genomics,* 36**,** 125-131.
623 NUGENT, S., MOTHERSILL, C. E., SEYMOUR, C., MCCLEAN, B., LYNG, F. M. & MURPHY, J. E. J. 2010.
624 Altered mitochondrial function and genome frequency post exposure to γ-radiation and
625 bystander factors. *International Journal of Radiation Biology,* 86**,** 829-841.
626 OKUNIEFF, P., SWARTS, S., KENG, P., SUN, W., WANG, W., KIM, J., YANG, S., ZHANG, H., LIU, C. &
627 WILLIAMS, J. P. 2008. Antioxidants reduce consequences of radiation exposure. *Oxygen*
628 *Transport to Tissue XXIX.* Springer.
629 PHILLIPS, N. R., SPROUSE, M. L. & ROBY, R. K. 2014. Simultaneous quantification of mitochondrial
630 DNA copy number and deletion ratio: a multiplex real-time PCR assay. *Sci Rep,* 4**,** 3887.
631 POLYAK, E., ZHANG, Z. & FALK, M. J. 2012. Molecular profiling of mitochondrial dysfunction in
632 Caenorhabditis elegans. *Mitochondrial Disorders.* Springer.
633 ROGOUNOVITCH, T. I., SAENKO, V. A., SHIMIZU-YOSHIDA, Y., ABROSIMOV, A. Y., LUSHNIKOV, E. F.,
634 ROUMIANTSEV, P. O., OHTSURU, A., NAMBA, H., TSYB, A. F. & YAMASHITA, S. 2002. Large
635 deletions in mitochondrial DNA in radiation-associated human thyroid tumors. *Cancer*
636 *Research,* 62**,** 7031-7041.
637 RYCHLIK, W. 1995. Selection of primers for polymerase chain reaction. *Molecular Biotechnology,* 3**,**
638 129-134.
639 SAWYER, D. E. & VAN HOUTEN, B. 1999. Repair of DNA damage in mitochondria. *Mutation*
640 *Research/DNA Repair,* 434**,** 161-176.

641 SPITZ, D. R., AZZAM, E. I., LI, J. J. & GIUS, D. 2004. Metabolic oxidation/reduction reactions and
642 cellular responses to ionizing radiation: a unifying concept in stress response biology. *Cancer*
643 *and Metastasis Reviews,* 23**,** 311-322.
644 STIERNAGLE, T. 1999. Maintenance of C. elegans. *Wormbook,* 2**,** 51-67.
645 YAKES, F. M. & VAN HOUTEN, B. 1997. Mitochondrial DNA damage is more extensive and persists
646 longer than nuclear DNA damage in human cells following oxidative stress. *Proceedings of*
647 *the National Academy of Sciences,* 94**,** 514-519.
648 YE, J., COULOURIS, G., ZARETSKAYA, I., CUTCUTACHE, I., ROZEN, S. & MADDEN, T. L. 2012. Primer-
649 BLAST: a tool to design target-specific primers for polymerase chain reaction. *BMC*
650 *bioinformatics,* 13**,** 134.

651

652

653

654 Supporting material

655 Development of droplet digital PCR method for the assessment
656 of mitochondrial DNA copy number variation in response to
657 ionizing radiation in the nematode *Caenorhabditis elegans*

658

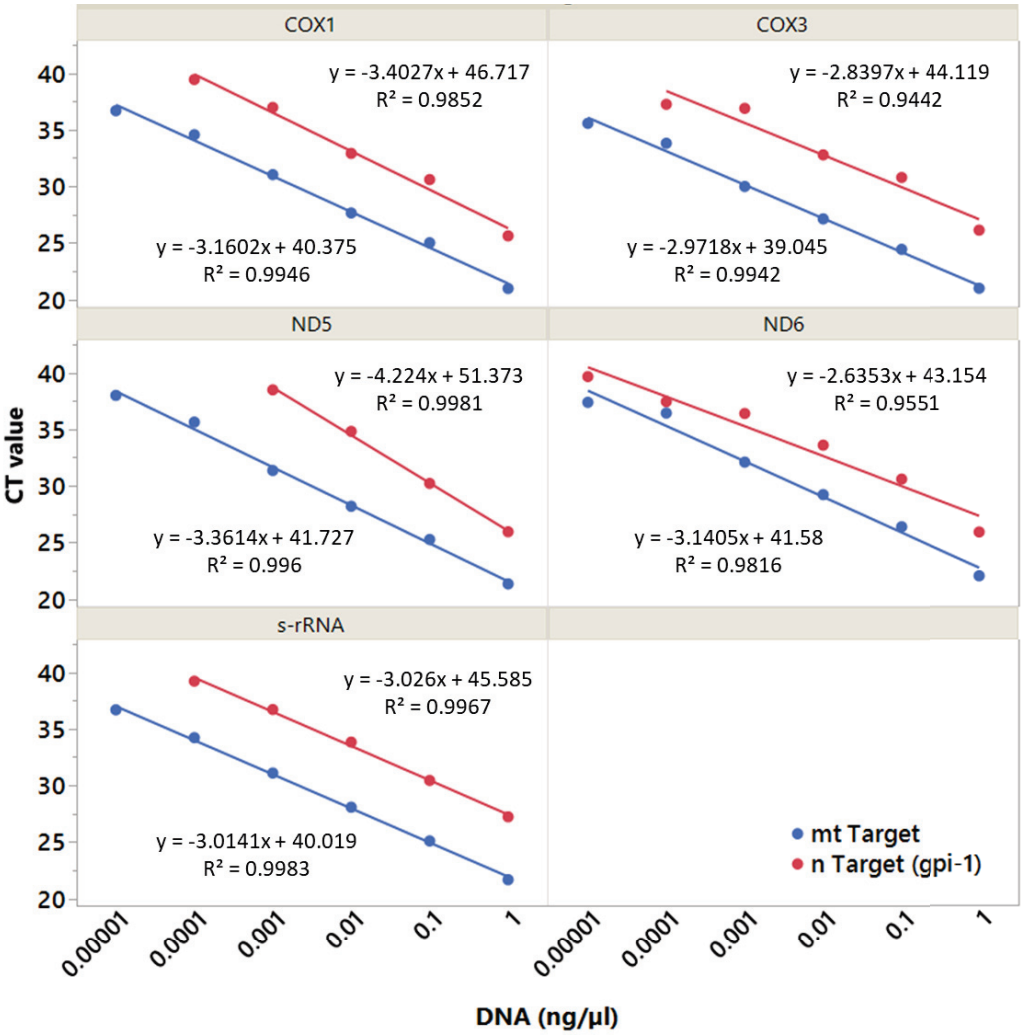

Figure S.1. CT values measured at different concentrations of DNA template (ng/µl) with qPCR duplex assay using five mitochondrial targets (COX1, COX3, ND5, s-rRNA, tRNA-val/ND6) and *gpi-1* as nuclear reference gene.

Table S.1. Amplification efficiency (Ex (%)) calculated for each mitochondrial target and for the nuclear reference gene *gpi-1*, from a linear regression analysis based on a duplex qPCR experiment performed with a serial dilution of DNA template (**Fig. S.1**).

		mtTarget	*gpi-1*
s-rRNA	Slope	-3.01	-3.03
	E_x (%)	108.7	108.0
	R^2	0.99	0.99
COX1	Slope	-3.16	-3.40
	E_x (%)	100.1	88.0
	R^2	0.99	0.98
COX3	Slope	-2.97	-2.84
	E_x (%)	111.4	120.6
	R^2	0.99	0.94
ND5	Slope	-3.36	-4.22
	E_x (%)	89.9	59.8
	R^2	0.99	0.99
tRNA-val/ND6	Slope	-3.14	-2.64
	E_x (%)	101.2	137.6
	R^2	0.98	0.95

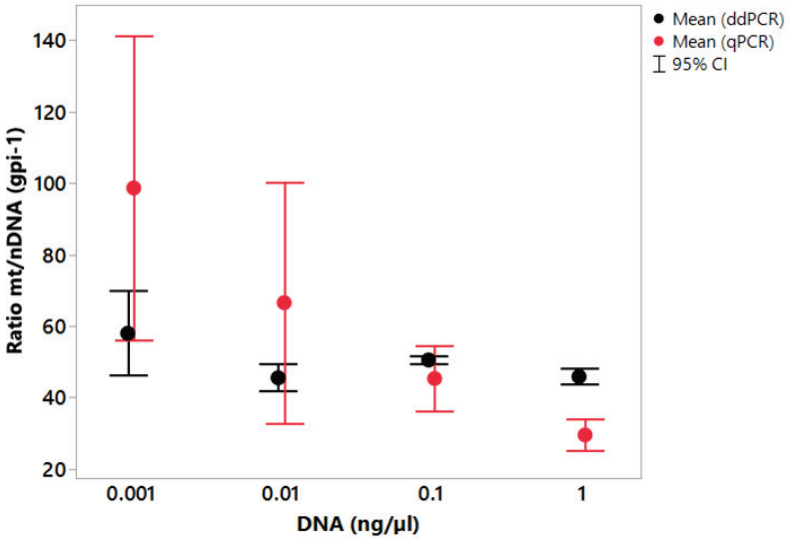

672

673 **Figure S.3** Comparison between qPCR and ddPCR for the quantification of mt/nDNA ratios, measured as
674 average of five mitochondrial targets and a nuclear reference gene (*gpi-1*) at different concentrations of
675 DNA template (ng/µl) (from three biological replicates and three technical replicates per concentration).

676

677

678

679

680

681

682

683

684 **Table S.2.** Dose-rates and total doses of exposure employed for the low and high dose-range chronic
685 gamma irradiation of *C. elegans*. Exposure to low dose-rage was performed from L1 stage, similarly to
686 exposure to high dose-range for 72 hours. Exposure for 24 and 48 hours was performed at ~L2/L3 and
687 L4 stages, respectively.

688

Total Dose (Gy)			
	Exposure time (hours)		
Dose-rate (mGy/hr)	24	48	72
0	-	-	0
0.43	-	-	0.03
1.1	-	-	0.08
10.8	-	-	0.78
40.8	-	-	2.94
99.9	-	-	7.19
1000	24.0	48.0	72.0

689

ISBN: 978-82-575-1674-1
ISSN: 1894-6402

Norwegian University
of Life Sciences

Postboks 5003
NO-1432 Ås, Norway
+47 67 23 00 00
www.nmbu.no

105962 / ANDVORDGRAFISK.NO